VOLUME 75 DECEMBER 23, 1971 NUMBER 26

JPCHAx

THE JOURNAL OF

PHYSICAL CHEMISTRY

PUBLISHED BIWEEKLY BY THE AMERICAN CHEMICAL SOCIETY

THE JOURNAL OF

PHYSICAL CHEMISTRY

BRYCE CRAWFORD, Jr., *Editor*
STEPHEN PRAGER, *Associate Editor*
ROBERT W. CARR, Jr., FREDERIC A. VAN-CATLEDGE, *Assistant Editors*

EDITORIAL BOARD: A. O. ALLEN (1970–1974), R. BERSOHN (1967–1971), J. R. BOLTON (1971–1975), S. BRUNAUER (1967–1971), M. FIXMAN (1970–1974), H. S. FRANK (1970–1974), J. R. HUIZENGA (1969–1973), M. KASHA (1967–1971), W. J. KAUZMANN (1969–1973), W. R. KRIGBAUM (1969–1973), R. A. MARCUS (1968–1972), W. J. MOORE (1969–1973), J. A. POPLE (1971–1975), B. S. RABINOVITCH (1971–1975), H. REISS (1970–1974), S. A. RICE (1969–1975), R. E. RICHARDS (1967–1971), F. S. ROWLAND (1968–1972), R. L. SCOTT (1968–1972), R. SEIFERT (1968–1972)

CHARLES R. BERTSCH, *Manager, Editorial Production*

AMERICAN CHEMICAL SOCIETY, *1155 Sixteenth St., N.W., Washington, D. C. 20036*
FREDERICK T. WALL, *Executive Director*

Books and Journals Division
JOHN K CRUM, *Director (Acting)*
JOSEPH H. KUNEY, *Head, Business Operations Department*
RUTH REYNARD, *Assistant to the Director*

©Copyright, 1971, by the American Chemical Society. Published biweekly by the American Chemical Society at 20th and Northampton Sts., Easton, Pa. 18042. Second-class postage paid at Washington, D. C., and at additional mailing offices.

All manuscripts should be sent to *The Journal of Physical Chemistry*, Department of Chemistry, University of Minnesota, Minneapolis, Minn. 55455.

Additions and Corrections are published once yearly in the final issue. See Volume 74, Number 26 for the proper form.

Extensive or unusual alterations in an article after it has been set in type are made at the author's expense, and it is understood that by requesting such alterations the author agrees to defray the cost thereof.

The American Chemical Society and the Editor of *The Journal of Physical Chemistry* assume no responsibility for the statements and opinions advanced by contributors.

Correspondence regarding accepted copy, proofs, and reprints should be directed to Editorial Production Office, American Chemical Society, 20th and Northampton Sts., Easton, Pa. 18042. Manager: Charles R. Bertsch. Assistant Editor: Edward A. Borger. Editorial Assistant: William T. Boyd.

Advertising Office: Century Communications Corporation, 142 East Avenue, Norwalk, Conn. 06851.

Business and Subscription Information

Remittances and orders for subscriptions and for single copies, notices of changes of address and new professional connections, and claims for missing numbers should be sent to the Subscription Service Department, American Chemical Society, 1155 Sixteenth St., N.W., Washington, D. C. 20036. Allow 4 weeks for changes of address. Please include an old address label with the notification.

Claims for missing numbers will not be allowed (1) if received more than sixty days from date of issue, (2) if loss was due to failure of notice of change of address to be received before the date specified in the preceding paragraph, or (3) if the reason for the claim is "missing from files."

Subscription rates (1971): members of the American Chemical Society, $20.00 for 1 year; to nonmembers, $40.00 for 1 year. Those interested in becoming members should write to the Admissions Department, American Chemical Society, 1155 Sixteenth St., N.W., Washington, D. C. 20036. Postage to Canada and countries in the Pan-American Union, $4.00; all other countries, $5.00. Single copies for current year: $2.00. Rates for back issues from Volume 56 to date are available from the Special Issues Sales Department, 1155 Sixteenth St., N.W., Washington, D. C. 20036.

This publication and the other ACS periodical publications are now available on microfilm. For information write to: MICROFILM, Special Issues Sales Department, 1155 Sixteenth St., N.W., Washington, D. C. 20036.

Notice to Authors printed in this issue

THE JOURNAL OF
PHYSICAL CHEMISTRY

Volume 75, Number 26 December 23, 1971

Symposium on Polymer Chemistry, Southeast–Southwest Regional Meeting of the American Chemical Society, New Orleans, La., December 1970

Thermodynamic and Morphological Properties of Crystalline Polymers . . . . **L. Mandelkern** 3909

Molecular Mechanism of Chain Rupture in Strained Crystalline Polymers . . . . **A. Peterlin** 3921

Theoretical Models for Peak Migration in Gel Permeation Chromatography . . . . **Edward F. Casassa** 3929

The Kinetics of Chlorine Fluoride at High Temperatures
. . . **J. A. Blauer, W. C. Solomon, and V. S. Engleman** 3939

Primary and Secondary Rate Processes in the Acetone–Silane Photochemical System
. . . **H. Edward O'Neal, Spyros Pavlou, Tom Lubin, Morey A. Ring, and L. Batt** 3945

Studies on the Formation of Primary Yields of Hydrogen Peroxide and Molecular Hydrogen ($G_{H_2O_2}$ and G_{H_2}) in the γ Radiolysis of Neutral Aqueous Solutions . . . . **Z. D. Draganić and I. G. Draganić** 3950

Interlamellar Metal Complexes on Layer Silicates. I. Copper(II)–Arene Complexes on Montmorillonite
. . . **Thomas J. Pinnavaia and M. M. Mortland** 3957

A Proton Magnetic Resonance Study of the Hydrogen Bonding of Alkylated Bases to Dimethyl Sulfoxide
. . . **Raymond C. Fort, Jr., and Ted R. Lindstrom** 3963

Field-Dependent Contributions to Carbon-13 Nuclear Relaxation
. . . **James R. Lyerla, Jr., David M. Grant, and Richard D. Bertrand** 3967

Some Observations Concerning Nuclear Magnetic Resonance Proton Shifts of Polar Solutes
. . . **Paul H. Weiner and Edmund R. Malinowski** 3971

A Study of Phosphorus–Sulfur Compounds by Inner-Orbital Photoelectron Spectroscopy: Thiono–Thiolo Sulfur
. . . **Wojciech J. Štec, William E. Moddeman, Royal G. Albridge, and John R. Van Wazer** 3975

Transition Probabilities of Europium in Phosphate Glasses
. . . **R. Reisfeld, R. A. Velapoldi, L. Boehm, and M. Ish-Shalom** 3980

Matrix-Isolation Study of the Pyrolysis of Bromochloromethyl-Substituted Organomercury Compounds. Infrared Spectra of Bromochlorocarbene and the Free Radicals CCl_2Br and $CClBr_2$
. . . **A. K. Maltsev, O. M. Nefedov, R. H. Hauge, J. L. Margrave, and D. Seyferth** 3984

The Infrared Spectrum of Polyethylene Irradiated at 4°K . . . . **David C. Waterman and Malcolm Dole** 3988

Low-Frequency Modes in Molecular Crystals. XVII. Torsional Motions and Barriers to Internal Rotation in Some Ethylsilanes, Ethylgermanes, and Ethanol . . . . **J. R. Durig and C. W. Hawley** 3993

Vibrational Energy Transfer in the Hydrogen Molecule–Helium Atom System . . . . **Hyung Kyu Shin** 4001

Proton-Transfer Reactions. A Mechanism for the Absorption of Ultrasound in Aqueous Solutions of Proteins
. . . **Matthew Hussey and Peter D. Edmonds** 4012

Proton Transfer in the Two-Step Electrochemical Reduction of Oxygen in *N,N*-Dimethylformamide
. . . **Helen J. James and Robert F. Broman** 4019

Transport Processes in Low Melting Salts. The $AgNO_3$–$TlNO_3$ System
. . . **G. J. Janz, R. P. T. Tomkins, H. Siegenthaler, K. Balasubrahmanyam, and S. W. Lurie** 4025

The Analysis of Solution Kinetics Data Coupled with Thermal Transients in an Adiabatic Calorimeter. I
. . . **E. D. West and W. J. Svirbely** 4029

The Analysis of Solution Kinetics Data Coupled with Thermal Transients in an Adiabatic Calorimeter. II. First-Order Reactions . . . . **W. J. Svirbely, E. D. West, and F. A. Kundell** 4039

Vapor–Liquid Equilibria of Binary Mixtures of Carbon-14-Labeled Hexane with Aliphatic Ketones . . . **Bogdan Magiera and Witold Brostow** 4041

Heats of Formation of Nitroaromatics. Group Additivity for Solids . . . . **Robert Shaw** 4047

Vacuum Vaporization Studies of Lithium Fluoride Single Crystals . . . **D. L. Howlett, J. E. Lester, and G. A. Somorjai** 4049

The Reaction of O(^{3}P) with Dideuterioacetylene . . . . **David G. Williamson** 4053

NOTES

A Nuclear Magnetic Resonance Study of the Protolysis Kinetics of 5-Dimethylaminonaphthalene-1-sulfonic Acid and Its *N*-Methylsulfonamide . . . . **J. F. Whidby, D. E. Leyden, C. M. Himel, and R. T. Mayer** 4056

Raman Spectrum of Purple Sulfur . . . . **Robert E. Barletta and Chris W. Brown** 4059

Fluorine Nuclear Magnetic Resonance Study of the Conformation of a Polyethylenimine Derivative . . . **Timothy W. Johnson and Irving M. Klotz** 4061

COMMUNICATIONS TO THE EDITOR

Electron Spin Resonance Signals of Abnormal Alkyl Radicals Trapped on Porous Vycor Glass Surfaces Coated with Metal Oxides at 77°K. . . . . **Takashi Katsu, Michiyasu Yanagita, and Yuzaburo Fujita** 4064

Additions and Corrections 4066

Author Index to Volume 75, 1971 . . . . 1A

Key Word Index to Volume 75, 1971 . . . . 1K

Compound Index to Volume 75, 1971 . . . . 1C

AUTHOR INDEX

Albridge, R. G., 3975

Balasubrahmanyam, K., 4025
Barletta, R. E., 4059
Batt, L., 3945
Bertrand, R. D., 3967
Blauer, J. A., 3939
Boehm, L., 3980
Broman, R. F., 4019
Brostow, W., 4041
Brown, C. W., 4059

Casassa, E. F., 3929

Dole, M., 3988
Draganić, I. G., 3950
Draganić, Z. D., 3950
Durig, J. R., 3993

Edmonds, P. D., 4012
Engleman, V. S., 3939

Fort, R. C., Jr., 3963
Fujita, Y., 4064

Grant, D. M., 3967

Hauge, R. H., 3984
Hawley, C. W., 3993
Himel, C. M., 4056
Howlett, D. L., 4049
Hussey, M., 4012

Ish-Shalom, M., 3980

James, H. J., 4019
Janz, G. J., 4025
Johnson, T. W., 4061

Katsu, T., 4064
Klotz, I. M., 4061
Kundell, F. A., 4039

Lester, J. E., 4049
Leyden, D. E., 4056
Lindstrom, T. R., 3963
Lubin, T., 3945
Lurie, S. W., 4025
Lyerla, J. R., Jr., 3967

Magiera, B., 4041
Malinowski, E. R., 3971
Maltsev, A. K., 3984
Mandelkern, L., 3909
Margrave, J. L., 3984
Mayer, R. T., 4056
Moddeman, W. E., 3975
Mortland, M. M., 3957

Nefedov, O. M., 3984

O'Neal, H. E., 3945

Pavlou, S., 3945
Peterlin, A., 3921
Pinnavaia, T. J., 3957

Reisfeld, R., 3980
Ring, M. A., 3945

Seyferth, D., 3984
Shaw, R., 4047
Shin, H. K., 4001
Siegenthaler, H., 4025
Solomon, W. C., 3939
Somorjai, G. A., 4049
Stec, W. J., 3975
Svirbely, W. J., 4029, 4039

Tomkins, R. P. T., 4025

Van Wazer, J. R., 3975
Velapoldi, R. A., 3980

Waterman, D. C., 3988
Weiner, P. H., 3971
West, E. D., 4029, 4039
Whidby, J. F., 4056
Williamson, D. G., 4053

Yanagita, M., 4064

In papers with more than one author the name of the author to whom inquiries about the paper should be addressed is marked with an asterisk in the by-line.

NOTICE TO AUTHORS

I. General Considerations

The Journal of Physical Chemistry is devoted to reporting both experimental and theoretical research dealing with fundamental aspects of physical chemistry. Space limitations necessitate giving preference to research articles dealing with previously unanswered basic questions in physical chemistry. Acceptable topics are those of general interest to physical chemists, especially work involving new concepts, techniques, and interpretations. Research that may lead to reexaminations of generally accepted views is, of course, welcome.

Authors reporting data should include an interpretation of the data and its relevance to the theories of the properties of matter. However, the discussion should be concise and to the point and excessive speculation is to be discouraged. Papers reporting redeterminations of existing data will be acceptable only if there is reasonable justification for repetition: for example, if the more recent or more accurate data lead to new questions or to a reexamination of well known theories. Manuscripts that are essentially applications of chemical data or reviews of the literature are, in general, not suitable for publication in *The Journal of Physical Chemistry*. Detailed comparisons of methods of data analysis will be considered only if the paper also contains original data, or if such comparison leads to a genesis of new ideas.

Authors should include an introductory statement outlining the scientific rationale for the research. The statement should clearly specify the questions for which answers are sought and the connection of the present work with previous work in the field. All manuscripts are subject to critical review. It is to be understood that the final decision relating to a manuscript's suitability rests solely with the editors.

Symposium papers are sometimes published as a group, but only after special arrangement with the editor.

Authors' attention is called to the "Handbook for Authors," available from the Special Issues Sales Department, American Chemical Society, 1155 Sixteenth St., N.W., Washington, D. C. 20036, in which pertinent material is to be found.

II. Types of Manuscripts

The Journal of Physical Chemistry publishes two types of manuscripts: *Articles* and *Communications.*

A. Articles should cover their subjects with thoroughness, clarity, and completeness. However, authors should also strive to make their *Articles* as concise as possible, avoiding unnecessary historical background. Abstracts to *Articles* should be brief—300 words is a maximum—and should serve to summarize the significant data and conclusions. The abstract should convey the essence of the *Article* to the reader.

B. Communications are of two types, *Letters* and *Comments.* Both types are restricted to three-quarters of a page (750 words or the equivalent) including tables, figures, and text, and both types of *Communications* are subject to critical review, but special efforts will be made to expedite publication.

Letters should report preliminary results whose immediate availability to the scientific community is deemed important, and whose topic is timely enough to justify the double publication that usually results from the publication of a *Letter*.

Comments include significant remarks on the work of others. The editors will generally permit the authors of the work being discussed to reply.

The category of *Notes* has been discontinued since the handling of such manuscripts was precisely the same as that of *Articles* save for the requirement of an Abstract, and since even a short *Article* will need an Abstract ultimately, it seems as well to ask the author to provide this. Short *Articles* will of course continue to be welcome contributions.

III. Introduction

All manuscripts submitted should contain brief introductory remarks describing the purpose of the work and giving sufficient background material to allow the reader to appreciate the state-of-knowledge at the time when the work was done. The introductory remarks in an *Article* should constitute the first section of the paper and should be labeled accordingly. In *Communications,* the introductory material should not be in such a separate section. To judge the appropriateness of the manuscript for *The Journal of Physical Chemistry,* the editors will place considerable weight on the author's intentions as stated in the Introduction.

IV. Functions of Reviewers

The editors request the scientific advice of reviewers who are active in the area of research covered by the manuscript. The reviewers act only in an advisory capacity and the final decision concerning a manuscript is the responsibility of the editors. The reviewers are asked to comment not only on the scientific content, but also on the manuscript's suitability for *The Journal of Physical Chemistry.* With respect to *Communications,* the reviewers are asked to comment specifically on the urgency of publication. Authors are encouraged to suggest, when submitting a manuscript, names of scientists who could give a disinterested and informed and helpful evaluation of the work. All reviews are anonymous and the reviewing process is most effective if reviewers do not reveal their identities to the authors. An exception arises in connection with a manuscript submitted for publication in the form of a comment on the work of another author. Under such circumstances the first author will, in general, be allowed to review the communication and to write a rebuttal, if he so chooses. The rebuttal and the original communication may be published together in the same issue of the journal. Revised manuscripts are generally sent back to the original reviewers, who are asked to comment on the revisions. If only minor revisions are involved, the editors examine the revised manuscript in light of the recommendations of the reviewers without seeking further opinions. For the convenience of reviewers, authors are advised to indicate clearly, either in the manuscript or in a covering letter, the specific revisions that have been made.

V. Submission of Manuscripts

All manuscripts must be submitted in triplicate to expedite handling. Manuscripts must be typewritten, double-spaced copy, on $8^1/_2 \times 11$ in. paper. Legal sized paper is not acceptable. Authors should be certain that copies of the manuscript are clearly reproduced and readable. **Authors submitting figures must include the original drawings or photographs thereof, plus three xerographic copies for review purposes. These reproductions of the figures should be on $8^1/_2 \times 11$ in. paper.** Graphs must be in black ink on white or blue paper. Lettering at the sides of graphs may be penciled in and will be typeset. Figures and tables should be held to a minimum consistent with adequate presentation of information. All original data which the author deems pertinent must be submitted along with the manuscript. For example, a paper reporting a crystal structure should include structure factor tables for use by the reviewers.

Footnotes and references to the literature should be numbered consecutively within the paper; the number should also be placed in parentheses in the left margin opposite the line in which the reference first appears. A complete list of references should appear at the end of the paper. Initials of the authors referred to in the citations should be included in the complete reference at the back of the paper. Nomenclature should conform to that used in *Chemical Abstracts* and mathematical characters should be underlined for italics, Greek letters should be annotated, and subscripts and superscripts clearly marked.

Papers should not depend for their usefulness on unpublished material, and excessive reference to material in press is discouraged. References not readily available (*e.g.*, private technical reports, preprints, or articles in press) that are necessary for a complete review of the paper must be included with the manuscript for use by the reviewers.

VI. Revised Manuscripts

A manuscript sent back to an author for revision should be returned to the editor within 6 months; otherwise it will be considered withdrawn and treated as a new manuscript when and if it is returned. Revised manuscripts returned to the editor must be submitted in triplicate and all changes should be made by typewriter. **Unless the changes are very minor, all pages affected by revision must be retyped.** If revisions are so extensive that a new typescript of the manuscript is necessary, it is requested that a copy of the original manuscript be submitted along with the revised one.

VII. Supplementary Material

From time to time manuscripts involve extensive tables, graphs, spectra, mathematical material, or other "supplementary material" which, though of value to the specialized reader who needs all the data or all the detail, does not help and often hinders the effective presentation of the work being reported. The American Chemical Society has instituted a policy of including such supplementary material in the *microfilm* editions of its journals, which are available in many scholarly libraries; in addition, interested readers will be able to obtain the microfilm material directly at nominal cost. Authors are encouraged to make use of this resource, in the interests of shorter articles (which mean more rapid publication) and clearer, more readable presentation.

Supplementary material for inclusion in the microfilm edition should accompany a manuscript at the time of its original submission to an editor. It should be clipped together and attached at the end of the manuscript, along with a slip of paper clearly indicating that the material is "supplementary material for the microfilm edition." A footnote should appear in the paper indicating the nature of the supplementary material and the means by which the interested reader might be able to obtain copies of the data without use of the microfilm edition itself. The following is an example:

(3) Listings of structure factors, coordinates, and anisotropic temperature factors will appear immediately following this article in the microfilm edition of this volume of the journal. Single copies may be obtained from the Business Operations Office, Books and Journals Division, American Chemical Society, 1155 Sixteenth Street, N. W., Washington, D. C. 20036, by referring to author, title of article, volume, and page number. Remit check or money order for $0.00 for photocopy or $0.00 for microfiche.

The amount of money to be indicated in the blanks will be filled in by the Editorial Office at Easton, Pa., after the acceptance of an article.

VIII. Proofs and Reprints

Galley proofs, original manuscript, cut copy, and reprint order form are sent by the printer directly to the author who submitted the manuscript. The attention of the authors is directed to the instructions which accompany the proof, especially the requirement that all corrections, revisions, and additions be entered on the proof and not on the manuscript. Proofs should be checked against the manuscript (in particular all tables, equations, and formulas, since this is not done by the editor) and returned as soon as possible. No paper is released for printing until the author's proof has been received. Alterations in an article after it has been set in type are made at the author's expense, and it is understood that by entering such alterations on proofs the author agrees to defray the cost thereof. The filled-out reprint form must be returned with the proof, and if a price quotation is required by the author's organization a request for it should accompany the proof. Since reprinting is generally done from the journal press forms, all orders must be filed before press time. None can be accepted later, unless a previous request has been made to hold the type. Reprint shipments are made a month or more after publication, and bills are issued by the printer subsequent to shipment. Neither the editors nor the Washington office keeps any supply of reprints. Therefore, only the authors can be expected to meet requests for single copies of papers.

A page charge is assessed to cover in part the cost of publication. Although payment is expected, it is not a condition for publication. Articles are accepted or rejected only on the basis of merit, and the editor's decision to publish the paper is made before the charge is assessed. The charge per journal page is $50.

THE JOURNAL OF

PHYSICAL CHEMISTRY

Registered in U. S. Patent Office *© Copyright, 1971, by the American Chemical Society*

VOLUME 75, NUMBER 26 DECEMBER 23, 1971

Thermodynamic and Morphological Properties of Crystalline Polymers[1]

by L. Mandelkern

Department of Chemistry and Institute of Molecular Biophysics, The Florida State University, Tallahassee, Florida 32306

(Received May 24, 1971)

Publication costs borne completely by The Journal of Physical Chemistry

A variety of physical chemical properties of linear polyethylene, crystallized either in bulk or from dilute solution, are reviewed. The importance of utilizing molecular weight fractions is demonstrated, and a diversity of properties are discussed in terms of crystallite size and interfacial structure. The properties of solution-formed crystals cannot be explained in terms of a regularly folded, regularly structured interface. A disordered amorphous overlayer, which is consistent with the electron micrographs and other morphological studies, is required. Bulk crystallized samples of high molecular weight are characterized by a very high interfacial free energy consistent with a diffuse and distorted interfacial region. In addition there exists an interzonal region where the chain units are in nonordered conformations and connect crystallites.

General Introduction

It has been well demonstrated that the crystallization–melting process involving long-chain molecules can be treated as a first-order phase transition which is similar in all its major aspects to the behavior of monomeric substances.[2] Similarly, the crystallization kinetics from the pure melt has been shown to adhere to the general mathematical formulation for the kinetics of phase changes as developed by Avrami.[2,3] Although these very important results establish the physical chemical framework and give the proper perspective within which to study crystalline polymers, certain important kinds of problems cannot be resolved solely from these general conclusions. Deviations from equilibrium theory are the norm as a consequence of kinetic factors which control the crystallization process, so that a polycrystalline system with an attendant complex morphology results. Therefore, in order to understand the properties of crystalline polymers, whether they be thermodynamic, spectral, mechanical, or other kinds, the relation to morphological features and the deviations from equilibrium must be established. It is our objective here to attempt to establish such relationships.

Investigations over the past decade have established that virtually all homopolymers of regular structure crystallize from dilute solution in the form of thin lamella-like platelets. Typically, such crystals are several microns in lateral dimensions and are the order of 100 Å thick. The crystallite thickness is found to be very sensitive to the crystallization temperature. Furthermore, selected area diffraction studies have demonstrated that the chain axes are preferentially oriented normal to the wide faces of the crystals. Since this crystal habit and dimensions are found for chains of very high molecular weight, a given chain molecule must traverse a crystallite many times. There is, therefore, a reentrant requirement for the chain to the crystallite of origin. From these observations and the external form of the crystals, the conclusion was

---

(1) (a) The first three papers of this issue were presented at the Southeast–Southwest Regional ACS Meeting held in New Orleans, La., on Dec 2–4, 1970. The are being published as part of our experimental series of review articles on significant areas in physical chemistry. We invite our readers to let us know their views on the desirability of such contributions continuing to appear from time to time in this journal.—The Editors. (b) This work was supported by a grant from the Army Research Office (Durham).

(2) L. Mandelkern, "Crystallization of Polymers," McGraw-Hill, New York, N. Y., 1964.

(3) (a) M. Avrami, *J. Chem. Phys.*, 7, 1103 (1939); (b) *ibid.*, 8, 212 (1940).

reached, and is still being argued in some quarters, that the chains comprising the crystallites are regularly folded so that the 001 basal plane is a smooth surface of regular folds.[4]

Lamella-like crystallites are also a well-established and characteristic morphological form for homopolymers crystallized in bulk, *i.e.*, from the pure melt. The concept of regularly folded chains has therefore also been carried over to the bulk crystallized systems.[4b-d] Here it is also argued that a chain is regularly folded and confined to a single crystallite. This proposal continues with the concept that there are no chain units in nonordered conformations which connect crystallites; *i.e.*, amorphous or interzonal regions are absent. In this view the well-known and generally accepted deviations in thermodynamic quantities from those of a perfect crystal, the halos observed in wide-angle X-ray diffraction, and the observations of certain infrared bands, for example, are attributed to contributions from the smooth interface of the small crystals and from defect structures within the crystallite interior.[4b-d]

Certain important aspects of morphology such as the interfacial structure, the existence of chain units between crystallites, and the role of defect structure cannot be established solely from the appearance of electron micrographs. The major reason for postulating a set of regularly folded chains appears to reside in an effort to explain the external shape of the platelets formed in dilute solution. There is an obvious large gap in attempting to relate the external habit of crystals to molecular fine structure. The present state of electron microscopic technique is such that, for example, a discrimination as to the nature of the interfacial structure cannot be made. Physical chemical measurements and deductive reasoning power must be brought to bear on the problem. We shall try to accomplish this by considering the properties of crystals formed from the two major modes of crystallization, *i.e.*, from dilute solution and from the pure melt. Any conclusions that are reached must of course be in accord with the general nature of the electron microscope observations and of the crystallite habit.

Crystallization from Dilute Solution

Introduction. Two extreme types of chain reentry have been envisaged.[5,6] In one of these, the regularly folded array, each molecule crystallizes to the fullest extent possible so that crystallization is complete except for the number of chain elements required to make the sharp fold between crystalline sequences. Crystalline sequences from the same molecule are thus adjacent to one another and a regularly folded or pleated 001 interface is formed. Alternatively it has been proposed that adjacent reentry does not occur. Instead the crystalline sequences are connected more or less at random with the connecting loops also being of random length. A chain would thus traverse a nonordered or amorphous overlayer before rejoining the crystal lattice. According to this model the lamella are not completely crystalline but contain a disordered amorphous overlayer.[5,6] Two variants of these extremes have also been proposed which still require adjacent reentry. In one of these the regular folds are maintained but the sequence lengths are allowed to deviate from the mean.[7] A somewhat more irregular surface would thus be formed. However, we must recognize that only minor deviations can be tolerated in order to be consistent with the regularity evidenced in the four orders of low-angle X-ray diffraction that are observed. The other variant removes the regular fold requirement and replaces it with a loose loop of disordered chain units.[8]

Crystallite Size–Crystallization Temperature Relation. Before discussing the properties of solution formed crystals it is instructive to examine the relation between the crystallite thickness ζ and the crystallization temperature T_c. These data set a basis for a proper understanding of the properties. It is found, in detailed studies with linear polyethylene, that the crystallite thickness is independent of molecular weight for molecular weights greater than about 15,000.[9,10] Consequently, all properties which depend only on size are also molecular weight independent. For isothermal crystallization, the crystallite thickness is found to be independent of time from the earliest measurements that are possible to very long periods of storage at the crystallization temperature.[9] The postulated isothermal thickening of such crystals does not manifest itself in experimental reality. Properties which depend on thickness will thus also be independent of time.

Figure 1 is a composite plot of the crystallite thickness ζ, in ångströms, as a function of temperature, for linear polyethylene, crystallized from different solvents. The data represent the reports from several different laboratories, all of which are in essential agreement.[9,11-13] The dependence of the crystallite size

---

[4] (a) A. Keller, *Kolloid-Z. Z. Polym.*, **231**, 386 (1969); (b) J. D. Hoffman, *SPE* (*Soc. Plast. Eng.*) *J.*, **4**, 315 (1964); (c) P. H. Geil, "Polymer Single Crystals," Interscience, New York, N. Y., 1963; (d) P. H. Lindenmeyer, *Science*, **147**, 1256 (1965).

[5] P. J. Flory, *J. Amer. Chem. Soc.*, **84**, 2857 (1962).

[6] L. Mandelkern, *Progr. Polym. Sci.*, **2**, 165 (1970).

[7] J. D. Hoffman, J. J. Lauritzen, Jr., E. Passaglia, G. S. Ross, L. J. Frolen, and J. J. Weeks, *Kolloid-Z. Z. Polym.*, **231**, 564 (1969).

[8] H. G. Zachmann and A. Peterlin, *J. Macromol. Sci., Phys.*, **3**, 495 (1969).

[9] J. F. Jackson and L. Mandelkern, *Macromolecules*, **1**, 546 (1968).

[10] H. F. Bair and R. Salovey, *J. Macromol. Sci., Phys.*, **3**, 3 (1969).

[11] (a) H. E. Bair and R. Salovey, *Macromolecules*, **3**, 677 (1970); (b) T. Kawai and A. Keller, *Phil. Mag.*, [8] **11**, 1165 (1965).

[12] A. Nakajima, F. Hamada, S. Hayaski, and T. Sumida, *Kolloid-Z.*, **222**, 10 (1968).

[13] R. K. Sharma, J. F. Jackson, and L. Mandelkern, *Polym. Prepr., Amer. Chem. Soc., Div. Polym. Chem.*, **10** (2), 1327 (1969).

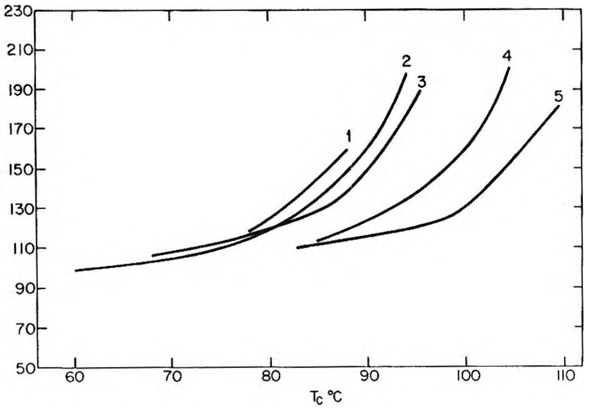

Figure 1. Plot of crystallite thickness ζ against crystallization temperature T_c, for different solvents: (1) decalin, (2) toluene, (3) xylene, (4) n-octane, (5) n-hexadecane.

on the crystallization temperature is readily apparent. The relatively flat portions of the curves, which are obtained at the lower crystallization temperatures, are a consequence of the fact that the crystallization is not isothermal in this temperature range. Dilatometric measurements show that the crystallization rate is very rapid at these temperatures,[14,15] and direct temperature measurements demonstrate that the actual crystallization is nonisothermal.[9,16] Therefore, theories based on isothermal crystallization, no matter how detailed or sophisticated they are, which attempt to join or connect this nonisothermal region with the higher temperature region, are inappropriate.[7]

At the higher crystallization temperatures there is a very strong dependence of ζ on T_c for all the crystallizing solvents. The crystallite thickness increases almost twofold for a 10° increase in T_c. Experimental studies of the crystallization kinetics from dilute solution have shown that this process is characterized by a large negative temperature coefficient typical of nucleation control. A direct correlation between the nucleation parameters governing the crystallization rate and the observed crystallite size has been made.[15] The general hypothesis can then be put forth that the crystallite size in the chain direction, ζ, can be identified with ζ^*, the critical size of the nucleus in the chain direction. With this assumption and the very general proposition, common to all nucleation theories, that ζ^* is inversely related to the free energy of fusion, we can write

$$\zeta = \zeta^* = \frac{1}{\Delta f_u(v_2, T_c)} \simeq \frac{\kappa T_s^\circ}{\Delta H_u(T_s^\circ - T_c)} \qquad (1)$$

Equation 1 is of a very general form which is common to all known nucleation theories. It is, therefore, highly nonspecific. This is a very important fact since adherence to the form of eq 1 does not uniquely specify a particular type of nucleation process. In eq 1 T_s° is the equilibrium dissolution temperature (melting temperature in a dilute solution), and ΔH_u is the enthalpy of fusion per chain repeating unit. The parameter κ, which is a function of the interfacial free energies involved, specifies the type of nucleation that is size and rate controlling.

In order to analyze the data of Figure 1 by means of eq 1, a determination of T_s° independent of this set of data needs to be made. Although this quantity cannot be measured directly, it can be obtained by extrapolation methods from other kinds of experiments. The details of these methods and the data obtained have previously been reported.[9,13,17] A compilation of the values for T_s°, for the solvents of Figure 1, is given in Table I.

We can see from this table that the different and independent extrapolation methods yield very concordant values for T_s° for each of the solvents. From these results a plot, according to the suggestion of eq 1, of ζ against $T_s^\circ/(T_s^\circ - T_c)$ is given in Figure 2. The plot in this figure demonstrates that, when examined according to the fundamentals of nucleation theory, the data can be reduced to a single relation. Therefore, we can conclude that the interfacial free energy governing nucleation is independent of the crystallizing solvent. The single relation of Figure 2 encompasses both the nonisothermal and isothermal regions. This indicates that at the lower temperatures the deviations from linearity are dependent on the undercooling (and thus the crystallization rate) rather than the absolute temperature.

When compared at identical values for the temperature variable $T_s^\circ/(T_s^\circ - T_c)$, the crystallite sizes are

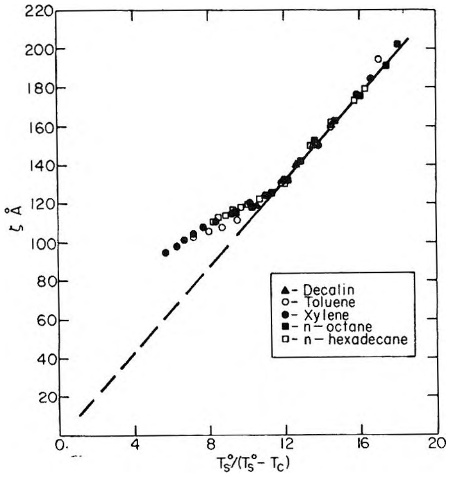

Figure 2. Plot of ζ against temperature variable $T_s^\circ/(T_s^\circ - T_c)$. Data are from Figure 1.

---

[14] L. Mandelkern, *Polymer*, 5, 637 (1964).

[15] C. Devoy, L. Mandelkern, and L. Bourland, *J. Polym. Sci., Part A-2*, 8, 869 (1970).

[16] H. Nagai and N. Kajikawa, *Polymer*, 9, 177 (1968).

[17] R. K. Sharma and L. Mandelkern, *Macromolecules*, 3, 758 (1970).

Table I:[17] The Values of $T_0°$ for Linear Polyethylene (°C)

Solvent	1 Density– ΔT	2 ΔH^*–ΔT regular-fold model	3 ΔH^*–ΔT (disordered interface)	4 Nucleation theory	5 Nucleation theory	6 Dissolution of soln crystals	7 Dissolution of bulk crystals
Decalin	114.6 ± 1			113.0 ± 1.5	114.5 ± 1	116.0 ± 1	116.5 ± 2
Toluene	116.9 ± 1	116.9 ± 1	116.9 ± 1	118.6 ± 2	116.9 ± 1	116.9 ± 1	117.2 ± 2
p-Xylene	118.6 ± 1	118.6 ± 1	118.6 ± 2	118.6 ± 2	118.6 ± 2	118.6 ± 2	118.6 ± 2
n-Octane	127.0 ± 1	125.6 ± 1	124.0 ± 2	127.7 ± 2	127.0 ± 1	125.6 ± 1	126.1 ± 2
n-Hexadecane	134.0 ± 2	134.0 ± 1	134.0 ± 1	133.1 ± 2	134.0 ± 1	134.6 ± 1	130.9 ± 2

thus the same irrespective of the wide range of crystallization temperatures that exist among the different solvents. Among these data are examples where smaller size crystallites are obtained at higher crystallization temperatures when the results from different crystallizing solvents are compared. The application of nucleation theory provides a powerful unifying factor in analyzing the data from the different solvents.

In order to analyze the linear, isothermal regions of Figure 2 in more detail, it is necessary to make an *a priori* assumption with respect to the mode of nucleation. This in turn involves specifying the parameter κ. Consistent with the specific assumption that is made, the interfacial free energy governing nucleation, σ_{en}, can be obtained. We shall consider two- and three-dimensional nucleations which are the two extreme types of size control. From the slope of the straight line of Figure 2, the value of κ yields the interfacial free energies which are listed in the last two rows of Table II. These interfacial free energies are given for several different values of $T_s°$ so that our conclusions will not be biased by the specific selection of this quantity. In this connection it should be noted that a linear relation in Figure 2 for high-temperature crystallization can be obtained for a range of values of $T_s°$. Thus as has been indicated above, the straight line of Figure 2 does not uniquely specify $T_s°$. The data in Table II serves as the major basis for the selection of this quantity. It is of fundamental importance to compare this value of the interfacial free energy with σ_{ec}, the interfacial free energy associated with the interfacial structure of the mature crystallites that are actually formed. These two quantities are not necessarily identical. This latter interfacial free energy can be determined in a straightforward manner, without the necessity of making any assumption about the interfacial structure, by measuring the solubility temperature as a function of crystallite thickness. It has been shown that these measurements can be carried out without any significant melting or other structural changes taking place during the time required to perform the dissolution temperature measurements.[9] The results of these measurements[9,13] have demonstrated that σ_{ec} is also independent of the crystallizing solvent. The values obtained for σ_{ec} are listed in the first row of Table II. An examination of the data in this table demonstrates rather clearly that irrespective of the values chosen for $T_s°$ and irrespective of whether a two- or three-dimensional nucleation process is size controlling, the interfacial free energy governing nucleation is distinctly different from that which is associated with the basal plane of the mature crystallite. We come to this conclusion without having to make any particular assumptions with regard to either interfacial structure. This difference in interfacial free energies must then reflect major differences in the two interfacial structures that are involved. Thus the assumption that the interfacial structures of the mature crystallite and the nucleus from which it is formed are the same is incorrect. This *a priori* identification has led to many misleading concepts.

Table II:[9] Deduced Values of the Interfacial Free Energies cal/mol of Sequence) for Different $T_s°$ in Xylene

	$T_s°$, °C			
	118.6	116.0	114.0	112.0
σ_{ec}	3400	2900	2600	2360
σ_{en} (3 dim)	2400	2160	1960	1760
σ_{en} (2 dim)	4800	4320	3920	3520

The studies of the crystallization kinetics[15] and the analysis of the relation between the crystallite size and the crystallization temperature that was given above clearly demonstrate that the crystallite thickness is nucleation controlled. However, since this conclusion is reached from the most general considerations of nucleation theory, one cannot logically argue from this kind of data alone for a particular type of nucleation. The answer to this important question must come from other sources and other kinds of experiments.

Properties. In this section we examine the properties of solution formed crystals in an effort to learn more about their interfacial structure. If the crystal formed from dilute solution possessed a regularly folded interfacial structure and were internally perfect, the measured density should be very close to 1.00 g cm^{-3}

which corresponds to the density of the unit cell.[18] Although there has in the past been a great deal of disagreement as to the value of the density, this question has recently been clarified.[19] Values of the measured densities range from 0.96 to 0.98, depending on the crystallization temperature.[19,20] These values represent substantial deviation from that of the unit cell. They correspond to levels of crystallinity as low as 80–85% as compared to the 95% level required for a regularly folded structure. The densities are found to be independent of molecular weight (for molecular weights greater than 15,000), to be dependent only on the crystallite size, and to be independent of the crystallizing medium. As is indicated in Figure 3 the density is inversely proportional to ζ for crystallization from different solvents at different temperatures. The crystallite size is thus the sole determining factor. Similar results have also been reported by Fischer and Schmidt,[21] Fischer and Hinrichsen,[22] and Blackadder and Roberts.[23] For an infinite size crystal, $1/\zeta = 0$, these data extrapolate to the density of the unit cell. Thus the density deviations from the unit cell are solely size dependent and there is no evidence for contributions from internal lattice defects. These results give strong support to the presence of an amorphous overlayer. This conclusion is substantiated by the work of Fischer, *et al.*, on the determination of the absolute intensity of the low-angle X-ray scattering of crystals formed from dilute polyethylene solutions.[24] The fluctuations in electron density required to explain the scattering data can be directly and quantitatively related to the macroscopic density difference between the crystalline and amorphous states and the degree of crystallinity.

The enthalpies of fusion of these crystals are also independent of molecular weight,[17,25] independent of the crystallizing solvent,[17] and inversely proportional to ζ.[17,25,26] This size relation adheres to the requirement of either the regularly folded or disordered interfacial model. From these data alone a discrimination can only be made on the basis of the deduced interfacial enthalpy. For either model, the extrapolated value for the infinite-size crystal is 69 ± 1 cal/g.[17,25] This is in excellent accord with theoretical expectation[27] and other experimental results.[28] These measurements again show no detectable contribution of internal lattice defects to the measured enthalpy of fusion.

Conventional infrared analysis for the degree of crystallinity, utilizing either the 1894-cm^{-1} crystalline band, the 1368-, 1352-, and 1303-cm^{-1} noncrystalline bands, or a combination of these, yields levels of crystallinity in the range 77–85%. These results are in very good agreement with the values calculated from the density measurements.[29] The extinction coefficients of the 1894-cm^{-1} crystalline band for solution crystals and normal paraffins are the same. Thus we can conclude that the interior of the crystals of long-chain molecules, formed in dilute solution, is very similar to that of the normal paraffins. The internal defect level is thus about the same so that the nonordered chain units must be assigned to an amorphous interfacial overlayer.

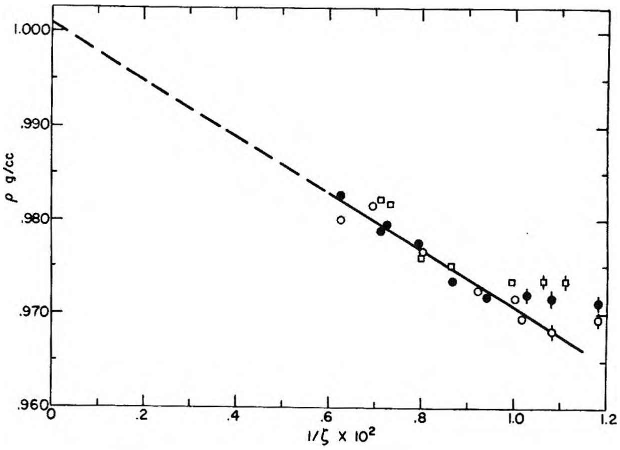

Figure 3. Plot of density as a function of the reciprocal crystallite thickness ζ, in CH_2 units, for samples crystallized from different solvents: toluene, ○; *n*-octane, ●; *n*-hexadecane, □. Short vertical lines represent nonisothermal crystallization. Data are from ref 17.

Schonhorn and Luongo[30] have studied the infrared spectrum of a cyclic hydrocarbon $C_{34}H_{68}$ and compared these results with those obtained from the melt of a normal hydrocarbon and from solution crystals of linear polyethylene. In the crystalline state the X-ray diffraction pattern of the cyclic hydrocarbon indicates that the conformation is that of a fully collapsed hoop having tight regular folds characteristic of adjacent chain reentry. Because of the sequence of bond orientations required to make this tight fold, an intense absorption band is observed at 1340 cm^{-1} as is illustrated in Figure 4. We note, however, in this

---

(18) C. W. Bunn, *Trans. Faraday Soc.*, **35**, 482 (1939).

(19) R. K. Sharma and L. Mandelkern, *Macromolecules*, **2**, 266 (1969).

(20) D. A. Blackadder and P. A. Lewell, *Polymer*, **9**, 249 (1968).

(21) E. W. Fischer and G. F. Schmidt, *Angew. Chem.*, **74**, 551 (1962).

(22) E. W. Fischer and G. Hinrichsen, *Kolloid-Z. Z. Polym.*, **219**, 93 (1966).

(23) D. A. Blackadder and T. L. Roberts, *Makromol. Chem.*, **126**, 116 (1969).

(24) E. W. Fischer, H. Goddar, and G. F. Schmidt, *J. Polym. Sci., Part B*, **5**, 619 (1967).

(25) L. Mandelkern, A. L. Allou, Jr., and M. R. Gopolan, *J. Phys. Chem.*, **72**, 309 (1968).

(26) H. E. Bair, T. W. Huseby, and R. Salovey in "Analytical Calorimetry," R. S. Porter and J. F. Johnson, Ed., Plenum Press, New York, N. Y., 1968, p 31.

(27) P. J. Flory and A. Vrij, *J. Amer. Chem. Soc.*, **85**, 3548 (1963).

(28) F. A. Quinn, Jr., and L. Mandelkern, *ibid.*, **80**, 3178 (1958); 81, 6355 (1959).

(29) T. Okada and L. Mandelkern, *J. Polym. Sci., Part B*, **4**, 1043 (1966).

(30) H. Schonhorn and J. P. Luongo, *Macromolecules*, **2**, 366 (1969).

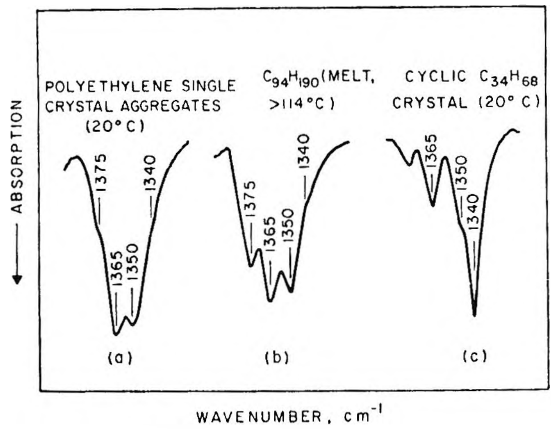

Figure 4. Spectra in 1400–1300-cm^{-1} region of polyethylene solution crystals at 20°; m-$C_{94}H_{190}$ melt (>114°) and crystalline cyclic hydrocarbon ($C_{34}H_{68}$) at 20°. Data are from ref 30.

figure that for the solution crystals of polyethylene the intensity of this band and the ratio of the intensity of this band to that of the usual gauche band at 1350 cm^{-1} is greatly reduced. In fact, the infrared spectra in the gauche band region is virtually identical with that of the melt of the normal hydrocarbon (middle spectrum of Figure 4). We can conclude from these observations that solution crystals of polyethylene do not display the infrared characteristics required of a folded structure with adjacent reentry. Based on this study[30] the interfacial structure of solution crystals is concluded to be the same as the melt of normal hydrocarbons.

Krimm and Bank[31,32] have recently reported other kinds of infrared analysis on solution-formed crystals of polyethylene. In one of their studies particular attention is given to the low-frequency interchain lattice vibration located in the vicinity of 71 cm^{-1}. This frequency is a function of the interactions between chains and thus of the lattice parameters within the crystal. Small shifts in this frequency, which correlated with changes in the lattice dimensions, were observed for unfractionated polyethylene when cast films and solution-crystallized samples were compared with bulk crystallized and samples crystallized under conditions of high temperature and pressure. It was assumed that these shifts reflected differences in the interfacial structure.[31] However, a very detailed, quantitative study has shown that for solution crystals the a and b axes systematically increase with a decrease in the crystallization temperature.[33] Thus, for these small-size crystals, 80–160 CH_2 units thick, the interfacial structure is influencing the unit cell dimensions although the basic nature of the interfacial structure is not changing. The interpretation given to the changes in the 71-cm^{-1} infrared band is, therefore, not unequivocal.[31] In fact it needs to be reexamined in light of the changes that are observed in the lattice dimensions for these crystals.

In another aspect of their work, Krimm and Bank[32] compared the splitting of the 720, 730-, and 1800-cm^{-1} modes for mixtures of $C_{36}H_{74}$ and $C_{36}D_{74}$ with corresponding mixtures of hydrogenated and deuterated polyethylene which was crystallized in different ways. Theoretically, splitting will be observed when there is a nonuniformity of the mass distribution of the two species within the crystal lattice.[32] Splittings were observed for polymer mixtures of certain given nominal compositions when they were not observed for corresponding compositions of the monomeric mixtures. The required nonuniformity of the mass distribution was attributed to a regularly folded crystal structure which of course yields the required mass distribution.[32] However, this is not a unique explanation. Further studies have shown that for both the monomeric and polymeric species, the hydrogenated samples possess a 4–6° greater melting temperature.[34] From simple considerations of phase equilibria it follows that at equilibrium the compositions of the crystal and the melt will not be the same. This partitioning of species upon crystallization will be further enhanced by the influence of the difference in melting temperatures on the crystallization kinetics.[34] Hence there is not an unequivocal interpretation to this set of infrared results.

Very strong evidence for the existence of a disordered interfacial structure comes from the direct observation of glass formation in solution crystals. Irrespective of the detailed theories of glass formation that have been proposed, it is agreed that it is a property of the disordered or amorphous regions where the chain units are in a nonordered conformation. Two distinctly different types of measurements demonstrate glass formation in solution-formed crystals. One set is dynamic mechanical measurements which have been contributed mainly by Takayanagi.[35,36] A detailed analysis of these results[37] demonstrates that loss peaks are observed at the same temperature for both solution- and bulk-crystallized samples. Further data, employing static methods, show that these loss peaks correspond to the glass temperature. In a quite different approach, Fischer, Kloos, and Lieser[38] have studied the temperature dependence of the absolute intensity

(31) M. I. Bank and S. Krimm, *J. Appl. Phys.*, **39**, 4951 (1968).

(32) M. I. Bank and S. Krimm, *J. Polym. Sci., Part A-2*, **7**, 1785 (1969).

(33) R. Kitamaru and L. Mandelkern, *ibid., Part A-2*, **8**, 2079 (1970).

(34) F. Stehling, E. Ergöz, and L. Mandelkern, *Macromolecules*, **4**, 672 (1971).

(35) M. Takayanagi, E. Imada, E. Nagai, T. Tatsumi, and T. Matsuo, *J. Polym. Sci., Part C*, **16**, 867 (1967).

(36) M. Takayanagi, *Proc. Int. Congr. Rheol.*, **4**, Part 2, 161 (1965).

(37) F. C. Stehling and L. Mandelkern, *J. Polym. Sci., Part B*, **7**, 255 (1969).

(38) E. W. Fischer, F. Kloos, and G. Lieser, *ibid., Part B*, **7**, 845 (1969).

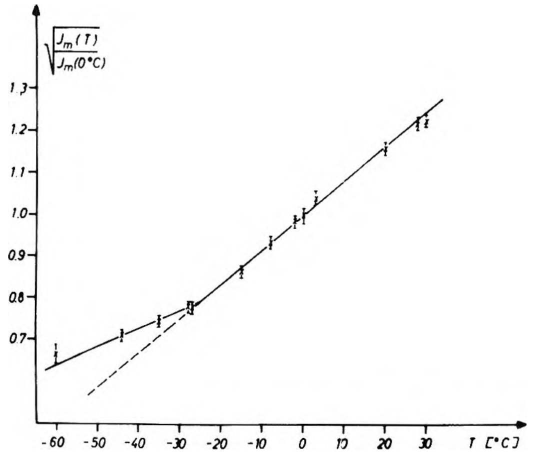

Figure 5. Temperature dependence of the square root of the relative intensity of the low-angle diffraction maximum for solution crystals of polybutene-1. Data are from ref 38.

of the low-angle scattering maximum. A plot of the square root of the ratio of the intensity maximum at temperature T to that at 0°, T_0, is given as a function of temperature in Figure 5 for solution crystals of polybutene-1. Theoretically, the slope in this plot is related to the difference in expansion coefficient of the amorphous and crystalline phases. A sharp discontinuity can be noted at $-25°$. This temperature corresponds to that generally accepted for the glass temperature of polybutene-1. Similar experiments, utilizing solution crystals of linear and branched polyethylene, also display discontinuities at temperatures corresponding to their respective glass temperatures.[39] Thus the evidence for glass formation in solution-grown crystals is quite strong.

Other properties, such as wide-angle X-ray diffraction,[40] yield noncrystalline content for polyethylene solution crystals of about 15–20%. Selective oxidation studies indicate that the interfacial layer contains about 15–25% of the chain units.[41–45] Broad-line nmr spectra of polyethylene crystals formed from dilute solution indicate the presence of a mobile or amorphous fraction. A refined analysis of such spectra by Bergmann and Nawotki[46] has shown that only about 85–90% of the material is within the crystal lattice.

The review of properties that have been given above makes abundantly clear that there is a large, if not overwhelming, body of evidence that indicates that solution crystals are only about 80–85% crystalline. There is an amorphous, disordered overlay, where the chain units are in a nonordered conformation, which comprises the remainder of the material. This conclusion and the major properties upon which it is based are completely compatible with the electron micrographs and are also consistent with the other major morphological observations. The lamella platelike character of the crystals formed is not in question. It should be clear, however, that their observation does not require the corollary assertion of regularly folded chains. Although the experimental evidence, from a nonmorphological viewpoint, with respect to the interfacial structure of solution-formed crystals, is quite substantial, other concepts are still being argued. The more detailed basis for these latter views can be found in the references already cited.[4a,c,7]

Crystallization from Melt

Introduction. A lamella-like crystallite is a well-established and accepted morphological form that develops upon the crystallization of a homopolymer from the pure melt. The analysis of the properties of solution-formed crystals indicates, however, that it would be premature to equate this morphology with an interfacial structure comprised of regularly folded chains and to dismiss the existence of chain units in nonordered conformations. The description of the interfacial and interzonal chain structure cannot be accomplished solely from morphological observations. Neither can any progress in understanding be expected solely from the analysis of isolated pieces of physical–chemical data. It is necessary that an overall view of properties be developed to see if a coherent understanding can be evolved.

In order to help elucidate this problem we have generated experimental data, which has involved a variety of experimental techniques for the same chemically constituted polymer, for samples crystallized under defined and controlled conditions. The necessary data have been produced by studying the properties of molecular weight fractions of linear polyethylene. The molecular weights studied covered the range 3×10^3 to 8×10^6, and samples were crystallized under controlled conditions, particularly at elevated temperatures for long time periods. In anticipation of our results, we find that, in marked contrast to crystallization from very dilute solution, the properties of polymers crystallized from the pure melt are very dependent on molecular weight.

Properties. The first property that we shall examine is the dependence of the density on molecular weight.[47,48] These results are presented in Figure 6 as

---

(39) E. W. Fischer and F. Kloos, *J Polym. Sci., Part B*, **8**, 685 (1970).

(40) W. O. Statton and P. H. Geil, *J. Appl. Polym. Sci.*, **3**, 357 (1960).

(41) A. Peterlin and G. Meinel, *J. Polym. Sci., Part B*, **3**, 1059 (1965).

(42) A. Peterlin, G. Meinel, and H. G. Olf, *ibid., Part B*, **48**, 399 (1966).

(43) F. H. Winslow, M. Y. Hellman, W. Matreyek, and R. Salovey, *ibid., Part B*, **5**, 89 (1967).

(44) D. J. Blundell, A. Keller, and T. M. Conner, *ibid., Part A-2*, **5**, 991 (1967).

(45) T. Williams, D. J. Blundell, A. Keller, and I. M. Ward, *ibid., Part A-2*, **9**, 1613 (1968).

(46) K. Bergmann and K. Nawatki, *Kolloid-Z.*, **219**, 132 (1967).

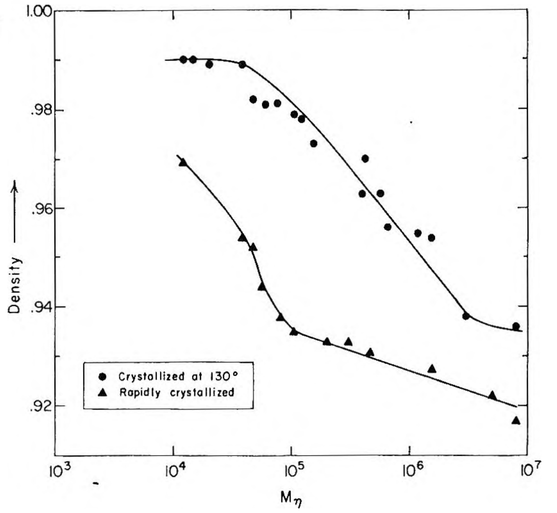

Figure 6. Plot of density, measured at room temperature, as a function of molecular weight for fractions of linear polyethylene.

the measured density at room temperature for two modes of crystallization. One of these involves long-time crystallization at 130°; the other was rapid crystallization achieved by quick cooling. The measured densities are conveniently compared with the density of the unit cell which is 1.00 g cm^{-3} at room temperature. We immediately note the wide range in values that can be achieved. After 130° crystallization, the densities at room temperature range from 0.99 to less than 0.94 g cm^{-3}. After rapid crystallization this value can be reduced to slightly less than 0.92. All these values are for the same polymer, crystalline linear polyethylene, so that clearly they are not restricted to any narrow limits as has been implied. These results illustrate the pitfalls that can be encountered in selecting isolated pieces of data and attempting to develop detailed theories from them.

We can also discern from Figure 6 that there is a very systematic change of the density with molecular weight. Within the present range of experimental data there are essentially three regions. At low molecular weights, less than 50,000–60,000, the observed densities are relatively high and approach that of the unit cell. As the molecular weight is increased, however, there is a significant monotonic decrease in the density up to $M = 1.2 \times 10^6$. At still higher molecular weights, a constant low value of the density is attained. The wide range in densities that can be achieved is not a trivial effect and is systematically dependent on molecular weight. The deviations in density from that of the unit cell clearly cannot be attributed to end groups acting as lattice imperfections. It is in fact for the lowest molecular weights, with the highest concentrations of end groups, that the density is closest to that of the unit cell.

If the densities are measured at the elevated crystallization temperatures, prior to cooling to room temperature, then a similar dependence on molecular weight is found but the density level is considerably less.[47,48] Upon cooling, further crystallization with an attendant increase in density is observed.[47,48] However, the relative magnitude of the change is much greater in the higher molecular weight range than in the lower. Put another way, relatively more crystallization occurs upon cooling for molecular weights greater than about 50,000. For the lower molecular weight range only a small increase in density takes place upon cooling.

Enthalpy of fusion measurements follow a pattern very similar to that of the density–molecular weight relations.[25,48] After high-temperature crystallization and cooling to room temperature, the measured enthalpies of fusion range from 69 cal/g for the lower molecular weights to 37.5 cal/g for the larger chains. The lower molecular weights thus yield values close to that expected for the macroscopic ideal crystal. After rapid crystallization of high molecular samples the measured enthalpy of fusion can be reduced to as low as 20–25 cal/g.

From these results we see that a wide range in thermodynamic properties can be realized. Very large deviations from those expected from the perfect crystal are observed. These deviations are not rarities, as has been implied, but are systematic with molecular weight and the crystallization conditions.

Degree of Crystallinity. The problem as to whether a crystalline polymer can be treated as a complete set of crystals of small thickness, with a large concentration of internal defects, or whether there are chain units in nonordered conformations which connect crystallites can be resolved in part by examining the validity of the degree of crystallinity calculations. Classically, this kind of calculation has been based on the assumption of the additivity of the crystalline and amorphous (interzonal) phases. We must now also consider possible contributions from the interfacial region and from defects within the crystallite interior. The wide range in properties that one has been able to generate by studying molecular weight fractions makes for an ideal set of data with which to test this concept. For example, on a strict additivity basis, the degrees of crystallinity, $1 - \lambda$, from the density measurements range from 0.50 to 0.95 for linear polyethylene.

We first compare the degree of crystallinity calculated from density, using just the additivity principle, with the values calculated in the conventional manner from infrared analysis. As has been previously reported[49,50] there is very good agreement between the two methods over the whole range. Therefore, for

---

(47) J. G. Fatou and L. Mandelkern, *J. Phys. Chem.*, **69**, 417 (1965).

(48) E. Ergöz, Ph.D. Dissertation, Florida State University, 1970.

(49) T. Okada and L. Mandelkern, *J. Polym. Sci., Part A-2*, **5**, 239 (1967).

(50) L. Mandelkern, *Polym. Eng. Sci.*, **7**, 232 (1967).

these two methods there do not seem to be any contributions from the interfacial region or from internal defects. Quantitative wide-angle X-ray diffraction studies, from several laboratories,[51-53] also show good agreement with the degree of crystallinity calculated from the density.

When the simple additivity rule is used, the enthalpy of fusion measurements, for samples cooled to room temperature, do not yield concordant values of the degree of crystallinity. Except for the samples with the very highest level of crystallinity a major disparity is found. The enthalpy measurements yield lower values for $1 - \lambda$ than the density. Since the enthalpy of fusion is calculated on a mass basis, this discrepancy cannot be attributed to voids within the sample. The source of this apparent discrepancy is realized when samples are analyzed at the crystallization temperature; *i.e.*, they are never cooled to room temperature. Under those conditions very good agreement between the two methods is found over a wide range in the degree of crystallinity.[25] The disparity is therefore a consequence of cooling from the crystallization temperature. Smaller crystallites will be formed on cooling so that there will be a substantial contribution from the interfacial enthalpy to the measured enthalpy of fusion. This will then yield an apparent lower value for $1 - \lambda$. Analysis of dilute-solution crystals show that the interfacial enthalpy is a significant quantity.[17,25]

A refined analysis of the broad-line nmr spectra[46] has shown that segmental motions of the interfacial region must be taken into account in addition to the usual broad and narrow components assigned to the crystalline and amorphous regions. For linear polyethylene of low density, about 10% of the material needs to be assigned to the interfacial region. The absolute low-angle intensity measurements of Schultz and Kavesh,[53] for a sample whose crystallinity is about 70%, indicate the possibility of contributions from the interfacial regions in this type of measurement.

We have already seen that the deviations in properties from that of the ideal crystal cannot be attributed to chain ends or to voids within the lattice. It remains to be ascertained whether the lattice parameters and unit cell dimensions, which would be sensitive to other kinds of internal defects, are perhaps changing. Detailed quantitative studies[33] have, however, demonstrated that for bulk-crystallized samples the lattice parameter and unit cell dimensions do not change over the wide range in macroscopic densities that are observed. We must conclude therefore that there are no defects present within the interior of the crystallites which would affect the lattice parameters.

The results described above lead to the general conclusion that the degree of crystallinity is a quantitative concept. This gives strong support for the existence of a well-defined amorphous or interzonal region where the chain units are in nonordered conformations and possess properties which are similar to that of the pure melt. The interzonal region is thus composed of portions of a chain and not complete molecules. These chain units, which connect crystallites, would not be straight or ordered as has been proposed.[54-56]

Character of Crystallites and Interfacial Free Energy. Electron microscope studies of fracture surfaces[57,58] and of the residue from selective oxidation[48] have shown that lamella-like crystallites are formed over the complete molecular weight range, from several thousand to several million. The fracture surface studies up to molecular weights of 570,000 show that the lamella are banded or striated irrespective of whether the crystallite thickness is comparable to the extended chain length or very much smaller.[57,58] The lamella also have the same character in polydisperse systems.[57] The wide range in molecular weights and crystallite sizes over which lamella are observed do not allow them to be *a priori* identified with regular folding or for any type of folding. Neither can the electron micrograph observations be used as an argument for molecular weight segregation during crystallization. One can also add that neither can the observation of multiple peaks, during differential calorimetry measurements, be used as an argument for molecular weight fractionation during crystallization.

An analysis can be made, from the fracture surfaces, of the lamella thickness as a function of molecular weight. The results are given in Figure 7. Here, in terms of the number of CH_2 units, the crystallite thickness ζ is plotted against the chain length x for samples crystallized at 130°. There is a very definite dependence of the crystallite size on molecular weight. For low molecular weights, $x \leq 900$ ($M \leq 12{,}500$), the average values of ζ are very close to x. Such crystallites are termed extended-chain crystals. As the molecular weight increases from 12,000 to 56,000, the average lamella thickness increases from about 600 units to about 900 units. The ratio $\langle\zeta\rangle/x$ thus decreases from 0.7 to 0.25 so that the crystallite thickness still represents a significant portion of the extended-chain length. For molecular weights from 200,000 to 570,000 the crystallite sizes increase only slightly, reaching an asymptotic value of 1000–1200 CH_2 units. This size

---

(51) H. Hendus and G. Schnell, *Kunststoffe*, **51**, 69 (1960).

(52) M. Gopalan and L. Mandelkern, *J. Polym. Sci., Part B*, **5**, 925 (1967).

(53) S. Kavesh and J. M. Schultz, *ibid., Part A-2*, **9**, 85 (1971).

(54) H. D. Keith, F. J. Padden, Jr., and R. G. Vadimsky, *ibid., Part A-2*, **4**, 267 (1966).

(55) H. D. Keith, F. J. Padden, Jr., and R. G. Vadimsky, *J. Appl. Phys.*, **37**, 4027 (1966).

(56) C. Devoy and L. Mandelkern, *J. Polym. Sci., Part B*, **6**, 141 (1968).

(57) F. R. Anderson, *J. Appl. Phys.*, **35**, 64 (1964).

(58) L. Mandelkern, J. M. Price, M. Gopalan, and J. G. Fatou, *J. Polym. Sci., Part A*, **4**, 385 (1966).

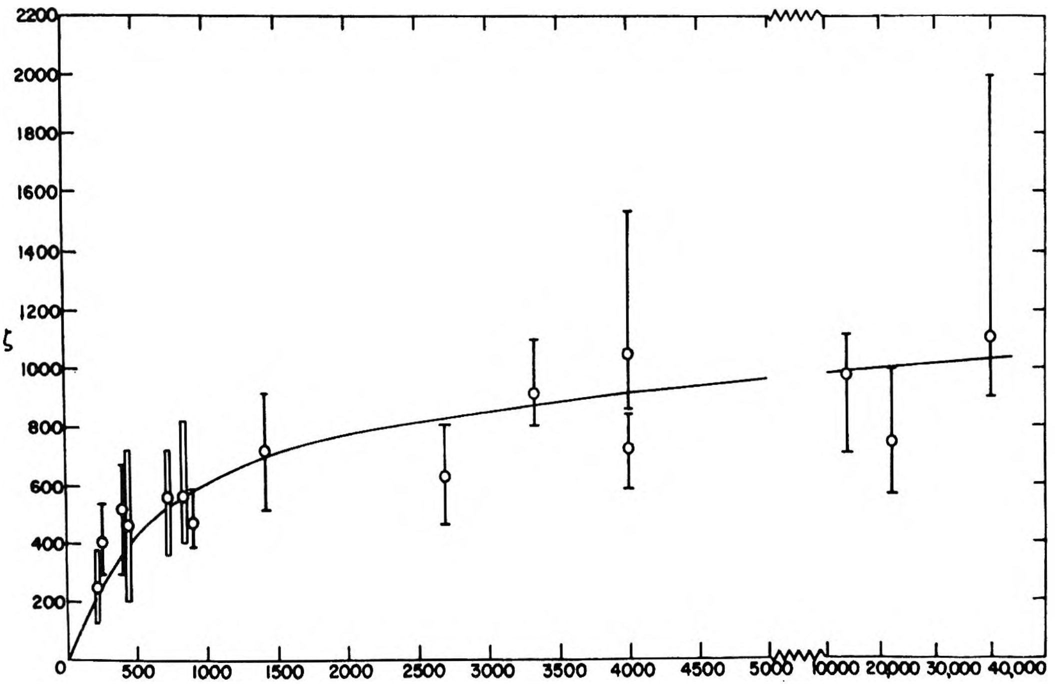

Figure 7. Plot of crystallite size ζ, in CH_2 units, against chain length x for molecular weight fractions of polyethylene crystallized at 130° and cooled to room temperature. Data are from ref 58.

range is consistent with low-angle X-ray measurement of Pollack, *et al.*,[59] and of Schultz.[53] At these higher molecular weights the crystallite thickness has now become exceedingly small when compared to the extended-chain length.

We should note that the molecular weight range where the density and enthalpy of fusion start to undergo their major decrease corresponds to the ratio $\langle\zeta\rangle/x$ beginning to deviate from unity. This ratio becomes progressively smaller as the molecular weight increases and the deviations in thermodynamic quantities from that of the unit cell increase. This is the kind of correlation we would expect for a fairly constant crystallite thickness and ever increasing amorphous or interzonal content. This conclusion is substantiated by fracture experiments. In the lower molecular range, where $\langle\zeta\rangle/x$ is approximately unity, fracture is easily accomplished at room temperature. However, for the higher molecular weight samples, where $\langle\zeta\rangle/x \ll 1$, fracture can only be accomplished at the temperature of liquid nitrogen which is below the glass temperature of linear polyethylene.[60]

From the measured crystallite thickness and from the directly determined melting temperatures the interfacial free energy, σ_{ec}, associated with the basal plane of the mature crystallites can be calculated in a straightforward manner.[61] The results are plotted in Figure 8 and two different sets of data, which are in very good agreement with one another, are presented. In one set of data the crystallite thickness and melting temperatures were determined from the low-angle diffraction maxima and the temperatures of their disappearance.[62] In the other the crystallite thickness was determined by electron microscopy, and the melting temperature by dilatometry.[58] For molecular weights greater than about 10^5 the interfacial free energy is independent of molecular weight and assumes its highest values. At

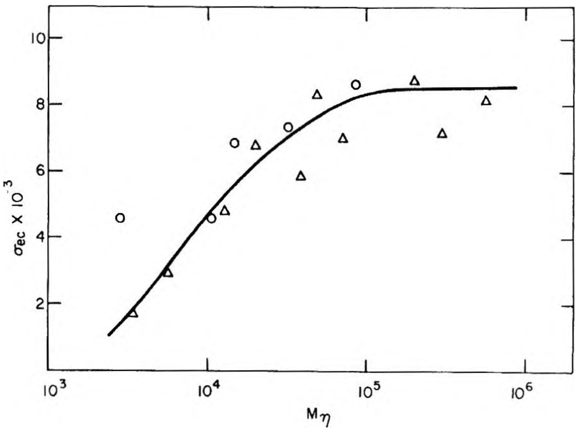

Figure 8. Plot of interfacial free energy σ_{ec} (cal/mol) against molecular weight for polyethylene crystals: △, electron microscopy from ref 58; ○, low-angle X-ray diffraction from ref 62.

---

(59) S. S. Pollack, W. A. Robinson, R. Chiang, and P. J. Flory, *J. Appl. Phys.*, **33**, 237 (1962).

(60) F. C. Stehling and L. Mandelkern, *Macromolecules*, 3, 242 (1970).

(61) We emphasize here, as we did in the discussion of solution crystals, the difference between the interfacial free energy governing nucleation and that which is associated with the mature crystals that are actually formed.

(62) J. M. Schultz, W. H. Robinson, and G. M. Pound, *J. Polym. Sci., Part A-2*, **5**, 511 (1967).

the lower molecular weights, one has the lowest interfacial free energies and there is a transition zone connecting the two regions. A similar molecular weight dependence has been found for the interfacial free energy governing spherulitic growth.[63]

The molecular weight dependence of the interfacial free energy is again a reflection of the ratio of the crystallite size to the extended-chain length. When this ratio is large, σ_{ec} has its smallest values although it is still large when compared to that for monomeric systems. When the ratio of the crystallite size to the extended-chain length becomes very small, the interfacial energy is correspondingly very large. Although this thermodynamic analysis cannot specify the molecular nature of the interfacial regions, they clearly must be different in the different molecular weight ranges, although lamella structures are observed throughout. The molecular nature of the interfacial region characteristic of the lower molecular weights, large $\langle\zeta\rangle/x$, will yield the most stable, higher melting systems since it has associated with it the lowest value of the interfacial free energy. Hence, if the crystallites formed from the higher molecular weight chains possessed this same interfacial structure, the melting temperatures would be greater than observed. In this high molecular weight range, $\langle\zeta\rangle/x \ll 1$, it is possible to postulate, solely from geometric considerations, an interface of regularly folded chains. However, if this interfacial structure did indeed exist, it would not do so because of any enhanced stability that is endowed by this structure.

Summary of Morphology. Since lamella-like crystallites are observed for the complete range of $\langle\zeta\rangle/x$, they cannot be automatically attributed to a regularly folded chain structure. For high molecular weights, when $\langle\zeta\rangle/x \ll 1$, it is possible, on a geometric basis, to postulate a regularly folded interfacial structure and the absence of interzonal regions. This postulate is clearly consistent with geometric considerations and visual observations. However, there are several compelling reasons which make this difficult, if not impossible to accept. As has already been pointed out, the very high values of the interfacial free energy associated with the basal plane argue against a regular, smooth interface. The concordance of the degree of crystallinity calculations, by a variety of methods, utilizing the properties of molten chains, argues very strongly for the presence of interzonal regions as does the low level of crystallinity that can be attained for linear polyethylene.

If one is prone to argue that the observed deviations in properties can be attributed to imperfections within the crystal lattice, and we should recall that these deviations can be rather large, they cannot be due to chain ends, voids, or changes in the lattice parameters. These have been the most popular kinds of imperfections that have been postulated. The claims are, however, without substance. Any other kinds of imperfections that might be postulated will have to satisfy certain conditions.

In the molecular weight range where $\langle\zeta\rangle/x \ll 1$ the crystallite thickness and melting temperature are essentially invariant although the density and enthalpy of fusion are continuously decreasing. Thus these defects would not be affecting the thermodynamic stability while their concentration would have to be continually increasing. This would represent a very unusual situation. Since the crystallite size and interfacial free energy are also invariant, in this region, these postulated defects cannot be attributed to changes in interfacial properties. There are undoubtedly defected structures within the interior of crystallites, as there are in monomeric substances, but the requirements that have to be met for the polymeric systems have yet to be theoretically expounded and experimentally demonstrated. The concept of an interfacial structure in which there is no change with molecular weight and in which interzonal connections are absent cannot be substantiated. Despite this evidence, other interpretations of structure, based in the main on restricted data, still argue for the absence of amorphous regions. These discussions can be found in the references cited.[4,64]

There are many compelling reasons that argue very strongly for the presence of interzonal regions. The concordant values obtained for the degree of crystallinity have already been mentioned. The fracture properties also require such regions, for when the molecular weight is greater than 56,000, $\langle\zeta\rangle/x \ll 1$ fracture requires the reduction in temperature below the glass temperature. The existence of a glass temperature for a semicrystalline polymer in general and its recent demonstration for linear polyethylene[60] also require amorphous regions. Thermal expansion and specific heat measurements of linear polyethylene of low density display classical glass temperature behavior, typical of amorphous polymers. A consistent and rational interpretation of both the broad-line nmr spectra and the dynamic mechanical properties as a function of sample density can only be made by quantitatively invoking the presence of amorphous regions.[60] The intensity ratio, in the infrared region, of the two major gauche bond absorptions are the same for bulk-crystallized linear polyethylene and the melt of normal hydrocarbons.[49,50] Hence, we must conclude that the nonordered regions in the polymer possess the same structure as the melt of normal hydrocarbons. This conclusion is, of course, consistent with the existence of amorphous regions.

Considering all the properties that have been discussed and recognizing the wide range in values that can be attained for a given property and, furthermore,

---

(63) C. Devoy and L. Mandelkern, *J. Polym. Sci., Part A-2*, **7**, 1883 (1969).

(64) P. Lindenmeyer, *Kolloid-Z. Z. Polym.*, **231**, 593 (1969).

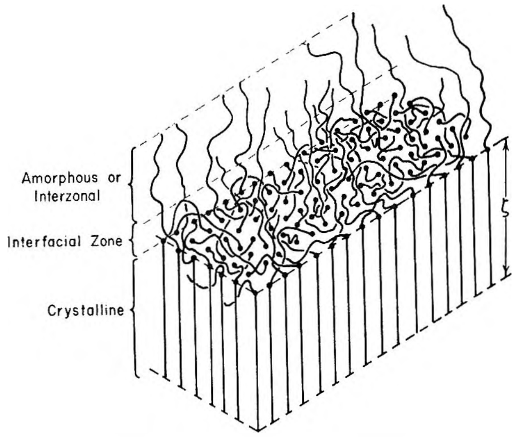

Figure 9. Schematic representation of crystallite.

requiring a consistency of interpretation among all the data, a schematic representation of a primitive crystallite, as is depicted in Figure 9, has evolved. Although admittedly highly schematic and oversimplified, it does represent the primary morophological entity. The vertical straight lines within the crystalline region represent the chain sequences in ordered conformation. In the amorphous or interzonal region, the chain units are in nonordered conformations and have thermodynamic, spectral, and mechanical properties similar to those of the pure melt. The chain units in this disordered array connect one crystallite with another. The interfacial region is a zone many units thick where the packing is very distorted and crowded. Some chains pass through this zone and thus form the interzonal region, while others return to the crystallite of origin but not necessarily in juxtaposition. Thus a disordered, highly irregular interfacial structure results which is consistent with the high value for the interfacial free energy associated with the basal plane when $\langle\zeta\rangle/x \ll 1$. On the other hand, when $\zeta \rightarrow x$ the interzonal region will no longer be present and there will be very little necessity for a chain to return to the crystallite of origin. In this situation the distortion and crowding of the interfacial region will be significantly reduced as is indeed reflected in the lower values obtained for the interfacial free energy.

The model of the rudimentary crystallite and the associated chain units that has been presented can explain all of the thermodynamic, mechanical, and spectroscopic properties that have been reported as well as the broad-line nmr and dynamical mechanical results. Moreover, it is completely consistent with the electron microscopy observations.

Molecular Mechanism of Chain Rupture in Strained Crystalline Polymers

by A. Peterlin

Camille Dreyfus Laboratory, Research Triangle Institute, Research Triangle Park, North Carolina 27709

(Received April 2, 1971)

Publication costs borne completely by The Journal of Physical Chemistry

In conventional tensile test of crystalline polymers at room temperature the unoriented microspherulitic sample usually necks and draws. By this operation one transforms a fraction or even the whole specimen into the highly oriented fiber structure. Its basic element is the microfibril composed of folded-chain crystal blocks connected in the axial direction by a great many intrafibrillar tie molecules. In the tensile test the load is nearly uniformly distributed among the microfibrils. A stress concentration occurs at the point of line defects of the microfibrillar superlattice, *i.e.*, at the ends of microfibrils, and at the areas of defective lateral cohesion of microfibrils. In such places at sufficiently high strain some tie molecules are so much elongated that the force concentration is sufficient for the rupture of the covalent chemical bond in the main chain. The broken ends with unpaired electrons act as radicals detectable by electron spin resonance. At room temperature the primary radicals are so extremely short-lived that one is able to detect merely the secondary radicals obtained by hydrogen abstraction from the unbroken chains. The radicals are formed over the whole strained specimen. Their number, increasing more than exponentially with strain, is a function of strain and not of stress. It is a direct measure of tie molecules strained up to the breaking point. The low anisotrophy of the esr spectrum and the accessibility of radicals to solvents corroborate the assumption that the radicals formed under strain are located in the moderately oriented amorphous layer between crystal blocks in contrast with radicals formed by γ irradiation which are primarily located in the highly oriented crystals.

Elongation of crystalline polymers up to fracture involves some polymer chain rupture which can be detected by electron spin resonance (esr) investigation of radicals formed as the chains are broken.[1-10] The spectra[11-13] and their anisotropy[14] permit the identification and determination of orientation of radicals.[7] At room temperature one has merely secondary radicals formed by hydrogen abstraction on moderately oriented or completely unoriented unbroken chains. The number and location of radicals as function of strain is closely connected with the molecular and supercrystalline structure of the sample.[5-7] Therefore one has first to describe the morphology of a crystalline polymer before one can proceed with the interpretation of the data on chain rupture.

It turns out that the unoriented spherulitic samples in the conventional fracture experiment gets first transformed into the fiber structure before it breaks.[15] The transformation is only local if the conditions of the experiment produce a high local stress concentration, as for instance in front of the tip of a crack or notch in the tensile or shear test. However, even in low-temperature fracture, with very little large-scale plastic deformation, one may have on a microscopic scale some transformation from spherulitic to fiber structure. Therefore, one has to know the basic facts of such a transformation and the properties of the resulting fibrous material before one can reasonably discuss the mechanism of molecular fracture in crystalline polymers.

Plastic Deformation of Crystalline Polymers

Many unoriented, more or less spherulitic crystalline polymers are highly ductile at room temperature and still more at elevated temperature up to the melting point. The load–elongation curve exhibits a very short Hookean region which, at about 1 or 2% elongation, already shows signs of irreversible plastic deformation. The strain softening rapidly increases with strain thus leading to the maximum in the load–elongation curve at the yield point. Further elongation proceeds at a nearly constant drawing load which is smaller than the yield load. Depending on tempera-

---

(1) S. N. Zhurkov, A. Ya. Savostin, and E. E. Tomashevskii, *Dokl. Akad. Nauk SSSR*, **159**, 303 (1964).

(2) S. N. Zhurkov and E. E. Tomashevskii, *Phys. Basis Yield Fract., Conf., Proc., 1967*, 200 (1968).

(3) D. Campbell and A. Peterlin, *J. Polym. Sci., Part B*, **6**, 481 (1968).

(4) D. K. Roylance, K. L. DeVries, and M. L. Williams, "Fracture," Chapman and Hall, London, 1969, p 551.

(5) J. Becht and H. Fischer, *Kolloid-Z. Z. Polym.*, **229**, 167 (1969).

(6) G. S. P. Verma and A. Peterlin, *ibid.*, **236**, 111 (1970).

(7) G. S. P. Verma and A. Peterlin, *J. Macromol. Sci., Phys.*, **4**, 589 (1970).

(8) J. Becht and H. Fischer, *Kolloid-Z. Z. Polym.*, **240**, 766 (1970).

(9) K. L. DeVries, D. K. Roylance, and M. L. Williams, *J. Polym. Sci., Part A-1*, **8**, 237 (1970).

(10) H. H. Kausch-Blecken von Schmeling, *J. Macromol. Sci., Rev. Macromol. Chem.*, **4**, 243 (1970).

(11) S. Bresler, A. Osminskaya, and A. Popov, *Kolloid. Zh.*, **20**, 403 (1958).

(12) S. Bresler, A. Osminskaya, and A. Popov, *Zh. Tekh. Fiz.*, **29**, 358 (1959).

(13) P. Butyagin and A. Berlin, *Vysokomol. Soedin*, **1**, 865 (1959).

(14) M. Kashiwagi, *J. Polym. Sci., Part A-1*, 189 (1963).

(15) See, for instance, "Encyclopedia of Polymer Science and Technology," Vol. 7, Wiley, New York, N. Y., 1967, p 261.

ture, elongation rate, and material, the amount of drawing, *i.e.*, the draw ratio, varies in wide limits, 4–6 in nylon and 10–30 in polyethylene. It is homogeneous at high temperature (hot drawing) and inhomogeneous with a neck at low temperature (cold drawing). At the end of drawing the load starts to increase as a consequence of strain hardening up to the final break at the so-called natural draw ratio of the material.

In the inhomogeneous cold drawing the necking produces in one step a very much stronger, nearly completely oriented fibrous material which deforms little during the rest of the drawing experiment.[16] In the neck each volume element gets extended almost to the natural draw ratio. Hence the cross section of the sample is reduced and the stress is increased by the same factor. In spite of the drastic increase of stress, the deformation of the necked material is insignificant if compared with the large deformation in the neck. If, however, one further increases the load, the drawn material cannot extend very much but breaks instead. The fracture is brittle or fibrous, with a rough surface in the former[17] and extensive fibrillation[18] in the latter case.

The homogeneous hot drawing does not involve such dramatic changes as necking. Nevertheless, it produces a strain-hardened and oriented fibrous material by a gradual transformation of the spherulitic structure of the starting material. Neither the draw ratio nor the strength attained are as high as in cold drawing with a neck.

The new material obtained by drawing is highly oriented as shown by small- and wide-angle X-ray scattering, optical birefringence, or dichroism and by the high anisotropy of mechanical properties. The chains in the crystals are oriented almost perfectly in the draw direction, and the lamellae, as a rule, perpendicular to it.[19] A substantial although less complete orientation is detectable by ir dichroism in the amorphous component.[20] However the orientation is only the consequence of the microfibrillar structure of the new material and not the decisive factor determining the physical properties. This distinction is quite important. One can achieve almost the same degree of orientation by proper sedimentation of crystals formed from dilute solution during cooling. The single crystal mat so obtained has the lamellae parallel to the surface of the mat and the chain axes perpendicular to it. Since there is no material connection between adjacent lamellae in the chain direction, the cohesion is based merely on the relatively weak van der Waals forces of the amorphous surface layers. The small- and wide-angle X-ray scattering pattern is very similar to that of the fibrous material. The chain orientation is less perfect and the lamella packing is better. However, the mechanical properties are completely different: very low elastic modulus and strength in the chain direction in contrast with the values in the fiber. The properties perpendicular to the chain direction differ in the opposite sense. In spite of the mosaic structure the blocks of each single crystal are fully connected with each other by the folded macromolecules. Such connections are missing at the outer boundary of each crystal. In the fiber structure, however, the crystal blocks of adjacent microfibrils have practically no material connection. Hence the oriented single crystal mat does not show any fibrillation tendency in contrast with the fibrous material which fibrillates easily and, particularly in the fatigue test, breaks in the characteristic fibrous manner.

The basic element of the fiber structure is the microfibril which is produced by the micronecking process at the cracks of the ribbonlike lamellae of the spherulitic structure.[21] Each microneck transforms a certain width of lamella into one microfibril. Since there is not energy enough for complete unfolding of chains, one must imagine that blocks of folded chains are broken away from the lamella and incorporated into the microfibril. The chains at the lateral boundary of the block which are bridging the interblock fracture crack are partially unfolded during the separation (Figure 1). They are essential not only for the micronecking process, *i.e.*, for the pulling of the next block and breaking it off from the lamella, but also for the axial cohesion of the microfibril as connectors of blocks in the axial direction. Since, as a rule, each microneck transforms a width of the lamella larger than the width of the microfibril, the blocks cannot be incorporated in the microfibril in exactly the same order as they were located in the lamella.[22] That means that originally adjacent blocks no longer immediately follow each other in the microfibril. This spatial separation of blocks causes the unfolded chains to act as intrafibrillar tie molecules across more than one amorphous layer sandwiched between the crystal cores of consecutive blocks. This effect increases the fraction β of tie molecules per amorphous layer by a factor $p + 1$ if p is the number of blocks separating in the microfibril the originally adjacent blocks connected by a string of molecules (Figure 2). As a consequence of the high tensile stress acting on the

---

[16] G. Meinel and A. Peterlin, *J. Polym. Sci., Part A-2*, **9**, 67 (1971).

[17] J. W. S. Hearle and P. M. Cross, *J. Mater. Sci.*, **5**, 507 (1970).

[18] See, for instance, G. M. Bartenev and Yu. S. Zuyev, "Strength and Failure of Viscoelastic Materials," Pergamon Press, Oxford, 1968, p 94.

[19] P. H. Geil, "Polymer Single Crystals," Interscience, New York, N. Y., 1963.

[20] W. Glenz and A. Peterlin, *J. Macromol. Sci., Phys.*, **4**, 473 (1970).

[21] A. Peterlin, *J. Polym. Sci., Part C*, **9**, 61 (1965); **15**, 427 (1966); **18**, 123 (1967).

[22] A. Peterlin, *J. Mater. Sci.*, **6**, 490 (1971).

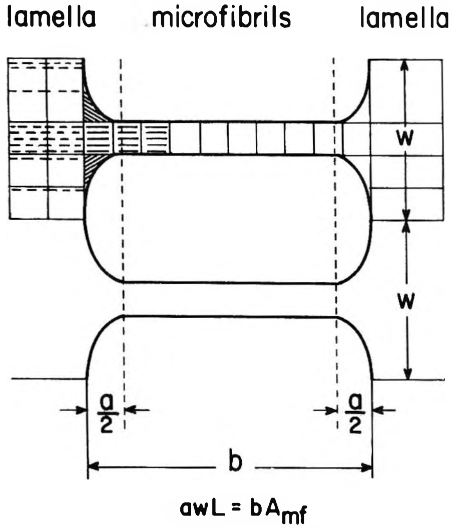

Figure 1. Microfibril formation by micronecking at a single-crystal crack. An area of width w and breadth a is transformed into a microfibril of length b. For the sake of simplicity the mosaic blocks are assumed as identical squares with the folds (short dashes) perpendicular to the crack. The chains (long dashes) in the crystal blocks of the microfibril are fully oriented.

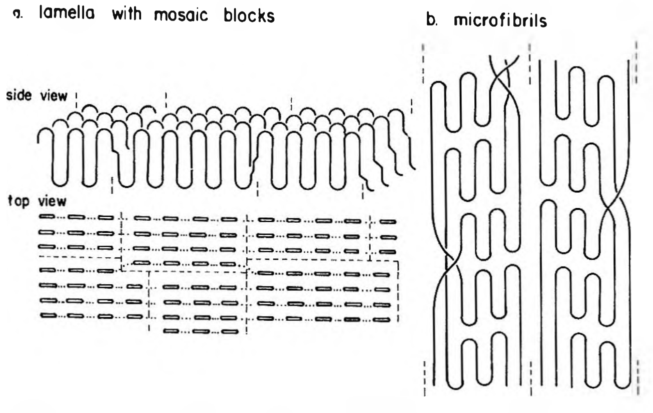

Figure 2. Connection of blocks of folded chains by tie molecules in (a) the original lamella and (b) the microfibril.

chains during unfolding in the microneck and subsequently in the newly formed microfibril, one expects the sections of tie molecules passing through the amorphous layer to be highly stretched. In the case of polyethylene that means a strong preference for trans conformations and suppression of gauche conformations below the frequency expected in a unoriented liquid in thermal equilibrium.

The separation p and hence the number of tie molecules are larger if the width w of lamella per microneck increases, *i.e.*, if the number of microneck per unit length of crack decreases. If the microfibrils have a nearly constant average cross section A_{mf}, the length and hence the draw ratio λ_{mf} of the microfibril also increase linearly with the width of lamella per microneck. The total length depends on the total length of the ribbonlike lamella in the direction perpendicular to the crack. A very rough estimate yields

$$\lambda_{mf} = wL/A_{mf} = (p + 1)L/A_{mf}^{1/2} \qquad (1)$$

$$p + 1 = w/A_{mf}^{1/2}$$

$$\beta_{\lambda} = (p + 1)\beta_1$$

Here L is the thickness of lamella which, for sake of simplicity, is assumed to be also the length of the blocks in the microfibril and β_1 is the fraction of molecules connecting adjacent blocks in the undeformed lamella. Since the nearly extended tie molecules contribute much more to the elastic modulus and strength than the randomly oriented chain folds and free chain ends, one can conclude that the modulus and the stress to break of the microfibril increase nearly linearly with the draw ratio of the microfibril. Since a minimum molecular length is necessary for the micronecking, below which the number of molecular ties between the adjacent blocks is not yet sufficient for pulling out of blocks and above which the chances for that are rapidly increasing, the number of micronecks and microfibrils per unit length of crack is increasing with molecular weight. According to eq 1 that reduces the draw ratio and hence the tensile strength of the microfibrils in perfect agreement with experiments.[23-26]

The maximum length of the microfibril is determined by the maximum extension a_{max} of lamella in the direction perpendicular to the crack, *i.e.*, by the expression wLa_{max}/A_{mf}. Because there are practically no material connections from one crystal to the next one, the micronecking process ends as soon as it has transformed the whole strip of lamella of width w into one single microfibril. One can even imagine that by some accidental agglomeration of crystal defects the micronecking is stopped earlier yielding a shorter microfibril.

The tendency of microfibrils for lateral coalescence and the pretty good fit of blocks caused by the tendency to minimize the free surface energy on the boundary between adjacent microfibrils produce folded-chain lamellae more or less perpendicular to the draw direction which yield the characteristic two- or four-point small-angle X-ray scattering pattern. They can be also detected by electron microscopy on etched fiber surfaces.[27] However, they are a secondary feature, more an artifact than a true structural element. There are practically no molecules connecting laterally

---

[23] G. R. Williamson, B. Wright, and R. N. Haward, *J. Appl. Chem.*, **14**, 131 (1964).

[24] R. N. Haward and J. Mann, *Proc. Roy. Soc., Ser. A*, **282**, 120 (1964).

[25] R. N. Haward and G. Thackray, *ibid., Ser. A*, **302**, 453 (1968).

[26] J. M. Andrews and I. M. Ward, *J. Mater. Sci.*, **5**, 411 (1970).

[27] A. Peterlin and K. Sakaoku, "Clean Surfaces," G. Goldfinger, Ed., Marcel Dekker, New York, N. Y., 1970, p 1.

adjacent blocks of the same lamella which end up in different microfibrils. In a stack of individually grown lamellae or in a spherulite all material connections among the blocks are lateral, perpendicular to the chain direction, and in the fibrous material they are axial, parallel to the chain direction. In the other direction, *i.e.*, in the chain direction in the former and in the direction perpendicular to it in the latter case, the connections are merely by van der Waals forces between more or less noncrystalline chains in the surface layers of the blocks.

There are some interlamellae tie molecules connecting the stacked lamellae of the spherulitic structure.[28] Their number increases with molecular weight and rate of crystallization. After micronecking, in the drawn material, they connect adjacent microfibrils. Some interfibrillar links may be generated also by the boundary fluctuation between adjacent micronecking regions.

Radical Formation in the Fiber under Load

If a highly oriented fiber or film of nylon is loaded up to the final fracture, one detects by electron spin resonance the formation of radicals. Their number increases with increasing load.[1,2] Upon load application the intensity of the esr spectrum very rapidly increases to a constant value which does not change with time.[4-6] Load removal and reloading does not change the intensity until the sample is elongated to the maximum strain of the previous loading. Straining beyond this point again produces new radicals. One concludes that the stationary number of radicals is a function of strain and not of stress. It seems to increase more than exponentially with strain.[7]

The radicals are formed in the whole strained sample so that their number observed by esr yields the density of radical population as function of strain. Depending on the size of the sample, the maximum radical density at the break of the material, and the sensitivity of the esr spectrometer one can first detect the radical formation at very much differing relative strain levels. In nylon 6 with a high yield of radicals one can make good measurements at strains which are about 40% of the strain to break.

The radicals have a finite lifetime. It is maximum in an inert atmosphere and at low temperature. Heating and the presence of oxygen reduce it quite drastically. A correction has to be applied to experimental data in order to obtain the radical concentration as a function of strain without the effect of finite lifetime.[4,9]

The esr spectrum is basically identical with that obtained in the same temperature range on γ-irradiated samples. At room temperature it is characteristic of secondary radicals formed by hydrogen abstraction from chain groups and not of the primary radicals formed by chain scission. With nylon the rupture of C–C bond of the main chain yields as primary radicals[29]

$$-CH_2CONH\dot{C}H_2 + \dot{C}H_2CH_2-$$

I

which at room temperature are so short-lived that they are not observed at all. Instead the spectrum observed corresponds to the secondary radical[1-14]

$$-CH_2CONH\dot{C}HCH_2-$$

II

obtained by proton abstraction from the CH_2 chain group. In the case of rubber the amount of hydrogen generated under applied stress is so large that one can observe gas bubble formation.[30] Esr data indeed show an extremely high density of radicals up to $10^{20}/cm^3$ which is about three orders of magnitude higher than in nylon.[31]

There is a remarkable difference between the mechanically strained and γ-irradiated nylon as far as radical orientation is concerned. In a biaxially oriented γ-irradiated nylon 66 strip Kashiwagi[14] found the esr spectrum to be a sextet, triplet, and quartet if the magnetic field is (1) perpendicular to the film, (2) in the film plane perpendicular, and (3) parallel to the machine direction, respectively. This anisotropy reflects the orientation of the radicals in the biaxially oriented crystal lattice. The irradiation creates radicals uniformly in the amorphous and crystalline regions of the sample. Their average orientation is hence identical with that of polymer chains. It even increases with time if, as is indeed the case, the lifetime of radicals in the amorphous component is shorter than in the crystalline regions. In strained nylon 66, however, the orientation is much less conspicuous.[7] The observed spectrum rather well agrees with the radical spectrum averaged over all orientations, *i.e.*, to the sum (1) + (2) + (3) as shown in Figure 3. This lack of radical orientation leads to the conclusion that the secondary radicals are located on chains in the amorphous component which is substantially less oriented than the crystalline component of the sample. Such a location also follows from experiments of Becht and Fischer[5] on strained nylon immersed in acrylic acid which penetrates the amorphous nylon but not the nylon crystals. The radicals triggered the polymerization of the acid and were completely consumed during this process.

Upon stretching up to fracture, radicals were observed in fibers and/or oriented films of nylon 6, nylon 66, silk, polyethylene, and polyethylene terephthalate (Table I). The data of different investigators dis-

---

(28) H. D. Keith and F. J. Padden, Jr., *J. Polym. Sci.*, **41**, 525 (1959).

(29) V. A. Zakrevskii, E. E. Tomashevskii, and V. V. Baptizmanskii, *Sov. Phys.-Solid State*, 9, 1118 (1967).

(30) E. H. Andrews and P. E. Reed, *J. Polym. Sci.*, *Part B*, **5**, 317 (1967).

(31) K. L. DeVries, private communication.

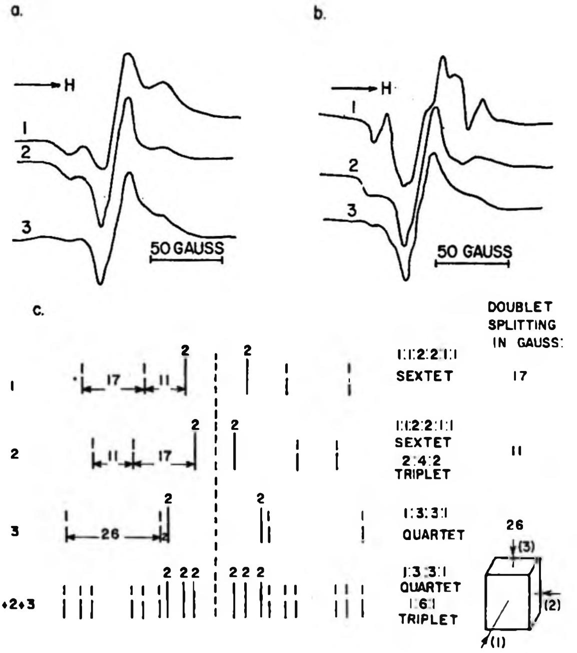

Figure 3. Esr spectrum of (a) highly strained (Verma) and (b) γ-irradiated (Verma–Peterlin[6]) biaxially oriented nylon 6 film as function of magnetic field orientation. (c) Model of spectrum for oriented (1, 2, 3) and unoriented (1 + 2 + 3) radicals according to the data by Kashiwagi.[14]

agree very much as far as the maximum density of radicals is concerned. Becht and Fischer[8] found a high density of radicals in nylon 6 but some orders of magnitude smaller values in nylon 12, polyethylene, polypropylene, and polyethylene terephthalate. They supported their findings by the observation of intrinsic viscosity which drops by 15% in nylon 6, corresponding to a drop of molecular weight by 25%. No reduction of molecular weight was observable with other samples. They concluded that with exception of nylon 6 no or very few chains are broken in the fracture experiment and explained this result by a low ratio of activation energy for chain rupture and cohesive energy of crystal lattice in the former case and a high ratio in the rest of the samples.

Table I: Radical Concentration at Break for Different Fibers

	Zhurkov–Tomashevskii[2]	Campbell–Peterlin[3]	Becht–Fischer[6,8]
Nylon 6	5×10^{17} (−30, 20°)		11×10^{17}
Nylon 66		$\sim 10^{17}$ (20°)	
Nylon 12			$<5 \times 10^{16}$ (20°)
Silk	7×10^{17} (−30°)		
Polyethylene	5×10^{16} (−30°)		$<5 \times 10^{15}$ (20°)
Polyethylene terephthalate	8×10^{16} (−30°)		$<10^{16}$ (20°)

Such a disagreement may be also caused by the differences in antioxidants, stabilizers, and other additives which enormously influence the lifetime and even the nature of radicals. A nylon 66 sample investigated by Campbell and Peterlin[3] contained an unidentified additive yielding predominantly a single-line esr spectrum upon irradiation or stretching but hardly any trace of the spectrum of the radical II in the latter case. This observation was explained by the preferential presence of the additive in the amorphous layers between the crystals so that all radicals in this component are transformed into radicals with a single-line esr spectrum. The normal radical II is hence detectable only with an irradiated sample as a consequence of the fact that a sufficiently large fraction of radicals are in the crystalline regions which are not as much affected by the additive as the amorphous regions.

Radical Formation by Crushing and Cutting

Bresler, *et al.*,[11,12] and Butyagin and Berlin[13] were the first to detect by esr radicals formed in polymers (polyethylene, nylon, poly(methyl methacrylate)) during crushing in an oxygen-free atmosphere at low temperature. The esr measurements were performed at low temperature so that indeed the spectra of primary radicals could be observed corresponding to unpaired electrons on the ends of the broken chains. With increasing temperature of the crushed sample the spectra change to those of secondary radicals. In the presence of oxygen one mainly obtains peroxide radicals upon heating to room temperature. Concurrently the intensity of the esr spectrum decreases as radicals are destroyed.

The crushing creates a new surface which is not easy to measure precisely. A better definition of the new surface is achieved by slicing a rod with a sharp knife.

A quantitative study of the number of radicals formed per square centimeter of cutting surface was performed by Backman and DeVries[32] on nylon 66, polyethylene, and polyethylene terephthalate. In all three cases they obtained at low temperature about 10^{13} radicals/cm^2. This number drastically decreases as one approaches the glass transition temperature of the material. On the other hand, Pazonyi, *et al.*,[33] investigated the number of radicals formed by cutting of low- and high-density polyethylene and plasticized poly(vinyl chloride) (PVC) not by esr but by dye extinction caused by the radicals. They used a 10^{-4} *M* solution of diphenylpicrylhydrazyl in alcohol as scavenger and measured photometrically the decrease of dye intensity. At 30° they obtained about 10^{15} radicals/cm^2 which is 100 times more than the number

---

(32) D. V. Backman and K. L. DeVries, *J. Polym. Sci., Part A-1*, **7**, 2125 (1969).

(33) T. Pazonyi, F. Tüdős, and M. Dimitrov, *Angew. Makromol. Chem.*, **10**, 75 (1970).

obtained by Backman and DeVries. The radical density in PVC decreases rapidly with increasing amount of plasticizer (dioctyl phthalate).

Crushing at sufficiently low temperature involves very little plastic deformation and transformation of spherulitic into fibrous structure. The cracks mainly occur through the regions of minimum strength, *i.e.*, through the boundary layers between adjacent spherulites, stacks of lamellae, parallel lamellae, and adjacent mosaic blocks of single lamellae. These boundaries contain less crystallizable rejected impurities and a minimum of tie molecules. Hence one expects a small number of ruptured chains per square centimeter of crack surface. Cutting with a sharp knife, however, involves a substantial amount of plastic shearing which locally, within a thin layer between a few microns and a few hundred microns, transforms the spherulitic to fibrous structure. A fraction of this layer is strained sufficiently close to fracture so that radicals are formed by chain rupture. Consequently, the surface density $[\mathrm{R}]_c/\mathrm{cm}^2$ of radicals in the cut sample represents the number of radicals in this fraction of surface layer

$$[\mathrm{R}]_c/\mathrm{cm}^2 = l[\mathrm{R}]_f/\mathrm{cm}^3 \tag{2}$$

where l is the equivalent thickness of such a layer which in uniform strain field would yield at the fracture the maximum density $[\mathrm{R}]_f$ of radicals.

If l is assumed to be $10\ \mu = 10^{-3}$ cm, then eq 2 yields $10^3[\mathrm{R}]_c$ for $[\mathrm{R}]_f$, *i.e.*, $10^{16}/\mathrm{cm}^3$ with the data of Backman and DeVries and $10^{18}/\mathrm{cm}^3$ with the data of Pazonyi, *et al.* With a larger l these figures for radical volume density are proportionately reduced. One may expect that they must be lower than those obtained in the fracture of fibrous material because in the not yet perfectly oriented areas, plastically deformed during cutting, the crack can better avoid the areas of high concentration of tie molecules than in the material with fibrous structure.

Molecular Interpretation of Rupture Data

Some important conclusions about chain rupture in the stretching experiment can be derived in a straightforward manner from the maximum number of radicals observed. The fracture plane of oriented nylon or polyethylene contains $\beta/A \approx 10^{14}$ tie molecules/cm^2 if β is assumed to be 20% and $A = 20$ Å.[2] That would yield 2×10^{14} radicals/cm^2. The actually observed values are $(2\text{–}5) \times 10^{17}/\mathrm{cm}^3$ which is equivalent to at least 1000 fracture planes/1-cm length of the sample. On the other hand, the number of amorphous layers alternating with crystal blocks in each microfibril is $1/L$. In nylon with $L \approx 100$ Å that yields $1/L = 10^6\ \mathrm{cm}^{-1}$. If all the tie molecules in the amorphous layers were broken during the fracture experiment, one would expect $2\beta/LA \approx 2 \times 10^{20}$ radicals/cm^3, *i.e.*, 1000 times more than actually observed. One sees that only a tiny fraction, 0.1%, of all tie molecules are ruptured at the fracture so that the sample, with exception of the fracture area, is very little damaged by chain rupture. The majority of the sample is practically unaffected, and the tie molecules are unbroken. Any direct correlation among elastic modulus, strength, and the number of ruptured chains as function of strain is misleading because the actual failure of the sample is primarily the consequence of local fluctuation of the stress field caused by inherent structure defects and tie molecule distribution.

If a load is applied in the fiber direction, it could be very uniformly distributed among the microfibrils according to their cross section if the microfibrils indeed extended through the whole length of the sample. However, since their length is limited by the dimensions of the original ribbonlike lamellae, the problem of load transfer among well-aligned microfibrils of limited length becomes quite important. The surface-to-volume ratio of the microfibril, with an average diameter of about 200 Å or even less, makes the van der Waals cohesive forces between adjacent microfibrils quite sufficient for such a transfer. Their action is supported by the interfibrillar tie molecules. The finite elongation of the sample before break is much larger than the possible elongation of the microfibril and hence requires some sliding motion of microfibrils. It is opposed by the friction forces in the boundary layer between the microfibrils and by the connecting interfibrillar tie molecules which must be either ruptured or partially unfolded during such a deformation.

The nonuniform lateral cohesion of microfibrils and their final length introduce an element of inhomogeneity in the stress distribution. Particularly at the end of a microfibril which represents something like a *linear or point dislocation* in the microfibrillar superlattice, a local stress concentration is created on the adjacent microfibrils which may overstrain the load bearing elements in them (Figure 4). The crystal blocks as strongest element are not very much affected. They mainly serve as load transmitters to the connecting intrafibrillar tie molecules in the amorphous layer between subsequent blocks.

In the ideal case the load would be uniformly distributed among the tie molecules so that each would have to carry a load

$$F_{\mathrm{tm}} = (A/\beta)\sigma_{\mathrm{mf}} \tag{3}$$

As a rule the stress σ_{mf} on the microfibril at the linear dislocation is by a factor $q > 1$ larger than the average stress σ = load/cross section of the loaded sample. In thermal equilibrium according to Tobolsky and Eyring[34] the average lifetime of a strained bond is

$$t_\sigma = t_0 \exp(U_0 - g\sigma)/kT \tag{4}$$

where U_0 is the activation energy for bond rupture and

---

[34] A. Tobolsky and H. Eyring, *J. Chem. Phys.*, **11**, 125 (1943).

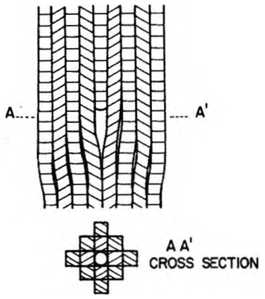

Figure 4. Superlattice of aligned microfibrils with a point dislocation at the end of a microfibril.

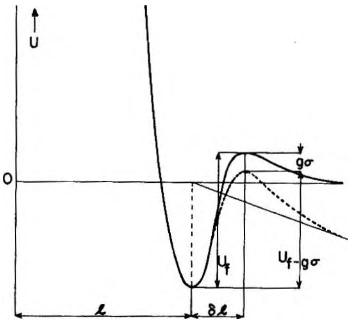

Figure 5. The energy well of a covalent bond of length l and activation energy for rupture U_f under the influence of a bulk tensile stress σ lowering U_f to $U_f - g\sigma$.

g a coefficient which correlates the applied stress σ to the work of the force F_{tm} on the covalent chemical bond during stretching by δl from the equilibrium position to the position of the maximum of the bonding energy curve (Figure 5). From eq 3 one has

$$g = q(A/\beta)\delta l \qquad (5)$$

The radical population derived from the radical formation rate

$$\mathrm{d}R/\mathrm{d}t = (2n - R)/t_\sigma \qquad (6)$$

turns out to be

$$R(t) = 2n(1 - e^{-t/t_\sigma}) \qquad (7)$$

where n is the number of strained tie molecules. The factor 2 takes into account the fact that the bond rupture produces two free ends, *i.e.*, two radicals. If the experiment extends over the lifetime t_σ, one would rupture 0.63 of the strained tie molecules, in twice that time 0.86, and so on.

The initial increase of radical population upon straining the sample and the early saturation can be described by eq 7. According to such an interpretation the stationary radical concentration equals twice the number n of loaded tie molecules. They are all broken and the load must be borne by other structure elements, *e.g.*, by microfibrils farther away from the linear dislocations of the microfibrillar superlattice where the first stress concentration occurred and was high enough for chain rupture.

Since the number of microfibrils affected increases with the distance from the point dislocation, each one has to carry a smaller fraction of the load so that at a given strain very soon the situation is reached that no unbroken microfibril is overstrained. Load removal and reloading up to the same strain does not change the situation. By increasing the strain beyond the maximum value of previous loading new microfibrils become strained up to the breaking point. The accumulation of damage at the point dislocations hence creates weak areas with gradually increasing extension in the plane perpendicular to the applied stress. As soon as the cross section of any of such area reaches the critical dimensions for crack propagation according to Griffith, the strained sample fails catastrophically.

The stepwise fracture of microfibrils during the nucleation stage as described above is very similar to that postulated by Bueche and Halpin[35] for polymer rubbers. They assumed that bundles of a few hundred chains are broken in succession until the crack becomes critical. If the diameter of the bundle is a fraction $1/p$ of the critical crack size, the time to produce such a crack is p times the time t_b' to fracture the bundle. The number p of steps is of the order of magnitude between 10^4 and 10^7. The short time t'/p needed for such a single step shifts the time range of the master curve of creep compliance $\Gamma(t)$ *vs.* t/a_T by many decades to the left. The reduction of the compliance is less than the reduction of time so that the crack nucleus grows to the critical size in a significantly shorter time than in the case that the whole nucleation ought to be completed in one single step. The choice of step length, however, is completely arbitrary and can be justified *a posteriori* by fit with experimental data. In contrast to that, a crystalline polymer with fibrous structure has the microfibrils as elementary units which are independent enough from the rest of the sample that they can and must be broken individually. At such a single-step fracture $n_{mf} = \beta A_{mf}/A$ chains are broken. The number of ruptured chains per unit volume as function of strain is proportional to the number of single steps, *i.e.*, to the number of broken microfibrils.

Such a mechanism of fracture needs some modification because the tie molecules in any amorphous layer between subsequent crystal cores may differ in length and hence get differently strained at any axial strain of the microfibril. The nonuniform strain of the microfibril being maximum in the close vicinity of a point dislocation and minimum in a regular area of the microfibrillar superlattice will, of course, bring more tie molecules to rupture in the most strained amorphous layers. However, the statistical variation of length of tie molecules will be sufficient for some of them to be at the strain to break even in the less strained layers although the majority of such cases will be in the most

---

(35) F. Bueche and J. C. Halpin, *J. Appl. Phys.*, 35, 36 (1964).

strained layers. The strain dependence of radical density of the sample is hence reflecting the strain distribution of tie molecules in the loaded sample caused by the variation of extensibility of tie molecules in each amorphous layer and by the strain variation of microfibrils as a consequence of defects of microfibrillar superlattice.

If one has a variety of tie molecules with different length and strain, one has to sum eq 7 over all of them

$$R(t) = 2\int_0^n (1 - e^{-t/t_\sigma(\epsilon)})\mathrm{d}n(\epsilon') \qquad (8)$$

where $\mathrm{d}n(\epsilon')$ is the number of molecules which at a given load σ or sample elongation ϵ have reached the same strain ϵ'. The lifetime $t_\sigma(\epsilon')$ in such a case reads

$$t_\sigma(\epsilon') = t_0 \exp(U_0 - g\sigma)/kT \qquad (9)$$

$$g\sigma = q(A/\beta)\sigma\delta l = F(\epsilon')\delta l$$

$$F(\epsilon') = q(a/\beta)\sigma = f(\epsilon')\sigma$$

where $F(\epsilon')$ is the force acting on a tie molecule with a strain ϵ'. One assumes in this case that the crystal blocks and the fixation of tie molecules in the crystal lattice are strong enough for the stress concentration described by the factor $f(\epsilon')$. Actually the situation is reversed. The molecule can be strained to a value ϵ' if the force can reach the value $F(\epsilon')$. The stress concentration factor $f(\epsilon')$ is higher than $q(A/\beta)$ corresponding to uniform length and spatial distribution of tie molecules. That is schematically represented in Figure 6 for an amorphous layer at three levels of strain. Almost all the stress is initially concentrated on one tie molecule. After it is broken, two tie molecules are bearing the load and at a later stage one has three tie molecules in such a position. That means that the factor replacing A/β is just the whole area of the microfibril in the first stage, one-half and one-third the area in the second and third stage, respectively.

In evaluating the time dependence of radicals at a given stress or strain according to eq 8 one sees that the expression in the parentheses is zero for large and 1 for small $t_\sigma(\epsilon')$. That means that tie molecules of the former type do not contribute to the radical population and those of the latter type contribute fully. The transition between these two extremes is rather abrupt as a consequence of the exponential dependence of lifetime on ϵ'. Highly strained tie molecules rupture very fast and those with low concentration factor remain unaffected during the experiment. In observing the number of radicals formed one hence measures primarily the distribution function $\mathrm{d}n/\mathrm{d}\epsilon$ and not the effect of stress on the lifetime of an average covalent bond.

Moreover one must not forget completely the role of interfibrillar tie molecules formed during drawing from interlamellae tie molecules of the spherulitic starting material. In sliding motion of microfibrils they get easily strained up to the breaking point and hence contribute to the radical population of the strained fibrous material. Again a separation of this effect from that of intrafibrillar tie molecules seems not to be possible without some new data selectively concentrating on different types of tie molecules. From a purely formal point of view all types of tie molecules can be included in eq 8, and their dependence on ϵ can be derived from the experimentally obtained function $R(\epsilon)$.

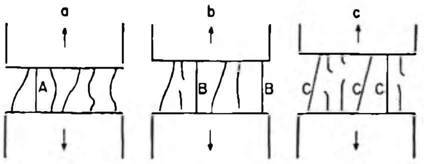

Figure 6. Tie molecules in the "amorphous" layer between subsequent crystal blocks of the microfibril. At low strain (a) a single tie molecule (A), at medium strain (b) two tie molecules (B), and at the highest strain (c) three tie molecules (C) are stretched up to the rupture point.

The low number of radicals in fractured polyethylene as compared with nylon 6 cannot be explained by a different resistance of chains to rupture. More likely the difference resides with the greater ease of sliding motion of polyethylene chains through the crystal lattice. At sufficiently high force exerted on the chain it may be easier to pull the chain to some extent through the crystal lattice and thus relieve the strain on the tie molecules section in the amorphous layer. Thus instead of chain rupture one has a partial relaxation of the most strained section by a longitudinal displacement of the chain in the crystal. Such an effect reduces but does not exclude chain fracture. It seems to be more predominant in polyethylene than in nylon with hydrogen bonding adding to the forces opposing sliding motion of chains through the lattice.

In linear polyhydrocarbons the lateral cohesive forces between adjacent chains are about 1% of the covalent forces in the chain direction. Hence a line of 100 chain units will have a binding energy equivalent to one covalent chain bond. That means that a crystal of such thickness can bind the chain so strongly and concentrate enough stress on it that the chain section in the amorphous layer can be broken. On the other hand, chain defects, as for instance the Reneker-type defect[36] or Pechhold's kinken,[37] can travel along the chain in the lattice with the final effect that the whole chain is displaced along its axis by one or more chain groups. By such a motion and ensuing chain translation the strain of tie molecule can be efficiently reduced and the molecule relaxed even in the case that the length of the crystallized straight section would provide a stronger lateral bonding than needed for the stress concentration up to chain rupture. Instead of covalent bond failure the chain is stepwise pulled out of the crystal lattice not as a rigid unit but by material transport in

---

(36) D. H. Reneker, *J. Polym. Sci.*, 59, 39 (1962).

(37) W. Pechhold, *Kolloid-Z. Z. Polym.*, 228, 1 (1968).

the form of a chain defect traveling along the chain through the lattice. Such a transport is easy in all cases where the translational period in the chain direction is small. It is not so in nylon 6 where the translation by two carbon–carbon distances does not restore the equilibrium location. It instead breaks a hydrogen bond which can be restored only by a translation over the whole chain period with six chain elements. This factor makes the longitudinal chain displacement by the motion of chain defects much more difficult in nylon 6 than in polyethylene with two chain elements per period. It hence favors chain rupture in the former and the pulling out of chains in the latter case.

More likely, however, the difference in radical population between nylon and polyethylene or polypropylene originates in the different crack propagation as a consequence of the microfibrillar superstructure. In polyethylene the high shear compliance favors longitudinal crack growth which ruptures very few tie molecules in contrast with nylon 6 and 66 where as a consequence of the strong hydrogen bonding between adjacent microfibrils the cracks mainly grow in the direction perpendicular to the fiber axis. In this case the microfibrils have to be fractured with the rupture of all tie molecules in at least one cross section of each microfibril.

Theoretical Models for Peak Migration in Gel Permeation Chromatography[1]

by Edward F. Casassa

Department of Chemistry, Mellon Institute of Science, Carnegie-Mellon University, Pittsburgh, Pennsylvania 15213

(Received May 13, 1971)

Publication costs assisted by the Air Force Materials Laboratory and Carnegie-Mellon University

The idea that the elution volume of a macromolecular species in a gel chromatogram is, under ordinary conditions, determined primarily by the equilibrium partition coefficient of the species between the mobile phase and a stationary phase inside micropores in the column packing has been put in question recently by the contention of Verhoff and Sylvester that gel permeation chromatography is a "hydrodynamic fractionation" method. Their theory is shown to differ from a similar derivation of Guttman and DiMarzio only because of certain approximations. With these removed, the Verhoff–Sylvester theory is brought into complete harmony with the other and becomes indistinguishable from an equilibrium model when the flow velocity through the pores is very slow compared to that in the mobile phase. Modification in the same spirit of a theory based on restricted diffusion in narrow channels is shown to bring it also into agreement with the equilibrium model.

Introduction

Explicit recognition of the possibility of chromatographic separations based on differences in the ability of solute molecules of different size to penetrate into voids within beads of a microporous column packing dates at least from Synge's discussion[2] of the "molecular sieve" effect and reports of elution of polysaccharides and polypeptides in inverse order of molecular weight from starch gel columns by Lindqvist and Storgårds[3] and Lathe and Ruthven.[4] The idea that size differences alone between solute molecules and pores could provide a means for effecting separations enjoyed rapid practical exploitation, and an extensive literature soon grew up on separation of biological macromolecules by passage of aqueous solutions through columns packed with swollen gels. Less than a decade ago this kind of chromatography also became a practical possibility for synthetic organic polymers when cross-linked polystyrene gels with controlled pore size were developed[5] and made commercially available. In a very few years, gel permeation chromatography (GPC)—to use the most popular of several names for the method[6-10]—has become the

---

(1) Work supported by the Air Force Materials Laboratory under Contract No. F33615-70C-1058. Presented in part at the Combined Southeast–Southwest Regional Meeting of the American Chemical Society, New Orleans, La., Dec 1970.

(2) R. L. M. Synge, "Les Protéines: Rapports et Discussions," Neuvieme Conseil de Chimie, Bruxelles, 1953, p 163.

(3) B. Lindqvist and T. Storgårds, *Nature (London)*, **175**, 511 (1955).

(4) G. H. Lathe and C. R. L. Ruthven, *Biochem. J.*, **60**, xxxiv (1955).

(5) J. C. Moore, *J. Polym. Sci., Part A*, **2**, 835 (1964).

(6) By adopting this conventional nomenclature we do not mean to imply that the column has to be packed with a "gel" in the sense that this word is usually understood. The term "exclusion chromatography" suggested by Pedersen[8] perhaps best reflects our point of view about the GPC process.

(7) J. Porath and P. Flodin, *Nature (London)*, **183**, 1657 (1959).

most widely used means of analytical polymer fractionation and has recently been adapted to preparative-scale fractionation. The success of GPC has inspired innumerable specific applications studies and a variety of investigations of operating variables in practical chromatography. The desirability of being able to characterize polymers from chromatographic data has motivated an empirical search for parameters to "calibrate" a column for elution of polymers generally from data on standard samples. However, despite the large volume of quantitative information that has been amassed, no consensus has been achieved concerning the dominant mechanism in GPC separation, except for the evident fact that it is somehow effected on the basis of molecular size.

The following presentation has as its purpose a comparison of diverse lines of thought on the basic question of how the fractionation in GPC comes about. Its scope is limited: the discussion is focused on what determines the position of the elution peak in the chromatogram of a homogeneous substance, the questions of peak broadening and peak shape being mentioned only in passing.

A logical starting point is the equation for the average elution volume $\bar{V}_e$

$$\bar{V}_e = V_0 + K_{GPC}V_i \tag{1}$$

We imagine the conventional experiment in which a thin layer of solution is introduced at the top of a packed column filled with solvent. Then liquid is withdrawn at a fixed rate from the bottom while more solvent is added at the same rate at the top. The volume of liquid eluted at the point in the chromatogram corresponding to the center of gravity of the elution peak for a particular solute is $\bar{V}_e$ for that species; thus, $\bar{V}_e$ is a measure of the average residence time of a solute molecule in the column.[11] The volumes V_0 and V_i are constants for a given column material and solvent, but the dimensionless parameter K_{GPC} depends on these and on the solute. In terms of the familiar simple physical model of a GPC column, V_0 represents the volume of the "mobile phase" outside the beads of the packing material and V_i is the volume contribution due to the micropores, "the stationary phase," within the beads. Thus, $V_0 + V_i$ is the total volume in the column, exclusive of the actual volume of solid in the packing and of any "blind" pores inaccessible alike to solute and solvent. However literally one may be inclined to take these definitions, the volumes can be defined by experiment. Very large particles, too large to enter any of the micropores, pass through the column "seeing" only the volume V_0 at which their elution peak appears. If the flow through the column is sufficiently slow, small molecules that can permeate the micropores completely—*e.g.*, radioactively labeled solvent—pass through the entire volume of the column and elute at $V_0 + V_i$. Molecules similar in order of size to the micropores effectively permeate some fraction K_{GPC} of the total void volume, and they elute somewhere in the range between V_0 and $V_0 + V_i$. Thus K_{GPC} is a number between zero and unity that measures the apparent fractional permeation of the void space by the solute. Experimentally K_{GPC} could conceivably turn out to be greater than unity. Such an event, a retardation of solute greater than that of the solvent, might be the result of adsorption on the surface of the microporous packing. For the present discussion we assume that such anomalous effects need not be considered.

The most noteworthy thing to be said about eq 1 is that this form implies virtually nothing about the content of a model for retardation of a species relative to one that passes through the external volume V_0 alone. All the theories that we shall mention can be cast into this form. Any process that "traps" molecules out of the interstitial phase temporarily—to constrain them to a far slower average velocity, to immobilize them completely, or to permit them to be transported only by diffusion—will produce a retardation that can be expressed by eq 1, at least to a good approximation. The meaningful content of any theory subsists in what it predicts about K_{GPC}: how this quantity depends on the structure of the column material, on solvent and solute, and on operating parameters. Our concern will therefore be with theories for K_{GPC} and comparison with experiment. It is useful to classify theoretical treatments under three headings—as they relate to equilibrium models, hydrodynamic models, or diffusion models for GPC separation—even though these do not represent completely exclusive categories, either in terms of concepts or in terms of likely processes in real chromatographic columns. The main focus of our discussion is on equilibrium and flow models: on their interrelations and on the elucidation of some apparent differences among recent theories. Since our interest here is confined to specific basic aspects of GPC, we simplify matters quite ruthlessly, essentially ignoring the mobile phase by assuming that all molecules in it pass down the column at a single uniform rate and ignoring similarly all instrumental effects that may influence real chromatograms. These limitations and others mentioned below must be kept in mind in judging comparisons with experiment.

---

(8) K. O. Pedersen, *Arch. Biochem. Biophys., Suppl.*, **No. 1**, 157 (1962).

(9) S. Hjerten and R. Mosbach, *Anal. Biochem.*, **3**, 104 (1962).

(10) R. L. Steere and G. K. Ackers, *Nature (London)*, **196**, 475 (1962).

(11) It is more usual to define the elution volume as the maximum of the peak—*i.e.*, the most probable elution volume—but the theories analyzed below are best discussed in terms of the average $\bar{V}_e$. In our theoretical discussion this is more a logical nicety than a necessity, for we shall be concerned chiefly with circumstances such that the elution peaks approach the limiting symmetrical (Gaussian) form.

Equilibrium Theory

The easiest assumption to make is that the elution volume of a macromolecular solute is determined by the equilibrium partitioning between the interstitial phase of macroscopic dimensions and the phase in micropores.[12-15] In this view K_{GPC} is just an equilibrium constant, the ratio of solute concentration inside pores to that outside if the solution is dilute. The concept is attractive because equilibrium calculations are inherently easier than nonequilibrium ones. One can employ elementary statistical mechanics to get explicit results with simple geometrical models without concern about the actual processes of trapping and release of molecules. An incontrovertible support of this point of view is the fact that the equilibrium condition must represent the limiting behavior of a long column at sufficiently low rate of flow. Thus, even if real columns should operate with large deviations from equilibrium behavior, it is important to know what bound is set by equilibrium.

Some insight into the significance of the equilibrium assumption can be gained by considering the general theory of adsorption chromatography. The most useful formulation for this purpose is the stochastic theory of Giddings and Eyring.[16,17] They determined the distribution of residence times in a column for molecules subject to random alternating steps of immobilization by adsorption on identical independent binding sites and release to the mobile phase where travel along the column takes place at a steady rate. As Carmichael[18] pointed out, this formalism is immediately translatable into the terminology of GPC. The result for the average elution volume is that $K_{\mathrm{GPC}} = K$, the equilibrium distribution coefficient for solute between stationary and mobile phases, regardless of the value of $\bar{N}$, the number of entrapments that the average molecule undergoes as it progresses throgh the column.[16-18] The elution volume V_e defined by the maximum in the elution peak is related to $\bar{V}_e$ by[16,18]

$$V_e/\bar{V}_e \approx 1 - (KV_i/\bar{V}_e)(3/2\bar{N}) \tag{2}$$

If $\bar{N}$ is at least of the order of 10^2—and if the idealized process envisaged here describes GPC—the peak shape will not differ significantly from Gaussian. The same theory shows that peak spreading is directly proportional to $\bar{N}$. The idea that elution volume is determined by equilibrium partitioning of solute is generally accepted for adsorption chromatography where the intimate contact between the stationary and mobile phases and the fact that one is dealing with small molecules both suggest that equilibrium may be well approximated.[17] That this might be so for GPC of macromolecules is less apparent in view of their low diffusion rates and the relative inaccessibility of micropores deep within beads.

The exclusion of compact molecules such as proteins from micropores obviously suggests that the effect might be substantially accounted for on straightforward geometrical grounds. For example, in Figure 1A, we depict in cross section a spherical macromolecule of radius r inside a hollow cylinder of radius a. The center of the sphere cannot approach the wall of the cavity more closely than the distance r; that is, the sphere "sees" a cavity of radius $a - r$, rather than the entire volume. At equilibrium the concentration of spheres in the smaller effective volume is equal to that in unbounded space outside the void. Thus, the average concentration of spheres inside the cavity is less than that outside and the distribution of spheres between the two phases satisfies the equilibrium constant

$$K = \left(\frac{a - r}{a}\right)^2 \tag{3}$$

for an infinite cylinder (*i.e.*, with neglect of end effects).

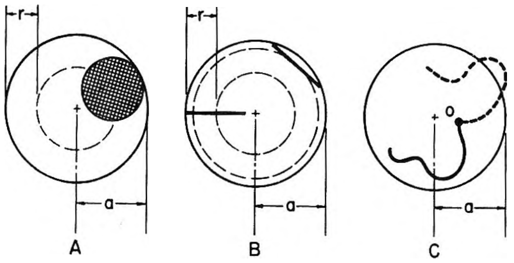

Figure 1. Schematic diagrams illustrating exclusion effect in cylindrical void of radius a: (A) hard sphere of radius r; (B) thin rod of length $2r$ in two orientations in the plane of the cross section; (C) random-flight chain with one end at point O, showing allowed conformation (solid curve) and forbidden conformation (dotted curve).

A more complicated example is illustrated in Figure 1B. A thin uniform rod-shaped molecule of length $2r$ inside the hollow cylinder has its axis perpendicular to the cylinder axis. When the center of mass of the rod is at distance $x > r$ from the wall of the cavity, the rod cannot touch the wall. In an intermediate region $r > x > [(a^2 + r^2)^{1/2} - a]$ the rod can be accommodated, but it is not free to assume all rotation angles. Every x smaller than the last limit represents a class of entirely forbidden conformations. This kind of exclusion problem has been worked out by Giddings, *et al.*,[15] for rigid particles of various shapes in simple voids.

Finally, Figure 1C represents a random-flight polymer chain in the cylindrical cavity. Now any part of the

---

(12) R. L. Pecsok and D. Saunders, *Separ. Sci.*, **1**, 613 (1966).

(13) T. C. Laurent and J. Killander, *J. Chromatogr.*, **14**, 317 (1964).

(14) E. F. Casassa, *J. Polym. Sci.*, *Part B*, **5**, 773 (1967).

(15) J. C. Giddings, E. Kucera, C. P. Russell, and M. N. Myers, *J. Phys. Chem.*, **72**, 4397 (1968).

(16) J. C. Giddings and H. Eyring, *ibid.*, **59**, 416 (1955).

(17) J. C. Giddings, "Dynamics of Chromatography," Marcel Dekker, New York, N. Y., 1965, Part 1.

(18) J. B. Carmichael, *J. Polym. Sci.*, *Part A-2*, **6**, 517 (1968); *Polym. Prepr., Amer. Chem. Soc., Div. Polym. Chem.*, **9**, 572 (1968).

molecule can be in any part of the cavity, but the presence of the wall still decreases the conformational freedom of the chain. With one end of the chain at point O some conformations that would be possible in the absence of the boundary are forbidden because some part of the chain would cross the boundary.

The three cases illustrated all concern the effect of a barrier on the availability of conformations available to a macromolecule. Case A exemplifies the ordinary "steric exclusion" that has characterized idealized models for GPC of biological molecules. Cases B and C are more complicated but not essentially different if we consider not merely exclusion from Cartesian space (which is the only possibility for an isotropic spherical particle whose conformation is completely specified by the locus of a single point) but rather exclusion from a part of the configuration space of all coordinates of the particle[15]—three Cartesian coordinates plus two angles for a rod (in three dimensions), $3N$ coordinates for a random flight of N steps. The result in each case is a distribution coefficient $K \leq 1$. The calculation for case A is trivial; that for B is only a little more intricate. The calculation for C is more difficult but it can be done by solving the partial differential equation for a particle undergoing Brownian motion subject to appropriate boundary conditions.[14] The result can be written in the series form

$$K = 4 \sum_{m=1}^{\infty} \beta_m^{-2} \exp[-\beta_m^2(Nb^2/6a^2)] \qquad (4)$$

for the statistical chain of N steps each of rms effective length b. The β_m are roots of the equation $J_0(\beta) = 0$, $J_0(\beta)$ denoting the Bessel function of the first kind of order zero. The parameters N and b become physically meaningful in the combination $Nb^2/6$, the mean-square molecular radius of gyration. Relations analogous to eq 4 have also been derived for spherical and slab-shaped voids.[14,19] Throughout the ensuing discussion, we confine our attention to idealized models in which a column contains identical micropores and the solution is so dilute that solute molecules never interact.

From the point of view of this discussion, the distinction[4] that has sometimes been maintained betwen partition chromatography[20] in gel columns and the effect of exclusion from micropores is rather artificial. The models for exclusion are merely very simple models for a certain kind of partitioning process. They attribute the standard free energy change for transporting a macromolecule from the outer phase to the interior of a micropore entirely to the entropy change connected with the constraint imposed on the macromolecule by the presence of rigid, impenetrable barriers defining the pores. There is no other entropy contribution and no heat of interaction between solute and the gel material. Most likely, reality will often be found to be more complicated than such models would allow.

In principle, a direct test of the concept that equilibrium partitioning governs elution from a GPC column is available without regard to the properties of a specific model. The K_{GPC} derived from elution experiments can be compared with the true equilibrium constant obtained from static equilibrium experiments.[19,21–23] If an aliquot of solution is mixed with a known amount of the column packing material and allowed to equilibrate with it, any resulting change in concentration of solute in the supernatant serves as a means of determining K provided the internal pore volume V_i is also determined. This can be done as mentioned above by column experiments or by equilibration experiments with solute molecules so large that they cannot appreciably permeate the pores. The quantities involved can be defined unambiguously by the experimental procedures, but it should be remembered that the geometrical meaning of "pore volume" has to remain somewhat imprecise. Any bulky solute molecule is excluded from any surface in a column, say the outer surface of beads, by a distance that varies with the size of the molecule; and this distance measures a layer whose volume is implicitly included in the measured pore volume.

Few direct comparisons of K with K_{GPC} have been attempted, and it must be remembered the reported experimental values of the latter are derived from V_e not $\bar{V}_e$. With a series of narrow-distribution polystyrenes in chloroform solution and porous glass beads, Yau, *et al.*,[22] found excellent agreement between static and elution experiments and no dependence on flow rate under ordinary operating conditions for GPC columns. On the other hand, elution of polystyrenes in a higher molecular weight range from columns of cross-linked polystyrene showed deviations from predictions based on static experiments and measurable dependence on flow rate. Ackers[21] studied the behavior of proteins and virus particles on Sephadex (dextran gel) columns. For these aqueous systems K and K_{GPC} were in good agreement in tightly cross-linked gels, but large differences appeared with very highly swollen, loosely cross-linked gels. The experiments suggest that elution under ordinary conditions from materials with a comparatively rigid pore structure—porous glass and silica gel columns representing the extreme—is governed by equilibrium partitioning but that nonequilibrium effects are important when the gel phase can be described as a network of thin flexible filaments meeting at infrequent junctions and enclosing a very large amount of liquid. Later, Brumbaugh and Ackers[23] devised a direct optical scanning technique to determine total solute

(19) E. F. Casassa and Y. Tagami, *Macromolecules*, **2**, 14 (1969).

(20) A. J. P. Martin, *Ann. Rev. Biochem.*, **19**, 517 (1950).

(21) G. K. Ackers, *Biochemistry*, **3**, 724 (1964).

(22) W. W. Yau, C. P. Malone, and S. W. Fleming, *J. Polym. Sci., Part B*, **6**, 803 (1968).

(23) E. E. Brumbaugh and G. K. Ackers, *J. Biol. Chem.*, **243**, 6315 (1968).

concentration at any point within a gel column. They found excellent agreement between K_{GPC}, determined for several proteins on a Sephadex column by measurements of peak velocity within the column, and the equilibrium K measured on the same column saturated (*i.e.*, operated with an input at constant solute concentration until the effluent exhibited the same concentration as the feed).

Another way to verify the equilibrium theory is obviously to calculate K, *ab initio*, for a model and then compare this with the experimental K_{GPC}. The drawback of this approach is the difficulty of treating, or even defining, a sufficiently realistic pore model. Even if partitioning of solute can be attributed simply to steric hindrance, the morphology of real pores is hardly likely to resemble any simple geometrical shape. A comparison of this kind has been made with data of Moore and Arrington[24] on elution of narrow-distribution polystyrenes in a Θ solvent from two porous-glass columns of different pore size.[25,26] The polymer molecules can be represented adequately as random-flight chains, and their unperturbed mean-square dimensions are known. A measure of the mean pore size in the glass is obtained by mercury intrusion measurements. Combining all this information with the theoretical function for random-flight chains in any chosen pore model, one is able to obtain values of K. The comparison displayed in Figure 2 shows that K_{GPC} from the work of Moore and Arrington is larger than the theoretical K for random-flight chains in cylindrical cavities, but perhaps no better agreement should be expected in view of the certainly oversimple character of the model and a considerable uncertainty in the pore size measurements. The experimental points in Figure 2 happen, in fact, to agree well with the theoretical K for linear chains in slab-shaped cavities[14] (of thickness $2a$); but it is hard to see how the slab model could be physically realistic.

A third kind of test of equilibrium theory utilizes model calculations but largely avoids the difficulty in characterizing pore structure accurately. Since molecular conformation of polymer chains can be described more satisfactorily than real pore goemetry, one can investigate theoretically the differences in K for different molecular models in the same model pore.[15,19] One hopes that approximately the same comparative behavior between different molecules will prevail in a variety of pores; and since the polymer chemist is usually interested in characterizing polymer molecules rather than pore structures, lack of information about the pores need not be counted a serious deficiency. A theoretical comparison of this sort among branched and linear polymer chains yields semiquantitative agreement with results of GPC experiments and reveals something about the basis for "universal calibration"[27,28] of columns. Calculation of K for a particular class of branched polymers—"star" molecules formed by identical linear-chain arms joined at a common point—in simple cavities is not significantly more difficult than for linear chains. It is found[19] that values of K in pores of a given shape for random-flight linear chains and for star chains with a moderate number of branches define fairly well a single master curve when plotted against any function of the dimensionless variable

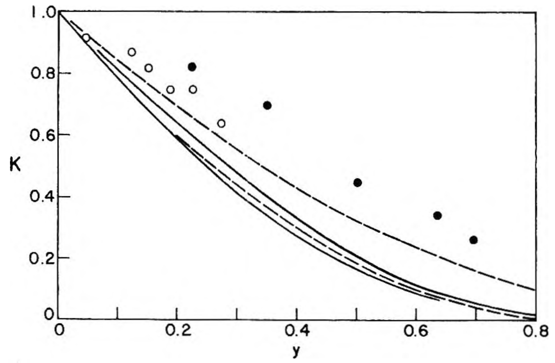

Figure 2. Plots of partition coefficients for permeation of random-flight polymer chains into cylindrical voids: K for linear chains (lower solid curve) and 12-branch star molecules (upper solid curve); K_η for linear chains for $\Phi = 39.4 \times 10^{21}$ (upper dashed curve) and $\Phi = 90.2 \times 10^{21}$ (lower dashed curve). The points are data of Moore and Arrington[24] (*cf.* ref 14).

$$y = (Nb^2/6a^2)^{1/2}g^{1/6} \qquad (5)$$

where N, b, and a have the meanings given above and g is the ratio of mean-square radii of linear and branched chains of the same mass and chemical structure in a Θ solvent (so that random-flight statistics applies for long chains). Plots of K for linear chains and star molecules with twelve branches in cylindrical cavities are compared on this basis in Figure 2. The curves for stars with three, four, and six branches are virtually coincident with that for linear chains. Analogous results for spherical and slab-shaped cavities appear in ref 19.

The importance of this theoretical correlation lies in the relations

$$[\eta]M = (\pi N_A/30)R_\eta^3 = \Phi y^3 a^3 \qquad (6)$$

The first equality defines a hydrodynamic molecular radius R_η proportional to be the cube root of the product of intrinsic viscosity $[\eta]$ (expressed in eq 6 in the customary units 100 ml/g) and molecular weight, N_A denoting Avogadro's number. The second equality depends on the familiar Flory–Fox relation[29,30] between

---

[24] J. C. Moore and M. C. Arrington, International Symposium on Macromolecular Chemistry, Tokyo and Kyoto, 1966, Preprints of Scientific Papers, VI-107.

[25] W. Haller, *Nature* (*London*), **206**, 693 (1965).

[26] W. Haller, *J. Chromatogr.*, **32**, 676 (1968).

[27] H. Benoit, Z. Grubisic, P. Rempp, D. Decker, and J. G. Zilliox, *J. Chim. Phys.*, **63**, 1507 (1966); Z. Grubisic, P. Rempp, and H. Benoit, *J. Polym. Sci.*, *Part B*, **5**, 753 (1967).

[28] K. A. Boni, F. A. Sliemers, and P. B. Stickney, *ibid.*, *Part A-2*, **6**, 1579 (1968).

$[\eta]$ and mean-square molecular radius for linear polymers and the approximate theory of Zimm and Kilb[31] for the intrinsic viscosity of star-branched chains. Since Φ is a universal numerical constant,[30] the construction of a master curve from the theoretical relations for linear and branched chains implies that two different polymers with the same value of the product $[\eta]M$ will have the same elution volume on any given column. This correlation was, in fact, proposed by Benoit, *et al.*,[27] on the basis of elution data on various linear and branched polymers. The support given this proposal by our theoretical work rests entirely on equilibrium thermodynamics, presuming that the connection between intrinsic viscosity and chain dimensions can be considered firmly enough established. The correlation with an equivalent hydrodynamic size does not *per se* argue that GPC depends on hydrodynamic effects in micropores.

In anticipation of the discussion below, it is of interest to inquire whether R_η might be taken to represent an equivalent hard-sphere radius for exclusion of a polymer chain from the vicinity of an impenetrable surface: for a chain in a cylindrical void, does the quantity

$$K_\eta = (1 - R_\eta/a)^2 \tag{7}$$

with R_η obtained from the second equality in eq 6, approximate the correct equilibrium constant given by eq 4? In Figure 2, K_η is plotted against y for two values of Φ. The best theoretical value,[32] $\Phi = 39.4 \times 10^{21}$ for a nondraining chain, is in good agreement with experimental values[33] deduced from viscosity measurements; but it makes K_η somewhat greater than K. The other plot is determined by $\Phi = 90.2 \times 10^{21}$, the value that makes the initial slope coincide with that of K for a linear chain. The result shows that the two functions are brought very nearly into coincidence by proper scaling.

Despite argument about the correct value of Φ to use in eq 6, there is no warrant for a value greater than 39.4 $\times 10^{21}$ to relate $[\eta]M$ and the molecular radius of gyration. However, there is also no reason to assume that Φ from intrinsic viscosity is the correct quantity to use to relate chain dimensions to the exclusion effect. To put the matter another way, R_η defined by the intrinsic viscosity certainly need not be the same as the effective radius for the exclusion effect, and Figure 2 indicates that the former is smaller than the latter—just as the effective hydrodynamic radius for sedimentation of polymer chains is different from R_η.[30] The question of the magnitude of the effective radius to be substituted in the equilibrium expression does not affect the proposition that the quantity $[\eta]M$ is an elution parameter independent of the polymer: all that is required is that the proper radius be proportional to y (or to R_η).

Flow Models

The arguments outlined above seem to us to constitute a strong case for the position that the elution volume in GPC, as ordinarily carried out, is determined primarily, if not exclusively, by the equilibrium distribution coefficient. However, since detailed theories emphasizing mass flow effects have recently been put forward, it seems necessary to take account of this other point of view—which in fact has a close relation to older work on ultrafiltration.

Red blood cells have long been known to move faster than the plasma through capillaries.[34] A qualitative explanation can be found in the existence of a flow velocity profile across a narrow tube filled with flowing liquid. The corpuscles, being of appreciable size in comparison with the tube diameter, are constrained to travel preferentially near the center of the tube where the flow rate of the liquid medium is greater than it is near the tube walls. If the corpuscles do not distort the flow lines too drastically, they will have a mean velocity greater than that of the plasma. Recalling this phenomenon, Pedersen[8] suggested that something similar might play a role in GPC (and was able to observe a chromatographic effect by passing solutions of large protein molecules through a column packed with very small *solid* glass spheres).

Since the velocity effect envisaged by Pedersen depends on hydrodynamics, it does not appear to be the equivalent of an equilibrium model for GPC separation. However, the two situations are far from unrelated. The flow separation should vanish if the large suspended particles (more precisely their centers of mass) are able to occupy equally all regions of the tube cross section. That is, the effect depends (among other things) on a difference in flow rates in the middle of the tube and at the periphery and also on the fact that the size of the particle excludes them from the latter. It appears then that the peripheral region behaves like a stationary phase—and we recall in this connection that it is not really possible operationally to distinguish between a stationary phase inside pores and a surface region at any boundary of the mobile phase. Pedersen's idea is not worked out by him in quantitative fashion, and this verbal description has to be supplemented by more exact analysis in order to make clear what is involved.

The most comprehensive discussion of "separation by flow" has been given in a series of papers under that title by DiMarzio and Guttman.[35-37] They first

---

[29] P. J. Flory and T. G. Fox, *J. Amer. Chem. Soc.*, **73**, 1904 (1951); *J. Polym. Sci.*, **5**, 745 (1950).

[30] P. J. Flory, "Principles of Polymer Chemistry," Cornell University Press, Ithaca, N. Y., 1953, Chapter 14.

[31] B. H. Zimm and R. W. Kilb, *J. Polym. Sci.*, **37**, 19 (1959).

[32] C. W. Pyun and M. Fixman, *J. Chem. Phys.*, **42**, 3838 (1965).

[33] G. C. Berry, *ibid.*, **46**, 1338 (1967).

[34] A. C. Burton in "Medical Physiology and Biophysics," T. C. Ruch and J. F. Fulton, Ed., W. B. Saunders, Philadelphia, Pa., 1966, Chapter 29.

[35] E. A. DiMarzio and C. M. Guttman, *J. Polym. Sci., Part B*, **7**, 267 (1969).

[36] E. A. DiMarzio and C. M. Guttman, *Macromolecules*, **3**, 131 (1970).

consider a suspension of particles (polymer molecules) in a continuous medium passing through a uniform circular cylindrical tube.[35,36] The fluid velocity is governed by Poiseuille flow, and the parabolic velocity profile is unaffected by the particles. To calculate the particle velocity, DiMarzio and Guttman use an analysis of Debye[38] with the refinement of including a quadratic component of the shear field. For the ratio of the mean velocity $\langle u_p \rangle$ of a spherical particle of effective radius r to the mean velocity $\langle u \rangle$ of solvent, they obtain

$$\langle u_p \rangle / \langle u \rangle = 2 - (1 - r/a)^2 - \gamma (r/a)^2 \qquad (8)$$

where $r < a$. The last term on the right arises from the quadratic contribution to the shear field. The coefficient γ depends on the molecular model (*e.g.*, on the permeability of a polymer molecule represented as a diffuse sphere) but lies between zero and 0.4. If $\gamma = 0$, $\langle u_p \rangle$ is determined merely by constraint of the center of mass of a particle to distances greater than r from the wall of the tube, the particle traveling with the velocity of the streamline passing through its center.

We note at this point that the process just described constitutes a model for ultrafiltration.[39] We need but imagine the suspension of spheres forced from a large reservoir through a battery of identical tubes in tandem. A sphere cannot enter a tube if its center lies on a streamline that passes closer than a distance r from the wall of the tube at its mouth. Accordingly, the effective tube cross section for capture of spheres has a radius $a - r$. Competing effects thus operate: exclusion from a tube decreases transport of spheres through it, but confining spheres to the central part of the fluid velocity profile enhances transport of spheres that can enter the tube. Calculation of the net output of spheres from a tube gives the sieve constant φ, defined as the ratio of the concentration of particles in the filtrate to that in the feed. For spheres in cylindrical tubes this is

$$\varphi = (1 - r/a)^2 \langle u_p \rangle / \langle u \rangle \qquad (9)$$

In the DiMarzio–Guttman theory $\langle u_p \rangle / \langle u \rangle$ is given by eq 8, but this specific model is not required for the validity of eq 9.

Equation 8 indicates that large particles in a tube must travel faster, on the average, than small ones. If a mixture of large and small particles is introduced as a pulse into the flowing liquid, the different species will emerge in two peaks if the tube is long enough. Thus, flow in a tube provides, as DiMarzio and Guttman propose, a possible means of separation according to particle size. In the form just described, however, their model is clearly not a model for GPC separation. It will suffice to mention two considerations. (1) The advancement of large particles relative to small ones in a chromatogram from a bundle of identical tubes in parallel can be by a factor of 2 at most (assuming $\gamma = 0$) and this optimum is approached for the limiting case of a particle almost filling the tube—for which the assumptions of the theory must be meaningless. (2) To effect separation of macromolecules, the tubes have to be roughly of macromolecular dimensions (say 500–5000 Å): it is an easy matter to show that for tubes of reasonable length in parallel, an enormous pressure head is needed to produce the kind of flow rates that are usual in GPC columns.

To adapt their flow model to GPC, Guttman and DiMarzio[37] describe a column model made up of banks of cylindrical tubes. Each bank contains tubes of two sizes, large and small, mounted in parallel and all the same length l. A large number of banks is stacked in series to form a column with a mixing chamber between successive banks. The numbers of each kind of tube are the same in each bank. The small tubes of radius a are of such size, relative to particles represented as spheres of effective radius r suspended in the liquid-filled column, that the flow effect expressed by eq 8 can be important; but the large tubes are so large that particles and solvent are transported in them at the same average velocity (which is high compared to the flow velocity in small tubes). Every molecule is required to pass through the same total number of tubes, but the number of tubes of one kind that the molecule enters is characterized by a probability distribution. Particles and carrier fluid spend negligible time in mixing chambers. Formulating conservation equations for flow through the column, Guttman and DiMarzio obtain the average elution volume for the spheres. The problem can be stated thus:[37] to evaluate

$$\bar{V}_e = Qnl \left[\frac{p_l}{\langle u_p \rangle_l} + \frac{p_s}{\langle u_p \rangle_s} \right] \qquad (10)$$

where Q is the total carrier fluid flow (volume/time), n is the fixed number of tubes that each particle must traverse to get through the column, $\langle u_p \rangle_l$ and $\langle u_p \rangle_s$ are the mean velocities of particles in large and small tubes, and p_l and p_s are normalized probabilities ($p_l = 1 - p_s$) that a particle travels through a large tube or a small tube, respectively, as it passes through any cross section of the column. It is assumed that the suspension is very dilute so that the carrier fluid volume differs only infinitesimally from the entire volume of material passing through the column. It follows that

$$Qnl = \langle u \rangle_l V_l + \langle u \rangle_s V_s \qquad (11)$$

V_l and V_s denoting the volume of the column in large and small tubes, and $\langle u \rangle_l$ and $\langle u \rangle_s$, the respective carrier fluid velocities.

Guttman and DiMarzio proceed from eq 10 to evaluate the probabilities p_s and p_l for two limiting situations. (A) The concentrations of particles in any cross section of the column are locally in equilibrium;

---

(37) C. M. Guttman and E. A. DiMarzio, *Macromolecules*, **3**, 681 (1970).

(38) P. Debye, *J. Chem. Phys.*, **14**, 636 (1946).

(39) J. D. Ferry, *J. Gen. Physiol.*, **20**, 95 (1936).

i.e., the concentration in a small tube is less by a factor of the equilibrium constant K—or $(1 - r/a)^2$ for equivalent spheres—than that in a large tube. (B) The particles travel through the tubes in such fashion that a volume of solution above a tube, large or small, simply passes into it without composition change, except that particles are completely excluded from small tubes if $r > a$.

For case A, the p_s required by flow continuity can be written

$$p_s = \frac{N_s\langle u_p\rangle_s a^2 K}{N_s\langle u_p\rangle_s a^2 K + N_l\langle u\rangle_l w^2} \tag{12}$$

where N_l and N_s are numbers of large and small tubes in the column and w is the radius of a large tube. At infinite dilution of particles, this p_s, with eq 10 and 11, yields the elution volume

$$\bar{V}_e = V_l + KV_s + [\langle u\rangle_s/\langle u\rangle_l]V_s \times [1 + (V_s/V_l)][1 - \varphi] + O[(\langle u\rangle_s/\langle u_l\rangle)^2] \tag{13}$$

where φ is the sieve constant of eq 9. If, in addition, the flow effect on mean particle velocity is given by eq 8, eq 13 becomes equivalent to eq 3.17 of Guttman and DiMarzio, although it is cast in a different form here for convenience in the ensuing discussion. The coefficient of the term in $\langle u\rangle_s/\langle u\rangle_l$ is evidently of the order of V_s. Then since $\langle u\rangle_s$ must be much smaller than $\langle u\rangle_l$ if the model is to be at all realistic for a GPC column, eq 13 reduces for practical purposes to

$$\bar{V}_e \approx V_l + KV_s \tag{14}$$

or the equilibrium result, as Guttman and DiMarzio point out.

For case B, the Guttman–DiMarzio theory gives

$$\bar{V}_e = V_l + V_s[2 - (1 - r/a)^2 - 2\gamma(r/a)^2]^{-1} \tag{15}$$

provided $r < a$. This relation should be applicable at the limit of no equilibration of concentrations through the column cross section, thus at flow rates so high that diffusion is unimportant. This limit is therefore not comparable physically with the equilibrium situation and will not be further interest here. It does illustrate, however, that the form of eq 1 can be obtained, as already mentioned, without reference to equilibrium and that the coefficients of V_s in the two limiting cases are not radically different except as r approaches a.

Another recent flow theory for GPC is that of Verhoff and Sylvester.[40] In their scheme, a GPC column is characterized by relatively rapid flow of liquid through wide channels (the interstitial phase between the packed beads) and slow flow through narrow channels inside the porous beads. The channels intersect frequently so that a given particle traveling through the column finds itself in turn in various narrow and wide channels as it proceeds through the column. The model is therefore like that used in discussing equilibrium theory, with the single important difference that mass flow is explicitly taken to occur in the "stationary phase."

To make their model more amenable to calculation, Verhoff and Sylvester specify that the column be made up of uniform cylindrical tubes of but two diameters and all of the same length l, as in the Guttman–DiMarzio model. Each particle passes through the same number of tubes but the division between small and large tubes is determined statistically. Verhoff and Sylvester define the quantity

$$P_e = Qnlp_s\langle u\rangle_s \tag{16}$$

and assume that particle velocities are the same as carrier fluid velocities in *both* kinds of tubes. Then, in effect, using eq 11 and 16 with eq 10, they obtain

$$\bar{V}_e = V_l + P_eV_s + [\langle u\rangle_s/\langle u\rangle_l]V_s(1 - P_e) \tag{17}$$

or

$$\bar{V}_e \approx V_l + P_eV_s \tag{18}$$

inasmuch as $\langle u\rangle_s \ll \langle u\rangle_l$.

Thus Verhoff and Sylvester recover the form of eq 1. They identify P_e as the sieve constant and first assume for it a result derived by Ferry[39]

$$\begin{aligned} P_e = \varphi' &\equiv 2(1 - r/a)^2 - (1 - r/a)^4 \\ &= (1 - r/a)^2[1 + (2r/a) - (r/a)^2] \end{aligned} \tag{19}$$

in a theory of ultrafiltration. As before, a and r are radii of the small tubes and of the effective spheres representing suspended particles. It will be noted that φ' differs from φ in the DiMarzio–Guttman model only through the absence of the quantity $2\gamma(r/a)^2$ in the bracketed factor in eq 19.

Suggesting that Brownian motion tends to cancel out the last two terms within brackets in eq 19, Verhoff and Sylvester also propose as a further approximation, appropriate for extremely small tubes

$$P_e = (1 - r/a)^2 \tag{20}$$

which is merely the equilibrium constant for partitioning of rigid spheres between cylindrical pores and a macroscopic solution phase. With the final approximation of eq 20, their hydrodynamic GPC theory, at least for hard spheres, seems to have no content apart from what is in the equilibrium theory.

Although the result expressed by eq 20 with eq 18 is equivalent to eq 14 for case A of Guttman and DiMarzio, the question remains: why is the primary result of Verhoff and Sylvester, eq 17 with P_e given according to eq 19, different from eq 13? Apart from the important difference between K and the sieve constant, it is also not immediately apparent why the coefficient of $\langle u\rangle_s/\langle u\rangle_l$ in eq 17 lacks the factor $1 + V_s/V_l$ in eq 13. The genesis of the first discrepancy lies in two inconsis-

---

(40) F. H. Verhoff and N. D. Sylvester, *J. Macromol. Sci., Chem.*, **4**, 979 (1970).

tent assumptions in the derivation by Verhoff and Sylvester. By assuming $\langle u_p\rangle_s = \langle u\rangle_s$, they ignore the flow effect discussed by DiMarzio and Guttman (and implicitly by Ferry). However, at the same time using Ferry's sieve constant, they presume the flow effect to be operative. The inconsistency is easily removed. Letting $\langle u_p\rangle_s/\langle u\rangle_s$ be given by φ'/K for hard spheres (or, similarly, φ/K according to DiMarzio and Guttman) but following Verhoff and Sylvester in every other respect—using eq 11 and 16 in eq 10—we obtain in place of eq 17

$$\bar{V}_e = V_l + P_e(K/\varphi')V_s + (\langle u\rangle_s/\langle u\rangle_l)V_s(1 - P_e) \qquad (21)$$

Now, with $P_e = \varphi'$, the equilibrium result is unambiguously recovered when the third term becomes insignificant. The remaining unimportant divergence of this term from the corresponding one in eq 13 is accounted for by the fact that the P_e entirely consistent with the model is not exactly φ (or φ'). Maintaining the definition of P_e by eq 16 and eliminating p_s by eq 12, we find after some manipulation that

$$P_e = K\frac{\langle u_p\rangle_s}{\langle u\rangle_s}\left(1 + \frac{\langle u\rangle_s V_s}{\langle u\rangle_l V_l}\right)\left(1 + K\frac{\langle u_p\rangle_s V_s}{\langle u\rangle_l V_l}\right)^{-1}$$
$$= K\frac{\langle u_p\rangle_s}{\langle u\rangle_s}\left[1 + \frac{\langle u\rangle_s V_s}{\langle u\rangle_l V_l}\left(1 - K\frac{\langle u_p\rangle_s}{\langle u\rangle_s}\right) + \ldots\right] \qquad (22)$$

Letting $K\langle u_p\rangle_s/\langle u\rangle_s = \varphi$ and putting eq 22 into eq 21, we regain the form of eq 13 (and exactly the Guttman–DiMarzio result if φ' is replaced by φ).

Even though the dependence on $\langle u\rangle_s/\langle u\rangle_l$ in eq 13 and 21 is surely unimportant practically, the manner of dismissal is logically somewhat unsatisfactory. This dependence does not represent a nonequilibrium effect in the formalism of the hydrodynamic theory because, if the liquid velocities are determined by Poiseuille flow, the ratio $\langle u\rangle_s/\langle u\rangle_l$ stays fixed as $\langle u\rangle_l$ becomes vanishingly small—and K_{GPC} does not identically approach K. The answer to this difficulty lies in the consideration that at some sufficiently small $\langle u\rangle_s$ the hydrodynamic model itself becomes untenable. At the limit, Poiseuille flow behavior must be obliterated by Brownian motion; and then there seems to be no difficulty in conceiving of the phase within pores as truly stationary with respect to the mobile phase—so that $\langle u\rangle_s/\langle u\rangle_l$ can in fact approach zero at least as rapidly as $\langle u\rangle_l$ does.

Verhoff and Sylvester use eq 18 and 20 for a number of comparisons with available GPC data on linear-chain polymers. The agreement they present between the data of Moore and Arrington[24] and eq 20 *appears* to be much better than we achieved with the same data and eq 4. However, in accomplishing this: they assume a value of Φ about 22% smaller than what we regard as the best value; with this Φ and Mark–Houwink viscosity parameters they calculate the rms molecular end-to-end distance; they arbitrarily substitute this dimension (2.45 times the rms radius) into eq 20; and finally in place of the experimental values, they use pore sizes adjusted to make the data fit the theory. The effective molecular radii they use are thus much larger than values that would make eq 20 agree with the equilibrium relation, eq 4. The adjustment of the pore sizes can be defended on the ground that the change is in the direction compensating for the expected systematic error in measurements by mercury porosimetry,[26] but in our work we chose to avoid taking any parameter as arbitrary. In this connection, it must be remarked that the correlation of P_e with experiments in this way can hardly constitute a unique triumph of the hydrodynamic theory since, as we have shown above, free adjustment of r or a will bring eq 20 into excellent agreement with eq 4.

Diffusion

An extensive analysis of the effects of diffusion in GPC lies beyond the intent of the present discussion, but some remarks are pertinent to what we have already said.

Qualitative suggestions that GPC is a diffusion-controlled process have perhaps been motivated by correlations of elution volumes with diffusion coefficients,[41,42] just as correlations with another measure of molecular size, the hydrodynamic volume, seem to have inspired suggestions of a hydrodynamic process. Such arguments are suggestive, but they are hardly persuasive.

In a quantitative treatment, Ackers[21] combines steric exclusion of large particles from narrow pores with the effect of frictional resistance to diffusion of the particles within pores.[43,44] If we imagine that flow of carrier fluid occurs through the pores, his model becomes formally analogous to that of Verhoff and Sylvester, but with a *retardation* of large particles relative to small ones due to restricted diffusion replacing the *advancement* predicted from Poiseuille flow. Like Verhoff and Sylvester (in the version of their theory identifying P_e with φ' of eq 13), Ackers identifies K_{GPC} with a sieve constant; *i.e.*, for equivalent spheres in a cylindrical tube

$$K_{GPC} = \varphi'' \equiv (1 - r/a)^2 \times [1 - 2.104(r/a) + O(r^3/a^3)] \qquad (23)$$

in which the quantity in brackets[42] arises from restricted diffusion. As it stands, this result presents the obvious difficulty that there is no flow-rate dependence and thus no way for K_{GPC} to approach the equilibrium value $(1 - r/a)^2$ at the limit of slow flow. The logic outlined above in the case of the Verhoff–Sylvester theory applies

---

(41) A. Polson, *Biochim. Biophys. Acta*, **50**, 565 (1961).

(42) W. R. Smith and A. Kollmansberger, *J. Phys. Chem.*, **69**, 4157 (1965).

(43) J. R. Pappenheimer, *Physiol. Rev.*, **33**, 387 (1953).

(44) E. M. Renkin, *J. Gen. Physiol.*, **38**, 225 (1955).

here too. If we take account of the difference in mean velocities of particles and carrier fluid in small tubes by writing

$$\langle u_p \rangle_s / \langle u \rangle_s = \varphi''(1 - r/a)^{-2} \tag{24}$$

and put this into eq 10 together with eq 11 and 12, we obtain precisely the form of eq 13 with φ'' in place of φ'. Thus, K_{GPC} differs from K only by a contribution $O(\langle u \rangle_s / \langle u \rangle_l)$ that is quantitatively insignificant for $\langle u \rangle_s \ll \langle u \rangle_l$. As in the other cases, the model has to fail at extremely low flow rate so that K_{GPC} should correctly approach K at the limit.

In a derivation by Yau and Malone,[45] GPC separation is attributed to lateral diffusion in the column. In their mathematical formalism the solute is pictured as undergoing unidimensional diffusion from a fixed concentration in the mobile phase into a semiinfinite gel medium. The problem is thus reduced to a standard one in diffusion theory, and the result is yet another expression of the form of eq 1, but with K_{GPC} a complicated function of the diffusion coefficient in the gel and the flow rate. Although arbitrary adjustment of parameters enables this theory to conform fairly well to typical GPC data on the molecular weight dependence of elution volume for flexible-chain polymers,[45] it is not obvious what correspondence the model might have to the physical situation in ordinary small-zone chromatography. Logically, but unrealistically, this diffusion model requires K_{GPC} to approach unity at slow flow rate; thus in succeeding papers Yau, *et al.*, [22,46] combine it with the equilibrium theory by writing K_{GPC} as a product of the equilibrium K and the distribution coefficient given by the diffusion model. Yau[46] uses φ'' (eq 23) to represent the ratio of the diffusion coefficient in the gel to that in the mobile phase.

The most satisfactory theoretical treatments of diffusion in the stationary phase are due to Kubin[47] and Hermans[48] who picture the gel phase rather abstractly as composed of isotropic spheres into which solute particles can diffuse up to a certain equilibrium concentration. Hermans' results indicate that the effect of nonequilibrium in the gel phase can be expected to appear in spreading and skewing of elution peaks, and at low flow rate K_{GPC} unambiguously represents the equilibrium partition coefficient. Giddings, *et al.*,[15] summarize arguments supporting this view for ordinary GPC experiments.

Summary and Conclusions

In the analysis recounted above, we have undertaken an examination of the interrelations among partly divergent points of view about the basis of separation in GPC. In particular, this enterprise was motivated by the apparent differences between two recent "flow" theories by Verhoff and Sylvester and by Guttman and DiMarzio, both based on models including Poiseuille flow through micropores pictured as fine capillaries. The differences are traced to approximations in the Verhoff–Sylvester derivation, and once these are eliminated, the two theories agree in showing that K_{GPC} is related to the equilibrium partition coefficient of a solute between pores and the mobile phase by an expression of the form

$$K_{\mathrm{GPC}} = K + O(\langle u \rangle_s / \langle u \rangle_l) \tag{25}$$

Although the (trivially small) second term on the right-hand side of eq 25 does not vanish with decreasing $\langle u \rangle_l$ in the context of the hydrodynamic theory, it must do so in fact as Brownian motion ultimately vitiates the hydrodynamic model. Hence, eq 20, which Verhoff and Sylvester suggest for reasons that are not made completely clear, together with eq 18, does represent a quantitatively correct result for their theory (and for case A of the Guttman–DiMarzio theory) in the absence of Brownian motion and an exact result with it. The presumption that r in eq 20 represents an equivalent radius defined so as to make eq 3 satisfy the equilibrium constant of eq 4 leads us to assert that the Verhoff–Sylvester theory in the final form reduces to the equilibrium theory. In this circumstance, the latter has the advantage of being stated in a general context that transcends specific model geometry and avoids uncertain approximations beyond the basic postulate that K_{GPC} is to be identified with the equilibrium constant. Of course, it might be argued that the Verhoff–Sylvester theory is not an equilibrium theory because r in eq 20 is explicitly taken by the authors to be the "hydrodynamic radius." In reply we can say that Verhoff and Sylvester do not in fact use the hydrodynamic radius. Further it is hard to see how a molecular radius other than that defined by equilibrium exclusion can be logically justified for a theory that is intended to be applicable when the liquid velocity in the pore phase is small. For these reasons we do not regard the theory of Verhoff and Sylvester as establishing the hydrodynamic character of GPC separation; and, therefore, we cannot accept their proposal that ordinary GPC should be renamed "hydrodynamic fractionation." This, or the term "separation by flow" that Guttman and DiMarzio use, is more appropriate for case B of the Guttmann–DiMarzio theory where an ultrafiltration effect depends directly on the character of Poiseuille flow through narrow channels.

Since a reinterpretation of the "restricted diffusion" model of Ackers makes his theory parallel exactly the structure of the Veroff–Sylvester theory that we have criticized, the only difference being the substitution of φ'' of eq 24 in place of φ' of eq 19 to represent P_e in eq

---

[45] W. W. Yau and C. P. Malone, *J. Polym. Sci., Part B*, **5**, 663 (1967).

[46] W. W. Yau, *ibid., Part A-2*, **7**, 483 (1969).

[47] M. Kubin, *Collect. Czech. Chem. Commun.*, **30**, 1104, 2900 (1965).

[48] J. J. Hermans, *J. Polym. Sci., Part A-2*, **6**, 1217 (1968).

18, we suggest that this model too, properly considered, leads to the equilibrium relation at low flow rates. To put our criticism another way, Ackers, like Verhoff and Sylvester, identifies K_{GPC} with a sieve constant; and this is what is basically at issue. As eq 22 shows, P_e defined by eq 16 is indeed (almost) the sieve constant; but as eq 21 shows, it is incorrect to equate P_e with K_{GPC}.

According to the form of eq 13, any first-order hydrodynamic contribution to K_{GPC} could only increase it since the sieve constant is between zero and unity on the basis of any of the models we have discussed—even though the effect of relative flow velocities of particles and carrier fluid increases the sieve constant in the flow models and decreases it in the restricted-diffusion model. These contrary effects on transport of suspended particles through narrow tubes obviously prompt a question as to which kind of model might be the more realistic. Reasonably, both effects might be included; indeed Renkin[44] suggested that the sieve constant should be $\varphi''[1 + (2r/a) - (r/a)^2]$. However, it would be outside the ambit of this paper to delve further into the difficult problem of the actual behavior of suspensions flowing through small channels.[43,44,49]

Unlike the hydrodynamic contribution to K_{GPC}, true nonequilibrium effects in partitioning, as expressed by the idealized stochastic theory, do not affect the average elution volume for a solute; but according to eq 2 they tend to shift the maximum of the peak toward a smaller volume. The preponderance of evidence is that nonequilibrium has only a minor effect on elution peak maxima in ordinary columns, but under certain experimental conditions nonequilibrium behavior of the qualitative character predicted by the stochastic theory can become prominent.[21-23] The corollary of the insensitivity of mean and most probable elution volumes to flow and nonequilibrium phenomena is that detailed study can most profitably be directed toward the shape and breadth of peaks, on which both classes of phenomena will have more direct effects. There is the interesting consideration, pointed out by Guttman and DiMarzio,[37] that flow and diffusion tend to compensate: mass flow through pores will clear them of solute in a finite time and thus act to counter the skewing and tailing of peaks characteristic of diffusion-limited transport.

---

(49) See, for example, a review by H. L. Goldsmith and S. G. Mason in "Rheology: Theory and Applications," Vol. 4, F. R. Eirich, Ed., Academic Press, New York, N. Y., 1967, Chapter 2.

The Kinetics of Chlorine Fluoride at High Temperatures

by J. A. Blauer, W. C. Solomon,* and V. S. Engleman

Technology Division, Air Force Rocket Propulsion Laboratory, Edwards, California 93523

(Received April 29, 1971)

Publication costs assisted by the Air Force Rocket Propulsion Laboratory

Two-body emission from chlorine atoms has been used to follow the thermal decomposition of ClF occurring behind incident shock waves in the temperature range of 1700–2200°K. The initial reaction rates were interpreted in terms of the bimolecular rate constant for the reaction $ClF + M = Cl + F + M$ and may be expressed in the form $k_3[\text{initial}] = 10^{14.6 \pm 0.3} \exp(-61{,}300 \pm 3000/RT)$ cc/mol-sec. However, if the competing exchange reaction $Cl + ClF = Cl_2 + F$ is very fast, then the rate expression for $ClF + M = Cl + F + M$ becomes $k_3 = 10^{14.5 \pm 0.4} \exp(-57{,}500 \pm 3000/RT)$ cc/mol-sec. The latter value for k_3 is in better agreement with all of the available data.

Introduction

Although there have been theoretical predictions concerning the behavior of the ClF system,[1,2] there are currently few actual rate data available. Global rates for the reaction occurring between Cl_2 and F_2 have been reported;[3] however, no attempt was made to attribute experimental significance to the rates of individual reaction steps. The present shock tube study is the third in a series of kinetic measurements on the related systems ClF_5, ClF_3, and ClF being conducted in these laboratories.[4,5]

---

(1) S. W. Benson and C. R. Haugen, *J. Amer. Chem. Soc.*, **87**, 4036 (1965).

(2) R. M. Noyes, *ibid.*, **88**, 4311 (1966).

(3) E. A. Fletcher and B. E. Dahneke, *ibid.*, **91**, 1603 (1969).

(4) J. A. Blauer, H. G. McMath, and F. C. Jaye, *J. Phys. Chem.*, **73**, 2683 (1969).

(5) J. A. Blauer, H. G. McMath, F. C. Jaye, and V. S. Engleman, *ibid.*, **74**, 1183 (1970).

We have selected an experimental procedure which is based upon a measurement of the intensity of the two-body emission from Cl atoms behind incident shock waves. Our use of 5000 Å as the point of observation is based upon the results of Carabetta and Palmer.[6] They found that at the latter wavelength the emission intensity is independent of temperature and linearly dependent on the square of the Cl-atom concentration.

Experimental Section

The shock tube and associated apparatus have been described adequately elsewhere.[7] In the present instance, spectral isolation was by means of a Beckman DU monochromator, and detection of radiation was accomplished with a 1P28 photomultiplier tube.

Gaseous ClF having a purity of 98.0% was purchased from Ozark-Mahoning Co. and was further purified by trap-to-trap distillation at −100°. High-purity Cl_2 and HF (*ca.* 99.5% min) were purchased from Matheson and were treated by cooling to −100°, followed by removal of all permanent gases *in vacuo*. Argon having a minimum stated purity of 99.9% was also purchased from Matheson and was used without further purification. Chlorine trifluoride having a minimum purity of 98% was purchased from Matheson. The gas was further purified by forming the KF complex, $KClF_4$, at ambient temperatures. The pure ClF_3 was recovered by vacuum distillation at 200°. The purity of the ClF_5 used in these experiments was the same as that discussed in our previous paper.[5]

After a gaseous mixture with argon had been prepared, its ClF, F_2, and Cl_2 contents were determined by measuring the optical densities at 2600, 2850, and 3250 Å, respectively. A solution of the resulting three simultaneous equations gave the initial concentrations of the aforementioned species. The ClF_3 and ClF_5 concentrations were obtained from pressure measurements.

Results and Discussion

A typical emission trace is shown in Figure 1. It may be seen that after 150 μsec of test time drift due to nonidealities appeared in some traces making it necessary to estimate the equilibrium intensity as early as possible (*ca.* ~100–150 μsec). In accordance with the results of Carabetta,[6] the Cl-atom concentration was related to the emission intensity, I, by means of the expression, $[\mathrm{Cl}] = A(I)^{1/2}$. Here, A is the proportionality constant which was evaluated from the equilibrium conditions. Values of $A = [\mathrm{Cl}]_{\mathrm{equil}}/(I)^{1/2}$ for binary mixes of ClF in Ar were normalized to a standard value obtained for a binary mixture of Cl_2 in Ar. Both of the above-mentioned values of A were acquired on the same day. The results are found in Table I. It is seen that even over a factor of 50 variation in the value for $[\mathrm{Cl}]_{\mathrm{equil}}$ these proportionality constants showed little drift. Similarly, although the F-atom concentrations vary over a factor of 20, their presence had only a slight effect upon the emission intensity. These observations precluded any significant contribution to the radiancy from such two-body processes as

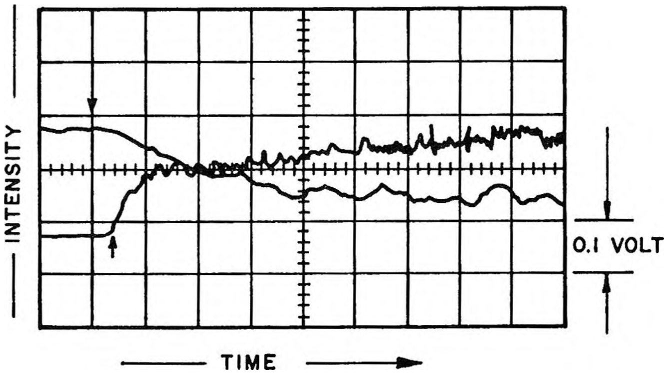

Figure 1. Emission trace for test no. 22, 0.1 V/ordinate division, 10 μsec and 50 μsec/abscissa division, 2.0% ClF in Ar. Incident shock temperature and pressure at the front of 1878°K and 22.7 atm, respectively. The arrows show the extrapolated point of shock incidence and direction of increasing intensity.

$$\mathrm{Cl} + \mathrm{F} = \mathrm{ClF} + h\nu \tag{1}$$

$$\mathrm{F} + \mathrm{F} = \mathrm{F_2} + h\nu \tag{2}$$

and demonstrated conclusively that the emission intensity was a true measure of the Cl-atom concentration. This conclusion has been further corroborated by the data obtained with ClF_3 and ClF_5 (see Table I).[8,9]

Resort is made to the method of initial slopes to estimate the rate constants for the processes

$$\mathrm{ClF} + \mathrm{M} = \mathrm{Cl} + \mathrm{F} + \mathrm{M} \tag{3}$$

$$\mathrm{Cl_2} + \mathrm{M} = \mathrm{Cl} + \mathrm{Cl} + \mathrm{M} \tag{4}$$

It is found that plots of $(I)^{1/2}$ *vs.* time are linear over at least 50% of the reaction, making the evaluation of initial rates from the first 10% of the reaction profile a relatively simple process. The point of shock incidence is found by extrapolating these plots to zero intensity. Density corrections are made in the manner outlined by Palmer.[10] The resulting experimental rate constants are found in Table I and plotted as func-

---

(6) R. A. Carabetta and H. B. Palmer, *J. Chem. Phys.*, **46**, 1333 (1967).

(7) J. A. Blauer and W. C. Solomon, *J. Phys. Chem.*, **72**, 2307 (1968).

(8) It has been reported[9] that the emission intensity from shock-heated HF* is altered in the presence of Cl atoms. Experiments (see Table I) with Cl–HF mixtures seen herein show no such behavior for the radiancy from the two-body recombination of Cl atoms. Similarly, the presence of HF has no effect upon the dissociation rate of Cl_2; see Figure 2.

(9) J. A. Blauer, V. S. Engleman, and W. C. Solomon, 13th International Symposium on Combustion, Salt Lake City, Utah, 1970, p 109.

(10) H. B. Palmer and D. F. Hornig, *J. Chem. Phys.*, **26**, 98 (1957).

Table I: Initial Reaction Rate Data

Test	T_2, °K	$(Ar)_0 \times 10^3$, mol/cc	$(ClF)_0 \times 10^6$, mol/cc	$(Cl_2)_0 \times 10^6$, mol/cc	$(F)_{equil} \times 10^6$, mol/cc	$[(Cl)/\sqrt{I}]/[(Cl)/\sqrt{I}]_s$[c]	$k \times 10^{-7}$, cc/mol-sec
17	1779	0.143	0.291	...	0.085	0.91	0.91
18	1692	0.141	...	0.288	...	1.00	1.4
20	2176	0.039	...	0.079	...	1.02	38
21	1924	0.145	0.295	...	0.124	1.26	3.2
22	1878	0.144	0.294	...	0.112	1.03	2.2
23	1796	0.114	0.232	...	0.074	1.12	1.4
24	1676	0.094	0.191	...	0.036	1.20	0.26
25	2196	0.039	...	0.079	...	0.98	32
26	2236	0.040	...	0.082	...	1.00	51
27	1786	0.076	0.399	...	0.048	1.26	1.0
28	1810	0.071	0.373	...	0.092	1.13	1.3
29	2167	0.039	0.205	...	0.123	1.00	18
30	2145	0.046	...	0.094	...	1.03	28
31	1902	0.056	...	0.296	0.100	1.03	2.7
32	2042	0.018	0.096	...	0.046	1.12	15
33	2274	0.061	...	0.125	...	0.99	62
34	1986	0.098	...	0.201	...	1.08	10
35	1951	0.099	...	0.203	...	1.02	9.9
36	1768	0.094	...	0.192	...	1.06	3.1
37	1759	0.095	...	0.195	...	1.06	3.2
38[d]	1921	0.071	...	0.145	...	0.99	9.1
39	1916	0.070	...	0.146	...	1.01	12
40	1834	0.089	...	0.181	...	0.99	6.3
41	1776	0.095	...	0.193	...	0.98	4.9
42	1559	0.111	...	0.226	...	1.02	0.65
43[d]	1750	0.094	...	0.195	...	1.01	3.3
44	1757	0.094	0.242	...	0.068	0.95	0.80
46	1912	0.130	0.334	...	0.114	1.11	4.1
47	2133	0.024	0.060	...	0.047	...	24
49[a]	1718	0.154	0.314	...	0.633	...	0.47
50[a]	2047	0.093	0.189	...	0.441	0.93	8.9
51[a]	2150	0.057	0.115	...	0.296	1.10	21
54	1847	0.114	...	0.233	...	1.00	5.5
57	2248	0.101	...	0.206	...	1.00	72
59[b]	1938	0.077	0.156	...	0.664	1.04	4.5
67	2540	0.051	...	0.104	...	1.08	245

[a] Binary mixes of ClF_3 and Ar. [b] Binary mix of ClF_5 and Ar. [c] $[(Cl)/\sqrt{I}]_s$ refers to measurements made with a binary mixture of Cl_2 and Ar on the same day as the datum point in question. [d] Contains 2.0% HF.

tions of temperature in Figures 2 and 3. The temperature dependencies of these rate constants can be expressed in the forms

$$k_3[\text{initial}] = 10^{14 \pm 0.3}(\exp(-61{,}300 \pm 3000/RT) \quad \text{cc/mol-sec}$$

$$k_4[\text{initial}] = 10^{13.3 \pm 0.2}(\exp(-46{,}450 \pm 1500/RT) \quad \text{cc/mol-sec}$$

The latter expression is in good agreement with the earlier findings of Carabetta,[6] Thiel,[11] and Jacobs.[12] The use of the above expression as an estimate of the rate constant for reaction 3 is clouded by the possible occurrence of the two exchange reactions.

$$ClF + Cl = Cl_2 + F \qquad \Delta H = +3 \text{ kcal/mol} \quad (5)$$

$$ClF + F = Cl + F_2 \qquad \Delta H = +23 \text{ kcal/mol} \quad (6)$$

In an effort to account for these additional reaction paths, we have used the following experimental approach.

Experimentally, a study of ClF decomposition in the presence of Cl and Cl_2 has been attempted. However, the fact that the emission intensity is a linear function of the square of the Cl-atom concentration negates the advantage of the addition of Cl_2 to a reaction mixture containing ClF. Nevertheless, *F atoms* in the form of ClF_3 or ClF_5 could be added. (Consideration of the results of our previous work[4,5] showed that under the conditions of the present study ClF_3 and ClF_5 would completely decompose into ClF and F atoms within the interval of 2 μsec.) Accordingly, exchange reactions −5 and 6 could be investigated. However, reaction −5 could be examined only by a consideration

---

(11) M. Thiel, D. J. Seery, and D. Britton, *J. Phys. Chem.*, **69**, 834 (1965).

(12) T. A. Jacobs and R. R. Giedt, *J. Chem. Phys.*, **39**, 749 (1963).

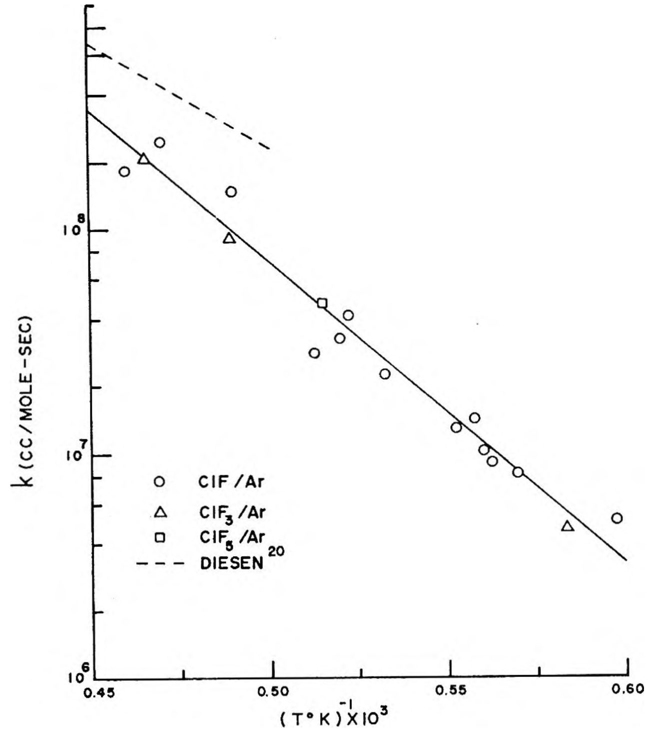

Figure 2. Temperature dependence of initial reaction rate constant for the thermal decomposition of ClF.

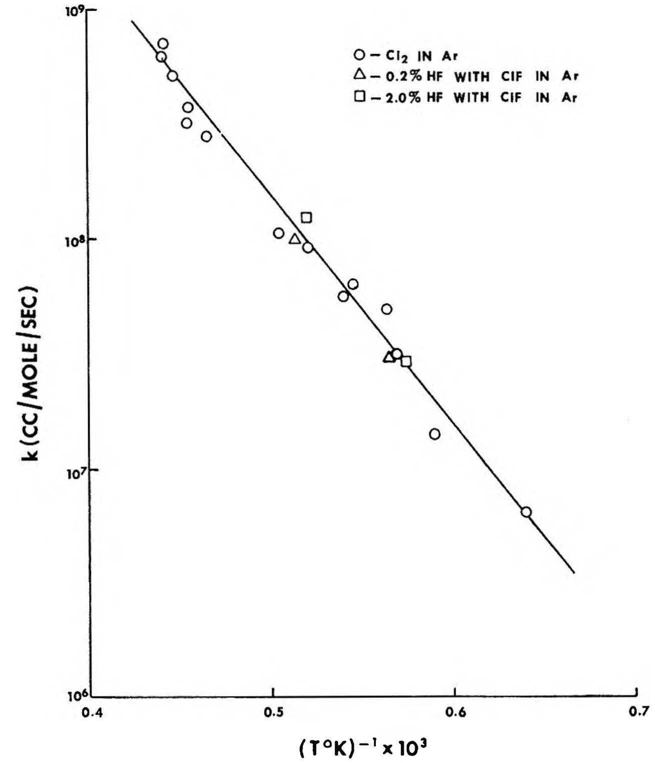

Figure 3. Temperature dependence of apparent initial reaction rate constants for the thermal decomposition of Cl_2 (argon diluent).

of the entire reaction profile. The effect of these large amounts of added F atoms upon the initial reaction rate is illustrated graphically in Figure 2. Since the added F atoms produce no discernible positive drift in the value of k_3[initial], a significant early contribution of reaction 6 to the overall decomposition can be readily excluded. Furthermore, the absence of any marked inhibition of the initial reaction rate by F atoms seems to rule out any large early contribution from reaction 5. This tentative conclusion would be incorrect if steps 5 and 6 are proceeding simultaneously over the temperature range of this study (a canceling effect would be operating). Two general analytical approaches for evaluating the above-mentioned rate constants from reaction profiles have been followed.

Approach I. Recently, Warnatz[13] has made direct measurements to obtain a value for the exchange reaction −5. The value which he obtains is $5.7 \times 10^{14} \exp(-1400/RT)$ cc/mol-sec. In view of these recent results we must reexamine the assumption that the initial rate data provide a good measure of k_3.

To give a more definitive value to k_3, the reaction mechanism consisting of steps 3, 4, and 6 was subjected to numerical integration by means of a nonequilibrium computer program[14] which solves the conservation equations simultaneously with the reaction rate equations. Rates of reverse reactions were obtained from the principle of detailed balancing. In this analysis the experimental value obtained by Warnatz[13] for k_{-5} is held constant while the value for k_3 is obtained by iteration. The value selected for step 5 is that which is obtained from the initial slope in the Cl_2 experiments reported herein. Figure 4 gives the fit to the computed reaction profile data which is obtained when $k_3 = 3.0 \times 10^{14\pm0.4} \exp(-57{,}500 \pm 3000/RT)$ cc/mol-sec. Figure 5 shows the nature of the agreement with experiment which one obtains when the latter value for k_3 is used and F atoms are present in large excess. Good fits to the experimental data are obtained in both instances in which the above rate constants were employed. Agreement with experimental reaction profiles was satisfactory throughout the entire range of experimental conditions employed in this study. The activation energy which is obtained from approach I for reaction 3 is not unreasonable when compared to the currently accepted bond dissociation energy for ClF of 60 ± 1 kcal/mol at 2000°K.[15] Indeed, according to the present analysis, the thermal dissociation of ClF would appear to be unclouded by anomalies such as those which appear in the data concerning the dissociation of Cl_2.[11,12]

In Table II[15,16] are gathered the results of several

---

(13) J. Warnatz, H. Gg. Wagner, and C. Zetzsch, *Ber. Bunsenges. Phys. Chem.*, 75, 119 (1971).

(14) Furnished by Dr. T. A. Jacobs, Aerospace Corp., El Segundo, Calif.

(15) "JANAF Thermochemical Tables," Dow Chemical Co., Midland, Mich., June 1970.

(16) V. H. Dibeler, J. A. Walker, and K. E. McCollah, *J. Chem. Phys.*, 50, 4592 (1969).

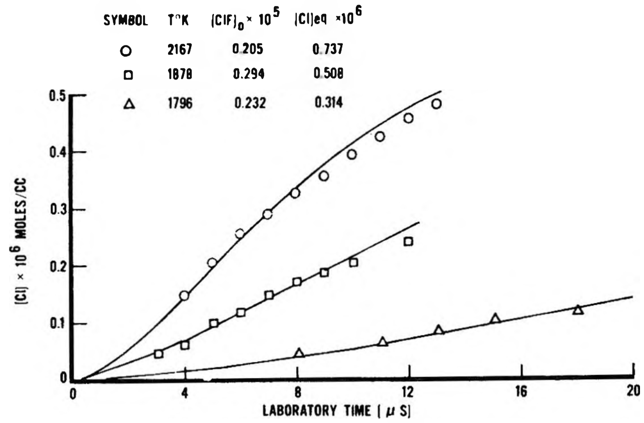

Figure 4. Comparison of computed reaction profiles with experimental data for binary mixes of ClF and Ar. Assumed rate constants were $k_4 = 0.3 \times 10^{15} \exp(-57{,}432/RT)$ and $k_{-8} = 0.57 \times 10^{15} \exp(-1400/RT)$.

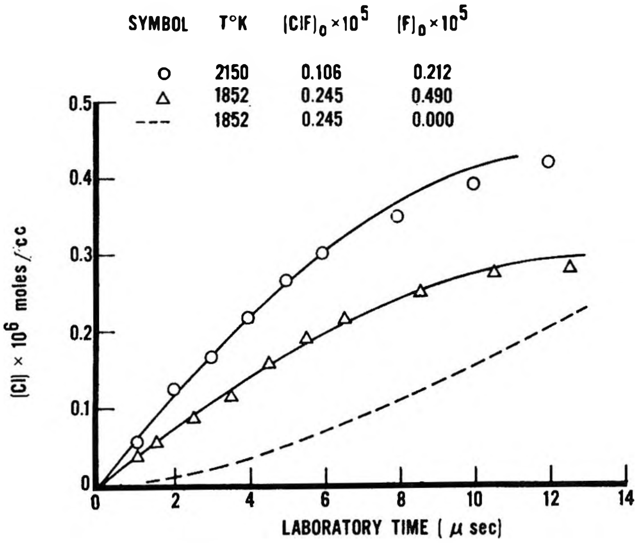

Figure 5. Comparison of computed reaction profiles with experimental data for binary mixes of ClF_3 and Ar. Assumed rate constants were $k_4 = 0.3 \times 10^{15} \exp(-57{,}432/RT)$ and $k_8 = 0.57 \times 10^{15} \exp(-1400/RT)$.

investigations concerning the thermal dissociation of the elemental halogens in shock tubes. With the possible exception of F_2, the apparent activation energies tend to be well below the bond dissociation energies. Accordingly, unless approach I gives an overestimate of the activation energy for ClF dissociation, the number presented herein is anomalous when compared to the results for the related diatomic molecules of the series. Indeed, McIntyre[17] has recently estimated k_3

$$k_3 = 10^{12.9} \exp(-41{,}500/RT) \text{ cc/mol-sec}$$

Although this equation reproduces our results to within a factor of 3 in the temperature range of overlap for the two studies (see Figure 2), it does imply an activation energy significantly lower than that deduced from approach I. This discrepancy can be due, at least in part, to the rather large amount of scatter generally encountered in shock-tube measurements. Indeed agreement between the two studies is not unusually bad, since our k_3[initial] predicts within a factor of 2 the values for k_3 given by McIntyre.[17]

Table II: Published Arrhenius Parameters for the Dissociation of Diatomic Halogens

Halogen	Temp, °K	E_a, kcal/mol	D_0,[a] kcal/mol	Reference
F_2	1200–2700	27–35	29–37	17, 18
Cl_2	1600–2600	45	57	11
Br_2	1200–2200	32.3	45	10
I_2	1000–1600	29.4	34	19

[a] Dissociation energies taken from ref 15 and 16.

Approach II. We proceed with numerical integration as before, *vide ut supra.* In this case, however, values for both k_3 and k_4 result from the initial slope measurements. The activation energy for k_5 is estimated[18] according to the Evans–Polanyi rule at 12 kcal/mol. Only the value of A_5 (preexponential for step 5) was varied during the course of the calculations. The computed reaction profile was found to be very insensitive to the values assigned to A_5 for those tests corresponding to binary mixtures containing ClF_3 and Ar. The opposite was true for binary mixtures containing ClF and Ar; see Figures 6 and 7. The above behavior is traced to a nearly complete suppression of reaction 5 in the former case (excess of F atoms). One may now extract a value for A_5 from the ClF and Ar data which is $10^{11\pm1}$ cc/mol-sec. Thus, if initial slope data can be relied upon to estimate k_3, an unusually small value must be assigned to k_5.

Finally, it is of interest to compare the rate constants for reaction −3 with those computed from theoretical considerations given by Benson and Fueno.[19] In Table III there are tabulated the results for a few such calculations along with the observed values. From the above calculations it is apparent that the theory overestimates the rate constants in both instances. A similar situation is found if one compares the results of F-atom recombination[20–22] with the theory. The agreement is somewhat better for Cl-atom recombination.[6,11,12]

---

(17) J. A. McIntyre and R. W. Diesen, *J. Phys. Chem.*, **75**, 1765 (1971).

(18) N. N. Semenov, "Some Problems of Chemical Kinetics and Reactivity," Vol. 1, Pergamon Press, Elmsford, N. Y., 1958, p 27.

(19) S. W. Benson and T. Fueno, *J. Chem. Phys.*, **36**, 1957 (1962).

(20) R. W. Diesen, *J. Phys. Chem.*, **72**, 108 (1968).

(21) T. Just and G. Rimple, Deutsche Luft-und Raumfahrt Report 70-02 (1970).

(22) D. Britton, N. Davidson, W. Gehman, and G. Schott, *J. Chem. Phys.*, **25**, 804 (1956).

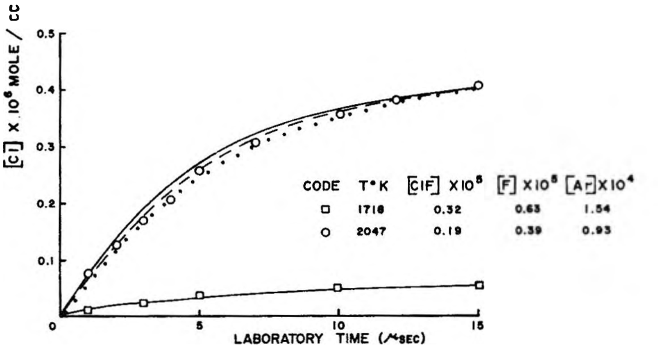

Figure 6. Computed *vs.* observed reaction profiles for binary mixes of ClF_3 and Ar: ——, $A_8 = 0$; - - -, $A_8 = 10^{12}$ cc/mol-sec; ——, $A_8 = 10^{13}$ cc/mol-sec.

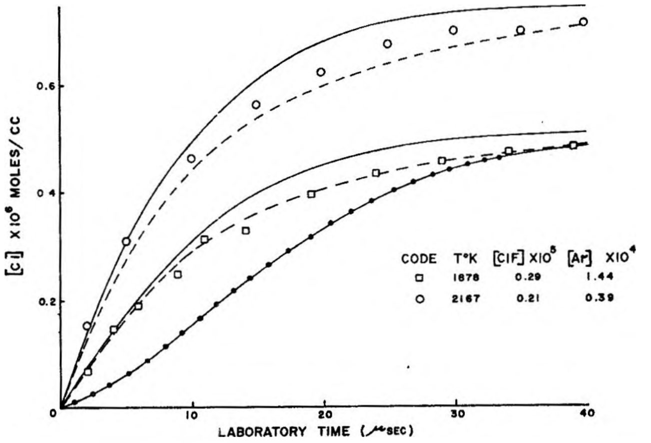

Figure 7. Computed *vs.* observed reaction profiles for binary mixes of ClF and Ar: ——, $A_8 = 0$; - - -, $A_8 = 10^{11}$ cc/mol-sec; ●-●-●, $A_8 = 10^{12}$ cc/mol-sec.

Conclusions

The rate constants from analysis II are based upon the validity of the initial slope assumption. The result from the first treatment is obtained by employing an experimental number for step -5 which was obtained near room temperature. However, the experimental data collected herein allow no clear choice between the two mechanisms. Nevertheless, the argument in favor of approach I seems to be the stronger. Thus, an activation energy of 61 kcal/mol for step 3 is higher than would be expected based upon experience with other diatomic molecules. There is no consistency in the values provided by approach II and the direct experimental measurement of step -5 by Warnatz.[13] The data provided by McIntyre[17] also indicate that approach II underestimates k_{-5}. Further, the

$$Cl + Cl_2O = Cl_2 + ClO \tag{7}$$

$$Cl + NOCl = Cl_2 + NO$$

closely related reactions are known to be very fast.[23-26] A theoretical estimate of the lower limit for the bimolecular A factor for k_5, obtained from methods outlined by Benson,[27] is $10^{14.0}$ cc/mol-sec. The latter value is consistent with the results obtained by following approach I. Finally, the theory of Benson and Fueno[19] for atomic recombination gives somewhat better agreement with the value of k_{-3} obtained from approach I than with that used in approach II. This study would appear to be an example in which strong reliance on the initial slope assumption can lead to significant error.

Table III: Comparison of Observed Recombination Rate Constants with the Values Computed from Theory, k_{-8}

T, °K	k_r(obsd) × 10^{-14} cc^2/mol^2-sec Approach I	 Approach II	 Theory
1779	0.63	0.31	4.0
1902	0.64	0.32	3.8
2167	0.64	0.32	3.6

[a] Method II-A of ref 19 employed.

---

(23) C. G. Freeman and L. F. Phillips, *J. Phys Chem.*, **72**, 3028 (1968).

(24) K. H. Homann, W. C. Solomon, T. Warnatz, H. G. Wagner, and C. Zetzsch, *Ber. Bunsenges. Phys. Chem.*, **74**, 589 (1970).

(25) E. A. Ogryzlo, *Can. J. Chem.*, 39, 2556 (1961).

(26) W. G. Burns and F. S. Dainton, *Trans. Faraday Soc.*, **48**, 52 (1952).

(27) S. W. Benson, "Thermochemical Kinetics," Wiley, New York, N. Y., 1968, p 97.

Primary and Secondary Rate Processes in the Acetone–Silane Photochemical System

by H. Edward O'Neal,* Spyros Pavlou, Tom Lubin, Morey A. Ring, and L. Batt

Department of Chemistry, San Diego State College, San Diego, California 92115 *(Received December 17, 1970)*

Publication costs borne completely by The Journal of Physical Chemistry

The photolysis (3130 Å) of acetone in the presence of silane has been investigated at 25, 65, and 100°. Rate constant parameters for the H-abstraction reactions from silane by the methyl and the 2-hydroxy-2-propyl radical were obtained: $\log k_1$ (l./mol-sec) = 8.24 − (6.17 ± 0.37)/θ and $\log k_6$ (l./mol-sec) = 8.75 − (9.0 ± 1)/θ, respectively. Spontaneous decomposition quantum yields were also measured and found to be consistent with the primary process mechanism proposed earlier. Mechanisms for the formations of isopropyl alcohol and *tert*-butyl alcohol, two unusual reaction products, are proposed, and some values for the various reaction processes involved are deduced.

Introduction

Primary processes in the acetone photochemical system have been fairly well elucidated.[1,2] One of the most interesting conclusions of the prior studies was that the acetone triplet could behave much like a free radical. Thus the acetone triplet was observed to undergo H-abstraction reactions from hydrogen bromide with a rate comparable to that of the corresponding methyl radical reaction. The purpose of the present study was to investigate the radical trapping abilities of silane toward the acetone triplet and also to obtain the H-abstraction Arrhenius parameters for the reaction of methyl radicals with silane.

Experimental Section

Silane was prepared by the reduction of tetrachlorosilane with $LiAlH_4$.[3] Separation was achieved from the reaction mixture by passing the products through a −160° trap (which retained unreacted tetrachlorosilane) and into a silica gel trap cooled to −195°. Of the two principal contaminants, HCl was irreversibly absorbed on the silica gel and hydrogen was removed by pumping at liquid N_2 temperatures. The silane recovered on warming was found to be chromatographically pure to within 0.05 mol %. Experimental procedures employed in the photolysis were, with few exceptions, the same as those described elsewhere.[1] The light source was an Osram 200-W super high-pressure Hg lamp. Radiation, passed through a nickel–cobalt sulfate and a potassium biphthalate filter solution, was centered in the 3130-Å region. Transmitted light intensities were monitored by an RCA-931 phototube whose output was suitably recorded. Analyses were made with a Perkin-Elmer Model 154D vapor phase chromatograph with both thermal and flame ionization detectors. Methane and ethane were analyzed on a PE-J (silica gel) column, and all other products were analyzed on both a PE-R(Ucon oil LB-550-X) column and a PE-t (β,β-oxydipropionitrile) column. Analytical accuracies were estimated between 5 and 10%.

Results

Major products of the photolysis were methane, ethane, carbon monoxide, isopropyl alcohol, and *tert*-butyl alcohol. Minor products were hydrogen, disilane, methyl ethyl ketone, biacetyl, acetaldehyde, and ketene. Data are shown in Table I.

Reactions 1–12, listed in Table II, seem to account for the most important features of the photolysis system.

Methyl H Abstraction from Silane. Silane is a relatively effective trap for methyl radicals, as evidenced by the marked decrease in ethane yields with increasing silane concentration. If one assumes that methyl radical concentrations are sufficiently low to minimize methane yields from radical–radical disproportionation reactions and that methane was produced *only via* methyl H abstraction from silane and acetone, one obtains from the relative rates of methane and ethane formation (eq 1, 2, 3) the usual expression

$$Q = \frac{Y(\mathrm{CH_4})}{[Y(\mathrm{C_2H_6}) \times t]^{1/2}[\mathrm{A}]} = \frac{k_2}{k_3^{1/2}} + \frac{k_1}{k_3^{1/2}}\frac{[\mathrm{SiH_4}]}{[\mathrm{A}]} \quad \text{(I)}$$

where $Y(\mathrm{X})$ is the yield of X in moles per liter.

Plots of the data according to eq I were made and the rate constants for H abstraction of methyl from silane were calculated. The data give

$$k_1(25°) = 3.76 \pm 0.21 \times 10^3$$

and

---

(1) C. W. Larson and H. E. O'Neal, *J. Phys. Chem.*, **70**, 2475 (1966).

(2) H. E. O'Neal and C. W. Larson, *ibid.*, **73**, 1011 (1969).

(3) A. C. Finholt, A. C. Bond, Jr., K. E. Welyback, and H. I. Schlesinger, *J. Amer. Chem. Soc.*, 69, 2692 (1947).

Table I: Data on Photolysis of Acetone in the Presence of Silane

Reactants (mol/l.) × 10^4	Yields (mol/l.) × 10^6								
CH_3COCH_3	SiH_4	$(\overline{SiH_4}/A)^a$	CH_4	C_2H_6	CO	*tert*-BuOH	*i*-PrOH	$I_a{}^b$	$t \times 10^{-4\,c}$
				$T = 25°$					
6.80	4.4	0.65	3.45	2.13	1.91	0.37	0.35	42	2.50
5.30	10.2	1.92	8.42	5.50	1.47	0.37	0.84	35.2	1.80
9.20	10.2	1.11	11.9	9.27	4.40	0.91	2.02	79	1.80
8.87	10.2	1.15	4.63	1.15	3.10	0.44	0.59	27.6	1.59
6.50	20.3	3.12	8.00	1.36	...	0.36	2.34	22.2	1.42
33.7	20.0	0.59	5.14	0.95	None	1.18	2.06	93	1.08
13.8	43.4	2.88	11.0	0.48	7.15	0.27	8.05	24.6	2.08
18.2	76.5	4.20	6.05	0.059	3.16	0.20	9.05	27.2	1.60
				$T = 65°$					
27.6	12.8	0.46	101	15.3	69.6	13.7	35.8	269	1.77
22.3	18.4	0.82	88.4	7.82	53.4	10.0	29.2	297	1.20
32.3	11.6	0.36	90.5	21.5	77.6	20.2	28.6	308	1.29
				$T = 100°$					
31.2	2.79	0.066	59.5	45.7	68.8	32.5	22.4	352	1.11
34.6	7.40	0.204	150	40.3	128	47.3	38.6	278	1.54
7.38	28.2	3.58	64.0	0.603	30.6	1.04	28.0	59	1.79
13.9	7.18	0.69	226	56.2	194	27.1	44.5	238	1.85
17.2	10.4	0.54	63.4	9.15	45.1	7.00	18.6	144	0.73
25.4	8.50	0.34	131	38.6	82.5	23.0	29.6	248	1.08
37.4	0.30	0.005	23.2	39.8	48.2	3.24	2.7	186	1.04

[a] Average silane to acetone ratios in a run (see text). [b] Units are (einsteins/l.-sec) × 10^{10}. [c] Units are sec.

$$k_1(100°) = 34.3 \pm 0.32 \times 10^3$$

for k_1 in units of l./mol-sec. In Arrhenius form, these give

$$\log k_1(\text{l./mol-sec}) = 8.24 - (6.17 \pm 0.37)/\theta$$

The rate constant errors, which represent 95% confidence limits (*i.e.*, $\pm 2\sigma$), are rather large. Good mass balances were not obtained in this photolysis system, and these errors undoubtedly reflect the appreciable experimental scatter in the data. Nevertheless, the Arrhenius parameters for the H abstraction by methyl from silane are in reasonable agreement (roughly within the limits of error) with those obtained in prior studies.[4,5]

$$\log k_1 \text{ (l./mol-sec)} = 8.8 - (6.99 \pm 0.56)/\theta \quad \text{(SJSG)}$$

$$(\log k_1 \text{ (l./mol-sec)} = 8.82 - 6.89 \pm 0.16)/\theta \quad \text{(MT)}$$

In the latter studies methyl radicals were generated using the photolysis of azomethane. The systems were apparently cleaner and better behaved, and in view of the good agreement obtained, their results should be considered the more reliable. One of the inconsistencies in our data, which may have had some effect on our rate constant determinations of k_1, is that appreciably more than stoichiometric amounts of silane were reacted. The measured amount of silane in the system after reaction was always less than the amount expected on the basis of initial concentrations and the extent of photolysis. Since an appreciable amount of hydrogen and disilane were also produced in some runs, it is possible that some silyl radical induced decomposition of silane was occurring (eq II). This process has been proposed by Purnell and Walsh[6] and also by Ring, Puentes, and O'Neal[7] to explain the thermal decomposition kinetics of silane.

$$\begin{gathered} SiH_3 + SiH_4 \longrightarrow H + Si_2H_6 \\ H + SiH_4 \longrightarrow SiH_3 + H_2 \end{gathered} \qquad \text{(II)}$$

Primary Decomposition Quantum Yields. Decomposition quantum yields, calculated from the equation

$$\varphi_d = Y[CH_4 + 2C_2H_6 + \textit{tert}\text{-BuOH} + \text{MEK–CO}]/I_a \cdot t$$

were found to be much lower than those of acetone without inhibitors. They were independent of the silane concentration and strongly temperature dependent. Average values at the three temperatures were $\varphi_d \simeq 0.10$ (25°), $\varphi_d \simeq 0.22$ (65°), and $\varphi_d \simeq 0.37$ (100°) (see Table III). These observations are consistent with equations d*, S, and T where spontaneous decomposi-

---

(4) O. P. Strausz, E. Jakubowski, H. S. Sandhu, and H. E. Gunning, *J. Chem. Phys.*, **51**, 552 (1969).

(5) E. R. Morris and J. C. J. Thynne, *J. Phys. Chem.*, **73**, 3294 (1969).

(6) J. H. Purnell and R. Walsh, *Proc. Roy. Soc., Ser. A*, **293**, 543 (1966).

(7) M. A. Ring, M. J. Puentes, and H. E. O'Neal, *J. Amer. Chem. Soc.*, **92**, 4845 (1970).

Table II

	Rate constants[a]
Primary processes	
CH_3COCH_3 (A) + $h\nu$ (3130 Å) $\longrightarrow$ $^3A^*$	Ia[b]
Decompositions	
$^3A^* \xrightarrow{d^*} CH_3\cdot + CH_3\dot{C}O$	$k(\epsilon^*)$
$(M) + {}^3A \xrightarrow{d} CH_3\cdot + CH_3\dot{C}O + (M)$	$^3k_d = \dfrac{10^{9.81 - 5.95/\theta}}{(1 + ZM/k(\epsilon^*))}$
Stabilization	
$^3A^* + M \xrightarrow{s} {}^3A + M$	$Z\cdot M \simeq 10^{11}\cdot M$
Secondary processes	
$CH_3\cdot + SiH_4 \xrightarrow{1} CH_4 + SiH_3\cdot$	$k_1 = 10^{8.33 - 6.33/\theta}$ [c]
$CH_3\cdot + A \xrightarrow{2} CH_4 + \cdot CH_2COCH_3$	$k_2 = 10^{8.6 - 9.7/\theta}$ [d]
$CH_3\cdot + CH_3\cdot \xrightarrow{3} C_2H_6$	$k_3 = 10^{10.34}$ [e]
$CH_3\dot{C}O + R\cdot \xrightarrow{4} CH_2CO + RH$	$k_4 = \simeq 10^{11}$ [f]
$CH_3\dot{C}O + (M) \xrightarrow{5} CH_3\cdot + CO + M$	k_5[g]
Isopropyl alcohol formation	
$SiH_4 + {}^3A \xrightarrow{T} CH_3\dot{C}(OH)CH_3(\cdot AOH) + SiH_3\cdot$	$^3k_T \geq 10^{9 - 3.6/\theta}$ [c]
$SiH_4 + \cdot AOH \xrightarrow{6} CH_3CHOHCH_3 + SiH_3\cdot$	$k_6 = 10^{8.77 - 9.0/\theta}$ [c]
tert-Butyl alcohol formation	
$CH_3\cdot + {}^3A \underset{-7}{\overset{7}{\rightleftharpoons}} {}^1(tert\text{-}BuO\cdot{}^*)$	$k_7 \geq 10^{12.2}$ [c]
	$k_{-7} \geq 10^{8.7}$ [c]
$^1(tert\text{-}BuO\cdot{}^*) + M \xrightarrow{8} {}^1(tert\text{-}BuO\cdot) + M$	$k_8\ (sec^{-1}) \simeq Z\cdot M$
$^1(tert\text{-}BuO\cdot) \xrightarrow{9} A^* + CH_3\cdot$	$k_9 \geq 10^{3.2}$ [c,h]
$SiH_4 + {}^1(tert\text{-}BuO\cdot) \xrightarrow{10} tert\text{-}BuOH + SiH_3\cdot$	$k_{10} \simeq 10^{9 - 5.6/\theta}$ [c,h]
$R\cdot + \cdot AOH \xrightarrow{11} A + RH$	$k_{11} = 7.2 \times 10^{10}$ [f]
$R\cdot + \cdot R \xrightarrow{12}$ products	$k_{12} = 3.6 \times 10^{10}$ [f]

[a] Units are sec^{-1} (unimolecular) or l./mol-sec (bimolecular). [b] Probably a multiple step isoergotic process proceeding through an upper singlet state. [c] See text. [d] A. F. Trotman-Dickenson and G. S. Milne, "Tables of Bimolecular Reactions," NSRDS-NBS 9, U. S. Government Printing Office, Washington, D. C., 1967. [e] A. Shepp, *J. Chem. Phys.*, **24**, 939 (1956). [f] R· is any radical, but probably primarily silyl. [g] Decomposition in the pressure fall-off region under normal experimental conditions, see H. E. O'Neal and S. W. Benson, *J. Chem. Phys.*, **36**, 2196 (1962). [h] $^1(tert\text{-}BuO\cdot)^*$ indicates here the first excited state of the *tert*-butoxy radical.

tion of vibrationally excited triplet state acetone molecules competes with collisional stabilization, and *all* thermally equilibrated triplet state acetone molecules are trapped by silane. This mechanism was proposed to explain the nondependence on inhibitor concentrations observed in the photolysis of acetone in the presence of hydrogen bromide.[1] It has also been shown to be quantitatively consistent with the variations of triplet state phosphorescence caused by total pressure, temperature, and wavelength changes.[2]

Table III: Spontaneous Decomposition Quantum Yields

T, °C	System	φ_d^*	$\dfrac{k(\epsilon^*)}{Z\cdot M}$	M[b]	$\dfrac{k(\epsilon^*)}{Z}$[c]	ϵ[d]
25	A + SiH_4	0.10	0.11	5.5	0.61	4.23
65	A + SiH_4	0.22	0.28	7.4	2.07	6.35
100	A + SiH_4	0.37	0.58	6.7	3.88	6.35
44	A + HBr[a]	0.08	0.087	6.6	0.57	1.97
96	A + HBr	0.18	0.22	6.8	1.50	...
126	A + HBr	0.25	0.33	7.5	2.48	2.38

[a] See ref 1. [b] M is the average total pressure for all runs at each of the temperatures indicated. Units are cm. The silane collision efficiency relative to acetone was assumed to be 0.33. [c] Units are cm. [d] Units of the extinction coefficient (ϵ) are l./mol-cm.

Ratios of spontaneous decomposition rates relative to stabilization rates can be obtained from the relation, $k(\epsilon^*)/ZM = \varphi_d^*/(1 - \varphi_d^*)$. These are compared with prior results of the acetone–HBr photolysis system in Table III. Arrhenius plots of the spontaneous decomposition to collisional stabilization rate constant ratios for the two photolysis systems give roughly comparable temperature dependencies ($E \simeq 4.4$ kcal/mol); however, spontaneous decomposition rates are about a factor of 2 faster (at the same temperatures) in the acetone–silane system. The shift, according to the mechanism, corresponds to an increase in the vibrational energy content of the acetone triplets of only 0.6 kcal/mol. This is equivalent to a difference in average wavelength of absorbed radiation of about 20 Å in the 3130-Å region. On consideration of the differences in the experimental extinction coefficients for the two systems (column 7, Table III; higher ϵ signifying shorter average λ absorption), it is apparent that the spontaneous decomposition yields observed in the two systems are qualitatively, if not quantitatively, consistent.

Isopropyl Alcohol Formation. According to the mechanism, isopropyl alcohol is formed *via* a two-step trapping of the acetone triplet with silane (reactions T and 6). In general, quantum yields of isopropyl alcohol seldom exceeded 0.15; thus most of the ·AOH radicals formed by the trapping of the acetone triplet with silane (reaction T) did not react further with silane (reaction 6), but rather by some other route (presumably reaction 11). In support of the proposed mechanism, two runs at 100°, made with added toluene, gave isopropyl alcohol quantum yields of between 0.65 and 0.70 (*i.e.*, near the theoretical of $\Sigma\varphi_i = 1$). An identical increase in φ(*i*-PrOH) was observed with added toluene in the A + HBr photolysis.[1] Photolysis of acetone in the presence of toluene alone does *not* produce any isopropyl alcohol (1). The explanation in both systems is the same. In the absence of toluene, the predominant radicals in the system ($SiH_3\cdot$ or $Br\cdot$) disproportionate with the $\cdot AOH$ intermediates. This appears as *no reaction*. With added toluene, the silyl (or $Br\cdot$) radicals *are metathesized to benzyl* ($C_6H_5CH_2\cdot$) (reaction 13), which recombine rather than disproportionate

$$SiH_3\cdot + C_6H_5CH_3 \xrightarrow{13} SiH_4 + C_6H_5CH_2\cdot \quad (13)$$

Theoretical trapping of the $\cdot AOH$ radicals by silane then occurs. If the above is correct, one can place a lower limit on the first bond dissociation energy in silane, since *if* the H-abstraction reaction of silyl from toluene were endothermic it is unlikely that it could compete with the disproportionation reaction (reaction 11). Thus $DH°(SiH_3\text{–}H) \geq DH°(C_6H_5CH_2\text{–}H) = 87$ kcal/mol. The electron impact measurements of this bond dissociation energy[8] (*i.e.*, $DH°(SiH_3\text{–}H) \cong 94$ kcal/mol) therefore seem quite reasonable.

Steady-state treatment of the mechanism gives the following relation

$$\frac{d(i\text{-PrOH})}{dt} = \frac{Y(i\text{-PrOH})}{t} = \frac{k_6 k_{12}^{1/2}(1 - \varphi_d^*)I_a^{1/2}[SiH_4]}{k_{11}} \quad (III)$$

The above relation implies $k_d \ll k_T(SiH_4)$ and that $k_6(SiH_4) \ll k_{11}(R\cdot)$. Reaction 12 represents all termination processes. These assumptions are consistent with the experimental observations. Plots of the data at 25 and 100° according to the above relation are shown in Figure 1. Although some scatter is apparent, the above relation is the only one of many for which the data showed any kind of reasonable behavior. From the slopes one can obtain values for $k_6k_{12}^{1/2}/k_{11}$. Assuming $k_{11} \simeq 2k_{12} \simeq 2k_3$, one can obtain the Arrhenius parameters of reaction 6 (*i.e.*, H abstraction of the $\cdot AOH$ radical from silane). The result is $\log k_6$ (l./mol-sec) $= 8.75 - (9.0 \pm 1)/\theta$. The *A* factor is quite reasonable, although possibly slightly high when compared to our value for A_1. The activation energy of 9 kcal/mol (2.7 kcal/mol higher than E_1) is also reasonable on the basis of the greater endothermicity of reaction 6 relative to reaction 1.

tert-Butyl Alcohol Formation. Perhaps the most interesting product, and certainly the most difficult to explain, is *tert*-butyl alcohol. One can postulate at least three modes of formation for this product: recombination of $CH_3\cdot$ and $\cdot AOH$ radicals (reaction 14); addition of methyl to ground state acetone followed by trapping with silane (reactions 15 and 16); and addition of methyl to triplet acetone molecules followed by collisional stabilization and trapping with silane (reactions 7–9).

$$CH_3\cdot + \cdot AOH \xrightarrow{14} tert\text{-BuOH} \quad (14)$$

$$CH_3\cdot + A \overset{15}{\rightleftharpoons} tert\text{-BuO}\cdot \quad (15)$$

$$SiH_4 + tert\text{-BuO}\cdot \xrightarrow{16} tert\text{-BuOH} + SiH_3\cdot \quad (16)$$

If reaction 14 were the primary source of the alcohol, one would expect isopropyl alcohol, *tert*-butyl alcohol,

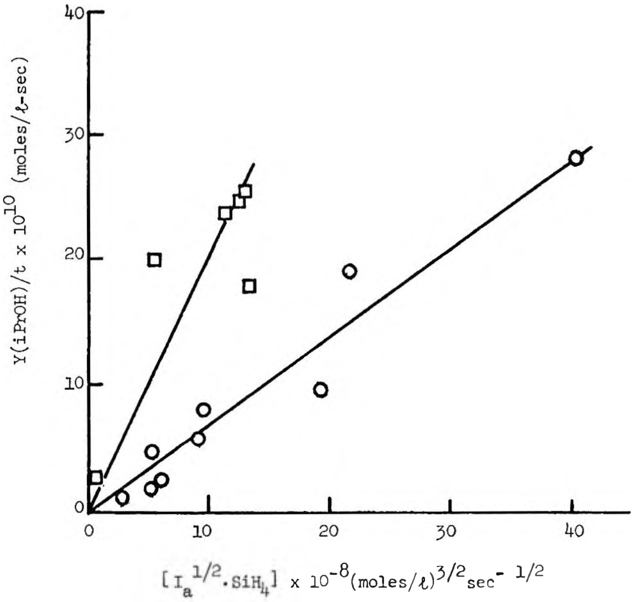

Figure 1. Isopropyl alcohol formation (eq III): □, data at 100°; ○, data at 25°. Values shown for $[Y(i\text{-PrOH})/t]$ at 25° have been multiplied by 5 for representational purposes. Slope $= [k_6k_{12}^{1/2}(1 - \phi_d^*)/k_{11}]$.

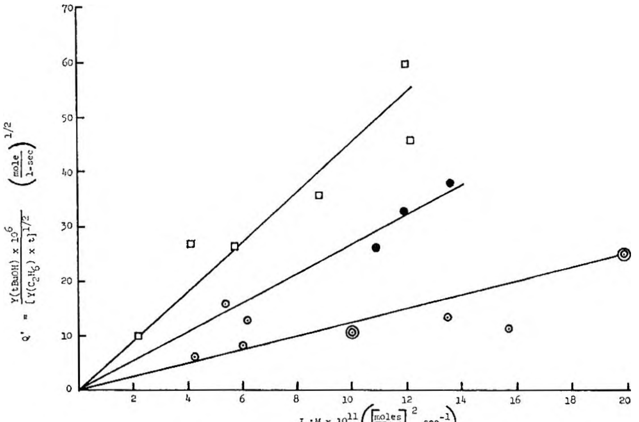

Figure 2. *tert*-Butyl alcohol formation (eq IV): ⊙, 25° data (All Q' values have been multiplied by 5 and $I_a \cdot M$ values multiplied by 10 for representational purposes. Double circled points were scaled down from $I_a \cdot M$ values of 51.2 and 26.4, respectively.) Slope $= 2.13 \times 10^5$ (mol/l.)$^{-3/2}$ sec$^{1/2}$; ●, 65° data, slope $= 2.68 \times 10^5$ (mol/l.)$^{-3/2}$ sec$^{1/2}$; □, 100° data, slope $= 4.50 \times 10^5$ (mol/l.)$^{-3/2}$ sec$^{1/2}$; M = total pressure (*i.e.*, SiH_4 + acetone).

---

[8] W. C. Steele and F. G. A. Stone, *J. Amer. Chem. Soc.*, **84**, 441, 3599 (1962); F. E. Saalfeld and H. J. Svec, *J. Phys. Chem.*, **70**, 1753 (1966).

and ethane yields to obey eq IV. Such is quite definitely *not* the case.

$$\frac{Y(tert\text{-BuOH}) \times t^{1/2}}{Y(i\text{-PrOH})\,[Y(\mathrm{C_2H_6})]^{1/2}} = \frac{k_{14}k_3^{1/2}}{k_\epsilon} \times \left(\frac{1}{[\mathrm{SiH_4}]}\right) \quad \text{(IV)}$$

nitely *not* the case. One cannot, however, completely exclude this mode of formation at "low" silane pressures. Reactions 15 and 16 can also be excluded as a possible mode of *tert*-butyl alcohol formation if the existing thermochemical and kinetic data[9] for reaction −15 are accepted. Thus using Quee and Thynne's value[10] for the *tert*-butoxy radical decomposition rate constant, one can calculate k_{15} (l./mol-sec) = $10^{7.7\ -\ 19.6/\theta}$. With a maximum methyl radical concentration of 10^{-10} mol/l. and setting [A] = 5 × 10^{-3} mol/l., this gives a maximum value for the rate of *tert*-butyl alcohol formation of 10^{-19} mol/l.-sec (*i.e.*, more than nine orders of magnitude lower than that observed).

Steady-state analysis of the third pathway, *i.e.*, methyl radical addition to the acetone triplet (reactions 7–10), gives eq V.

$$Q' = \frac{Y(tert\text{-BuOH})}{[Y(\mathrm{C_2H_6}) \times t]^{1/2}} = \frac{k_7k_8k_{10}(1 - \varphi_\mathrm{d}^*)(\mathrm{SiH_4})(I_\mathrm{a}\cdot M)}{(k_9 + k_{10}\mathrm{SiH_4})(k_{-7} + k_8\mathrm{M})({}^3k_\mathrm{d} + k_7\mathrm{CH_3} + {}^3k_\mathrm{T}\mathrm{SiH_4})k_3^{1/2}} \quad \text{(V)}$$

Evaluation of this mode of formation is obviously complicated by the numerous mechanistic possibilities. However the only relation which seems consistent with the data follows from the following approximations

$$^3k_\mathrm{T}(\mathrm{SiH_4}) > {}^3k_\mathrm{d};\quad k_{-7} > k_8\mathrm{M};\qquad k_9 > k_{10}(\mathrm{SiH_4}) \quad \text{(VI)}$$

The first of the above is consistent with the invariance of the decomposition quantum yields with silane pressure. Thus eq V simplifies to

$$Q' = \frac{k_7k_8k_{10}(1 - \varphi_\mathrm{d}^*)[I_\mathrm{a}\cdot M]}{k_9k_{-7}{}^3k_\mathrm{T}k_3^{1/2}} \quad \text{(VII)}$$

Plots of Q' *vs.* $I_\mathrm{a}\cdot M$ are shown in Figure 2. Slopes of the lines, and therefore the rate constant ratio $R = k_7k_8k_{10}/k_9k_{-7}{}^3k_\mathrm{T}k_3^{1/2}$, are not very temperature dependent. In fact $R(100)/R(65)/R(25) \simeq 3{:}1.45{:}1$, which corresponds to an overall activation energy of only about 2 ± 1 kcal/mol. From the kinds of processes involved, it would appear that this activation energy would have to be placed between reactions 10 and T. Thus $E_{10} - E_\mathrm{T} \simeq 2 \pm 1$ kcal/mol.

Examination of the assumptions (eq VI) permits the assignment of limiting values on various rate constants. Thus with $^3k_\mathrm{d} = 10^{9.81\ -\ 5.95/\theta}[\mathrm{M}]/(1 + ZM/k(\epsilon^*))$,[2] $0.3 < ([\mathrm{A}]/[\mathrm{SiH_4}]) < 10$, $[\mathrm{M}] \le 5 \times 10^{-3}$ mol/l., $[\mathrm{SiH_4}] \le 3 \times 10^{-3}$ mol/l., and assuming $A_\mathrm{T} = A_{10} \simeq 10^9$ l./mol-sec, one obtains from the 100° condition that

$$^3k_\mathrm{T} \ge 10^{6.9} \text{ and } E \le 3.6 \text{ kcal/mol}$$

$$k_9 \ge 10^{3.2}\ \mathrm{sec^{-1}} \text{ if } E_{10} \simeq E_\mathrm{T} + 2 \le 5.6 \text{ kcal/mol}$$

$$k_{-7} \ge 10^{8.7}\ \mathrm{sec^{-1}} \text{ with } k_8 \simeq Z \simeq 10^{11} \text{ l./mol-sec}$$

These are all reasonable limits for the kinds of processes depicted. The lifetime of the upper electronic state of the *tert*-butoxy radical, primarily determined by the rate of internal conversion (reaction 9), must be longer than $10^{-3.2}$ sec. Also, activation energies for alkoxy radical H abstractions from silane must be appreciably less than alkyl radical H abstractions, which is reasonable. Finally, direct substitution of the assumptions into R and rearrangement leads to a limiting condition for the rate constant of methyl addition to the acetone triplet. Thus

$$k_7 \ge 10^{12.2} \text{ l./mol-sec}$$

Reaction 7 is basically a radical–radical recombination reaction which would be expected to proceed on almost every collision (*i.e.*, $Z \simeq 10^{11.2}$ l./mol-sec). The above condition is too high by a power of 10, but may not be too unreasonable. The effective collision diameter could be larger than "normal" collision frequency values, and the conditions of eq V may be only barely met at 100°. If one substitutes the average rather than maximum value for M into R, one obtains $k_7 \ge 10^{11.4}$ l./mol-sec. It should also be noted that the lower temperature restrictions which can be calculated for k_7 are quite reasonable (*i.e.*, $k_7 \ge 10^{9.6}$ l./mol-sec).

Formation of *tert*-butyl alcohol may, of course, occur *via* some other route entirely. However, we have been unable to propose any other logical route consistent with either the data or with theory.

Acknowledgment. This work was supported by a National Science Foundation Grant, No. GP-7371.

---

[9] S. W. Benson and H. E. O'Neal, "Kinetic Data on Gas Phase Unimolecular Reactions," NSRDS-NBS 21, U. S. Government Printing Office, Washington, D. C., p 597, 1970.

[10] M. Y. Quee and J. C. J. Thynne, *Trans. Faraday Soc.*, 63, 2970 (1967), give $k_{-15} = 10^{14.7\ -\ 22.8/\theta}\ \mathrm{sec^{-1}}$.

Studies on the Formation of Primary Yields of Hydrogen Peroxide and Molecular Hydrogen ($G_{H_2O_2}$ and G_{H_2}) in the γ Radiolysis of Neutral Aqueous Solutions

by Z. D. Draganić and I. G. Draganić*

Boris Kidrič Institute of Nuclear Sciences, Belgrade, Yugoslavia *(Received June 22, 1971)*

Publication costs borne completely by The Journal of Physical Chemistry

The formation of $G_{H_2O_2}$ and G_{H_2} was studied in γ-irradiated aqueous solutions containing selected mixtures of scavengers for both oxidizing and reducing primary free radicals. Experimental verification was made of various assumptions based on the free-radical model of water radiolysis. It was confirmed that efficient scavenging of OH radicals not only reduces $G_{H_2O_2}$ but also increases G_{H_2} by depressing the extent of water re-forming reactions and making more e_{aq}^- available for increased H_2 formation. Similarly, it was shown that the removal of e_{aq}^- leads not only to a decrease in G_{H_2} but also to an increase in $G_{H_2O_2}$. These effects are additive, and empirical relations were proposed to correlate the expected primary molecular yields with the reactivities toward OH and e_{aq}^-. Unifying curves were obtained for the dependence of observed fractional yield changes, G_M/G_M°, on reactivities. They point out that the secondary spur reactions of radicals with products of radical–solute scavenging reactions are rather exceptions even at solute concentrations of about 1 M and reactivities of 10^{10} sec^{-1}.

Introduction

The free-radical model of water radiolysis,[1] which has furnished satisfactory explanations for most of the experimental observations,[2-4] assumes that in irradiated aqueous solutions the primary free radicals (OH, e_{aq}^-, H) disappear mainly by the following reactions.

$$OH + OH \longrightarrow H_2O_2 \qquad (1)$$

$$OH + e_{aq}^- \longrightarrow OH^- \qquad (2)$$

$$OH + H \longrightarrow H_2O \qquad (3)$$

$$OH + S_1 \longrightarrow P_1 \qquad (4)$$

$$e_{aq}^- + e_{aq}^- \xrightarrow{2H_2O} H_2 + 2OH^- \qquad (5)$$

$$e_{aq}^- + H_3O^+ \longrightarrow H + H_2O \qquad (6)$$

$$e_{aq}^- + H \xrightarrow{H_2O} H_2 + OH^- \qquad (7)$$

$$e_{aq}^- + S_2 \longrightarrow P_2 \qquad (8)$$

$$H + H \longrightarrow H_2 \qquad (9)$$

$$H + S_3 \longrightarrow P_3 \qquad (10)$$

Accordingly, the formation of primary hydrogen peroxide ($G_{H_2O_2}$) is in reaction 1, and the reactions 5, 7, and 9 account for the major part of primary yield of molecular hydrogen (G_{H_2}). In neutral water or dilute aqueous solutions $G_{H_2O_2}$ = 0.67 and G_{H_2} = 0.45, as derived from various measurements.[1]

Recent studies have clearly confirmed that an increase in concentration of an efficient OH scavenger, S_1, leads to a decrease in $G_{H_2O_2}$ which is proportional only to $v_{OH} = k_{OH+S_1}[S_1]$, in reciprocal seconds.[5] Also the observed decrease of G_{H_2} was found to be proportional to the reactivity toward the hydrated electrons, $v_{e_{aq}^-} = k_{e_{aq}^-+S_2}[S_2]$, in reciprocal seconds, regardless of the chemical nature of S_2.[6]

The above findings represent an important argument for the assumption that the origin of primary molecular yields should be sought in recombination reactions (eq 1, 5, 7, and 9). However, new sources of primary molecular products and some limitations of the diffusion model (eq 1–10) have been suggested in recent considerations of very early effects of water radiolysis.[7] It was, therefore, interesting to get further information concerning the formation of primary H_2O_2 and H_2. If the recombination reactions are indeed of importance for the origin of $G_{H_2O_2}$ and G_{H_2}, then the yield decreases should also be observed in solutions containing simultaneously larger amounts of scavengers for both oxidizing and reducing primary species (S_1, S_2, and S_3); in the above-mentioned studies, the irradiated solutions contained only the scavenger reacting with the precursor of the molecular product measured (*i,e.*, OH scavenger in H_2O_2 or e_{aq}^- in H_2 studies).

---

[1] A. O. Allen, "The Radiation Chemistry of Water and Aqueous Solutions," Van Nostrand, Princeton, N. J., 1961; I. G. Draganić and F. D. Draganić, "The Radiation Chemistry of Water," Academic Press, New York, N. Y., 1971.

[2] A. Mozumder and J. L. Magee, *Radiat. Res.*, **28**, 215 (1966).

[3] A. Kuppermann in "Radiation Research 1966," G. Silini, Ed., North-Holland Publishing Co., Amsterdam, 1967, p 212.

[4] H. A. Schwarz, *J. Phys. Chem.*, **73**, 1928 (1969).

[5] Z. D. Draganić and I. G. Draganić, *ibid.*, **73**, 2571 (1969).

[6] E. Peled and G. Czapski, *ibid.*, **74**, 2903 (1970).

[7] W. H. Hamill, *ibid.*, **73**, 1341 (1969); P. L. T. Bevan and W. H. Hamill, *Trans. Faraday Soc.*, **66**, 2533 (1970); T. Sawai and W. H. Hamill, *J. Phys. Chem.*, **74**, 3914 (1970).

The model represented by eq 1–10 could also be tested by experimental verifications of the following assumptions. (a) Efficient removal of e_{aq}^- should not only reduce G_{H_2} but also increase $G_{H_2O_2}$. The reason is that more OH radicals should remain available for reaction 1 because of the depression of reactions 2 and 3. (b) Efficient removal of OH radicals should not only reduce $G_{H_2O_2}$ but also increase G_{H_2} by depressing the extent of water reforming reactions (eq 2 and 3) and making more e_{aq}^- available for increased formation of H_2 in reactions 5 and 7.

The purpose of this study was the experimental verification of the above assumptions. Simultaneous presence of larger amounts of scavengers for both oxidizing and reducing primary species (reactivities up to 10^{10} sec^{-1}) made the conditions in most of the cases studied deliberately more complex than in other studies on the origin of primary molecular products. It was expected that in some cases P_1, P_2, and P_3 would react with primary oxidizing and/or reducing radicals. This should cause each system to behave quantitatively different, making the reaction scheme more complex than given above by eq 1–10. Also, it was interesting to compare these experimental results with theoretical predictions of the diffusion model, derived for simpler conditions (initial concentrations of S_1, S_2, and S_3 set equal to 1×10^{-3} *M*), where the secondary spur reactions of radicals with products of radical–solute scavenging reactions are not expected to occur.

Experimental Section

All the chemicals used in this study were (Merck or BDH products) of the highest purity available and were not subjected to any additional purifications. The purification of water and the sample preparation were carried out by the standard procedures previously described.[5] Because of acetone loss on degassing its concentration was always determined; under well standardized working conditions a good reproducibility (±2%) was reached (*e.g.*, 0.60 *M* starting concentration gave 0.41 *M* acetone in deaerated solution).

Irradiations were carried out using a 3000-Ci (nominal) radioactive cobalt source giving 2.4×10^{19} eV g^{-1} hr^{-1}. Absorbed doses varied from 2×10^{17} to 12×10^{17} eV g^{-1} and were corrected for the electron density of the solution studied.

Hydrogen peroxide was determined by the KI method[8] with an accuracy of ±2%; exceptionally it was ±4% in the case of very large amounts of scavengers present and low yields measured. The optical density measurements were made in 4-cm cells and against water. Reference samples contained the solutes at the concentrations under study and the reagent; they were prepared and measured simultaneously with irradiated samples. Before the analysis some H_2O_2 (about 1×10^{-6} *M*) was always added to eliminate the errors due to the presence of trace amounts of reducing impurities. Optical densities were stable with time except for solutions containing both formate and acetone, where the measurement conditions had to be standardized. Molar extinction coefficients were between 23,800 and 21,720 M^{-1} cm^{-1} at 350 nm and 24°. The value of 23,800 M^{-1} cm^{-1} was found to be correct for the dilute solutions of all of the scavengers studied in this work as well as for 1 *M* solutions of NO_3^-, ethanol, isopropyl alcohol, and their mixtures. For 0.41 *M* acetone and its mixtures with ethanol and isopropyl alcohol ϵ_{350} = 23,250 M^{-1} cm^{-1}. In the case of 1 *M* solutions of $HCOO^-$ and NO_3^- the molar extinction coefficient was 22,060 M^{-1} cm^{-1}; ϵ_{350} 21,720 M^{-1} cm^{-1} was found for 1 *M* formate solutions.

Molecular hydrogen was measured by gas chromatography;[9] hydrogen was separated on a 6-m column of silica gel at 50° and argon as the carrier gas. The accuracy was ±2%.

The accuracy in all radiation chemical yield measurements was better than ±4%.

Results

Table I summarizes the yields of hydrogen peroxide measured in aqueous solutions containing various combinations of substances known as efficient scavengers for OH and e_{aq}^-. The yields of molecular hydrogen measured in irradiated solutions of selected mixtures of free-radical scavengers are presented in Table II. Table III shows how the yields of H_2O_2 and H_2 depend on the concentration of one solute which is at the same time efficient scavenger for both oxidizing and reducing primary radicals. The yields given in Tables I–III were calculated from concentration–dose plots which were linear over the studied absorbed dose range. In some of the H_2O_2 measurements the dosage plots were not straight lines, and the corrected values had to be used as the initial yields. These were obtained as the $G(H_2O_2)$ readings at zero dose on diagrams where point-by-point peroxide yields were plotted against dose.

Discussion

The systems used in the present study were chosen in such a way that the measured values of $G(H_2O_2)$ and $G(H_2)$ represent the corresponding primary yields, $G_{H_2O_2}$ and G_{H_2}. In constructing the yield–reactivity curves (Figures 1–4) the experimental values from Tables I–III were directly used. The reactivities were calculated as the products of scavenger concentration and the rate constant. Table IV summarizes the values of rate constants used in these calculations. It

---

(8) A. O. Allen, C. J. Hochanadel, J. A. Ghormley, and T. W. Davis, *J. Phys. Chem.*, 56, 575 (1952); H. A. Schwarz and A. J. Salzman, *Radiat. Res.*, 9, 502 (1958).

(9) Lj. Petković, M. Kosanić, and I. Draganić, *Bull. Inst. Nucl. Sci., Boris Kidrič (Belgrade)*, 15, 9 (1964).

Table I: Yields of Hydrogen Peroxide Measured in Deaerated Aqueous Solutions Containing Various Concentrations of Efficient Scavengers for OH and e_{aq}^-

$NaNO_3$

Scavenger for OH, *M*	$G(H_2O_2)$ measured in the presence of e_{aq}^- scavenger, *M*								
	2.5×10^{-3}	5×10^{-3}	1×10^{-2}	2.5×10^{-2}	5×10^{-2}	0.1	0.25	0.5	1.0
C_2H_5OH									
1×10^{-3}	0.67	0.66	0.67	0.71	0.71	0.75	0.77	0.78	...
2.5×10^{-3}	0.67	...	...	0.69	...	...	0.76	...	...
5×10^{-3}	0.63	...	...	...	...	...	...	...	...
1×10^{-2}	...	...	...	0.66	...	...	0.72	...	...
2.5×10^{-2}	0.58	...	...	0.60	...	...	0.66	...	...
0.1	0.50	...	0.51	0.54	...	0.58	0.59	...	0.65
0.25	...	...	...	0.48	...	...	...	...	...
0.3	0.47	...	...	...	...	...	...	...	...
1.0	0.34	...	0.36	0.37	...	0.38	0.41	...	0.48
2.5	0.28	...	...	...	...	...	...	...	...
$HCOO^{-}$[a]									
2.5×10^{-3}	...	...	...	...	...	...	0.76	...	...
1×10^{-2}	...	...	...	...	...	...	0.72	...	...
2.5×10^{-2}	...	...	...	...	...	...	0.67	...	...
0.1	...	...	...	...	...	...	0.61	...	...
0.25	...	...	...	...	...	...	0.54	...	...
1.0	...	0.30	0.32	...	0.34	...	0.37	...	0.40

$(CH_3)_2CO$

Scavenger for OH, *M*	$G(H_2O_2)$ measured in the presence of e_{aq}^- scavenger, *M*								
	5×10^{-3}	1×10^{-2}	2.5×10^{-2}	5×10^{-2}	0.10	0.41	0.50	0.55	1.5
C_2H_5OH									
2×10^{-3}	0.67	0.68	...	0.72	0.74	...	0.80	...	...
1×10^{-2}	...	...	...	...	...	0.72	...	...	...
0.1	...	...	...	...	...	0.59	...	...	...
1.0	...	0.35	0.36	...	...	0.39	...	0.43	0.47
$(CH_3)_2CHOH$									
1×10^{-3}	...	...	...	...	...	0.77	...	...	...
2.5×10^{-2}	...	...	...	...	...	0.66	...	...	...
2.5×10^{-1}	...	...	...	...	...	0.53	...	...	...

[a] These data have been obtained by Mrs. N. Mrkić as a part of her B.Sc. thesis at the University of Belgrad, Yugoslavia, 1971.

should be noted that for e_{aq}^- reactivities the dependence of the rate constant on the ionic strength was taken into account.[6] Also, in calculating the OH reactivities account was taken of recent findings concerning the pH dependence of rate constants of reactions between halide ions and OH radicals.[10]

Dependence of Measured $G_{H_2O_2}$ on Reactivities toward OH and e_{aq}^-. Figure 1 summarizes the results on the effect of OH scavenger concentration on $G_{H_2O_2}$ measured in the presence of a constant amount of e_{aq}^- scavenger. It can be seen that increased reactivity toward OH radicals leads to a decrease in the observed H_2O_2 yields also in the presence of larger amounts of e_{aq}^- scavenger: 0.25 *M* nitrate (curve 1), 0.025 *M* nitrate (curve 2), and 0.0025 *M* (curve 3). In the presence of larger amounts of e_{aq}^- scavenger the absolute values of H_2O_2 are larger, pointing to an increased formation which takes place even at high OH reactivities. Curves 1–3 are practically parallel, indicating that the mechanism of formation of primary hydrogen peroxide is practically the same.

In most of the cases presented in Figure 1 ethanol in various concentrations was used as OH scavenger. To verify the general character of the effect observed, ethanol was replaced in some experiments by sodium formate or isopropyl alcohol (2.5×10^{-3} to 1 *M*), both efficient OH scavengers. Also, acetone (0.41 *M*) was used instead of nitrate in some irradiations. These cases are also presented in Figure 1. It can be seen that the data fit well the yield–reactivity curves, confirming that the effect observed does not depend on the chemical nature and the combination of the scavengers used; it is dependent on the reactivity only.

Figure 2 shows how the increased reactivity toward e_{aq}^- leads to an increase in measured $G_{H_2O_2}$ in the pres-

---

(10) M. Kosanić and I. Draganić in "Proceedings of the Third Tihany Symposium on Radiation Chemistry," J. Dobo and P. Hedvig, Ed., Academiai Kiado, Budapest, 1971.

Table II: Yields of Molecular Hydrogen Measured in Deaerated Aqueous Solutions Containing Various Concentrations of Efficient Scavengers for e_{aq}^- and OH

Scavenger for e_{aq}^-, M	$G(H_2)$ measured in the presence of OH scavenger, M 5×10^{-4}	0.1	0.5	1.0	
NO_3^-		I^-			
2.5×10^{-4}	0.45	0.44	0.50	0.54	
2.5×10^{-3}	0.43	...	...	...	
2.5×10^{-2}	0.34	...	...	0.44	
0.25	0.19	0.21	0.24	0.29	
1.0	0.09	...	...	0.16	
NO_3^-		Br^-			
2.5×10^{-4}	...	...	0.49	...	
0.25	...	...	0.23	...	
NO_3^-		CNS^-			
2.5×10^{-4}	...	0.44	...	0.40	
	1×10^{-3}	0.1	0.5	1.0	1.5
H_2O_2[a]		Br^-			
2×10^{-4}	0.45	0.46	0.48	0.51	0.54
2×10^{-3}	0.43	...	...	...	0.53
2×10^{-2}	0.38	...	...	...	0.48
0.2	0.27	0.28	0.30	0.34	0.37
2.0	0.17	...	...	...	...
Cu^{2+}			Br^-		
1×10^{-4}	0.47	...	0.47	0.49	0.53
1×10^{-3}	0.40	...	...	...	0.51
1×10^{-2}	0.34	...	...	...	0.45
0.1	0.29	...	0.32	0.33	0.38
1.0	0.22	...	...	...	...

[a] These data have been obtained by Mrs. N. Mrkić as a part of her B.Sc. thesis at the University of Belgrade, Yugoslavia, 1971.

Table III: Yields of Hydrogen Peroxide and Molecular Hydrogen Measured in Deaerated Aqueous Solutions of Acrylamide

Solute, M	$G(H_2O_2)$	$G(H_2)$
2×10^{-4}	0.68	...
2.5×10^{-4}	...	0.46
1×10^{-3}	0.65	...
2.5×10^{-3}	0.63	0.42
1×10^{-2}	0.60	...
2.5×10^{-2}	0.54	0.32
5×10^{-2}	0.53	...
0.1	0.47	0.28
0.25	0.41	...
0.5	0.36	0.19

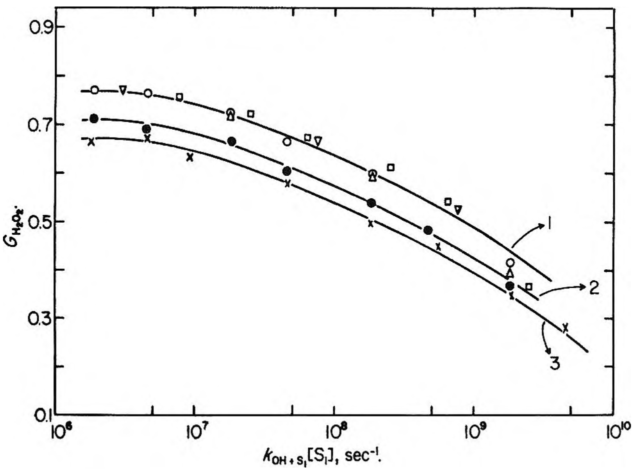

Figure 1. Dependence of observed primary hydrogen peroxide yield on hydroxyl radical reactivity in deaerated solutions containing e_{aq}^- scavenger. Curve 1: ○, 0.25 M NO_3^- + C_2H_5OH; △, 0.41 M $(CH_3)_2CO$ + C_2H_5OH; ▽, 0.41 M $(CH_3)_2CO$ + $(CH_3)_2CHOH$; □, 0.25 M NO_3^- + $HCOO^-$. Curve 2: ●, 0.025 M NO_3^- + C_2H_5OH. Curve 3: ×, 0.0025 M NO_3^- + C_2H_5OH.

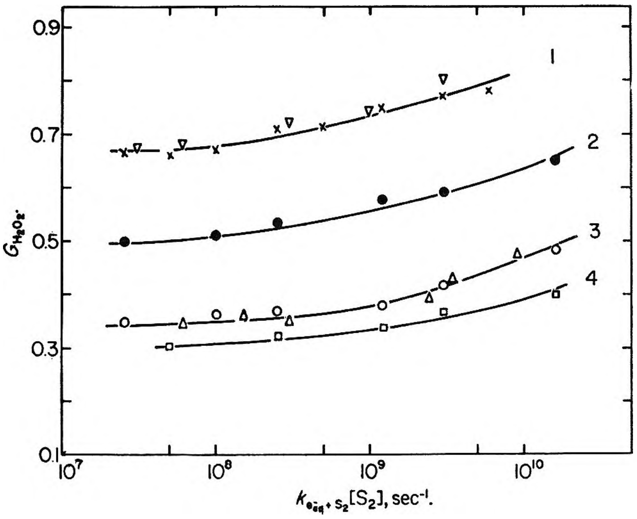

Figure 2. Dependence of observed primary hydrogen peroxide yield on hydrated electron reactivity in deaerated solutions containing OH scavenger. Curve 1: ×, 1×10^{-3} M C_2H_5OH + NO_3^-; ▽, 1×10^{-3} M C_2H_5OH + $(CH_3)_2CO$. Curve 2: ●, 0.1 M C_2H_5OH + NO_3^-. Curve 3: ○, 1.0 M C_2H_5OH + NO_3^-; △, 1.0 M C_2H_5OH + $(CH_3)_2CO$. Curve 4: □, 1.0 M $HCOO^-$ + NO_3^-.

ence of larger amounts of OH scavenger: 1 M ethanol (curve 3), 0.1 M ethanol (curve 2), and 1×10^{-3} M (curve 1). Curve 4 represents the data with 1 M formate ion instead of ethanol. The data with acetone (1×10^{-2} to 1.5 M), used instead of nitrate as hydrated electron scavenger, agree well with the available yield–reactivity curves. As in the above case, we see that the formation of primary hydrogen peroxide yields depends on the reactivity only and not on the chemical nature or the combinations of the scavengers used.

Dependence of Measured G_{H_2} on Reactivities toward e_{aq}^- and OH. Figure 3 shows that increasing reactivity toward e_{aq}^- causes a decrease in G_{H_2} also in the presence of larger amounts of OH scavengers. The absolute values of the yields increase with increasing OH scavenger concentration: 1 M iodide or 1.5 M bromide (curve 1), 5×10^{-4} M iodide, or 1×10^{-3} M bromide (curve 2). The trends of yield–reactivity curves are

Table IV: Rate Constants Used in the Reactivity Calculation[a]

Scavenger	k_{OH+S}, M^{-1} sec^{-1}	$k_{e_{aq}^{-}+S}$, M^{-1} sec^{-1}	k_{H+S}, M^{-1} sec^{-1}
C_2H_5OH	1.83×10^{9} [b]	$\leqslant 400$ [c]	1.6×10^{7}
$HCOO^-$	2.5×10^{9}	$<10^{6}$	2.5×10^{8}
$(CH_3)_2CHOH$	2.9×10^{9} [d]	...	5×10^{7}
$(CH_3)_2CO$	6.2×10^{7}	5.9×10^{9}	6×10^{5}
NO_3^-	$<5 \times 10^{5}$	1.05×10^{10}	1×10^{7}
0.1 M NO_3^-	...	1.3×10^{10} [e]	...
1.0 M NO_3^-	...	1.6×10^{10} [e]	...
$CH_2CHCONH_2$	6×10^{9} [f,g]	2×10^{10} [f]	1.8×10^{10} [g]
Br^-	7.5×10^{9} [h]	...	...
I^-	1.4×10^{10} [h]	...	...
CNS^-	2×10^{10}	...	...
H_2O_2	4.5×10^{7}	1.23×10^{10}	5×10^{7}
Cu^{2+}	3.5×10^{8}	4.5×10^{10}	4.2×10^{7}
0.01 M Cu^{2+}	...	2.7×10^{10} [e]	...
0.1 M Cu^{2+}	...	1.7×10^{10} [e]	...
1.0 M Cu^{2+}	...	0.91×10^{10} [e]	...

[a] If not otherwise indicated, the rate constant values were taken from the compilation made by M. Anbar and P. Neta, *Int. J. Appl. Radiat. Isotopes*, **18**, 493 (1967). [b] P. Neta and L. M. Dorfman, *Advan. Chem. Ser.*, **No. 81**, 222 (1968). [c] B. Hickel and K. Schmidt, *J. Phys. Chem.*, **74**, 2470 (1970). [d] Calculated according to Neta and Dorfman (footnote *b*). [e] Reference 6. [f] Reference 5. [g] K. W. Chambers, E. Collinson, and F. S. Dainton, *Trans. Faraday Soc.*, **66**, 142 (1970). [h] Reference 10.

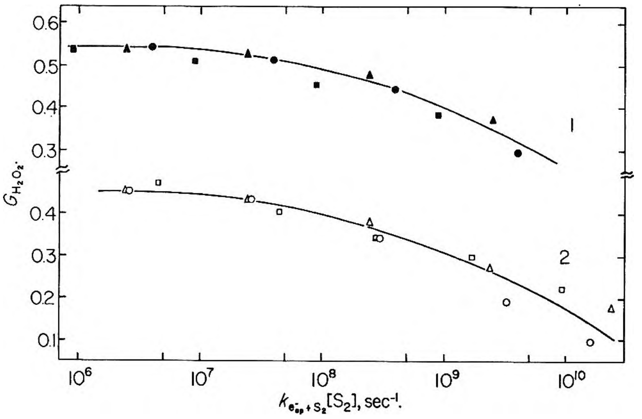

Figure 3. Dependence of observed primary molecular hydrogen yield on hydrated electron reactivity in deaerated solutions containing OH scavenger. Curve 1: ●, 1.0 M I^- + NO_3^-; ▲, 1.5 M Br^- + H_2O_2; ■, 1.5 M Br^-+ Cu^{2+}. Curve 2: ○, 5 × 10^{-4} M I^- + NO_3^-; △, 1 × 10^{-3} M Br^- + H_2O_2; □, 1 × 10^{-3} M Br^- + Cu^{2+}.

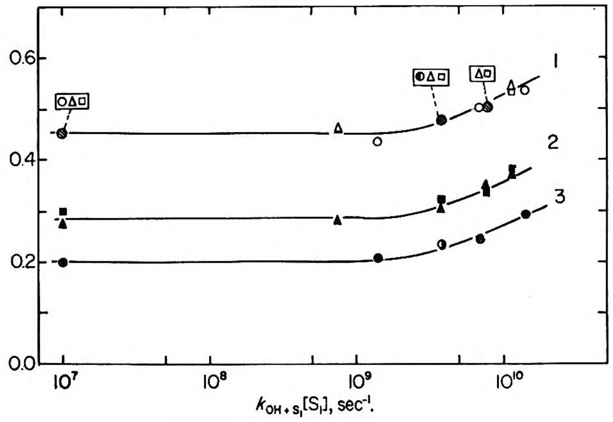

Figure 4. Dependence of observed primary molecular hydrogen yield on hydroxyl radical reactivity in deaerated solutions containing e_{aq}^- scavenger. Curve 1: ○, 2.5 × 10^{-4} M NO_3^- + I^-; ◐, 2.5 × 10^{-4} M NO_3^- + Br^-; △, 2 × 10^{-4} M H_2O_2 + Br^-; □, 1 × 10^{-4} M Cu^{2+} + Br^-. Curve 2: ▲, 0.2 M H_2O_2 + Br^-; ■, 0.1 M Cu^{2+} + Br^-. Curve 3: ●, 0.25 M NO_3^- + I^-; ◑, 0.25 M NO_3^- + Br^-.

the same and point out that the formation of primary H_2 yields is not disturbed by the presence of larger amounts of efficient OH scavengers. Only the G_{H_2} measured in 1 M nitrate solution containing 1 mol/l. of iodide is not plotted in Figure 3 because the value of the rate constant at the corresponding ionic strength is not established. However, as can be seen in Table II, it also confirms the general trend.

Figure 4 shows the effect of OH scavenger concentration on G_{H_2} measured in the presence of larger amounts of e_{aq}^- scavengers. It can be seen that the molecular hydrogen yields increase with increasing reactivity toward OH also in the presence of hydrated electron scavengers. The absolute values were found to be lower when more e_{aq}^- scavenger was present (curves 2 and 3), but the trend of yield-reactivity curves is practically the same, pointing out that the mechanism of increased H_2 formation is the same.

It should be pointed out that the increase of KCNS concentration in irradiated solutions does not lead to an increase in H_2 yields (Table II) although this substance is known as a good OH scavenger, and here was used in larger concentrations (0.1 and 1 M). This observation calls for further study, and its explanation should be sought in secondary spur reactions of primary radicals with products of radical-solute scavenging reactions.

Unifying Curves for Reactivity Dependence of Frac-

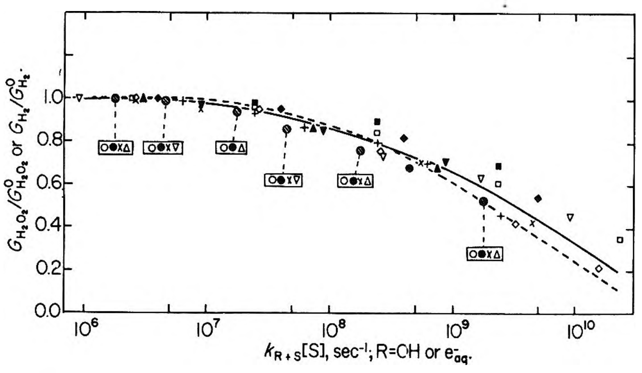

Figure 5. Unifying curve for the decrease of $G_{H_2O_2}/G^\circ_{H_2O_2}$ or $G_{H_2}/G^\circ_{H_2}$ with increasing reactivity toward OH or e_{aq}^-. Hydrogen peroxide: ○, 0.25 M NO_3^- + C_2H_5OH; ●, 0.025 M NO_3^- + C_2H_5OH; ×, 2.5 × 10^{-3} M NO_3^- + C_2H_5OH; △, 0.41 M $(CH_3)_2CO$ + C_2H_5OH; +, 0.25 M NO_3^- + $HCOO^-$; ▲, 0.41 M $(CH_3)_2CO$ + $(CH_3)_2CHOH$. Molecular hydrogen: ◇, 5 × 10^{-4} M I^- + NO_3^-; ◆, 1.0 M I^- + NO_3^-; □, 1 × 10^{-3} M Br^- + H_2O_2; ■, 1.5 M Br^- + H_2O_2; ▽, 1 × 10^{-3} M Br^- + Cu^{2+}; ▼, 1.5 M Br^- + Cu^{2+}. The dotted line is the diffusion kinetic theoretical curve according to Kuppermann.[3]

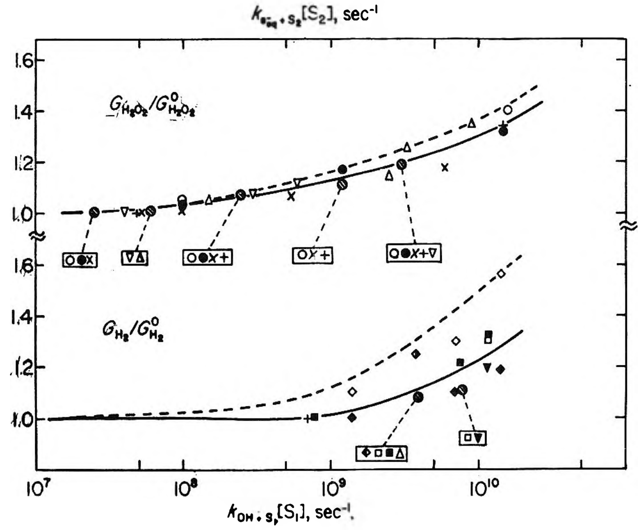

Figure 6. Unifying curve for the increase of $G_{H_2O_2}/G^\circ_{H_2O_2}$ or $G_{H_2}/G^\circ_{H_2}$ with increasing reactivity toward e_{aq}^- or OH radicals. Hydrogen peroxide: ○, 1.0 M C_2H_5OH + NO_3^-; ●, 0.1 M C_2H_5OH + NO_3^-; ×, 1 × 10^{-3} M C_2H_5OH + NO_3^-; +, 1.0 M $HCOO^-$ + NO_3^-; △, 1.0 M C_2H_5OH + $(CH_3)_2CO$; ▽, 1 × 10^{-3} M C_2H_5OH + $(CH_3)_2CO$. Molecular hydrogen: ◆, 0.25 M NO_3^- + I^-; ◇, 2.5 × 10^{-4} M NO_3^- + I^-; ◐, 0.25 M NO_3^- + Br^-; ◑, 2.5 × 10^{-4} M NO_3^- + Br^-; □, 0.2 M H_2O_2 + Br^-; ■, 2 × 10^{-4} M H_2O_2 + Br^-; ▲, 0.1 M Cu^{2+} + Br^-; ▼, 1 × 10^{-4} Cu^{2+} + Br^-. The dotted line is the diffusion kinetic theoretical curve according to Kuppermann.[3]

tional Changes of Primary Yields, G_M/G_M°, where M was H_2O_2 or H_2. Various studies on the origin of primary molecular yields have confirmed that the ratio of primary molecular yield measured in the presence of the scavenger of its precursor, G_M, to that observed in dilute solution when the scavenger has no effect, G_M°, depends only on the reactivity of the scavengers used. The analysis of the present data (Figures 1–4) shows that the unifying curves can also be obtained here when G_M° is the yield measured in solution where the reaction of solute with the precursor of M can be neglected.

Figure 5 summarizes all the results on G_M decreases with increasing reactivities toward the precursors of M. It can be seen that a unifying curve is obtained for fractional lowering of both primary yields, H_2O_2 and H_2.

Figure 6 summarizes all the results on G_M increases. The upper curve concerns the fractional increase of H_2O_2 yields with increasing reactivities toward e_{aq}^-. We see that a fairly satisfactory correlation between the $G_{H_2O_2}/G_{H_2O_2}^\circ$ and reactivities could be obtained although the observations were made on solutions containing larger amounts of scavengers for hydroxyl radical. The lower curve concerns the fractional increase of H_2 yields with increasing reactivities toward OH. The straggling of these data is larger than in the previous case and, as we mentioned before, deserves further studies. It seems evident, nevertheless, that one can correlate the increase of fractional yields of primary molecular hydrogen with reactivity toward OH even in systems containing large amounts of scavengers for e_{aq}^-, the precursor of primary H_2.

The data shown in Figures 1–6 point out the scarcity of secondary reactions which could be expected to take place under our experimental conditions between the products of radical–solute scavenging reactions and the primary radical which is the precursor of G_M. Except for H_2 measured in the presence of KCNS, where no increase was found, and some deviations when H_2O_2 was present, the assumed decreases or increasing of G_M were easily observable and G_M/G_M° correlated with reactivities.

The dotted lines in Figures 5 and 6 represent the theoretical curves,[3] also adjusted to the G_M/G_M° form. They were calculated from a diffusion model of water radiolysis which essentially consisted of reactions 1–10; however, initial reactivities of S_1 and S_2 were 6 × 10^6 sec^{-1} only, while in the experiments they amounted up to 10^{10} sec^{-1}. The quite reasonable agreement between the experimental findings and theoretical predictions might not be purely fortuitous. This could be one more confirmation that even at reactivities of about 10^{10} sec^{-1}, and the simultaneous presence of scavengers for both primary free radicals, no significant secondary reactions take place in the spurs in the γ-irradiated aqueous solutions.

On the Origin of Primary Molecular Products. It has recently been proposed[7] that the origin of primary H_2O_2 and H_2 yields in water radiolysis is in prompt recombination of dry charged species (H_2O^+ or H_3O^+) and of dry electrons (e^-). These reactions were assumed to be in competition with hydration and reactions with some suitable scavengers. It was suggested that these reactions are very fast and should not overlap the time scale considered by the diffusion model of radiation chemistry of aqueous solutions. However, it was concluded that the spur diffusion model should not be applied to solutions containing more than 0.1 M scavenger because of intervention in the early ionic processes.

This concentration limit does not seem to be justified according to the present results: we have shown that the yields measured in solutions containing up to 1.5 M solutes fit the unifying curves reasonably well. Also, if we are dealing at larger concentrations with dry charged species and dry electrons instead of OH and e_{aq}^-, then their behavior must be very similar. This means that their recombination reactions should be influenced in a similar way and that their reactivities toward the scavengers should be very close. Recent observations on picosecond scale[11] do not support this assumption; they show that the dry and the hydrated electron are not scavenged with similar efficiency by a given solute.

Taking into account data presented in this work on primary molecular products formation, and in the absence of more information concerning the prompt recombinations of "dry" species leading to H_2O_2 and H_2, we think that the origin of $G_{H_2O_2}$ and G_{H_2} under the conditions studied, the half-life of fastest scavenger reaction about 50 psec, should be in reactions 1, 5, 7, and 9. Furthermore, this study has confirmed that the reaction mechanism given by eq 1–10 represents adequately the phenomena observed. One advantage of this approach is that the nature of reacting species assumed and the rate constants of their reactions used have been well established in numerous independent studies.

Dependence of Primary Molecular Yield on Reactivities toward OH and e_{aq}^- and the Additivity of Effects Observed. We have seen how the experiments carried out in this work confirm the assumption that the efficient removal of a free-radical precursor of a given molecular product leads not only to a decrease in its yield, but simultaneously causes an increase in the other primary molecular product yield. It is also evident that $G_{H_2O_2}$ was depressed by the presence of an OH scavenger and increased if an efficient e_{aq}^- scavenger was present in irradiated solution. Similarly, the observed yield of primary H_2 depended on the reactivity both toward e_{aq}^- and OH scavengers. The analysis of experimental data (Figures 1–4) suggests the following empirical relations

$$G_{H_2O_2} = 0.67 - (\Delta G_{H_2O_2})_{v_{OH}} + (\Delta G_{H_2O_2})_{v_{e_{aq}^-}} \quad (11)$$

$$G_{H_2} = 0.45 - (\Delta G_{H_2})_{v_{e_{aq}^-}} + (\Delta G_{H_2})_{v_{OH}} \quad (12)$$

Here $G_{H_2O_2}$ and G_{H_2} are the primary molecular yields predicted for solutions containing the scavengers for both primary oxidizing and reducing species. The ΔG values represent the corresponding yield changes due to the presence of primary radical scavenger. They are proportional to the reactivity, v_{OH} or $v_{e_{aq}^-}$ in reciprocal seconds and should be derived from the calibration yield–reactivity curves. These curves, representing G_M as the function of reactivity toward the primary radical concerned, could be constructed from the results published in this work and elsewhere.[5,6] The values 0.67 and 0.45 are, respectively, $G_{H_2O_2}$ and G_{H_2}, measured in dilute solutions where the solutes have no effect.

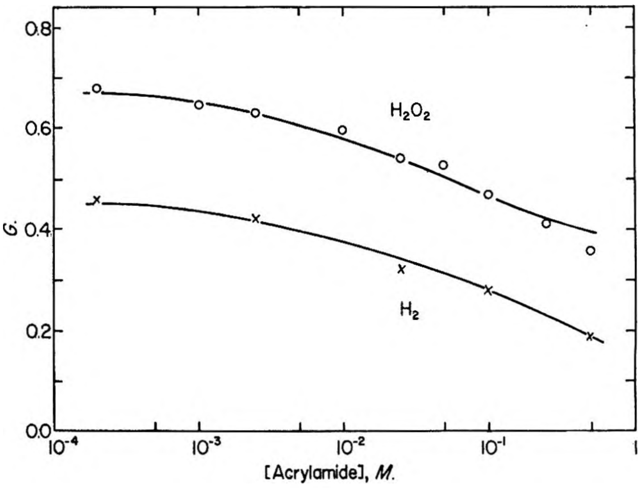

Figure 7. The dependence of $G_{H_2O_2}$ and G_{H_2} on increasing concentration of acrylamide in deaerated neutral aqueous solutions. The solid lines were calculated according to eq 11 and 12.

We have checked these empirical relations (eq 11 and 12) by measuring $G_{H_2O_2}$ and G_{H_2} in deaerated acrylamide solution (Figure 7). Our previous study[5] indicated this solute, which is known as an efficient scavenger for both primary oxidizing and reducing species. In the calculation we have neglected its reactivity toward H atoms and the effect of the reaction 10 on primary molecular yields formation. According to recent studies the hydrogen atom contribution to the effects observed is not significant.[4,12] As can be seen, the experimental and calculated values agree very well in the concentration range studied. At higher concentrations the irradiated solutions become so viscous that the analysis is impracticable. Other solutes at larger concentrations, *e.g.*, nitrite ion, should be tried to get a more pronounced effect, especially in the case of molecular hydrogen.

Concluding Remarks

1. The recombination reactions of primary oxidizing and reducing free radicals leading to the formation of H_2O_2 and H_2 take place also in the simultaneous presence of larger amounts (up to 1.5 M) of scavengers for both oxidizing and reducing primary species.

2. Efficient removal of OH radicals reduces $G_{H_2O_2}$

---

[11] R. K. Wolff, M. J. Bronskill, and J. W. Hunt, *J. Chem. Phys.*, **53**, 4211 (1970).

[12] E. Peled, U. Mirski, and G. Czapski, *J. Phys. Chem.*, **75**, 31 (1971).

and increases G_{H_2}. Efficient removal of e_{aq}^- reduces G_{H_2} and increases $G_{H_2O_2}$. These effects are additive and empirical equations were proposed: they make it possible to predict a primary molecular yield formed in an irradiated solution containing simultaneously larger concentrations of efficient scavengers for both free-radical precursors (OH and e_{aq}^-).

3. Unifying curves were obtained for $G_M/G_M{}^\circ$ dependence on reactivities toward OH or e_{aq}^-. These experimental plots agree reasonably well with the diffusion-kinetic theoretical predictions which were calculated for experimental conditions where the secondary spur reactions are not expected to occur.

Acknowledgments. The authors are indebted to Dr. A. O. Allen (Brookhaven National Laboratory, Upton, N. Y.) for his interest in this work and to Mr. M. Borovičanin for technical assistance in the experiments.

Interlamellar Metal Complexes on Layer Silicates. I. Copper(II)-Arene Complexes on Montmorillonite

by Thomas J. Pinnavaia* and M. M. Mortland*

Department of Chemistry and the Departments of Crop and Soil Sciences and Geology, Michigan State University, East Lansing, Michigan 48823

(Received August 4, 1971)

Publication costs assisted by Michigan State University

The adsorption of toluene and other methyl-substituted benzenes on the interlamellar surfaces of copper(II) montmorillonite has been studied by spectroscopic methods. In addition to physically adsorbed molecules interacting with the silicate surface there are present chemisorbed species which are coordinated through π electrons to the exchangeable copper(II) ions. In each case the coordinated species is similar to that in the previously studied type I benzene complex in which the ring is planar and aromaticity is retained on coordination. None of the methyl-substituted benzenes formed complexes analogous to the type II benzene complex in which the ring is distorted and aromaticity is lost. Possible structures for the type I complexes are discussed.

Introduction

Montmorillonite is a naturally occurring layer aluminosilicate whose structure is similar to that of pyrophyllite except that there is isomorphous replacement of Al^{3+} by Mg^{2+} in the octahedral sheet. The resulting negative charge is balanced by exchangeable cations positioned between the aluminosilicate layers, and the large internal surface area (*ca.* 800 m^2/g) thus becomes available for the adsorption of a variety of molecules. The adsorption mechanisms, which have been recently reviewed,[1] differ considerably, depending on the nature of the interlamellar cation and the adsorbate molecule.

In the case of transition metal ion exchange forms of the mineral and adsorbate molecules containing donor atoms, mechanisms involving the formation of discrete donor-acceptor complexes are common. The coordination chemistry of the metal ion is often related to that of the ion in homogeneous solution, but it can sometimes be greatly influenced by the unique environment at the silicate surface. A case in point is the formation of two types of copper(II)-arene complexes[2,3] in the adsorption of benzene on copper(II) montmorillonite. One complex possesses an apparent "green" color (type I), and the other is "red" (type II). Under conditions where the type I complex is formed, the degree of hydration of the mineral is higher than that needed to form the type II complex. Thus the two complexes can be interconverted simply by adding or removing controlled amounts of water. The nature of the coordinated benzene in the two complexes differs markedly, as judged by infrared spectroscopy. In the type I complex the benzene ring is planar and retains its aromaticity, whereas in the type II complex the ring is greatly distorted and the π electrons are probably localized. These two chemisorbed species are especially interesting in view of the fact that no copper(II)-arene complexes have yet been observed in homogeneous solution. Moreover, the donation of π

[1] M. M. Mortland, *Advan. Agron.*, 22, 75 (1970).

[2] H. E. Doner and M. M. Mortland, *Science*, 166, 1406 (1969).

[3] M. M. Mortland and T. J. Pinnavaia, *Nature (London)*, 229, 75 (1971).

electrons from an aromatic hydrocarbon to a metal ion acceptor has not been previously observed for an adsorption process on layer aluminosilicates and related three-dimensional zeolites.

The present study investigates by spectroscopic means the nature of adsorbed toluene and other methyl-substituted benzenes on copper(II) montmorillonite in order to establish their relationships, if any, to the two types of benzene complexes.

Experimental Methods

Materials. Naturally occurring montmorillonite (Wyoming bentonite, API No. 25) was purchased from Ward's Natural Science Establishment. The copper(II) exchange form was prepared by treating the <2-μg fraction of the mineral with 1.0 *N* $CuCl_2$, centrifuging, and discarding the supernatant liquid. The procedure was repeated three times to maximize the exchange of the original cations (mainly Na^+). Excess $CuCl_2$ was removed by washing with distilled water until no test for Cl^- was obtained with $AgNO_3$. The approximate composition of the anhydrous mineral is $Cu_{0.19}[Al_{1.53}Fe_{0.16}Mg_{0.33}][Al_{0.05}Si_{3.95}]O_{10}(OH)_2$.

Arene–copper(II) montmorillonite complexes were prepared by placing a sample of the air-dried mineral, usually in the form of a film, in a P_2O_5 desiccator containing a beaker of the appropriate reagent grade aromatic hydrocarbon. The deeply colored complexes were formed within 24 hr under these conditions.

Infrared Spectra. Spectra in the region 4000–600 cm^{-1} were obtained on a Beckman IR-7 spectrophotometer. Samples were prepared by evaporating in the open atmosphere aqueous suspensions of the mineral on a polyethylene surface. The resulting thin, self-supporting films (*ca.* 1 mg/cm^2) were then peeled away from the polyethylene surface and used to form the desired complex. The films were mounted in a brass cell equipped with NaCl windows in order to protect them from atmospheric moisture.

Since the film samples are highly oriented with the planes of the silicate sheets lying parallel to the film surface, it was possible to investigate pleochroic effects by observing differences in absorption intensities with the film positioned 90 and 45° to the path of the spectrophotometer beam. All differences in absorbance and relative optical densities were estimated from band heights.

Electronic Spectra. Electronic spectra of mull samples in the region 26,000–250 nm were obtained on a Cary 14 spectrophotometer. The mulls were prepared by evaporating a suspension of copper(II) montmorillonite directly onto a quartz glass window, forming the desired complex, and then coating the sample with mineral oil. All spectra were run against a reference sample of copper(II) montmorillonite in order to compensate for radiation losses due to scattering and adsorptions of the mineral itself. The spectrum of each complex was obtained on at least two independent samples to ensure reproducibility of the absorption bands. It was not possible to observe the internal transitions of the aromatic ligands below 250 nm because of the absorptions of physically bound species also present on the surface and severe radiation scattering in this region.

Esr Spectra. The esr spectrum of the copper(II)–toluene complex was recorded at room temperature on a Varian E-4 spectrometer. The sample was prepared by freeze-drying a suspension of the mineral in a quartz-glass esr tube fitted with a Teflon stopcock and then forming the complex.

X-Ray Diffraction. Powder diffraction patterns were obtained by conventional means on a Phillips X-ray diffractometer using Cu radiation and an Ni filter.

Results

When the exchangeable alkali metal and alkaline earth cations of naturally occurring montmorillonite are replaced by copper(II), the layer silicate mineral adopts the pale blue color characteristic of aqueous Cu^{2+}. At room temperature and *ca.* 50% relative humidity the 001 spacing (12.4 Å) indicates that the interlamellar surface occupied by the cation is also covered with a monolayer of water. The water content corresponds to *ca.* 14 water molecules per copper(II) ion. The metal ion may achieve a coordination number of 6 by binding to three of these water molecules and to three oxygen atoms of the silicate structure. The remaining water molecules occupy outer spheres of coordination. Recent studies by Farmer and Russell[4] on copper(II) and other cation-exchange forms of montmorillonite indicate that the adsorbed water is highly structured with the water in outer spheres of coordination forming dielectric links *via* hydrogen bonding between the cation and the negatively charged silicate structure. Dehydration of the mineral by evacuation at temperatures below 150° or by drying over P_2O_5 leads to preferential removal of outer-sphere water and frees some of the silicate surface for the adsorption of a variety of neutral molecules. The removal of all interlamellar water causes adjacent silicate layers to come together, and internal adsorption of many molecules is prevented or greatly retarded.

Copper(II) montmorillonite dried over P_2O_5 at room temperature binds toluene by physical adsorption to the silicate structure and by complex formation with the copper(II) ions. A 001 spacing of 15.8 Å upon adsorption verifies that the binding occurs on the interlamellar surfaces. The two forms of bound toluene are readily distinguished by infrared spectroscopy. The infrared bands characteristic of both forms are identified in spectrum C of Figure 1. Included in the

---

[4] V. C. Farmer and J. D. Russell, *Trans. Faraday Soc.*, **67**, 2737 (1971).

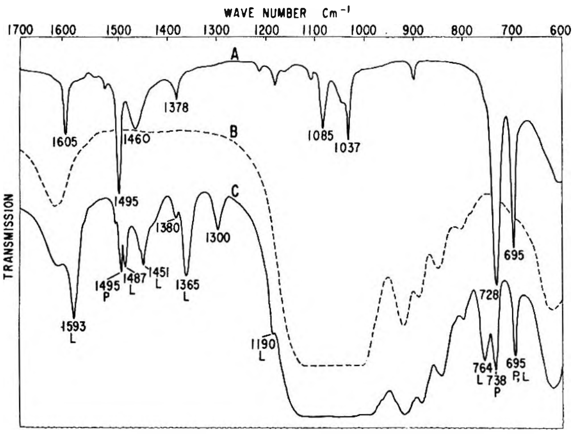

Figure 1. Infrared spectra for (A) liquid toluene, (B) copper(II) montmorillonite, and (C) the toluene–copper(II) montmorillonite complex. Bands labeled "P" and "L" are assigned to physically adsorbed and ligand toluene, respectively.

figure are spectra for liquid toluene and copper(II) montmorillonite. Although we are lacking quantitative equilibrium data, the ratio of ligand to physically adsorbed toluene increases with decreasing degree of hydration. In addition, there is a differential loss of the two species upon heating at 105°, the ligand being relatively stable while the physically adsorbed toluene is greatly diminished. Thus the assignment of bands in spectrum C was facilitated by interconverting the two forms as well as observing their relative stabilities.

Four normal modes are observed in the region 1700–600 cm^{-1} for physically adsorbed toluene: the C–C stretching vibrations ν_{19a}[5] and ν_{19b}, respectively, at 1495 and ~1458 cm^{-1}, the C–H out-of-plane deformation ν_{11} at 738 cm^{-1}, and the out-of-plane skeletal vibration ν_4 at ~695 cm^{-1}. The other normal modes expected in this region either are too weak to observe or are obscured by vibrations of the adsorbed water or of the silicate structure. At least one internal vibration of the CH_3 group is also observed, *viz.*, the symmetric deformation at 1380 cm^{-1}. The asymmetric CH_3 deformation probably lies near the ν_{19b} vibration at ~1458 cm^{-1}. Little or no pleochroism (*cf.* Experimental Section) was observed for the symmetric CH_3 deformation and the ν_{19a} and ν_{19b} vibrations for which the transition moments lie in the plane of the aromatic ring. However, an appreciable pleochroic effect (*ca.* 20% increase in absorbance) was observed for the ν_{11} vibration in which the transition moment is perpendicular to the ring. Much larger pleochroic effects would be expected if the plane of the molecule was perfectly parallel to the silicate surface. Thus the plane of the physically adsorbed toluene is tilted but probably more nearly parallel than perpendicular to the silicate surface. All of the observed vibrational frequencies are essentially unshifted (<2 cm^{-1}) relative to those for liquid toluene, except the ν_{11} vibration which is shifted to higher energy by 10 cm^{-1}. The latter mode is known to be quite sensitive to environment. Comparable shifts in ν_{11} are observed, for example, for toluene in the solid state[6] and for toluene in certain clathrate compounds.[7]

In comparison with liquid toluene, the ligand form of toluene on copper(II) montmorillonite exhibits marked frequency shifts and changes in relative intensities for all vibrational bands. Frequency assignments and relative optical densities are given in Table I. Unlike the physically bound form, all of the C–C stretching modes of the complexed toluene are shifted to lower energy by 7–12 cm^{-1} and the CH_3 deformations are shifted in the same direction by 13–25 cm^{-1}. Moreover, the high-energy shift for the ν_{11} vibration is 3.6 times larger than that observed for the physically adsorbed form. One strong band at 1300 cm^{-1} in the spectrum of the complexed toluene has no obvious counterpart in the spectrum of liquid toluene. This band is tentatively assigned to a C–H in-plane deformation (ν_3) which has been observed by others[6] as a very weak band at 1312 cm^{-1}. The marked difference in intensity would require a change in transition moment upon complexation. That such changes do indeed occur is especially well illustrated by the differences in intensities among the ν_{8a}, ν_{19a}, and ν_{11} vibrations.

Table I: Assignments and Relative Optical Densities for the Vibrational Frequencies of Toluene in the Liquid State and as a Coordinated Ligand on Copper(II) Montmorillonite

Liquid		Cu(II) complex on mineral		
Freq, cm^{-1}	Rel OD	Freq, cm^{-1}	Rel OD	Assignment[a]
1605	100	1593	100	C–C str (ν_{8a})
1495	300	1487	36	C–C str (ν_{19a})
1460	80	1451	36	C–C str (ν_{19b})
1460		~1435 sh	. . .	Asym CH_3 def
1378	37	1365	56	Sym CH_3 def
		1300	25	C–H in-plane def (ν_3)?
1212	17	1190	. . .	C–H in-plane def (ν_{13})
728	780	764	59	C–H out-of-plane def (ν_{11})

[a] Assignments for liquid toluene were taken from ref 6.

In view of the great changes in frequencies and intensities of CH and CH_3 deformation vibrations of ligand toluene, important effects on the CH stretch-

---

(5) Frequency designations for the vibrational modes of toluene and the other aromatic molecules discussed herein are described by G. Varsányi in "Vibrational Spectra of Benzene Derivatives," Academic Press, New York, N. Y., 1969.

(6) N. Fuson, C. Garrigou-Lagrange, and M. L. Josien, *Spectrochim. Acta*, 16, 106 (1960).

(7) T. Iwamoto, T. Nakano, M. Morita, T. Miyoshi, T. Miyamoto, and Y. Sasaki, *Inorg. Chim. Acta*, 2, 313 (1968).

Table II: Frequencies (cm^{-1}) of C–C Stretching and C–H Out-of-Plane Deformation Modes for Aromatic Molecules in the Liquid State and Adsorbed on Copper(II) Montmorillonite

	C–C str (ν_{19})			C–H out-of-plane def (ν_{11})		
Compd	Liquid	Physically adsorbed on silicate surface	Cu(II) complex on silicate surface	Liquid	Physically adsorbed on silicate surface	Cu(II) complex on silicate surface
Toluene	1495	1495	1487	728	738	764
o-Xylene	1495	1495	1483	743	750	773
p-Xylene	1517	1516	1503	795	800	817
m-Xylene	1481	1480	1473	769	777	803
Mesitylene	1473	1473	1463	837	844	~890[a]
Benzene	1478	1478	1470[b]	675	688	706[b]

[a] Obscured by a vibration of the silicate lattice. [b] Frequencies for the type I benzene complex.

ing vibrations might also be expected. The ligand toluene had much reduced absorption intensities for the CH stretching vibrations in comparison with liquid toluene. These very low absorption intensities plus the background of the montmorillonite itself precluded a detailed study in this region of the spectrum. No significant pleochroic effects were observed for any of the in-plane or out-of-plane vibrational bands of ligand toluene. Such a result would occur if the plane of the ring was inclined relative to the silicate surface at an angle near 45°.

Physical adsorption and complex formation are also involved in the adsorption of the xylenes and of mesitylene on copper(II) montmorillonite. In each case the relationship among the vibrational frequencies for the complexed, physically bound, and liquid states is similar to that described above for toluene. A comparison of the C–C stretching vibration (ν_{19a} or ν_{19b}) and the C–H out-of-plane deformation (ν_{11}) for the three states is given in Table II, along with those for the "green" type I benzene complex. For all of the physically adsorbed aromatic molecules the C–C stretching vibrations are unshifted relative to the liquid state but the out-of-plane C–H deformation is shifted to higher energy by 5–13 cm^{-1}. All of the complexed molecules, on the other hand, show 8–14 cm^{-1} low-energy shifts for the C–C stretch and 23–~53 cm^{-1} high-energy shifts for the C–H out-of-plane deformation.

The vibrational spectra clearly indicate that the coordinated methyl-substituted benzenes are analogous to the ligand benzene in the type I complex insofar as the ring is planar and aromaticity is retained. The sacrifical role of the aromatic hydrocarbon in the bonding, however, is evident from the low-energy shifts of the C–C stretching frequencies. No evidence was obtained for the formation of methyl-substituted benzene complexes similar to the type II benzene complex. The vibration spectrum of this latter complex is markedly unlike that expected for a planar benzene ring even under very low site symmetry. Two C–C stretching vibrations, for example, occur as very strong broad bands at 1540 and 1480 cm^{-1}, indicating that the π electrons of the C_6H_6 moiety are much less delocalized over the ring than they are in the uncoordinated molecule.

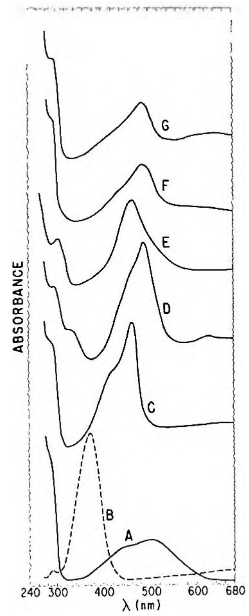

Figure 2. Visible–uv spectra of arene–copper(II) montmorillonite complexes (mulls): (A) benzene (type II), (B) benzene (type I), (C) toluene, (D) mesitylene, (E) *p*-xylene, (F) *m*-xylene, and (G) *o*-xylene.

All of the copper(II)–arene complexes are deeply colored. Their uv–visible spectra are shown in Figure 2, and the band maxima are listed in Table III. The methyl-substituted benzene complexes show at least two visible bands, which may arise from transitions of the metal ion. A uv band between 285 and 335 nm shifts to higher energy with increasing ionization potential[8] of the arene in the order mesitylene < *p*-xylene < *o*,*m*-xylene < toluene. Thus, the band can be reasonably assigned to a charge-transfer transition. The mesitylene complex exhibits two additional bands at 625 and 298 nm. No bands were detected in the region 700–26,000 nm for any of the complexes.

---

(8) R. S. Mulliken and W. B. Person, "Molecular Complexes," Wiley-Interscience, New York, N. Y., 1969, p 135.

Table III: Electronic Absorption Bands of Copper(II) Arene Complexes on Montmorillonite

Ligand	ν_{max}, cm^{-1}				
Mesitylene	33,600	29,900	~22,500	20,100	16,000
p-Xylene		33,000	21,700	~19,400	
o-Xylene		34,300	~23,000	20,700	
m-Xylene		34,500	~23,000	20,500	
Toluene		35,100	23,500	21,700	
Benzene (type I)			27,200		
Benzene (type II)		35,700	22,200	19,900	~3,400[a]

[a] From data in ref 3.

The electronic spectra of the types I and II benzene complexes differ greatly. The type II complex gives two visible and one uv band similar to the methyl-substituted benzene complexes, but it is distinguished from these latter complexes by a very low-energy transition in the ir region at ~3400 cm^{-1}. Electronic absorption bands in the ir region are very unusual, but in the case of copper(II) such a band at 4500 cm^{-1} has been observed previously[9] for the $d_{xy} \rightarrow d_{xz}, d_{yz}$ transition[10] of $CuCl_4^{2-}$ in a distorted tetrahedral configuration. The type I complex exhibits only one symmetrical band positioned at 368 nm. It is noteworthy that the apparent green color which is normally observed under conditions where mostly type I and little type II complex are present[3] is not the expected complement of the 368-nm absorption. The true color of the complex is pale yellow, and this color can be observed by carefully drying the montmorillonite at room temperature under vacuum before exposing it to benzene vapor. The green color occurs when the mineral is interstratified with some silicate layers containing the yellow type I complex and others containing uncomplexed, pale blue copper(II).

The esr spectra of the type I benzene and toluene complexes, as well as the type II benzene complex,[3] consist of a single asymmetric line with a half-width of ~250 G. The intensity of the line is essentially identical with that for uncomplexed copper(II) on montmorillonite. Thus it appears that no appreciable amounts of copper(I) or organic cation radicals are formed in the adsorption processes.

Discussion

Aromatic molecules have been previously known to bond to silica,[11,12] layer silicates,[13-15] and three-dimensional zeolites[16-19] *via* physical adsorption processes. Thus our observation of physically bound benzene and its methyl-substituted derivatives on copper(II) montmorillonite was not unexpected. There is, however, an interesting similarity between the vibrational frequencies of these molecules on the silicate surface and those for the same molecules physically adsorbed on silica[11] and different metal ion exchange forms of zeolites.[16,18,19] On all three types of adsorbents, the in-plane C-C stretching vibration, as well as other in-plane vibrations, are essentially unshifted relative to the liquid state, whereas the ν_{11} out-of-plane C-H deformation always shifts to higher energy by 5-15 cm^{-1}. It has been suggested in the case of silica[11] and the zeolites[16,18] that important adsorption forces result from an interaction of the π electrons of the adsorbate and the hydroxyl groups or oxygen atoms of the adsorbent. A similar interaction may occur on copper(II) montmorillonite because in the case of physically adsorbed benzene[3] and toluene the plane of the aromatic ring is inclined at the silicate surface. It is to be noted, however, that the interaction of π electrons with silicate oxygen atoms cannot be expected to explain the physical adsorption of *all* aromatic molecules on montmorillonite. Early X-ray diffraction studies,[13] for example, have shown that aromatic molecules can adopt perpendicular as well as inclined orientations on montmorillonite, depending on the nature of substituents on the aromatic ring and the adsorption conditions.

Crystallographic data for known metal-arene complexes indicate that benzene may act as a formal two-, three-, four-, or six-π-electron donor. Each type of bonding mechanism can be envisioned for the copper(II)-arene complexes formed in the adsorption processes, depending on the assumed symmetry of the metal ion. Sandwich-type bis(π-arene)copper(II) species seem initially attractive because they would be isoelectronic with the known noncentrosymmetric complex $Co[C_6(CH_3)_6]_2$,[20,21] but their existence is precluded by the basal spacings of the mineral. If we make the reasonable assumption that the effective thickness of a benzene ring (3.4 Å) and of an alkyl-substituted benzene ring (4.0 Å) would contract by as much as 0.5 Å upon π bonding to copper(II) and concomitant interaction with silicate oxygens, then interlamellar heights of at least 5.8 and 7.0 Å, respectively, would be required to accommodate a bis(π-benzene)- and bis(π-toluene)-copper(II) complexes. These values, of course, are

---

(9) D. M. Gruen and R. L. McBeth, *Pure Appl. Chem.*, **6**, 23 (1963).

(10) W. E. Hatfield and T. S. Piper, *Inorg. Chem.*, **3**, 84 (1964).

(11) G. A. Galkin, A. V. Kiselev, and V. I. Lygin, *Trans. Faraday Soc.*, **60**, 431 (1964).

(12) M. J. Rosen and Gandler, *J. Phys. Chem.*, **75**, 887 (1971).

(13) R. Green-Kelly, *Trans. Faraday Soc.*, **51**, 412 (1955).

(14) R. M. Barrer and K. E. Kelsey, *ibid.*, **57**, 452 (1961).

(15) R. M. Barrer and K. Brummer, *ibid.*, **59**, 959 (1963).

(16) C. L. Angell and M. V. Howell, *J. Colloid Interface Sci.*, **28**, 279 (1968).

(17) C. L. Angell and P. C. Schaffer, *J. Phys. Chem.*, **69**, 3463 (1965).

(18) G. A. Galkin, A. V. Kiselev, and V. I. Lygin, *Russ. J. Phys. Chem.*, **36**, 951 (1962).

(19) V. N. Abramov, A. V. Kiselev, and V. I. Lygin, *ibid.*, **37**, 613 (1963).

(20) E. O. Fischer and H. H. Lindner, *J. Organometal. Chem.*, **2**, 222 (1964).

(21) B. J. Nicholson and H. C. Longuet-Higgins, *Mol. Phys.*, **9**, 461 (1965).

based on the further assumption that the planes of the aromatic rings lie parallel to the silicate sheets, whereas in the case of the toluene complex the ring is in fact inclined by as much as 45°. The basal spacings of copper(II) montmorillonite are 15.8 and 15.0 Å, respectively, when the toluene complex and types I and II benzene complexes occupy the interlamellar regions. Since the basal spacing is *ca.* 9.6 Å under conditions where the interlamellar height is determined solely by the van der Waals radii of silicate oxygen atoms, the observed spacings for the toluene and benzene complexes are inconsistent with sandwich-type structures. Thus only one aromatic ring can be above a copper(II) ion on the surface.

Similar arguments allow us to rule out structures analogous to $(C_6H_6HgAlCl_4)_2$[22] or $(C_6H_6PdAl_2Cl_7)_2$[23] in which a metal–metal unit is contained between two arene rings acting formally as three-electron donors to each of the two metal atoms. The fact that no decrease in electron spin density on copper is observed for the two benzene complexes and the toluene complex, of course, precludes any structures containing a copper–copper interaction.

In the case of the type I arene complexes, in which the aromatic ring is planar and the π electrons are delocalized, the copper(II) ion may be bonded either to the center of the aromatic ring or to a ring edge as in $C_6H_6AgClO_4$.[24] Due largely to the work of Amma and his coworkers,[25-28] a considerable number of edge-bonded arene complexes of silver(I) and copper(I) are known, but unfortunately very sparse spectroscopic data are available. However, a comparison of vibrational frequencies is possible for the type I copper(II)–benzene complex,[3] known π-bonded benzene complexes,[29] and $C_6H_6AgClO_4$.[30,31] Among the three types of complexes the ir spectra in the 1500–1200- and 800–600-cm^{-1} regions are qualitatively similar with the C–C stretching frequencies shifted to lower energy and the out-of-plane C–H deformations shifted to higher energy. The magnitudes of the shifts for the type I benzene complex (-8 and $+31$ cm^{-1}) lie nearer those for (C_6H_6)-$AgClO_4$ (~-20 cm and $+33$ cm—^{1}) than for those normally observed for π-bonded C_6H_6 rings (~-50 and $\sim+100$ cm^{-1}) and tend to support an edge-bonded structure. Important differences in other spectral regions occur between $C_6H_6AgClO_4$ and π-bonded C_6H_6 rings, but these regions were not observable for the type I benzene–copper(II) complex due to absorptions of the silicate lattice.

Amma has emphasized the importance of metal–anion interactions in determining the stability of edge-bonded arene complexes. The silicate structure obviously plays an important role in stabilizing the type I copper(II)–arene complexes observed here as they immediately decompose when displaced from the surface by $N(CH_3)_4^+$ ions. Since the 1630-cm^{-1} deformation frequency of water is always observed in the presence of the type I complexes, the copper(II) ion may not be directly bonded to silicate oxygens but instead linked to these atoms through bridging water molecules. Many models can be proposed for the environment of copper(II) on the silicate surface. For example, based on the known lower hydrate phases of divalent cations exchange forms of montmorillonite,[4,32] it is reasonable to suppose that there are three water molecules per cation in a type I complex. Under these conditions the coordinated water molecules may hydrogen bond to the three oxygens on an SiO_4 tetrahedral face and provide a C_{3v} environment suitable for overlap of the empty 4s or sp^3 orbital on copper(II) and the highest filled e_1 orbital on benzene. A similar environment is found for copper(I) in $C_6H_6CuAlCl_4$.[25]

We do not wish to imply, however, that 1:1 complexes are expected in all cases. The situation could easily be as complicated as that for crystalline arene complexes of silver(I). In $(C_6H_6)AgClO_4$ the cation is bonded to the edges of two C_6H_6 rings and the anion is passive, whereas in $(C_6H_6)AgAlCl_4$ five-coordination of silver(I) is achieved by bonding to four chlorine atoms of an infinite $AlCl_4^-$ sheet and to an edge of one C_6H_6 ring. *m*-Xylene, on the other hand, forms a 2:1 complex with $AgClO_4$ in which the cation is tetrahedrally coordinated to two chlorine atoms and to the edges of two benzene rings. Similar variations in the coordination of copper(II) among the type I complexes may account for the differences in the electronic spectra, especially those between benzene and the methyl-substituted derivatives.

We have no cogent explanation for the failure of methyl-substituted benzenes to form complexes analogous to the type II benzene complex, except to suggest that steric factors may hinder the ring distortions necessary for localization of the π electrons in the C_6 ring and subsequent coordination to the metal ion. The localization of π electrons is indeed rare in metal–arene complexes, but it is definitely known to occur in $(\pi\text{-}C_5H_5)Rh[C_6(CF_3)_6]$,[33] wherein the metal forms two σ bonds to two carbon atoms and one π bond to a localized C=C bond on the dihedral ring.[34]

(22) R. W. Turner and E. L. Amma, *J. Inorg. Nucl. Chem.*, **28**, 2411 (1966).

(23) G. Allegra, A. Immirzi, and L. Porri, *J. Amer. Chem. Soc.*, **87**, 1394 (1965).

(24) H. G. Smith and R. E. Rundle, *ibid.*, **80**, 5075 (1958).

(25) R. W. Turner and E. L. Amma, *ibid.*, **88**, 1877 (1966).

(26) R. W. Turner and E. L. Amma, *ibid.*, **88**, 3243 (1966).

(27) I. F. Taylor, Jr., E. A. Hall, and E. L. Amma, *ibid.*, **91**, 5745 (1969).

(28) E. A. Hall and E. L. Amma, *ibid.*, **91**, 6538 (1969).

(29) H. P. Fritz, *Advan. Organometal. Chem.*, **1**, 240 (1964).

(30) L. W. Daasch, *ibid.*, **15**, 726 (1959).

(31) G. Karagounis and O. Petter, *Z. Elektrochem.*, **63**, 1120 (1959).

(32) G. F. Walker, *Clays Clay Miner.*, **4**, 101 (1956).

(33) R. S. Dickson and G. Wilkinson, *J. Chem. Soc.*, 2699 (1964).

(34) M. R. Churchill and R. Mason, *Proc. Chem. Soc., London*, 365 (1963).

A Proton Magnetic Resonance Study of the Hydrogen Bonding of Alkylated Bases to Dimethyl Sulfoxide

by Raymond C. Fort, Jr.,* and Ted R. Lindstrom

Department of Chemistry Kent State University, Kent, Ohio

(Received June 18, 1971)

Publication costs borne completely by The Journal of Physical Chemistry

Iterative computer programs have been devised to treat the data obtained in a proton magnetic resonance study of 1-methyluracil, 1-methylcytosine, 9-ethyladenine, and 9-ethylguanine in dimethyl sulfoxide-d_6. Thermodynamic data for the hydrogen bonding of the NH protons of these bases to the dimethyl sulfoxide are derived thereby. The method appears capable of extension to the determination of intrinsic base-pairing energies.

A number of groups have applied proton magnetic resonance spectroscopy to the study of interactions involving purine or pyrimidine bases.[1-17] Although associations by means of hydrogen bonds, etc., are qualitatively easy to detect by this means, difficulties arise when one tries to evaluate equilibrium constants and enthalpies for the associations.

A serious obstacle to the application of the typical pmr approach to hydrogen-bonding equilibria is that the computations[18-23] which yield the thermodynamic parameters require a knowledge of the chemical shifts of the unassociated species under consideration. Because the purine and pyrimidine bases do not dissolve to an extent detectable by pmr spectroscopy in any solvent with which they do not associate, such data are experimentally unavailable. For this reason, it has been customary to take a hydrogen-bonded solute–solvent complex as a reference state and to assume for base-pairing purposes that no free monomer is present.[11] This assumption is almost certainly incorrect,[20] and base-pairing energies obtained by employing it are therefore incorrect.

We felt that an evaluation of the solute–solvent interactions themselves would be a valuable first step toward making available the precise energetics involved in various base-pairing schemes. For reasons of solubility, we chose to investigate first the alkylated bases 1-methyluracil, 1-methylcytosine, 9-ethyladenine, and 9-ethylguanine in dimethyl sulfoxide-d_6 solution.

Experimental Section

The 1-methyluracil, 1-methylcytosine, 9-ethyladenine, and 9-ethylguanine were purchased from Cyclo Chemical Corp., Los Angeles, and were dried before use in an Abderhalden pistol charged with P_2O_5. Dimethyl sulfoxide-d_6 was purchased from Merck Sharpe and Dohme and stored over Linde 4A molecular sieves. No water was detectable by pmr spectroscopy.

Samples were prepared directly in 5-mm pmr tubes by weighing, and trace quantities of tetramethylsilane and cyclohexane added to serve as a double internal standard. The tubes were then sealed. The entire sample preparation was conducted in a glove box under dry nitrogen. When these precautions were not taken, NH resonance lines were appreciably broadened, apparently by exchange.

The pmr measurements were made with a Varian As-

---

[1] C. D. Jardetzky and O. Jardetzky, *J. Amer. Chem. Soc.*, **82**, 222 (1960).

[2] O. Jardetzky, P. Pappas, and N. G. Wade, *ibid.*, **85**, 1657 (1963).

[3] F. J. Bullock and O. Jardetzky, *J. Org. Chem.*, **29**, 1988 (1964).

[4] J. P. Kokko, J. H. Goldstein, and L. Mandel, *J. Amer. Chem. Soc.*, **83**, 2909 (1961).

[5] L. Gatlin and J. C. Davis, *ibid.*, **84**, 4464 (1962).

[6] S. I. Chan, M. P. Schweizer, P. O. P. Ts'o, and G. M. Helmkamp, *ibid.*, **86**, 4182 (1964).

[7] M. P. Schweizer, S. I. Chan, and P. O. P. Ts'o, *ibid.*, **87**, 5241 (1965).

[8] B. W. Bangerter and S. I. Chan, *ibid.*, **91**, 3910 (1969).

[9] L. Katz and S. Penman, *J. Mol. Biol.*, **15**, 220 (1966).

[10] L. Katz, *ibid.*, **44**, 279 (1969).

[11] R. Newmark and C. Cantor, *J. Amer. Chem. Soc.*, **90**, 5010 (1968).

[12] R. R. Shoup, H. T. Miles and E. D. Becker, *Biochem. Biophys. Res. Commun.*, **23**, 194 (1966).

[13] S. M. Wang and N. C. Li, *J. Amer. Chem. Soc.*, **90**, 5069 (1968).

[14] Y. Inoue and S. Aoyagi, *Biochem. Biophys. Res. Commun.*, **28**, 973 (1967).

[15] J. H. Prestegard and S. I. Chan, *J. Amer. Chem. Soc.*, **91**, 2843 (1969).

[16] F. K. Schweighardt, C. Moll, and N. C. Li, *J. Mag. Res.*, **2**, 35 (1970).

[17] The above listing is intended to be representative, rather than complete.

[18] R. J. Abraham, *Mol. Phys.*, **4**, 369 (1971).

[19] M. W. Hanna and A. L. Ashbaugh, *J. Phys. Chem.*, **68**, 811 (1964).

[20] D. Porter and W. S. Brey, *ibid.*, **71**, 3779 (1967); **72**, 650 (1968).

[21] P. O. Groves, P. J. Huck, and J. Homer, *Chem. Ind. (London)*, 915 (1967).

[22] J. Homer and P. J. Huck, *J. Chem. Soc. A*, 277 (1968).

[23] R. C. Fort, Jr., and T. R. Lindstrom, *Tetrahedron*, **23**, 3227 (1967).

sociates A-60 spectrometer. Because of the low concentration of the bases (0.004 to 0.028 mole fraction), sensitivity enhancement with a Varian C-1024 computer of average transients was necessary. Chemical shifts reproducible to ±1.0 Hz were obtained by modulating the spectrometer field with a Hewlett-Packard 200 AB audiooscillator so that the sample peak was bracketed by the side bands of TMS and cylohexane. A Hewlett-Packard 5512A frequency counter was used to monitor the modulating frequency.

Temperature measurements were made with the standard charts supplied by Varian, and calibration was checked occasionally with a Leeds and Northrup recording thermocouple (for the loan of which we thank the KSU Physics Department). Reported temperatures are the average of readings obtained before and after the spectrum was taken, and are probably accurate to ±1.0°.

For each sample, the chemical shift was measured as a function of temperature at eight to ten intervals over the whole liquid range of the solvent. The data so obtained were used as input to our FORTRAN IV programs, processed on a Burroughs 5500 computer in the KSU Computer Center.

Results and Discussion

Figures 1–4 present the observed variations of chemical shift with temperature for the four bases. The observed upfield shift with increasing temperature is typical for the disruption of hydrogen bonds;[24] *a priori* it could arise from disruption of hydrogen bonds to the solvent or from shifting of a monomer–dimer equilibrium involving only the base. These two possibilities can be distinguished by considering the concentration dependence of the chemical shifts.

Dimerization requires a significant variation of shift with concentration, even when the latter is small. For hydrogen bonding to the solvent, which is present in large excess, the chemical shift should become essentially independent of concentration at low concentrations.[24] Table I shows that in fact, the chemical shift *is* independent of concentration in the range employed in this study. Therefore the chemical shift changes are

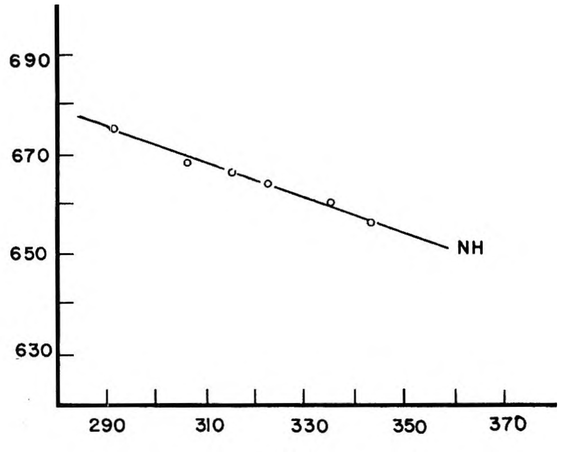

Figure 1. Temperature dependence of the chemical shift of 1-methyluracil.

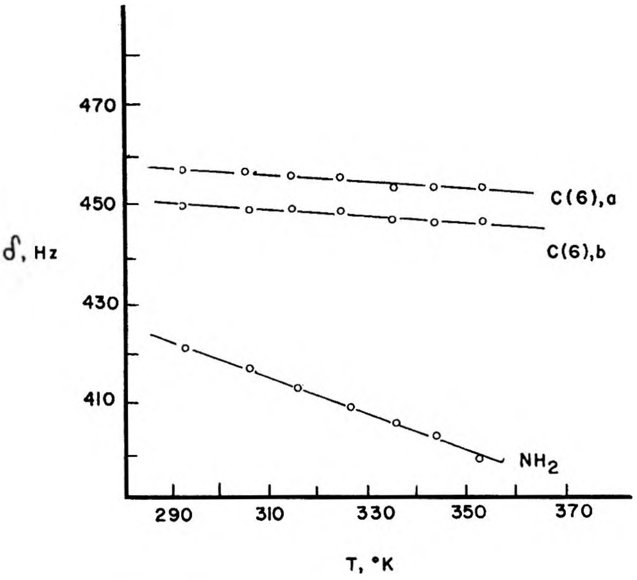

Figure 2. Temperature dependence of the chemical shifts of 1-methylcytosine; C(6), a and C(6), b are the two lines of the hydrogen on C(6).

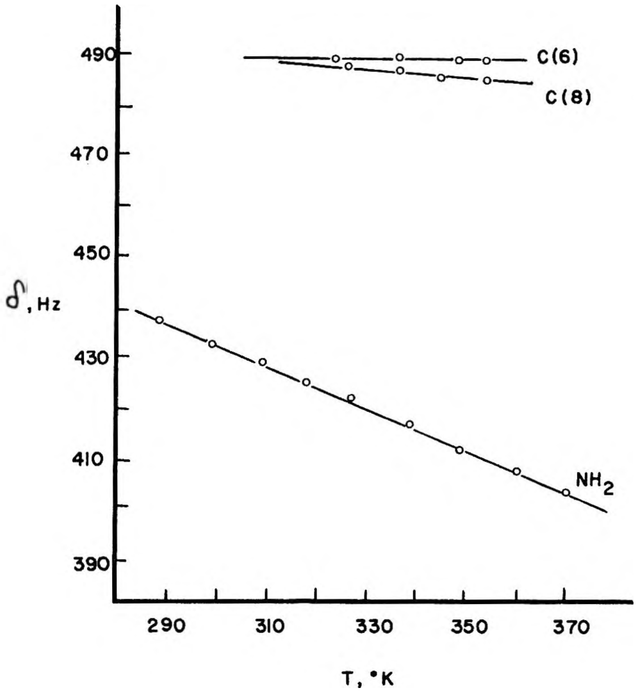

Figure 3. Temperature dependence of the chemical shifts of 9-ethyladenine; C(6) and C(8) are the two hydrogens on carbon.

---

[24] *Cf.* J. A. Pople, W. G. Schneider, and H. J. Bernstein, "High Resolution Nuclear Magnetic Resonance," McGraw-Hill, New York, N. Y., 1959, Chapter 15.

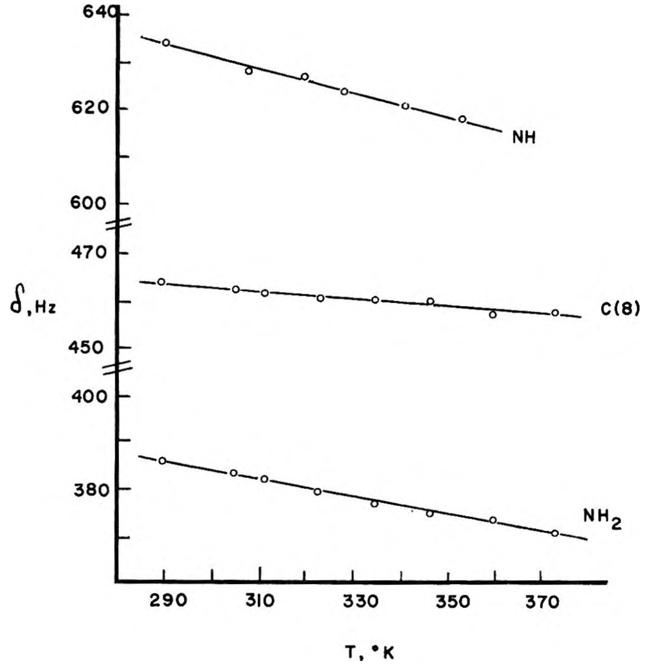

Figure 4. Temperature dependence of the chemical shifts of 9-ethylguanine; C(8) is the hydrogen on carbon.

Table I: Concentration Dependence of Chemical Shifts

Base	Concn[a]	T, °K	δ_{NH}[b]	δ_{NH_2}[b]
1-Methyluracil	0.00824	291	675.2	...
	0.01270	291	675.2	...
	0.01830	291	675.0	...
	0.0286	290	675.0	...
1-Methylcytosine	0.0049	292	...	419.4
	0.0070	293	...	419.6
	0.0142	292	...	421.4
	0.0183	292	...	420.8
9-Ethyladenine	0.0059	289	434.0	...
	0.0080	289	433.1	...
	0.0123	289	434.3	...
9-Ethylguanine	0.0040	290	634.6	386.9
	0.0070	290	636.7	388.0
	0.01175	290	637.6	388.9

[a] Mole fraction solute. [b] In Hz downfield from TMS at 60 MHz; ±1.0 Hz.

attributable to the equilibrium

$$\text{solute} + \text{solvent} = \text{complex} \qquad (1)$$

The derivation of the thermodynamic constants for equilibrium 1 was approached in the following fashion. Abraham[18] has shown that eq 2 and 3 may be applied

$$K = \frac{\delta_{\text{obsd}} - \delta_{\text{F}}}{\delta_{\text{C}} - \delta_{\text{F}}} \qquad (2)$$

$$K = e^{-\Delta H/RT} e^{\Delta S/R} \qquad (3)$$

to the determination of association constants by pmr spectroscopy. Here K is the association constant, δ_C is the chemical shift of a proton in the complex, and δ_F is the chemical shift of that proton in the unassociated state.

In our study, δ_F is an unknown, for reasons discussed above, and likewise δ_C cannot be directly obtained because the usual procedure of extrapolating a chemical shift *vs.* temperature plot to absolute zero is probably invalid.[23,25,26] We therefore devised several iterative computer programs to analyze the data.

The program HBCOMP/HBFREE uses eq 2 and 3 and treats the problem as follows. Starting values of δ_C and δ_F are chosen and employed with the observed chemical shifts to compute a series of K's for the various temperatures. A van't Hoff plot is then made, and the standard deviation from the best least-squares fit is obtained. A new value of δ_C is now chosen according to a predetermined scheme, and the computations are repeated; the value of δ_F remains the same. That value of δ_C which gives the minimum error in the van't Hoff plot is then held constant, while δ_F is varied in a search for the minimum error. This alternation is repeated over the whole range of reasonable values for the two shifts. The minimum deviation from the van't Hoff plot over this whole range is taken to be that associated with the "true" values of the thermodynamic parameters for the solute–solvent association. Table II contains the results of the application of this program.

Table II: Thermodynamic Constants and Calculated Chemical Shifts, HBCOMP/HBFREE

Site	$-\Delta H$, kcal/mol[a]	K_{25}[b]	δ_{comp}[c]	δ_{free}[c]
1-Methyluracil NH	1.74	6.80	715.0	388.5
1-Methylcytosine NH_2	2.29	3.92	456.5	274.5
9-Ethyladenine NH_2	2.42	3.84	469.0	286.5
9-Ethylguanine NH	1.76	4.90	675.0	447.5
9-Ethylguanine NH_2	2.27	3.92	408.5	307.5

[a] ±0.2 kcal. [b] Computed using concentration in mole fraction. [c] In Hz downfield from TMS on 60 MHz, calculated.

It is extremely important in such an approach as this, with so many variables affecting the shape of the potential energy surface, to establish that one is looking at a true minimum in the error function—*i.e.*, that one has fallen into the deepest well on the surface. To this end, the starting points and assigned ranges of δ_C and δ_F were varied widely; always the error minima were found at the locations described in Table II.

Nonetheless, further confirmation was sought, and a second program was devised. This program, HYBOND, begins by assuming values for δ_C, δ_F, ΔH, and ΔS. The enthalpy and entropy values are used in eq 3 to calcu-

---

(25) P. Laszlo and D. H. Williams, *J. Amer. Chem. Soc.*, **88**, 2799 (1966).

(26) I. D. Kuntz and M. D. Johnson, *ibid.*, **89**, 6008 (1967).

late an association constant for each temperature. The K's are then used with the assumed chemical shifts in eq 4[27] to calculate the expected chemical shift at each temperature. The difference between the observed and calculated chemical shifts is noted. Each of the four unknown quantities is then varied in turn, and the resultant change in the difference between observed and calculated chemical shifts is noted for each. Finally, each of the variables is altered by an amount proportional to the effect it had on the error function. This cycle is repeated until a minimum difference is observed. The results derived in this manner are given in Table III.

Table III: Thermodynamic Constants and Calculated Chemical Shifts, HYBOND

Site	$-\Delta H$, kcal/mol[a]	K_{25}[b]	δ_{comp}[c]	δ_{free}[c]
1-Methyluracil NH	1.72	6.00	715.2	379.9
1-Methylcytosine NH_2	2.27	4.00	456.5	269.4
9-Ethyladenine NH_2	2.36	3.00	469.7	279.1
9-Ethylguanine NH	1.73	5.00	675.3	439.8
9-Ethylguanine NH_2	2.15	4.00	409.3	297.6

[a] ±0.2 kcal. [b] Computed using concentration in mole fraction. [c] In Hz downfield from TMS at 60 MHz, calculated.

It is gratifying to find that the results from the two methods of computation are virtually identical. The ability of two different programs to arrive at the same set of values gives confidence in the conclusion that these parameters do describe the hydrogen-bonding interactions of the bases with dimethyl sulfoxide.

In discussing the data in Tables II and III, it would be useful to have available similar data for simple amines and amides with which to compare our results. Regrettably, such information is essentially nonexistent. Porter and Brey[20] determined the enthalpies of association of succinimide and pyrrole with dimethyl sulfoxide to be -5.0 and -3.0 kcal, respectively; however, the succinimide value is measured with respect to the solvated succinimide dimer, rather than the monomer, and thus is not directly comparable. The enthalpy of -3.4 kcal obtained for the association between *N*,*O*-dibenzylhyhydroxylamine and DMSO[28] involves too dissimilar a compound to be of comparative value.

Comments upon our observation that amide NH bonds of uracil and guanine appear to form weaker hydrogen bonds than amine NH's of cytosine, adenine, and guanine must therefore be limited. Acidity, the most common indicator of propensity for hydrogen bond formation, would suggest that the reverse order is to be expected. Thus, the pK_a's of the amide protons in 1-methyluracil and 9-methylguanine are both about 9.8,[29] and a pK_a near 12 is likely for the NH_2 groups of cytosine and adenine.[29] On the other hand, the stronger amine hydrogen bonds agree with the results of molecular orbital calculations by Pullman and Pullman.[30] The net σ charges on the amine hydrogens of cytosine, adenine, and guanine are $+0.229$, $+0.230$, and $+0.231$, respectively, while the net σ charges for the amide hydrogens of uracil and guanine are $+0.195$ and $+0.196$, respectively. The greater positive charge on the amine hydrogens implies that they should form stronger hydrogen bonds with a given acceptor, in accord with our data.

Although the data are not comparable in any strict sense, our results can be used in conjunction with the results of Newmark and Cantor[11] to estimate the guanine–cytosine interaction energy. Newmark and Cantor determined that the enthalpy change for conversion from the base–solvent (dimethyl sulfoxide) associations to the base–base association is -5.7 kcal/mol. From Table III, ΔH for the dissociation of the guanine/DMSO hydrogen bonds is $2.2 + 1.7 = +3.9$ kcal/mol, and for the cytosine/DMSO hydrogen bond, $\Delta H = +2.3$ kcal/mol. Thus interactions totaling 6.2 kcal/mol are disrupted to allow base pairing. The entire process liberates $+5.7$ kcal/mol, so that the actual ΔH for base pairing is -11.9 kcal/mol, or about 4 kcal/mol of hydrogen bonds.

As noted above, there are no data available with which to compare the result of this analysis. Nonetheless, it appears that the approach developed in this paper may make available, readily, a wide range of data regarding the hydrogen-bonding capabilities of purine and pyrimidine bases. Further studies are in progress.

Acknowledgments. We wish to extend our most sincere thanks to Dr. John Reed for his extensive and invaluable assistance in the early stages of our programming efforts. T. R. L. acknowledges the fellowship support of the National Aeronautics and Space Administration.

---

(27) This is a rearranged version of eq 2.

(28) H. Feuer, D. Pelle, D. M. Braunstein, and C. N. R. Rao, *Spectrochim. Acta, Part A*, **25**, 1393 (1969).

(29) A. Albert, "Physical Methods in Heterocyclic Chemistry," A. R. Katritzky, Ed., Academic Press, New York, N. Y., 1963.

(30) A. Pullman and B. Pullman, *Advan. Quant. Chem.*, **4**, 267 (1968).

Field-Dependent Contributions to Carbon-13 Nuclear Relaxation

by **James R. Lyerla, Jr., David M. Grant,* and Richard D. Bertrand**

Department of Chemistry, University of Utah, Salt Lake City, Utah 84112 *(Received April 26, 1971)*

Publication costs assisted by the National Institutes of Health

The effect of field-dependent relaxation mechanisms on carbon-13 spin-lattice relaxation times has been examined for CS_2 and seven members of the halomethane series. Field-dependent and temperature-dependent studies indicate the anisotropy mechanism does contribute to the relaxation in CS_2. Field-dependent studies, carbon-hydrogen dipole-dipole relaxation times, and C-H nuclear Overhauser effects demonstrate the existence of an efficient scalar-coupling mechanism in the bromomethanes which is absent in the chloromethanes and small in the iodomethanes.

I. Introduction

The spin-lattice relaxation process for spin $^1/_2$ nuclei is subject to a variety of contributing relaxation mechanisms. Assuming the absence of paramagnetic impurities, the nuclear relaxation in pure diamagnetic liquids may be determined by inter- and intramolecular nuclear dipole-dipole, spin-rotation, chemical shift anisotropy, and scalar-coupling interactions. All or any combination of the above mechanisms may operate in a particular liquid. Most investigations of spin-lattice relaxation times (T_1) in spin $^1/_2$ systems have illustrated that the dipole-dipole and spin-rotation pathways usually dominate the relaxation process. Conversely, few systems have been investigated in which the chemical shift anisotropy or scalar-coupling process contribute to T_1. As these two mechanisms depend on the magnitude of the applied magnetic field, they are readily identified from other relaxation modes by field-dependent studies. Herein are reported the results of such studies on the role of field-dependent mechanisms in determining carbon-13 spin-lattice relaxation times in representative chemical systems.

II. Experimental Section

All the experiments were performed at two field strengths: 14.1 kG using a Varian AFS-60 spectrometer and 23.5 kG using a Varian XL-100-15 spectrometer. Selective and pseudo-random noise proton decoupling was available on both instruments. Adiabatic rapid passage techniques[1] were used to determine T_1 values. Nuclear Overhauser measurements were determined in the manner previously described.[2,3] Temperature-dependent studies on CS_2 were performed on the XL-100-15, and the reported temperatures are accurate within ±3°.

The degassed CS_2 sample, ~60% enriched in the ^{13}C isotope, was obtained from Pro Chem Ltd. The halomethanes studied were obtained from standard sources. All samples were thoroughly degassed *via* freeze-pump-thaw techniques and sealed in 10 mm o.d. nmr tubes prior to determining T_1.

III. Results and Discussion

A. Chemical Shift Anisotropy. The carbon disulfide (CS_2) molecule presents a unique system in which to study the potential importance of the chemical shift anisotropy mechanism as no opportunity exists for the dipole-dipole or scalar-coupling relaxation processes to operate. Hence the T_1 of CS_2 is subject to only spin-rotation and chemical shift anisotropy mechanisms. As the spin-rotation contribution is independent of field strength, the anisotropy contribution should be reflected in the field dependence of T_1. The results for T_1 at 14.1 and 23.5 kG and at 311°K are reported in Table I.

The close agreement of the T_1 values at the two different fields indicates a negligible contribution of anisotropy to T_1 at fields up to 23.5 kG, and it must be assumed that the relaxation process is totally dominated by the spin-rotation mode at room temperature. This finding fails to support the earlier[4] relaxation work on CS_2 obtained at 9.3 and 14.1 kG. Based on these former results a contribution of 20.9 sec is predicted for the shift anisotropy process at 23.5 kG and room temperature in contradiction to the findings reported herein.

To further investigate the contribution of chemical shift anisotropy to the carbon-13 relaxation in CS_2 a temperature-dependent study of T_1 at 23.5 kG was performed. As the spin-rotation and shift anisotropy mechanisms have opposite dependence on temperature, a plot (an Arrhenius temperature dependence is as-

---

(1) T. D. Alger, S. C. Collins, and D. M. Grant, *J. Chem. Phys.*, **54**, 2820 (1971).

(2) J. R. Lyerla, Jr., D. M. Grant, and R. K. Harris, *J. Phys. Chem.*, **75**, 585 (1971).

(3) K. F. Kuhlmann, D. M. Grant, and R. K. Harris, *J. Chem. Phys.*, **52**, 3439 (1970).

(4) A. Olivson, E. Lippmaa, and J. Past, *Est. NSV Tead. Aka. Toim., Fuus.-Mat.*, **16**, 390 (1967).

Table I: Carbon-13 Relaxation Results for CS_2

Temp.[a] °K	T_1,[b] sec	T_{1a},[c] sec	T_{1sr},[c] sec
311[d]	35.0		
311	33.8	2049	34.4
292	43.0	1593	44.2
277	50.0	1356	51.9
254	67.7	967	72.8
238	79.4	799	88.2
221	89.3	686	102.7
207	98.3	600	118.0
191	110.0	500	141.0
180	119.6	418	168.0

[a] Temperature is accurate to ±3°. [b] The error in individual T_1 measurements ranged from 5 to 12%. [c] Calculated using eq 4 and 5. [d] Result from AFS-60 spectrometer operating at 14.1 kG; all other results are from the XL-100-15 at 23.5 kG.

sumed) of log T_1 *vs.* inverse temperature should result in considerable deviations from linearity whenever both mechanisms are operative. The temperature-dependent T_1 results given in Table I for CS_2 (covering most of the range from the boiling to the freezing points) are illustrated in Figure 1 and found to exhibit the proposed curvature. Even though the spin-rotation process dominates over the whole temperature range due to its greater efficiency at the temperatures studied, the shift-anisotropy mechanism becomes significant at temperatures below ~221°K. At low temperature, the slower tumbling motions or increased correlation time for the anisotropy mechanism increases the efficiency of this process.

The explicit form of the two relaxation processes can be written for a linear molecule as

$$1/T_{1a} = \frac{2}{15}\omega_c^2(\Delta\sigma)^2\tau_a \tag{1}$$

and

$$1/T_{1sr} = \frac{8\pi^2}{3h^2}kTC^2I\tau_{sr} \tag{2}$$

where T_{1a} and T_{sr} denote the relaxation rates due to anisotropy and spin-rotation, respectively, ω_c the resonance frequency of ^{13}C at 23.5 kG, $\Delta\sigma$ the anisotropy in the chemical shielding of CS_2, τ_a the correlation time for molecular reorientation, I the moment of inertia, C the spin-rotation interaction constant, and τ_{sr} the angular momentum correlation time. Hubbard[5] has derived a relation between the two correlation times whenever the molecular reorientation is diffusion controlled. If this result is assumed to hold for CS_2, then

$$\tau_{sr}\tau_a = I/6kT \tag{3}$$

where $\tau_a \gg \tau_{sr}$ and the rate due to spin rotation can be written in terms of T_{1a}. Note, the two correlation times are the only nonconstant terms in eq 1 and 2 as the explicit temperature dependence in eq 2 is eliminated when the Hubbard relation is used. Employing the usual reciprocal relation between T_1 and the various contributions

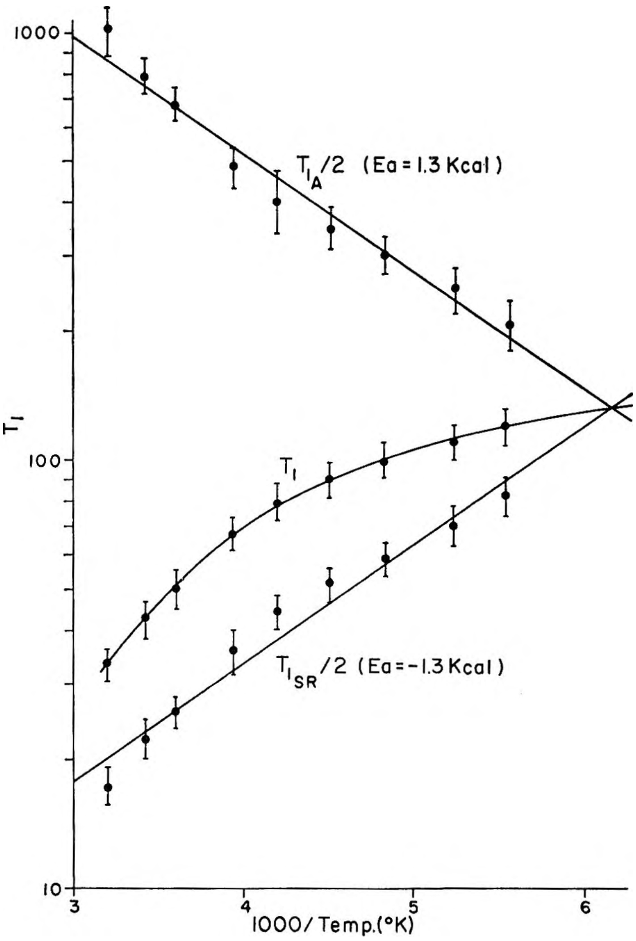

Figure 1. Illustration of the temperature-dependent ^{13}C T_1 results for CS_2 and the respective contributions of the shift-anisotropy (T_{1a} and spin-rotation (T_{1sr}) mechanisms to T_1.

$$1/T_1 = 1/T_{1sr} + 1/T_{1a} \tag{4}$$

and eq 1, 2, and 3, the following expression for T_{1a} is obtained

$$T_{1a}^2 - \frac{T_{1a}}{\lambda T_1} + 1 = 0 \tag{5}$$

where

$$\lambda = \frac{16\pi^2}{135}\frac{(CI)^2}{h^2}\omega_c^2(\Delta\sigma)^2$$

The values of $\Delta\sigma$ and C for CS_2 were calculated by referencing to the known rotation constant and shielding anisotropy in the CO molecule[6] *via* the method suggested by Flygare.[7-9] The estimated values for

---

(5) P. S. Hubbard, *Phys. Rev.*, **131**, 1155 (1963).

(6) I. Ozier, L. M. Crapo, and N. F. Ramsey, *J. Chem. Phys.*, **49**, 2314 (1968).

(7) W. H. Flygare, *ibid.*, **41**, 793 (1964).

Table II: Carbon-13 Relaxation Data for Some Halomethanes

Compound	Low field (14.1 kg)			High field (23.5 kg)		
	T_1, sec	η	T_{1D}, sec	T_1, sec	η	T_{1D}, sec
CH_3Br	8.5 ± 0.6	0.30 ± 0.03	56 ± 5	11.6 ± 1.8	0.43 ± 0.06	54 ± 5
CH_3I	11.1 ± 0.4	0.42 ± 0.05	52 ± 5	12.8 ± 0.6	0.51 ± 0.04	50 ± 5
CH_2Cl_2	18.0 ± 1.3	1.07 ± 0.07	32 ± 3	16.6 ± 1.5	1.00 ± 0.10	33 ± 3
CH_2Br_2	4.1 ± 0.4	0.36 ± 0.08	22 ± 4	5.9 ± 0.6	0.50 ± 0.09	24 ± 4
CH_2I_2	3.9 ± 0.5	1.55 ± 0.12	5 ± 2	4.3 ± 0.9	1.60 ± 0.16	5 ± 2
$CHCl_3$	23.8 ± 1.8	1.47 ± 0.11	32 ± 4	24.0 ± 1.5	1.53 ± 0.30	31 ± 6
$CHBr_3$	2.0 ± 0.3	0.30 ± 0.05	13 ± 3	2.2 ± 0.6	0.33 ± 0.08	13 ± 4

CS_2 using this approximate method are $C = 2.07$ kHz and $\Delta\sigma = -430$ ppm. Equation 5 was solved quadratically for T_{1a} at each T_1 value and the value of T_{1sr} deduced from the reciprocal relation given in eq 4. The respective values are also reported in Table I. The plus root was used from the quadratic expression to determine T_{1a} as the minus root predicted a physically untenable temperature dependence for T_{1a}. Also plotted in Figure 1 is the temperature dependence of the calculated shift-anisotropy and spin-rotation contributions. These plots roughly have a linear dependence on reciprocal temperature with an activation parameter of 1.2–1.3 kcal for both processes, which is in good agreement with the value of 1.4 kcal predicted from microviscosity theory[10] using temperature-dependent viscosity and density data for CS_2. This result tends to substantiate the use of a diffusion equation to describe the molecular reorientation in CS_2. Finally these results point out that even at 180°K the anisotropy mechanism constitutes only 30% of the total relaxation rate in CS_2. Hence the anisotropy mechanism while definitely demonstrable in CS_2 still assumes a minor role in the relaxation process at 23.5 kG.[11]

B. Scalar Coupling. The possibility of scalar-coupling contributions to C-13 spin–lattice relaxation times has been examined by considering several members of the halomethanes. Since the chlorine, bromine, and iodine nuclei are subject to relaxation by a fast quadrupolar mechanism, the carbon in the respective halomethanes may relax through a scalar interaction of the second kind, as defined by Abragam.[12] The halomethanes are also subject to C–H and C–X dipole–dipole and spin-rotation relaxation processes which could also affect T_1.

To demonstrate the existence of the scalar-coupling mechanism, the T_1's of seven members of the halomethane series were determined at 14.1 and 23.5 kG under proton-decoupled conditions by adiabatic rapid passage (ARP). The T_1's of the degassed samples were determined at 311°K. The relaxation results including nuclear Overhauser enhancement factors are reported in Table II. These data indicate that only the bromomethanes show a measurable field dependence, while a small field effect only slightly greater than experimental error is observed for CH_3I. The trend to longer relaxation times at higher fields is consistent with the inverse-field dependence of the scalar-coupling process which is given in the following equation

$$1/T_{1sc} = \frac{8}{3}\pi^2 J^2 S(S+1)\frac{T_{1Q}}{1 + (\Delta\omega)^2 T_{1Q}^2} \qquad (6)$$

where J is the scalar-coupling constant, $\Delta\omega$ the difference in resonance frequency of the two-coupled spins, S the spin quantum number of the quadrupolar nucleus, and T_{1Q} the corresponding spin–lattice relaxation time. If the denominator in eq 6 is such that $(\Delta\omega)^2 T_{1Q}^2 \gg 1$ then the mechanism will have a quadratic field dependence; if the two terms are comparable the field dependence of T_1 will be somewhat less than quadratic; and if $(\Delta\omega)^2 T_{1Q}^2 \ll 1$, the field dependence will be negligible over the usual field strengths employed in nmr spectroscopy and thus it is possible for T_1 to have *no field* dependence even though the scalar-coupling relaxation mechanism operates.

To determine whether scalar coupling is significant in the T_1's showing no field dependence and to calculate the magnitude of the scalar contribution in the bromine compounds, eq 6 is used to estimate T_{1sc}. This requires reasonable values for J and T_{1Q}, quantities not readily available for the majority of compounds studied here. J_{C-X} may be estimated from the relation

$$J_{C-X} = \frac{\gamma_X}{\gamma_H} J_{C-H} \qquad (7)$$

where J_{CH} is the known[13–15] carbon–hydrogen cou-

---

(8) W. H. Flygare and J. Goodisman, *J. Chem. Phys.*, **49**, 3122 (1968).

(9) C. Deverell, *Mol. Phys.*, **18**, 319 (1970).

(10) K. T. Gillen and J. H. Noggle, *J. Chem. Phys.*, **53**, 801 (1970).

(11) This conclusion is consistent with results reported at the "12th Experimental NMR Conference" at Gainesville, Fla., Feb 18–20, 1971, by H. W. Spiess. Evidence from CS_2 relaxation studies at 15, 30, and 62 MHz indicated small anisotropy relaxation contributions at the two lower fields while major contributions were found at 62 MHz.

(12) A. Abragam, "The Principles of Nuclear Magnetism," Oxford University Press, London, 1961, Chapter VIII.

(13) N. Muller and D. E. Pritchard, *J. Chem. Phys.*, **31**, 1471 (1959).

(14) E. R. Malinowsky, *J. Amer. Chem. Soc.*, **83**, 4479 (1961).

(15) G. S. Reddy and J. H. Goldstein, *J. Chem. Phys.*, **38**, 2736 (1963).

pling constant for a particular member of the halomethane series. An approximate value for T_{1Q} may be calculated from the relation[12]

$$1/T_{1Q} = \frac{3}{40}\,\frac{2S+3}{S^2(2S-1)}\,4\pi^2\left(\frac{e^2Qq}{h}\right)^2\tau_c \qquad (8)$$

where e^2Qq/h is the quadrupolar coupling constant and τ_c the molecular reorientation time. Microviscosity and density data[10,16,17] were used to estimate τ_c for the highly anisotropic CH_3Br and CH_3I molecules. In evaluating T_{1Q} for the remaining molecules, the value of τ_c was determined from the proton carbon-13 dipolar relaxation times, T_{1D}. This requires the separation of T_{1D} from T_1 *via* the relation[1-3]

$$T_{1D} = \frac{T_1}{2\eta}\,\frac{\gamma_H}{\gamma_C} \qquad (9)$$

where γ_H/γ_C is the ratio of magnetogyric ratios and η is the nuclear Overhauser enhancement factor. Values of T_{1D} are given in Table II, along with the experimental values for T_1 and η at two different field strengths. It is worth noting that T_{1D} for each molecule at both field strengths exhibits within experimental error the expected field invariance. These values of T_{1D} were then used to evaluate τ_c *via* the standard expression[12]

$$\frac{1}{T_{1D}} = \sum_i \frac{\gamma_H{}^2\gamma_C{}^2\tau_c{}^2}{r_{CH_i}{}^6} \qquad (10)$$

where the sum is over all directly bound protons. These various estimates for τ_c and quadrupolar couplings along with the ensuing values for T_{1Q} are given in Table III. The values of T_{1sc} calculated with eq 6 from the estimated J's and T_{1Q}'s, outlined above, are also reported in Table III.

The predicted T_{1sc} values for both isotopes of bromine (79 and 81) and of chlorine (35 and 37) are given in Table III as they are of comparable abundance in both cases. Strictly considered, the decay patterns of isotopic mixtures will be characterized by linear combinations of exponential terms with different relaxation constants, but since experimental deviations from simple exponential relationship were negligible, the data were treated with a single "effective" T_1. A more detailed study with isotopically pure species is required for a specific study of isotopic effects. Even so, the estimates given in Table III discriminate between the various isotopic species, and it is observed that the predicted T_{1sc} values indicate that the ^{79}Br isotope contributes significantly to the carbon relaxation process through scalar coupling. Furthermore, the predicted field dependence of T_{1sc} indicates a dependence much less than quadratic as $(\Delta\omega)^2T_{1Q}{}^2$ is not greater than one in the three bromo compounds. The high efficiency of T_{1sc} in bromo compounds arises from the relatively small $\Delta\omega$. The ^{13}C resonance frequency is 15.087 MHz, and the ^{79}Br value is 15.023 MHz. In the other compounds and in general for most scalar couplings with quadrupolar nuclei $\Delta\omega$ is much larger, leading to a low efficiency in the scalar-coupling mechanism for T_1. Thus, the carbon-13–bromine pair of nuclei are rather unique because of the close proximity of their resonance frequencies.[18]

Table III: Predicted Values of T_{1sc} at 14.1 and 23.5 kG for Some Halomethanes[a]

Compound	$\tau_c{}^b \times 10^{+12}$, sec	e^2qQ/h,[c] MHz	$T_{1Q} \times 10^{+7}$, sec	$T_{1sc}{}^{14.1}$, sec	$T_{1sc}{}^{23.5}$, sec
$CH_3{}^{79}Br$	0.87	553	9.4	8.3	9.7
$CH_3{}^{81}Br$		462	13.5	476	1326
CH_3I	1.1	1850	2.8	518	1440
$CH_2{}^{35}Cl_2$	0.64	72	707	3.2×10^6	14×10^6
$CH_2{}^{37}Cl_2$		57	1230	6.5×10^6	27×10^6
$CH_2{}^{79}Br_2$	0.84	586	8.8	3.1	3.6
$CH_2{}^{81}Br_2$		490	12.6	157	435
CH_2I_2	3.7	1993	0.72	36	78
$CH^{35}Cl_3$	1.2	79	339[d]	0.9×10^6	2.5×10^6
$CH^{37}Cl_3$		62	560	1.9×10^6	5.0×10^6
$CH^{79}Br_3$	2.8	629	2.3	5.3	5.5
$CH^{81}Br_3$		523	3.3	24	61

[a] Values are given only for the isotopically pure species. The scalar-coupling relaxation times for the mixed species such as $CH_2{}^{79}Br^{81}Br$ may be obtained from the approximate average of the reciprocal times recorded for the isotopically pure compounds. [b] These correlation times are calculated from eq 10 using the T_{1D} values given in Table II except for the very anisotropic CH_3Br and CH_3I. In these latter two cases τ_c was taken from microviscosity and density data (see ref 10). As the T_{1D} values are for normally occurring isotopic compositions, the corresponding τ_c values, therefore, will be isotopically weighted averages. While the various isotopic species of each compound will have slightly different moments of inertia and, therefore, different rotational diffusion constants, this variation should be negligible compared with the other errors encountered in this calculation. [c] Average value of gas and solid data taken from Y. Saito, *Can. J. Chem.*, **43**, 2430 (1965), and B. P. Dailey, *J. Chem. Phys.*, **33**, 1641 (1960). [d] This estimated value for T_{1Q} in the liquid state compares favorably with the 350×10^{-8} sec value obtained by W. T. Huntress, Jr., *J. Phys. Chem.*, **73**, 103 (1969). This agreement lends support to the process of estimating the quadrupole couplings and correlation times.

---

(16) E. Hatscheck, "The Viscosity of Liquids," Van Nostrand, Princeton, N. J., 1928.

(17) "Viscosity and Density Data from International Critical Tables," McGraw-Hill, New York, N. Y., 1933.

(18) Because of the second term in $1/T_{2sc} = {}^4/_3\pi^2J^2S(S+1)[(T_{1Q}/1 + (\Delta\omega)^2T_{1Q}{}^2) + T_{1Q}]$, T_{2sc} times of spin $^1/_2$ nuclei are generally very efficient when coupled with a quadrupole nucleus. However, it is to be noted that $T_{1sc} = T_{2sc}$ whenever $(\Delta\omega)^2T_{1Q}{}^2 \ll 1$. As $(\Delta\omega)^2T_{1Q}{}^2 \approx 0.1$ for ^{79}Br in this study one may expect $T_{1sc} \approx T_{2sc}$. R. Freeman and H. Hill (preprint of talk given at the 5th Conference on Molecular Spectroscopy, Brighton, England, Sept 22, 1971) have observed this general equivalence of T_1 and T_2 along with the significant shortening of T_1 for the carbon attached to bromine in *p*-bromobenzonitrile. We are very appreciative for this prepublication information and valuable discussions with Dr. Freeman regarding this important point which corroborates the dominance of the scalar-coupling mechanism for carbons attached to bromine atoms.

The theoretical estimates of T_{1sc} for CH_3I and CH_2I_2 indicate that for these species the scalar coupling could account for 3 and 10% of the respective overall T_1 values. Thus, some of the shortening in CH_2I_2 may be attributable to this mechanism even though the experimental errors do mask the effect. However, in the instance of CH_3I, the 1.7 sec lengthening in T_1 at high fields cannot be completely ascribed to the field dependence of the scalar-coupling mechanism and may reflect an unfavorable combination of errors. The error-free values probably are much closer together.

Also of importance in this study are the trends observed in the C–H dipolar relaxation times. These values are consistent with the structural features such as the reduction of $1/T_{1D}$ in CH_3Br and CH_3I due to the facility of motion about the C_3 axis. The effect of increased moments of inertia and/or viscosity in going from CH_2Cl_2 to CH_2I_2 and continuing in $CHCl_3$ and $CHBr_3$ is also reflected in the T_{1D} values as these changes should result in longer correlation times and more efficient dipolar relaxation rates. The normal T_{1D} values found for the bromomethanes when the overall $1/T_1$ rates are so unusually high provides confirmatory evidence that some other relaxation mechanism operates in the bromomethanes. As the spin-rotation contributions in the bromomethanes should be intermediate between the chloro and iodo species in the respective $CH_{4n}X_n$ compounds, one may rule out the possibility of the spin-rotation mechanism producing the very efficient T_1 process required in the bromomethanes. Bromine–carbon-13 dipolar relaxation of the carbon-13 nucleus is not dominant due to the rather large C–Br bond distance which is raised to the inverse sixth power even though the magnetic moment is one of the largest comparing favorably with that of the proton.

The above arguments, although in some instances qualitative, do provide substantial support for the scalar-coupling mechanism as the dominant relaxation mechanism for carbons bound to bromine. A small effect from this mechanism may be present in some iodine compounds, but chlorine is not expected to affect T_1. Further investigations are being carried out on other C–Br systems and a more quantitative evaluation considering the two Br isotopes is to be conducted.

Acknowledgment. This research was supported by the National Institutes of Health under Grant No. GM-08521.

Some Observations Concerning Nuclear Magnetic Resonance Proton Shifts of Polar Solutes[1]

by Paul H. Weiner and Edmund R. Malinowski*

Department of Chemistry and Chemical Engineering, Stevens Institute of Technology, Hoboken, New Jersey 07030

(Received July 29, 1971)

Publication costs borne completely by The Journal of Physical Chemistry

The proton chemical shifts of polar solutes in a variety of solvents are reported. Various factors which contribute to the solvent effect are discussed. It is found that the reaction-field contribution involves an effective dielectric constant which makes this contribution vanish in the case of nonpolar solvents. When the solute molecule and solvent molecules possess permanent dipoles a dipole–dipole effect is observed. The nature of this effect is discussed.

Introduction

Recently, the technique of factor analysis has been applied to the problem of solvent effects in nuclear magnetic resonance of both polar[2] and nonpolar[3a,b] solutes. By means of factor analysis the proposition of Buckingham, Schaefer, and Schneider,[4] that the chemical shift of a solute can be expressed as a linear sum of factors, was shown to be valid. Factor analysis also indicated that three factors were sufficient to span the solvent effect space concerning the chemical shifts

---

[1] Based, in part, on a thesis submitted by P. H. Weiner to Stevens Institute in partial fulfillment for a Ph.D. degree.

[2] P. H. Weiner, E. R. Malinowski, and A. R. Levinstone, *J. Phys. Chem.*, **74**, 4537 (1970).

Table I: Chemical Shifts (Corrected for Bulk Susceptibility) of Substituted Methane Solutes, Relative to External HMD[a]

	Solvents											Gas[c]
Solutes	CH_3CN	CH_2Cl_2	$CHCl_3$	CCl_4	CS_2	CH_2Br_2	$CHBr_3$	CH_3I	CH_2I_2	$(CH_3)_2CO$	$(CH_3)_2SO$	phase
CH_3CN	119.4	116.6	121.9	120.4	125.8	129.5	138.2	128.3[b]	148.6	113.3[b]	128.6[b]	86.4[d]
CH_3Cl	183.4	179.0	182.1	181.8	187.6	189.0	195.0	186.0	206.1	173.0	188.6	154.0[e]
CH_2Cl_2	328.7	318.4	319.3	320.1	324.9	328.0	332.7	327.9	343.3	327.8	349.2	289.0[e]
$CHCl_3$	457.5	437.5	438.0	438.0	443.5	447.6	450.5	451.5	461.2	471.7[b]	503.0	410.9[e]
CH_3Br	162.2	157.4	160.6	160.6	166.8	168.1	173.8	165.0	185.0	152.3	167.7	130.5[e]
CH_2Br_2	307.0	296.2	297.4	298.4	303.9	307.1	309.9	306.4	320.8	307.7[b]	329.0[b]	268.6[e]
$CHBr_3$	427.2	411.4	411.9	412.2	417.9	419.4	421.9	422.0	430.7	442.6	466.7	390.5[e]
CH_3I	132.2	127.9	131.5	131.9	139.5	139.1	144.6	136.4	155.5	122.3[b]	136.2[b]	102.6[d]
CH_2I_2	239.9	232.2	234.0	235.2	243.1	241.7	245.5	240.9	254.8	238.7	244.9[b]	214.6[d]
CHI_3	305.1	294.4	296.4	297.7	304.1	300.7	303.4	301.4	308.0	313.4	319.8	285.4[d]
CH_2BrCl	319.7	309.8	311.3	311.3	317.4	320.7	323.3	320.2	335.4	320.3	342.3	281.9[d]
$CHBrCl_2$	421.5	433.1	434.1[b]	433.2	438.9	442.8	443.9	445.0	454.7	464.8	493.5	...
CH_2ClCN	258.6	246.8	248.0	247.2	253.9	259.1	263.9	260.7	277.6	265.0	286.7	...

[a] In Hz at 60 MHz. Positive shifts are downfield shifts from external hexamethyldisiloxane. [b] Deuterated solvent. [c] Gas-phase shifts are relative to external HMD. [d] Estimated by factor analysis, Ph.D. Thesis, P. H. Weiner. [e] T. Vladimiroff, Ph.D. Thesis, Stevens Institute of Technology, Hoboken, N. J.; *Diss. Abstr. B*, 28 (8), 3248 (1968).

of polar solutes,[2] relative to internal tetramethylsilane. The gas-phase shift of a solute was identified to be a true measure of the shift of an unperturbed molecule. For nonpolar solute shifts, relative to external hexamethyldisiloxane, the solvent anisotropic effect was successfully separated from the van der Waals contribution and quantitative values of solvent anisotropy were determined for many common solvents.[3a] The theoretical formulation for the van der Waals shift proposed by Howard, Linder, and Emerson[5] was reexamined by factor analysis and was found to be a reasonable approximation to the real situation.[3b]

In the present paper we examine the effects of solvent upon the proton shifts of polar solutes in light of information gained from the factor-analysis studies[2,3] of nonpolar solutes.

Experimental Section

Solutions were prepared by adding a trace of solute to the solvent, thus approximating infinite dilution. All chemical shifts were referenced with respect to external hexamethyldisiloxane (HMD) and were corrected for bulk susceptibility by the spinning coaxial sample technique described in detail in the earlier work.[6] Measurements were made at a probe temperature of 39 ± 1°. Experimental proton shift data for the polar solutes in a variety of solvents are shown in Table I. These shifts are accurate to within ±1 Hz. A positive value indicates a downfield shift from external HMD.

Discussion

The Buckingham, Schaefer, and Schneider equation[4] for the chemical shift of solute i in solvent α is given as

$$\delta(\mathrm{i},\alpha) = \delta_\mathrm{g}(\mathrm{i}) + \sigma_\mathrm{b}(\alpha) + \sigma_\mathrm{w}(\mathrm{i},\alpha) + \sigma_\epsilon(\mathrm{i},\alpha) + \sigma_\mathrm{a}(\alpha) \quad (1)$$

Here $\delta_\mathrm{g}(\mathrm{i})$ is the gas-phase shift of solute i, $\sigma_\mathrm{b}(\alpha)$ is the bulk susceptibility effect of solvent α, $\sigma_\mathrm{w}(\mathrm{i},\alpha)$ is the van der Waals interaction shift, $\sigma_\epsilon(\mathrm{i},\alpha)$ is the reaction-field effect due to the presence of a dipolar group in the solute, and $\sigma_\mathrm{a}(\alpha)$ is a shift caused by the anisotropy of the solvent. When corrected for bulk-magnetic effects the shift becomes

$$\delta_\mathrm{c}(\mathrm{i},\alpha) = \delta(\mathrm{i},\alpha) - \sigma_\mathrm{b}(\alpha) = \delta_\mathrm{g}(\mathrm{i}) + \sigma_\mathrm{w}(\mathrm{i},\alpha) + \sigma_\epsilon(\mathrm{i},\alpha) + \sigma_\mathrm{a}(\alpha) \quad (2)$$

Equation 2 can be rearranged to give the gas-to-solution shift, $S(\mathrm{i},\alpha)$.

$$S(\mathrm{i},\alpha) = \delta_\mathrm{c}(\mathrm{i},\alpha) - \delta_\mathrm{g}(\mathrm{i}) = \sigma_\mathrm{w}(\mathrm{i},\alpha) + \sigma_\epsilon(\mathrm{i},\alpha) + \sigma_\mathrm{a}(\alpha) \quad (3)$$

In our previous examination of the anisotropy term,[3a] we restricted our attention to nonpolar solutes. In such cases the reaction field term $\sigma_\epsilon(\mathrm{i},\alpha)$ is negligible. The solvent anisotropy of carbon tetrachloride is generally assumed to be zero because of molecular symmetry. Furthermore, the van der Waals term has been shown[3b,6] to be a product function of solute and solvent terms, $\sigma_\mathrm{w}(\mathrm{i},\alpha) = \sigma_\mathrm{w}(\mathrm{i})\ \sigma_\mathrm{w}(\alpha)$. Hence, from eq 3 we deduce the following expression for the gas-to-solution shift of a nonpolar solute

$$S(\mathrm{i},\alpha) = \frac{\sigma_\mathrm{w}(\alpha)}{\sigma_\mathrm{w}(\mathrm{CCl_4})} S(\mathrm{i},\mathrm{CCl_4}) + \sigma_\mathrm{a}(\alpha) \quad (4)$$

For nonpolar solutes, a plot of $S(\mathrm{i},\alpha)$ *vs.* $S(\mathrm{i},\mathrm{CCl_4})$

---

(3) (a) P. H. Weiner and E. R. Malinowski, *J. Phys. Chem.*, **75**, 1207 (1971); (b) *ibid.*, **75**, 3160 (1971).

(4) A. D. Buckingham, T. S. Schaefer, and W. G. Schneider, *J. Chem. Phys.*, **32**, 1227 (1960).

(5) B. B. Howard, B. Linder, and M. T. Emerson, *ibid.*, **36**, 485 (1962).

(6) E. R. Malinowski and P. H. Weiner, *J. Amer. Chem. Soc.*, **92**, 4193 (1970).

should be linear, having a slope equal to the ratio of van der Waals solvent terms and an intercept equal to the anisotropy of solvent α. Such behavior has been observed.[3a]

In order to extend the graphical analysis to include polar solutes we first define a new quantity $S^*(\mathrm{i},\alpha)$ in the following way.

$$S^*(\mathrm{i},\alpha) = S(\mathrm{i},\alpha) - \sigma_\epsilon(\mathrm{i},\alpha) = \sigma_\mathrm{w}(\mathrm{i},\alpha) + \sigma_\mathrm{a}(\alpha) \quad (5)$$

If we subtract the reaction field term from the solute gas-to-solution shift, then for polar solutes we obtain an expression analogous to eq 4, namely

$$S^*(\mathrm{i},\alpha) = \frac{\sigma_\mathrm{w}(\alpha)}{\sigma_\mathrm{w}(\mathrm{CCl_4})} S^*(\mathrm{i},\mathrm{CCl_4}) + \sigma_\mathrm{a}(\alpha) \quad (6)$$

For nonpolar solutes we notice that $S(\mathrm{i},\alpha) = S^*(\mathrm{i},\alpha)$. Equation 6 represents a general expression which is applicable to both polar and nonpolar solutes.

According to Buckingham, Schaefer, and Schneider,[4] the reaction field shift is given by the equation

$$\sigma_\epsilon(\mathrm{i},\alpha) \cong -k\left(\frac{\epsilon - 1}{2\epsilon + 2.5}\right)\frac{\mu}{\alpha}\cos\theta \quad (7)$$

Here, μ is the dipole moment of the solute in the gas phase, α is the solute molecular polarizability, θ is the angle between the solute dipole and the C–H bond containing the proton in question, ϵ is the static dielectric constant, and k is a bond parameter. Becconsall and Hampson[7] point out that it is unreasonable to use the static dielectric constant in eq 7 since the solute molecule has rotational freedom. Instead, an effective dielectric constant, ϵ', should be used. Unfortunately, they proposed a crude graphical procedure for estimating ϵ'. Gerhold and Miller,[8] upon studying the temperature dependence of the solvent Stark effect in electron absorption spectra, proposed the following equation which gives a better estimate of the effective dielectric constant

$$\frac{\epsilon - 1}{2\epsilon + 2} - \frac{n^2 - 1}{2n^2 + 2} = \frac{\epsilon}{(\epsilon + 2)(2\epsilon + 1)} \times \frac{(2\epsilon' + 1)(\epsilon' - 1)}{\epsilon'} \quad (8)$$

Here n is the solvent index of refraction. Although this model may not be totally applicable to the present study, it should afford a more reasonable estimate of the effective dielectric constant that should be used for calculating the reaction field shift experienced by a rotating polar solute molecule. Table II contains the observed dielectric constants of some common polar and nonpolar solvents along with the calculated effective dielectric constants determined from eq 8.

The reaction field formula written in terms of an effective dielectric constant is

$$\sigma_\epsilon(\mathrm{i},\alpha) = -k\left(\frac{\epsilon' - 1}{2\epsilon' + 2.5}\right)\frac{\mu}{\alpha}\cos\theta \quad (9)$$

Table II: Comparison of Dielectric Constants and Effective Dielectric Constants Calculated by the Method of Gerhold and Miller[a]

Solvent	Dielectric constant,[b] ϵ	Effective dielectric constants, ϵ'
CH_3CN	37.5	29.9
CH_2Cl_2	8.47	5.7
$CHCl_3$	4.8	3.3
CCl_4	2.234	1.06
CS_2	2.635	1.01
CH_2Br_2	6.85	3.88
$CHBr_3$	4.38	2.1
CH_3I	6.62	3.81
CH_2I_2	5.23	2.2
$(CH_3)_2CO$	20.7	15.3
$(CH_3)_2SO$	4.6	32.4

[a] G. A. Gerhold and E. Miller, *J. Phys. Chem.*, **72**, 2737 (1968). [b] Dielectric constants taken from the "Handbook of Chemistry and Physics."

This equation predicts that the reaction field shift for polar solutes in nonpolar solvents is negligibly small since $\epsilon' \approx 1$ for nonpolar solvents as seen in Table II.

After using eq 9 to evaluate the reaction field term as shown in Table III, we calculated $S^*(\mathrm{i},\alpha)$ and made the following plots: $S^*(\mathrm{i},\mathrm{CS_2})$ *vs.* $S^*(\mathrm{i},\mathrm{CCl_4})$; $S^*(\mathrm{i},(\mathrm{CH_3})_2\mathrm{CO})$ *vs.* $S^*(\mathrm{i},\mathrm{CCl_4})$; and $S^*(\mathrm{i},(\mathrm{CH_3})_2\mathrm{SO})$ *vs.* $S^*(\mathrm{i},(\mathrm{CH_3})_2\mathrm{CO})$ (see Figures 1, 2, and 3). In Figure 1, $S^*(\mathrm{i},\alpha) = S(\mathrm{i},\alpha)$ since $\sigma_\epsilon(\mathrm{i},\alpha) \approx 0$ for CS_2 and CCl_4. Here we see that the polar and nonpolar solutes behave identically as predicted by eq 6.

Table III: Reaction Field Contribution of Polar Solutes in Acetone and Dimethyl Sulfoxide Solvents

Solute	$\sigma_{\epsilon'}$(i, acetone)	$\sigma_{\epsilon'}$(i, DMSO)	Solute	$\sigma_{\epsilon'}$(i, acetone)	$\sigma_{\epsilon'}$(i, DMSO)
CH_3Cl	−4.1	−4.8	$CHBr_3$	−3.9	−4.3
CH_2Cl_2	−4.8	−5.3	CH_3I	−3.0	−3.4
$CHCl_3$	−4.4	−5.0	CH_2I_2	−3.3	−3.8
CH_3Br	−3.6	−4.1	CHI_3	−4.0	−4.7
CH_2Br_2	−4.3	−4.9	CH_3CN	−7.9	−9.0

For $S^*(\mathrm{i},(\mathrm{CH_3})_2\mathrm{CO})$ *vs.* $S^*(\mathrm{i},\mathrm{CCl_4})$ we find a dramatically different behavior. The first striking observation is that four straight lines can be drawn, one connecting all nonpolar solute points and one connecting all monodipolar solutes. All four lines intersect at a common point where the gas-to-solution shift in carbon tetrachloride is zero. The slopes increase as the number of dipoles in the solute molecules increases. This behavior is not unique to the acetone–carbon tetra-

---

(7) J. K. Becconsall and P. Hampson, *Mol. Phys.*, **10**, 21 (1965).

(8) G. A. Gerhold and E. Miller, *J. Phys. Chem.*, **72**, 2737 (1968).

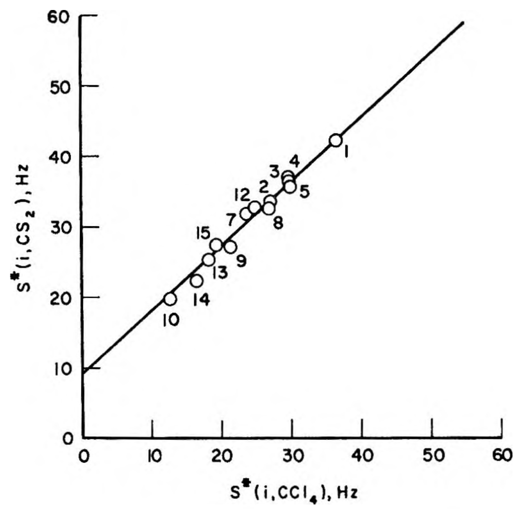

Figure 1. Gas-to-solution shifts, corrected for reaction field effects, in carbon disulfide *vs.* the corresponding shifts in carbon tetrachloride. Solutes: 1, CH_3CN; 2, CH_3Cl; 3, CH_3Br; 4, CH_3I, 5, CH_2Cl_2; 6, CH_2Br_2; 7, CH_2I_2; 8, $CHCl_3$; 9, $CHBr_3$; 10, CHI_3; 11, CH_4; 12, CH_3CH_3; 13, $C(CH_3)_4$; 14, C-C_6H_{12}; 15, $Si(CH_3)_4$.

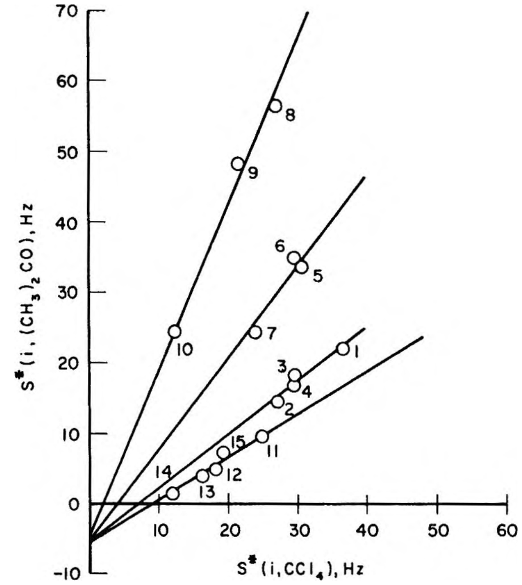

Figure 2. Gas-to-solution shifts, corrected for reaction field effects, in acetone *vs.* the corresponding shifts in carbon tetrachloride. (See Figure 1 for key.)

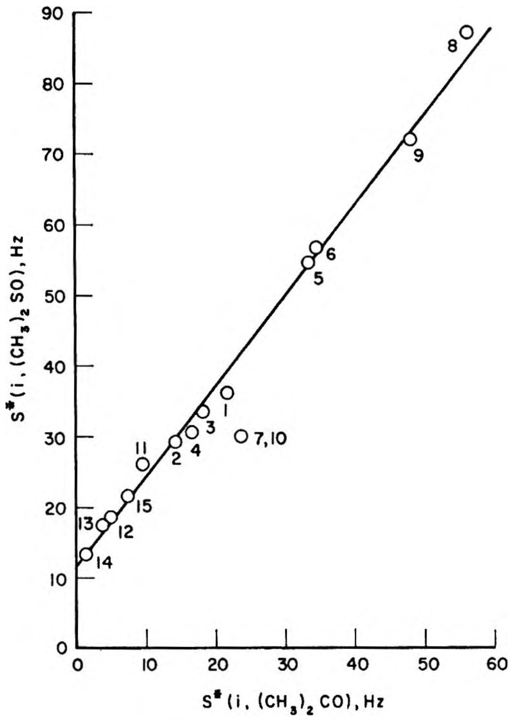

Figure 3. Gas-to-solution shifts, corrected for reaction field effects, in dimethylsulfoxide *vs.* the corresponding shifts in acetone. (See Figure 1 for key.)

chloride system. The same behavior is observed when $S^*(i,\alpha)$ for acetonitrile and dimethyl sulfoxide solvents are plotted against those in carbon tetrachloride. For methyl iodide–carbon tetrachloride the polar solutes deviate only slightly from the nonpolar solute line. In all cases studied the common intersection point implies that the solvent anisotropy effect is independent of the polar nature of the solute (see eq 6). Systematic deviations of the polar solutes from the nonpolar line indicate that a new type of solute–solvent interaction is present in acetone, dimethyl sulfoxide, and acetonitrile solvents which does not seem to occur in carbon disulfide or carbon tetrachloride. This excess shift can be explained on the basis of dipole–dipole orientation during collision. Conceivably the solute dipole aligns itself with the solvent dipole so that the solute hydrogens strike the π-electron rich region of the solvent molecule. In solvents such as acetone, dimethyl sulfoxide, and acetonitrile the π electrons lie along the dipole axis. For the trihalogenated methane solutes the collision is most likely to occur at the single hydrogen atom. For disubstituted methanes the collision energy would be shared equally between two hydrogens on the solute. In monosubstituted methanes the three hydrogens would share in the collision process. The shift could be caused by a distortion of the electron cloud surrounding the hydrogen on the solute. The distortion would be greatest when there is only one solute hydrogen present as in the trisubstituted solutes.

Figure 3 is a plot of $S^*(i,(CH_3)_2SO)$ *vs.* the corresponding shifts in acetone solvent. Both polar and nonpolar solutes fall on the same line. This plot indicates that the shape of the solvent molecule is quite important in determining the magnitude of the excess polar solute shifts. Acetone and dimethyl sulfoxide solvent are structurally similar compounds. This observation provides a clue in the theoretical development of solvent effects upon polar solutes.

From these observations we recognize that an additional effect is operative when both solute and solvent molecules possess permanent dipole moments. This effect is exceedingly enhanced when the polar solvent molecule contains π electrons as in acetone and dimethyl sulfoxide. To explain the graphical observations we contend that this dipole–dipole interaction must be of the following form.

$$\sigma_d(i,\alpha) = \sigma_d(i)\sigma_d(\alpha) \tag{10}$$

Concerning Figure 2 the vertical deviations from the nonpolar line represent the contributions due to the dipole–dipole interactions. For a given class of solutes (*i.e.*, mono-dipolar, di-dipolar or tri-dipolar) this dipole–dipole effect must be proportional to the solvent part of the van der Waals term since linear lines can be passed thru each class of solutes, the lines intersecting at a common point where $S^*(i,CCl_4)$ equals zero. The differences in slopes are accounted for by $\sigma_d(i)$ which must be a function of the number of dipoles in the solute molecule as well as the geometrical shape.

The fact that all solute points lie on the same linear line in the acetone–dimethyl sulfoxide plot (Figure 3) also suggests that the solvent dipole term is proportional to the solvent van der Waals term. That is

$$\sigma_d(\alpha) = P_d(\alpha)\sigma_w(\alpha) \tag{11}$$

where $P_d(\alpha)$ takes into consideration the shape of the solvent molecule, its dipole moment, the π-electron configuration, and other factors. For acetone and dimethyl sulfoxide the probability term $P_d(\alpha)$ must be nearly identical because of the similarities in geometrical structure, in their π-electron distribution, and in the location of the dipoles.

In conclusion, then, we propose that the solvent effect on proton magnetic resonance of the molecules studied here can be accounted for the by expression

$$\delta(i,\alpha) = \delta_g(i) + \sigma_a(\alpha) + \sigma_b(\alpha) + \sigma_w(i,\alpha) + \sigma_{\epsilon'}(i,\alpha) + \sigma_d(i,\alpha)$$

Here $\sigma_{\epsilon'}(i,\alpha)$ is a modified reaction-field term, having zero value for nonpolar solvents. The last term, $\sigma_d(i,\alpha)$, accounts for the dipole–dipole interaction between the solute and solvent molecules. This term is found to be proportional to the van der Waals term. The exact nature of this term is not fully understood.

Acknowledgment. This investigation was supported in part by the U. S. Army Research Office (Durham) under Contract No. DA-31-124-ARO-D-90.

A Study of Phosphorus–Sulfur Compounds by Inner-Orbital Photoelectron Spectroscopy: Thiono–Thiolo Sulfur

by Wojciech J. Stec,[1] William E. Moddeman,[2] Royal G. Albridge, and John R. Van Wazer*[3]

Departments of Chemistry and Physics, Vanderbilt University, Nashville, Tennessee 37203 *(Received April 7, 1971)*

Publication costs borne completely by The Journal of Physical Chemistry

The binding energies of the "2s" and "2p" orbitals of sulfur and the "2p" orbitals of phosphorus have been measured for a series of covalent phosphorus compounds in which a sulfur atom substitutes for an oxygen either as an electron-pair acceptor for the phosphorus (*i.e.*, in the "isolated" position) or as a bridge between two phosphorus atoms. For this series of compounds, the measured sulfur inner-orbital binding energies are higher by about 1 eV for the P–S–P linkage than for the P=S arrangement. The position of the sulfur in the molecule has a smaller effect on the phosphorus "2p" binding energy. Comparison of these results with similar data on related compounds shows that the findings cannot be simply related from one series of compounds to another. Some new ^{31}P nmr data are also presented.

I. Introduction

Because the chemistry of compounds involving a sulfur bonded to phosphorus still poses many unresolved problems concerning whether or not the sulfur is in a bridging position between the phosphorus and another atom (thiolo) or is in an isolated position (thiono) on the phosphorus,[4] we thought that the relatively new technique of inner-orbital photoelectron spectroscopy[5] might be a fruitful one for study of this topic. Although a considerable amount of data has resulted from sulfur inner-orbital photoelectron spectroscopy of sulfur compounds[5,6] and there is also some information on the binding energies of phosphorus inner orbitals of phosphorus–sulfur compounds,[7,8] the possibility of characterizing a sulfur atom as thiono or thiolo has not previously been investigated by this technique.

---

[1] On leave of absence for 1970 from the Polish Academy of Sciences, Łodz.

[2] Postdoctoral Fellow 1970–1971.

[3] To whom reprint requests should be addressed.

Emphasis in this study has been on the derivatives of 5,5-dimethyl-1, 3-dioxaphosphorinanyl, since these compounds are high-melting solids having low vapor pressures, and their structures seem to be reasonably well demonstrated by the chemical reactions whereby they were obtained (see the pertinent references in the Experimental Section), as well as by infrared and proton nuclear magnetic resonance (nmr) data.[9–12] These compounds have the following structures

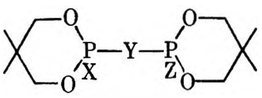

I

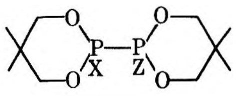

II

a, $X = Y = Z = O$
b, $X = S;\ Y = Z = O$
c, $X = Z = S;\ Y = O$
d, $X = Z = O;\ Y = S$
e, $X = Y = S;\ Z = O$

a, $X = Z = O$
b, $X = S;\ Z = O$

II. Experimental Section

Photoelectron Spectroscopy. The photoelectron spectrometer used in this study with magnesium and aluminum X-ray sources has been previously described.[13] The spectra were calibrated using the carbon "1s" binding energy and the experimental energy resolution was 0.17%. All of the carbon "1s" lines for compounds Ia to Ie, IIa, and IIb of Table I showed partially resolved line structures in which there was a main peak about twice as high as an overlapped secondary peak, the latter exhibiting a binding energy about 2.1 eV higher than the main peak. Since this main peak was the only one to grow with increasing time (due to buildup of "pump oil"[14] on the sample), it was assumed that this peak would exhibit a binding energy of 285.0 eV, which is the accepted value for the carbon "1s" line of aromatic and aliphatic hydrocarbons.[15] For compounds V and VI of Table I, the carbon reference peak was arbitrarily assigned the same binding energy of 285.0 eV, and this was also done for the compounds VII through IX, where the carbon was presumed to be attributable to residual carbon vapor.

Peak widths at half-height were measured for the observed lines to adjudge whether or not a given line might consist of two coalesced peaks. Unfortunately the entire set of measurements were made over a 6-month period so that the settings of the slit defining the electron beam were, because of mechanical difficulties, not always identical. Therefore the observed line widths have only qualitative meaning. Both magnesium and aluminum were employed as anodes in the X-ray source and each anode was used for every compound to assure that the peak-width measurements were not affected by the presence of a foreign line, such as an Auger peak. Note that the $\beta\rho$ used for the aluminum anode was 116.780 and for the magnesium anode 104.500 G-cm.[16]

Nuclear Magnetic Resonance Spectroscopy. The ^{31}P nmr studies were carried out on a Varian XL-100-15 spectrometer, with the sample being contained in a 5-mm tube centered in a 12-mm tube. The annular space between the tubes was filled with deuteriochloroform to maintain a heteronuclear lock on the deuterium nucleus, plus a small amount of triphenyl phosphite as an "external" ^{31}P reference for the sample. All measurements were converted into 85% phosphoric acid as the reference standard (with positive shifts being upfield), on the basis that the shift of triphenyl phosphite under the conditions of measurement is 180.1 ppm downfield from H_3PO_4.

---

(4) For example, see D. E. C. Corbridge, "Topics in Phosphorus Chemistry," Vol. 3, M. Grayson and E. J. Griffith, Ed., Interscience, New York, N. Y., 1966, p 309. Also see E. Fluck, "Topics in Phosphorus Chemistry," Vol. 4, M. Grayson and E. J. Griffith, Ed., Interscience, New York, N. Y., 1967, p 370.

(5) K. Siegbahn, C. Nordling, A. Fahlman, R. Nordberg, K. Hamrin, J. Hedman, G. Johansson, T. Bergmark, S. E. Karlsson, I. Lindgren, and B. Lindberg, *Nova Acta Regiae Soc. Sci. Upsal.*, [4] **20**, 1 (1967).

(6) J. Hedman, P. F. Heden, R. Nordberg, C. Nordling, and B. J. Lindberg, *Spectrochim. Acta, Part A*, **26**, 761 (1970).

(7) W. E. Morgan, W. J. Stec, R. G. Albridge, and J. R. Van Wazer, *Inorg. Chem.*, **10**, 926 (1971).

(8) M. Pelavin, D. N. Hendrickson, J. M. Hollander, and W. L. Jolly, *J. Phys. Chem.*, **74**, 1116 (1970).

(9) For compounds Ia, Ib, Ic, and Ie, see K. D. Bartle, R. S. Edmundson, and D. W. Jones, *Tetrahedron*, **23**, 1701 (1967).

(10) For compounds Ib and Id, see A. R. Katritzky, M. R. Nesbit, J. Michalski, A. Zwierzak, and Z. Tulimowski, *J. Chem. Soc. B*, 140 (1970).

(11) For compound IIb, see R. K. Harris, J. R. Wolpin, and W. J. Stec, *Chem. Commun.*, 1391 (1970).

(12) Additionally, the structures of compounds IIa and IIb have been fully proven by X-ray analysis, see Z. Gatdecki and J. Wojciechowska, paper submitted for publication.

(13) A. Fahlman, R. G. Albridge, R. Nordberg, and W. M. LaCasse, *Rev. Sci. Instrum.*, 41, 596 (1970); R. Nordberg, H. Brecht, R. G. Albridge, A. Fahlman, and J. R. Van Wazer, *Inorg. Chem.*, **9**, 2469 (1970).

(14) Since our spectrometer uses a turbo-molecular pump instead of an oil pump, this commonly used phrase is a misnomer. Also, silicone O-rings and silicone greases are used throughout the spectrometer so that one might imagine that the "pump oil" line might be attributable to the carbon of dimethylsiloxanes, which does not exhibit a "1s" binding energy of 285.0 eV. However, a study using magnesium fluoride as the substrate for the "pump oil" showed the usual buildup of the carbon "1s" line but no evidence for the concomitant appearance of any silicon lines even after 12 hr. Thus, we believe that the residual carbon appearing in our spectrometer is due to stray organic vapor (perhaps volatiles coming from the adhesives on the Scotch tape) which has a sufficient number of methyl and methylene groups (as well as aromatic groups having only one or two noncarbon substituents per ring) so that the value of 285.0 eV is applicable for its "1s" binding energy.

(15) U. Gelius, P. F. Hedén, J. Hedman, B. J. Lindberg, R. Manne, R. Nordberg, C. Nordling, and K. Siegbahn, *Phys. Scripta*, **2**, 70 (1970).

(16) K. Siegbahn in "Beta and Gamma Ray Spectroscopy," Vol. I, K. Siegbahn, Ed., North-Holland Publishing Co., Amsterdam, 1965, Chapter III.

Table I: Observed Inner-Orbital Electronic Binding Energies of Phosphorus and Sulfur

Compd	Structure	Binding energies, eV Phosphorus "2p"	Sulfur "2s"	Sulfur "2p"
Ia	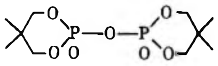	134.3	...	...
Ib	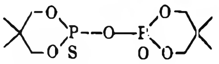	134.2 ± 0.2	227.2	162.7 ± 0.2
Ic	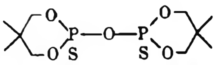	134.3 ± 0.2	227.1	162.6 ± 0.2
Id	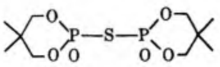	133.9 ± 0.2	228.0	163.8 ± 0.2
Ie	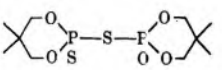	133.9 ± 0.2	227.3	163.2 ± 0.3[a]
IIa	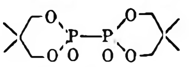	133.4	...	...
IIb	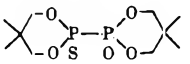	133.5 ± 0.1	...	162.7 ± 0.1
III	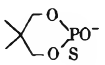 $(H_3NC_6H_{11})^+$	133.4 ± 0.2	...	162.0 ± 0.2
IV	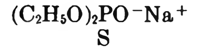 $(C_2H_5O)_2\underset{S}{P}O^-Na^+$	134.3 ± 0.1	...	163.2 ± 0.1
V	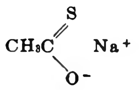	...	...	162.5 ± 0.4
VI	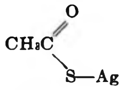	...	...	161.8 ± 0.3
VII	P_4S_3	134.9 ± 0.1	...	163.1 ± 0.4
VIII	P_4S_{10}	134.5 ± 0.3	...	163.4 ± 0.1
IX	S_8		227.9 ± 0.1	163.9 ± 0.1

[a] Graphical resolution of this wide peak led to two peaks exhibiting binding energies of 163.6 and 162.3 eV.

Sample Preparation. All of the compounds used in this study were fully crystalline materials which (except for the salts) had been recrystallized at least once. Each sample was prepared by grinding a batch of crystals in a small vibrating ball-mill. The resulting powder was dusted onto a piece of Scotch-brand permanent-mending tape which was then tapped several times; more powder was sprinkled on, followed by a final tapping to affix the powder so that none of the underlying Scotch tape would be exposed to the X-ray beam. At least three replicates from start to finish were run for each sample in Table I, where the observed standard deviations between repeated measurements are shown. The 5,5-dimethyl-1,3-dioxaphosphorinanyl derivatives were synthesized according to the methods given in the literature. These include a preparation[17] for Ia, Ic, and III; another [18] for Ib, and one for Id.[19] Compounds IIa and b were made according to another reference.[20] Compounds V and VI were prepared by appropriate neutralization of commercially available thioacetic acid. The P_4S_3 was a commercial sample; whereas the P_4S_{10} and S_8 were recrystallized from commercial samples.

III. Results and Discussion

Inner-Orbital Binding Energies. The experimentally determined inner-orbital-electron binding energies of phosphorus and sulfur are reported in Table I for the compounds studied herein. It should first be noted that the difference between the highest and the lowest reported "2p" binding energy is 1.5 eV for phosphorus and 2.1 eV for sulfur. Thus, we are dealing with small changes that lie within the width at half-height (ranging from 2.5 to 4.0 eV) of any of the peaks. The presence of two different kinds of phosphorus or two different

---

(17) R. S. Edmundson, *Tetrahedron*, 21, 2379 (1965).

(18) R. S. Edmundson, *Chem. Ind.* (*London*), 784 (1963).

(19) J. Michalski, M. Mikolajczyk, B. Mlotkowska, and A. Zwierzak, *Angew. Chem., Int. Ed.*, 6, 1079 (1967).

(20) W. Stec and A. Zwierzak, *Can. J. Chem.*, 45, 2513 (1967).

kinds of sulfur atoms in a molecule generally resulted in a widening of the respective spectral peaks, with no evidence of separation into two peaks.

The phosphorus "2p" data on compounds Ia through e demonstrate that substitution of a bridging oxygen atom by a sulfur reduces the "2p" binding energy of the phosphorus by *ca.* 0.5 eV, whereas, for a similar substitution in the isolated position on the phosphorus, the change in binding energy is inappreciable (≤ 0.1 eV). Likewise the thiolo sulfur exhibits a binding energy which is *ca.* 1 eV higher than the thiono. Clearly, the difference between thiono and thiolo shows up more distinctly in the sulfur rather than the phosphorus "2p" binding energy. Note that, in conformity with previous experience, the changes in the sulfur "2s" binding energies reasonably parallel those in the sulfur "2p" binding energies.

Because compounds Ib, Ie, and IIb contain phosphorus in two chemically different positions and compound Ie has two distinguishable sulfur atoms, it should be expected that the respective "2p" peaks would be unusually wide. This was not found to be the case for the phosphorus in compounds Ib, Ie, and IIb but was observed for the sulfur in compound Ie. Further, an equimolar mixture of compounds Ib and d was run several times, and the results were compared with the binding-energy spectrum of compound Ie. Both the phosphorus and sulfur "2p" peaks of the mixture were unusually wide (with the sulfur peak being about as broad as that observed for compound Ie), and the sulfur "2p" binding energy was 163.2 ± 0.3 eV and the phosphorus 133.9 ± 0.2 eV. Graphical resolution of the broad sulfur "2p" peaks of the mixture and of compound Ie indicated that the thiolo and thiono binding energies differ by *ca.* 1 eV—the same value which was obtained from separate peak measurements on compounds Ib or Ic *vs.* Id.

For compounds IIa and b, it is again seen that the substitution of sulfur for oxygen in the isolated position has no appreciable effect on the phosphorus "2p" binding energy. Further, the sulfur "2p" binding energy of the thiono sulfur is the same whether the adjacent phosphorus is bonded to another phosphorus atom (compound IIb) or is connected to that phosphorus through an oxygen bridge (compounds Ib and c). Compound III exhibits a phosphorus "2p" binding energy which is *ca.* 1 eV smaller than that of compound Ic, indicating that converting from a bridging to a negatively charged oxygen in the structure leads to reduction in the positive charge[5] on the phosphorus atom. This is also accompanied by a change in the same direction, although smaller, in the charge borne by the thiono sulfur.

The observed differences in measured binding energies between compounds III and IV are difficult to interpret since they may be attributable in some part to small differences in the carbon "1s" reference peak.[21] This also applies to a direct comparison of the data of compounds V and VI with the other binding energies shown in Table I. However, it is important to note that the sulfur "2p" energy of compound V is larger than that of compound VI; whereas that of compound Ib is smaller than that of compound Id. If we accept the common view that the silver atoms of silver thioacetate will be bonded to the sulfur atoms, whereas the sodium atoms of sodium thioacetate will be ionized to leave a preponderance of negative charge on the oxygens, the data of Table I suggest that a sulfur atom bridging between a carbon and a silver atom has a different binding energy than a sulfur bridging between two phosphorus atoms. This corresponds to a greater electron-withdrawing effect on the sulfur by the phosphorus atoms in compound Id or e than by the silver and carbon atoms in compound VI.

Compounds VII through IX are included in Table I for reference purposes. Since the carbon peak observed for these structures is surely attributable to residual carbon, the reported binding energies may not be directly comparable to those of the other structures, owing to small differences in the absolute value of the binding energy corresponding to the center of the carbon "1s" peak. However, it is interesting to note that the reported "2p" binding energies for the sulfur bridging between two phosphorus atoms in compound Id and for the sulfur bridging between two sulfur atoms in S_8 (compound IX) are close to each other, although these values are 0.8 eV higher than the reported sulfur "2p" binding energy for P_4S_3 (compound VII) in which each sulfur atom bridges between two phosphorus atoms.

^{31}P Chemical Shifts. The nuclear magnetic resonance spectroscopy results on compounds Ia through e and for IIa and b are given in Table II from which it can be seen that the ^{31}P chemical shift of the phosphorus bearing the phosphoryl oxygen lies in an entirely different region of the spectrum (-10 to -25 ppm) than that of the phosphorus bearing the thiono sulfur (-65 to -40 ppm). It is obvious from the data of Table II that nuclear magnetic resonance spectroscopy is a much more powerful tool for differentiating between these various structures than is inner-orbital photoelectron spectroscopy. By analogy to known compounds, the values of the chemical shifts shown in Table II can be roughly predicted. Thus, from the shifts of $+1$, -26, -68, -95, and $+9$ ppm of $OP(OR)_2$, $OP(OR)_2(SR)$, $SP(OR)_3$, $SP(OR)_2(SR)$, and

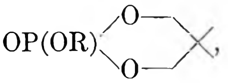

, where $R = C_2H_5$, obtained from the literature,[22] we would estimate the following shifts for

---

(21) The carbon bonded to an oxygen will exhibit a different binding energy (*ca.* 287 eV) than the other carbon atoms in a purely hydrocarbon environment (285 eV). Thus, the average peak position may vary depending on the ratio of carbon to oxygen atoms in the alkoxyl groupings.

the compounds shown in Table II: Ia, +10; Ib, +10, −59; Id, −17; and Ie, −17, −86 ppm. Note that these estimated values (which are systematically low by about 10 ppm) are based on the assumption that the effect of the C–O–P linkage on the ^{31}P chemical shift of the phosphorus would not be much different than that of a P–O–P linkage.

Table II: ^{31}P Nmr Data Taken on Saturated Solutions in Deuteriochloroform

Compd[a]	Chemical shifts,[b] ppm		Coupling constants, Hz	
	δ_{OP}	δ_{SP}	J_{HCOP}	J_{PP}
Ia	21.5		16	
Ib[c]	21.9	−43.6		
Id	−6.0		26	
Ie	−6.0	−64.5		
IIa	1.7		12	
IIb	5.5	−58.9	20 (O) 18 (S)	491

[a] Because of very low solubilities in $CHCl_3$, $CDCl_3$, C_6H_6, $[(CH_3)_2N]_2CO$, and CF_3COOH, no measurements were made on compound Ic. [b] Referenced to 85% H_3PO_4, with positive shifts being upfield. [c] Edmundson[18] has reported shifts corresponding to +22.5 and −45.5 ppm, with J_{HCOP} = 28 Hz.

Since the variations in the inner-orbital binding energies are primarily sensitive[5] to the diagonal terms corresponding to the chosen atom in the charge-bond order matrix[22] while the nmr chemical shift of a nucleus such as phosphorus depends mainly on the p and d contributions (including cross terms) to this matrix,[22] these properties exhibit quite different dependencies on the molecular wave function. Therefore, although we have interrelated these properties in another paper[7] (*via* a calculation of atomic charges), it does not seem profitable to do this again for the data given in Tables I and II.

IV. Conclusions

The results reported herein are disappointing in that the differences in inner-orbital binding energies from one compound to another are small relative to the precision of the measurements. However, the reported data do indicate experimentally that the switching of a sulfur atom from the thiono to the thiolo position has a small electron-donating effect on the phosphorus atom, coupled with electron removal from the sulfur. The major value of inner orbital photoelectron spectroscopy lies in the fact that there is a reasonably good correlation between the measured binding energy and the atomic charge.[5] Thus the method, although crude and inherently not capable of a large increase in precision, furnishes unique data of chemical interest and hence serves as a qualitative check on theoretical predictions as to charge assignments in molecules.

Acknowledgment. We wish to thank the National Science Foundation for partial support of this work.

[22] M. M. Crutchfield, C. H. Dungan, J. H. Letcher, V. Mark, and J. R. Van Wazer, "P^{31} Nuclear Magnetic Resonance," Wiley-Interscience, New York, N. Y., 1967.

Transition Probabilities of Europium in Phosphate Glasses

by R. Reisfeld,* R. A. Velapoldi, L. Boehm,

Department of Inorganic Chemistry, The Hebrew University of Jerusalem, Israel

and M. Ish-Shalom

Israel Ceramic and Silicate Institute, Haifa, Israel *(Received July 28, 1971)*

Publication costs borne completely by The Journal of Physical Chemistry

Absorption, excitation, and emission spectra of europium have been measured in metaphosphate glasses. The oscillator strengths of the transitions of the $^7F_0$ and $^7F_1$ levels are calculated and compared with the values for aqueous solutions. The intensities and half-bandwidths of fluorescence from the $^5D_0$ levels are compared with those of silicate glasses and aqueous solutions. The influence of the crystal fields of the glass on the hypersensitive $\Delta J = 2$ transition is discussed. The point symmetry of Eu in phosphate glass was found to be C_s. The broadening of the spectral lines in glasses and aqueous solutions has been attributed to a multiplicity of sites with the same symmetry and various crystal field parameters.

Introduction

The objectives of this work were (1) to study the influence of the glass host on the transition probabilities of Eu^{3+} and (2) to compare the broadening of the europium fluorescence in glasses with the broadening in aqueous systems.

The characteristics of glasses with rare earth ions as the fluorescent center are of particular interest since these species are used as laser amplifiers and oscillators. A systematic study of the luminescent characteristics of glasses containing rare earths was done in this laboratory.[1-8]

There has been considerable spectroscopic investigation involving europium activated phosphors for several reasons. The phosphors are of practical use in color television and more information about crystal levels can be obtained for even-electron systems than those with odd-electron systems. Rice and DeShazer[9] have used the fluorescence of europium as an indicator of site symmetry of rare earth ions in glasses.

The quantum efficiencies of the fluorescence of the $^5D_0$ level of europium in liquid solvents was studied by Dawson and Kropp[10] and Haas and Stein.[11] In a later work we will discuss the quantum efficiencies and nonradiative energy dissipations of europium in various glass matrices.

Spectral Intensities: Theory

The ground level electronic configuration of trivalent europium is f^6. Transitions within the f shell are responsible for the crystal spectra. Transitions are forbidden in a free ion by the parity rule for electric dipole transitions. In a crystal or glass, forced electric transitions become allowed as a consequence of coupling of odd electronic wave functions due to the odd parity terms in the crystal field expansion. Considering the static field approximation in the theory developed by Ofelt[12] and Judd,[13] the contribution of the odd parity part of the crystal field is calculated by mixing states of different parity.

Judd's result for oscillator strength P, corresponding to the induced electric dipole transition $\psi J \rightarrow \psi' J'$ at energy σ (cm^{-1}), may be written

$$P = \sum T_\lambda \sigma (f^N \psi J || U^{(\lambda)} || f^N \psi' J')^2 \quad (\lambda = 2, 4, 6) \qquad \text{(I)}$$

where $U^{(\lambda)}$ is a tensor operator of rank λ. The three quantities T_λ are related to the radial parts of $4f^N$ wave functions, the wave functions of perturbing configurations, the refractive index of the medium, and the ligand-field parameters which characterize the environment of the ion.

The measured intensity of an absorption band is related to P by the following expression[14]

$$P = 4.318 \times 10^{-9} \int \epsilon_i(\sigma) d\sigma \qquad \text{(II)}$$

where ϵ is the molar absorptivity at the energy σ (cm^{-1}).

---

(1) R. Reisfeld, A. Honigbaum, G. Michaeli, L. Harel, and M. Ish-Shalom, *Israel J. Chem.*, **7**, 613 (1969).

(2) R. Reisfeld and E. Greenberg, *Anal. Chim. Acta*, **47**, 155 (1969).

(3) R. Reisfeld, Z. Gur-Arieh, and E. Greenberg, *ibid.*, **50**, 249 (1970).

(4) R. Reisfeld and E. Biron, *Talanta*, **17**, 105 (1970).

(5) R. Reisfeld, E. Greenberg, and S. Kraus, *Anal. Chim. Acta*, **51**, 133 (1970).

(6) R. Reisfeld, E. Greenberg, L. Kirshenbaum, and G. Michaeli, *8th Rare Earth Conf.*, **2**, 743 (1970).

(7) R. Reisfeld and L. Boehm-Kirshenbaum, *Israel J. Chem.*, **8**, 103 (1970).

(8) R. A. Velapoldi, R. Reisfeld, and L. Boehm, *9th Rare Earth Conf.*, **1**, 488 (1971).

(9) D. K. Rice and L. G. DeShazer, *Phys. Rev.*, **186**, 387 (1969).

(10) W. R. Dawson and J. L. Kropp, *J. Opt. Soc. Amer.*, **55**, 822 (1965).

(11) Y. Haas and G. Stein, *J. Phys. Chem.*, in press.

(12) G. S. Ofelt, *J. Chem. Phys.*, **37**, 511 (1962).

(13) B. R. Judd, *Phys. Rev.*, **127**, 750 (1962).

(14) W. T. Carnall, P. R. Fields, and K. Rajnak, *J. Chem. Phys.*, **49**, 4412 (1968).

Table I: Oscillator Strengths and Quantum Efficiencies of Europium(III) in Phosphate Glass and in Aqueous Solution

Transition assignment	Wave number, cm^{-1}	Oscillator strength × 10^7			Quantum efficiency (this work)
			Literature[a] (HClO$_4$)		
		This work	Exptl	Calcd	
$^7F_2 \rightarrow {}^5D_0$	16,319	0.015	...	...	
$^7F_1 \rightarrow {}^5D_0$	16,771	0.089	...	...	
$^7F_0 \rightarrow {}^5D_0$	17,256	0.013	0	0	0.953
$^7F_1 \rightarrow {}^5D_1$	18,700	0.505	...	...	
$^7F_0 \rightarrow {}^5D_1$	18,993	0.146	0.14	0.14	0.822
$^7F_0 \rightarrow {}^5D_2$	21,493	1.248	0.21	0.21	0.693
$^7F_0 \rightarrow {}^5D_3$	24,009	0.547	...	...	0.612
$^7F_0 \rightarrow {}^5L_6$	25,380	8.981	17.7	17.7	0.581
$^7F_1 \rightarrow {}^5G_5$, $^5G_6$	26,041	6.019	4.3	5.6	
$^7F_0 \rightarrow {}^5G_3$	26,507	2.726	...	...	
$^7F_1 \rightarrow {}^5L_8$	27,285	0.391	...	...	
$^7F_0 \rightarrow {}^5D_4$	27,567	1.926	1.7	1.7	
$^7F_1 \rightarrow {}^5H_3$	30,464	1.242	...	...	
$^7F_1 \rightarrow {}^5H_5$	31,152	3.001	...	...	
$^7F_0 \rightarrow {}^5H_6$	31,397	6.776	7.3	8.0	

[a] Reference 14.

In cases where the transitions occur wholly or partially by a magnetic dipole mechanism following the selection rules $\Delta J = 1$, $\Delta L = 0$, $\Delta S = 0$, and $\Delta l = 0$

$$P_{\text{exptl}} = P_{\text{md}} + P_{\text{ed}} \qquad \text{(III)}$$

where P_{exptl} is the experimentally observed oscillator strength, P_{ed} is the induced electric dipole transition, and P_{md} is the magnetic dipole transition. The intensities of radiative transitions of Eu(III) in aqueous solution have been calculated using the above considerations.[15]

In the present work, the oscillator strength of Eu^{III} in glasses was measured and compared to the results obtained in aqueous solution by Carnall, *et al.*[15] The results which follow allow us to derive conclusions concerning glasses and aqueous solutions with respect to the following parameters: (1) change in line intensity, (2) shift of spectral lines, and (3) splitting and broadening of the spectral lines.

From the experimentally determined oscillator strengths given in Table I and a theoretical calculation of the reduced matrix elements appearing in Judd's formula, eq I, it is possible to obtain the T coefficients by a method similar to that used by Carnall. A knowledge of these coefficients would give insight into the crystal field strength of glasses.

Experimental Section

Materials. Sodium dihydrogen phosphate monohydrate, $NaH_2PO_4 \cdot H_2O$, Mallinckrodt, 99.5% purity, and Eu_2O_3, Molycorp., 99.9% purity, were used. A mixture of the phosphate with 2 wt % europium was prepared and homogenized in an electric vibrator. The mixture was melted in a platinum crucible at 1100° and poured into a stainless steel mold, producing a rectangular prism of glass, approximately 10 × 10 × 40 mm. The glass was annealed at 300° for 3 hr followed by polishing of the six faces with diamond powder. The final size of the glass sample was 10 × 10 × 40 mm.

The absorption spectra of the glasses were recorded on a Cary 14 recording spectrophotometer using undoped phosphate glass as a blank. All measurements were made at room temperature. Emission spectra were obtained on a spectrofluorometer previously described[1] and a Turner 210 spectrofluorometer which gives corrected spectra.

Results

Table I gives the oscillator strengths and spectral assignments of Eu^{III} in phosphate glasses compared to those in aqueous solution.[14] The last column lists comparative quantum efficiencies of the fluorescence from the $^5D_0$ level excited to selected levels; these values will be discussed in later work. Figure 1 is the part of the absorption spectrum from which the relative populations of the ground-state multiplets were calculated.

The values obtained in this work are corrected for the population distribution of total concentration in $^7F_0$, $^7F_1$, and $^7F_2$. The correction was made using the following formula

$$C_j/C_T = (g_j/g_0) \exp[-(E_j - E_0)/kT] \qquad \text{(IV)}$$

where $C_T = \Sigma_0{}^2 C_j$, C_j is the concentration of atoms in $^7F_{0,1,2}$, and $g_j = 2J + 1$. From our experimental results (Figure 1), $E_1 - E_0 = 279$ cm^{-1} and $E_2 - E_0 = 917$ cm^{-1}. The corresponding fractions of populations represented by C_j/C_T are $C_0 = 0.792$, $C_1 = 0.200$, and $C_2 = 0.008$.

---

(15) W. T. Carnall, P. R. Fields, and K. Rajnak, *J. Chem. Phys.*, **49**, 4450 (1968).

Table II: Relative Intensities and Half-Bandwidths of $^5D_0$ Emissions of Europium(III)

	Water					Europium(III) in						
		Eu(ClO$_4$)$_3$		Eu(NO$_3$)$_3$		Phosphate			Silicate			
Transition assignments	Band max, nm	RI	½BW,[a] cm^{-1}	RI	½BW,[a] cm^{-1}	Band max, nm	RI	½BW,[a] cm^{-1}	Band max, nm	RI	½BW,[a] cm^{-1}	LaF$_3$ RI[b]
$^5D_0 \rightarrow {}^7F_0$	580.0	...	...	...	...	578.5	0.036	119	579.7	0.130	149	0.060
$^5D_0 \rightarrow {}^7F_1$	592.5	1.00	258	1.00	232	591.9	1.000	313	592.2	1.000	313	1.000
$^5D_0 \rightarrow {}^7F_2$	617.0	0.80	368	2.10	317	612.1	3.000	289	610.2	4.255	295	0.814
$^5D_0 \rightarrow {}^7F_3$	652.0	...	...	...	...	654.7	0.219	234	655.7	0.314	381	0.029
$^5D_0 \rightarrow {}^7F_4$	695.0	1.00	310	1.00	332	692.3	1.026	142	693.2	0.398	121	0.434

[a] Half-bandwidth. [b] Reference 16.

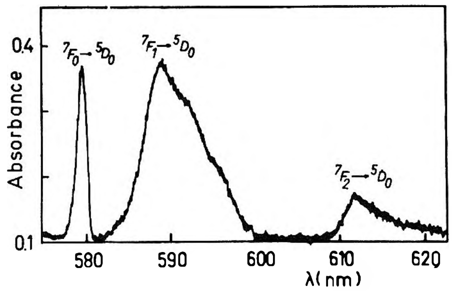

Figure 1. Part of the absorption spectrum of Eu^{III} in phosphate glass.

Table II gives the wavelength maxima, relative intensities, and half-bandwidths for fluorescence from $^5D_0$ to the ^7F multiplets for Eu^{III} in water solution[11] and in phosphate and silicate[8] glasses. The last column in the table presents relative intensities for the emissions of Eu^{III} in LaF$_3$ in which the symmetry is C_{2v}.[16]

Discussion

In general, the oscillator strengths obtained for glasses are higher than those obtained for aqueous solutions with the exception of the $^7F_0 \rightarrow {}^5L_6$.

We note that the oscillator strength for the $^7F_0 \rightarrow {}^5D_0$ transition in the glass is relatively large compared to the zero value reported for the europium perchlorate solution.[14] This transition has been reported to exist in cases where the site symmetry allows an electric dipole process. The symmetries allowing such a process are C_s, C_n, and C_{nv}.[17] This is consistent with the results of Rice and DeShazer,[9] who deduced that Eu^{III} was situated in a C_s symmetry. By comparing the half-bandwidth of the $^7F_0 \rightarrow {}^5D_0$ transition in an europium sesquioxide crystal, which is about 2 cm^{-1}, to the half-bandwidths of these transitions in glasses (Table II, Figure 2) which are 119 cm^{-1} in phosphate glass and 149 cm^{-1} in silicate glass, it is concluded that there are approximately 50 slightly different sites of C_s symmetry in these glasses. The slight differences in environment are caused by small variations in the crystal field parameters. The energy-level shifts for ions in different environments lead to slight changes in the transition wavelengths producing the broadening of the spectra. We believe that a similar situation exists in solution where the broadening of the $^5D_0 \rightarrow {}^7F_1$ and $^5D_0 \rightarrow {}^7F_2$ bands resulted in a variety of sites for the same symmetry due to a slight change in the distances between the ligands (water, nitrate, or perchlorate) and the rare earth ions.

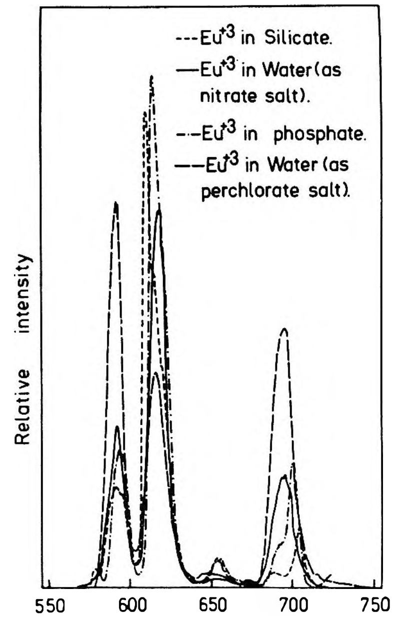

Figure 2. Corrected emission spectra of Eu^{III} in various media.

In glasses, the europium is surrounded by nonbridging oxygens in the phosphate tetrahedra,[18] and the relative positions of tetrahedra with relation to Eu may be slightly distorted simply by a change in the Eu-O distance.

The difference between solutions and glasses in the $^7F_0 \rightarrow {}^5D_2$ oscillator strengths and intensities can be seen in Tables I and II, respectively. It should also be noted that the relative electric dipole intensities of Eu^{III} in LaF$_3$ are smaller than those in glasses with C_s symmetries (Table II).

---

(16) M. J. Weber, "Optical Properties of Ions in Crystals," H. M. Crosswhite and H. W. Moos, Ed., 1967, p 467.

(17) W. C. Niewpoort, G. Blasse, and A. Bril, ref 16, p 161.

(18) R. Reisfeld and J. Hormodaly, *9th Rare Earth Conf.*, 1, 123 (1971).

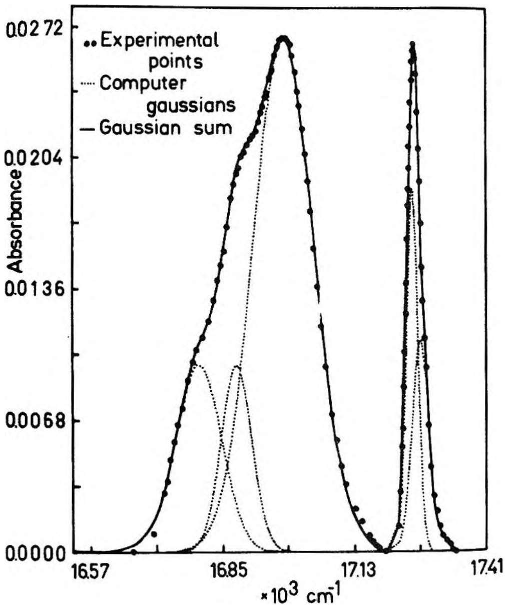

Figure 3. Gaussian analysis of absorption spectrum of Eu^{III} in phosphate glass for the $^7F_{0,1} \rightarrow {}^5D_0$ transitions.

It is known that the absorption bands of europium in solution due to 2 ⟷ 0 transitions are intensified by a factor of about 10 when the aquo ions are replaced by other complexing ions.[19] Jørgensen has named these as "hypersensitive" transitions.[20] Judd pointed out that only the following symmetries will give rise to hypersensitive transitions: C_s, C_1, C_2, C_{2v}, C_{3v}, C_{4v}, and C_6.[21] It is therefore of interest to compare the hypersensitivity of the $^5D_0 \rightarrow {}^7F_2$ and $^7F_0 \rightarrow {}^5D_2$ transitions in media other than solutions (Table II).

By comparing the relative intensity of the $^5D_0 \rightarrow {}^7F_2$ transition from the emission spectra, we also see that although the site symmetry of Eu^{III} is C_s in phosphate and silicate glasses, the forced electric dipole is stronger for Eu^{III} in the silicate glass.

Another striking observation from Figure 2 and Table II is the relatively high transition probability of the $^5D_0 \rightarrow {}^7F_4$ transition with $\Delta J = 4$ for the perchlorate solution. The selection rules for electric dipole transitions induced in those cases where the symmetry group of the Eu site does not contain the inversion operation should be 2, 4, and 6.[17] Therefore, if the $^5D_0 \rightarrow {}^7F_4$ were an electric dipole transition, its intensity should be higher in glasses than in the perchlorate solution which has relatively high symmetry. The fact that this transition intensity is higher in perchlorate solution than in glasses may be due, in our opinion, to a quadrupole transition.[21] The electric quadrupole operator has an even symmetry, and therefore such a transition is allowed within the 4f shell.

Figure 3 presents the results of Gaussian analyses of the $^7F_0 \rightarrow {}^5D_0$ and $^7F_1 \rightarrow {}^5D_0$ transitions. The first peak is not degenerate, and therefore, if only one site were present, it should be a very narrow band (1–2 cm^{-1}). We fitted it by two Gaussians as did Rice and DeShazer;[9] however, it should be realized that a large number of Gaussians (~50) would give an even better fit. Similarly, the $^7F_0 \rightarrow {}^5D_1$ transition is triply degenerate, and the Gaussian distribution resolved three major peaks, each of which can be individually resolved into a large number of Gaussians. This indicates that each Gaussian obtained represents a large number of different sites.

Acknowledgment. The authors are deeply grateful to Professor A. B. Scott for reading the manuscript and making useful suggestions and to Mrs. L. Harel for preparing the phosphate glass. The work was performed under NBS contract (G)-103.

---

(19) S. P. Sinha, "Europium," Springer-Verlag, Berlin 1967.

(20) C. K. Jørgensen and B. R. Judd, *Mol. Phys.*, **8**, 281 (1964).

(21) B. R. Judd, *J. Chem. Phys.*, **44**, 839 (1966).

Matrix-Isolation Study of the Pyrolysis of Bromochloromethyl-Substituted Organomercury Compounds. Infrared Spectra of Bromochlorocarbene and the Free Radicals CCl_2Br and $CClBr_2$

by A. K. Maltsev, O. M. Nefedov,

N. D. Zelinsky Institute of Organic Chemistry, Academy of Science of the USSR, Moscow, U.S.S.R.

R. H. Hauge, J. L. Margrave,*

Department of Chemistry, Rice University, Houston, Texas 77001

and D. Seyferth

Department of Chemistry, Massachusetts Institute of Technology, Cambridge, Massachusetts 02139

(Received July 5, 1971)

Publication costs assisted by the U. S. Atomic Energy Commission

The compounds $C_6H_5HgCCl_2Br$ (I) and $C_6H_5HgCClBr_2$ (II) have been pyrolyzed in the gas phase at temperatures from 250 to 450°. Pyrolysis in both cases was essentially complete at 360° and produced C_6H_5HgBr and the carbenes CCl_2 and CClBr from compounds I and II, respectively. The free radicals CCl_2Br and $CClBr_2$ were also produced but in smaller amounts. Band assignments for the parent compounds and pyrolysis products are presented for the 400–1000-cm^{-1} spectral range. All pyrolysis products have been previously reported and band center measurements agree well with published values. However, isotopic splitting due to chlorine isotopes is generally better resolved than in previous studies and provides strong evidence for the number of chlorine atoms present in each species.

Introduction

Recently, trichloromethyl derivatives of mercury have been shown to decompose during pyrolysis in the gas phase producing reactive intermediates CCl_2 and CCl_3 which were detected directly by matrix-isolation ir spectroscopy.[1-3] Thus pyrolysis of $RHgCCl_3$ compounds was found to be a new source of these species and is expected to be important in studies of their gas-phase chemical reactions and structures. It is of interest to study the pyrolysis of other halomethylmercury compounds in order to produce different halocarbenes and free radicals in the gas phase. Seyferth, *et al.*,[4] have found that $C_6H_5HgCCl_2Br$ (I)[5] and $C_6H_5HgCClBr_2$ (II)[5] react rapidly in organic solvents at *ca.* 80° with a variety of compounds forming C_6H_5HgBr (III) and final products resulting from reaction with CCl_2 and CClBr, respectively. Kinetic studies of $C_6H_5HgCCl_2Br$–olefin reactions in benzene solution indicated that free CCl_2 was an intermediate in these reactions.[6] Vibrational spectra of matrix-isolated CCl_2 are now well known,[2,7,8] while that of bromochlorocarbene CBrCl has been described without details in a paper[9] devoted to the spectrum of CBr_2. Free radicals CCl_2Br and $CClBr_2$ have been produced previously by lithium atom reaction with a mixed halocarbon species.[10] CCl_2Br has also been matrix isolated from pyrolysis of CCl_3Br.[11] In the present study we have investigated ir spectra of matrix isolated gas-phase pyrolysis products of I and II. Spectra of parent molecules I, II, and final product III were also recorded for assignment.

Experimental Section

Samples of I and II were synthesized as described earlier.[5] Both compounds and a commercial sample of C_6H_5HgBr (III) (Alpha Inorganics) were analyzed by mass spectrometry with a Bendix time-of-flight spectrometer. Spectra were recorded at ionizing voltages between 20 and 50 V and the identities of all compounds were confirmed from their molecular peaks.

---

(1) A. K. Maltsev, R. G. Mikaelian, and O. M. Nefedov, *Bull. Acad. Sci. USSR, Div. Chem. Sci.*, 199 (1971).

(2) A. K. Maltsev, R. G. Mikaelian, O. M. Nefedov, R. H. Hauge, and J. L. Margrave, *Proc. U. S. Nat. Acad. Sci.*, in press.

(3) A. K. Maltsev, R. G. Mikaelian, and O. M. Nefedov, *Proc. Acad. Sci. USSR, Chem. Sect.*, (1971).

(4) D. Seyferth, J. M. Burlitch, R. J. Minasz, J. Y.-P. Mui, H. D. Simmons, Jr., A. J. H. Treiber, and S. R. Dowd, *J. Amer. Chem. Soc.*, **87**, 4259 (1965).

(5) D. Seyferth and R. L. Lambert, Jr., *J. Organometal. Chem.*, **16**, 21 (1969).

(6) D. Seyferth, J. Y.-P. Mui, and J. M. Burlitch, *J. Amer. Chem. Soc.*, **89**, 4953 (1967).

(7) D. E. Milligan and M. E. Jacox, *J. Chem. Phys.*, **47**, 703 (1967).

(8) L. Andrews, *ibid.*, **48**, 979 (1968).

(9) L. Andrews and T. G. Carver, *ibid.*, **49**, 896 (1968).

(10) L. Andrews, *ibid.*, **48**, 972 (1968).

(11) J. H. Current and J. K. Burdett, *J. Phys. Chem.*, **73**, 3504 (1969).

$C_6H_5HgCCl_3$ and C_6H_5HgBr impurities were found in I and II and C_6H_5HgCl in III. The percentage of impurities was estimated as approximately 5%. The amount of C_6H_5HgBr in I and II increased during heating of the samples in the mass spectrometer at 50° probably as a result of decomposition in the solid phase.

Methods of evaporation, low-pressure pyrolysis of samples, and the construction of the liquid helium flow cryostat have been described in detail previously.[2,12] Molecules were trapped in an Ar matrix on a polished copper surface and spectra were recorded with a Beckman IR-9 spectrophotometer in the region 400–1000 cm^{-1} where the most important vibrations of the phenyl ring C–Cl and C–Br bonds are found.

The matrix gas to sample mole ratio was calculated by making the following assumptions. The amount of sample used per half-hour trapping was approximately 10 mg or 23 μmol of $PhHgCCl_2Br$. With the furnace orifice located 4 in. from the trapping surface and assuming a cosine distribution of beam intensity one calculates that 1.5% or 0.34 μmol of the total flux reaches the 0.625×1.5 in. trapping surface. The most commonly used trapping rate of Ar was 3.5 cc/min or 4.5 mmol/0.5 hr. All of the Ar is not trapped out, however, as the background pressure of the system rises to 5×10^{-5} mm at this trapping rate. A matrix to sample ratio can be calculated if one makes the reasonable assumption that at least one-third of the Ar introduced is trapped on the same surface as the sample. This gives a ratio of 4400 which suggests that in general sample molecules are well isolated from one another.

Results

C_6H_5HgBr (III). The infrared spectrum of III in an Ar matrix at 15 K is shown in part in Figure 1c and band centers are listed in Table I. All frequencies agree well with the published spectra of III in the crystalline state, in solution, and with the spectrum of matrix-isolated C_6H_5HgCl[3] for vibrations assigned to the phenyl group.

$C_6H_5HgCCl_2Br$ (I). All the reproducible absorptions which occur with constant relative intensities in the spectrum of I in an Ar matrix at 15 K may be divided into several groups (Figure 1a and Table I).[13] The first group corresponds to the well known frequencies[14,15] of the monosubstituted phenyl ring, C_6H_5Hg: 449.0, 694.8, 729.3, 999.5, and 1025.0 cm^{-1}. The second group labeled "d" and "e" absorptions, has band splittings, relative intensities, and band center positions similar to that of $C_6H_5HgCCl_3$ in an Ar matrix.[2] They are assigned to antisymmetric (d) and symmetric (e) stretching vibrations of the CCl_2 portion of I. The three bands of group "f" are completely absent in the $C_6H_5HgCCl_3$ spectrum and thus can be assigned to vibrations which involve the Br atom. Of three bands in group f, the broad one at 646 cm^{-1} increases during matrix warm-up, while the narrow bands at 642.1 and 653.9 cm^{-1} decrease. Thus these two frequencies are believed to be stretching vibrations of the C–Br bond and the 646-cm^{-1} broad band to be due to some associated form.

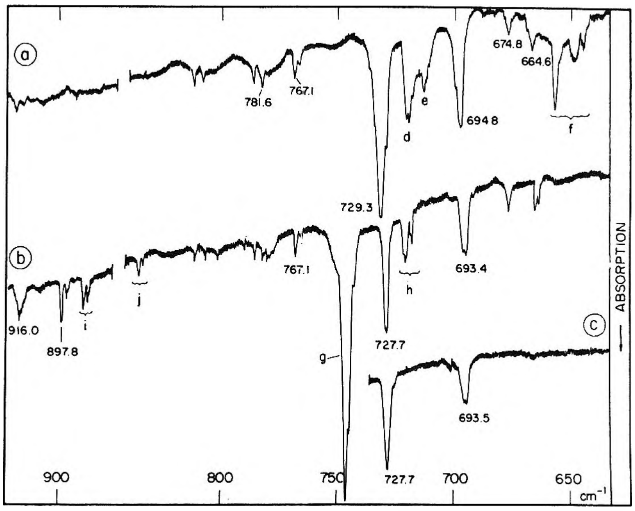

Figure 1. a, $C_6H_5HgCCl_2Br$ in an Ar matrix at 15 K; b, products from pyrolysis of $C_6H_5HgCCl_2Br$ in an Ar matrix at 15 K; c, C_6H_5HgBr in an Ar matrix at 15 K.

In addition there are several weak absorptions in spectrum 1a (664.6, 674.8, and 767.1 cm^{-1}) which change in relative intensity and are absent in some experiments after partial evaporation of the sample in a vacuum. They were assigned to solvent impurities; in particular the 767-cm^{-1} band is due to chloroform. Bands 781.6, 916.0 and probably 785.3, 806.4, and 810.9 cm^{-1} belonging to C_2Cl_4[2,12] appear as a result of thermal decomposition of I in the solid phase.[4] At temperatures higher than 70° this process is much faster such that a half-life of I is thought to be about 1 hr or less.

Pyrolysis of $C_6H_5HgCCl_2Br$. The study of the pyrolysis of I within the temperature range 250–450° has shown that complete decomposition in the gas phase occurs at temperatures higher than 360°. This is evidenced by the absence of f bands (C–Br bond) in spectra of the pyrolysis products (Figure 1b). Bands at 693.4 and 727.7 cm^{-1} are easily assigned to the final product C_6H_5HgBr by comparison with Figure 1c. Weak bands at 664.5, 674.8, 767.1, 779.7, 781.6, 785.3, 806.4, and 810.9 cm^{-1} are essentially the

---

[12] R. H. Hauge, J. W. Hastie, and J. L. Margrave, unpublished results.

[13] Listings of band center measurements and their assignment will appear immediately following this article in the microfilm edition of this volume of the journal. Single copies may be obtained from the Reprint Department, ACS Publications, 1155 Sixteenth Street, N.W., Washington, D. C. 20036. Remit check or money order for $3.00 for photocopy or $2.00 for microfilm.

[14] J. H. S. Green, *Spectrochim. Acta*, **24A**, 863 (1968).

[15] J. Mink, Ph.D. Thesis, Moscow State University, USSR, 1968.

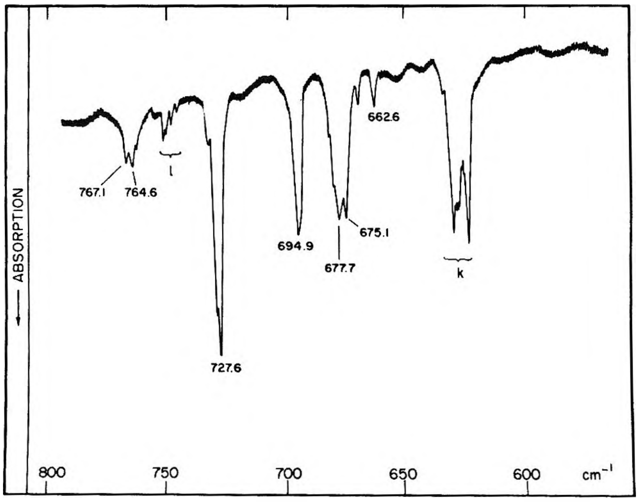

Figure 2. $C_6H_5HgCClBr_2$ in an Ar matrix at 15 K.

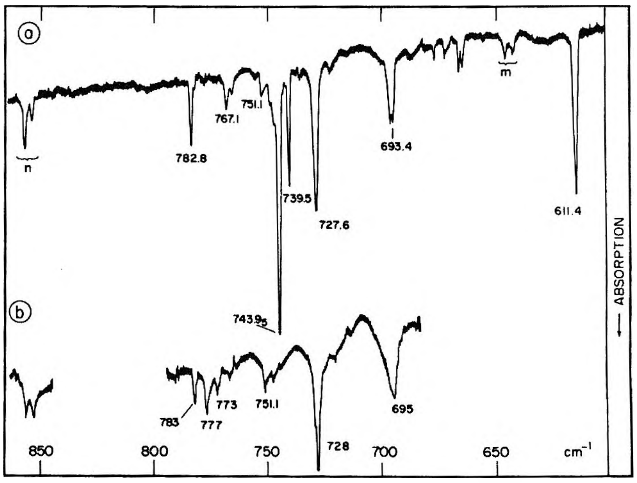

Figure 3. a, Products from pyrolysis of $C_6H_5HgCClBr_2$ in an Ar matrix at 15 K before warm-up; b, after warm-up and recooling to 15 K.

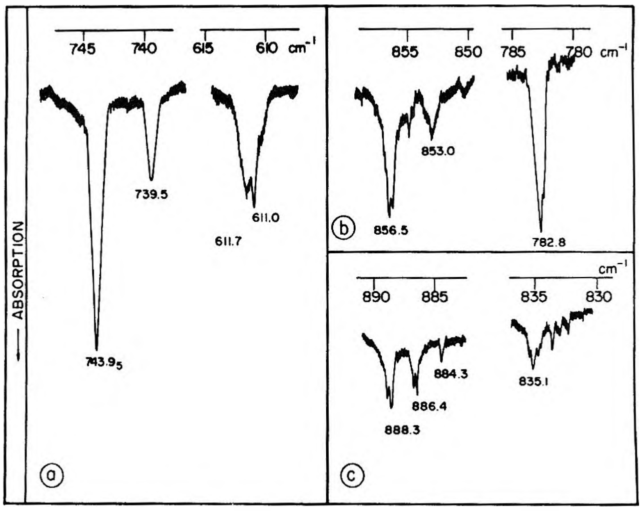

Figure 4. Chlorine and bromine isotope splitting of bands in an Ar matrix at 15 K: a, CClBr; b, $CClBr_2$; c, CCl_2Br.

same as in the spectrum before pyrolysis (Figure 1a) and were also observed in $RHgCCl_3$ pyrolysis studies.[2]

There are four new band groups labeled g-j in Figure 1b. The two strong absorptions g and h correspond well with ν_3 and ν_1 stretching vibrational bands of dichlorocarbene, CCl_2, recently obtained in high resolution.[2] As a result of the $C_6H_5HgCCl_3$ impurity in sample I, as mentioned above, there is also an 897.8-cm^{-1} band of the CCl_3 radical in Figure 1b. Consequently there is a small contribution to the CCl_2 absorption from $C_6H_5HgCCl_3$ pyrolysis. Frequencies and relative intensities of i and j bands agree well with bands previously assigned[10] to the radical CCl_2Br. (No chemical evidence for formation of this radical was obtained when $PhHgCCl_2Br$ reacted with olefins in benzene solution at 80°.[4])

$C_6H_5HgCClBr_2$ (II). Absorptions assigned to II in the 400–940-cm^{-1} region are listed in Table II[13] and shown in Figure 2. There are the known bands of the phenyl ring vibrations (448.8, 694.9, 727.6–728.6 cm^{-1}) and some impurity lines (662.6, CO_2; 767.1, $CHCl_3$) which are the same as in spectra presented above and also in a previous paper.[2] The group of weak bands marked l is also present in pyrolysis products spectra and does not vary in proportion to other bands, and thus it is believed to be caused by an impurity, $CClBr_3$.[9] Another weak impurity absorption occurs at 669.6 cm^{-1}. By analogy to other strong bands of carbon–halogen stretching vibrations, the group k is thought to be a C–Br bond stretch and the 675.1–677.7 bands primarily due to a C–Cl stretch. During warm-up of the matrix, relative intensities within both these groups change similarly such that the low-frequency lines, 623.3 and 675.1, respectively, become much stronger.

Pyrolysis of $C_6H_5HgCClBr_2$. The pyrolysis of II is almost complete at temperatures of 300–320° as seen from the absence of parent compound bands in Figure 3a. However, new absorptions appear which include the 693.4 and 727.6-cm^{-1} features of C_6H_5HgBr. The bands of group n and the 782.8-cm^{-1} peak may be clearly assigned to the $CClBr_2$ radical by comparison with Andrews' data[10] and by the presence of two bands 856.0 and 853.0 with a frequency separation and relative intensities as expected from the presence of a single chlorine atom with natural isotopic abundance (Figure 4b).

The matter of greatest interest is an assignment of the three strongest bands centered at 611.4, 739.5, and 743.9 cm^{-1}. All three lines grow with constant relative intensities during trapping and should belong to the same molecule. A high-resolution study has shown a 0.7-cm^{-1} splitting of the 611.4 into two peaks with equal intensities and an absence of splitting of the two other bands (Figure 4a). The ratio of intensities was found to be $I_{743.9}:I_{739.5}:I_{611.4} = 1:0.34:0.69$.

Experiments with a warm-up of the matrix have been run to study the relative reactivity of this molecule. The three bands in question diminished simultaneously with every consecutive increase of the temperature from 15 K. Their rate of reduction was found to be more rapid than absorptions of $CClBr_2$ and complete disappearance occurred at a lower temperature. New bands grew in at 777, 773, 686, and 652 (broad) cm^{-1}.

Discussion

CCl_2Br and $CClBr_2$ Radicals. The chlorine isotopic splitting and relative intensities for the i absorption at 885-890 cm^{-1} (Figures 1b and 4c) agree with that expected for two equivalent chlorine atoms with natural abundances of $^{35}Cl_2$, $^{35}Cl^{37}Cl$, and $^{37}Cl_2$ isotopic combinations.

For the n absorption near 855 cm^{-1} (Figures 3a and 4b) the chlorine isotopic splitting into two bands and their relative intensities indicate the presence of a single chlorine atom in the molecule. The expected bromine isotopic splitting is apparently smaller than the 1-cm^{-1} half-width of the 855-cm^{-1} bands.

Bands j near 835 cm^{-1} (Figures 1b and 4c) and the 782.8-cm^{-1} band (Figures 3a and 4b) grow during trapping and disappear after warm-up of the matrix in a similar manner to i and n bands, respectively. Thus j and i bands have been assigned to CCl_2Br and the n and 782.8-cm^{-1} bands to $CClBr_2$.

In a paper devoted to a study of the CCl_3 radical[10] Andrews has suggested that reactions of CCl_3Br, CCl_2Br_2, and $CClBr_3$ with lithium atoms lead to the formation of CCl_2Br and $CClBr_2$ free radicals. The good agreement (within 1 cm^{-1}) between frequencies observed by Andrews[10] and our results gives added confidence to the current assignments (Tables I and II). The 620-cm^{-1} band labeled C_3 in ref 9 and assigned to the symmetric stretching vibration of the CCl_2Br radical was not observed in the present study and thus supports a planar structure for the radical. However, this could be due to the small amount of CCl_2Br present.

Dichlorocarbene. The high-resolution ir spectrum of dichlorocarbene CCl_2 in an Ar matrix has been given in an earlier publication.[2] A $C^{35}Cl_2$-$C^{37}Cl_2$ splitting of 4.0 ± 0.4 cm^{-1} was found for the ν_3 stretching vibration which gives a bond angle of $\sim$108°. However, CCl_2 was observed along with strong bands of the CCl_3 radical in contrast to the present study where CCl_2 band intensities were at least ten times stronger than band intensities of any other radical (Figure 1b). (The much higher reactivity of $PhHgCCl_2Br$ as a CCl_2 source—compared to $PhHgCCl_3$—has been noted in solution studies at 80°.[4]) Thus a clearer chlorine isotopic splitting pattern was obtained and therefore a slightly better measurement of the ν_3 splitting (4.1 ± 0.2 cm^{-1}).

Bromochlorocarbene. The three strongest bands at 743.9, 739.5, and 611.4 cm^{-1} resulting from $C_6H_5HgCClBr_2$ pyrolysis are assigned to the same molecular species. The band intensity ratio of $I_{743.9}:I_{739.5}$ = 1:0.34 agrees well with ^{35}Cl-^{37}Cl isotopic natural abundance for a molecule with a single chlorine atom (1:0.33). The observed value of the isotopic shift of 4.45 cm^{-1} is similar to those found for monochloroalkyl molecules.[16] Both bands are shown in Figure 4a with half-widths of $\sim$1 cm^{-1}. The above observations support an assignment of the 743.9 and 739.5 cm^{-1} absorptions to a vibration involving a single chlorine atom. The third band centered at 611.4 cm^{-1} shows a partially resolved splitting of 0.7 cm^{-1} (Table II, Figure 4a) which can be explained by the presence of ^{79}Br-^{81}Br isotopes in a molecule with a single bromine atom. The 740-cm^{-1} region is close to that found for a C-Cl bond stretching vibration in monochloroalkyl molecules while the frequency region near 611 cm^{-1} is reasonable for a C-Br stretch. The matrix warm-up experiments have shown the reactivity of the molecule under consideration to be much greater than that of $CClBr_2$ free radical. All of the above observations are consistent with the absorbing species being CClBr. This molecule would have three vibrational frequencies with a bending mode in the far-infrared spectral region.

Recently, Andrews and coworkers have obtained very interesting results for a number of different radicals and carbenes,[17] particularly CCl_2Br, $CClBr_2$, and CBrCl, by using alkali metal atom reactions with mixed halocarbon species in rate gas matrices.[17] This method seems to have many advantages and a bright future. However, in the case of reactions with mixed chlorobromomethanes the alkali metal atoms (M) may withdraw either halogen to form two different free radicals and possibly two carbenes simultaneously. This situation tends to produce overlapping features, strong interference from the molecular precursor, and some band broadening due to the necessity of working with a matrix gas to reactive molecule ratio of the order of 300-600 rather than typical ratios of 1000-10,000 as in the present experiments. In contrast, matrix spectra obtained from pyrolysis of $RHgCX_3$ compounds usually give only weak absorptions from molecules other than carbenes. For these reasons it is felt that the production of halocarbenes from pyrolysis of $RHgCX_3$ compounds allows more accurate measures of band position and isotopic splitting.

Pyrolysis Mechanism. The mechanism of the gas-phase pyrolysis reaction is similar to one described for $RHgCCl_3$ molecules[2,3] and includes the formation of a carbene and in part a radical. The observation of dichlorocarbene, CCl_2, and the absence of CBrCl bands

---

(16) S. T. King, *J. Chem. Phys.*, **40**, 1321 (1968).

(17) See, for example, ref 8-10.

in spectra from pyrolysis of I has proved that the dissociation process goes primarily through formation of C_6H_5HgBr rather than of C_6H_5HgCl, in agreement with reactions of I in solution and its decomposition in the solid phase.[4] It may be concluded from the study of the pyrolysis of $C_6H_5HgCCl_2Br$ that this reaction is at present the best source of dichlorocarbene in the gas phase.

Acknowledgments. This work was supported by the U. S. Atomic Energy Commission. Liquid helium was supplied by a grant from the Office of Naval Research. The experimental part of this work was done at the Department of Chemistry, Rice University, while one of us (A. K. M.) was a Visiting Scientist under auspices of the U. S. S. R. and U. S. A. Academies of Science.

The Infrared Spectrum of Polyethylene Irradiated at 4°K

by David C. Waterman

Department of Chemistry and Materials Research Center, Northwestern University, Evanston, Illinois 60201

and Malcolm Dole*

Department of Chemistry, Baylor University, Waco, Texas 76703 *(Received July 26, 1971)*

Publication costs assisted by the U. S. Atomic Energy Commission

Both ultraviolet and infrared measurements were made at 4°K on a high-density polyethylene after irradiation with 1-MeV electrons at 4°K. No significant changes were observed in the uv spectrum due to the irradiation. On warming to 77°K a small shoulder appeared at 258 nm equivalent to about 4% of the allyl free radical ultimately formed after annealing at room temperature. In the ir spectra two overlapping absorption bands at about 973 and 966 cm^{-1} were produced at 4°K, but on warming to 77°K the two bands were transformed into the single sharp band characteristic of the vinylene group at 966 cm^{-1}. The total area of the double band was almost exactly equal to that of the single band. The new band at 973 cm^{-1} is tentatively assigned to the transient, the $—CH{=}C^{+}H—$ ion. Irradiations at 77°K with subsequent heating to room temperature demonstrated that there is no decay of the *trans*-vinylene group during low-temperature irradiations.

Introduction

In this paper both the ultraviolet and infrared spectra are reported of linear polyethylene irradiated with 1-MeV electrons at liquid helium temperature and at 77°K. The uv observations will be described, but they were not as interesting as the changes in the ir spectra; hence the emphasis in this report will be on the latter. As far as we are aware, there has hitherto been no observations of the uv or ir spectra at 4°K of polyethylene (PE) irradiated at that temperature. Rexroad and Gordy[1] irradiated PE at liquid helium temperature and examined its esr spectrum to see if hydrogen atoms could be formed and trapped at 4°K, but none was found. Aulov, *et al.*,[2] studied the radiothermoluminescence on heating to higher temperatures of both low- and high-density polyethylene irradiated at liquid helium temperature.

Experimental Section

Marlex 6002 PE which was used in our previous studies[3,4] was melted onto nickel wire mesh having a reported transparency of 80%. By supporting the PE in this way rapid heat transfer could be achieved between the thin layer of PE, its nickel support, and the copper block to which the nickel mesh was clamped with the nickel mesh side in contact with the fixed half of the block. A liberal application of Apiezon grease N around the edge of the nickel mesh improved the thermal contact. In the case of the irradiations at 77°K, Marlex-6002 films 0.26 and 0.023 mm in thickness were used.

The combined irradiation and spectroscopic cell is illustrated in Figure 1. It was an adaptation of the cell previously used[3] at 77°K. A and B are the filling tubes for the liquid nitrogen, C, and helium, D, reservoirs, respectively. Inasmuch as the cell was held at an angle of about 30° under the electron beam generator so that the stream of electrons could pass through the

---

[1] H. N. Rexroad and W. Gordy, *Phys. Rev.*, **125**, 242 (1962).

[2] V. A. Aulov, F. F. Sukhov, I. V. Chernyak, and N. A. Slovokhotova, *Khim. Vys. Energ.*, **2**, 191 (1968); **3**, 452 (1969).

[3] D. C. Waterman and M. Dole, *J. Phys. Chem.*, **74**, 1906 (1970).

[4] D. C. Waterman and M. Dole, *ibid.*, **74**, 1913 (1970).

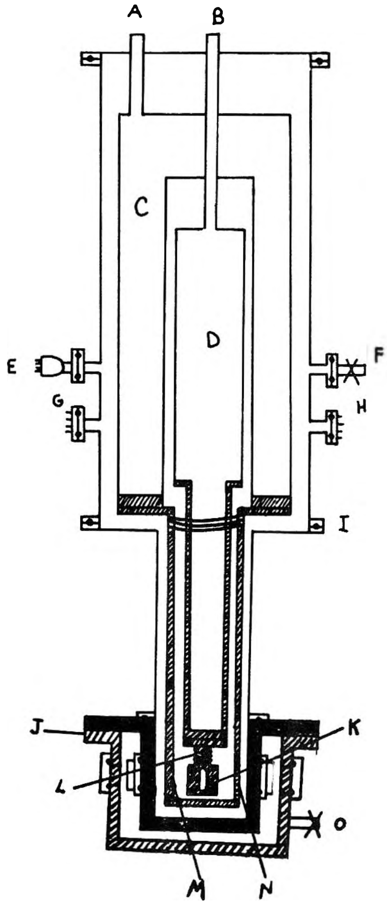

Figure 1. Low-temperature combined irradiation and spectroscopic cell. Parts shaded with slant marks were made out of copper while the completely shaded areas were made of brass. Other parts were made of stainless steel.

windows of the cell and the PE sample in a vertical direction, the cell windows on jacket J of Figure 1 should be rotated through 90° about the vertical axis in the figure to conform to actual practice. E is a port containing the electrical connections for a thermocouple vacuum gauge; F is the connection to the vacuum pump. G contains the electrical leads to the chromel–alumel thermocouples on the liquid nitrogen shield and to the carbon resistor (used to measure the temperature) on the sample holder. H contains the leads to the heaters on the nitrogen radiation shield and sample holder, respectively. At point I are the bolts that hold the lower section surrounding the sample holder to the liquid helium reservoir. Evacuation of the gas in the space surrounding the liquid helium reservoir D takes place through holes at the bottom of the radiation shield at M and N. The outer section which is attached at J after the irradiation is evacuated through the port O. When this is accomplished, the titanium windows through which the electron beam passed during the irradiation fall off and can be rolled aside. Atmospheric pressure then holds the outer windows in place for the spectroscopic observations. In this way the cell windows can be changed after the irradiation and before the spectroscopic observations without raising the temperature of the sample or losing the vacuum about it. K is the sample holder which can be heated by the heating elements at L. Irradiation doses were 20 and 40 Mrads at a dose rate of about 100 Mrads hr^{-1}.

After the sample had been irradiated its uv or ir spectrum was observed, first at 4°K and again at 4°K after heating the sample to 77°K. No attempt was made to exclude visible light from the irradiation–spectroscopic cell during any of this work.

One experiment was done with a dose of 5 Mrads in order to observe any possible changes in the uv, visible, or near-ir part of the spectrum.

Results and Discussion

Irradiations at 4°K. First of all, it can be said that within the accuracy of our experiments no difference in the spectra taken at 77 and 4°K of unirradiated PE could be observed. In the case of the uv, visible, and near-ir study, after the PE sample was irradiated to a dose of 5 Mrads its spectrum was taken at 4°K; it was then heated to 77°K and its spectrum was again taken after recooling to 4°K. There was no change in the intensity of the alkyl radical ($-CH_2\dot{C}HCH_2-$) absorption band at 215 nm during the heating and cooling process, nor was there any change of the intensity of the spectrum in the region of the conjugated diene absorption, about 236 nm. A small shoulder in the spectrum appeared at 258 nm, which is the wavelength attributed by Waterman and Dole[3] to the allyl free radical in irradiated PE, $-\dot{C}HCH{=}CH-$. This shoulder was definitely not present in the spectrum immediately after the irradiation at 4°K, and it demonstrates the slight formation of the allyl radical on heating from 4 to 77°K. The amount of allyl radical formed was about 4% of the total amount observed after heating to room temperature and after all of the alkyl free radicals had decayed.[4]

No other changes were observed in the spectrum from 200 to 2000 nm. Cooling the irradiated sample from 77 to 4°K had little effect on the intensity of the allyl or dienyl absorbance, and in general the uv studies were rather unproductive of significant observations. No indication of absorptions due to trapped electrons was observed; they may have been bleached by visible light before the spectrum was taken.[5] Shida and Hamill[6] studied the absorption spectra of positive olefin ions trapped in γ-irradiated organic glasses and found that vinyl-type positive ions were not detectable and probably could not be trapped as such. Vinylene and vinylidene positive ions exhibited rather broad ab-

(5) R. M. Keyser, J. Lin, K. Tsuji, and F. Williams, *Polym. Prep., Amer. Chem. Soc., Div. Polym. Chem.*, 9, 227 (1968).

(6) T. Shida and W. H. Hamill, *J. Amer. Chem. Soc.*, 88, 5376 (1966).

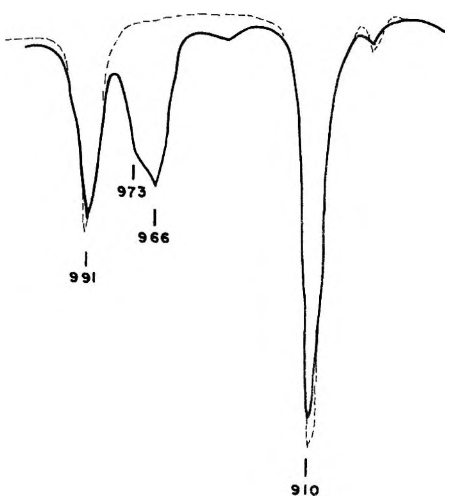

Figure 2. Infrared spectrum of unirradiated Marlex-6002 polyethylene at 4°K, dashed line. Solid line is the infrared spectrum of the same sample taken at 4°K after an irradiation to 40 Mrads at 4°K.

sorption spectra in the range 600–800 nm. In the case of 5 mol % cyclohexene in *sec*-BuCl, the absorption was quite weak with a broad maximum at 700 nm. The absorption band of the positive olefinic ion in pure hexene-2 was stronger with a small maximum around 650 nm and a broad more intense maximum around 1600 nm. Perhaps such absorption bands could have been observed in this work if doses larger than 5 Mrads had been used.

More interesting were the ir absorbances. In Figure 2 the 4°K spectra of unirradiated PE and PE irradiated to 40 Mrads at 4°K are compared. It can be seen that there was a small amount of vinyl group decay, about 14%, during the 4°K irradiation. However, there was no further decay of the vinyl group, Figure 3, on heating from 4 to 77°K. This is in contrast to the significant amount of vinyl decay that occurs on heating from 77°K to room temperature.[4] Inasmuch as allyl free radicals were probably formed[4] by reaction of an alkyl free radical with a double bond, the double bond involved in the allyl free radical formation on heating from 4 to 77°K must have been the vinylene group. Shida and Hamill[6] attribute the lack of absorption spectra characteristic of positive olefinic ions in the case of vinyl type unsaturation such as in hexene-1 to a rapid dimerization type reaction of a vinyl positive ion with a neutral vinyl group as postulated by Chang, Yang, and Wagner.[7]

No diene absorption in the ir at 988 cm^{-1} could be detected, either after the irradiation at 4°K or after heating to 77°K. However, diene was formed on heating from 77°K to room temperature. Partridge[8] proposed that the diene could be produced by the scission of two CH bonds on one carbon atom. The liberated H atoms would then be required to abstract H atoms from adjacent carbon atoms followed by a shift of a

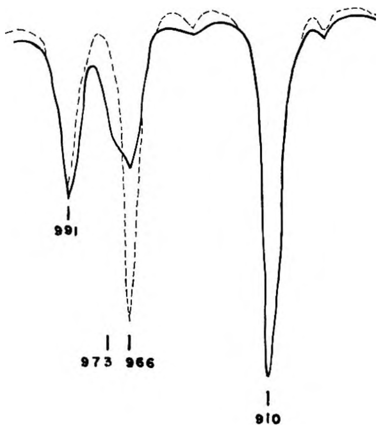

Figure 3. Solid line same as the solid line in Figure 2; dashed line, infrared spectrum of polyethylene taken at 4°K after an irradiation at 4°K to 40 Mrads and after heating briefly to 77°K.

hydrogen atom two positions along the chain or to abstract H atoms from one adjacent carbon atom and from one β to the free radical followed by a shift of one H atom one position along the chain. As calculated by Dole, Böhm, and Waterman,[9] H-atom migration along a chain is unlikely to happen, even at room temperature unless the $-CH_2-$ group exists in an excited state. Fallgatter and Dole[10] suggested that two hydrogen molecules might be liberated in the same act to form bicyclo[1.1.0]butane

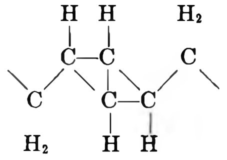

which is unstable and reverts to the diene. At 4°K or 77°K the bicyclobutane might be stable enough not to revert to the diene.

In Figure 2 can be seen what are apparently two overlapping ir absorption bands in the neighborhood of 966 cm^{-1}, the frequency of the absorption due to the vinylene group. This double absorption band merges to a single band on heating from 4° to 77°K (Figure 3) with the position of the peak of the absorption band accurately at the wave number expected for the *trans*-vinylene group. As a tentative suggestion for the assignment of the transient absorption band at about 973 cm^{-1} we wish to suggest that the band could be due to the $—CH{=}C^{+}H—$ cation. On warming from 4° to 77°K the cations could reunite with trapped electrons to become the *trans*-vinylene group. Mitigating against this hypothesis is the fact that no spectra due to trapped electrons could be detected, but their absorption may have been too broad or too weak to have been detected in the uv studies. On the other hand the total area of the two overlapping bands at 973 and 966 cm^{-1} of Figure 2 is almost exactly equal to the area of the single band of Figure 3 at 966 cm^{-1}. This strongly suggests that the transient species giving rise to the 973 band is converted quantitatively into the *trans*-vinylene group and that its extinction coefficient must be very nearly equal to that of the *trans*- vinylene band at 966 cm^{-1}. Furthermore, in the published report of the radio thermoluminescence studies of Aulov, *et al.*,[2] on PE irradiated at 4°K a small shoulder on the luminescence curve at about 60 to 70°K can be seen. This is consistent with the postulate that the conversion of the 973-cm^{-1} band to the 966-cm^{-1} band is due to the untrapping of electrons below 77°K.

---

[7] P. C. Chang, N. C. Yang and C. D. Wagner, *J. Amer. Chem. Soc.*, 81, 2060 (1959).

[8] R. H. Partridge, *J. Chem. Phys.*, 52, 1277 (1970).

[9] M. Dole, G. G. A. Böhm, and D. C. Waterman, *Eur. Polym. J. Suppl.*, 93 (1969).

[10] M. B. Fallgatter and M. Dole, *J. Phys. Chem.*, 68, 1988 (1964).

Boustead and Charlesby[11] studied thermoluminescence curves above 77°K and concluded that a glow peak at 102°K was associated with trapping at a vinyl group, and a second peak at 104°K at a vinylene group. Boustead and Charlesby calculated from the equation $E(\text{ev}) = 2 \times 10^{-3}T(°\text{K})$ where E is the infrared vibrational stretching energy of the vinyl group frequency, 1650 cm^{-1}, that this energy corresponded to 102°K, the approximate temperature at which the vinyl glow peak was observed. Using 973 cm^{-1}, the frequency of the low-temperature ir absorption band observed here, we obtain 60°K as a predicted temperature for a glow peak associated with the 973-cm^{-1} band. This temperature is in the temperature range where the 973 band disappeared. Campbell[12] γ-irradiated both low- and high-density polyethylenes at 77°K and examined their esr spectra before and after irradiation and after photobleaching with light of wavelength greater than 750 or 1000 nm. He discovered a simultaneous decay of triplet and singlet esr spectra, the latter due to trapped electrons and the former to a postulated positive ionic species associated with vinylidene unsaturated groups. The latter could not have been the species responsible for the 973-cm^{-1} absorption band observed here, because its intensity reached a maximum at a dose of 0.5 Mrad whereas in our case the concentration of the postulated ionic species was linear with dose up to 40 Mrads. Furthermore, we had no vinylidene unsaturation in our sample. However, it would be interesting to measure the esr spectra of polyethylene irradiated at 4°K and maintained in the dark to prevent optical bleaching. In the work of Rexroad and Gordy[1] mentioned above no signal due to trapped electrons was observed at 4°K after an irradiation at that temperature, "only a broad central resonance with $g = 2.00$." The electron spectrum is a sharp singlet, but Rexroad and Gordy apparently made no effort to exclude light from their cryostat or esr cavity.

To summarize, we believe that the 973-cm^{-1} band is to be attributed to the —CH=C$^+$H— group because (a) it appears in the region of the spectrum expected for a C–H wagging vibration; (b) as judged from the magnitude of the absorption bands it appears to be quantitatively converted to the —CH=CH— absorption band on heating to 77°K; (c) the band apparently has an extinction coefficient close to that of the *trans*-vinylene group; and (d) Aulov, *et al.*,[2] detected radiothermoluminescence occurring in the 70°K range.

The intensity of the 966-cm^{-1} band after heating to 77°K and after a dose of 40 Mrads was twice that of a sample similarly treated but given a dose of only 20 Mrads. Thus it would appear that the growth of the *trans*-vinylene group is linear with dose after the transient at 973 cm^{-1} has been converted to the *trans*-vinylene group.

It should be noted that the ir absorption band of the postulated -CH=C$^+$H— ion occurs at slightly higher frequency than that of the —CH=CH— group itself; however, the difference is very small, only about 5 to 7 wave numbers. It is very difficult to predict the shift in the maximum of the absorption band because of the fact that the observations concern the out of plane bending frequency of the C–H group in the solid state. Possibly the removal of an electron from the —CH=CH— group, if it is an anti- or nonbonding electron, will increase the bond energy in the resulting cation. While we do not have values for the bond energy of the C–H bond in the neutral or positively charged vinylene group in solid polyethylene, there are examples where the bond energy is greater in the cation than in the neutral molecule; *e.g.*, CH$^+$ has a bond energy of 85 kcal mol^{-1} as compared to 81 kcal mol^{-1} for CH.[13]

Irradiations at 77°K. Because of the double reservoirs of the combined irradiation–spectroscopic cell illustrated in Figure 1, it was convenient to carry out irradiations of PE film to very high doses, 225 Mrads at liquid nitrogen temperature. After each irradiation the film was heated to room temperature and the concentration of the *trans*-vinylene group produced by the irradiation was measured by means of the ir absorption band at 966 cm^{-1}. Figure 4 illustrates the data obtained where it can be seen that the yield of *trans*-vinylene groups was linear with dose up to 225 Mrads. The data of Figure 4 can be assumed to represent values obtained at 77°K because there was very little change in the *trans*-vinylene concentration on heating to room temperature after the irradiation at 77°K as the data of Table I demonstrate.

Slovokhotova, *et al.*,[14] also noted no significant

---

[11] I. Boustead and A. Charlesby, *Proc. Roy. Soc., Ser. A*, 316, 291 (1970).

[12] D. Campbell, *J. Polym. Sci. Part B*, 8, 313 (1970).

[13] S. W. Benson, *J. Chem. Educ.*, 42, 502 (1965).

[14] N. A. Slovokhotova, A. T. Koritskii, V. A. Kargin, N. Ya. Buben, V. V. Bibikov, Z. F. Il'icheva, and G. V. Rudnaya, *Polym. Sci., U.S.S.R.*, 4, 1244 (1963).

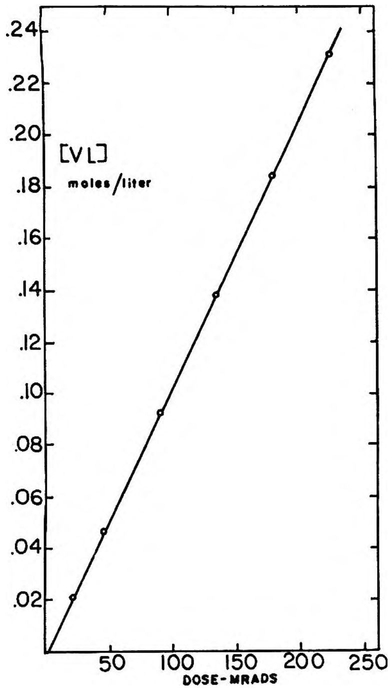

Figure 4. Growth of the *trans*-vinylene group as a function of dose in Marlex-6002 polyethylene. Irradiations at 77°K followed by infrared analysis at room temperature.

Table I: Absorbances of Polyethylene at 910 and 966 cm^{-1} after Irradiations at 77°K before and after Heating to Room Temperature

Dose, Mrads	Treatment of film	Absorbance	
		910 cm^{-1}	966 cm^{-1}
0	As received	0.644	0.00
35	Not heated above 77°K	0.475	0.241
35	After heating to 25°	0.296	0.254
70	Not heated above 77°K	0.385	0.503
70	After heating to 25°	0.261	0.510

change in the absorption band at 966 cm^{-1} on heating to room temperature after an irradiation at 77°K. On the other hand, as found previously,[15] the vinyl group concentration as measured by the ir band at 910 cm^{-1} decreased materially during the post-irradiation heating.

It should be mentioned that at low doses the thicker Marlex-6002 film was used and at the high doses the 0.023-mm film. Data obtained from the two films overlapped well and the linearity of the data of Figure 4 demonstrate that there was no effect of film thickness on the results.

The yield of *trans*-vinylene unsaturation was considerably less at 77°K than at room temperature. From the slope of the straight line of Figure 4, $G(t\text{-Vl})$ was calculated to be 1.03 in contrast to the value of 2.4 found by Kang, Saito, and Dole[16] by extrapolating data for 35° irradiations to zero dose. Slovokhotova, *et al.*,[14] concluded that the yield of *trans*-vinylene double bonds was the same for irradiations at room temperature as at 77°K. However, they were apparently referring to the overall yield including decay of *trans*-vinylene groups due to the irradiation. At a 27-Mrad dose, for example, Kang, *et al.*,[16] measured an average $G(t\text{-Vl})$ value of only 1.4, a decrease of one G unit from the extrapolated value at zero dose. Kang, *et al.*,[16] used 139 l. cm^{-1} mol^{-1} for the extinction coefficient of the *trans*-vinylene group in polyethylene while a more up to date value of 169[17] was used in this research. Kang's $G(t\text{-Vl})$ value at zero dose would be reduced to 2.0 if 169 were used in their calculations.

The data of Figure 4 demonstrate that there is no destruction of vinylene unsaturation by irradiation at 77°K. Partridge[18] had concluded that decay of *trans*-vinylene groups was independent of temperature and this conclusion was in agreement with his theory of excitation energy transfer in polyethylene. It would appear, however, that at 77°K or lower there is apparently insufficient chain mobility for the *trans*-vinylene groups to react, even though they become activated by exciton migration.

Acknowledgments. This research was supported by the U. S. Atomic Energy Commission, first at Northwestern University and then at Baylor University, and by income from the chair in Chemistry at Baylor University endowed by a gift from The Robert A. Welch Foundation. We are also indebted for support provided by the Advanced Research Projects Agency of the Department of Defense through the Northwestern University Materials Research Center. Dr. J. A. Reid of the Phillips Petroleum Company kindly supplied the polyethylene samples. We acknowledge with thanks a stimulating conversation with Dr. R. H. Partridge.

---

(15) M. Dole, D. C. Milner, and F. Williams, *J. Amer. Chem. Soc.*, **80**, 1580 (1958).

(16) H. Y. Kang, O. Saito, and M. Dole, *ibid.*, **89**, 1980 (1967).

(17) R. J. de Kock, P. A. H. M. Hol, and H. Boz, *Z. Anal. Chem.*, **205**, 371 (1964).

(18) R. H. Partridge, *J. Chem. Phys.*, **52**, 2501 (1970).

Low-Frequency Modes in Molecular Crystals. XVII.[1a] Torsional Motions and Barriers to Internal Rotation in Some Ethylsilanes, Ethylgermanes, and Ethanol[1b]

by J. R. Durig* and C. W. Hawley

Department of Chemistry, University of South Carolina, Columbia, South Carolina 29208

(Received July 19, 1971)

Publication costs borne completely by The Journal of Physical Chemistry

The far-infrared spectra of solid $CH_3CH_2SiH_3$, $CH_3CH_2SiD_3$, $CH_3CH_2SiCl_3$, $CH_3CH_2GeH_3$, $CH_3CH_2GeCl_3$, CH_3CH_2OH, and CH_3CD_2OD have been recorded. The low-frequency Raman spectra were also recorded for all the solids except ethanol. The interesting CH_3 torsional modes were observed in the spectra of the solids at 211, 210, 257, 189, 245, 282 and 251, and 198 and 184 cm^{-1}, with corresponding barriers of 2.82, 2.88, 4.41, 2.33, 4.03, 4.05, and 4.04 kcal/mol for ethylsilane, ethylsilane-d_3, ethyltrichlorosilane, ethylgermane, ethyltrichlorogermane, ethanol, and ethanol-d_6, respectively. The SiH_3 and GeH_3 torsional modes were observed at 142 and 113 cm^{-1}, which leads to respective barrier heights of 1.99 and 1.37 kcal/mol. Assignments are proposed for the other low-frequency modes. The trends in the barriers are discussed in terms of present theory.

I. Introduction

In some recent publications we have demonstrated the utility of the far-infrared spectra of molecular solids for the direct observation of torsional transitions.[2,3] There have been several recent theoretical papers in which barriers to internal rotation of the methyl moiety have been predicted.[4-10] However, in some cases there are no reliable experimental data for comparison or the theoretical values were compared to incorrect experimental ones. In several of these papers predictions for barrier heights are given for molecules which contain two or three halogen atoms or row three or four elements. However, microwave studies have usually been limited to first row elements and only fluorine substitution in the case of the halogen atoms. In most cases fluorine substitution has not caused dramatic changes in the barrier heights from those obtained for the corresponding hydrogen analogs. Therefore, if potential barrier changes are going to be discussed in familiar chemical terms such as electronegativity, induction, and resonance, there is a real need to find molecules which show marked barrier changes with changes in substituents. It is expected that chlorine and heavy atom changes should produce these marked effects. Thus, we have undertaken a study of the low-frequency vibrations of ethylsilane, ethylgermane, ethyltrichlorosilane, ethytrichlorogermane, and ethanol for the purpose of obtaining the methyl torsional frequencies with the corresponding barriers restricting internal rotation of the methyl group.

II. Experimental Section

Ethylsilane and ethylgermane were produced by the $LiAlH_4$ reduction of corresponding trichlorides as described by Mackay and Watt,[11] except that *n*-butyl ether was used as the solvent. Ethylsilane-d_3 was prepared similarly using $LiAlD_4$ for the reduction. The purity of the compounds was checked by comparing the mid-infrared spectra to those published earlier;[11] no extraneous bands were observed. Ethyltrichlorosilane and ethyltrichlorogermane were purchased commercially and purified by trap-to-trap distillation. Again, the purity was checked by comparing the mid-infrared spectra with those published earlier.[12,13] The ethanol and ethanol-d_6 were obtained from commercial sources with stated purities of 99+% and were used without further purification.

The far-infrared spectra of solid samples were re-

---

[1] (a) For part XVI, see *J. Chem. Phys.*, in press. (b) Taken in part from the thesis of C. W. Hawley to be submitted to the Department of Chemistry in partial fulfillment of the Ph.D. degree.

[2] (a) J. R. Durig, S. M. Craven, and J. Bragin, *J. Chem. Phys.*, **51**, 5663 (1969); (b) *ibid.*, **52**, 2046 (1970).

[3] J. R. Durig, C. M. Player, Jr., and J. Bragin, *ibid.*, **54**, 460 (1971).

[4] J. P. Lowe and R. G. Parr, *ibid.*, **44**, 3001 (1966).

[5] W. H. Fink and L. C. Allen, *ibid.*, **46**, 2261 (1967).

[6] W. H. Fink and L. C. Allen, *ibid.*, **46**, 2271 (1967).

[7] R. A. Scott and H. A. Scheraga, *ibid.*, **42**, 2209 (1965).

[8] W. H. Fink and L. C. Allen, *ibid.*, **46**, 3270 (1967).

[9] V. Magnasco, *Nuovo Cimento*, **24**, 425 (1962).

[10] For an up to date review of theoretical treatments of internal rotations, see J. P. Lowe in "Progress in Physical Organic Chemistry," A. Streitwieser, Jr., and R. W. Taft, Ed., Vol. 6, Interscience, New York, N. Y., 1968, pp 1-109.

[11] K. M. Mackay and R. Watt, *Spectrochim. Acta*, **23A**, 2761 (1967).

[12] S. E. Rudakova and Yu. A. Pentin, *Opt. Spectrosc.*, 18, 339 (1965).

[13] B. M. Gibson, M. S. Thesis, University of South Carolina, 1967.

Table I: Low-Frequency Vibrations and Assignments for Ethylsilane, Ethylsilane-d_3, and Ethylgermane

$CH_3CH_2SiH_3$				$CH_3CH_2SiD_3$					$CH_3CH_2GeH_3$				
Infrared solid		Raman liquid (−180°)		Infrared solid		Raman liquid (−180°)			Infrared solid		Raman liquid (−180°)		
$\bar{\nu}$, cm^{-1}	Rel int	$\Delta\bar{\nu}$, cm^{-1}	Rel int	$\bar{\nu}$, cm^{-1}	Rel int	$\Delta\bar{\nu}$, cm^{-1}	Rel int	Shift factor	$\bar{\nu}$, cm^{-1}	Rel int	$\Delta\bar{\nu}$, cm^{-1}	Rel int	Assignment
...		...		424	m	420	m	...					SiD_3 rock
412	w	...		391	w	...		...					2 × 211 = 422
357	w	...		...		...		...					211 + 142 = 353
237	m	240	m	220	m	230	m	1.08	241	s	232	s	CCX deformation
211	m	...		210	m	...		1.00	189	w	...		CH_3 torsion
142	w	...		101	w	...		1.41	113		116	m	XH_3 torsion
92	m	...		90	m	...		1.02					Translation
49	m	...		46	m	...		1.06					Libration

Table II: Low-Frequency Vibrations and Assignments of Ethyltrichlorosilane and Ethyltrichlorogermane

$CH_3CH_2SiCl_3$					$CH_3CH_2GeCl_3$					
Infrared (solid)		Raman (solid)			Infrared (solid)		Raman (solid)			
$\bar{\nu}$, cm^{-1}	Rel int	$\Delta\bar{\nu}$, cm^{-1}	Rel int	Depol.[a] ratios (liquid)	$\bar{\nu}$, cm^{-1}	Rel int	$\Delta\bar{\nu}$, cm^{-1}	Rel int	Depol.[b]	Assignment
...		...			294	m	291	m	p	CCGe deformation
257	w	251	w		245	w				CH_3 torsion
222	s	221	m	dp	179	m	171	s	dp	XCl_3A' symmetric deformation
189	w	176	w	dp	157	s	146	s	dp	XCl_3A'' antisymmetric defor.
180	m									XCl_3A' antisymmetric defor.
159	w	155	w	dp	140	w	132	m	dp	XCl_3A'' rock
...		124	w	0.70						XCl_3A' rock
75	w	72	w	?	58	w				XCl_3 torsion
61					69	w				Lattice
52	w									Lattice

[a] Depolarization ratios taken from ref 26. [b] Depolarization ratios taken from ref 13.

Table III: Low-Frequency Vibrations and Assignments of Ethanol and Ethanol-d_6

CH_3CH_2OH Infrared (solid)		CD_3CD_2OD (Infrared Solid)											
		Assignment (Mikawa, *et al.*[31])				Assignment I				Assignment II			
$\bar{\nu}$, cm^{-1}	Rel int	$\bar{\nu}$, cm^{-1}	Rel int	Shift factor	Motion[a]	$\bar{\nu}$, cm^{-1}	Rel int	Shift factor	Motion[a]	$\bar{\nu}$, cm^{-1}	Rel int	Shift factor	Motion[a]
292	w	...				258	w	1.13	L	258	w	1.13	L
282	m	258	w	1.09	L	235	vs	1.20	L	198	m	1.42	Torsion
251	m	235	vs	1.07	L	184	m	1.37	Torsion	184	m	1.36	Torsion
222	vs	198	m	1.12	L	198	m	1.12	L	235	vs	0.94[b]	L
192	w	184	m	1.04	T	~179	vw	1.07	T	~179	vw	1.07	T
141	m	133	m	1.06	L	133	m	1.06	T	133	m	1.06	T
119	w	107	m	1.11	L	107	m	1.11	L	107	m	1.11	L
85	vw	79	w	1.07	T	79	w	1.07	T	79	w	1.07	T

[a] For the motions, L is libration, T is translation, and torsion refers to the methyl torsion. [b] This strong band is assigned as the $R_y(A_u)$ hydrogen bonding stretching motion.

corded on a Beckman IR-11 spectrophotometer. The instrument was purged with dry air and was calibrated with atmospheric water vapor using the assignments of Dowling and Hall.[14] The cold cell, which uses liquid nitrogen as a coolant, has been previously described.[15] Samples were vaporized *in vacuo* and condensed on a cold (−194°) polycrystalline silicon substrate. The substrate was maintained in good thermal contact with the refrigerated sink by using Cry-Con conductivity

---

(14) R. T. Hall and J. M. Dowling, *J. Chem. Phys.*, **47**, 2454 (1967).

(15) F. G. Baglin, S. F. Bush, and J. R. Durig, *ibid.*, **47**, 2104 (1967).

grease. An iron–constantan thermocouple was used to monitor the temperature of the brass block with which the silicon plate was in thermal contact. The observed frequencies are listed in Tables I–III and are believed to be accurate to ± 1 cm^{-1} for sharp bands.

The Raman spectra were recorded on a Cary Model-81 Raman spectrophotometer using the 6328-Å excitation line of a Spectra-Physics 125 He-Ne laser. The low-temperature Raman cell has been described previously.[16] The temperature was monitored with an iron–constantan thermocouple attached to the sample block. The spectrometer was calibrated with a neon lamp throughout the spectral range and the observed frequencies, which are listed in Tables I–III, are believed to be accurate to ±2 cm^{-1} for all sharp lines. Figures 1–8 contain far-infrared and low-frequency Raman spectra of the various solids studied in this investigation.

III. Results

A. Ethylsilane ($CH_3CH_2SiH_3$) *and Ethylsilane-*d_3 ($CH_3CH_2SiD_3$). Mackay and Watt[11] have reported the infrared spectra of ethylsilane and ethylsilane-d_3 in the gas phase and proposed a vibrational assignment. However, the frequencies for the skeletal bending and the two torsional modes were not obtained in the earlier study. In general, torsional oscillations are usually quite anharmonic and because of their low frequency several excited states are populated at room temperature This results in very broad bands that are difficult to detect in the spectra of the fluid states. Also, because of the small polarizability change associated with methyl torsions, they usually appear weak, if at all, in the Raman effect. However, the skeletal bending vibration should have an appreciable polarizability change and should appear relatively intense in the Raman spectrum. Thus, a study of both the far-infrared and Raman spectra should provide data for the confident assignment for the three low-frequency fundamentals. Due to the close proximity and equivalent intensities of the skeletal bending mode and methyl torsional mode, it was necessary to record the infrared and Raman spectra of ethylsilane-d_3 to differentiate between these two modes. This isotopic substitution also allowed an appraisal to be made as to the degree of kinetic energy coupling between the two tops.

In Figure 1 are shown the far-infrared spectra of ethylsilane in the vapor and solid states, and for comparison that of solid ethylsilane-d_3 is also given. An inspection of the spectra of the gas and solid shows that the two bands at 49 and 92 cm^{-1} in the spectrum of the solid are lattice modes. However, the two pronounced bands at 211 and 237 cm^{-1} in the spectrum of the solid have comparable bands in the spectrum of the vapor. The band appearing in the vapor is quite broad with a pronounced Q-branch at 206 cm^{-1} and a broad central maximum at 230 cm^{-1}. In the spectrum of the solid the higher frequency band appearing at 237 cm^{-1} in the "light" molecule shifts to 220 cm^{-1} with deuteration. The observed shift factor of 1.08 compares well with the theoretical value of 1.09 calculated for the skeletal

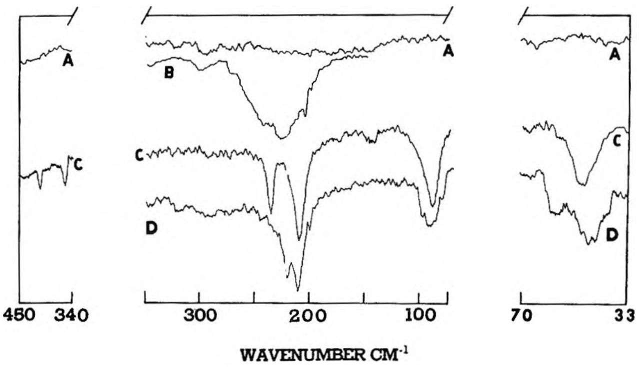

Figure 1. A, Generalized background absorption; B, far-infrared spectrum of ethylsilane vapor; C, far-infrared spectrum of ethylsilane solid (−190°); D, far-infrared spectrum of ethylsilane-d_6 solid (−190°). Ordinate in arbitrary units of absorption.

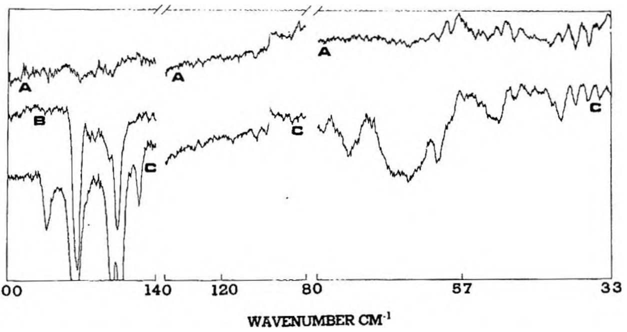

Figure 2. Far-infrared spectrum of ethyltrichlorosilane solid (−190°). Ordinate in arbitrary units of absorption.

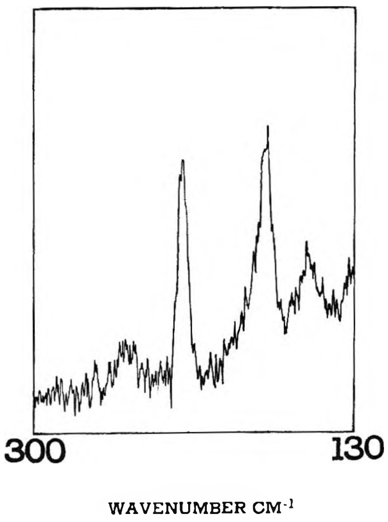

Figure 3. Low-frequency Raman spectrum of ethyltrichlorosilane solid (−190°). Ordinate in arbitrary units of scattering intensity.

---

(16) D. J. Antion and J. R. Durig, *J. Chem. Phys.*, **47**, 2104 (1967).

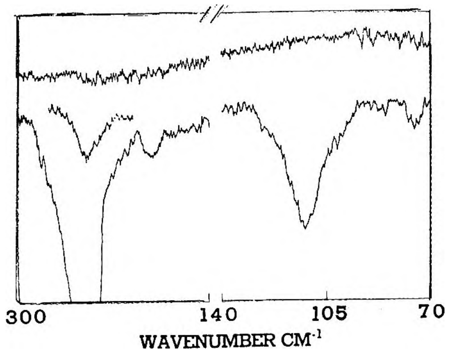

Figure 4. Far-infrared spectrum of ethylgermane solid (−190°). Ordinate in arbitrary units of absorption.

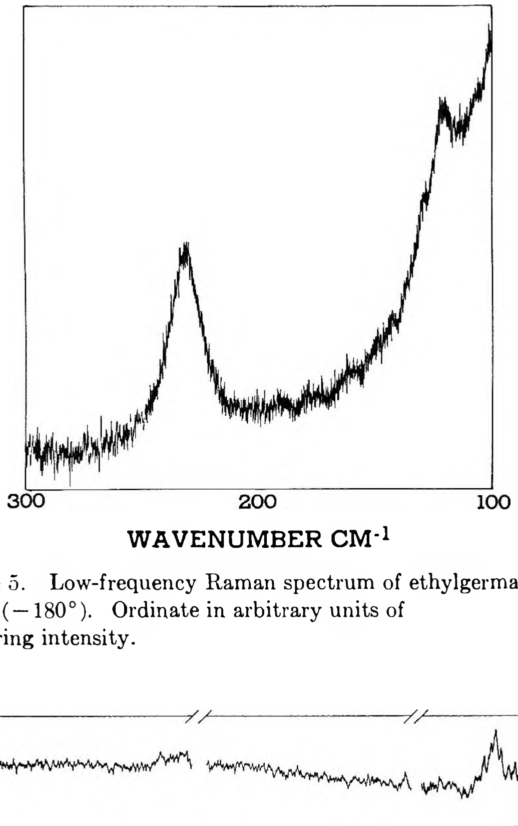

Figure 5. Low-frequency Raman spectrum of ethylgermane liquid (−180°). Ordinate in arbitrary units of scattering intensity.

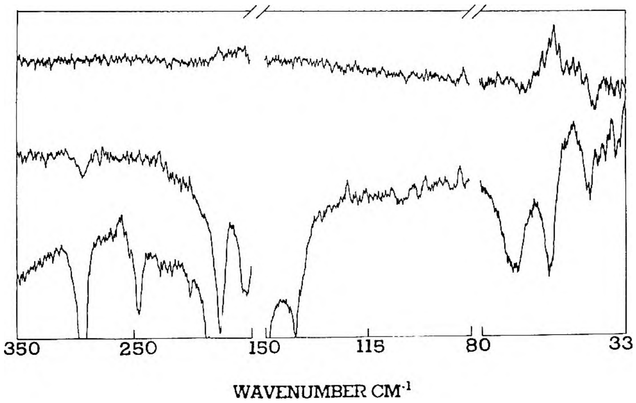

Figure 6. Far-infrared spectrum of ethyltrichlorosilane solid (−190°). Ordinate in arbitrary units of absorption.

bending mode. Thus, the bands appearing at 211 cm^{-1} (206 cm^{-1} in the vapor) in the "light" molecule and 210 cm^{-1} in the d_3 molecule are confidently assigned to the methyl torsions for the respective compounds.

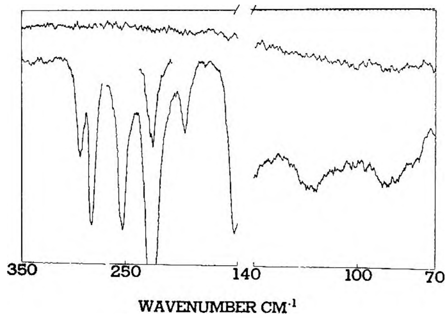

Figure 7. Far-infrared spectrum of ethanol solid (−190°). Ordinate in arbitrary units of absorption.

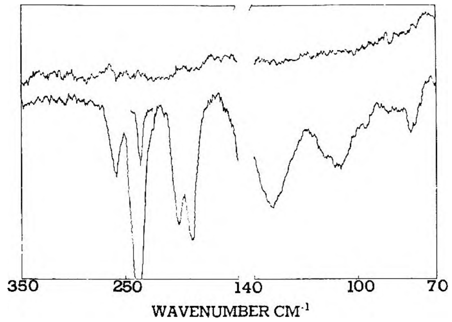

Figure 8. Far-infrared spectrum of ethanol-d_6 solid (−190°). Ordinate in arbitrary units of absorption.

It is seen from the small shift in the methyl torsional frequency on deuterating the silyl group that there is no coupling between the tops. To calculate the torsional barrier, we have assumed a cosine type potential of the form $V(\alpha) = {}^1/_2\, V_3(-\cos 3\alpha)$ with all terms higher than threefold being considered negligible. Because of the absence of coupling the barriers were calculated by applying the method of Fateley and Miller[17] to each top separately. The barriers were obtained using the tables of Matheiu eigenfunctions prepared by Herschbach.[18] The reduced moment of inertia constant ($F = h^2/8\pi^2 I_r$) of the methyl group was calculated to be 5.7 cm^{-1} from the assumed structural parameters given in Table IV. The resulting barrier to internal rotation of the methyl group is 2.82 kcal/mol for the solid and 2.70 kcal/mol for the gas. These values compare quite well with a barrier obtained from a microwave study by Petersen and Pierce[19] of 2.65 kcal/mol for the gas.

An inspection of Figure 1 shows a very weak band at at 142 cm^{-1} in the spectrum of solid ethylsilane and 101 cm^{-1} in the deuterated species. These bands are assigned as arising from the $SiH_3(D_3)$ torsion on the basis of their shift factor (1.41). The frequency of 142 cm^{-1} and an F value of 3.67 cm^{-1} gives a barrier to internal

---

[17] W. G. Fateley and F. A. Miller, *Spectrochim. Acta*, **17**, 857 (1961).

[18] D. R. Herschbach, "Tables for Internal Rotation Problem," Department of Chemistry, Harvard University, 1957.

[19] D. H. Petersen and L. Pierce, Paper N10, Symposium on Molecular Structure and Spectroscopy, Columbus, Ohio, June 1962.

Table IV: Structural Parameter Assumed in Calculation of Barrier Heights[a]

	C-H$_\alpha$	C-H$_\beta$	C-C	C-X	XH	X-Cl	F_{CH_3}	F_{xy_3}
Ethylsilane	1.093	1.093	1.540	1.867	1.484	...	5.76	3.67
Ethylgermane	1.093	1.093	1.540	1.960	1.529	...	5.67	3.50
Ethyltrichlorosilane	1.093	1.093	1.540	1.871	...	2.008	5.30	0.635
Ethyltrichlorogermane	1.093	1.093	1.540	1.950	...	2.13	5.29	0.612
Ethanol	1.100	1.093	1.524	1.428	0.956	...	5.26	...

[a] All angles assumed tetrahedral except $\sphericalangle$ COH = 104.77°; all tops stagger relative to CH_2.

rotation of 1.99 kcal/mol. This compares with the gas phase value of 1.98 kcal/mol obtained previously.[19]

B. Ethyltrichlorosilane ($CH_3CH_2SiCl_3$). Several infrared and Raman papers have appeared previously on ethyltrichlorosilane.[12,20-27] The observations here are similar to those of Durig and Hellams,[27] but the two studies differ in that for the present work all three deformations of the $SiCl_3$ group are observed, and the methyl torsion is assigned.

The band appearing at 222 cm^{-1} is assigned, as in the previous work,[27] to the A′ symmetric $SiCl_3$ deformation. The band appearing at 182 cm^{-1} in the liquid had been previously assigned as degenerate. This band gives rise in the solid to two bands at 180 and 189 cm^{-1}. These two bands are then assigned to the A″ and A′ antisymmetric $SiCl_3$ deformations. It should be mentioned that any attempt to distinguish which of these two bands arises from the A′ and A″ motions would be rather arbitrary on the basis of the available data. The band at 159 cm^{-1} is assigned as formerly to the $SiCl_3$ A″ rock.[27] The band appearing at 124 cm^{-1} in the Raman spectrum is assigned to the A′ rock.

The band appearing at 75 cm^{-1} has been previously observed in the liquid[27] and is assigned to the torsion about the C–Si bond. Again from the structural parameters of Table IV, an F value of 0.63 cm^{-1} is obtained, and from the observed frequency of 75 cm^{-1} a barrier of 2.94 kcal/mol is obtained. This value must be considered tentative for two reasons. First it must be pointed out that this low-frequency band in the liquid may arise from intermolecular motions of the partially structured liquid. Second if indeed the band results from the $SiCl_3$ torsional mode then one might expect it to be shifted to a higher frequency due to intermolecular forces, compared to a gas phase value. Thus, the barrier obtained from the data on the condensed phases may reflect contributions from both intramolecular and intermolecular forces.

The only band appearing outside the lattice region not yet assigned occurs at 257 cm^{-1} in the infrared spectrum of the solid. Since all internal vibrations have been assigned, except the methyl torsional mode, and this frequency is outside the range of the "group frequencies" established for the bending modes of trichlorosilanes by Durig and Hellams,[27] this band is assigned to the CH_3 torsion. It should be noted that this band appears in the Raman spectrum of the solid; however, it is very weak and does not appear except at a very low temperature ($\sim -190°$). From the assumed structure the F value for the methyl group is calculated to be 5.30 cm^{-1} which gives a periodic barrier of 4.41 kcal/mol. The methyl torsional mode is also thought to give rise to the infrared band at 240 cm^{-1} in the liquid phase. From this frequency a barrier of 3.88 kcal/mol is calculated. This lower barrier reflects the dependence of the barrier height on the physical state. Thus, the relatively high value for the barrier compared to the corresponding one in ethylsilane should not be considered as arising solely from the addition of the chlorines on the silicon atom.

C. Ethylgermane ($CH_3CH_2GeH_3$). An extensive vibrational investigation of ethylgermane has been reported by Mackay and Watt.[11] In this study the bands appearing at 170 and 150 cm^{-1}, in the Raman spectrum of the liquid, were assigned as the methyl and germyl torsions, respectively. Both of these lines are well characterized "ghosts" of the Cary Model-81 Raman spectrometer equipped with a mercury arc source and are shown by our investigation to have been incorrectly assigned by the previous workers.

Three bands appear in the far-infrared spectrum of the solid at 241, 189, and 113 cm^{-1} (*cf.* Figure 4). The band observed at 241 cm^{-1} corresponds to the 239-cm^{-1} band previously observed in the Raman spectrum of the liquid[11] and is similarly assigned to the skeletal bending mode.

It has been previously shown[2,3] that the methyl torsional mode is usually quite weak in the far-infrared spectrum and is seldom observed in the Raman effect. Because of this, the weak infrared feature at 189 cm^{-1} is assigned as the methyl torsion. It should be noted (see Figures 4 and 5) that this is the only low-frequency

---

(20) A. L. Smith, *Spectrochim. Acta*, **16**, 87 (1960).

(21) J. Goubeau and H. Siebert, *Z. Anorg. Chem.*, **261**, 63 (1950).

(22) H. Murata, R. Okawava, and T. Watase, *J. Chem. Phys.*, **18**, 1308 (1950).

(23) H. Murata, *J. Chem. Soc. Jap.*, **73**, 465 (1952).

(24) L. Savidan, *Bull. Soc. Chim. Fr.*, 411 (1953).

(25) M. I. Batuev, A. D. Petrov, V. A. Ponomarenko, and A. D. Matveeva, *Izv. Akad. Nauk SSR, Otd. Khim. Nauk*, 1070 (1956).

(26) H. Murata, *Sci. Ind.*, **30**, 164 (1956).

(27) J. R. Durig and K. L. Hellams, *Appl. Spectrosc.*, **22**, 153 (1968).

infrared band which has no Raman counterpart. This frequency, with an F value of 5.67 cm^{-1}, gives a calculated barrier to internal rotation of the methyl group of 2.33 kcal/mol. It should be noted that this value is significantly lower than the corresponding value of 2.82 kcal/mol found for the methyl torsional barrier in ethylsilane. The intermolecular effects are expected to be insignificant for ethylgermane as they were for ethylsilane. Methyl torsional modes have always been shown to shift to higher wave numbers due to intermolecular forces; thus, if these effects are more pronounced in the germanium compound than for the silane, the barrier differential would even be greater.

The band appearing at 113 cm^{-1} in the infrared spectrum of the solid is assigned as the germyl torsional mode. This band is shown not to be a lattice mode by its appearance at 116 cm^{-1} in the Raman spectrum of the liquid (−180°). With a reduced moment of inertia constant of 3.50 cm^{-1}, the barrier obtained is 1.37 kcal/mol. This value will be shown to be consistent with other barriers for germyl torsional modes in the discussion section.

D. Ethyltrichlorogermane ($CH_3CH_2GeCl_3$). Previous vibrational studies have been reported on ethyltrichlorogermane,[13,28–30] but the two torsional modes have not been satisfactorily assigned. The most comprehensive work of the previous studies is that of Lippincott, *et al.*[29] In that study a band appearing at 291 cm^{-1} in the Raman effect was assigned as the methyl torsional mode. However in our study this line is shown to be polarized and because of its position and intensity it is assigned to the CCGe deformation. This assignment is consistent with that given for the corresponding modes in the other molecules studied herein.

The bands appearing at 179, 157, and 140 cm^{-1} all appear as depolarized lines in the Raman effect.[13] Thus, if these bands are to be assigned to the bending motions of the $GeCl_3$ group, then the A″ modes are most probably degenerate with the A′ modes. On this basis the A′ symmetric deformation is assigned to the band at 179 cm^{-1}. The A′ and A″ antisymmetric deformations correspond to an E mode under local C_{3v} symmetry and are assigned as being degenerate at 157 cm^{-1}. The A′ and A″ rocking motions which also correspond to an E mode for the C_{3v} point group are assigned as being degenerate at 140 cm^{-1}. These assignments are consistent with the depolarization data and are reasonable on the basis of the local symmetry of the $GeCl_3$ group.

There are three additional bands (245, 69, 58 cm^{-1}) in the far-infrared spectrum of the solid which have not been previously observed. Again it is expected that the methyl torsion would appear as the least intense fundamental in the far-infrared. On this basis the band at 245 cm^{-1} is assigned as the methyl torsion. From the assumed structural parameters (Table IV), an F value of 5.29 cm^{-1} is obtained, and with the frequency of 245 cm^{-1} a barrier of 4.03 kcal/mol is calculated. It should be pointed out that this barrier is close to, but a little lower than that obtained in the corresponding silicon compound.

Previously, a band at ~110 cm^{-1} had been assigned by Lippincott and Tobin[29] as the torsion about the C–Ge bond. This band was not observed in our study in either the infrared or the Raman spectra when a pure sample was used. However, when the sample was exposed to the air, this band could be observed in the Raman spectrum. Thus, this band is taken as arising from a low-frequency mode of the hydrolysis product. Two bands remain to be assigned in the far-infrared spectrum of the solid, one of which may be the $GeCl_3$ torsion. An unambiguous assignment of one of these bands as the torsion cannot be made on the basis of our data, since neither band was observed in the infrared or Raman spectrum of the liquid and upon doing a temperature study the peaks tend to merge. If the 69-cm^{-1} band is assigned as the torsion, the barrier would be 2.64 kcal/mol, whereas if the 58-cm^{-1} band is assigned to this motion the calculated barrier is 1.86 kcal/mol. If one compares the torsional barriers with those for the other molecules studied, one sees neither of these values is unacceptable.

E. Ethanol (CH_3CH_2OH). There has recently appeared an infrared study (250–4000 cm^{-1}) of a single crystal and a far-infrared study (below 300 cm^{-1}) of a polycrystalline sample of ethanol and two of its deuterated derivatives.[31] From this study it was shown that the crystal consists of unit cells with double chains of four molecules each, with a factor group symmetry of C_{2h}^6. From this symmetry, it is predicted that there would be three infrared active translations and six infrared active librations. Since, we had also studied the far-infrared spectrum of this molecule and our results differ somewhat from those previously reported, we are including our data in this study.

The infrared spectrum of polycrystalline ethanol is shown in Figure 7 and that of the "d_6" compound in Figure 8. The relatively sharp, medium intensity band at 292 cm^{-1} was not observed in the previous study. Also, there are considerable differences in the frequencies and the relative intensities of the remaining bands. It was found to be necessary to hold the ethanol sample 5° below its melting point for ~2 hr to obtain a reproducible spectrum; thus, these differences are felt to be due to differences in the degree of crystallinity in the samples used in the two studies.

The observation of the band at 292 cm^{-1} requires a

---

(28) M. I. Batuev, V. A. Ponomarenko, A. D. Matveeva, and G. Ya. Vzenkova, *Izv. Akad. Nauk SSR, Otd. Khim. Nauk*, 2120 (1959).

(29) E. R. Lippincott, P. Mercier, and M. C. Tobin, *J. Phys. Chem.*, **57**, 939 (1953).

(30) N. A. Chumaevskii, *Opt. Spectrosc.*, **13**, 37 (1962).

(31) Y. Mikawa, J. W. Brasch, and R. J. Jakobsen, *Spectrochim. Acta*, **27A**, 529 (1971).

reassignment of the bands observed between 150 and 300 cm^{-1}. It appears that the 292-cm^{-1} band shifts to 258 cm^{-1} with deuteration giving a shift factor of 1.13, and is thus assigned as a librational mode. The shifting of the 192-cm^{-1} band to the low-frequency shoulder of the 184-cm^{-1} band in the spectrum of the deuterium compound is consistent with the assignment of this band to a translational mode. There is considerable doubt as to the correct assignment of the three bands at 282, 251, and 222 cm^{-1}. There are two possible assignments (see Table III), one of which requires a large intensity reversal whereas the other assignment requires a "blue" shift of one of the bands with deuteration.

It was noted by Mikawa, *et al.*,[31] that most of the intramolecular fundamentals appeared as doublets in their study of single crystal ethanol. It has been found that methyl torsional modes give rise to much larger factor group splittings than do the other internal fundamentals.[6] Thus, one would expect from the results of Mikawa, *et al.*,[31] to observe splitting for this mode in ethanol. Also, in a study of the ethyl halides[3] in the solid phase, it was observed that for these molecules the calculated barrier heights are approximately 0.8 kcal/mol higher in the solid than those obtained for these molecules in the gas. Because of these considerations the present authors favor assignment II listed in Table III, where the torsion is assigned as split with frequencies of 282 and 251 cm^{-1} for the "light" molecule and 198 and 184 cm^{-1} for the "heavy" species. Using the average frequency the torsional barrier height for solid ethanol is calculated to be 4.05 kcal/mol. This compares with a value of 3.37 kcal/mol obtained from a microwave study of the gas.[32] It is therefore seen that assignment II is favored on the basis of the splitting observed for the torsion and the gas to solid shift in the barrier height. The major argument against assignment II is the shift of the 222-cm^{-1} band to 235 cm^{-1} on deuteration. Such an assignment has been proposed for the most intense low-frequency band in the vibrational spectrum of 2-propanol.[33,34] Such shifts, although impossible for an uncoupled oscillator, are readily explained if the vibration is assumed to be coupled. Further vibrational studies of CD_3CH_2OH and CD_3CD_2OH might help determine which of these possible assignments is correct. Also a neutron inelastic scattering study could probably be used to distinguish the methyl torsional mode from the external vibrations.

IV. Conclusions

Many theoretical papers have appeared on the subject of torsional barriers, some utilizing quantum mechanical formalism[4-6,35-38] and others using a more empirical approach.[7-9,39-41] The quantum mechanical calculations, especially in terms of bond function analysis, should be very enlightening as to the forces contributing to the barrier. Although there have been several barriers calculated using the quantum mechanical approach which are in good agreement with experiment, it is generally agreed that this agreement is largely due to a cancellation of errors when the conformational energy difference is taken. The barrier height is often several orders of magnitude lower than the error in the total energy; thus, the analyses based on these calculations are somewhat questionable.

The semiempirical approaches usually have attempted to interpret torsional oscillations in terms of potential functions applicable to other types of internal vibrations or intramolecular interaction potential functions. With this approach, the intramolecular interaction constants are usually transferred from data obtained from intermolecular interaction studies. Since the barrier is most probably due to secondary overlap or nonbonded interactions, it would seem that, with the proper choice of coefficients, such potential functions should give reasonable results.

From the data presented in Table V it is seen that there is a gradual decrease in the barrier to the rotation of the methyl group as one goes from propane to ethylsilane to ethylgermane. This decrease is as one would expect on the basis of secondary overlap because of the longer more diffuse C–X bond formed as one transcends the group IVa series. One would also expect this decrease on the basis of nonbonded interaction since the forces exerted on the methyl group would also be expected to decrease with the increasing C–X bond length. Assuming no interaction from the heavy atom hydrogens and extrapolation of this effect, the methyl group should, in the limit of an infinite C–X bond length, experience an interaction field equivalent to that of a CH_2 group. Thus, the limiting low barrier for $CH_3CH_2XY_n$ molecules as one transcends a given family of elements would be $^2/_3$ the barrier of the methyl derivative of the first member of the series. On the basis of this the limiting barrier for the propane type molecules would be 1.95 kcal/mol.

On going to the trichlorides it is seen that for these molecules there must be a third-order effect from the interactions of the heavy atom chlorines with the methyl hydrogens to cause such a drastic increase in the

---

(32) L. M. Imanov and Ch. O. Kadzhar, *Izv. Akad. Nauk Azerb. SSR, Ser. Fiz.-Tekn. Mat. Nauk*, 33 (1967).

(33) J. R. Durig, C. B. Pate, Y. S. Li, and D. J. Antion, *J. Chem. Phys.*, **54**, 4863 (1971).

(34) J. R. Durig, C. M. Player, Jr., Y. S. Li, J. Bragin, and C. W. Hawley, *ibid.*, in press.

(35) M. Cignitto and T. Allen, *J. Phys. Chem.*, **68**, 1292 (1964).

(36) R. Hoffman, *J. Chem. Phys.*, **39**, 1397 (1963).

(37) R. M. Pitzer, *ibid.*, **41**, 2216 (1964).

(38) A. J. Sovers, C. W. Kern, R. M. Pitzer, and M. Karpus, *ibid.*, **49**, 2592 (1968).

(39) E. A. Mason and M. M. Kreevoy, *J. Amer. Chem. Soc.*, **77**, 5808 (1955).

(40) R. E. Wyatt and R. G. Parr, *J. Chem. Phys.*, **41**, 3263 (1964); **43**, S217 (1965); **44**, 1529 (1966).

(41) J. P. Lowe and R. G. Parr, *ibid.*, **43**, 2565 (1965).

Table V: Comparison of Barriers for Ethane and Propane Type Molecules

	Barrier, kcal/mol		Barrier, kcal/mol CH$_3$	XH$_3$
CH_3CH_3	2.928[a]	$CH_3CH_2CH_3$	3.33	3.33[e]
CH_3SiH_3	1.70[b]	$CH_3CH_2SiH_3$	2.82	1.99[f]
CH_3GeH_3	1.24[c]	$CH_3CH_2GeH_3$	2.33	1.37[f]
CH_3SnH_3	0.65[d]	$CH_3CH_2SnH_3$	...	...

[a] S. Weiss and G. E. Leroi, *J. Chem. Phys.*, **48**, 962 (1968). [b] R. W. Kilb and L. Pierce, *ibid.*, **27**, 108 (1957). [c] V. W. Laurie, *ibid.*, **30**, 1210 (1959). [d] P. Cahill and S. S. Butcher, *ibid.*, **35**, 2255 (1962). [e] E. Hirota, C. Natsumura, and Y. Morino, *Bull. Chem. Soc. Jap.*, **40**, 1124 (1967). [f] This work.

barrier of the chlorides relative to the corresponding hydrides. It has been mentioned earlier that part of this apparent increase may reflect intermolecular contributions; however, in the view of the empiricist, those forces with directional character which contribute to the intermolecular interaction are also those forces which contribute to the barrier. Thus, it is felt that this increase is at least qualitatively significant. This strong chlorine interaction is also reflected in the heavy atom tops where the barrier in the ethyltrichlorosilane is approximately equal to the methyl barrier in ethane, even though the bonds are diffuse and the nonbonded distance is considerably greater. This strong chlorine effect is also demonstrated in the chlorine derivatives of ethane.[3,42] It should be noted that for the two trichlorides there is a decrease in the barrier height obtained for both the methyl and heavy atom tops on going from the silane to the germane derivative.

Another interesting observation is that the proportionate drop in the barrier heights for the heavy atom tops, as one goes from propane to ethylsilane to ethylgermane, is approximately equal to the proportion decrease in the barrier for the methyl derivatives. This again is as expected, since the nonbonded distance changes for the heavy tops in both the methyl and ethyl derivatives are approximately the same, and the change in barrier should simply reflect the proportionate effect of this distance change on the effective field exerted by the ethyl or methyl groups on the tops. (See Table VI.)

Table VI: Summary of Barriers

	CH$_3$	XY$_3$
$CH_3CH_2SiH_3$	2.82	1.99
$CH_3CH_2SiCl_3$	4.41	2.94
$CH_3CH_2GeH_3$	2.33	1.37
$CH_3CH_2GeCl_3$	4.03	1.86
CH_3CH_2OH	4.05	...

Finally, it should be pointed out that the group IVa elements provide a rather favorable series for studying the effect of the change of the nonbonded distance on the barrier because, for this group, the complexities of the changes in the hybridization are minimal and the angles remain essentially tetrahedral. The effect of the hybridization changes on the barrier heights is dramatically demonstrated for the group Va and VIa elements by a comparison of the barriers for methylamine[43]–methylphosphine[44] and methanol[45]–methanethiol,[46] where the respective barriers are 1.98, 1.96, 1.07, and 1.27 kcal/mol.

Acknowledgment. The authors gratefully acknowledge the financial support given to this work by the National Science Foundation under Grant No. GP-20723.

(42) J. R. Durig, S. M. Craven, K. K. Lau, and J. Bragin, *J. Chem. Phys.*, **54**, 479 (1971).

(43) D. Kivelson and D. R. Lide, Jr., *ibid.*, **27**, 353 (1957).

(44) T. Kajima, E. L. Breig, and C. C. Lin, *ibid.*, **35**, 2139 (1961).

(45) K. T. Hecht and D. M. Dennison, *ibid.*, **26**, 48 (1957).

(46) T. Kojima and T. Nishikawa, *J. Phys. Soc. Jap.*, **12**, 680 (1957).

Vibrational Energy Transfer in the Hydrogen Molecule–Helium Atom System[1a]

by Hyung Kyu Shin

Department of Chemistry,[1b] *University of Nevada, Reno, Nevada 89507* *(Received May 24, 1971)*

Publication costs assisted by the U. S. Air Force Office of Scientific Research

Vibrational energy transfer in H_2 + He is studied by use of the accurate *a priori* interaction potential. An expression for the vibrational transition probabilities is obtained by solving the Schrödinger equation for the perturbed oscillator states. The expression explicitly shows the dependence of the transition probability on molecular orientations, oscillator anharmonicity, and multiquantum transitions. Detailed numerical study for the $0 \rightarrow 1$ vibrational transition in the electron-volt range is carried out to show the dependence of the transition probability on the relative collision energy and the orientation angle. At higher energies, the introduction of the anharmonicity correction decreases the vibrational transition probability by large factors. The temperature dependence of the transition is also discussed with the angle and energy-averaged transition probability. Vibration–rotation energy transfer is not considered, but the amount of energy transfer to the anharmonic oscillator is calculated as a function of the initial orientation angle.

Introduction

In recent years, with the advent of large memory high-speed computers, accurate *a priori* interaction potential energy functions have become available for the calculation of probabilities of molecular energy transfer.[2–5] Among them are the relatively simple forms for H_2 + He computed by Krauss and Mies[2b] and by Gordon and Secrest.[5] Recently, Lester[4] obtained a lengthy function for $Li^+ + H_2$ by employing accurate self-consistent field wave functions. These functions, which show detailed orientation dependences, are obtained for the regions which are appropriate for the study of vibrational excitations. Since such exact potential functions are becoming available, we can now make rigorous calculations of vibrational transition probabilities and related quantities. Mies[6] used the H_2 + He potential in his numerical evaluation of the $0 \rightarrow 1$ vibrational transition probability within the framework of the distorted wave approximation (DWA), and compared the result with that of model potentials to show the inadequacy of the latter forms in describing the H_2 + He collision. Although the calculation revealed new features of the transition process, it is generally known that the DWA cannot be used to calculate the vibrational transition probabilities in the region of high collision energies,[7–9] where the approximation may lead to the situation that the probabilities exceed unity. The DWA, which is simple to use, normally gives acceptable results for low probabilities.

The *a priori* H_2 + He potential function is in a simple form, which can be readily used for accurate calculation of the transition probabilities. In the present paper, we developed a method for the calculation of vibrational transition probabilities for H_2 + He. The method involves the solution of the Schrödinger equation describing the perturbed oscillator states in an explicit form. We shall use the potential function obtained by Krauss and Mies. Although numerical calculation of the transition probabilities will be shown, we shall consider the development of the method in detail; the development will be made such that the method can be readily used with other collision systems for which accurate forms of the interaction potentials are available.

Potential Energy Functions

The *a priori* interaction energy for H_2 + He determined by Krauss and Mies is

$$U(x,q,\theta) = C \exp(-\alpha x + \alpha_1 xq)[A(\theta) + B(\theta)q] \quad (1)$$

where q is the displacement of the oscillator from its equilibrium position R_e, x the distance between the center of mass of H_2 and He, $\alpha = 1.86176$ au^{-1}, $\alpha_1 = 0.3206$ au^{-2}, $C = 198.378$ eV, $A(\theta) = 1.0 + 0.30124 \cos^2 \theta$, and $B(\theta) = -0.59932 + 0.21517 \cos^2 \theta$ au^{-1}. This function accurately represents the H_2 + He interaction for the ranges $0 \leq q + R_e \leq 2$ au and $2.5 \leq x \leq 3.8$ au.

In using eq 1 for the formulation of vibrational transition probabilities, we face mathematical difficulty due to the appearance of the q dependence both in the pre-exponential and exponential parts. However, this difficulty can be avoided by expanding $\exp(\alpha_1 xq)$ in a

---

[1] (a) This work was supported by the Directorate of Chemical Sciences, the U. S. Air Force Office of Scientific Research, under Grant AFOSR-68-1354. (b) Theoretical Chemistry Group Contribution No. S-1033.

[2] (a) C. S. Roberts, *Phys. Rev.*, **131**, 203 (1963); (b) M. Krauss and F. H. Mies, *J. Chem. Phys.*, **42**, 2703 (1965).

[3] W. A. Lester, *ibid.*, **53**, 1511 (1970); **53**, 1611 (1970).

[4] W. A. Lester, *ibid.*, **54**, 3171 (1971).

[5] M. D. Gordon and D. Secrest, *ibid.*, **52**, 120 (1970).

[6] F. H. Mies, *ibid.*, **42**, 2709 (1965).

[7] K. Takayanagi, *Advan. Mol. At. Phys.*, **1**, 149 (1965).

[8] D. Rapp and T. Kassal, *Chem. Rev.*, **69**, 61 (1969).

[9] D. Secrest and B. R. Johnson, *J. Chem. Phys.*, **45**, 4556 (1966).

power series and taking the first several terms. For the range in which eq 1 is valid the exponential part exp$(\alpha_1 xq)$ lies in the range from exp$(0.8015q)$ to exp$(1.2182q)$. If we take q as large as +0.6 au, these two limits are 1.6175 and 2.0771, respectively. In the expansion, when we take the first four terms of the upper limit, exp$(0.7309) \simeq 2.0631$ while its exact value is 2.0771. On the other hand, for $q = -0.6$ au, exp$(-0.7309) \simeq 0.4711$ while its exact value is 0.4814. The equilibrium value R_e is 1.4 au, and probably the range of the displacement of the vibrational amplitude of the displacement of the vibrational amplitudes of interest is ±0.3 au. Therefore, the error caused by the expansion of exp$(\alpha_1 xq)$ should be very small, and to a good approximation we can express the exponential part as

$$\exp(\alpha_1 xq) = 1 + \alpha_1 xq + {}^1/_2(\alpha_1 x)^2q^2 + {}^1/_6(\alpha_1 x)^3q^3 + {}^1/_{24}(\alpha_1 x)^4q^4 \qquad (2)$$

With this expression we now write the modified interaction potential as

$$\begin{aligned} U(x,q,\theta) = {} & CA(\theta)\exp(-\alpha x) + C\exp(-\alpha x)\{[A(\theta)\alpha_1 x + B(\theta)]q + \\ & [{}^1/_2A(\theta)(\alpha_1 x)^2 + \alpha_1 B(\theta)x]q^2 + \\ & [{}^1/_6A(\theta)(\alpha_1 x)^3 + {}^1/_2B(\theta)(\alpha_1 x)^2]q^3 + \\ & [{}^1/_{24}A(\theta)(\alpha_1 x)^4 + {}^1/_6B(\theta)(\alpha_1 x)^3]q^4\} \equiv \\ & U(x,0,\theta) + U'(x,q,\theta) \qquad (3) \end{aligned}$$

where the q-dependent part $U'(x,q,\theta)$ is responsible for vibrational transitions, while $U(x,0,\theta)$ essentially controls the relative translational motion of the collision partners. We shall express the q-dependent terms in the form

$$U'(x,q,\theta) = \sum_{i=1}^{4} \eta_i(x)q^i \qquad (4)$$

We are therefore concerned with the interaction of H_2 with He through the perturbation energy $\Sigma\eta_i(x)q^i$, which explicitly includes vibration–rotation coupling. In setting up the problem, we shall parametrize x in the time t, so that the sum can be considered to be a time-dependent perturbation energy. The Hamiltonian takes the form

$$H = \frac{p^2}{2M} + U(q) + \sum_{i=1}^{4} \eta_i(t)q^i \qquad (5)$$

where p is the momentum and M is the reduced mass of the oscillator and $U(q)$ is the intramolecular potential function. If we assume the harmonic motion of the oscillator, then the latter function is simply ${}^1/_2M\omega^2q^2$, where ω is the vibrational frequency. In studying vibrational energy transfer problems, we therefore need to know, in addition to $U(x,q,\theta)$, the intramolecular potential energy of the oscillator. Such a potential must reproduce the oscillator's anharmonicity, which might exert an important influence on the vibrational energy transfer. Potentials such as the Morse function $U(q) = D_e[1 - \exp(-\phi q)]^2$ can be used here, where ϕ is a range parameter to be determined and D_e is the dissociation energy. However, the Morse function is difficult to handle in the method described below, but without causing any serious error we can expand it about q and take the first several terms. By defining the force constant by $[\mathrm{d}^2U(q)/\mathrm{d}q^2]_{q=0}$, we can then approximate the H_2 molecule by an anharmonic oscillator with the potential

$$U(q) = {}^1/_2M\omega^2q^2 - {}^1/_2M\omega^2\phi q^3 + {}^7/_{24}M\omega^2\phi^2q^4 \qquad (6)$$

The second and third terms on the right-hand side are assumed to reproduce the anharmonicity of the molecule. Therefore we shall replace $U(q)$ in the Hamiltonian by ${}^1/_2\,M\omega^2q^2 + \Sigma_{j=3}{}^4\,\lambda_jq^j$, where $\lambda_3 = -{}^1/_2\,M\omega^2\phi$ and $\lambda_4 = {}^7/_{24}\,M\omega^2\phi^2$. We then have

$$H = \frac{p^2}{2M} + {}^1/_2M\omega^2q^2 - F(t)q + \sum_{j=3}^{4}\lambda_jq^j + \sum_{i=2}^{4}\eta_i(t)q^i \qquad (7)$$

where $-F(t) = \eta_1(t)$.

Perturbed Wave Function

The oscillator is perturbed by the energy $U'(x,q,\theta)$ during the course of collision, and we now need to find the wave function representing the perturbed state. Since the quantum system under the influence of $U'[x(t),q,\theta]$ evolves in an exactly predictable manner, we can determine the wave function $\psi(t)$ representing its dynamical state at time t by specifying $\psi(t_0)$ for the initial state at t_0. The wave function $\psi(t)$ then represents the perturbed state and can be obtained by solving the Schrödinger equation

$$i\hbar\dot{\psi}(t) = H\psi(t) \qquad (8)$$

where the Hamiltonian is given by eq 7. If we discard the two sums in eq 7, the subsequent solution of eq 8, which is well known, will describe the case of the forced harmonic oscillator.[10,11] We should therefore be able to take into account explicitly the effect of oscillator anharmonicity on the solution $\psi(t)$ with the j sum. The appearance of the sums in eq 7 greatly complicates the solution of eq 8. To facilitate the solution, we introduce the operators **a** and **a**$^+$, which are hermitian conjugates of each other satisfying the commutation relation $[\mathbf{a},\mathbf{a}^+] = 1$. The position variable q and the mo-

---

(10) I. I. Gol'dman and V. D. Drivchenkov, "Problems in Quantum Mechanics," Addison-Wesley, Reading, Mass., 1961, pp 103–106. Also see D. ter Haar, "Selected Problems in Quantum Mechanics," Academic Press, New York, N. Y., 1964, pp 152, 153.

(11) C. E. Treanor, *J. Chem. Phys.*, **43**, 532 (1965); **44**, 2220 (1966).

mentum p are linear combinations of these operators[10,12]

$$q = \left(\frac{\hbar}{2M\omega}\right)^{1/2}(\mathbf{a}^+ + \mathbf{a}) \tag{9}$$

$$p = i\left(\frac{M\hbar\omega}{2}\right)^{1/2}(\mathbf{a}^+ - \mathbf{a}) \tag{10}$$

In terms of these operators we can write the Hamiltonian as

$$H = (\mathbf{N} + {}^1/_2)\hbar\omega - \left(\frac{\hbar}{2M\omega}\right)^{1/2}F(t)(\mathbf{a} + \mathbf{a}^+) + \sum_{j=3}^{4}\left(\frac{\hbar}{2M\omega}\right)^{j/2}\lambda_j(\mathbf{a} + \mathbf{a}^+)^j + \sum_{i=2}^{4}\left(\frac{\hbar}{2M\omega}\right)^{i/2}\eta_i(t)(\mathbf{a} + \mathbf{a}^+)^i \tag{11}$$

where $\mathbf{N} = \mathbf{a}^+\mathbf{a}$. By use of the commutation relation and the identity $[(\mathbf{a}^+)^n, \mathbf{a}] = -n(\mathbf{a}^+)^{n-1}$, we can expand $(\mathbf{a} + \mathbf{a}^+)^i$ and $(\mathbf{a} + \mathbf{a}^+)^j$ in the form $\Sigma_{m,n}\, c_{m,n}(\mathbf{a}^+)^m\mathbf{a}^n$; *e.g.*, $(\mathbf{a} + \mathbf{a}^+)^2 = \mathbf{a}^2 + 2\mathbf{a}^+\mathbf{a} + \mathbf{a}^{+2} + 1$. Such expansions will be used in obtaining eq 14–17 from eq 13 below.

We shall first look for the solution of eq 8 in the form[10,11,13]

$$\psi(t) = c(t)\exp[f(t)\mathbf{a}^+]\exp[g(t)\mathbf{a}]\exp[h(t)\mathbf{N}]\psi(t_0) \tag{12}$$

We assume the initial wave function $\psi(t_0)$ by the harmonic oscillator wave function and write it in the form $\psi_m(q)$, m representing the initial oscillator state. Therefore, eq 12 can be obtained as a linear combination of the unperturbed harmonic oscillator wave function with the coefficients determined by the time-dependent energy terms as well as the anharmonicity terms. The square of the coefficient of a particular state (say n) is then the probability that the oscillator is in the state n at time t; the probability at $t = +\infty$, p_{mn}, can be obtained by evaluating the coefficient at $t = +\infty$.

With the time derivative of eq 12 and by use of the commutation relation and $[(\mathbf{a}^+)^n, \mathbf{a}] = -n(\mathbf{a}^+)^{n-1}$ in the expanded form[10] of $\exp[f(t)\mathbf{a}^+]\exp[g(t)\mathbf{a}]\exp[h(t)\mathbf{N}]$, we find the following equation[14] from eq 8

$$i\hbar\Big\{\dot{h}(t)\mathbf{N} + [\dot{f}(t) - \dot{h}(t)f(t)]\mathbf{a}^+ - [\dot{g}(t) + \dot{h}(t)g(t)]\mathbf{a} + \frac{\dot{c}(t)}{c(t)} - \dot{h}(t)f(t)g(t) - \dot{g}(t)f(t)\Big\}\psi(t) = \Big[(\mathbf{N} + {}^1/_2)\hbar\omega - F(t)\left(\frac{\hbar}{2M\omega}\right)^{1/2}(\mathbf{a} + \mathbf{a}^+) + \sum_{j=3}^{4}\left(\frac{\hbar}{2M\omega}\right)^{j/2} \times \lambda_j(\mathbf{a} + \mathbf{a}^+)^j + \sum_{i=2}^{4}\left(\frac{\hbar}{2M\omega}\right)^{i/2}\eta_i(t)(\mathbf{a} + \mathbf{a}^+)^i\Big]\psi(t) \tag{13}$$

By equating the coefficients of the operators $\mathbf{N}$, $\mathbf{a}^+$, and $\mathbf{a}$ of the both sides of this equation, we find

$$\dot{h}(t) = -\left[i\omega + \frac{i}{M\omega}\eta_2(t)\right] \tag{14}$$

$$\dot{f}(t) + i\left[\omega + \frac{\eta_2(t)}{M\omega}\right]f(t) = \frac{iF(t)}{(2M\hbar\omega)^{1/2}} + \frac{3i}{\hbar}\left(\frac{\hbar}{2M\omega}\right)^{3/2}[\lambda_3 + \eta_3(t)] \tag{15}$$

$$\dot{g}(t) - i\left[\omega + \frac{\eta_2(t)}{M\omega}\right]g(t) = \frac{iF(t)}{(2M\hbar\omega)^{1/2}} + \frac{3i}{\hbar}\left(\frac{\hbar}{2M\omega}\right)^{3/2}[\lambda_3 + \eta_3(t)] \tag{16}$$

$$\frac{\dot{c}(t)}{c(t)} = -\frac{i\omega}{2} - \frac{i}{2M\omega}\eta_2(t) + \frac{3\hbar i}{(2M\omega)^2}[\lambda_4 + \eta_4(t)] + \left\{\frac{iF(t)}{(2M\hbar\omega)^{1/2}} + \frac{3i}{\hbar}\left(\frac{\hbar}{2M\omega}\right)^{3/2}[\lambda_3 + \eta_3(t)]\right\}f(t) \tag{17}$$

The coefficients of the operators which are in higher orders of $\mathbf{a}^+$, $\mathbf{a}$, and $\mathbf{N}$ appeared on the right-hand side of eq 13 are set equal to zero, but the resulting relations do not contribute to the formulation of the relevant equations given above. In deriving the differential equations, eq 14 has been used to simplify the three other equations. It is obvious that the solution of eq 15 is the complex conjugate of that of eq 16. With the initial conditions ($t_0 = -\infty$), $h(-\infty) = 0$, $f(-\infty) = 0$, and $c(-\infty) = 1$, we find the solutions

$$h(t) = -i\omega t - \frac{i}{M\omega}\int_{-\infty}^{t}\eta_2(t)\mathrm{d}t \tag{18}$$

$$f(t) = \frac{i}{(2M\hbar\omega)^{1/2}}\exp\left[-i\omega t + \frac{i}{M\omega}\int_{-\infty}^{t}\eta_2(t')\mathrm{d}t'\right]\int_{-\infty}^{t}\mathrm{d}t'\left\{F(t') + \frac{3\hbar}{2M\omega}[\lambda_3 + \eta_3(t')]\right\}\left\{\exp\left[i\omega t' + \frac{i}{M\omega}\int_{-\infty}^{t'}\eta_2(t'')\mathrm{d}t''\right]\right\} \tag{19}$$

$$g(t) = -f^*(t) \tag{20}$$

---

(12) A. Messiah, "Quantum Mechanics," Vol. I, North-Holland Publishing Co., Amsterdam, 1968, Chapter 12.

(13) P. Pechukas and J. C. Light [*J. Chem. Phys.*, **44**, 3897 (1966)] solved the problem of the linearly forced harmonic oscillator in terms of the operators $\mathbf{a}^+$ and $\mathbf{a}$.

(14) H. Shin, *Chem. Phys. Lett.*, **5**, 137 (1970).

$$c(t) = \exp\left[-\frac{i\omega t}{2} - \frac{i}{2M\omega}\int_{-\infty}^{t}\eta_2(t')\mathrm{d}t' + \frac{3i\lambda_4\hbar t}{(2M\omega)^2} + \frac{3\hbar i}{(2M\omega)^2}\int_{-\infty}^{t}\eta_4(t')\mathrm{d}t'\right]\left[\exp\left\{\frac{i}{(2M\hbar\omega)^{1/2}} \times \int_{-\infty}^{t}\mathrm{d}t' \exp\left[-i\omega t' - \frac{i}{M\omega}\int_{-\infty}^{t'}\eta_2(t'')\mathrm{d}t''\right] \times \left\{\frac{iF(t')}{(2M\hbar\omega)^{1/2}} + \frac{3[\lambda_3 + \eta_3(t')]}{\hbar}\left(\frac{\hbar}{2M\omega}\right)^{3/2}\right\}\int_{-\infty}^{t'}\mathrm{d}t'' \times \left\{F(t'') + \frac{3\hbar}{2M\omega}[\lambda_3 + \eta_3(t'')]\right\}\exp[i\omega t'' + \frac{i}{M\omega}\int_{-\infty}^{t''}\eta_2(t''')\mathrm{d}t''']\right\}\right] \quad (21)$$

With the solutions for the coefficients given above, we now solve eq, 12 for $\psi(t)$ as a particular combination of the unperturbed harmonic oscillator wave functions. The coefficients of such a combination will depend on the functions given by eq 18–21. For the wave function $\psi_m(q)$ we have the following recursion relations[12]

$$\mathbf{a}^+\psi_m = (m + 1)^{1/2}\psi_{m+1} \quad (22)$$

$$\mathbf{a}\psi_m = m^{1/2}\psi_{m-1}\ (m \neq 0);\ \mathbf{a}\psi_0 = 0 \quad (23)$$

$$\mathbf{N}\psi_m = m\psi_m \quad (24)$$

Since the operator $\mathbf{a}^+$ transforms the state m into the state $m + 1$, $\mathbf{a}^+$ may be called an "excitation" operator. The operator $\mathbf{a}$, on the contrary, transforms the state into the lower state $m - 1$, thus acting as a "deexcitation" operator. Hence, in eq 12 each operator in the exponent will operate on $\psi_m(q)$ to generate the wave functions $\psi_0(q)$, $\psi_1(q)$, $\psi_2(q), \ldots$, $\psi_n(q)$, ... By expanding the exponential part of eq 12[10] and by generating the functions with the recursion relations given above, we obtain the wave function $\psi(t)$ in the form

$$\psi(t) = c(t)\exp[mh(t)]\sum_{s=0}^{m}\frac{[g(t)]^s}{s!} \times \sqrt{\frac{m!}{(m-s)!}}\sum_{r=0}^{\infty}\frac{[f(t)]^r}{r!} \times \sqrt{\frac{(m-s+r)!}{(m-s)!}}\psi_{m-s+r} = c(t)\sum\sum K(t|s,r|m,n)\psi_n \quad (25)$$

where in the second relation n represents $(m - s + r)$. For the oscillator initially in the lowest state $m = 0$, this equation reduces to

$$\psi(t) = c(t)\sum_{r=0}^{\infty}\frac{[f(t)]^r}{\sqrt{r!}}\psi_r \quad (25\text{a})$$

Transition Probability

The probability of the $m \rightarrow n$ vibrational transition can be obtained from eq 25 by squaring the coefficient $K(\infty|s,r|m,n)$. However, there can be more than one term contributing to the final state n so that the squaring should include the sum of all such terms. For example, for the transition $3 \rightarrow 4$, there are four terms leading to the ψ_4 state, namely $(s,r) = (0,1)$, $(1,2)$, $(2,3)$, and $(3,4)$. We generalize this situation to obtain the final expression of the vibrational transition probability as

$$P_{mn} = |c(\infty)|^2|f(\infty)|^{2|n-m|}m!n! \times \left.\sum_{s=0}^{\min(m,n)}\frac{(-1)^s|f(\infty)|^{2s}}{s!(m-s)!(n-m+s)!}\right|^2 \quad (26)$$

in which the s sum is from zero to $\min(m,n)$, the lower of m or n. We must note that this equation satisfies the principle of detailed balance $P_{mn} = P_{nm}$ and that the probability is conserved; $\Sigma_{n=0}^{\infty} P_{mn} = 1$. For the oscillator initially in the ground state, eq 26 reduces to the simple form

$$P_{on} = \frac{|c(\infty)|^2|f(\infty)|^{2n}}{n!} \quad (27)$$

which can also be obtained from eq 25a.

From eq 19 and 21, we have

$$|f(\infty)|^2 = \frac{1}{2M\hbar\omega}\left|\int_{-\infty}^{\infty}\mathrm{d}t\left\{F(t) + \frac{3\hbar}{2M\omega}[\lambda_3 + \eta_3(t)]\right\} \times \exp\left\{i\omega t + \frac{i}{M\omega}\int_{-\infty}^{t}\eta_2(t')\mathrm{d}t'\right\}\right|^2 \equiv \frac{\Delta E}{\hbar\omega} \quad (28)$$

$$|c(\infty)|^2 = \exp\left[-\frac{1}{2M\hbar\omega}\left|\int_{-\infty}^{\infty}\mathrm{d}t\left\{F(t) + \frac{3\hbar}{2M\omega}[\lambda_3 + \eta_3(t)]\right\}\exp\left\{i\omega t + \frac{i}{M\omega}\int_{-\infty}^{t}\eta_2(t')\mathrm{d}t'\right\}\right|^2\right] \equiv \exp\left(-\frac{\Delta E}{\hbar\omega}\right) \quad (29)$$

where ΔE may be defined as the amount of the energy transferred to the oscillator driven by the perturbation energy $\Sigma\eta_i(t)q^i$. We note the appearance of the anharmonicity effect λ_3 in ΔE while λ_4 does not. If we set $\eta_2(t)$, $\eta_3(t)$, and the anharmonicity term λ_3 to zero, then the expression of ΔE reduces to the well known form[15]

$$\Delta E^\circ = \frac{1}{2M}\left|\int_{-\infty}^{\infty}F(t)\exp(i\omega t)\mathrm{d}t\right|^2 \quad (30)$$

for the harmonic oscillator driven by the force $F(t)$.

For an explicit calculation of P_{mn} we need to find the time dependence of $\eta(x)$'s from the x–t relation by solving the equation of motion as

$$t = \left(\frac{\mu}{2}\right)^{1/2}\int_{x^*}^{x}\frac{\mathrm{d}x}{[E - U(x,q,\theta)]^{1/2}} \quad (31)$$

---

(15) D. Rapp, *J. Chem. Phys.*, **32**, 735 (1960).

where μ is the reduced mass of the collision system, E the relative translational energy, and x^* the largest root of $E - U(x,q,\theta) = 0$. This equation determines the trajectory of the relative motion as a function of θ and q, but we neglect the effect of the oscillator's displacement on the trajectory. Since we wrote

$$U(x,q,\theta) = CA(\theta)\exp(-\alpha x) + U'(x,q,\theta) \tag{3}$$

the potential function appropriate for determining the trajectory can be taken to be $CA(\theta)\exp(-\alpha x)$, and use it in eq 31. The essential part of the integrals in eq 27 and 28 will then have the form

$$\int_{-\infty}^{\infty} \exp[-\alpha x(t) + i\omega t]\mathrm{d}t$$

which can be computed by contour integration.[16] As $x \rightarrow 0$, the potential energy $U(x,0,\theta)$ tends to $CA(\theta)$, where $C = 198.378$ eV. Since $A(\theta)$ is not significantly different from unity, this limiting value lies in a strongly repulsive region. By defining the collision time as[17]

$$\tau = \left(\frac{\mu}{2}\right)^{1/2} \int_{x_0}^{x^*} \frac{\mathrm{d}x}{[U(x,0,\theta) - E]^{1/2}} \tag{32}$$

we can solve eq 31 as

$$t = i\tau - \frac{i}{\alpha}\left(\frac{2\mu}{U}\right)^{1/2} \tag{33}$$

or

$$[CA(\theta)\ \exp(-\alpha x)]^{1/2} = \frac{(2\mu)^{1/2}}{\alpha i}\frac{1}{(t - i\tau)} \tag{34}$$

In eq 32 the lower limit x_0 represents the distance at which $U(x,0,\theta)$ becomes strongly repulsive. A different choice of this integration limit would not alter the result; the necessary condition for the choice is $U(x_0,0,\theta) \gg E$. For $U(x,,\theta) = CA(\theta)\exp(-\alpha x)$, the integration in eq 32 is trivial; the result is simply

$$\tau = \frac{\pi}{\alpha}\left(\frac{\mu}{2E}\right)^{1/2} \tag{35}$$

Since the collision time is determined from the relative motion of the incoming atom with respect to the center of mass of the oscillator, the situation that the collision time is independent of the angle θ is certainly expected in the present approximation. In eq 28 and 29 the term

$$\frac{i}{M\omega}\int_{-\infty}^{t} \eta_2(t')\mathrm{d}t'$$

appeared in the exponent of ΔE is due to the term proportional to q^2 of $U(x,q,\theta)$. The appearance of this term is seen in eq 14 indicating that the frequency varies with the time,[18] *i.e.*, $\omega + \eta_2(t)/M\omega$. Except at very high collision energies, the time-varying term is small, so that we can expand this exponential part in a power series and take the first three terms. In the following calculation section, we will find that this expansion is satisfactory. Then, the amount of energy transfer can be given in the form

$$\begin{aligned}\Delta E = \frac{1}{2M}\Bigg|\int_{-\infty}^{\infty} \mathrm{d}t\ \exp(i\omega t)\left\{F(t) + \frac{3\hbar}{2M\omega}[\lambda_3 + \right.\\ \left.\eta_3(t)]\right\} + \frac{i}{M\omega}\int_{-\infty}^{\infty} \mathrm{d}t\ \exp(i\omega t)\left\{F(t) + \right.\\ \left.\frac{3\hbar}{2M\omega}[\lambda_3 + \eta_3(t)]\left[\int_{-\infty}^{t} \eta_2(t')\mathrm{d}t'\right]\right\} - \\ \frac{1}{2(M\omega)^2}\int_{-\infty}^{\infty} \mathrm{d}t\ \exp(i\omega t)\left\{F(t) + \right.\\ \left.\frac{3\hbar}{2M\omega}[\lambda_3 + \eta_3(t)]\left[\int_{-\infty}^{t} \eta_2(t')\mathrm{d}t'\right]^2\right\}\Bigg|^2\end{aligned} \tag{36}$$

where the explicit forms of $F(t)$, $\eta_2(t)$, and $\eta_3(t)$ are, respectively

$$F(t) = -C[\alpha_1 A(\theta)x + B(\theta)]\exp(-\alpha x)$$

$$\eta_2(t) = C[{}^1/_2 A(\theta)\alpha_1{}^2x^2 + \alpha_1 B(\theta)x]\exp(-\alpha x)$$

$$\eta_3(t) = C[{}^1/_6 A(\theta)\alpha_1{}^3x^3 + {}^1/_2 B(\theta)\alpha_1{}^2x^2]\exp(-\alpha x)$$

The right-hand side of these relations will be converted into the corresponding time-dependent forms by use of the relation

$$x = -\frac{2}{\alpha}\ln\left\{\left[\frac{2\mu}{CA(\theta)}\right]^{1/2}\frac{1}{\alpha(\tau + it)}\right\} \tag{37}$$

and eq 34 itself. The resulting equation will contain integrals of the forms

$$\int_{-\infty}^{\infty} \frac{\exp(i\omega t)}{(t - i\tau)^{\beta}}\mathrm{d}t$$

and

$$\int_{-\infty}^{\infty} \ln{}^{\gamma}\left\{\left[\frac{2\mu}{CA(\theta)}\right]^{1/2}\frac{1}{\alpha(\tau + i\tau)}\right\}\frac{\mathrm{d}t}{(t - i\tau)^{\beta}}$$

where β and γ are integers. Since there is a branch cut from $i\tau$ along the imaginary axis to $i\infty$, we cannot simply replace the above integrals by their residues at the pole. Therefore, we replace the integration by an integration along a contour, which extends from $+i\infty$, encircles the singular point, $i\tau$, and then follows a branch cut in the complex t plane.[16] The latter form of the two integrals given above eventually reduces to the former when a successive use of the L'Hospital rule is made before letting $t \rightarrow i\tau$. Carrying out the integration, we find

$$\int_{-\infty}^{\infty} \frac{\exp(i\omega t)}{(t - i\tau)^{\beta}}\mathrm{d}t = \frac{2\pi(i\omega)^{\beta}}{\omega\Gamma(\beta)}\exp(-\omega\tau) \tag{38}$$

---

[16] E. E. Nikitin, *Opt. Spektrosk.*, **6**, 141 (1959); English transl., *Opt. Spectrosc.*, **6**, 93 (1959).

[17] H. Shin, *J. Phys. Chem.*, **73**, 4321 (1969).

[18] A. Zelechow, D. Rapp, and T. E. Sharp, *J. Chem. Phys.*, **49**, 286 (1968).

The integral $\int_{-\infty}^{t} \eta_2(t)\mathrm{d}t$ may be written in the form

$$\int_{-\infty}^{t} \eta_2(t)\mathrm{d}t = \int_{-\infty}^{t} [{}^1\!/_2 CA(\theta)\alpha_1{}^2x^2 + \alpha_1 CB(\theta)x] \exp(-\alpha x)\mathrm{d}t \quad (39)$$

which can be explicitly evaluated when $\mathrm{d}t$ is replaced by $\mathrm{d}x$ through eq 37. The result can be readily converted back to a time-dependent form by use of eq 34 for the evaluation of ΔE. We note that the leading term of the anharmonicity in eq 36 appears as

$$\lambda_3 \int_{-\infty}^{\infty} \exp(i\omega t)\mathrm{d}t$$

which is an integral representation of the δ function and vanishes in this case. Therefore, the first nonvanishing term of the anharmonicity contribution is

$$\lambda_3 \int_{-\infty}^{\infty} \exp(i\omega t)\mathrm{d}t \int_{-\infty}^{t} \eta_2(t')\mathrm{d}t'$$

By use of eq 38 followed by lengthy but elementary operations and simplifications, we finally obtain the following expression for the amount of energy transfer

$$\Delta E = \frac{8}{M}\left(\frac{\pi\omega\mu}{\alpha^2}\right)^2\left[\frac{B(\theta)}{A(\theta)}\right]^2 g(\theta) \exp\left[-\frac{\pi\omega}{\alpha}\left(\frac{2\mu}{E}\right)^{1/2}\right] \quad (40)$$

where

$$\begin{aligned} g(\theta) = \Bigg\{ & 1 + 2\left(\frac{\alpha_1}{\alpha}\right)\left(\frac{A}{B}\right) + \frac{6\hbar}{M\omega}\left(\frac{\alpha_1}{\alpha}\right)^2 + \\ & \frac{12\hbar}{M\omega}\left(\frac{\alpha_1}{\alpha}\right)^3\left(\frac{A}{B}\right) + \frac{3\hbar\phi}{M\omega}\left[\left(\frac{\alpha_1}{\alpha}\right)^2\frac{A}{B} + \frac{1}{2}\frac{\alpha_1}{\alpha}\right] - \\ & \frac{4\mu}{M\alpha^2}\left[\left(\frac{\alpha_1}{\alpha}\right)^2 + \frac{\alpha_1}{2\alpha}\frac{B}{A}\right] - \frac{6\mu}{M\alpha^2}\left(\frac{A}{B}\right) \times \\ & \left[4\left(\frac{\alpha_1}{\alpha}\right)^3 + 4\left(\frac{B}{A}\right)\left(\frac{\alpha_1}{\alpha}\right)^2 + \left(\frac{B}{A}\right)^2\frac{\alpha_1}{\alpha}\right] - \\ & \frac{22\mu}{M\alpha^2}\left(\frac{\alpha_1}{\alpha}\right)^2\left[\frac{3\hbar}{M\omega}\left(\frac{\alpha_1}{\alpha}\right)^2 + \frac{3\hbar}{2M\omega}\left(\frac{\alpha_1}{\alpha}\right)\left(\frac{B}{A}\right) + \right. \\ & \left. 2\left(\frac{\alpha_1}{\alpha}\right)\left(\frac{A}{B}\right) + \frac{3}{2}\right] - \frac{90\mu}{M\alpha^2}\left(\frac{\alpha_1}{\alpha}\right)^3\left(\frac{A}{B}\right)\left[\frac{\hbar}{M\omega}\left(\frac{\alpha_1}{\alpha}\right)^2 + \right. \\ & \left. \frac{2\hbar}{M\omega}\left(\frac{\alpha_1}{\alpha}\right)\left(\frac{B}{A}\right) + \frac{3\hbar}{4M\omega}\left(\frac{B}{A}\right)^2 + \frac{1}{2}\right] - \\ & \frac{180\mu}{M\alpha^2}\left(\frac{\alpha_1}{\alpha}\right)^4\left(\frac{A}{B}\right)\left(\frac{\hbar}{M\omega}\right)\left(\frac{\alpha_1}{\alpha} + \frac{5}{4}\frac{B}{A}\right)\Bigg\}^2 \end{aligned}$$

The lengthy expression for $g(\theta)$ is due to the inclusion of higher-order terms in q in the Hamiltonian. For practical purposes, higher-order terms in (α_1/α), particularly those containing $\mu/M\omega^2$ and/or $\hbar/M\omega$, can be neglected. Our problem of finding an explicit solution of P_{mn} is now completed with eq 26, 28, 30, and 40, and numerical computation ΔE, and in turn P_{mn} as a function of E and θ is simple. The energy constant C of the overall interaction does not appear in the above expression of ΔE, while the angle-dependent functions $A(\theta)$ and $B(\theta)$ enter in a complicated way. We also note that in the function $g(\theta)$, the first term is due to $B(\theta)q$ of the overall potential while the second term results from $A(\theta)\alpha_1 xq$ which is from the first q-dependent term of the expansion of $\exp(\alpha_1 xq)$. These two terms are the most important part of the potential causing vibrational transitions, *i.e.*, $g(\theta) \simeq [1 + 2(\alpha_1/\alpha)A(\theta)/B(\theta)]^2$.

Effects of Anharmonicity and Multi-quantum Transitions

In the above derivation we have discussed the effect of the oscillator anharmonicity on vibrational energy transfer. However, the effect was not fully accounted for in the derivation of the vibrational transition probability. Equation 36 shows that if $\eta_2(t)$ were zero, the anharmonicity correction would vanish, but the anharmonicity should contribute to the vibrational energy transfer even if $\eta_2(t)$ is zero. The form of $\psi(t)$ given by eq 12 is not sufficient for a rigorous calculation of the anharmonicity since it does not contain all the operators which act on the initial wave function to generate the anharmonicity. The leading part of the anharmonicity correction is proportional to $\lambda_3(\mathbf{a} + \mathbf{a}^+)^3$, which can be expanded as $\lambda_3(\mathbf{a}^3 + \mathbf{a}^{+3} + 3\mathbf{a}\mathbf{a}^{+2} + 3\mathbf{a}^2\mathbf{a}^+ - 3\mathbf{a}^+ - 3\mathbf{a})$. In the expansion $\mathbf{a}\mathbf{a}^{+2}$ and $\mathbf{a}^2\mathbf{a}^+$ also act as one-quantum transition operators, but only the operators $\mathbf{a}$ and $\mathbf{a}^+$ were included in the above derivation of P_{mn}. The cubic operators $\mathbf{a}^3$ and $\mathbf{a}^{+3}$ are three-quantum deexcitation and excitation operators, respectively. For the oscillator initially in the ground state, $\mathbf{a}^2\mathbf{a}^+$ and $\mathbf{a}^3$ should be discarded since they generate the ψ_{-1} and ψ_{-3} states. In the quadratic term, $(\mathbf{a} + \mathbf{a}^+)^2$ can be expanded as $\mathbf{a}^2 + \mathbf{a}^{+2} + 2\mathbf{a}^+\mathbf{a} + 1$, where $\mathbf{a}^2$ and $\mathbf{a}^{+2}$ are two-quantum transition operators, but these operators were not included in the above derivation.

Therefore, a more rigorous form of the wave function is

$$\psi(t) = c(t) \exp[f(t)\mathbf{a}^+] \exp[g(t)\mathbf{a}] \exp[h(t)\mathbf{N}] \times \exp[u(t)\mathbf{a}^{+2}] \exp[v(t)\mathbf{a}\mathbf{a}^{+2}]\psi(t_0) \quad (41)$$

This expression includes the one-quantum transition operator $\mathbf{a}\mathbf{a}^{+2}$ responsible for the leading effect of the anharmonicity and the two-quantum transition operator $\mathbf{a}^{+2}$. The latter operator represents the leading effect of multiquantum transitions. For the oscillator initially in the ground state, eq 41 contains all important information needed to determine the vibrational transition probability. By expanding the exponential operators and by generating the functions with the recursion relations as above, we obtain a lengthy expression for the wave function

$$\psi(t) = c(t) \sum_{l=0}^{\infty} \frac{[v(t)]^l}{l!} \frac{(m + 2l)!}{\sqrt{m!(m + l)!}} \times$$
$$\sum_{k=0}^{\infty} \frac{[u(t)]^k}{k!} \sqrt{\frac{(m + l + 2k)!}{(m + l)!}} \exp[(m + l + 2k)h(t)] \times$$
$$\sum_{s=0}^{m+l+2k} \frac{[g(t)]^s}{s!} \sqrt{\frac{(m + l + 2k)!}{(m + l + 2k - s)!}} \times$$
$$\sum_{r=0}^{\infty} \frac{[f(t)]^r}{r!} \sqrt{\frac{(m + l + 2k - s + r)!}{(m + l + 2k - s)!}} \psi_{m+l+2k-s+r} \equiv$$
$$\sum_{l} \sum_{k} \sum_{s} \sum_{r} K(t|l,k,s,r|m,n)\psi_n \quad (42)$$

In the second relation n, the final state, represents $(m + l + 2k - s + r)$, and the sums are arranged in the order of their generation from the initial state ψ_m. Because of the relation $n = m + l + 2k - s + r$, one of the indices in the middle group of the coefficient K need not be determined in carrying out the summations. If we also introduced the operators $\mathbf{a}^2$ and $\mathbf{a}^2\mathbf{a}^+$ in eq 41, there will be two additional sums appearing in eq 42. Such a treatment should, of course, be made in a more rigorous calculation. However, in the present paper, the inclusion of $\mathbf{a}^{+2}$ and $\mathbf{aa}^{+2}$ in $\psi(t)$ is sufficient in determining the leading effects of multiquantum transitions and anharmonicity.

By evaluating the time dependent functions in eq 41 at $t = \infty$, we can write the transition probability as

$$P_{mn} = |c(\infty)|^2 n! \Bigg| \sum_{l=0}^{\infty} \frac{[v(\infty)]^l}{l!} \frac{(m + 2l)!}{\sqrt{m!(m + l)!}} \times$$
$$\sum_{k=0}^{\infty} \frac{[u(\infty)]^k}{k!} \sqrt{\frac{(m + l + 2k)!}{(m + l)!}} \exp[(m + l + 2k)h(\infty)] \times$$
$$\sum_{s=0}^{m+l+2k} \frac{[g(\infty)]^s [f(\infty)]^{n-m-l-2k+s} \sqrt{(m + l + 2k)!}}{s!(m + l + 2k - s)!(n - m - l - 2k + s)!} \Bigg|^2 \quad (43)$$

which reduces to eq 26 when $v(\infty)$ and $u(\infty)$ are set equal to zero. To determine the functions $v(t)$ and $u(t)$, we need to obtain the time derivative $\psi(t)$ as follows

$$\dot{\psi}(t) = \dot{c}(t) \exp[f(t)\mathbf{a}^+] \exp[g(t)\mathbf{a}] \exp[h(t)\mathbf{N}] \times$$
$$\exp[u(t)\mathbf{a}^{+2}] \exp[v(t)\mathbf{aa}^{+2}]\psi(t_0) + c(t)\dot{f}(t)\mathbf{a}^+ \times$$
$$\exp[f(t)\mathbf{a}^+] \exp[g(t)\mathbf{a}] \exp[h(t)\mathbf{N}] \exp[u(t)\mathbf{a}^{+2}] \times$$
$$\exp[v(t)\mathbf{aa}^{+2}]\psi(t_0) + c(t)\dot{g}(t) \exp[f(t)\mathbf{a}^+] \times$$
$$\mathbf{a} \exp[g(t)\mathbf{a}] \exp[h(t)\mathbf{N}] \exp[u(t)\mathbf{a}^{+2}] \times$$
$$\exp[v(t)\mathbf{aa}^{+2}]\psi(t_0) + c(t)\dot{h}(t) \exp[f(t)\mathbf{a}^+] \times$$
$$\mathbf{a} \exp[g(t)\mathbf{a}]\mathbf{N} \exp[h(t)\mathbf{N}] \exp[u(t)\mathbf{a}^{+2}] \times$$
$$\exp[v(t)\mathbf{aa}^{+2}]\psi(t_0) + c(t)\dot{u}(t) \exp[f(t)\mathbf{a}^+] \times$$
$$\exp[g(t)\mathbf{a}] \exp[h(t)\mathbf{N}]\mathbf{a}^{+2} \exp[u(t)\mathbf{a}^{+2}] \times$$
$$\exp[v(t)\mathbf{aa}^{+2}]\psi(t_0) + c(t)\dot{v}(t) \exp[f(t)\mathbf{a}^+] \times$$
$$\exp[g(t)\mathbf{a}] \exp[h(t)\mathbf{N}] \exp[u(t)\mathbf{a}^{+2}]\mathbf{aa}^{+2} \times$$
$$\exp[v(t)\mathbf{aa}^{+2}]\psi(t_0) \quad (44)$$

The fifth and sixth terms, which contain the effect of multiquantum transitions and oscillator anharmonicity, can be converted into

$$\dot{u}(t)\{1 + 2h(t) + [h(t)]^2\}[\mathbf{a}^{+2} + 2g(t)\mathbf{a}^+ + g(t)^2]\psi(t)$$

and

$$\dot{v}(t)[1 + h(t)]\{\mathbf{aa}^{+2} - f(t)\mathbf{a}^{+2} + 2g(t)\mathbf{a}^+\mathbf{a} -$$
$$2g(t)f(t)\mathbf{a}^+ + [g(t)]^2\mathbf{a} - f(t)[g(t)]^2 + 2g(t)\}\psi(t)$$

We thus add these two terms (after multiplication by $i\hbar$) to the left-hand side of eq 13, and obtain

$$[1 + h(t)]\dot{v}(t) = \frac{3}{i\hbar}\left(\frac{\hbar}{2M\omega}\right)^{3/2} [\lambda_3 + \eta_3(t)] \quad (45)$$

and

$$\{1 + 2h(t) + [h(t)]^2\}\dot{u}(t) -$$
$$[1 + h(t)]f(t)\dot{v}(t) = -\frac{i}{2M\omega}\eta_2(t) \quad (46)$$

from the coefficients of $\mathbf{aa}^{+2}$ and $\mathbf{a}^{+2}$, respectively. For the 0 → 1 vibrational transition, the transition probability is then

$$P_{01} = \lim_{t \to \infty} |c(t)|^2 |f(t)|^2 |1 + 2f(t)v(t) \exp[h(t)]|^2 \quad (47)$$

where higher-order terms ($\ll 1$) in the square brackets have been neglected; such terms would become important in high energy collisions, however. Since the function $v(\infty)$ can be obtained from eq 45 as

$$v(\infty) = \frac{6\pi}{\hbar\omega}\left(\frac{\hbar}{2M\omega}\right)^{3/2} \lambda_3 i \quad (48)$$

the transition probability becomes

$$P_{01} = |c(\infty)|^2 |f(\infty)|^2 \left[1 - \left(\frac{12\pi\lambda_3}{\hbar\omega}\right)^2 \left(\frac{\hbar}{2M\omega}\right)^3 |f(\infty)|^2\right] \quad (49)$$

where the second term in the square brackets represents the effect of the anharmonicity. The expression can also be expressed as

$$P_{01}(E) = \frac{\Delta E}{\hbar\omega}\left[1 - \left(\frac{12\tau\lambda_3}{\hbar\omega}\right)^2 \left(\frac{\hbar}{2M\omega}\right)^3 \left(\frac{\Delta E}{\hbar\omega}\right)\right] \times$$
$$\exp\left(-\frac{\Delta E}{\hbar\omega}\right) \quad (50)$$

For $\lambda_3 = 0$, this expression reduces to the well-known form[8] $P_{01}(E) = (\Delta E/\hbar\omega) \exp(-\Delta E/\hbar\omega)$.

The energy transfer ΔE derived above depends only on the initial relative translational energy and not on the final relative energy. This dependence results because the trajectory $x(t)$ calculated above is independent of the collision system's final state. There-

Table I: Calculated Values of $P_{01}(E)$

$E \times 10^{12}$, erg	Orientation angles (θ)									
	0°	10°	20°	30°	40°	50°	60°	70°	80°	90°
1	8.77 (10)[a]	8.46 (10)	7.47 (10)	5.72 (10)	3.35 (10)	1.05 (10)	3.79 (14)	1.03 (10)	3.26 (10)	4.60 (10)
2	2.92 (5)	2.82 (5)	2.49 (5)	1.91 (5)	1.12 (5)	3.49 (6)	1.26 (9)	3.46 (6)	1.11 (5)	1.53 (5)
3	4.92 (4)	4.75 (4)	4.20 (4)	3.21 (4)	1.88 (4)	5.89 (5)	2.13 (8)	5.83 (5)	1.86 (4)	2.58 (4)
4	2.20 (3)	2.13 (3)	1.88 (3)	1.44 (3)	8.45 (4)	2.64 (4)	9.56 (8)	2.61 (4)	8.37 (4)	1.16 (3)
5	5.82 (3)	5.61 (3)	4.96 (3)	3.79 (3)	2.22 (3)	6.96 (4)	2.52 (7)	6.88 (4)	2.20 (3)	3.05 (3)
6	1.16 (2)	1.12 (2)	9.91 (3)	7.59 (3)	4.45 (3)	1.39 (3)	5.03 (7)	1.37 (3)	4.41 (3)	6.10 (3)
7	1.83 (2)	1.80 (2)	1.60 (2)	1.28 (2)	7.53 (3)	2.35 (3)	8.52 (7)	2.33 (3)	7.46 (3)	1.03 (2)
8	2.68 (2)	2.59 (2)	2.32 (2)	1.85 (2)	1.14 (2)	3.57 (2)	1.29 (6)	3.53 (3)	1.13 (2)	1.57 (2)
9	3.60 (2)	3.50 (2)	3.14 (2)	2.48 (2)	1.54 (2)	5.03 (2)	1.82 (6)	4.98 (3)	1.57 (2)	2.04 (2)
10	4.54 (2)	4.42 (2)	4.01 (2)	3.20 (2)	1.98 (2)	6.71 (3)	2.43 (6)	6.63 (3)	1.97 (2)	2.64 (2)
12	6.28 (2)	6.15 (2)	5.66 (2)	4.95 (2)	2.99 (2)	1.06 (2)	3.84 (6)	1.05 (2)	2.97 (2)	3.92 (2)
15	7.94 (2)	7.86 (2)	7.52 (2)	6.57 (2)	4.54 (2)	1.67 (2)	6.33 (6)	1.65 (2)	4.50 (2)	5.72 (2)
18	7.94 (2)	8.03 (2)	8.17 (2)	7.80 (2)	5.91 (2)	2.30 (2)	9.12 (6)	2.27 (2)	5.88 (2)	7.12 (2)
20	6.94 (2)	7.19 (2)	7.82 (2)	8.14 (2)	6.68 (2)	2.74 (2)	1.11 (5)	2.71 (2)	6.64 (2)	7.74 (2)

[a] Numbers in parentheses denote the negative power of 10; *e.g.*, 8.77 (10) = 8.77×10^{-10}.

fore, to avoid this physically unreasonable situation, we need to symmetrize[19] the energy by

$$\left[\frac{E^{1/2} + (E + \Delta)^{1/2}}{2}\right]^2$$

where Δ is the amount of energy transfer $|m - n|\hbar\omega$. We use this symmetrized energy in the calculation of the transition probabilities below. This symmetrization is equivalent to averaging the magnitudes of initial and final velocities.

Numerical Results and Discussion

For numerical analyses of the energy and angle dependence of the vibrational transition probability, we first show the values of $P_{01}(E)$ in Table I. For the calculation, we used the following constants:[6,20] $\nu\ (=\omega/2\pi) = 4159\ \text{cm}^{-1}$ and $\phi = 1.87824\ \text{Å}^{-1}$. The first eight terms of $g(\theta)$ were used in the calculation of ΔE. The fifth term represents the effect of the oscillator anharmonicity. When the constants are evaluated this term becomes $0.162\{0.106[A(\theta)/B(\theta)] + 0.163\}$. Since the ratio $A(\theta)/B(\theta)$ is not greatly different from unity (in atomic units) and since it is negative, the effect due to this term is not important. An important contribution of the anharmonicity comes from the second term of eq 50.

Table I shows several noteworthy features. The calculated transition probabilities cannot exceed unity, in contrast to the results of the usual perturbation theory.[8] In the limit of weak interaction the present result reduced to the first-order perturbation expression for the transition probability. The $P_{01}(E)$ takes a minimum value at the orientation angle of about 60°. Figure 1 shows the θ variation of the transition probability for several different values of E. A nearly symmetrical variation of $P_{01}(E)$ in the neighborhood of 60° is seen. At higher collision energies (*e.g.*, 3×10^{-11} erg) $P_{01}(E)$ is large at $\theta = 0°$ (collinear collision) and increases to a maximum value at ~30° followed by a sharp decrease to the minimum value at ~60°.

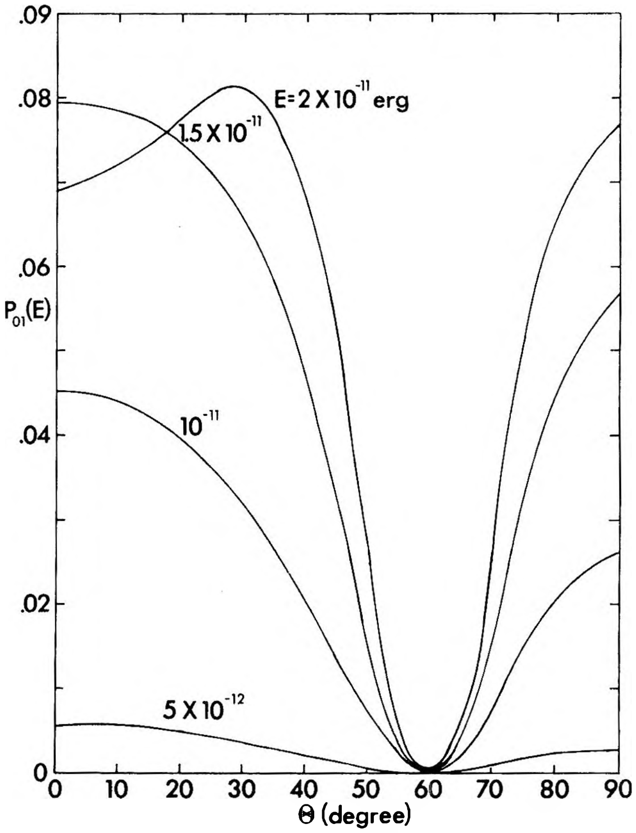

Figure 1. Angle dependence of P_{01} (E) at various values of E: $E = 5 \times 10^{-12}$, 10^{-11}, 1.5×10^{-11}, and 2×10^{-11} erg are chosen.

---

(19) T. L. Cottrell and J. C. McCoubrey, "Molecular Energy Transfer in Gases," Butterworths, London, 1961, Chapter 6.

(20) G. Herzberg, "Spectra of Diatomic Molecules," Van Nostrand, Princeton, N. J., 1950, Table 39.

As θ continues to increase, the probability sharply rises to a large value at $\theta = 90°$, the perpendicular orientation. While the actual shape is not exactly the same, the curves in Figure 1 (particularly that for $E = 2 \times 10^{-11}$ erg) are very similar to that of Mies.[6] At $E = 2 \times 10^{-11}$ erg, $P_{01}(E)$ is 6.94×10^{-2} at $\theta = 0°$ and increases to 8.14×10^{-2} at 30°. However, $P_{01}(E)$ at 90° is as large as 7.74×10^{-2}, which is larger than the value at the collinear collision. This situation can be explained as follows. The quantity ΔE is the amount of energy transfer when the anharmonicity correction is zero (the fifth term in $g(\theta)$ containing ϕ is very small). This quantity is always largest for the collision at $\theta = 0°$ (*e.g.*, $\Delta E/\hbar\omega = 0.256$, 0.167, and 0.134 at θ = 0, 30, and 90°, respectively, when the collision energy is 2×10^{-11} erg). However, the anharmonicity correction is most serious for the collinear collision (0.350 compared to the correction at 90° of 0.658). The increase of $P_{01}(E)$ with θ in the range from 0 to 30° results because $\Delta E/\hbar\omega$ varies only slightly while the anharmonicity correction changes significantly. [At lower energies, $P_{01}(E)$ does not take a maximum value in the P_{01}–θ plot, see Figure 1.]

In addition to the effect of the oscillator anharmonicity, the q dependence of $U(x,q,\theta)$ is also responsible for efficient energy transfer at 90°. As θ approaches 90°, $A(\theta)$ decreases toward unity from the maximum value 1.30124 at $\theta = 0°$ while $B(\theta)$ decreases toward its minimum value −0.59932 from the maximum value −0.38415 which also occurs at $\theta = 0°$. Since the latter function contributes to the overall interaction energy as $B(\theta)q$, the factor $[A(\theta) + B(\theta)q]$ would decrease only slowly as θ tends to 90° when q is negative. If q takes a large negative value, this factor can even increase as $\theta \rightarrow 90°$; this situation represents a compression of the H–H bond by a very large magnitude, but such a strong perturbation may not occur in the energy range considered here. Nevertheless, the θ and q dependences of $[A(\theta) + B(\theta)q]$ appear in such a way that the perturbation energy at 90° is not significantly small compared to the collinear case. It is important to point out that model potentials often assumed in the conventional calculations[6,21] give the transition probabilities at 90° very small compared to those at 0°.

In Figure 2 we compare our result with Mies' DWA calculation[6] for $\theta = 0°$ and find a satisfactory agreement; the results are reproduced from curve A of Figure 5 of ref 6. At lower energies, our result is larger than Mies' result by a factor of about 2. At higher energies, Mies' result exceeds ours and tends to increase beyond unity. (For comparison, we also show the case at $\theta = 90°$.) The transition probability at $\theta = 0°$ takes a maximum value at $\sim 1.6 \times 10^{-11}$ erg. The appearance of such a maximum was also noticed in Figure 1 where $P_{01}(E)$ for 1.5×10^{-11} erg is larger than that for 2×10^{-11} erg when the orientation angle is 0°. A similar $P_{01} - E$ variation is found for $P_{01}(E)$ below 30° in the energy range considered. For other orientation angles, $P_{01}(E)$ would take such a maximum value at still higher collision energies.

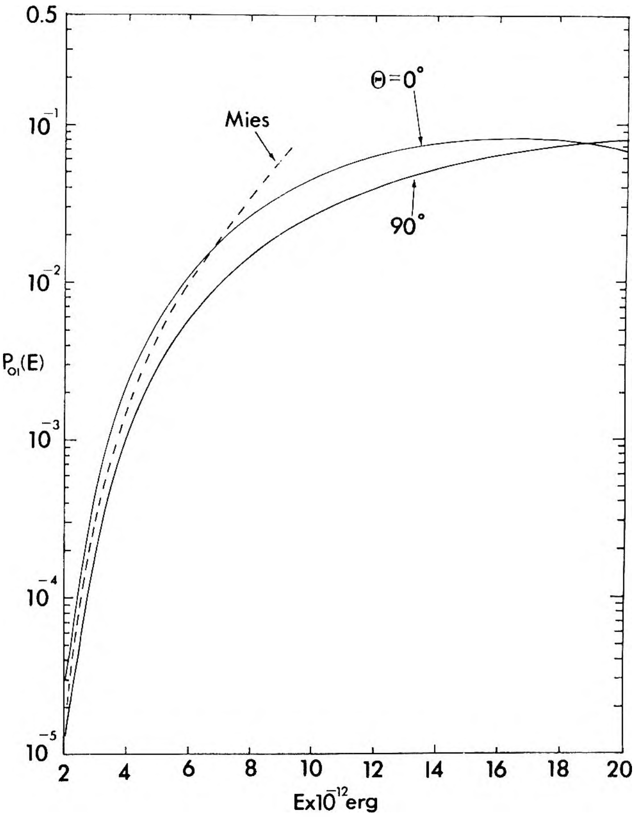

Figure 2. Plot of P_{01} (E) as a function of E for the collinear and perpendicular orientations. The dotted curve represents Mies' DWA calculation.

We have not investigated the problem of vibration-to-rotation energy transfer. The present approach does not appear to be suitable in investigating such a problem. There are theoretical methods that can be applied to the vibration-to-rotation energy transfer in H_2 + He.[22] Kelley and Wolfsberg[23] showed that rotational motion can significantly affect the probability of vibrational energy transfer. Assuming an exponential model potential, they calculated the amounts of vibrational and rotational energy transfer as a function of initial orientation angle. (It should be noted that Mies' result[6] that the model potential does not adequately describe the H_2 + He collision raises concern about the use of the model potential in general.) In the present work, we can also calculate the amount of vibrational energy transfer as a function of θ. Since θ is the angle at the instant of collision, it represents the initial orientation angle. As

---

(21) H. Shin, *J. Chem. Phys.*, **49**, 3964 (1968).

(22) H. Shin, *J. Phys. Chem.*, **75**, 1079, 3185 (1971).

(23) J. D. Kelley and M. Wolfsberg, *J. Chem. Phys.*, **53**, 2967 (1970).

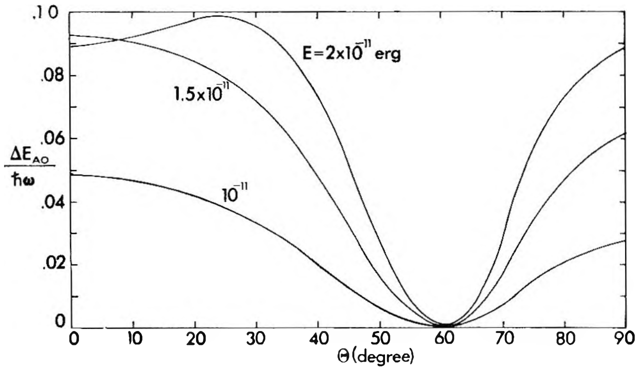

Figure 3. Plot of the amount of vibrational energy transfer for the anharmonic oscillator in units of $\hbar\omega$ as a function of the initial angle θ. The energies of 10^{-11}, 1.5×10^{-11}, and 2×10^{-11} erg are chosen.

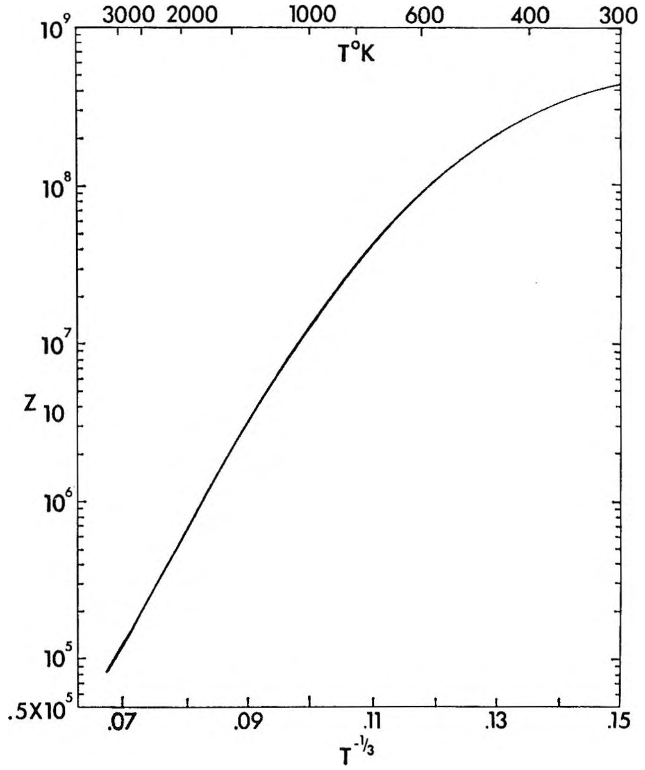

Figure 4. Temperature dependence of the collision number Z_{10}.

noted above, ΔE with $\lambda_3 = 0$ is the amount of energy transfer to (or from) the harmonic oscillator. The vibrational energy transfer for the anharmonic oscillator is, from eq 50, then

$$\Delta E_{\mathrm{AO}} = \Delta E\left[1 - \left(\frac{12\pi\lambda_3}{\hbar\omega}\right)^2\left(\frac{\hbar}{2M\omega}\right)^3\left(\frac{\Delta E}{\hbar\omega}\right)\right]$$

In Figure 3, we show the amount of energy transfer ΔE_{AO} in units of $\hbar\omega$ as a function of θ for several different collision energies. The variation of ΔE_{AO} with θ is similar to that of Kelley and Wolfsberg's work. The figure shows that at higher collision energies, the collinear collision is not the most efficient for energy transfer. Note that if $\Delta E_{\mathrm{AO}}/\hbar\omega$ is multiplied by exp($-\Delta E/\hbar\omega$) we obtain $P_{01}(E)$.

To discuss the temperature dependence of the vibrational transition probability we need to average $P_{01}(E)$ over a Boltzmann distribution of the initial energies. From the above calculation, we find that the collision time given by eq 35 varies from 1.39×10^{-14} sec at $E = 10^{-12}$ erg to 2.13×10^{-15} sec at 2×10^{-11} erg. If we define the vibrational period t_v by $1/\nu$, which is 7.63×10^{-15} sec, then $\tau \simeq t_v$ in the energy range considered. Although it is difficult to define the rotational period t_r, it can be significantly larger than τ. Since the colliding partners are approaching each other at all possible orientation angles, a useful expression is the angle and energy transition probability

$$P_{01}(T) = \frac{1}{kT}\int_0^{\pi/2} \sin\theta \mathrm{d}\theta \int_0^{\infty} P_{01}(E)\exp(-E/kT)\mathrm{d}E \tag{51}$$

Because of a complicated dependence of $P_{01}(E)$ on E and θ, we shall carry out the integrations numerically. The deexcitation probability $P_{10}(T)$ can be obtained as $P_{01}(T)\exp(+\hbar\omega/kT)$. Figure 4 shows the temperature dependence of the collision number Z_{10}, which is defined as $1/P_{10}(T)$. Above 800°K a linear relationship between log Z_{10} and $T^{-1/3}$ is found (often referred to as a Landau–Teller plot). A large deviation from the linearity at lower temperatures is seen. The figure also shows that the hydrogen molecule is difficult to deexcite (or excite) at ordinary temperatures.

Numerical integrations often have the disadvantage of giving only particular solutions for given initial conditions. Even if the solutions are approximate, on the other hand, analytical solutions can yield detailed information on the dependence of final expressions on relevant parameters which characterize the physical problem. Such solutions are therefore useful in the present problem in showing quantitatively the variation of the average transition probability on the temperature, anharmonicity, and other pertinent parameters. Such an approximate expression can be obtained from eq 51. As E increases the transition probability, $P_{01}(E)$ increases as exp($-$constant/$E^{1/2}$) while the Boltzmann factor decreases at low energies so that the integrand takes a maximum value at some energy (say E^*). For the energy range we are interested in, $\Delta E/\hbar\omega$ is small ($\ll 1$); *e.g.*, when $\theta = 0°$, $\Delta E/\hbar\omega$ increases from 1.45×10^{-6} at $E = 10^{-12}$ erg to 0.266 at 2×10^{-11} erg. At the energy where the integrand becomes largest, $\Delta E/\hbar\omega$ is significantly small compared to unity. Therefore, the exponential factor exp($-\Delta E/\hbar\omega$) in eq 51 can be expanded in a power series. By taking the terms in the integrand up to cubic in $\Delta E/\hbar\omega$, we have

$$P_{01}(T) = \frac{1}{kT}\int_0^{\pi/2} \sin\theta d\theta \left\{\int_0^{\infty} \epsilon\left[1 - \left(\frac{12\pi\lambda_3}{\hbar\omega}\right)^2 \times \left(\frac{\hbar}{2M\omega}\right)^3 \epsilon\right] \exp\left(-\epsilon - \frac{E}{kT}\right) dE\right\}$$

$$= \frac{1}{kT}\int_0^{\pi/2} \sin\theta d\theta \int_0^{\infty} \epsilon \exp\left(-\frac{E}{kT}\right) \times dE - \frac{G+1}{kT}\int_0^{\pi/2} \sin\theta d\theta \int_0^{\infty} \epsilon^2 \times \exp\left(-\frac{E}{kT}\right) dE + \frac{G}{kT}\int_0^{\pi/2} \sin\theta d\theta \times \int_0^{\infty} \epsilon^3 \exp\left(-\frac{E}{kT}\right) dE \quad (52)$$

where $\epsilon = \Delta E/\hbar\omega$ and $G = (12\pi\lambda_3/\hbar\omega)^2\ (\hbar/2M\omega)^3$. Each E integral can be evaluated by use of the Laplace method.[24] The energy E^* is then found by setting the first derivative of the exponent of the integrand with respect to E to zero. For the three integrals in eq 52, the maximum occurs, respectively, at

$$E^{*(1)} = \chi + {}^1/_2\hbar\omega \quad (53a)$$

$$E^{*(2)} = 2^{2/3}\chi + {}^1/_2\hbar\omega \quad (53b)$$

$$E^{*(3)} = 3^{2/3}\chi + {}^1/_2\hbar\omega \quad (53c)$$

where $\chi = [(\mu/2)^{1/2}(\pi\omega kT/\alpha)]^{2/3}$. The Laplace evaluation of eq 52 at these energies results in the average transition probability

$$P_{01}(T) = \left(\frac{4\pi}{3}\right)^{1/2}\left(\frac{\chi}{kT}\right)^{1/2} \exp(-\hbar\omega/2kT) \times \left[Q \exp\left(-\frac{3\chi}{kT}\right) - 2^{1/3}(G+1)Q' \exp\left(-\frac{2^{2/3}3\chi}{kT}\right) + \frac{3^{1/3}}{2}GQ^{2\prime\prime} \exp\left(-\frac{3^{5/3}\chi}{kT}\right)\right] \quad (54)$$

where

$$Q = \frac{8}{M\hbar\omega}\left(\frac{\pi\omega\mu}{\alpha^2}\right)^2 \int_0^{\pi/2} \left[\frac{B(\theta)}{A(\theta)}\right]^2 g(\theta)\sin\theta d\theta \quad (55)$$

$$\equiv \int_0^{\pi/2} G(\theta)\sin\theta d\theta \quad (55a)$$

$$Q' = \int_0^{\pi/2} [G(\theta)]^2 \sin\theta d\theta \quad (55b)$$

$$Q'' = \int_0^{\pi/2} [G(\theta)]^3 \sin\theta d\theta \quad (55c)$$

The θ integral in the latter equation includes the first eight terms of $g(\theta)$, and its graphical evaluation is simple. To obtain the average transition probability appropriate to a deexcitation of the oscillator, $P_{10}(T)$, rather than to an excitation, we have merely to replace $\exp(-\hbar\omega/2kT)$ by $\exp(+\hbar\omega/2kT)$.

By comparing the numerically integrated result with the calculated values of eq 54, we find that the approximate method is entirely satisfactory. At 300°K, the integrand of eq 51 takes a maximum value at $\sim 0.9 \times 10^{-12}$ erg so that in the integrand the transition probability can be replaced simply by ϵ; *i.e.*, the first integral of eq 52 is only important. Even at 3000°K the maximum value occurs at $\sim 2.6 \times 10^{-12}$ erg. By comparing these energies with those listed in Table I, we notice that when the thermal average is made the probability of vibrational energy transfer is affected very little by the parts due to the exponential factor $\exp(-\epsilon)$ and the anharmonicity correction. At 300°K, $3\chi/kT = 34.10$ and $(2)^{2/3}(3\chi/kT) = 54.15$ so that the first term in eq 52 is larger by a factor of about 10^7 than the second term, which contains the leading effect of the anharmonicity as well as that of the exponential part $\exp(-\epsilon)$; at 3000°K, the corresponding factor is about 4×10^2. Therefore, a useful expression of the average transition probability can be written in a particularly simple form

$$P_{01}(T) \simeq \left(\frac{4\pi}{3}\right)^{1/2}\left(\frac{\chi}{kT}\right)^{1/2} Q \exp\left(-\frac{3\chi}{kT} - \frac{\hbar\omega}{2kT}\right) \quad (56)$$

Finally, the approximate solutions reveal that the large deviation of log Z_{10} from the linearity at lower temperatures shown in Figure 4 is due to the contribution of the exponential part $\exp(+\hbar\omega/2kT)$; *e.g.*, at 300°K $\hbar\omega/2kT$ is as large as 10.55 whereas the leading term $3\chi/kT$ is 34.10.

---

[24] A. Erdélyi, "Asymptotic Expansions," Dover Publications, New York, N. Y., 1956, pp 36–39.

Proton-Transfer Reactions. A Mechanism for the Absorption of Ultrasound in Aqueous Solutions of Proteins

by Matthew Hussey*[1] and Peter D. Edmonds

Department of Biomedical Engineering, Moore School of Electrical Engineering, University of Pennsylvania, Philadelphia, Pennsylvania 19104 *(Received June 16, 1971)*

Publication costs assisted by the Department of Biomedical Engineering, Moore School of Electrical Engineering, University of Pennsylvania

This paper presents a first-order method of calculating the excess ultrasonic absorption due to proton-transfer reactions for solutions of proteins and polypeptides. The calculated results for three proteins—bovine serum albumin, human hemoglobin, and gelatin—and two polypeptides—polylysine and polyglutamic acid—are plotted and are shown to resemble qualitatively the experimental data from other authors. It is concluded that this mechanism is appreciable in the ranges pH <6 and pH >8. However, the calculation does need refinement and some ways to do so are recommended.

Introduction

Kessler and Dunn[2] have reported results of ultrasonic investigations on aqueous solutions of bovine serum albumin (BSA) at 20° over the frequency range 0.3–163 MHz and over the pH range 2.3–11.8. They found a sharp increase in the excess absorption outside the range $4.3 < \text{pH} < 10.5$. This effect was reversible and was more pronounced at the lower frequencies. They attributed the increase in absorption below pH 4.3 to the intermediate N–F′ transition discussed by Foster[3] and that above pH 10.5 to expansion of the molecule. Both sets of mechanisms represent conformational changes in the molecule.

Subsequently, Zana and Lang[4] reported results of their ultrasonic experiments on aqueous solutions of BSA, β-lactoglobulin, and lysozyme at 25° at 2.82 MHz and over the pH range 1.0–13.3. They concluded that proton-transfer reactions at the basic and acidic side chains constituted the mechanism most likely giving rise to the observed excess absorption in the ranges pH <4.0 and pH >10.0.

Some recent work by the present authors should help to shed some more light on this problem.[5-7] A theory of the pH dependence of the excess absorption due to proton-transfer reactions in aqueous solution was worked out and applied to the results of extensive ultrasonic measurements on solutions of glycine[5] and of lysine and arginine.[6] The measurements on glycine were at 22, 30, and 37°, covered the frequency range 10–130 MHz, and involved initial concentrations 0.25, 0.5, and 1.0 M at pH <5 and >8. The studies on lysine and arginine were at 22°, 0.25 M, pH >9, and frequencies between 10 and 130 MHz.

In this work it is proposed to apply the theory in a predictive manner to solutions of the following polypeptides and proteins for which ultrasonic absorption data already exist: BSA,[2,4] hemoglobin,[8,9] gelatin,[10,11] polylysine,[12] and polyglutamic acid.[13]

Summary of the Theory

The general form for the proton-transfer reaction between species A and B is

$$\mathrm{A} + \mathrm{X} \underset{k_{21}}{\overset{k_{12}}{\rightleftharpoons}} \mathrm{B} \qquad (1)$$

Here k_{12} and k_{21} are rate constants, forward and reverse, respectively. In aqueous solution X may be the hydrated hydrogen ion, H_3O^+, or the hydroxyl ion, OH^-.

For small displacements from equilibrium this reaction has a single relaxation time τ described as[14]

---

* To whom correspondence should be addressed at the Western Regional Hospital Board, Department of Clinical Physics and Bioengineering, Glasgow, C.4, Scotland.

(1) This work was done in partial fulfillment of the requirements for the Ph.D. degree in Biomedical Engineering at the University of Pennsylvania.

(2) L. W. Kessler and F. Dunn, *J. Phys. Chem.*, **73,** 4256 (1969).

(3) J. F. Foster, "Plasma Proteins," F. W. Putnam, Ed., Academic Press, New York, N. Y., 1960, Chapter 6.

(4) R. Zana and J. Lang, *J. Phys. Chem.*, **74,** 2734 (1970).

(5) M. Hussey and P. D. Edmonds, *J. Acoust. Soc. Amer.*, **49,** 1309 (1971).

(6) M. Hussey and P. D. Edmonds, *ibid.*, **49,** 1908 (1971).

(7) M. Hussey, Ph.D. Dissertation, University of Pennsylvania, Philadelphia, Pa., 1970.

(8) P. D. Edmonds, T. J. Bauld, J. F. Dyro, and M. Hussey, *Biochim. Biophys. Acta*, **200,** 174 (1970).

(9) W. D. O'Brien, private communication, 1969.

(10) H. Pauly and H. P. Schwan, accepted for publication in *J. Acoust. Soc. Amer.*

(11) Y. Wada, H. Sasabe and M. Tomono, *Biopolymers*, **5,** 887 (1967).

(12) R. C. Parker, L. J. Slutsky, and K. R. Applegate, *J. Phys. Chem.*, **72,** 3177 (1968).

(13) J. J. Burke, G. G. Hammes, and T. B. Lewis, *J. Chem. Phys.*, **42,** 3520 (1965).

$$\tau = [k_{12}(\bar{a}_A + \bar{a}_X + 1/K)]^{-1} \qquad (2)$$

where $\bar{a}_i$ is activity of species "i" at equilibrium and K is the equilibrium constant ($\equiv k_{21}/k_{12}$). Also

$$\bar{a}_i = y_i \bar{c}_i \qquad (3)$$

where $\bar{c}_i$ is equilibrium value of concentration of species "i" and y_i is the corresponding activity coefficient.

When a solution containing equilibrium 1 is irradiated by ultrasound, the equilibrium is disturbed. If the radiant power level is low ($\ll$1 W cm^{-2}), the displacement from equilibrium is small and the restoration of equilibrium is specified by the characteristic time given by eq 2. In the frequency domain this relaxational behavior is manifested as an excess absorption characterized by

$$\frac{\alpha^{ch}}{f^2} = A\frac{f_0^2}{f^2 + f_0^2} \qquad (4)$$

where α^{ch} is the excess amplitude absorption coefficient due to the reaction, f is frequency, f_0 is relaxation frequency, and A is relaxation amplitude.

$$f_0 = (2\pi\tau)^{-1} = \frac{k_{12}}{2\pi}\left(\bar{a}_A + \bar{a}_X + \frac{1}{K}\right) = \frac{k_{12}}{2\pi}D \qquad (5)$$

Here D represents the term in parentheses and

$$A = \frac{\pi\rho}{RTf_0}G(\Delta U)^2 \qquad (6)$$

where ρ is solution density, R is the gas constant, T is absolute temperature

$$G = \left[\frac{1}{\bar{c}_A} + \frac{1}{\bar{c}_X} + \frac{1}{\bar{c}_B}\right]^{-1} \qquad (7)$$

and

$$\Delta U = \Delta V - m\Delta H \qquad (8)$$

Here ΔV and ΔH are the partial molar volume and enthalpy, respectively, for the reaction and m is a constant for the medium at any temperature.[14]

If activity coefficients be assumed to equal unity, the D and G parameters may be calculated for any value of of pX ($\equiv -\log \bar{c}_X$) from eq 5 and 7 when one knows the equilibrium constant and the initial concentration C_0, where

$$C_0 = \bar{c}_A + \bar{c}_B \qquad (9)$$

Figure 1 illustrates the dependencies of the D and G parameters (and hence f_0 and A, respectively) on pX for three different values of C_0. Typical values for k_{12}, ΔU, and K were assumed in making the calculations for this figure.

Certain important features of the curves in Figure 1 should be noted. The range of pX in which appreciable excess ultrasonic absorption occurs covers about 1.2 pX units and falls on the low side of pK. The absorption magnitude parameter, G, peaks at a particular pX at which, for the same initial concentration value the relaxation frequency parameter, D, troughs. This special pX value, pX$_s$ is given approximately by

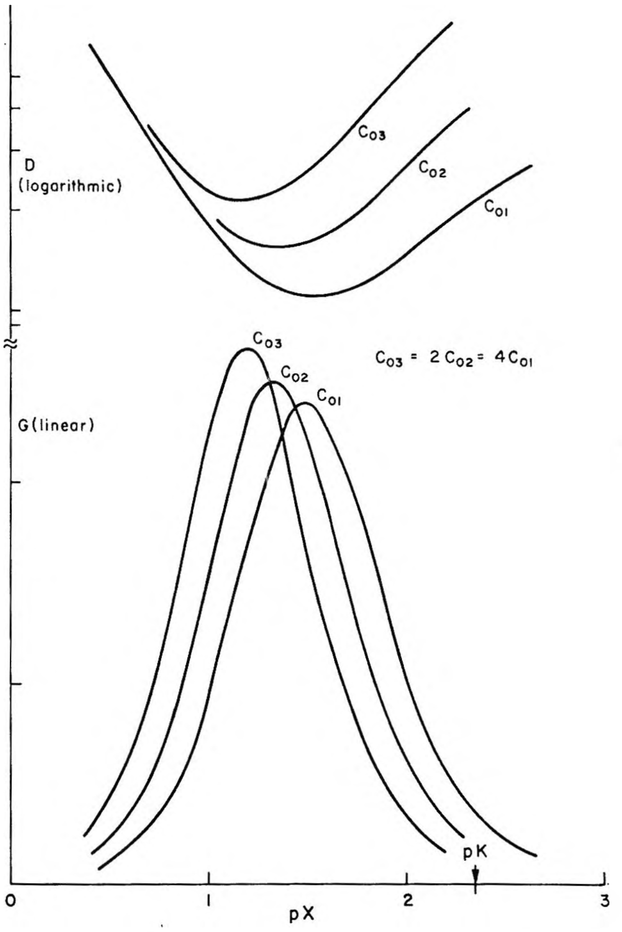

Figure 1. Dependence of the D and G parameters on pX for three different values of initial concentration, C_0.

$$\text{pX}_s = -\frac{1}{2}(\log K + \log C_0) = \frac{1}{2}(\text{p}K - \log C_0) \qquad (10)$$

Decreasing C_0 shifts pX$_s$ toward pK and diminishes, but not linearly, the peak value of G and the trough value of D. The introduction of activity coefficients[5] adds the term $-1/2 \log y_B$ to the right-hand side of eq 10. Conditions under which the activity coefficients would be appreciably less than unity (*e. g.*, high ionic strength) could thus introduce further shifts in the location of pX$_s$.

For the particular case of the proton-transfer reaction at a carboxyl group in aqueous solution, eq 1 becomes

$$\text{-COO}^- + \text{H}_3\text{O}^+ \rightleftharpoons \text{-COOH}\cdot\text{H}_2\text{O} \qquad (11)$$

Here pX becomes pH and the behavior of the appropriate D and G parameters is exactly as in Figure 1.

---

(14) M. Eigen and L. De Maeyer, in "Technique of Organic Chemistry," Vol. VIII, 2nd ed, Wiley-Interscience, New York, N. Y., 1963, Chapter XVIII.

For the reaction at an amino group equation 1 becomes

$$-NH_3^+ + OH^- \rightleftharpoons -NH_2 \cdot H_2O \qquad (12)$$

Here pX becomes pOH, so that on the pH scale (where $pH \equiv pK_w - pOH$ and where K_w is the ionization constant of water) the behavior of the D and G parameters is a mirror image of the curves in Figure 1 reflected through the line $pH = pK$ (where K is the appropriate acid equilibrium constant).

Application of This Theory to Polypeptide and Protein Solutions

A polypeptide consists of a long chain of amino acids artificially constructed, the sequence of which may be known. Thus polylysine consists of a backbone from which protrude side chains all terminated by ϵ-amino groups. Polyglutamic acid has a series of γ-carboxyl side-chain groups. The naturally occurring protein has a number of structural features but its primary structure is a chain of amino acids with side chains, some of which are carboxyl or amino or other ionizable types and some of which are not ionizable. The secondary, tertiary, and quaternary structures of the protein determine the location and orientation in space of the basic amino acid chain.

To apply eq 4–12 in a predictive manner to any general case, one must have fairly good approximate values at least for the following unknowns: k_{12}, ΔU, K, and C_0. In applying them, even in a strictly linear fashion to polypeptides and proteins, as it is proposed to do here, there are many difficulties to overcome.

One must know first what side-chain types are present and how many of each type. For most common proteins this information is now available from amino acid sequence studies.[15] However, since proteins are such complex three-dimensional structures, some of these side chains may be masked and so not available for proton transfer. Titration studies usually can reveal the number, n, of "available" side chains.[16–19] Titrimetric data can also provide mean pK values for particular types of ionizable side chains.[16–19] Rate constant values for individual side-chain types may be estimated from those of similar model compound.[5,6,20] ΔU values may be estimated, chiefly from dilatometric data on similar model compounds and on proteins[21–23] or from ultrasonic data on similar model compounds.[5,6,14] Knowing these parameter values for each side-chain type, one can apply eq 4–12 to calculate the contribution of this mechanism at each side chain to the excess ultrasonic absorption.

Simple summation provides a total predicted excess absorption. This calculation assumes independence of the different reactions and ignores possible variation in the environment around and parameters applying to side chains of the same type. These are major limitations to the validity of the calculation but it should allow a reasonably good qualitative picture to emerge.

Table I shows the parameter values used in the sample calculation for the aqueous solution of BSA, together with the sources of these parameter values. Tables II and III similarly treat solutions of human hemoglobin and gelatin, respectively. Table IV lists the pertinent parameters for polylysine and polyglutamic acid solutions.

Table I: Parameter Values Used to Calculate Contributions to Excess Absorption from Proton-Transfer Reactions at Side Chains in a 0.042 g/cm^3 BSA Solution at 25°[a]

Group	p$K^{16,17}$	$n^{16,17}$	$10^{10} \times k_{12}{}^{5,6,14,20}$ M^{-1} sec^{-1}	$\Delta U^{5,6,21-23}$ cm^3 mol^{-1}
α-Carboxyl	3.75	1	3	10
s-Carboxyl[b]	3.95	99	3	10
Imidazole	6.90	16	3	18
α-Amino	7.75	1	5	15
ϵ-Amino	9.80	57	5	15
Phenolic	10.35	19	2	17
Guanidine	12.50	22	5	15

[a] Molecular weight of BSA 65,000; $C_0 = 0.00063\ M$. [b] s refers to side chain.

Figures 2–6 show calculated excess absorption due to proton transfer at side chains and fairly directly comparable experimentally observed absorption (in excess of that in the region of pH 7) in the pertinent pH ranges for solutions of BSA, human hemoglobin, gelatin, polylysine, and polyglutamic acid, respectively.

Discussion

Qualitatively the calculated ultrasonic absorption behavior due to proton-transfer reaction at side chains in proteins is similar to that calculated and observed for glycine:[5] excess absorption occurs at high pH (>8) and at low pH (<6) with no appreciable contribution in between (6 < pH < 8). However there are major differences which arise from the composite nature of the results for proteins.

---

(15) M. O. Dayhoff, "Atlas of Protein Structure," National Biomedical Research Foundation, Silver Spring, Md., 1969.

(16) C. Tanford, *Advan. Protein Chem.*, **17**, 69 (1962).

(17) C. Tanford, S. A. Swanson, and W. S. Shore, *J. Amer. Chem. Soc.*, **77**, 6414 (1955).

(18) C. Tanford and Y. Nozaki, *J. Biol. Chem.*, **241**, 2832 (1966).

(19) P. Doty, A. Wada, J. T. Yang, and E. R. Blout, *J. Polym. Sci.*, **23**, 851 (1957).

(20) M. Sheinblatt and H. S. Gutowsky, *J. Amer. Chem. Soc.*, **86**, 4814 (1964).

(21) J. Rasper and W. Kauzmann, *ibid.*, **84**, 1771 (1962).

(22) W. Kauzmann, A. Bodanszky, and J. Rasper, *ibid.*, **84**, 1777 (1962).

(23) H. H. Weber and D. Nachmannsohn, *Biochem. Z.*, **204**, 215 (1928).

Table II: Parameter Values Used to Calculate the Contributions to Excess Absorption Due to Proton-Transfer Reactions at Side Chains in 0.15 g/cm^3 Human Hemoglobin Solution at 25°[a]

		[illegible]^{15,16,18}				
		pH values				
Group	p$K^{16,18}$	<4.5 >11.5	4.5 11.5	>4.5 <11.5	$10^{10}k_{12}$,^{5,6,14,20} M^{-1} sec^{-1}	ΔU,$^{5,6,21-23}$ cm^3 mol^{-1}
α-Carboxyl	3.7	4	4	4	3	10
s-Carboxyl	4.7	62	60	58	3	10
Imidazole	6.1	38	32	26	3	17
α-Amino	7.6	4	4	4	5	15.5
ε-Amino	10.4	44	43	42	5	15.5
Phenolic	9.6	12	12	12	2	17
Sulfhydryl	9.1	6	6	6	1	15
Guanidine	12.5	12	10	8	5	16

[a] Molecular weight of hemoglobin 68 000; $C_0 = 0.0022\ M$.

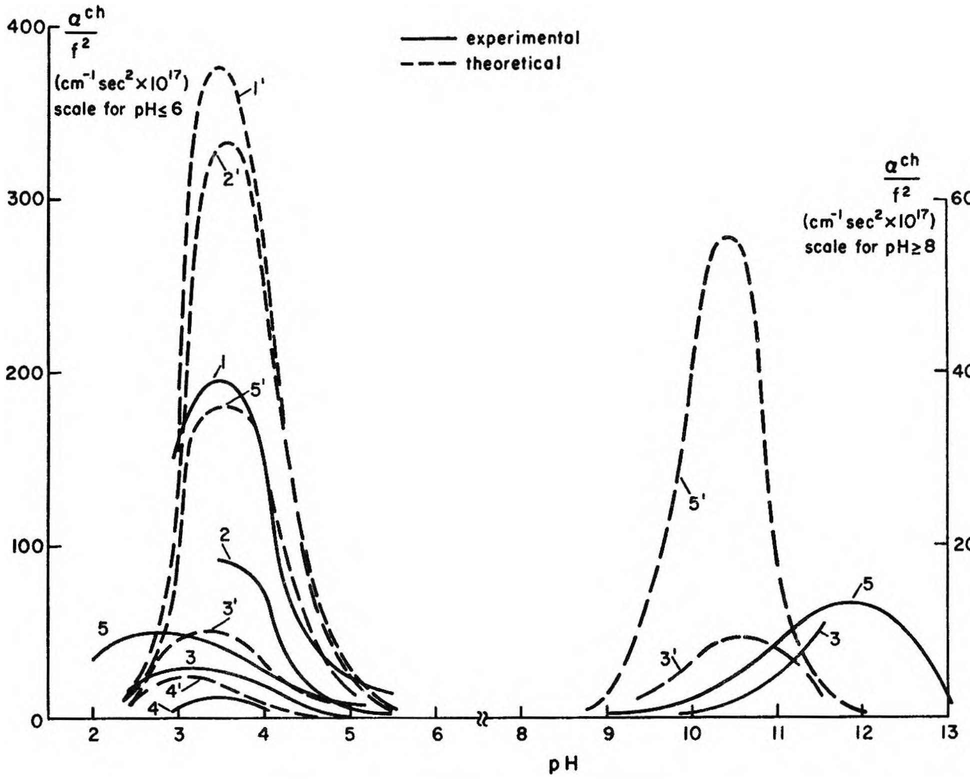

Figure 2. Excess absorption in aqueous BSA solutions in the pH ranges <6 and >8, over and above that in the region of pH 7: curves 1–4, derived from experimental data of Kessler and Dunn,[2] 20°, 0.042 g/cm^3 at 2.39, 4.43, 8.87, and 14.79 MHz, respectively; curve 5, derived from data of Zana and Lang,[4] 25°, 0.0116 g/cm^3 at 2.82 MHz; curves 1′–5′, calculated for proton-transfer reactions at side chains using parameter values in Table I, 25°, 0.042 g/cm^3 at 2.39, 4.48, 8.87, 14.79, and 2.82 MHz, respectively.

The range of pH over which the contribution from this mechanism in proteins is appreciable can extend over about three pH units. This range varies from protein to protein depending on the amino acid content and the pK values of the participating side chains. These factors also affect the amplitude of the absorption at any pH and frequency.

It is important to note that Figures 2–6 differ from Figure 1. To construct a figure analogous to Figures 2–6 for a simple model reaction requires a knowledge of the D and G parameter values for the reaction at each pX (or pH). These values must be inserted into eq 5, 6, and 4 in turn to obtain the single relaxation curve from which points may be selected for the required figure.

Clearly, therefore, eq 10 does not generally apply to the curves displayed in Figures 2–6. Use of this equation in this manner in ref 4 and 24 is not, therefore, acceptable without a clear specification of the use of the transformation process.

---

(24) F. Dunn and L. W. Kessler, *J. Phys. Chem.*, **74**, 2736 (1970).

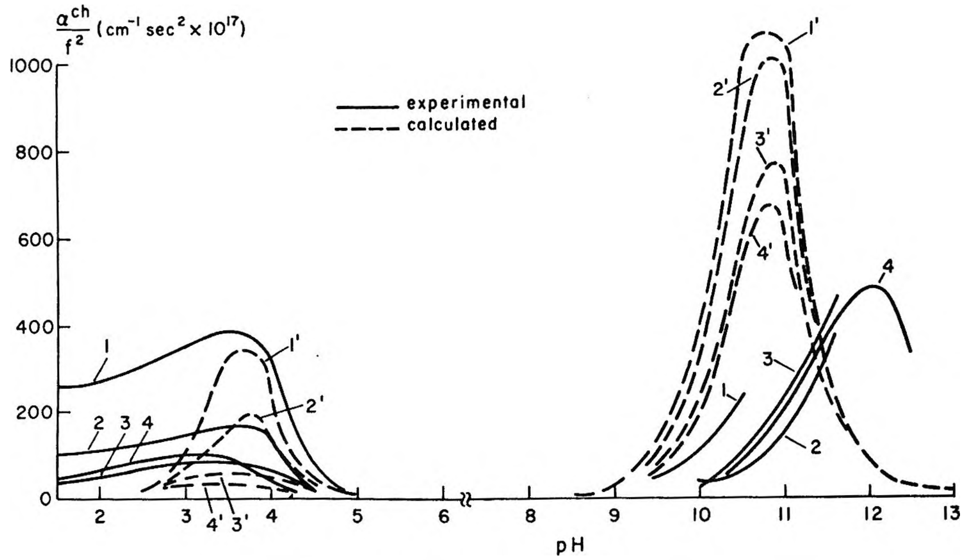

Figure 3. Excess absorption in aqueous hemoglobin solutions over and above that at pH 7: curves 1–4, processed from experimental data of O'Brien[9] on bovine hemoglobin, 10°, 0.15 g/cm^3 at 2.39, 4.43, 7.85, and 10.22 MHz, respectively; curves 1'–4', calculated for proton-transfer reactions using the parameter values in Table II, 25°, 0.15 g/cm^3 at 2.39, 4.43, 7.85, and 10.22 MHz, respectively.

Table III: Parameter Values Used to Calculate the Contributions to Excess Absorption Due to Proton-Transfer Reactions at Side Chains in 0.03 g/cm^3 Gelatin Solution at 25°[a]

Group	pK^{16}	n^{16}	10^{10} × k_{12},[5,6,14,20] M^{-1} sec^{-1}	ΔU,[5,6,21-23] cm^3 mol^{-1}
α-Carboxyl	3.8	1	3	10
s-Carboxyl	4.7	185	3	10
Imidazole	6.5	7	3	18
α-Amino	7.5	1	5	15
ε-Amino	10.2	55	5	15
Phenolic	9.8	2	2	17
Guanidine	12.5	73	5	15

[a] Molecular weight of gelatin 145,000; C_0 = 0.00021 M.

Table IV: Parameter Values Used to Calculate Contributions to Excess Absorption Due to Proton-Transfer Reactions at Side Chains in Polylysine (PL) and Polyglutamic acid (PGA) Solutions at 25°

	PL	PGA
Mol wt	86,300[12]	75,000[13]
Monomer molality	0.115 M	0.24 M
n	675[12]	560[19]
C_0	0.00017 M	0.00042 M
pK[a]	10.5[12]	5.5[19]
$10^{10}k_{12}$,[a] M^{-1} sec^{-1}	5[5,6,14]	3[5,6,14]
ΔU,[a] cm^3 mol^{-1}	15[5,6,21-23]	10[5,6,21-23]

[a] For pertinent side-chain types.

The original data of Kessler and Dunn[2] for BSA and O'Brien[9] for hemoglobin were in the form of plots of α/cf^2 *vs.* pH at different frequencies, where c is concentration of protein in grams per cubic centimeter. This normalization procedure was shown to be valid up to 0.1 g/cm^3 for BSA by Kessler and Dunn[2] and up to 0.15 gm/cm^3 for hemoglobin by Carstensen and Schwan[25] *in the neutral pH range.* Its validity must be called into question for measurements outside this range. In particular it has been shown not to apply to solutions in which proton-transfer reactions are a mechanism for excess absorption[5] since in these cases excess absorption is not linearly dependent on solute concentration. Therefore, for a full appreciation of the data of Kessler and Dunn[2] and of O'Brien[9] it is necessary to know the solute concentration to which the data apply.

Figures 2–6 indicate a broad qualitative resemblance between the dependence on pH of experimental excess absorption and that of calculated excess absorption due to proton-transfer reactions at side chains, for solutions of the three proteins and two polypeptides of interest here. In each case, at any frequency, excess absorption occurs at pH <6 and pH >8, goes to a peak within each of these ranges, and, generally, the height of the peak in the higher pH range is greater than that in the lower range. However, there are quantitative disagreements in particular cases on the magnitude of the peak and its location on the pH axis.

Figure 2 presents data of Kessler and Dunn[2] and of Zana and Lang,[4] together with comparable calculated curves for BSA solutions. The concentration used in the calculation was the same as that used to convert the data of Kessler and Dunn from α/cf^2 to α/f^2. In the low pH range the calculated data agree well with those

(25) E. L. Cartensen and H. P. Schwan, *J. Acoust. Soc. Amer.*, **31**, 305 (1959).

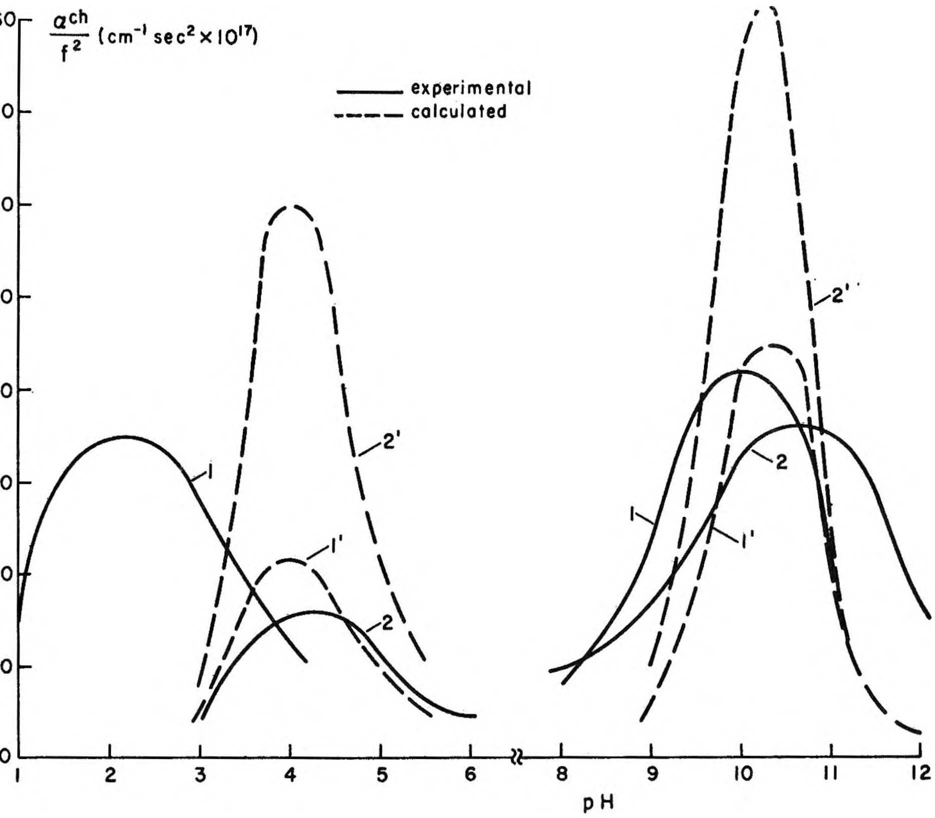

Figure 4. Excess absorption in the high and low pH ranges over and above that in the region of pH 7 for aqueous gelatin solutions: curve 1, experimental data derived from Pauly,[10] 35°, 0.2 g/cm^3 at 5 MHz; curve 2, derived from experimental data of Wada, *et al.*,[11] 40°, 0.03 g/cm^3 at 3 MHz; curves 1′ and 2′, calculated for proton-transfer reactions at side chains using the parameter values in Table III, 25°, 0.03 g/cm^3 at 5 MHz (1′) and 3 MHz (2′).

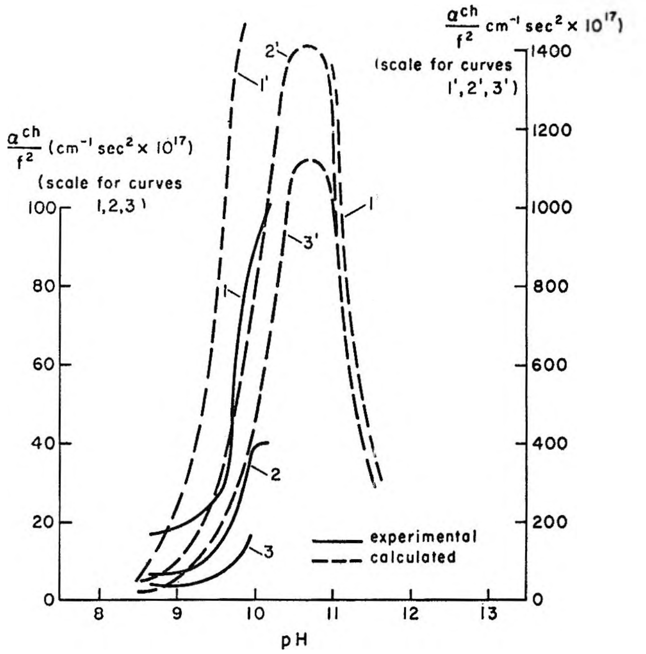

Figure 5. Excess absorption at pH >8 over and above that in the region of pH 7, for aqueous solutions of polylysine: curves 1–3, experimental data from Parker, *et al.*,[12] 25°, 0.115 *M* at 5.18, 9.4, and 13.52 MHz, respectively; curves 1′–3′, calculated from proton-transfer reactions at the ε-amino side chains, using the parameter values in Table IV, 25°, 0.115 *M* at 5.18, 9.4, and 13.52 MHz, respectively.

of Kessler and Dunn on the location of the absorption peak for each frequency, but in each case the magnitude of the calculated peak exceeds the experimental value by a factor of at least 2. There is both an amplitude and location discrepancy between the calculated curve and that of Zana and Lang. The latter data, of course, refer to a protein concentration much less than that for which the calculation was carried out. This would be expected to affect both of these comparable parameters. In the high pH range there is disagreement on both scores—location and amplitude of the absorption peak for the two frequencies shown.

The same kind of variants apply to the results for hemoglobin and gelatin (Figures 3 and 4, respectively)—some areas of agreement and some discrepancies between calculated and experimental data. It should be noted that the experimental curves for gelatin apply at temperatures much higher than 25°, the temperature for which the calculations were made. Extensive ultrasonic measurements have been made on solutions of hemoglobin in the physiologically "neutral" pH range $6 < \mathrm{pH} < 9$, and these have been summarized by Edmonds, *et al.*[8] From Figure 3, it is unlikely that proton-transfer reactions at side chains constitute a major mechanism contributing to observed excess absorption at "neutral" pH.

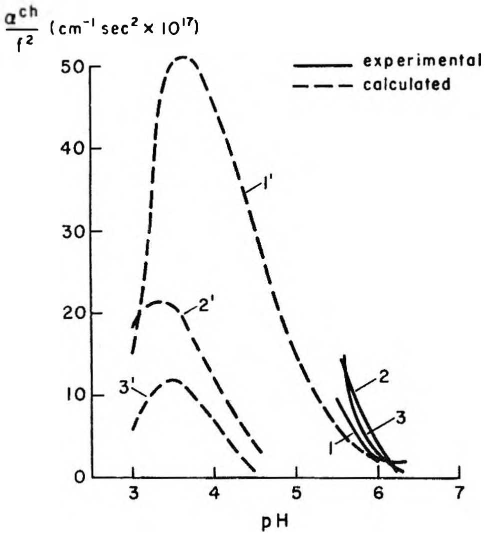

Figure 6. Excess absorption at pH <6, over and above that in the region of pH 7 for aqueous–dioxane (2:1) solutions of polyglutamic acid: curves 1–3, derived from the experimental data of Burke, *et al.*,[13] 25°, 0.24 *M* at 10, 20, and 40 MHz, respectively; curves 1′–3′, calculated for proton-transfer reactions at the carboxyl side chains, using the parameter values in Table IV, 25°, 0.24 *M* at 10, 20, and 40 MHz, respectively.

Parker, *et al.*,[12] used ultrasound to study the random coil–helix transition in poly-L-lysine. This conformational change occurs at pH >8. They observed a peaking of the excess absorption as pH was increased from 8. 65 to 10.2. Qualitatively, this is also predicted from our calculations on proton transfer at the side-chain ϵ-amino groups (see Figure 5).

These workers eliminated proton transfer as a mechanism to account for their observations "because the relaxation of the proton-transfer equilibrium is considerably faster than those observed" in their experiments. The present calculations show that proton-transfer reactions could very well be a major contributor to their observed excess ultrasonic absorption. In fact the calculations predict excess absorption more than an order of magnitude greater than that observed experimentally.

Figure 6 displays the calculated absorption data due to proton-transfer reactions in polyglutamic acid solutions. These may be compared with the experimental results of Burke, *et al.*[13] These workers were interested in studying the helix–random coil transition of this polypeptide and used pH values in the range $5.4 \leq \text{pH} \leq 9.0$. This range is almost all outside the range in which appreciable contributions from proton transfer would be expected to apply (see Figure 6). It is possible that they detected minor contributions from this mechanism at pH <6. However, extension of the experimental pH range to values <5 would be necessary before any definitive statement could be made in this respect. Indeed, extension of experimental ranges, of pH, temperature, solute concentration, frequency, etc., would be helpful in many cases for more clearly evaluating this mechanism.

In summary, it can be said that in no case (neither of the polypeptides, polyglutamic acid, and polylysine nor of the proteins, BSA, hemoglobin, and gelatin) do experimental results qualitatively conflict with the prediction of appreciable contribution to excess ultrasonic absorption from proton-transfer reactions in the ranges pH <6 and pH >8. However in each case it is likely that this is not the only mechanism in effect. Other mechanisms such as those mentioned by Zana and Lang[4] —solvation equilibria, conformational changes, and keto–enol equilibria—may have their contributions superimposed on those due to the proton-transfer processes, but certainly proton transfer cannot be eliminated from consideration.

The fact that in all cases the excess absorption from this mechanism calculated in the simple linear superposition manner displayed discrepancies from the measured absorption indicates that the calculation is not yet correct. Some cross coupling among the individual reactions and some variety in the parameter values even for side chains of the same type (*i.e.*, in k_{12}, ΔU, pK) most likely exist and should be taken into account. To do so thoroughly, however, would require that the three-dimensional structure of the molecule be taken into account and that the environment of each individual side chain be considered and evaluated. The work of Orttung[26] in evaluating titration data for hemoglobin should provide a pointer for this next step in improving the calculations of this work.

Further experimental work that would help to improve the reliability of these calculations would be the ultrasonic investigation of solutions of either or both the mentioned polypeptides but with varying degrees of polymerization. In this way the equations clearly applicable to the amino acid reactions[5,6] could be tested in sequentially more complex cases.

Proton transfer is not expected to contribute to excess absorption in the "neutral" pH range $6 < \text{pH} < 8$. In this range mechanisms such as those proposed by Zana and Lang[4] or those examined by Hammes and Pace[27] to account for relaxation in glycine, diglycine, and triglycine in solution at their isoelectric points must be invoked. However, much work yet remains to be done before these mechanisms can be quantified and the contributions from each evaluated.

Conclusions

Calculations indicate that proton-transfer processes are very likely a major mechanism contributing to excess ultrasonic absorption in the ranges pH <6 and pH >8 in solutions of proteins and polypeptides. The cal-

---

(26) W. H. Orttung, *J. Amer. Chem. Soc.*, **91**, 162 (1969).

(27) G. G. Hammes and C. N. Pace, *J. Phys. Chem.*, **72**, 2227 (1968).

culated data agree qualitatively with experimental results in these ranges. Likewise this mechanism is not expected to be appreciably applicable between these pH ranges.

However, these calculations need to be refined before they can be used subtractively to determine contributions from other mechanisms acting simultaneously with the proton-transfer processes.

Acknowledgments. This work was supported by Grants GM-12299 from the National Institute of General Medical Sciences and HE-01253 from the National Heart and Lung Institute.

Proton Transfer in the Two-Step Electrochemical Reduction of Oxygen in *N,N*-Dimethylformamide

by Helen J. James and Robert F. Broman*

Department of Chemistry, University of Nebraska, Lincoln, Nebraska 68508

(Received November 19, 1970)

Publication costs borne completely by The Journal of Physical Chemistry

Second-order rate constants for the chemical reaction in the ECE reduction of oxygen in *N,N*-dimethylformamide (DMF) with six different proton donors are determined by polarography. The mechanism of reaction during the lifetime of the polarographic mercury drop is shown to involve only a protonation of the superoxide ion and not of the hydroperoxide ion. The values of the second-order rate constants depend both on the acidity of the proton donor and on the proximity of a phenyl ring to the acidic proton within the proton-donor molecule. The phenyl ring is not a necessary requirement for the reaction to occur although it does increase the rate of reaction. Water is shown not to be a major contaminant since water strongly associates with DMF and is not available as a proton donor, even at moderately high water concentrations.

Introduction

The reduction of oxygen in protic and aqueous solutions has been postulated to proceed by an ECE reduction through an unstable superoxide intermediate.[1,2] Superoxide ion, O_2^-, has been shown to be a stable intermediate in the reduction of oxygen in solvents with a low availability of protons.[3,4] These solvents include dimethylformamide (DMF), dimethyl sulfoxide (DMSO), acetonitrile, and pyridine. The reduction of oxygen in such aprotic solvents in the presence of proton donors can be studied as an ECE mechanism in which the chemical step is the superoxide protonation.

An ECE mechanism, that is, a chemical reaction coupled between two electron transfers, has been investigated for a number of organic compound reductions.[5,6] In these studies the chemical reaction is the protonation of the organic anion of such compounds as anthraquinone, naphthalene, and benzophenone, and the reactions were studied in DMF solutions. The mathematical model for the ECE mechanism has been solved for chronopotentiometry,[7] potentiostatic electrolysis,[8] cyclic voltammetry,[9] and polarography.[10-12] Polarography is often the most convenient method to use since the data can be evaluated easily and the assumptions used in the theoretical calculations are the least limiting; therefore, polarography was used extensively in this work.

A proposed mechanism for oxygen reduction in DMF might be of the form

$$O_2 + e^- \longrightarrow O_2\cdot^- \qquad (1)$$

$$O_2\cdot^- + HX \xrightarrow{k} HO_2\cdot + X^- \qquad (2)$$

(1) J. P. Hoare, "The Electrochemistry of Oxygen," Interscience, New York, N. Y., 1965.

(2) F. Rallo and L. Rampazzo, *J. Electroanal. Chem.*, **16**, 61 (1968).

(3) D. L. Maricle and W. G. Hodgson, *Anal. Chem.*, **37**, 1562 (1965).

(4) M. E. Peover and B. S. White, *Chem. Commun.*, 183 (1965).

(5) P. H. Given and M. E. Peover, *J. Chem. Soc.*, 385 (1960).

(6) H. B. Mark, Jr., *Rec. Chem. Progr.*, **29**, 217 (1968).

(7) A. C. Testa and W. H. Reinmuth, *Anal. Chem.*, **33**, 1320 (1961).

(8) G. S. Alberts and I. Shain, *ibid.*, **35**, 1859 (1963).

(9) R. S. Nicholson and I. Shain, *ibid.*, **37**, 178 (1965).

(10) I. Tachi and M. Senda in "Advances in Polarography," I. Longmuir, Ed., Paragon Press, New York, N. Y., 1960, p 454.

(11) R. S. Nicholson, J. M. Wilson, and M. L. Olmstead, *Anal. Chem.*, **38**, 542 (1966).

(12) J. Janata and H. B. Mark, Jr., *J. Phys. Chem.*, **72**, 3616 (1968).

$$\mathrm{HO_2\cdot} + \mathrm{e^-} \longrightarrow \mathrm{HO_2^-} \qquad (3)$$

$$\mathrm{HO_2^-} + \mathrm{HX} \xrightarrow{k'} \mathrm{H_2O_2} + \mathrm{X^-} \qquad (4)$$

The competition of superoxide ion and hydrogen peroxide anion for the proton donor will determine whether the last step of this mechanism occurs or not during the drop lifetime; that is, if k' is considerably greater than k, the reaction will occur, and if k' is less than k, the reaction will not occur. Hydrogen peroxide has an acidity comparable to the phenols used in aqueous solutions and is less acidic than the carboxylic acids used in this study. Therefore, the second protonation step in the mechanism should not necessarily be disregarded.

Janata and Mark's development of the ECE mechanism[12] used a system similar to that above in which it was assumed that a second protonation did occur. An ECE mechanism shows a kinetic- as well as a diffusion-controlled portion of the limiting current. The limiting current can be given as

$$i_{\mathrm{lim}} = nF(\mathrm{d}N_{\mathrm{O_2}}/\mathrm{d}t)_{\mathrm{diff}} + nF(\mathrm{d}N_{\mathrm{HO_2\cdot}}/\mathrm{d}t)_{\mathrm{kin}} \qquad (5)$$

where n is the number of electrons transferred in each reduction step, F is the Faraday, N is the number of moles of reducible species at the electrode surface, and t is time in seconds, assuming that the chemical step of the mechanism is both fast and reversible. Nicholson, Wilson, and Olmstead[11] analytically solved an ECE mechanism under pseudo-first-order conditions, and Janata and Mark[12] developed their model using a reaction-layer concept. The following discussion is based on Janata and Mark's work as applied to the ECE mechanism in the reduction of oxygen in DMF. The reduction of oxygen to superoxide ion in eq 1 is the diffusion-controlled portion of the current and the combined eq 2 and 3 are the kinetic-controlled portion.

Using the reaction-layer theory and the assumption that the diffusion coefficients of oxygen and superoxide are approximately equal, Janata and Mark[12] derived the equation

$$i_{\mathrm{lim}} = nFqD_{\mathrm{O_2}}C_{\mathrm{O_2}}/(3\pi D_{\mathrm{O_2}}t/7)^{1/2} + nFqC^{\mu}{}_{\mathrm{O_2\cdot^-}}(10^{-3}kD_{\mathrm{O_2}}C^{\mu}{}_{\mathrm{HX}})^{1/2} \qquad (6)$$

where q $(=0.85(mt)^{2/3})$ is the surface of dme in cm^2, $D_{\mathrm{O_2}}$ is the diffusion coefficient of oxygen in cm^2/sec, $C_{\mathrm{O_2}}$ is the bulk concentration of oxygen in mM units, k is the second-order rate constant in M^{-1} sec^{-1}, $C^{\mu}{}_{\mathrm{O_2\cdot^-}}$ is the reaction volume concentration of superoxide, $C_{\mathrm{HX}}{}^{\mu}$ is the reaction volume concentration of HX, and t is the drop time corresponding to maximum current of an undamped polarogram. By defining

$$A_0 = (10^{-3}kD_{\mathrm{O_2}})^{1/2}$$

$$A_1 = (7D_{\mathrm{O_2}}/3\pi t)^{1/2}$$

$$I = i_{\mathrm{lim}}/2nFq$$

the expression becomes

$$2I = A_1C^{\mu}{}_{\mathrm{O_2\cdot}} + A_0C^{\mu}{}_{\mathrm{O_2\cdot^-}}(C^{\mu}{}_{\mathrm{HX}})^{1/2} \qquad (7)$$

For either case, that is whether the reaction represented by eq 4 occurs or not, the number of moles of oxygen reduced must equal the number of moles of unprotonated superoxide that diffuse away from the electrode. Thus

$$A_1C_{\mathrm{O_2}} = A_1C^{\mu}{}_{\mathrm{O_2\cdot^-}} + A_0C^{\mu}{}_{\mathrm{O_2\cdot^-}}(C^{\mu}{}_{\mathrm{HX}})^{1/2} \qquad (8)$$

If the reaction in equation 4 does occur, there are two moles of the proton donor consumed per mole of superoxide protonated and

$$A_2(C_{\mathrm{HX}} - C^{\mu}{}_{\mathrm{HX}}) = 2A_0C^{\mu}{}_{\mathrm{O_2\cdot^-}}(C^{\mu}{}_{\mathrm{HX}})^{1/2} \qquad (9)$$

where $A_2 = (7D_{\mathrm{HX}}/3\pi t)^{1/2}$. However, if the reaction in eq 4 does not occur, only 1 mol of proton donor is consumed per mole of superoxide protonated and

$$A_2(C_{\mathrm{HX}} - C^{\mu}{}_{\mathrm{HX}}) = A_0C^{\mu}{}_{\mathrm{O_2\cdot^-}}(C^{\mu}{}_{\mathrm{HX}})^{1/2} \qquad (10)$$

By solving eq 8 and either 9 or 10 for $C^{\mu}{}_{\mathrm{O_2\cdot^-}}$ and setting them equal, an equation that is cubic with respect to $(C^{\mu}{}_{\mathrm{HX}})^{1/2}$ is obtained. If the reaction in eq 4 occurs, the result is

$$(C^{\mu}{}_{\mathrm{HX}})^{3/2} + A_1C^{\mu}{}_{\mathrm{HX}}/A_0 + (2A_1C_{\mathrm{O_2}}/A_2 - C_{\mathrm{HX}})(C^{\mu}{}_{\mathrm{HX}})^{1/2} - A_1C_{\mathrm{HX}}/A_0 = 0 \qquad (11)$$

The equation is similar if the reaction in eq 4 does not occur but the coefficient of 2 is eliminated from the third term in the equation.

By use of a computer, these equations can be solved using a Newton iterative method for various values of k and concentrations of proton donor and oxygen. From these solutions, values for $C_{\mathrm{O_2\cdot^-}}$ and the limiting currents can be calculated. The calculated limiting currents can be compared to observed currents in order to approximate the rate constant, k, and to determine whether the reaction in eq 4 occurs during the lifetime of a drop.

Experimental Section

All chemicals were reagent grade. Solid reagents were dried over phosphorus pentoxide in a vacuum desiccator. Liquids were used as received. Stock solutions of 0.1 F tetraethylammonium perchlorate (TEAP) in DMF were made and used for all reagent solutions.

A multipurpose electroanalytical instrument as described by Goolsby and Sawyer[13] was used for all electrochemical experiments, along with a Clevite Mark 250 Brush recorder. A low-temperature bath maintained reaction solutions at 5° (±0.1°) where kinetic experiments were performed. The electrochemical cell had three compartments separated by medium-porosity sintered-glass frits. The compartments contained a dropping mercury electrode (dme), platinum electrode, and a saturated calomel electrode (sce), as the working, auxiliary, and reference electrode, respectively.

---

[13] A. D. Goolsby and D. T. Sawyer, *Anal. Chem.*, 39, 411 (1967).

Oxygen concentrations were determined by a modified Winkler method.[14] A revised sampling technique was necessary at 5° and consisted of placing 0.5–1.0 ml of deaerated DMF cooled in an ice bath into the sampling syringe before addition of the DMF sample to be analyzed. This prevented outgassing of the sample as it warmed to ambient temperature.

Results

Oxygen reduction in 0.1 F TEAP solutions of DMF in the absence of proton donors was performed to verify the formation of superoxide ion and to characterize its reduction parameters.[3,4] At 5° the polarographic $E_{1/2}$ was -0.84 V *vs.* sce and the plot of log $((i_d - i)/i)$ *vs.* E had a slope of 0.068. These parameters agree well with a reported $E_{1/2}$ of -0.87 V *vs.* sce in 0.1 F tetrabutylammonium perchlorate solutions of DMF[4] and with a slope of 0.070 reported for the reduction in 0.1 F TBAP solutions of DMSO.[3] The doubling of the limiting current with an added excess of proton donor also verifies the superoxide formation. The wave in the absence of proton donors can be classified as quasireversible and was found to have a transfer coefficient, α, equal to 0.75 and an electron-exchange rate constant, k^0, of 2.9×10^{-3} cm/sec, using the graphic method of Vavricka and Koryta.[15]

The polarographic diffusion coefficient at 25° was found to be 1.45×10^{-4} cm²/sec from the Ilkovic equation. This value is higher than expected compared with a value of 3.0×10^{-5} cm²/sec found in DMSO solutions.[16] Potentiostatic electrolysis also was used to determine diffusion coefficients from a plot of current *vs.* the reciprocal square root of time.[17] The value determined from the slope of this line is 7.44×10^{-5} cm²/sec. Values determined from the intercept and from the ratio of the intercept and slope agreed well with this latter value. The values determined by potentiostatic electrolysis were considerably lower than the value determined by polarographic limiting currents. We have no explanation for the unexpectedly high polarographic value and noted the same discrepancy between the two methods in 0.1 F aqueous TEAP solutions.

The polarographic reduction of oxygen in the presence of proton donors was studied using six compounds: phenol, 2-chlorophenol, 2,6-dimethylphenol, benzoic acid, phenylacetic acid, and acetic acid. A plot of the limiting current *vs.* the square root of the mercury height for oxygen solutions with and without a proton donor is shown in Figure 1. The nearly zero intercept in the absence of a proton donor indicates that the reaction is diffusion controlled, and the nonzero intercept in the presence of a proton donor shows a mixed kinetic- and diffusion-controlled process as expected for an ECE mechanism.

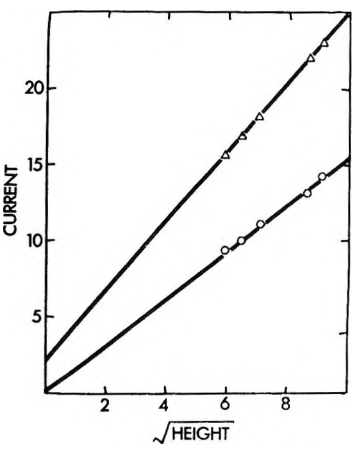

Figure 1. Polarographic limiting current (microamperes) at -1.2 V (*vs.* sce) as a function of the square root of the polarographic column height (cm$^{1/2}$): ○, oxygen (0.630 mM); △, oxygen (0.630 mM) and phenol (5.0 mM).

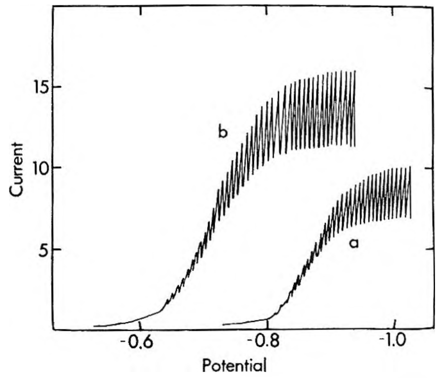

Figure 2. Effect of phenol on polarographic reduction of oxygen in DMF: a, oxygen (0.630 mM); b, oxygen (0.630 mM) and phenol (5.0 mM).

Typical polarograms of oxygen reduction in DMF with and without proton donors are shown in Figure 2. The significant changes in the presence of a proton donor are an increase in the limiting current and an anodic shift of the wave. Both of these factors are dependent upon the concentration of proton donor present. Polarographic maxima sometimes distorted the rising portion of the wave when proton donors were present and made an evaluation of $E_{1/2}$ difficult; therefore, the limiting current was used for a determination of the rate constant rather than $E_{1/2}$ values.[12]

The observed limiting currents were measured at -1.2 V *vs.* sce. The concentrations of oxygen and proton donor and the drop time of the DME were

---

(14) H. J. James and R. F. Broman, *Anal. Chim. Acta*, **48**, 411 (1969).

(15) S. Vavricka and J. Koryta, *Collect. Czech. Chem. Commun.*, **29**, 2251 (1964).

(16) E. L. Johnson, K. H. Pool, and R. E. Hamm, *Anal. Chem.*, **38**, 183 (1966).

(17) I. Shain and K. Martin, *J. Phys. Chem.*, **65**, 254 (1961).

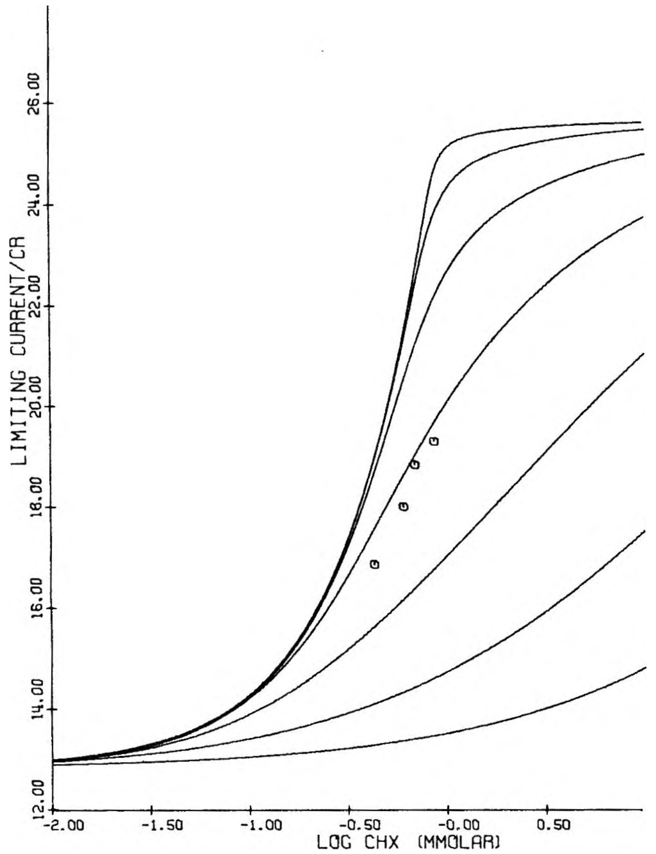

Figure 3. Single-protonation computed and observed currents for oxygen reduction (0.261 mM) in the presence of acetic acid as proton donor. The family of computed curves represent assigned values of k of 10^0, 10^1, 10^2, 10^3, 10^4, 10^5, and 10^6, increasing from bottom right to upper left. The ordinate is plotted as the limiting current divided by the oxygen concentration (μA l. mmol^{-1}), and the abscissa is the logarithm of the proton donor concentration in (mmol l.$^{-1}$). Drop time = 2.45 sec; m = 0.00132 g sec^{-1}.

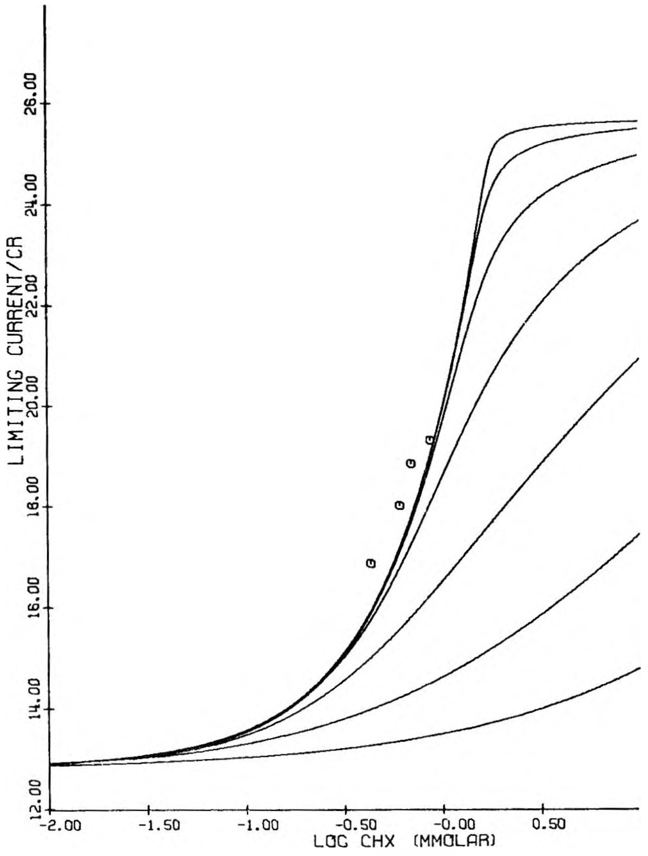

Figure 4. Double-protonation computed and observed currents for oxygen reduction (0.261 mM) in the presence of acetic acid. (See Figure 3 for description of the plots.)

varied in order to permit the observed currents to be increasing significantly with increasing proton donor concentrations.

The assumptions necessary to calculate the limiting currents for various values of k involve the values chosen for the diffusion coefficients of oxygen and the proton donors. These values for the proton donors are unknown at 5° and are only approximately known at 25°. If the assumption that the diffusion coefficients decrease by the same magnitude for all species involved in the reaction is valid, the values at 25° can be used. (Janata and Mark[12] used a value of 1.2×10^{-5} cm^2/sec for phenol derivatives at 25° and stated that as much as a 30% error in this value only slightly changed the calculated values.) Therefore, the values used in these calculations were $D_{O_2} = 1.45 \times 10^{-4}$ cm^2/sec and $D_{HX} = 1.2 \times 10^{-5}$ cm^2/sec.

The elucidation of the overall mechanism was performed by comparing calculated limiting currents for both possible mechanisms to observed currents. In many of the double-protonation model calculations, the observed currents were larger than the computed values. This would lead to the interpretation that were the double-protonation mechanism in effect, the overall electrode reaction was occurring more rapidly than permitted by mass transfer to a dropping mercury electrode. This particular effect is seen by comparing Figures 3 and 4. The experimental points fall within the family of computed curves for the single-protonation mechanism (Figure 3), but they fall outside the range in the double-protonation case (Figure 4). In addition, for a series of experiments using various concentrations of oxygen and proton donor, good consistency was found for a rate constant value to fit the experimental data using the single-protonation mechanism. On the other hand, a great degree of scatter was found for the rate constant when applying the double-protonation model. From these considerations, it was felt justifiable to assume that eq 4 is unimportant in the electrode reaction we are considering, and the rate constants reported below are based on the single-protonation mechanism.

The second-order rate constants described by a single protonation of superoxide ion for each donor can be considered only approximate. The determination of the rate constant was performed by comparing a series of calculated and observed currents for each proton donor and choosing the value of k which gave the best comparison. In each case at least four different oxygen concentrations were used and at each oxygen concentration the proton donor concentrations were varied. The values of k chosen are listed in Table I. The observed and calculated currents usually agreed to within ±5%. Another factor which makes the rate constants approximate is that small changes in these values do not greatly affect the calculated currents; therefore, the rate constants used to calculate theoretical currents differed by a multiplicative factor rather than an additive factor. It is estimated that these values can be considered to be known to no better than 50%.

Table I: Acid Dissociation Constants and Second-Order Rate Constants for the Proton Donors

Proton donor	K_a	k, M^{-1} sec^{-1}
Benzoic acid	6.5×10^{-13}	1.6×10^3
Phenylacetic acid	...	4×10^2
Acetic acid	6.5×10^{-14}	4×10^2
2-Chlorophenol	1.3×10^{-14}	1.6×10^3
Phenol	5×10^{-17}	8×10^2
2,6-Dimethylphenol	5×10^{-18}	2×10^2

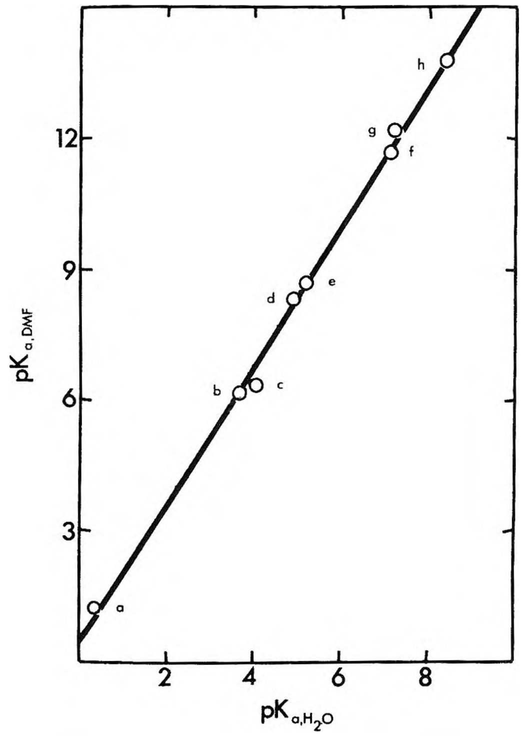

Figure 5. Relationship between pK_a values in DMF and in water for various phenols: a, picric acid; b, 2,6-dinitrophenol; c, 2,4-dinitrophenol; d, bromocresol green; e, 2,5-dinitro-phenol; f, 4-nitrophenol; g, 2-nitrophenol; h, 3-nitrophenol.

If a direct transfer of the proton occurs between the proton donor and the superoxide ion (eq 2) the reaction rate of this chemical step should be dependent upon the strength of the bond between the acidic proton and the rest of the molecule; *i.e.*, the reaction rates should correspond directly to the acidities of the proton donors. However, if an intermediate is formed through the association of the proton donor and superoxide ion, probably through a hydrogen bond, the overall rate of reaction is a composite of both the rate of formation of the intermediate and the rate of dissociation into the anion of the donor and the protonated superoxide. This mechanism can be expressed as

$$O_2\cdot^- + HX \rightleftharpoons [X\text{--}H\text{--}O_2\cdot]^- \qquad (12)$$

$$[X\text{--}H\text{--}O_2\cdot]^- \longrightarrow X^- + HO_2\cdot \qquad (13)$$

Therefore, a comparison of the acid dissociation constants and the rate constants should help to evaluate the mechanism of protonation.

The experimental evaluation of the acid dissociation constants is difficult due to their small values. pK values for acetic acid and benzoic acid have been evaluated in DMF as 13.3[18] and 12.2,[19] respectively. Phenylacetic acid would be expected to be a slightly weaker acid than benzoic acid in DMF since it is weaker in aqueous solution, and other carboxylic acids tend to have the same order in both solvents. pK_a values for the phenols used in this work can be estimated from a plot of other phenol acid dissociation constants in DMF and water.[20-22] This plot is shown in Figure 5 and is linear. From an extrapolation of this plot for the phenols used in this study, their acid dissociation constants can be approximated. The values of these estimated dissociation constants and the known values for benzoic and acetic acids are listed in Table I along with the second-order rate constants determined for all six proton donors.

A comparison of the acidities and reaction rates in Table I shows that there is not a direct correspondence, and a consideration of the factors influencing the stability of an intermediate is necessary. A delocalization of the charge on the intermediate ion in eq 12 would increase the stability of this intermediate. The electron-withdrawing power of the phenyl ring would provide a means to delocalize this charge. This inductive effect is related to the distance between the phenyl ring and the proton site. The fact that benzoic acid reacts only as fast as 2-chlorophenol, which is a much weaker acid, indicates that the inductive effect

---

(18) M. Teze and R. Schaal, *Bull. Soc. Chim. Fr.*, 1372 (1962).

(19) P. G. Segrs, R. K. Wolford, and L. R. Dawson, *J. Electrochem. Soc.*, **103**, 633 (1956).

(20) B. W. Clare, D. Cook, E. C. F. Ko, Y. C. Mac, and A. J. Parker, *J. Amer. Chem. Soc.*, **88**, 1911 (1966).

(21) S. M. Petrov and Yu. I. Umanskii, *Zh. Fiz. Khim.*, **41**, 1374 (1967).

(22) J. Juillard and A. Mallet, *C. R. Acad. Sci.*, **264**, 2098 (1967).

on the formation of an intermediate may be important to the overall reaction rate. A possible explanation for the fact that phenylacetic acid and acetic acid (which are estimated to have comparable acidities) have the same rate constants is that the phenyl ring is too far removed to influence the formation of the intermediate. The inductive effect of the chloro and methyl substituents in the phenols influences, in the same manner, both the acidities of these phenols and the formation of an intermediate. Although the individual rate constants in eq 12 and 13 cannot be resolved, the overall rate of protonation does appear to be dependent upon the proximity of a phenyl ring to the acidic proton in the proton donor molecule giving rise to a rate-enhancing inductive effect.

If water acts as a proton donor in DMF solutions, it could be a major contaminant in the study of the reactions of superoxide ion with other proton donors. Water does change the viscosity of DMF solutions.[23] In a 70 mol % water solution the viscosity is nearly 4 times that of pure DMF and this change can be attributed to an association of water and DMF. Ting, Wang, and Li[24] reported association constants between water and DMF in cyclohexane and suggested that as many as three DMF molecules may associate with one water molecule. This interaction would make water protons less available as donors in other reactions.

Jezorek and Mark[25] studied the reduction of anthracene and naphthalene in DMF with water present as a contaminant. This system is similar to oxygen reduction in this solvent as it too follows an ECE mechanism. These authors reported that very large concentrations of water were necessary (compared to phenol concentrations) in order to achieve significant increases in the limiting current. The increased viscosity lowers the diffusion coefficient of the oxidized species, and the current never attains the maximum expected height.

Water was added to the oxygen–DMF solutions to investigate its effect. For concentrations ranging from 0 to 56 mM in water, the $E_{1/2}$ values showed no significant change and the limiting current remained constant. Further addition of water caused a maximum to appear on the oxygen reduction wave and eventually one wave at more anodic potentials appeared with a much smaller total current height than the original wave. This decrease in the limiting current can be attributed to two factors: the increased viscosity lowers the diffusion coefficient, and since oxygen is less soluble in water than in DMF, the oxygen concentration is less in the mixed solvent. As expected, by making further additions until the solvent was almost aqueous, a typical two-electron reduction wave was observed. Thus contamination by water in small concentrations is not a serious handicap in the investigation of other proton donors.

Acknowledgments. We thank the National Science Foundation for partial support of this work through traineeships to H. J. J. (1967–1969) and through a development grant to the Department of Chemistry which made possible the construction of the electroanalytical instrument.

---

(23) J. M. Hale and R. Parsons in "Advances in Polarography," I. Longmuir, Ed., Paragon Press, New York, N. Y., 1960, p 829.

(24) S. F. Ting, S. M. Wang, and N. C. Li, *Can. J. Chem.*, **45**, 425 (1967).

(25) J. R. Jezorek and H. B. Mark, Jr., *J. Phys. Chem.*, **74**, 1627 (1970).

Transport Processes in Low Melting Salts. The $AgNO_3$–$TlNO_3$ System

by G. J. Janz,* R. P. T. Tomkins, H. Siegenthaler, K. Balasubrahmanyam, and S. W. Lurie

Department of Chemistry, Rensselaer Polytechnic Institute, Troy, New York 12181 *(Received June 1, 1971)*

Publication costs borne completely by The Journal of Physical Chemistry

An investigation of the viscosity and conductance and the laser Raman spectrum for molten mixtures of $AgNO_3$ and $TlNO_3$ is reported. The absence of new frequencies and the temperature invariance of the intensities for the observed Raman bands indicate that the symmetry of the NO_3^- ion in the mixtures does not differ significantly from that of the NO_3^- in the parent compounds. The "back-donation of electrons" from cations into the π system of the NO_3^- ions appears lessened in the molten mixtures, and this effect is greatest at the equimolar mixtures. From the viscosities, it is found that the simple mole fraction viscosity relationship is very nearly obeyed; *i.e.*, the polarization interactions are virtually zero, and the mixtures are thus nearly ideal. The electrical conductances of the mixtures can be accounted for if a term is introduced for ionic association, but in these mixtures this is found to be less than 4%. The results thus confirm small but finite noncoulombic contributions to the structural features and transport processes in such molten electrolytes.

The phase diagram for the $AgNO_3$-$TlNO_3$ system shows[1] the features of two low melting eutectic mixtures (52 mol % $TlNO_3$, mp 82.2°; 48 mol % $TlNO_3$, mp 82.5°) and a low melting compound of equimolar composition (mp 83°). There is, thus, the opportunity to investigate the liquid state properties of such mixtures from relatively low temperatures to temperatures where both the parent compounds themselves are molten (*e.g.*, $AgNO_3$, mp 210°; $TlNO_3$, mp 208°). In this communication, an investigation of the properties of viscosity and conductance of this system is reported from this viewpoint; the results are examined from the viewpoints of polarization and ionic size effects, together with some results from laser Raman spectroscopy.

Experimental and Results Section

For $AgNO_3$ and $TlNO_3$, NSRDS recommendations for viscosities, electrical conductance, and densities have been advanced recently[2] from critical assessments of the collected published data; the temperature-dependent equations are given in Chart I. The accuracies are estimated to be within the limits of 0.15-0.3% (density), 0.7-1.0% (conductance), and approximately 1.0% (viscosity).

Chart I

$AgNO_3$

$$\begin{array}{ll} \text{viscosity} & \eta = 11.59 \times 10^{-2} \exp(3620/RT) \text{ cP} \\ \text{conductance} & \begin{cases} \kappa = 11.745 \exp(-2749/RT)\ \Omega^{-1} \text{ cm}^{-1} \\ \Lambda = 587.9 \exp(-2898/RT)\ \Omega^{-1} \text{ cm}^{2} \end{cases} \\ \text{density} & \rho = 4.454 - 1.02 \times 10^{-3}T \text{ g cm}^{-3} \end{array}$$

$TlNO_3$

$$\begin{array}{ll} \text{viscosity} & \eta = 8.430 \times 10^{-2} \exp(3657/RT) \text{ cP} \\ \text{conductance} & \begin{cases} \kappa = 9.41_6 \exp(-3143/RT)\ \Omega^{-1} \text{ cm}^{-1} \\ \Lambda = 633.25 \exp(-3348.3/RT)\ \Omega^{-1} \text{ cm}^{2} \end{cases} \\ \text{density} & \rho = 5.804_1 - 1.873_7 \times 10^{-3}T \text{ g cm}^{-3} \end{array}$$

For binary mixtures of these two components, four investigations have been reported: Rabinowitsch (1921),[3] Sandonnini (1920),[4] Bokhovkin (1949),[5] and Brillant, *et al.* (1966, 1968).[6,7] The measurements of Rabinowitsch were limited to one composition (50 mol % $AgNO_3$) and a single temperature (373°K). The results of a critical evaluation of the latter two studies may be summarized as follows.

Density. The results of Bokhovkin[5] and Brillant[7] are at different compositions so that no direct comparison is possible except of the values for the single components. Such a comparison shows that the results of Brillant deviate somewhat less from the NSRDS recommended values[2] than those of Bokhovkin (approximately 0.2 and 0.8%, respectively). A statistical analysis of the results of Brillant[7] was undertaken to express the data simultaneously as a function of composition (c) and temperature (T, °K). The equation, thus derived, is

$$\rho = 5.80573 - 1.85467 \times 10^{-3}T - 1.10779 \times 10^{-2}C + 7.24708 \times 10^{-6}TC \text{ (g cm}^{-3}\text{)}$$

and may be used within the temperature range of 435–635°K, with a standard error of about 0.07% relative to the published data; the maximum departure is 0.2% and is noted at 485°K for the results reported for the 60 mol % $AgNO_3$ mixtures.

---

(1) C. Van Eyck, *Z. Phys. Chem. (Leipzig)*, **51**, 721 (1905).

(2) G. J. Janz, F. W. Dampier, G. R. Lakshminarayanan, P. K. Lorenz, and R. P. T. Tomkins, "Molten Salts," Vol. 1, NSRDS-NBS 15, U. S. Government Printing Office, Washington, D. C., Oct 1968.

(3) A. J. Rabinowitsch, *Z. Phys. Chem. (Leipzig)*, **99**, 417 (1921).

(4) C. Sandonnini, *Gazz. Chem. Ital.*, **50**, 289 (1920).

(5) I. I. Bokhovkin, *Zh. Obsch. Khim.*, **19**, 805 (1949).

(6) M. Bakes, S. Brillant, J. Brenet, J. DuPuy, J. Guion, Y. Nakamura, and J. Ruch, *J. Chim. Phys.*, **63**, 1491 (1966).

(7) S. Brillant, Ph.D. Thesis, Strasbourgh (1968); *J. Chim. Phys.*, **65**, 2138 (1968).

Conductance. Results reported[5–7] for the single components compare with the NSRDS recommended values as follows

Investigator	Deviation for NSRDS values
Sandonnini (1920)	$AgNO_3$ (2.2%); $TlNO_3$ (4.4%)
Bokhovkin (1949)	$AgNO_3$ (4.9%); $TlNO_3$ (3.3%)
Brillant (1968)	$AgNO_3$ (0.62%); $TlNO_3$ (0.60%)

For the binary mixtures, accordingly, the work of Brillant[7] is recommended; results for the single components and for five binary mixtures (containing 21, 35, 50, 70, and 90 mol % $TlNO_3$) were reported[7] and need not be detailed here. The derivation of an expression giving these results simultaneously as a function of temperature and composition (*cf.* density, preceding) was undertaken, but this work was without success.

Viscosity. The investigations appear limited to the studies of Bokhovkin[5] in which viscosities were reported for 13 binary mixtures (6.8 to 85.4 mol % $TlNO_3$; 398–498°K) and the single components, and that of Rabinowitsch[3] (one data point for 50 mol % $TlNO_3$ at 373°K). A comparison with the NSRDS value for molten $TlNO_3$ shows that the Bokhovkin result deviates by approximately 8%, and the estimate of uncertainty for the results of the binary mixtures is thus difficult without additional input. One of the eutectic mixtures (48 mol % $TlNO_3$; mp 82.5°) was selected for further study because of the larger temperature range available.

The eutectic mixture (above) was made up by weight from certified reagent grade chemicals which had been recrystallized from double-distilled water and oven dried (25°, 24 hr; 110°, 12 hr). All transfers of the dried chemicals were by desiccator techniques, in a dry N_2 glove box, or by vacuum manifold techniques. The viscosity measurements were with the modified Ostwald-type viscometer of this laboratory. Details of the design, the calibration procedures, and the silicone oil bath (160–250°), and molten salt bath (260–310°) have been given elsewhere by Timidei, *et al.*[8] All viscosity measurements were repeated at least three times to cross-check reproducibility of the flow times (±0.5%), and the temperatures were increased and decreased at random in the cycle to evaluate the temperature dependence of the viscosity data. The results are in Table I for the range investigated (160–310°).

Table I: Viscosity Data for $AgNO_3$–$TlNO_3$ Eutectic Mixture

T, °K	433	443	453	463	473	483
η, cP	7.441	6.523	5.863	5.263	4.712	4.384
T, °K	493	503	513	523	533	543
η, cP	4.027	3.714	3.461	3.215	3.081	2.900
T, °K	553	563	573	583		
η, cP	2.742	2.578	2.427	2.320		

The temperature dependence of these results was analyzed by the Arrhenius-type exponential relation and a power-series equation. The results are given by this expression

$$\eta = 122.59 \times 10^{-3} \exp(3407.2/RT) \text{ cP}$$

for the range of 503 to 583°K, and with the standard error of estimate equal to 2.06×10^{-2}; and over the complete temperature range by

$$\eta = 246.072 - 1.26600T + 2.216315 \times 10^{-3}T^2 - 1.306906 \times 10^{-6}T^3$$

(for 440 to 580°K) with the standard deviation, s, being 4.44×10^{-2}. The numerical coefficients above are cited to more figures than experimentally justified to ensure the analytical fit within the above precisions. Comparison with Bohkovkin[5] shows that the results are in good agreement at higher temperatures (*e.g.*, 1.5%, 225°) but deviate significantly in the lower temperature range (*e.g.*, 30%, 175°), and that the Bokhovkin data fall uniformly below the present results. The information is insufficient in the earlier work[6] for an explanation of these observations and while one might infer some systematic error in the earlier work from this trend, the matter cannot be resolved without additional information.

Raman Spectral Studies. The intensities of the symmetrical stretching frequency of the nitrate ion in melts of univalent nitrates (including $AgNO_3$ and $TlNO_3$) have been reported recently relative to the intensity in $NaNO_3$ by James and Leong.[9] In the present work the spectra for molten $AgNO_3$ and $TlNO_3$ were reinvestigated, together with three mixtures (33, 50, and 67 mol % $AgNO_3$) bridging the composition range of the two eutectics and the compound. The Raman spectra were recorded with the Jarrell-Ash Model 25-300 laser Raman facility of this laboratory, with both He-Ne (55 mW) and Ar^+ ion (125 mW) lasers as excitation sources. Details are reported elsewhere,[10] and it is sufficient to note that the frequencies in the molten mixtures fall, in general, between the frequencies of the pure molten $AgNO_3$ and $TlNO_3$. The absence of new frequencies in the mixtures and the temperature invariance of the intensities for the observed frequencies indicate clearly that the symmetry of the NO_3^- ion in the mixtures does not differ appreciably from that of the NO_3^- in the parent compounds. The molar intensities[10] of the ν_1 band (1037 cm^{-1}) relative to that of $TlNO_3$ were as follows

---

(8) A. Timidei, G. Lederman, and G. J. Janz, *Chem. Instrumentation*, 2, 309 (1970).

(9) D. W. James and W. H. Leong, *Trans. Faraday Soc.*, 66, 1948 (1970).

(10) K. Balasubrahmanyam and G. J. Janz, *J. Chem. Phys.*, in press.

$AgNO_3$ (mol %)	100	85	67	50	33	0
I_M	70	65	59	57	61	100

The molar intensity ratio for the single components, *i.e.*, (I_{TlNO_3}/I_{AgNO_3}), is 1.43; this is to be compared with that reported by James and Leong,[9] 1.37. The observation of the earlier study,[9] namely that intensities of the ν_1 mode for $AgNO_3$ and $TlNO_3$ are much greater than for melts of the alkali metal nitrates, are thus confirmed. The variations in the molar intensity with composition may be attributed to interionic interactions since the measurements were designed under conditions where the geometrical-optical effects and the refractive indices were essentially constant.

Discussion

The characterization of the interactions among the constituent ions is one of the central problems in molten electrolytes as well as in aqueous and nonaqueous electrolytes, since the structural, thermodynamic, and transport properties depend on the nature and the range of such interactions. From this viewpoint the discussion of James and Leong[9] on the structure of molten nitrates is informative. The high values of relative intensities of the symmetrical stretching mode, ν_1, for $AgNO_3$ and $TlNO_3$ are interpreted as due to an anion–cation covalent-type interaction, involving a donation of lone-pair electrons on the nitrate to vacant orbitals on the Ag^+ (5s) and Tl^+ (6p) much as in transition metal complexes, but with the onset of an additional effect, namely a "back-donation" of electrons from the filled d orbitals on the Ag^+ and Tl^+ into the π system of the nitrate ion. Because the additional electrons in the nitrate ion are in an antibonding π orbital, the resultant N–O bond has a lower bond order. It is thus more easily distorted while the π nature of the electrons makes them easily polarized. The effects of polarization by cation field, accordingly, are modified from the trend reported in the molten alkali metal nitrates.[11] In the present Raman investigation of the molten mixtures of Ag and Tl nitrates, the absence of new frequencies, and the temperature invariance of the intensities indicate clearly that the force field does not differ significantly from that in the melts of the single components, *i.e.* the symmetry of the nitrate ion is essentially unchanged, and the force field is predominantly coulombic in origin. It is to be noted that the molar intensities of the ν_1 band (1037 cm^{-1}) in the mixtures are less than for the parent compounds, and the significance of this, undoubtedly, lies in a hindrance to the back-donation of electrons (from the cations) into the π system of the nitrate ions. The anion–cation covalent-type interactions, advanced to explain the high values of I_M for molten $AgNO_3$ and molten $TlNO_3$,[9] are thus lessened significantly in the molten mixtures of these two salts, the effect being greatest at the equimolar ratio. The latter suggests that this hindrance lies in a nearest neighbor Ag^+, Tl^+ repulsion effect within the coordination sphere of the reference nitrate ion.

The transport properties of viscosity and conductance for molten nitrates and chlorides (as single salt melts) have been compared in a previous communication in this series.[12] The values of E_Λ (activation energy for conductance) for the series of nitrates are virtually invariant in contrast to the trend for the corresponding chlorides (E_Λ (kcal mol^{-1}): LiCl, 2.02; CsCl, 5.11; $LiNO_3$, 3.59; $CsNO_3$, 3.69); this near invariancy may be attributed to an "aggregate" or cooperative transport mechanism in which the differences in cationic mobilities are swamped by the enhanced anion–cation cooperative interactions, much as solvation damps out the size effect in aqueous cationic mobilities. The values of E_Λ for $AgNO_3$ and $TlNO_3$ noted in the present work (2.89_8 and 3.34_8), confirm that these two nitrates are no exceptions to the trend noted for the alkali metal nitrates. The calorimetric studies of molten nitrates, by Kleppa and coworkers,[13,14] confirm the need to consider a smaller, but significant, amount of dispersion force type interactions (covalency) to account for the observed enthalpies of mixing. This noncoulombic interaction energy was greater in molten $AgNO_3$ than in $TlNO_3$. While the lower value for E_Λ (above) may undoubtedly be attributed to such factors, the close correspondence of these two values with those for the alkali metal nitrates (*i.e.*, the near invariancy) is the more significant result. That the configurational changes in electrical transport are seated in highly cooperative effects receives further support from a comparison of the values of E_Λ and E_η. For $AgNO_3$ the ratio E_η/E_Λ is 1.06, and for $TlNO_3$, 1.09, respectively; this is to be compared with the range of values for the alkali metal nitrates[12] ($LiNO_3$, 1.42; $CsNO_3$, 1.20). From the process energetics, one infers that the configurational changes in these two transport processes are both highly cooperative and likely nearly equivalent.

It is of interest to examine the transport properties of molten mixtures of $AgNO_3$ and $TlNO_3$ relative to such viewpoints. The mole fraction equation for the viscosity of a mixture

$$\eta_{mixt} = X_1\eta_1 + X_2\eta_2$$

is predicted to be valid for a mixture of two nitrates under conditions where the cationic radii, r_1 and r_2, are equal. This follows directly from the generalizations advanced by Murgulescu and Zuca from their extensive studies[15–17] of the viscosities of binary mixtures of

---

(11) G. J. Janz, "Molten Salts Handbook," Academic Press, New York, N. Y., 1967.

(12) A. Timidei and G. J. Janz, *Trans. Faraday Soc.*, **64**, 202 (1968).

(13) O. J. Kleppa, R. B. Clarke, and L. S. Hersh, *J. Chem. Phys.*, **35**, 175 (1961).

(14) O. J. Kleppa and L. S. Hersh, *ibid.*, **36**, 544 (1962).

molten nitrates as a function of ionic radius. The polarization energy, defined after Lumsden,[18] as

$$E_p = -\frac{\alpha e^2}{2}\left[\frac{1}{r_{AB}^2} - \frac{1}{r_{AC}^2}\right]^2$$

will be zero if the two cations in the mixture have similar radii; *i.e.*, the system will be expected to behave as an ideal mixture. In Table II, the results of this calculation are summarized. The experimental limit of accuracy for the viscosity studies in the present work was estimated to be about 1%. Inspection shows that the mole fraction viscosity relationship is very nearly obeyed, *i.e.*, the mixture is virtually ideal from the viewpoints of the polarization interactions, and one would predict that $r_{Tl^+} \simeq r_{Ag^+}$ in these mixtures. The generally accepted radius for Ag^+ in molten electrolytes is 0.95 Å, from empirical observations; the Pauling radii are, respectively, Ag^+, 1.26 Å; Tl^+, 1.40 Å. It should be noted that the calculated viscosities (Table II), nevertheless, deviate from the observed values, the predicted viscosities falling uniformly below the experimental values, and that the deviation is just outside the estimated limits of accuracy. If significance is to be attached to this, it would imply a small but definite polarization interaction energy.

Table II: Additivity of Viscosities

T, °K	η_{AgNO_3}, cP	η_{TlNO_3}, cP	η_{calcd},[a] cP	η_{obsd}, cP	% departure
533	3.54	2.65	3.12	3.08	−1.30
543	3.32	2.50	2.93	2.90	−1.03
553	3.12	2.38	2.76	2.74	−0.73

[a] $\eta_{calcd} = X_1\eta_1 + X_2\eta_2$, where 1 and 2 are $AgNO_3$ and $TlNO_3$, respectively, and X_1, X_2 are 0.52 and 0.48.

If the conductances of the $AgNO_3$–$TlNO_3$ mixture are similarly examined, it is found that neither the mole fraction additivity expression nor the Markov equation[19]

$$\Lambda_{min} = X_1\Lambda_1 + X_2\Lambda_2$$

and

$$\Lambda_{mix} = X_1^2\Lambda_1 + X_2^2\Lambda_2 + 2X_1X_2A_{12}e^{-E_{\Lambda_{12}}/RT}$$
(Markov)

are adequate, but that the modified Markov equation[20]

$$\Lambda_{mix} = (1 - \theta)\Lambda_{Markov}$$
(Janz–Ward)

is found adequate for values of the θ parameter between 0.02 and 0.04. The results of these calculations are in Table III. Here the θ parameter corresponds to the Tobolsky parameter[21,22]

$$\theta = \left(\frac{d_2 - d_1}{d_1 + d_2}\right)^2$$

where d_1 and d_2 are distances of closest ionic approach; the values 0.02–0.04 correspond to a configuration in which the Ag^+ cation penetrates somewhat more than the Tl^+ ion into the sphere of influence of the NO_3^- ion. This is in accord with the enthalpies of mixing studies[13,14] (*i.e.*, the noncoulombic interaction energy is greater in molten $AgNO_3$ than in $TlNO_3$) and with the present Raman results. The significance of this to the electrical conductance is that the nonadditive factor corresponds to a fraction that no longer contributes to the process of conductance, much as the correction for ionic association in aqueous electrolytes. Details on the interaction sites and the geometry of the associated species are found in the previous communication.[20]

Table III: Additivity of Conductivities

T, °K	Λ_{AgNO_3}, Ω^{-1} cm^2	Λ_{TlNO_3}, Ω^{-1} cm^2	$\Lambda_{mol\ Fract}$,[a] Ω^{-1} cm^2	Λ_{Markov}, Ω^{-1} cm^2	Λ_{obsd},[b] Ω^{-1} cm^2	θ
513	34.1	23.4	29.1	29.1	28.4	0.024
553	42.3	30.1	36.5	36.5	35.2	0.040

[a] For $X_{AgNO_3} = 0.52$ and $X_{TlNO_3} = 0.48$. [b] From ref 7.

The transport properties of such molten electrolytes are influenced through both geometric and energetic factors. In molten nitrates, while the interaction forces are predominantly coulombic, the processes are significantly influenced by the symmetry of the nitrate ion, *i.e.*, through the various sites of differing anion–cation interaction energies. The very nearly ideal additivity of the viscosity for molten $AgNO_3$–$TlNO_3$ mixtures, the nonadditivity of the electrical conductances, and the Raman spectra confirm the importance of the small but finite noncoulombic contributions to the structural features and transport processes in such molten electrolytes.

Acknowledgments. The fused salt studies in this laboratory are made possible, in large part, by support received from the U. S. Navy, Office of Naval Research (transport processes) and the National Science Foundation (spectroscopy).

---

(15) I. G. Murgulescu and S. Zuca, *Electrochim. Acta*, **11**, 1383 (1966).

(16) I. G. Murgulescu and S. Zuca, *ibid.*, **15**, 1817 (1970).

(17) S. Zuca and B. Borcan, *ibid.*, **15**, 1817 (1970).

(18) J. Lumsden, *Discuss. Faraday Soc.*, **32**, 138 (1961).

(19) Yu. K. Delimarskii and B. F. Markov, "Electrochemistry of Fused Salts" (Eng. transl.), Sigma Press, New York, N. Y., 1961, pp 32, 33.

(20) A. T. Ward and G. J. Janz, *Electrochim. Acta*, **10**, 849 (1965).

(21) A. V. Tobolsky, *J. Chem. Phys.*, **10**, 187 (1942).

(22) O. J. Kleppa and L. S. Hersh, *ibid.*, **34**, 351 (1961).

The Analysis of Solution Kinetics Data Coupled with Thermal Transients in an Adiabatic Calorimeter. I

by E. D. West[1]

The National Bureau of Standards, Boulder, Colorado 80302

and W. J. Svirbely*

Department of Chemistry, University of Maryland, College Park, Maryland 20742 *(Received May 24, 1971)*

Publication costs borne completely by The Journal of Physical Chemistry

Calorimetric measurements of reaction rates in solution have generally suffered from inadequate treatment of the effects of the temperature gradient in the calorimeter. This paper is based on a more adequate theory of adiabatic calorimetry which predicts the effect of the thermal transients on the time–temperature observations from which rate constants must be calculated. The theory treats the calorimeter as a linear system with a characteristic response to an instantaneous energy input; in other words, the temperature output is related to an energy input through a kind of transfer function. The form of the characteristic response is predicted from the heat flow problem, and the necessary constants are determined experimentally. The forms of the time–temperature relationships are determined for first- and second-order reactions. The theory has been tested for the saponification reaction of ethyl acetate in aqueous ethanol. Rate constants calculated by simplified methods show large trends during the experiment. Calculations of rate constants by the relationship derived for second-order reactions are self-consistent throughout the experiment.

I. Introduction

The advantages of kinetic measurements by calorimetry have been set down by Sturtevant.[2] "Many physical methods require the use of relatively concentrated solutions in order that an appreciable change in the observed property be obtained. The great sensitivity attainable in calorimetric measurements would make it possible to work with dilute solutions even with reactions involving very small heat changes, and in many cases to obtain an accuracy not easily reached by other methods." One of the disadvantages has been that some of the data cannot be used in the analysis. For example, Sturtevant found it necessary to discard data taken in the first 20 min. We attribute this disadvantage to an inadequate theory of calorimetry. We propose a method of overcoming this disadvantage and other possible inadequacies of the method due to thermal transients in the calorimeter.

Applications have been made of calorimetry to thermochemistry and to kinetics.[3] Yet, the theory of calorimetric measurements used can hardly be called highly developed in the sense of starting from basic physics and proceeding rigorously to the details of the measurement.

A better theory might be expected to give some insight into the problem of evaluating the heat exchange due to thermal transients taking place during the reaction or some other heating process. For thermochemistry, the important question is whether or under what conditions the electrical calibration takes these transients into account. For kinetics, the problem is to relate the observed temperature as a function of time to the internal energy and the heat exchange.

Recently, West and Svirbely[4] have developed for adiabatic calorimeters a theory of measurement based on the first law of thermodynamics and the equations for heat transfer by conduction and radiation. They analyze the problem of heat flow in an adiabatic calorimeter and its effect on the temperature as a state variable as well as on the heat transfer and on the evaluation of the electrical and the mechanical work done on the calorimeter. In this paper, we develop the theory insofar as it applies to kinetics. We also present an analysis of the data obtained from a study involving the saponification of ethyl acetate in ethanol–water mixtures to test the theory.

II. Experimental Section

A. Chemicals. Ethyl Acetate. Reagent grade ester, obtained from J. T. Baker Chemical Co., was fractionally distilled. The middle, constant boiling fraction, bp 76.5°, was collected. Manufacturer's analysis of this lot showed water to be the largest impurity, 0.009%.

---

[1] Abstracted from the Ph.D. thesis of E. D. West, University of Maryland, 1969.

[2] J. M. Sturtevant, *J. Amer. Chem. Soc.*, **59**, 1528 (1937).

[3] (a) J. M. Sturtevant, *Physics*, **1**, 232 (1936); (b) G. Laville, *C. R. Acad. Sci.*, **240**, 1195 (1955); **240**, 1060 (1955); (c) E. Calvet and H. Prat, "Microcalometrie," Masson et Cie, Paris, 1956; (d) E. Calvet and F. Camia, *J. Chim. Phys.*, **55**, 818 (1958); (e) F. Becker and H. Hoffman, *Z. Phys. Chem. (Frankfurt an Main)*, **50**, 162 (1966); (f) F. Becker and F. Spalink *ibid.*, **26**, 1 (1960); (g) H. J. Borchardt and F. Daniels, *J. Amer. Chem. Soc.*, **79**, 41 (1957); (h) R. P. Bell and J. C. Clunie, *Proc. Roy. Soc., Ser. A*, **212**, 16 (1952); (i) C. H. Lueck, L. F. Beste, and H. K. Hall, *J. Phys. Chem.*, **67**, 972 (1963).

[4] E. D. West and W. J. Svirbely, to be published.

Sodium Hydroxide. Analytical reagent grade sodium hydroxide, obtained from J. T. Baker Chemical Co., was used. The concentrations of solutions of sodium hydroxide in ethanol–water mixtures were determined by titration against a dried and weighed amount of Mallinckrodt analytical reagent grade potassium hydrogen phthalate in 50 ml of water to a phenolphthalein end point. Results were as follows: solution 1, $N = 0.17420, 0.17435, 0.17429$; av, 0.17428; std dev, 0.00008; solution 2, $N = 0.19202, 0.19220, 0.19190$; av, 0.19204; std dev, 0.00015.

B. Calorimeter. The adiabatic calorimeter used in this research was designed applying the same principles that were used in the design of a high-temperature adiabatic calorimeter for heat capacity measurements.[5] A distinguishing feature of the high-temperature calorimeter was a surface separated from the sample container. The purpose of that construction was to ensure that the error in evaluating the heat exchange with the shield due to the temperature gradient would be proportional to the temperature rise and independent of the contents of the calorimeter. Several modifications have been made in that calorimeter for this research to accommodate the requirements of solution calorimetry.

A schematic diagram is shown in Figure 1. The calorimeter proper consists of two main parts, a permanently mounted part and a removable container which fits inside it. The cup portion of the container was made of copper. The top for closing the cup was made of inconel with inconel rods extending into the cup to support the arrangement which held the liquid reactant. The space between the lid and the cup was sealed with an "O" ring (Buna "N").

Stirrers for solution calorimetry usually have a drive shaft extending from the vitals of the calorimeter through the surrounding parts, such as an adiabatic shield or water bath. The shaft presents problems in evaluating the heat flow along it and in sealing the calorimeter to prevent evaporation. These difficulties have been overcome in the present case by driving a magnetic stirrer with an external driving magnet.

The arrangement for starting the reaction—"the mousetrap"—was made of inconel with Teflon gaskets and lubricating surfaces. The volatile solute liquid was contained in a hollow inconel cylinder of about 0.5-ml capacity, closed at both ends by Teflon gaskets. The gaskets were held in place by a lever arm with a catch and pin arrangement. When the pin was pulled, the catch released the lever, which let the gaskets and the hollow cylinder fall through the solution, rinsing out the solute as it fell. Arrangements which did not provide for such rapid dispersal of the solute gave unintelligible kinetic data, although they would probably be adequate for thermochemistry where timing is of less importance.

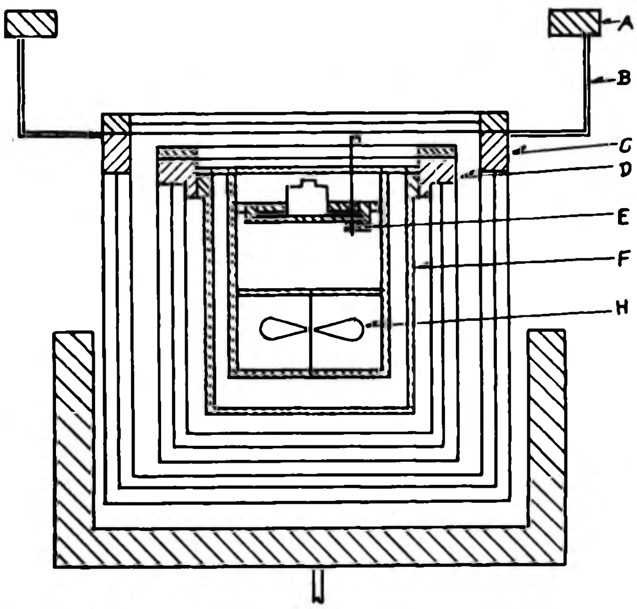

Figure 1. Cross section of the calorimeter. The calorimeter consists of the copper ring, D, with attached thin copper cups and lid, the solution container, F, which fits inside the ring, and the container lid with supports rods which position the "mousetrap," E, which contains the ester, and the propeller-type stirrer, H. The calorimeter is surrounded by the adiabatic shield, consisting of the copper ring, C, with attached copper cups and lid. The ring cools through the brass support B, to the heavy ring, A, which is in direct contact with the water bath.

The permanent part of the calorimeter was mounted on a copper ring about 0.125 in.^{2} in cross section. The ring was held in place by three small, thin-walled inconel tubes which offered the largest thermal resistance consistent with adequate mechanical support. Three thin-walled gold-plated copper cups were soldered to the ring to intercept heat transfer between the container and the adiabatic shield.

A thermopile measured the temperature difference between the copper ring of the calorimeter and a similar ring in the adiabatic shield. The thermopile was made of 19 junctions of chromel and constantan wires having a sensitivity of about 1200 μV/deg. The junctions were fastened to the copper ring with epoxy resin.

Provisions were made for a calorimeter heater to be located either on or in the container, *i.e.*, the heater wire was either wound on the outside wall and fastened in place with epoxy resin, or it was wound in an open loop and suspended directly in the solution from its own leads. The current leads for the calorimeter were brought through the copper rings and fastened in

---

(5) E. D. West and D. C. Ginnings, *J. Res. Nat. Bur. Stand.*, **60**, 309 (1958).

place with epoxy resin. Two potential leads were taken off the current leads midway between the two rings. The thermal contact between the current leads and the rings is the same for both rings.

The calorimeter was closed by a light lid consisting of two thin gold-plated copper disks held in a brass ring.

The adiabatic shield consisted of a copper ring and three thin gold-plated copper cups. The thermopile for temperature control was attached to the inside of the ring. The top of the shield was closed by a lid consisting of three thin gold-plated copper disks mounted in a brass ring.

C. Control of the Adiabatic Shield. The problem of controlling the temperature of the adiabatic shield for solution kinetics differs from the problem for heat capacity measurements.[5] The calorimeter may cool, so provision was made to cool the shield by providing a path of comparatively low thermal resistance from the adiabatic shield to the bath. A comparatively large power was required to maintain this temperature gradient. Power not supplied by the shield heater came from cooling the shield, so that rather rapid cooling could be obtained by decreasing the heater power. This technique required handling a larger power, but this was easily handled with transistors in contrast to the vacuum tubes used earlier.[5]

A block diagram of the control system is shown in Figure 2. The signal voltage from the 19 junction thermopile (1200 μV/deg) was compared to the dc reference voltage. The reference voltage was used to adjust the temperature difference so that heat is transferred to the adiabatic shield to balance out the stirring power. Under this condition, the temperature of the calorimeter changed slowly and could be read more accurately.

The reference voltage was supplied by a mercury cell kept in a dewar flask filled with oil to maintain its temperature reasonably constant. The stability of this source was not checked, other than by the precision of the kinetics experiments.

The error signal (difference between the thermopile and reference voltages) was amplified by a chopper-type dc amplifier, dependable to about 0.5 μV or 0.25 mdeg. The amplified signal was used to actuate a three-mode controller (proportional, integral, and derivative). The current output from the controller operated a simple transistor network which regulated the direct current to the shield heater.

D. Temperature Measurements. The temperature has two levels of significance in kinetic studies in a calorimeter. Reaction rates vary with temperature, but knowledge of the absolute temperature to 0.01° is adequate. This accuracy is easily achieved by ordinary resistance thermometry. However, the temperature as a measure of the concentration requires precision far better than 0.01°. In two experiments, for example, the total temperature rise was only about 0.03°. Since precision is more important than accuracy, a copper thermometer was used instead of a platinum thermometer.

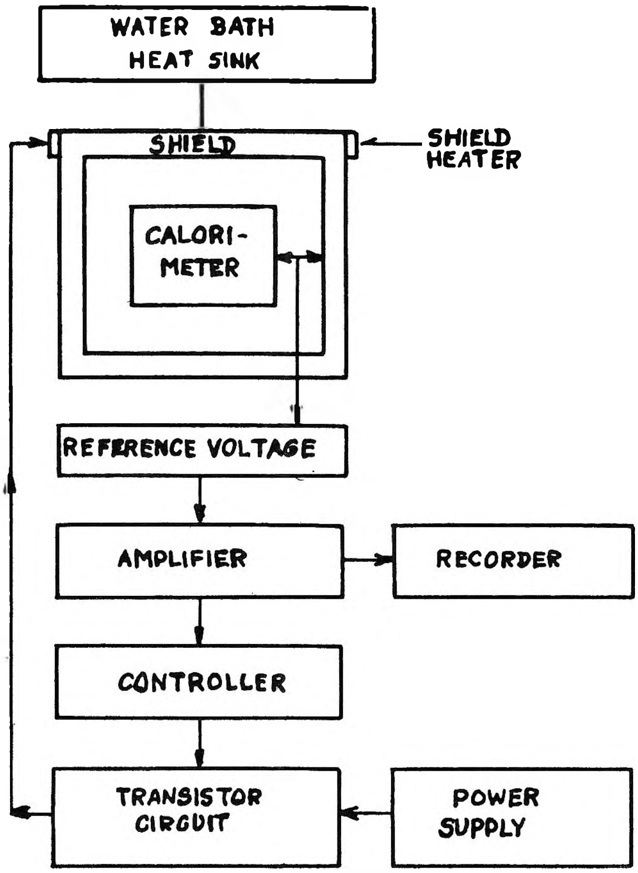

Figure 2. Schematic diagram of the adiabatic shield control system.

The copper thermometer was wound noninductively on the outside of the copper ring. It was calibrated against a capsule-type platinum resistance thermometer which has been certified by the National Bureau of Standards.

E. Experimental Procedure. The concentration of ester in an experiment depends on the weight of ester placed in the calorimeter. This was not a straightforward problem, because of the volatility of the ester. Smith and Levinson[6] have criticized the work of Evans, Gordon, and Watson[7] for lack of attention to the vaporization problem.

The amount of ethyl acetate was determined as follows. The "mousetrap" arrangement was washed, dried, assembled, and placed on an analytical balance until it came to constant weight. A quantity of ester was then forced into the "mousetrap" through a small opening by use of a hypodermic syringe. The opening was then closed with a small piece of Teflon. The weight of the assembly was then observed until it became constant. The difference between these two weights was taken as the weight of the ester.

---

[6] H. A. Smith and H. S. Levinson, *J. Amer. Chem. Soc.*, **61**, 1172 1939.

[7] D. P. Evans, J. J. Gordon, and H. B. Watson, *J. Chem. Soc.*, 1439 (1938).

The "mousetrap," the container lid, and the copper container cup were weighed next. The cup was then filled with the ethanol–water solution of sodium hydroxide. The lid with the attached "mousetrap" was put into place quickly to avoid loss by vaporization. Again the assembly was weighed. The difference between these two weights was taken as the weight of the solvent mixture.

The container was then assembled in the calorimeter. If the experiment was to be carried out below room temperature, the entire calorimeter was immersed in an ice bath. During immersion, the temperature could be followed with the copper resistance thermometer on the calorimeter. When this temperature was a few degrees below the desired starting temperature, the calorimeter was placed in the water bath, which had previously reached its operating temperature. The calorimeter was then heated with the electrical heater until the initial temperature was reached. During this heating period, the adiabatic shield control was placed in operation.

Some time after the heating was stopped, observations of the resistance were started. Although it was usually too early to determine the initial heat exchange rate accurately, the measurement was adequate to indicate whether the rate was abnormally negative, indicating evaporation from a leak in the container seals, or merely too large for convenient resistance measurements. In the latter case, the reference voltage was adjusted.

When the rate of resistance change became constant, the "mousetrap" was tripped on an integral minute as indicated by a timer with a sweep-second hand. At the beginning, resistance measurements were made every 30 sec. As the rate of change of the resistance decreased, the observations were taken at longer intervals of time until the rate of change was obscured by uncertainties in the heat leak rate.

F. Experimental Data. The resistances were first corrected for the small errors in the bridge dials, as found in the calibration. The corrected resistances were then converted into the equivalent resistance of the calibrating platinum resistance thermometer according to the formula developed in the comparison of the two thermometers. The equivalent platinum resistance was then converted into absolute temperature according to the Callendar interpolation formula for platinum resistance thermometers[8] and the constants given with the calibration by the National Bureau of Standards. The temperatures so obtained with the corresponding times are tabulated in Table I, along with other pertinent data, for one of the seven experiments performed.

Table I: Data for Kinetics Experiment[a]

Time, min	Temp, °C	Time, min	Temp, °C
0	25.0084	8	25.0513
0.5	25.004	10	25.0614
1	25.0034	10.5	25.0636
1.5	25.0063	11	25.0657
2	25.0094	11.5	25.0679
2.5	25.0132	14	25.0766
3	25.0171	14.5	25.0782
3.5	25.0211	15	25.0796
4	25.0253	15.5	25.0811
4.5	25.0293	19	25.0895
5	25.0329	19.5	25.0904
5.5	25.0364	20	25.0913
6	25.0395	20.5	25.0922
6.5	25.0429	24.75	25.0983
7	25.0458	34.75	25.106
7.5	25.0486	47.75	25.109

[a] Weight of ester, 0.1146 g; volume of solution, 84 ml; initial ester concentration, 0.01546 mol/l.; initial hydroxide concentration, 0.19174 mol/l.

The data for the first 20 min of the experiment are plotted in Figure 3. These data show the typical cooling due to endothermic heat of solution, followed by an increase in temperature due to the heat produced as the reaction proceeds. The observed temperature does not fall immediately, but decreases for about 2 min even though the reaction should be evolving heat at its greatest rate during this time.

III. Discussion

A. The Simple Theory of Adiabatic Calorimetry. The following state diagram (Scheme I) incorporates the processes which may occur when an isolated reaction takes place in an adiabatic calorimeter.

Scheme I

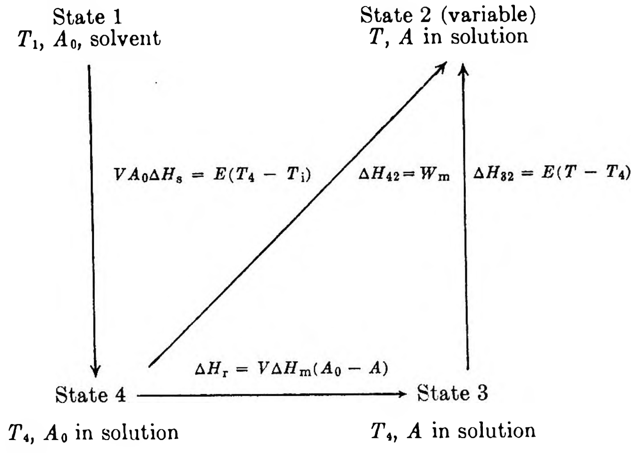

ΔH_r is the enthalpy of reaction, V is the volume of the solution, ΔH_m is the molar enthalpy of the reaction,

---

[8] H. F. Stimson, "Temperature, Its Measurement and Control in Science and Industry," Vol. 2, Reinhold, New York, N. Y., 1955.

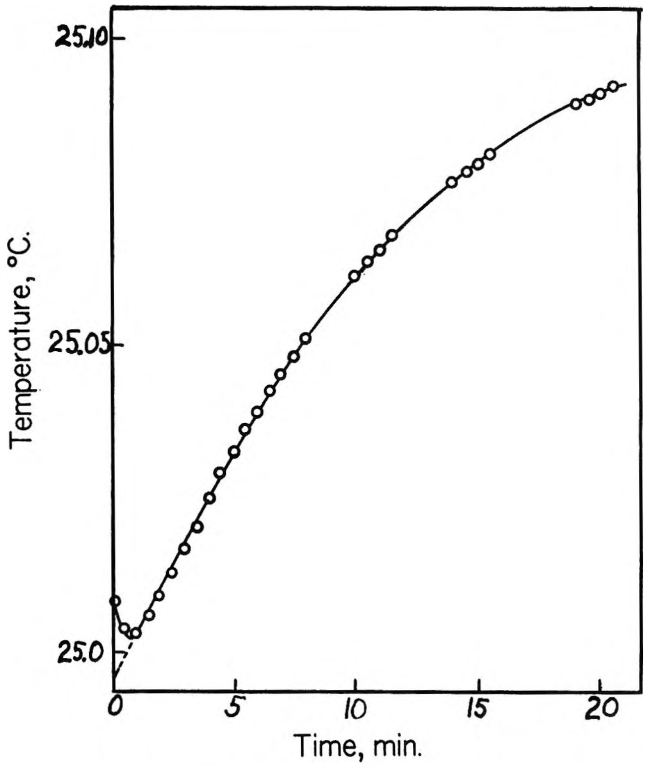

Figure 3. Typical temperature-time curve for the saponification of ethyl acetate.

A_0 and A are the initial and existing concentrations of the reactant A′ in moles per unit volume, respectively, ΔH_s is the molar heat of solution, E is the energy equivalent of the calorimeter, and W_m is the mechanical work of stirring.

The reaction is started by adding the reactant A′ to a solvent containing the other reactant. The addition is accompanied by a heat of solution as shown above in going from state 1 to state 4. If we assume the solution process to be endothermic, the calorimeter temperature drops from T_i to T_4. Both T_i and T_4 remain the same for all time. The reaction then proceeds in the calorimeter to state 2, which can also be reached by the path going through the hypothetical state 3. Based on the equality of these two paths, we obtain eq 1.

$$V\Delta H_m(A_0 - A) = W_m - E(T - T_4) \qquad (1)$$

Since

$$W_m = \dot{W}_m \Delta t \qquad (2)$$

eq 1 then becomes eq 3

$$A_0 - A = \frac{-E}{V\Delta H_m}\left(T - T_4 - \frac{\dot{W}_m \Delta t}{E}\right) \qquad (3)$$

On defining a "corrected temperature," T_c by $(T - (\dot{W}_m\Delta t/E))$ eq 3 becomes eq 4

$$A_0 - A = \frac{-E}{V\Delta H_m}(T_c - T_4) \qquad (4)$$

Since $T_c = T_\infty$ when $A = 0$, eq 4 leads to eq 5

$$A_0 = \frac{-E}{V\Delta H_m}(T_\infty - T_4) \qquad (5)$$

On dividing eq 4 by eq 5 we obtain eq 6

$$\frac{A}{A_0} = \frac{T_\infty - T_c}{T_\infty - T_4} \qquad (6)$$

Equation 6 is the familiar form encountered in kinetics when physical measurements[9] are made. It is also the relation which was used by Sturtevant.[2] Since A_0 is known, eq 6 is the required relationship connecting existing concentration with observed temperature, provided the *temperature gradient in the calorimeter can be neglected.*

The integrated form of a second-order rate equation involving two reactants is given by eq 7

$$kt(B_0 - A_0) = \ln \frac{A_0}{A}\left[1 - \frac{A_0}{B_0}\left(1 - \frac{A}{A_0}\right)\right] \qquad (7)$$

Combination of eq 6 and 7 leads to eq 8

$$kt(B_0 - A_0) = \ln \frac{(T_\infty - T_4)}{(T_\infty - T_c)}\left[1 - \frac{A_0}{B_0}\left(\frac{T_c - T_4}{T_\infty - T_4}\right)\right] \qquad (8)$$

The ultimate value of the corrected temperature, T_∞, after a very long time and the temperature, T_4, immediately following solution cannot be determined by direct observation but must be obtained either by an approximation or by some sort of extrapolation of the experimental data.

As a first approach to the calculation, the heat of solution is ignored and T_4 is taken to be the same as the initial temperature just before the experiment was started.

The determination of the ultimate temperature T_∞ is made by successive approximation. A rate constant is calculated for several intermediate temperatures assuming that the last observed temperature is the ultimate temperature. This approximate rate constant is then used to estimate how much ester remains at the last observed temperature. The total temperature rise, $(T_\infty - T_4)$, is then the corrected rise, $(T_c - T_4)$, at the last observation divided by the fraction of ester used up.

The data of Table I have been treated in this way. The calculated rate constant is plotted against the time of observation as curve 1 in Figure 4. The systematic trend is obvious and a better method of treating the data must be sought.

The next obvious step is to allow for the heat of solution. The data for the initial part of the reaction are simply extrapolated graphically in Figure 3 to obtain $T_4 = 24.9958°$. It must be emphasized that this is already a *departure from the simple theory.* If the temperature gradient were really negligible, the observed temperatures at 0.5 and 1 min would not lie above the extrapolated curve.

---

[9] A. A. Frost and R. G. Pearson, "Kinetics and Mechanism," 2nd ed, Wiley, New York, N. Y., 1961, p 29.

The rate constant has been calculated for the same set of data with this revised value for T_4 and plotted for comparison as curve 2 in Figure 4. Although the data are now much more self-consistent, the trend of the rate constant with time indicates that some systematic error remains.

B. Effect of the Temperature Gradient in Kinetic Studies. The effect of a temperature gradient in an adiabatic calorimeter has been studied in terms of the first law of thermodynamics and a generalized boundary value heat flow problem.[4] That study shows that for unit energy input at a time τ

$$E(T_c - T_i) = [1 - \sum a_i\phi_i^* e^{-b_i(t - \tau)}] \tag{9}$$

The term $(1 - \Sigma a_i\phi_i^* e^{-b_it})$ is independent of the sign and magnitude of the enthalpy change which eventually produces the temperature change $(T_\infty - T_i)$. The term is a characteristic of the calorimeter and will have to be evaluated. If T_∞ is the ultimate value of T_c, we may write for a heat of solution at time $t = 0$

$$\frac{T_c - T_i}{T_\infty - T_i} = 1 - \sum a_i\phi_i^* e^{-b_it} \tag{10}$$

Equation 10 provides a method for finding the a_i's and the b_i's. Equation 10 is derived in the thesis[1] and is labeled eq II-65. Reference 4 is an extension of the arguments in the thesis and leads to a theory of measurement for adiabatic calorimetry.

The calorimeter response to an instantaneous input of energy can be extended to time-dependent energies, such as the heat of reaction which is being released over the extended time of the reaction. When the solution is followed by a chemical reaction, we multiply the right-hand side of eq 9 by the energy input of the reaction $g(\tau)\mathrm{d}\tau$ at the time τ and integrate over all past time τ

$$E(T_c - T_i) = \int_0^t g(\tau)[1 - \sum a_i\phi_i^* e^{-b_i(t - \tau)}]\mathrm{d}\tau \tag{11}$$

The quantity $g(\tau)\mathrm{d}\tau$ is the heat of solution at time which we henceforth take to be $t = 0$ and, for $t > 0$, $g(\tau)$ is the rate at which heat is developed by the chemical reaction.

As shown on our state diagram, the heat of solution would be $V\Delta H_sA_0$ and, its proportional temperature response at the calorimeter ring would be

$$\frac{V\Delta H_sA_0}{E}(1 - \sum a_i\phi_i^* e^{-b_it})$$

Correspondingly, the input energy as a heat of reaction at a time, τ, would be $(V\Delta H_m\mathrm{d}A)$. However, the temperature response at the calorimeter ring determined at a time, t, as the result of the energy input at time, τ, would be

$$\frac{V\Delta H_m\mathrm{d}A}{E}(1 - \sum a_i\phi_i^* e^{-b_i(t - \tau)})$$

The observed temperature change in the calorimeter would include the contributions of the instantaneous heat of solution and the contributions of the heats of reaction for all times τ, leading to eq 12

$$(T_c - T_i) = -\frac{(V\Delta H_sA_0)}{E}[1 - \sum a_i\phi_i^* e^{-b_it}] - \frac{V\Delta H_m}{E}\int_0^t \frac{\mathrm{d}A}{\mathrm{d}\tau}(1 - \sum a_i\phi_i^* e^{-b_i(t - \tau)})\mathrm{d}\tau \tag{12}$$

On examining eq 12 we note that $(-V\Delta H_sA_0)/E$ is just the eventual temperature change $(T_4 - T_i)$ produced by the heat of solution, and

$$\frac{(V\Delta H_mA_0)}{E}$$

is just the eventual temperature change $(T_\infty - T_4)$ due to the heat of reaction. On making the above substitutions in eq 12 and carrying out part of the integration we obtain eq 13

$$(T_c - T_i) = (T_4 - T_i)(1 - \sum a_i\phi_i^* e^{-b_it}) + (T_\infty - T_4)\frac{(A_0 - A)}{A_0} + \frac{(T_\infty - T_4)}{A_0}\int_0^t \frac{\mathrm{d}A}{\mathrm{d}\tau}\sum a_i\phi_i^* e^{-b_i(t - \tau)}\mathrm{d}\tau \tag{13}$$

Equation 13 is the counterpart of eq 6 which assumes that there is no temperature gradient. One objective of this research was to compare the relative merits of the two equations.

C. Effect of a Temperature Gradient on a First-Order Reaction. If we are dealing with first-order kinetics, the rate equation at a time, τ, is given by eq 14

$$-\frac{\mathrm{d}A}{\mathrm{d}\tau} = kA_0e^{-k\tau} \tag{14}$$

Let us assume that eq 10 may be simplified to a single exponential (in an experiment this assumption must be checked), *i.e.*

$$(1 - \sum a_i\phi_i^* e^{-b_it}) = (1 - a_1\phi_1^* e^{-b_it})$$

On reference to eq 10 it can be seen that at $t = 0$, $T_c = T_i$, consequently, $\Sigma a_i\phi_i^* = 1$. It follows that for one exponential, $a_1\phi_1^* = 1$. The simplified response function is then given by $(1 - e^{-bt})$.

On substituting the simple response function and eq 14 into eq 13, we obtain eq 15

$$(T_c - T_i) = (T_4 - T_i)(1 - e^{-bt}) + (T_\infty - T_4) \times \frac{(A_0 - A)}{A_0} - (T_\infty - T_4)k\int_0^t e^{-k\tau}e^{-b(t-\tau)}\mathrm{d}\tau \quad (15)$$

After integration of the last term, rearrangement of eq 15 leads to eq 16

$$\frac{A_0 - A}{A_0} = \frac{(T_c - T_i) - (T_4 - T_i)(1 - e^{-bt})}{(T_\infty - T_4)} + \frac{k}{(b - k)}(e^{-kt} - e^{-bt}) \quad (16)$$

Equation 16 is the appropriate relation involving concentration and the observed temperature at various times t for a first-order reaction. However, if we assume that $T_4 = T_i$, *i.e.*, that there is no heat of solution, and if we use the relation for a first-order reaction, *i.e.*

$$\frac{(A_0 - A)}{A_0} = (1 - e^{-kt})$$

then eq 16 becomes eq 17

$$\frac{(T_\infty - T_c)}{(T_\infty - T_i)} = -\frac{ke^{-bt}}{b - k} + \frac{be^{-kt}}{b - k} \quad (17)$$

Rewrite eq 6 as eq 18

$$\frac{(T_\infty - T_c)}{(T_\infty - T_i)} = e^{-kt} \quad (18)$$

On comparing the right-hand sides of eq 17 and 18 it is apparent that (a) consideration of a temperature gradient leads to two exponential terms rather than one term to describe

$$\frac{(T_\infty - T_c)}{(T_\infty - T_i)}$$

(b) if $b \gg k$, as would be the case for a relatively slow reaction, eq 17 would decay to single exponential term. However, even then the two equations would not be identical due to the factor $b/(b - k)$. However, if

$$-\ln\left(\frac{T_\infty - T_c}{T_\infty - T_i}\right)$$

is plotted against t, a straight line would be obtained at large values of t. The slope of the linear section would be k (curve 1, Figure 5). However, a similar plot would be linear, with a slope of k, over the complete time range of the experiment if the temperature gradient is negligible (curve 2, Figure 5). The plots in Figure 5 are based on the assumed values of k and b equal to 0.0648 and 1.27 min^{-1}, respectively.

The significant conclusion deduced from Figure 5 is that, although the heat of solution is zero, there is an "incubation" period. The commonly observed "incubation" period can therefore be explained by the temperature gradient *by itself*. This is probably a general result, applicable whenever the observed system contains a delaying element.

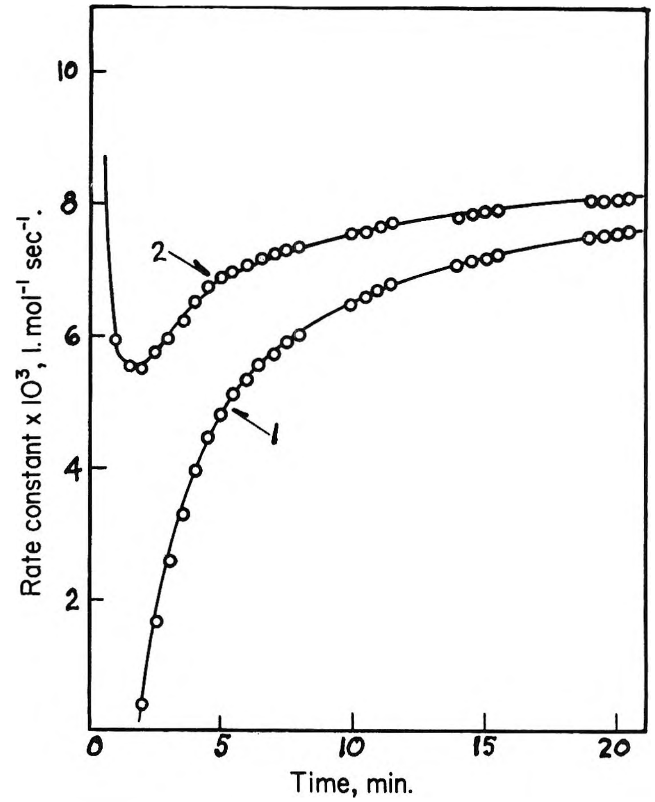

Figure 4. Rate constant calculated by the simple theory (eq 8).

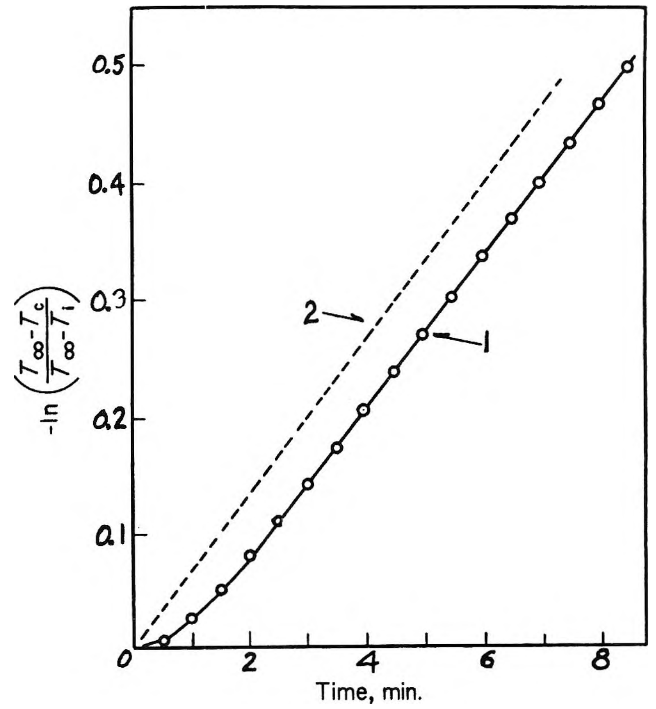

Figure 5. Effect of the thermometer response function on first-order reactions.

D. The Thermometer Response Function for Second-

Order Reactions. To apply the analysis developed in section IIIB to the kinetics data obtained in this research, it is necessary to determine the constants in the response function given by eq 10. To answer this question, two kinds of experiments were carried out—a series of solution experiments and a series of electrical heating experiments.

In the solution experiments, ethyl acetate was added to 85 wt % ethanol-water solution. A summary of the temperature measurements is recorded in Table II.

Table II: Data for Solution Experiments

Wt, g	Time, min	Temp, °C	$\frac{(T_\infty - T_c)}{(T_\infty - T_i)}$
0.4143	0	25.3048	
	0.5	25.2781	0.450
	1	25.2692	0.267
	1.5	25.2634	0.148
	2	25.2603	0.083
	∞	25.2562	
0.3082	0	25.2040	
	0.5	25.1848	0.470
	1	25.1775	0.269
	1.5	25.1733	0.154
	2	25.1705	0.077
	∞	25.1677	
0.4757	0	25.0599	
	0.5	25.0288	0.439
	1	25.0178	0.242
	1.5	25.0116	0.129
	2	25.0090	0.082
	∞	25.0044	
0.4134	0	25.1252	
	0.5	25.1009	0.514
	1	25.0881	0.258
	1.5	25.082	0.136
	2	25.0786	0.068
	∞	25.0752	

In the ratio of temperature differences in the last column, T_c is the observed temperature corrected for heat leak, T_∞ is the ultimate value of T_c, usually taken after about 10 min, and T_i is the initial value of T_c before the ester is added to the solution.

Our first problem is to determine how many terms of eq 10 are required to represent the data of Table II adequately. Equation 10 can be transformed to eq 10a

$$\frac{(T_\infty - T_c)}{(T_\infty - T_i)} = \sum a_i\phi_i e^{-b_it} \tag{10a}$$

To determine whether one exponential term is adequate, the logarithm of the ratio of the temperature differences is plotted against time. Reference to eq 10a shows that if one exponential term is adequate the plot should be a straight line with a slope equal to $-b$. Since such a linear relationship was obtained, the response of the thermometer function has been taken to include only one exponential term. A value of $b = 0.75\ \text{min}^{-1}$ was obtained.

The electrical heating experiments were devised to give the same information as the solution experiments discussed above. This can be done provided the electric heater immersed in the solution is the thermal equivalent of a heat of reaction. For this reason, the heater should have a very low heat capacity and should be in good thermal contact with the solution. The total energy supplied by an electrical heater operating at constant power, p, is the product of the power and the time, t. To find $T_c - T_i$ for constant power input, we perform the convolution of (pt) and the response to the step function given by eq 10. We obtain

$$T_c - T_i = \int_0^t \frac{p}{E}\left(1 - \sum a_i\phi_i^* e^{-b_i(t-\tau)}\right)d\tau \tag{19}$$

Because the constant p can be brought outside the integral, the integration can be performed to give eq 20

$$T_c - T_i = \frac{pt}{E} - \frac{p}{E}\sum\frac{a_i\phi_i^*}{b_i}(1 - e^{-b_it}) \tag{20}$$

If the power is held constant for a long time and then shut off at time, t', which is so large that all e^{-b_it} are negligible, the corrected temperature, T_c, for $t > t'$ is obtained[10] by adding to eq 20 the equivalent of eq 20 written for $-p$ and starting at t'. For $t > t'$ we obtain eq 21

$$T_c - T_i = \frac{p}{E}\left(t - \sum\frac{a_i\phi_i^*}{b_i}\right) - \frac{p}{E}\left[t - t' - \sum\frac{a_i\phi_i^*}{b_i}(1 - e^{-b_i(t-t')})\right] \tag{21}$$

Simplifying, we obtain

$$T_c - T_i = \frac{pt'}{E} - \frac{p}{E}\sum\left(\frac{a_i\phi_i^*}{b_i}\right)e^{-b_i(t-t')} \tag{22}$$

On defining $T' = T_c$ in eq 20 at the time t', and subtracting T' from both sides of eq 22, we obtain eq 23

$$T_c - T' = \frac{p}{E}\sum\left(\frac{a_i\phi_i^*}{b_i}\right)(1 - e^{-b_i(t-t')}) \tag{23}$$

When $t \gg t'$, T_c approaches a constant value which we define as T_∞. On dividing eq 23 by its equivalent for $t \gg t'$, we obtain eq 24

$$\frac{T_c - T'}{T_\infty - T'} = \frac{\sum\left(\frac{a_i\phi_i^*}{b_i}\right)(1 - e^{-b_i(t-t')})}{\sum\left(\frac{a_i\phi_i^*}{b_i}\right)} \tag{24}$$

For a single exponential term as was demonstrated to be valid in the solution experiments, the summations reduce to a single term and cancel. On subtracting the resulting equation from

---

(10) B. M. Brown, "The Mathematical Theory of Linear Systems," Wiley, New York, N. Y., 1961, p 82.

$$\frac{(T_\infty - T')}{(T_\infty - T')} = 1$$

we obtain

$$\frac{T_\infty - T_c}{T_\infty - T'} = e^{-b(t - t')} \tag{25}$$

Evidently, a plot of

$$\ln \frac{(T_\infty - T')}{(T_\infty - T_c)}$$

against t will have a slope of b.

Experimentally, the power is turned onto a heater coil of fine manganin wire suspended in the solution just above the stirrer. After 5–10 min, the power is turned off and the temperature is followed as a function of time. This experiment can be repeated much more readily than the solution experiments and permits repetition for exactly the same amount of solution. The data are plotted in Figure 6. From the graph, the value of $b = 0.84\ \text{min}^{-1}$ was obtained.

E. The Analysis of the Kinetics Data. On defining $k' = k(B_0 - A_0)$, eq 7 for a second-order reaction can be rewritten as eq 26

$$\frac{A}{A_0} = \frac{(B_0 - A_0)e^{-k't}}{(B_0 - A_0e^{-k't})} \tag{26}$$

where A_0, A, and B_0 represent the concentrations of starting ester, existing ester, and starting hydroxide ion, respectively. On taking the derivative of A with respect to the time, τ, the rate equation is given by eq 27

$$-\frac{dA}{d\tau} = A_0 \frac{(B_0 - A_0)}{B_0} \frac{k'e^{-k'\tau}}{\left(1 - \frac{A_0}{B_0} e^{-k'\tau}\right)^2} \tag{27}$$

On inserting this derivative into eq 13, along with the experimental condition that only one exponential term is required, we obtain eq 28

$$T_c - T_i = (T_4 - T_i)(1 - e^{-bt}) + (T_\infty - T_4) \times \left[\frac{(A_0 - A)}{A_0} - \frac{(B_0 - A_0)}{B_0} \int_0^t \frac{k'e^{-k'\tau}e^{-b(t - \tau)}}{\left(1 - \frac{A_0}{B_0} e^{-k'\tau}\right)^2} d\tau \right] \tag{28}$$

On rearrangement and solving for $(A_0 - A)/A_0$), we obtain eq 29

$$\frac{A_0 - A}{A_0} = \frac{(T_c - T_i) - (T_4 - T_i)(1 - e^{-bt})}{(T_\infty - T_4)} + \frac{(B_0 - A_0)}{B_0} k'e^{-bt} \int_0^t \frac{e^{-k'\tau}e^{b\tau}d\tau}{\left(1 - \frac{A_0}{B_0} e^{-k'\tau}\right)^2} \tag{29}$$

The temperature T_4, which would be reached by solution alone, is obtained from the solution experiments, and the constant b is obtained from the heating experiments. The integral is evaluated by numerical integration, using a value of k' obtained by successive approximation. The integral is in the nature of a correction term. For large values of t, either $e^{-k'\tau}$ or $e^{-b(t - \tau)}$ is small, so the integral will contribute less toward the end of the experiment than it will in the early part. For a calorimeter which equilibrates very rapidly, b is large and the integral will have a small effect.

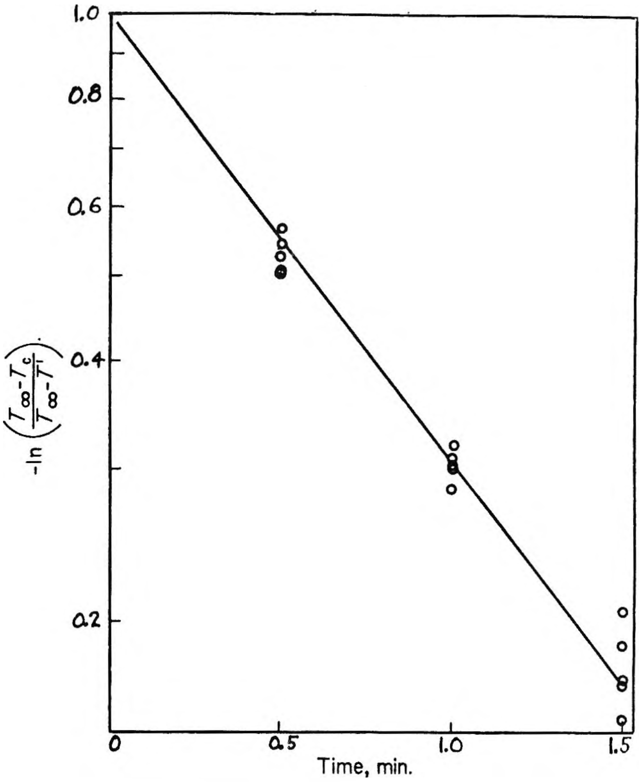

Figure 6. Determination of the thermometer response function from electrical heating experiments (eq 25).

As a check, we note that, if the effect of the temperature gradient in the calorimeter is neglected, eq 29 reduces to eq 6 which was developed from the simple theory.

The ultimate corrected temperature, T_∞, is estimated from the rate equation. On rearranging eq 8, we obtain eq 30

$$T_\infty = T_c + \left[(T_\infty - T_4) - \frac{A_0}{B_0}(T_c - T_4)\right]e^{-k't} \tag{30}$$

It is usually adequate to use the last observed temperature for T_∞ on the right-hand side, obtaining eq 31

$$T_\infty = T_c + (T_\infty - T_4)\left(1 - \frac{A_0}{B_0}\right)e^{-k't} \tag{31}$$

The data of Table I have been treated by eq 29 to obtain values for the concentration, A. These values are then used in eq 7 to calculate the rate constant, k. The results are tabulated in Table III. The third column of Table III represents the contribution of the first term on the right-hand side of eq 29 and the fourth column represents the integral correction. Together they represent the fraction of the ester used up. All of our experiments were carried out to at least 96% completion.

Table III: Rate Constant Calculations

Time, min	Rate constant $\times 10^3$, l. mol-sec^{-1}	$1 - A/A_0$, uncorrected	Correction term
0.5	9.00	0.014	0.036
1	8.49	0.039	0.054
1.5	8.92	0.080	0.062
2	8.73	0.116	0.065
2.5	8.66	0.154	0.065
3	8.58	0.190	0.063
3.5	8.52	0.226	0.061
4	8.57	0.264	0.059
4.5	8.59	0.298	0.056
5	8.56	0.330	0.054
5.5	8.54	0.361	0.051
6	8.45	0.387	0.049
6.5	8.48	0.416	0.046
7	8.43	0.441	0.044
7.5	8.41	0.466	0.042
8	8.39	0.490	0.040
10	8.41	0.577	0.033
10.5	8.40	0.595	0.031
11	8.41	0.614	0.030
11.5	8.44	0.632	0.028
14	8.44	0.708	0.022
14.5	8.45	0.721	0.021
15	8.45	0.734	0.020
15.5	8.47	0.747	0.019
19	8.56	0.819	0.014
19.5	8.56	0.827	0.014
20	8.57	0.835	0.013
20.5	8.56	0.842	0.012
24.75	8.65	0.896	0.008
34.75	8.88	0.961	0.003

To illustrate the effect of the integral term, the rate constants for the data of Table I have been calculated with and without the integral correction term. The lower curve in Figure 7 is a plot of the rate constant calculated without the correction, but after allowance for the heat of solution. For the upper curve, the rate constants were calculated using the correction. For the first 2 min, both curves appear to suffer from difficulties in accounting for the heat of solution, but the corrected values are strikingly more consistent than the uncorrected ones. After the first 2 min, the lower curve obviously undergoes a trend which is still evident at 20 min when the reaction is 84% complete.

By contrast, the rate constants represented by the upper curve are quite consistent. We take this as evidence for the correctness of the formulation by which they were calculated.

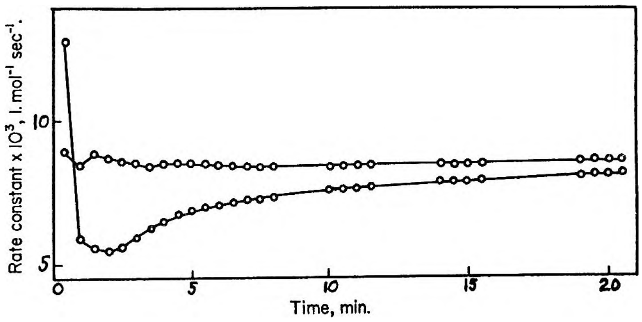

Figure 7. Effect of the correction term on the calculated rate constant.

Table IV: Summary of Rate Constants

Initial ester concn, mmol/l.	Initial hydroxide mmol/l.	Temp range, °C	wt % ethanol	$k \times 10^3$ l./mol-sec
17.48	173.98	0.1183	83	9.74
43.00	173.54	0.2995	83	9.85
39.28	173.60	0.2786	83	9.66
31.47	173.74	0.2193	83	9.75
4.537	174.21	0.0326	83	10.35
15.46	191.74	0.1006	85	8.55
4.011	192.00	0.0280	85	8.07

Table IV summarizes the rate constants for all of our experiments.

By interpolation of the data in the literature[6,7,11] for this reaction, k values of 6.21×10^{-3}, 7.05×10^{-3}, and 6.4×10^{-3} l./mol-sec in 85% ethanol–water mixtures and 7.3×10^{-3} l./mol-sec in 83% ethanol–water mixtures are obtainable. It does not appear that additional terms in the thermometer response function could account for the differences between these literature values and the values listed in Table IV. The corrected rate constant must be greater than the uncorrected value because the effect of the calorimeter is to delay the observed temperature rise, which therefore indicates too large a concentration and too small a rate.

Conclusion

When heat is evolved or absorbed during a reaction occurring in an adiabatic calorimeter, there is a delayed response in the observed temperature which should be a measure of the energy input or output. This delayed response can virtually destroy time–concentration data in kinetic studies unless recognition is taken of the temperature gradient. The treatment of the data by a linear theory of calorimetric measurements, which is developed in this paper for application to kinetic studies, gives rate constants which show very little trend with time during the entire experiment.

(11) E. Tommila, A. Koivisto, J. P. Lyra, K. Antell, and S. Heimo, *Suom. Tiedeakat. Toim.*, **47**, 3 (1952).

The Analysis of Solution Kinetics Data Coupled with Thermal Transients in an Adiabatic Calorimeter. II. First-Order Reactions

by **W. J. Svirbely,***

University of Maryland, College Park, Maryland 20742

E. D. West,

The National Bureau of Standards, Boulder, Colorado 80302

and F. A. Kundell

Salisbury State College, Salisbury, Maryland 21801

(Received May 24, 1971)

Publication costs borne completely by The Journal of Physical Chemistry

Calorimetric measurements of reaction rates in solution have generally suffered from inadequate treatment of the effects of the temperature gradient in a calorimeter. Recently we presented a theory of adiabatic calorimetry which predicts the behavior of the observed temperature as a function of time due to the combined effects of a heat of reaction, a heat of solution, and the thermal transients of the calorimeter. This paper demonstrates the utility of the theory for a pseudo-first-order reaction through use of the data obtained in the saponification of ethyl acetate in the presence of a large excess of hydroxide ion. The results are quite satisfactory, thus substantiating the calorimetric theory of kinetic measurements for first-order reactions.

I. Introduction

Calorimetric measurements of reaction rates in solution have generally suffered from an inadequate treatment of the effect of the temperature gradient in a calorimeter. A theory of measurement[1] has been recently developed for adiabatic calorimetry which predicts the behavior of the observed temperature as a function of time due to the combined effects of a heat of reaction, a heat of solution, and the thermal transients in the calorimeter. Appropriate equations were derived from the theory for first- and second-order reactions. The predictions of the theory for second-order reactions were tested by a study of the saponification of ethyl acetate in ethanol-water solutions. Calculations of the rate constants for that second-order reaction were self-consistent throughout the experiment.

In this paper we will test the predictions of the theory for first-order reactions.

II. Mathematical Procedure

The equation, which was developed[1] for first-order reactions, is shown by

$$\frac{A_0 - A}{A_0} = \frac{(T_c - T_i) - (T_4 - T_i)(1 - e^{-bt})}{(T_\infty - T_4)} + \frac{k}{b - k}(e^{-kt} - e^{-bt}) \quad (1)$$

where A_0 and A are starting and existing concentrations, respectively, of the reactant at time t; T_c, T_i, T_4, and T_∞ are observed temperature, initial temperature, temperature resulting from a heat of solution effect but prior to the beginning of the reaction, and temperature at infinite time, respectively; b is a constant of the calorimeter; and k is the first-order rate constant.

For a first-order reaction, the integrated form of the rate equation relating concentration to time is given by

$$A = A_0e^{-kt} \quad (2)$$

On substituting eq 2 into eq 1 and rearranging the resulting equation, one obtains eq 3

$$(T_c - T_\infty) + (T_4 - T_i)e^{-bt} = (T_\infty - T_4)\left[\frac{ke^{-bt}}{(b - k)} - \frac{be^{-kt}}{(b - k)}\right] \quad (3)$$

On defining $(T_4 - T_i)$ and $(T_\infty - T_4)$ by β and r, respectively, and on substituting these definitions in eq 3, one obtains eq 4

$$T_c = -\frac{rbe^{-kt}}{(b - k)} + \frac{rke^{-bt}}{(b - k)} - \beta e^{-bt} + T_\infty \quad (4)$$

A procedure for evaluating the rate constant, k, through direct use of eq 4 is already in the literature.[2] It is based on an estimate of k, expansion of eq 4 *via* Taylor's expansion, least-squares solution for the correction term to the first estimate, and repetition of the process using the corrected k as the new first estimate. A program was written to accomplish the calculations.

---

[1] E. D. West and W. J. Svirbely, *J. Phys. Chem.*, **75**, 4029 (1971).

[2] W. J. Svirbely and J. A. Blauer, *J. Amer. Chem. Soc.*, **83**, 4115 (1961).

III. Discussion and Results

If a reaction takes place between two reactants, first order in each reactant, and if one of the reactants, namely B, is present in large excess (at least tenfold), then the pseudo-first-order rate constant, k_1, is usually set equal to the product of the second-order rate constant, k_2, and the concentration of the reactant in excess, *i. e.*, $k_1 = k_2(\mathrm{B})$.

Some of the data we had obtained[1] for the saponification reaction of ethyl acetate was of this type and in those cases the reaction can be considered to be a pseudo-first-order reaction.

To save computer time, we selected for our first estimate of k_1 a value based on the k_2 value previously determined. Since values of T_4, T_i, T_∞, b, and time–temperature data were available, a corrected value of k_1 was obtained by the least-squares method based on eq 4. Values of T_c(calcd) were obtained next for each of the experimental times in an experiment through use of eq 4 and the first corrected value of k_1 for the experiment. The T_c(calcd) values were then compared with the T_c(obsd) values and the quadratic mean error of fit was obtained. The procedure was repeated using this first corrected value of k_1 as a new first estimate. The final results for one of the experiments are shown in Table I.

The third column of Table I lists values of T_c(calcd) obtained through use of the value of $k_1 = 0.0974\ \mathrm{min}^{-1}$. It is gratifying to see how well eq 4 duplicates the experimental temperatures, including the decrease at the start of the experiment due to the endothermic heat of solution and then the upswing in temperature due to the exothermic heat of reaction. The agreement demonstrates the adequacy of eq 1 to describe first-order kinetics when the temperature gradient is taken into account. This fact supports our calorimetric theory of kinetic measurements.

Table II summarizes the results for several experiments. The first-order rate constants in column 2 were obtained by the procedure just described. Column 5 represents the second-order rate constants which were calculated from the first-order rate constants in column 2 by means of the relation

$$k_2 = \frac{k_1}{60(\mathrm{OH})^-} \qquad (5)$$

Column 7 lists the second-order rate constants of the original paper.[1] The comparison of the values listed in columns 5 and 7 indicates quite good agreement and thus serves as a check on the overall procedure.

Table I: Time–Temperature Data for a Run

Time, min	Temp, °C (exptl)	Temp, °C (calcd)
0.00	25.0216	25.0216
0.50	25.0202	25.0206
1.00	25.0204	25.0205
1.50	25.0211	25.0209
2.00	25.0217	25.0217
2.50	25.0228	25.0226
3.00	25.0238	25.0236
3.50	25.0252	25.0247
4.00	25.0261	25.0257
5.00	25.0282	25.0278
5.50	25.0294	25.0289
6.00	25.0304	25.0298
6.50	25.0309	25.0308
8.00	25.0334	25.0334
8.50	25.0344	25.0341
9.00	25.0351	25.0349
9.50	25.0357	25.0356
11.00	25.0375	25.0375
11.50	25.0383	25.0381
12.00	25.0388	25.0387
12.50	25.0391	25.0392
14.00	25.0402	25.0407
14.50	25.0409	25.0411
15.00	25.0413	25.0415
15.50	25.0415	25.0419
18.00	25.0432	25.0436
18.50	25.0437	25.0439
19.00	25.0441	25.0442
19.50	25.0441	25.0445
23.75	25.0461	25.0463
28.75	25.0476	25.0477
38.75	25.0490	25.0491
48.75	25.0496	25.0496

$b = 0.84\ \mathrm{min}^{-1}$
$T_\infty = 25.0499°$
$T_4 = 25.0180°$
$T_i = 25.0216°$
$(\mathrm{OH})^-$ (concn) = 0.19200 mol/l.
Ester concn = 0.00401 mol/l.
$k_1 = 0.0974\ \mathrm{min}^{-1}$
Quadratic mean error of fit = 0.03%

Table II: Summary of Data

k_1,[a] min^{-1}	k_1,[b] min^{-1}	$(\mathrm{OH})^-$, mol/l.	Ester, mol/l.	$k_2 \times 10^3$, l./mol-sec	QME of fit, %	$k_2 \times 10^3$, l./mol-sec[c]
0.1002	0.0983	0.19174	0.01546	8.54	0.13	8.55
0.1030	0.1031	0.17398	0.01748	9.88	0.12	9.74
0.1166	0.1173	0.17421	0.004537	11.22	0.04	10.35
0.0974	0.0974	0.19200	0.004011	8.45	0.03	8.07

[a] First corrected value. [b] Second corrected value. [c] Reference 1.

Acknowledgment. We wish to express our appreciation to the Computer Science Center of the University of Maryland and the National Aeronautics and Space Administration for Grant NsG-398 applicable to computer time.

Vapor–Liquid Equilibria of Binary Mixtures of Carbon-14-Labeled Hexane with Aliphatic Ketones[1]

by Bogdan Magiera and Witold Brostow*

Instytut Chemii Fizycznej Polskiej Akademii Nauk, Warsaw 42, Poland

(Received February 17, 1971)

Publication costs borne completely by The Journal of Physical Chemistry

Equilibria of dilute solutions of *n*-hexane in turn in acetone and methyl ethyl, methyl propyl, and diethyl ketones have been studied. Isotherms and isobars linear with respect to composition were obtained, and thermodynamic consequences of such a behavior discussed. Activity coefficients and excess Planck functions of mixing were computed; some methods of obtaining the limiting values of activity coefficients at infinite dilution have been compared. A version of the quasilattice theory of mixtures, which may be called the model of dilute solutions of molecules of different sizes, was proposed and applied to describe the experimental data.

1. Introduction

Thermodynamic behavior of liquid phases containing very small quantities of one of the components is interesting for both fundamental and practical reasons. Consider a homogeneous binary mixture i–j containing very small amounts of component i; except for local concentration fluctuations which do not affect the averages, each molecule of i may be safely assumed to be surrounded by molecules of j only. From the point of view of the theory, instead of the usual three types of intermolecular interactions only two need to be considered: i–j and j–j. From the point of view of the industrial practice such as separation of components by rectification, information on the system in question enables us to obtain the substance j with a high degree of purity.

We have studied isothermal and isobaric vapor–liquid equilibria of dilute solutions of hexane in turn in acetone, methyl ethyl ketone, methyl propyl ketone, and diethyl ketone. The objects of particular attention were the limiting values of activity coefficients of hexane, $\lim_{x_1 \to 0} f_1$, where x_1 denotes the mole fraction of hexane in the liquid phase, obtained by our experimental procedure and also by other methods.

2. Experimental Section

Measurements were made in the vapor–liquid equilibrium still described previously by one of us[2a] and based on its construction on the Swietoslawski ebulliometer.[2b] The advantages in the use of such an apparatus have been discussed elsewhere.[3,4] The manostatic system used in both isobaric and isothermal determinations was the same as described in ref 5. Pressures were determined in a barometric ebulliometer[2b] filled in each case with the respective pure ketone. Temperatures were determined within ±0.02°K with Pt resistance thermometers (Heraeus, Hanau, West Germany) with Bundesanstalt (Braunschweig, West Germany) certificates; boiling point differences were measured with Roberteau thermometers, (Prolabo, Paris) within ±0.001°K. A dilute hexane solution was taken as one of the components, the respective pure ketone being the other one. The equilibrium determination procedure described in ref 2a was followed.

Advantages of the use of internal filling counters for ^{14}C assay have been discussed by Jordan and Lykourezos.[6] Before that, in the first determinations of compositions of organic liquid mixtures containing a ^{14}C-labeled component made in this laboratory[7] we have found such counters suitable for the purpose at hand; self-quenching mechanisms and properties of internal filling counters have been studied by Franke, *et al.*[8] Now, therefore, ^{14}C radioactivity was determined again in internal filling counters, switching however from the Geiger–Müller to proportional range. We have described elsewhere[9] the details of the ^{14}C-assay technique used in the present work.

The reagents used were purified by rectifying each twice through a laboratory column. ^{14}C-labeled hexane from Orlando Research Inc., in 5-mCi samples with specific acitivity 1.6 mCi/mmol, was diluted with a large excess of the inactive liquid. Refractive indices were measured with an Abbe-type refractometer, Carl Zeiss, Jena, East Germany; normal boiling points and ebulliometric degrees of purity were determined by the standard Swietoslawski procedure[2b] on a differential ebulliometer. The physicochemical characteristics of the reagents are given in Table I. To simplify the description, in the following text the substances will be designated by numbers given in the same table.

---

* To whom correspondence should be addressed at Départment de Chimie, Université de Montréal, Montreal 101, P. Q., Canada.

(1) Based on a dissertation submitted by B. Magiera to the Institute of Physical Chemistry of the Polish Academy of Sciences in partial fulfillment of the requirements for the D.Sci. (in chemistry) degree.

(2) (a) W. Brzostowski, *Bull. Acad. Pol. Sci., Ser. Sci. Chim.*, **8**, 291 (1960); (b) W. Swietoslawski, "Ebulliometric Measurements," Reinhold, New York, N. Y., 1945.

(3) W. Swietoslawski, K. Zieborak, and W. Brzostowski, *Bull. Acad. Pol. Sci., Cl. III*, **5**, 305 (1957).

(4) W. Brzostowski and W. Swietoslawski, *Zh. Fiz. Khim.*, **36**, 2090 (1962).

(5) A. Blinowska, W. Brzostowski, and B. Magiera, *Bull. Acad. Pol. Sci., Ser. Sci. Chim.*, **14**, 467 (1966).

(6) P. Jordan and Ph. A. P. Lykourezos, *Int. J. Appl. Radiat. Isotop.*, **16**, 631 (1965).

(7) W. Brzostowski, *Bull. Acad. Pol. Sci., Ser. Sci. Chim.*, **9**, 441 (1961).

(8) H. G. Franke, E. Huster, and O. Kraft, *Z. Phys.*, **188**, 274 (1965); H. G. Franke, *ibid.*, **188**, 339 (1965); H. G. Franke, E. Huster, and K. H. Rohe, *ibid.*, **188**, 519 (1965).

(9) W. Brzostowski and B. Magiera, *Nukleonika*, **12**, 781 (1967).

Table I: Properties of Reagents

No.	Substance	Bp, °K	$n^{20}D$	Ebulliometric degree of purity[a]
1	*n*-Hexane	341.90	1.3750	IV
2	Acetone	329.35	1.3588	IV
3	Methyl ethyl ketone	352.71	1.3786	V
4	Methyl propyl ketone	375.51	1.3905	IV
5	Diethyl ketone	374.85	1.3926	IV

[a] As defined in ref 2b.

3. Concentrational Relationships

For **1–2** mixtures four isotherms have been studied at 308.15, 318.15, 323.15, and 328.15°K. The results obtained are shown in Figure 1. The vapor phase is richer in the less volatile component, as at higher concentrations an azeotrope is formed—*cf.* Schäfer and Rall.[10] In the concentration ranges of the measurements linear behavior is observed, so that the total vapor pressure at given T is

$$P = P_{jj} + bx_1 \qquad (1)$$

Index j denotes here the component other than hexane. Generally, in this paper quantities without indices refer to a mixture, with a single index to a component in the mixture, and with a double index to a pure component.

For the remaining pairs of components studied, *i.e.*, **1–3**, **1–4**, and **1–5**, linear behavior was also found for all isotherms. The respective experimental values of constants P_{jj} and b in eq 1 for all systems and temperatures are listed in Table II. As the linear behavior is observed for both liquid and vapor curves, along each isotherm we have the ratio y_1/x_1 constant within the experimental error, with y_1 denoting mole fraction of hexane in the vapor phase; the respective values of these ratios are listed in the same table.

For each of the systems we have determined one isobar at a pressure close to atmospheric. The results are shown in Figure 2. For our dilute solutions linear concentration behavior is observed here too, so that at any P = constant we have y_1/x_1 = constant and

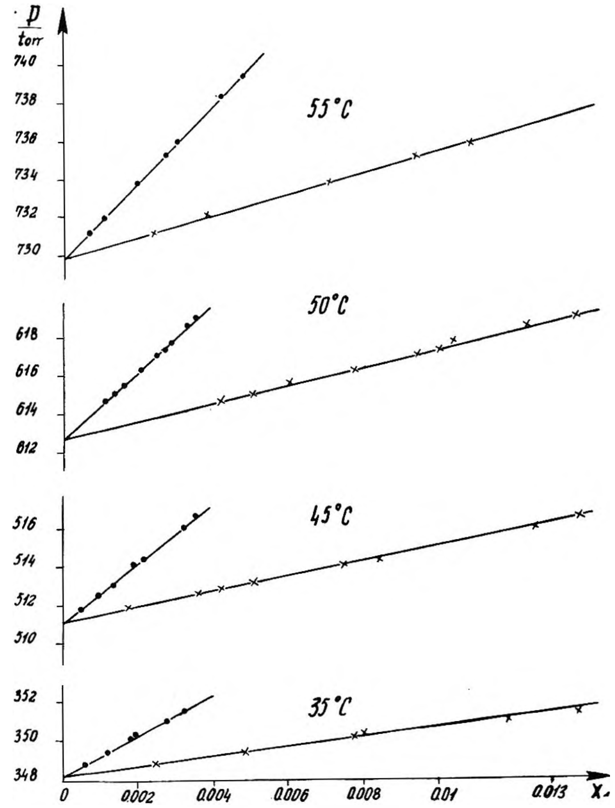

Figure 1. Isothermal vapor–liquid equilibria for **1–2** mixtures: ●, liquid points; ×, vapor points.

Table II: Constants in Eq 1

Components	T, °K	P_{jj},[a] Torr	b, Torr	y_1/x_1
1–2	308.15	348.2	1180	4.31
	318.15	511.1	1554	3.94
	323.15	612.7	1765	3.80
	328.15	729.8	2028	3.63
1–3	323.15	226.8	940	4.42
	333.15	389.8	1225	4.05
	343.15	554.6	1540	3.71
1–4	328.15	142.3	660	5.19
	343.15	257.2	950	4.70
	363.15	517.1	1650	4.12
1–5	328.15	144.8	616	5.11
	343.15	261.8	975	4.66
	363.15	526.2	1648	4.08

[a] We use 1 Torr = 0.00013332 J cm^{-3}.

$$T(x) = T_{jj} + b'x_1 \qquad (2)$$

Parameters of this equation are listed in Table III.

Consider now some consequences of eq 1. The relevant thermodynamic formula is

$$Py_if_i' = P_{ii}x_if_i \qquad (3)$$

---

(10) Kl. Schäfer and W. Rall, *Ber. Bunsenges. Phys. Chem.*, **62**, 1090 (1958).

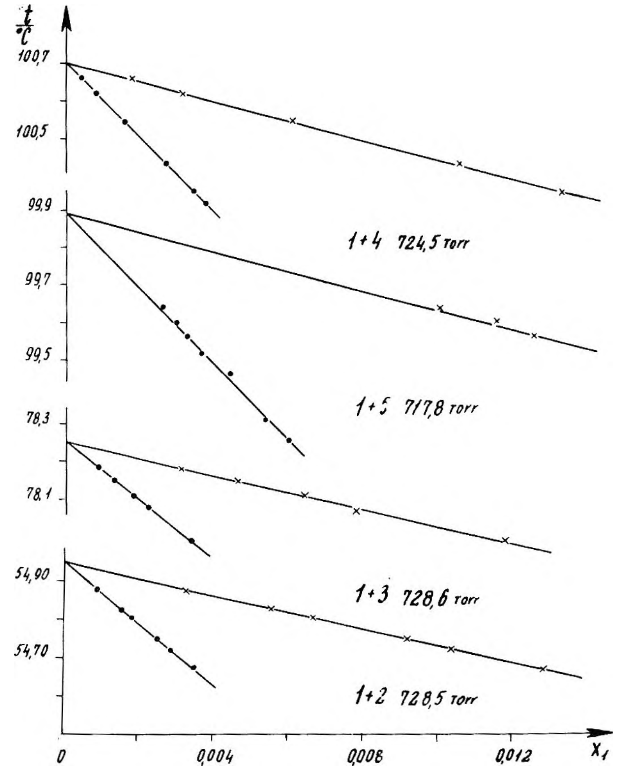

Figure 2. Isobaric vapor–liquid equilibria: ●, liquid points; ×, vapor points.

Table III: Constants in Eq 2

Components	P, Torr	T_{jj}, °K	b', °K	y_i/x_i
1-2	728.5	328.10	−80.7	3.62
1-3	728.6	351.40	−75.6	3.44
1-4	724.5	373.85	−98.5	3.84
1-5	717.8	373.04	−100.1	3.85

f_i' is the activity coefficient of ith component in the vapor phase; numerical values show that for our dilute solutions variations of f_i' with concentration may be neglected. We thus have

$$f_1 = \frac{y_1 f_1}{P_{11} x_1}(P_{jj} - b x_1) \tag{4}$$

i.e., f_1 along the isotherm varies linearly with x_1. Introduce now the excess Planck function of mixing Y^E, related to the more frequently used excess Gibbs function of mixing G^E by $Y^E = -G^E/T$, so that

$$-\frac{Y^E}{R} = x_i \ln f_i + x_j \ln f_j \tag{5}$$

where R is the gas constant. We have

$$\frac{\partial\left(-\frac{Y^E}{R}\right)}{\partial x_1} = \ln \frac{P_{jj} f_1' y_1}{P_{11} f_j' x_1} + \ln \frac{x_j}{y_j} \tag{6}$$

so that the first right-hand-side term is for our solutions concentration independent. Further

$$\frac{\partial^2\left(-\frac{Y^E}{R}\right)}{\partial x_1^2} = \frac{y_1 - x_1}{x_j y_j x_1} = \frac{b}{P x_j} \tag{7}$$

The last part of equality 7 follows, when one notices that according to the definition (5) for 1–j mixtures $\partial(-Y^E/R)/\partial x_1 = \ln(f_1/f_j)$; the Gibbs–Duhem equation gives for our case $\partial \ln f_j/\partial x_1 = -(x_1/xt)(\partial \ln P/\partial x_1)$, so that $\partial^2(-Y^E/R)/\partial x_1^2 = x_j^{-1}(\partial \ln P/\partial x_1)$. The last relation is used in conjunction with eq 1.

Zelvenskii and his collaborators in a series of studies[11–14] using ^{14}C- and ^{35}S-labeled compounds found the relative volatility β

$$\beta_{ij} = \frac{y_i x_j}{x_i y_j} \tag{8}$$

concentration independent. Using (3) and neglecting again variations of f_i' and f_j' with composition of dilute solutions, we find that the condition $\beta_{ij}(x) = \text{constant}$ leads to

$$\frac{f_i}{f_j}(x) = \text{constant} \tag{9}$$

Generally, (9) could be realized in the following cases: (I) $f_i = f_j = 1$; (II) one of the activity coefficients is different from unity, but both are concentration independent; (III) $\partial f_i/\partial x_i$ and $\partial f_j/\partial x_i$ are both $\neq 0$, with the same concentration dependence of f for both components. Case I is trivial as that of ideal solutions; case III violates the Duhem–Margules equation; the only case of interest is thus II. A further consequence of (9) under the same condition is

$$\frac{\partial \ln P}{\partial x_i} = \frac{-\partial \ln \frac{y_i}{x_i}}{\partial x_i} \tag{10}$$

The variant II for the component for which $f_i \neq 1$ leads to

$$\frac{\partial\left(-\frac{Y^E}{R}\right)}{\partial x_i} = \ln f_i \tag{11}$$

and hence

$$\frac{\partial^2\left(-\frac{Y^E}{R}\right)}{\partial x_i^2} = 0 \tag{12}$$

---

(11) Ya. D. Zelvenskii and V. A. Shalygin, *Zh. Fiz. Khim.*, **31**, 1501 (1957).

(12) Ya. D. Zelvenskii, V. A. Shalygin, and Yu. V. Golubkov, *Khim. Prom.*, **6**, 347 (1962); Ya. D. Zelvenskii and V. A. Shalygin, *ibid.*, **6**, 424 (1962).

(13) Ya. D. Zelvenskii, A. A. Titov, and V. A. Shalygin, *Khim. Tekhnol. Topliv Masel*, (4), 5 (1962); Ya. D. Zelvenskii, A. A. Titov, and V. A. Shalygin, *Khim. Tekhnol. Topl. Masel*, (3) 1 (1964).

Thus, considering the two types of experimental behavior, namely, y_i/x_i = constant and β_{ij} = constant in terms of the derivatives of the excess Planck function with composition, *i.e.*, comparing (6) with (11) and (7) with (12) we find differences in thermodynamic characteristics. It should be emphasized, however, that the differences at the level of Y^E itself are by no means pronounced. This is related to the fact that in the concentration ranges considered by us the differences between β_{ij} and y_i/x_i are small. For $x_i = 0.00001$ and $y_i/x_i = 3$, $\beta_{ij} - y_i/x_i = 0.002$ while for $y_i/x_i = 5$ the difference is 0.004. At $x = 0.01000$ the respective values of the difference are 0.060 and 4.210.

One might expect similar behavior, *i.e.*, independence of either β or y_i/x_i of composition in dilute solutions containing other components provided of course that they are zeotropic. In mixtures of benzene and hexane, studied previously, using ^{14}C-labeled benzene,[15] at the atmospheric pressure the azeotrope is formed with mole fraction of benzene $x = 0.00213$; in this case the variation of y_i/x_i with concentration is quite pronounced.

4. Activities

From (3), writing out the necessary terms explicitly

$$\ln f_i = \ln \frac{Py_i}{P_{ii}x_i} + \frac{(B_{ii} - V_{ii})(P - P_{ii}) + (2B_{ij} - B_{ii} - B_{jj})Py_j^2}{RT} \qquad (13)$$

For solutions studied we have calculated activity coefficients of components and excess Planck functions of mixtures using Tables II and III, eq 1, 2, 13, and 5. Further terms omitted in (13) are negligible. Vapor pressures of components P_{ii} were computed according to the formulas given in ref 16 for **1**, in ref 10 for **2**, and in ref 17 for **3** and **4**. Given a number of vapor pressure equations of hexane we have thus decided to rely on the critical compilation of Tatevskii, *et al.*;[16] as for acetone, we have chosen the formula of Schäfer and Rall,[10] as it is their data that we subsequently use for some comparisons. For diethyl ketone we have not found any equation in the literature. Two series of vapor pressure data, reported in ref 18 and 19, differ distinctly from one another (except giving the same normal boiling point). We have therefore performed measurements of our own, found them to agree with the Dreisbach and Shrader set,[19] and described both sets by

$$\log P_{55}(\text{Torr}) = 7.03583 - \frac{1313.9}{214.52 + t(^\circ\text{C})} \qquad (14)$$

Incidentally, the temperature dependence of vapor pressure is the same for the two isomers, *i.e.*, methyl propyl ketone and diethyl ketone. Molar volumes of liquids V_{ii} were computed from the density expansions, and second virial coefficients B_{ii} from a generalized principle of corresponding states[20] with the numerical coefficients from ref 21, *viz.*

$$\frac{B}{V_c} = 0.430 - 0.886\frac{T_c}{T} - 0.694 \times \left(\frac{T_c}{T}\right)^2 - 0.0375m\left(\frac{T_c}{T}\right)^{4.5} \qquad (15)$$

Index c refers to the critical state and m is a characteristic parameter, equal to 5 for hexane; we have computed $m(T)$ for the remaining components from the experimental values of B_{ii} for acetone,[22] methyl ethyl ketone,[23] and methyl propyl ketone;[23] for diethyl ketone we have assumed the same $m(T)$ as for its isomer.

It is still common to apply the Lewis and Randall rule, *i.e.*, to neglect the term involving the mixed virial coefficient B_{ij}. Errors resulting from such an assumption are known for hexane–chloroform mixtures from an earlier paper.[24] We have obtained B_{ij} from the same formula (15) assuming

$$T_{c_{ij}} = (T_{c_{ii}}T_{c_{jj}})^{0.5} \qquad (16)$$

$$V_{c_{ij}} = 0.125(V_{c_{ii}}^{1/3} + V_{c_{jj}}^{1/3})^3 \qquad (17)$$

$$m_{ij} = 0.5(m_{ii} + m_{jj}) \qquad (18)$$

The last of the combining rules has been recommended by Cruickshank, *et al.*[25] The results of calculations for hexane are shown in Figure 3.

Qualitatively, as expected, deviations from ideality decrease with decreasing polarity of ketone, *i.e.*, with substitution of one ketone solvent by another with a larger aliphatic part of the molecule. We notice that the values for the two isomers studied at a given temperature are relatively close to one another. Adequate quantitive description does not appear feasible at the present stage of the liquid-state theory.

Consider now in some detail values of $\lim_{x_1 \to 0} \ln f_1$, confining ourselves for a while to isotherms of **1**–**2** mixtures. First, by extrapolating the data shown in

---

(14) A. A. Efremov and Ya. D. Zelvenskii, *Zh. Prikl. Khim. (Leningrad)*, **38**, 2513 (1965).

(15) W. Brzostowski, *Bull. Acad. Pol. Sci., Ser. Sci. Chim.*, **9**, 471 (1961).

(16) V. M. Tatevskii, Ed., "Fizikokhimicheskie svoistva individualnykh uglevodorodov," Gostoptekhizdat, Moscow, 1960.

(17) T. E. Jordan, "Vapour Pressure of Organic Compounds," Interscience, New York, N. Y., 1954.

(18) D. R. Stull, *Ind. Eng. Chem.*, **39**, 514 (1947).

(19) M. Dreisbach and K. Shrader, *ibid.*, **41**, 2879 (1949).

(20) E. A. Guggenheim and C. J. Wormald, *J. Chem. Phys.*, **42**, 3775 (1965).

(21) M. L. McGlashan and D. J. B. Potter, *Proc. Roy. Soc., Ser. A*, **267**, 478 (1962).

(22) J. S. Rowlinson, *Trans. Faraday Soc.*, **45**, 974 (1949).

(23) J. K. Nickerson, K. A. Kobe, and J. J. McKetta, *J. Phys. Chem.*, **65**, 1037 (1961).

(24) W. Brzostowski and L. Verhoye, *Rocz. Chem.*, **42**, 507 (1968).

(25) A. J. B. Cruickshank, M. L. Windsor, and C. L. Young, *Trans. Faraday Soc.*, **62**, 2341 (1966).

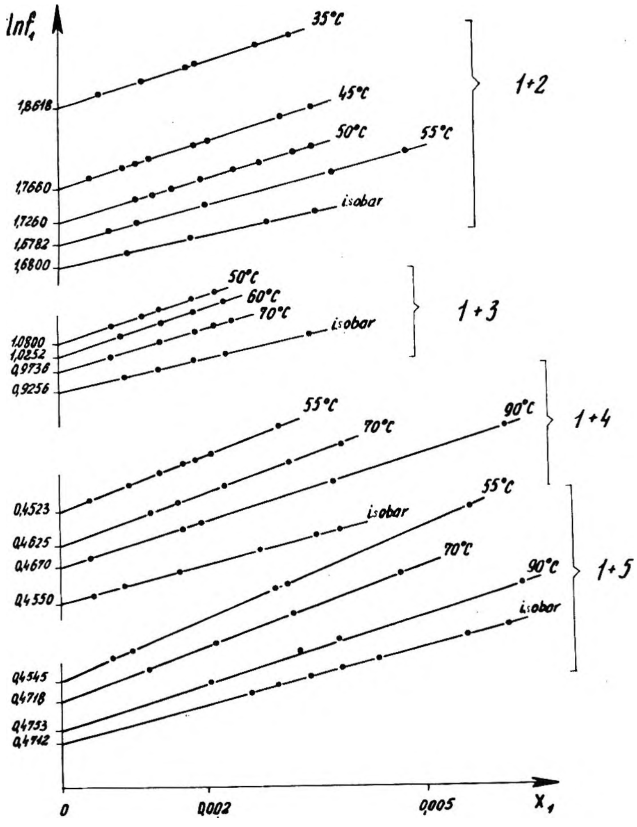

Figure 3. Activity coefficients of hexane in the liquid phases as functions of composition.

Figure 3, we obtain the values given in the second column of Table IV.

Table IV: Values of $\mathrm{Lim}_{x_1 \to 0}\,\mathrm{Ln}\,f_1$ for **1**–**2** Mixture

T, °K	$\mathrm{Lim}_{x_1\to 0}\ln f_1$				
	Exptl	Ref 10,26	Eq 20	Eq 20a	Eq 27
308.15	1.862	1.894	1.812	1.829	1.866
318.15	1.766	1.810	1.746	1.767	1.770
323.15	1.726	1.752	1.696	1.719	1.730
328.15	1.678	1.706	1.648	1.668	1.681

Another source of information on ln f_1 is the results of Schäfer and Rall.[10,26] These authors have measured vapor–liquid equilibria of concentrated **1**–**2** mixtures at a number of temperatures, calculated activity coefficients, and correlated their results with a Redlich–Kister type equation with explicit temperature dependence of the constants. Using their equation, we have obtained the values given in the third column of Table IV. All these values are higher than ours, but explanation of this is quite easy. Using the Redlich–Kister expansion we have made inter- and extrapolation with respect to temperature (except for 318.15°K). What is more important, we make concentration extrapolation; the actual range of Schäfer and Rall experiments at, say, 318.15°K was $0.0342 \leqslant x_1 \leqslant 0.9343$.

Using the data for both dilute and concentrated benzene–hexane mixtures,[15] calculations were made[27] which show the hazard involved in concentration extrapolation. Ideality in the Raoult sense cannot be assumed for dilute solutions either, as Edwards and Encina[28] have found for hexane–isooctane solutions with the mole fraction of isooctane $x \leqslant 0.00118$. Vernier and his colleagues[29] have obtained values of $\lim_{x_i \to 0} f_i$ for a number of systems by gas–liquid chromatography; when possible, they compared their results with those extrapolated from vapor–liquid equilibria of concentrated solutions; in some cases the differences were striking. It seems now, therefore, a safe conclusion that extrapolation from concentrated solutions should be avoided. When not, the behavior of dilute solutions but the limiting values alone are needed, then the chromatographic method is an alternative to such a method as used in the present work.

We conclude this section with comments on the Ellis and Jonah[30] method of obtaining $\lim_{x_i \to 0} f_i$. Rearranging eq 13 and introducing for the isothermal case the parameter

$$\Delta P = P - x_iP_{ii} - x_jP_{jj} \tag{19}$$

they have obtained the relation

$$\begin{aligned}\lim_{x_i\to 0} f_i = \frac{1}{P_{ii}}\Bigg\{\left[P_{ii} + \left(\frac{\Delta P}{x_ix_j}\right)_{x_i\to 0}\right] \times \\ \left(1 + P_{jj}\frac{B_{jj} - V_{jj}}{RT_{jj}}\right) - P_{jj}^2\frac{B_{jj} - V_{jj}}{RT_{jj}}\Bigg\} \times \\ \exp\left[\frac{(P_{ii} - P_{jj})(V_{ii} - B_{ii}) + (2B_{ij} - B_{ii} - B_{jj})P_{jj}}{RT_{jj}}\right]\end{aligned} \tag{20}$$

where $(\Delta P/x_ix_j)_{x_i\to 0}$ results from extrapolation of $P(x)$ data. Neglecting a term which is usually close to unity

$$\begin{aligned}\lim_{x_i\to 0} f_i = \frac{1}{P_{ii}}\Bigg\{\left[P_{ii} + \left(\frac{\Delta P}{x_ix_j}\right)_{x_i\to 0}\right] \times \\ \left(1 + P_{jj}\frac{B_{jj} - V_{jj}}{RT_{jj}}\right) - P_{jj}^2\frac{B_{jj} - V_{jj}}{RT_{jj}}\Bigg\}\end{aligned} \tag{20a}$$

We have performed calculations using eq 20 and 20a. The results are listed also in Table IV. We notice that (20a) does actually give values closer to experimental ones. This might be related to approximate character of calculations of second virial coefficients, in particular to the use of combining rules 16–18.

Analogous calculations using (20) and (20a) were also

---

(26) W. Rall and Kl. Schäfer, *Ber. Bunsenges. Phys. Chem.*, **63**, 1019 (1959).

(27) W. Brzostowski, *Rocz. Chem.*, **40**, 2021 (1966).

(28) J. Edwards and M. V. Encina, *Z. Naturforsch. A*, **25**, 45(1970).

(29) P. Vernier, C. Raimbault, and H. Renon, *J. Chim. Phys. Physicochim. Biol.*, **66**, 429 (1969).

(30) S. R. M. Ellis and D. A. Jonah, *Chem. Eng. Sci.*, **17**, 971 (1962).

made for **1–3**, **1–4**, and **1–5** mixtures. The pattern emerging is very much the same as for the **1–2** system; we therefore omit the respective numerical data. On the other hand, we have also applied the Ellis and Jonah[30] procedure for the isobaric case, with their parameter

$$\Delta T = T - x_i T_{ii} - x_j T_{jj} \tag{21}$$

The equation resulting from (13) obtained by Ellis and Jonah is in this case

$$\lim_{x_i \to 0} f_i = \frac{P_{jj}}{P_{ii}}\left\{1 - \frac{H_{jj}{}^{Z}}{RT_{jj}{}^{2}}\left[T_{ii} - T_{jj} + \left(\frac{\Delta T}{x_i x_j}\right)_{x_i \to 0}\right]\right\}\left[1 + P_{jj}\frac{B_{jj} - V_{jj}}{RT_{jj}}\right] \times \exp\left[\frac{(P_{ii} - P_{jj})(V_{ii} - B_{ii}) + (2B_{ij} - B_{ii} - B_{jj})P_{jj}}{RT_{jj}}\right] \tag{22}$$

Vaporization enthalpy $H_{jj}{}^{Z}$ of component j at its boiling point was computed using the Clausius–Clapeyron equation and the same $P_{jj}(T)$ relations as before. The results are shown in Table V.

Table V: Values of $\text{Lim}_{x_1 \to 0}$ Ln f_1 for Isobars

		$\text{Lim}_{x_1 \to 0}$ ln f_1		
			Eq 22	
Components	P, Torr	Exptl	Exponential term neglected	Vapor-phase nonideality neglected
1–2	728.5	1.680	1.660	1.685
1–3	728.6	0.926	0.873	0.854
1–4	724.5	0.455	0.418	0.358
1–5	717.8	0.471	0.447	0.387

5. Heat of Mixing

Schäfer and Rohr[31] have measured enthalpies of solution of hexane in acetone at 253.15 and 293.15°K. They have obtained the limiting values, which they denote by $({}^{i}W_L)_{A_\infty}$, related to the excess heat of mixing H^E by

$$({}^{i}W_L)_{A_\infty} = -\lim_{x_1 \to 0} \frac{H^E}{x_1} \tag{23}$$

From their calorimetric value at 293.15°K, we have $(RT^2)^{-1}(\lim_{x_1 \to 0}(H^E/x_1)) = 0.0094\ \text{deg}^{-1}$.

In our experimental range the dependence of $\lim_{x_1 \to 0}$ ln f_1 on temperature happens to be linear. Assuming that the linear relationship extends down to 293°K and using the thermodynamic formula

$$\frac{\lim\limits_{x_1 \to 0} \dfrac{H^E}{x_1}}{RT^2} = -\frac{\partial \lim\limits_{x_1 \to 0} \ln f_1}{\partial T} \tag{24}$$

we have obtained the value 0.0093 deg^{-1}. If instead of values in the second column of Table IV, the values from a version of the lattice theory (last column of the same table, but *cf.* next section) are used, the numerical result is exactly the same. It is comforting to find such an agreement of results obtained at different laboratories by two widely different methods.

6. Lattice Theory

From various possible approaches, we have chosen the quasilattice theory of solutions, as dealing in a straightforward way with combinational contributions and effect of size of molecules on thermodynamic functions.

We began with lattice theory equations such as are in use for the conventional range of concentrations. The results were not entirely satisfactory. It has to be remembered that the theory assumes the number of mixed pairs proportional to the product of mole fractions $x_i x_j$. This does not appear to be a good approximation for dilute solutions—*cf.* section 1 of this paper. Better results were obtained assuming the number of mixed pairs to be given simply by mole fraction of the dilute component x_i as suggested by Guggenheim in Chapter V of ref 32. Combining such an energetic term with combinatorial terms and denoting the dilute component by 1 we write

$$-\frac{Y^E}{R} = x_1 \ln \frac{\phi_1}{x_1} + x_j \ln \frac{\phi_j}{x_j} + \frac{w_1 x_1}{kT} \tag{25}$$

where k is the Boltzmann constant, w_1 the energetic parameter, and ϕ's are segment fractions expressed in terms of numbers of segments per molecule, r_i

$$\phi_i = \frac{r_i x_i}{r_i x_i + r_j x_j} \tag{26}$$

The combinatorial contribution is thus the usual lattice theory expression for molecules of different sizes with the coordination number z assumed to be infinity (*cf.* ref 32, Chapter X) and the ideal entropy of mixing already included in the logarithmic terms. If one assumes $r_i = r_j$ eq 25 reduces to a formula equivalent to relations used by Guggenheim in § 5.02 of his monograph.[32] Consequently (*cf.* definition 5) eq 25 gives

$$\ln f_1 = 1 - \frac{r_1}{r_1 x_1 + r_j x_j} + \ln \frac{r_1}{r_1 x_1 + r_j x_j} + \frac{w_1}{kT} \tag{27}$$

Calculations have been made using eq 27, as well as the corresponding formula for ln f_j, for all systems studied. A segment was assumed to consist of a carbon atom, with hydrogen atoms (or an oxygen atom) attached to it; thus $r_1 = 6$, $r_2 = 3$, $r_3 = 4$, and $r_4 = r_5 = 5$. For each isotherm (or isobar) an appropriate value of w_1/kT was assumed. The differences between experi-

---

(31) Kl. Schäfer and F. J. Rohr, *Z. Phys. Chem.* (*Leipzig*), **24**, 130 (1960).

(32) E. A. Guggenheim, "Mixtures," Clarendon Press, Oxford, 1952.

mental and calculated values were 3% in the worst cases. For 1–2 mixtures, dealt with in some detail above, we show the limiting values of $\ln f_1$ in the last column of Table IV; small differences result from the fact that the $\partial \ln f_1/\partial x_1$ derivative is slightly larger for the experimental set of data than for the set of data coming from eq 27. In any case, our calculations prove that what might be called the model of dilute solutions of molecules of different sizes—eq 25 and its consequences—render adequate representation of the experimental data.

7. Some Concluding Remarks

Throughout this paper we have been contrasting dilute solutions to concentrated ones. From the considerations in section 4, for instance, we have inferred that errors might occur if values of $\lim_{x_i \to 0} f_i$ are obtained by extrapolating data from concentrated solutions. Our quasilattice model of section 6 is also specifically for dilute solutions. This is not entirely meaningful until we specify what we mean by "dilute" and "concentrated." Qualitatively, diluteness may be related to the phenomenon customarily referred to in the literature as "breaking up the structure of a liquid" by introducing another component. We could then characterize diluteness in terms of preservation of essential features of the structure of the pure solvent; thus, for instance, experimentally accessible intermolecular distances could be used. The answers, however, would have to depend on the particular system studied and also on temperature. Clearly it would be difficult to give a general difinition of diluteness. If for practical purposes we would still insist on having one, we could follow the suggestion of Guggenheim,[32] reiterated earlier by one of us.[27] A dilute liquid mixture would then be such where $x_i < 0.01$.

Acknowledgment. For valuable discussions and advice, the authors wish to acknowledge their indebtedness to the late Professor Wtadystaw Malesiński.

Heats of Formation of Nitroaromatics. Group Additivity for Solids

by Robert Shaw

Physical Sciences Division, Stanford Research Institute, Menlo Park, California 94025

(Received March 22, 1971)

Publication costs assisted by Stanford Research Institute

Heats of formation for some solid nitroaromatic compounds have been estimated by group additivity, using both ideal gas group values with measured heats of sublimation and solid group values.

Heats of formation are the basis of many chemical thermodynamic and kinetic calculations. The ever increasing range of compounds of interest places a premium on fast, accurate, simple methods of estimation. Such a method, group additivity, has already been successfully applied to the estimation of heats of formation, entropies, and heat capacities from 300 to 1500°K of ideal gases[1] and heat capacities of liquids.[2] In principle, there are two methods of using group additivity to determine heats of formation of solids. If the groups are available, then the heat of formation of the ideal gas can be calculated. If the heat of sublimation is known, then the heat of formation of the solid follows. The second method is to develop group values for solids and to use these directly to calculate the required heat of formation. The heats of formation of some solid nitroaromatic compounds present an interesting example of the two approaches. The results suggest that the direct approach of using group values for solids is the better method at present.

The Ideal Gas Method

The heat of formation of a nitroaromatic compound in the ideal gas state requires that the C_B–NO_2 group be known (where C_B represents an aromatic, *i.e.*, benzene carbon atom). This group was not given in the recent ideal gas group additivity review.[1] The group may be obtained from the heat of formation of any nitroaromatic compound in the ideal gas state if the other groups are known. For example, $\Delta H_f^\circ(\mathrm{PhNO_2}) = 5(C_B\text{–}H) + 1(C_B\text{–}NO_2) = 16.9$ kcal mol^{-1} (Table I). From the known value of $(C_B\text{–}H) =$

---

[1] S. W. Benson, F. R. Cruickshank, D. M. Golden, G. R. Haugen, H. E. O'Neal, A. S. Rodgers, R. Shaw, and R. Walsh, *Chem. Rev.* 69, 279 (1969).

[2] R. Shaw, *J. Chem. Eng. Data*, 14, 461 (1969).

Table I: Measured and Estimated Heats of Formation of Various Compounds at 298°K (in kcal mol^{-1})

Compd	ΔH_f (crystal)	Ref	ΔH_f (liquid)	Ref	ΔH_{subl}	Ref	ΔH_{vap}	ΔH_f (ideal gas)	C_B–NO_2 group (ideal gas)	Estd ΔH_f(ideal gas)	$\Delta\Delta H_f$ (ideal gas), obsd − estd	Estd ΔH_f (crystal)	$\Delta\Delta H_f$ (crystal), obsd − estd
Nitrobenzene			3.8	9			13.1[a]	16.9	0.4	19.5	−2.6		
2,2′,4,4′,6,6′-Hexanitrostilbene (HNS)	13.9	5			43.0 at 457°K	7		56.9	2.7	58.6	−1.7		
trans-Stilbene (TS)	32.7	5			20.7	4		53.4					
2,4,6-Trinitrotoluene (TNT)	−15.4	5			28.3	5		12.9	3.2	12.2	0.7	−15.0	−0.4
					24.4	6		9.0	1.9	12.2	−3.2		
2,4,6-Trinitroaniline (TNA)	−17.8	9			27.7 at 350°K	7		9.9		12.9	−3.0	−18.0	+0.2
1,3-Diamino-2,4,6-trinitrobenzene (DATB)	−29.2	8			33.5 at 358°K	7		4.3		6.9	−2.6	−27.0	−2.2
1,3,5-Triamino-2,4,6-trinitrobenzene (TATB)	−36.9	8			40.2 at 426°K	7		3.3		0.9	2.4	−36.0	−0.9
m-Dinitrobenzene (MDB)	−6.2	9										−6.0	−0.2
1,3,5-Trinitrobenzene (TNB)	−9.6	3										−9.0	−0.6
p-Nitroaniline (PNA)	−10.0	9										−12.0	+2.0
2,4-Dinitroaniline (DNA)	−22.4	9										−15.0	−7.4
2,6-Dinitrotoluene (DNT)	−10.5	9										−12.0	+1.5
HNS minus TS	−18.8							3.5	3.5	0.6	2.9	−18.0	−0.8

[a] From the data given by Timmermans,[10] ΔH_{vap} = 11.34 kcal mol^{-1} at 450°K. For liquids like nitrobenzene,[2] C_p(liquid) − C_p(gas) = 12 cal mol deg^{-1}; so ΔH_{vap}(298°K) = 11.3 + 12(450 − 298) = 13.1 kcal mol^{-1}.

3.3 kcal mol^{-1}, (C_B–NO_2) = 16.9 − 16.5 = 0.4 kcal mol^{-1}. In Table I[2-10] the heats of formation of several nitroaromatic compounds in the ideal gas state are calculated from the measured heats of formation of the solid and the measured heats of sublimation. In cases where the heat of sublimation is not measured at 298°K, there should be a correction for the differences in heat capacities of the solid and ideal gas. The data required to make these corrections are not available but in general it is expected that the corrections will be small and can be neglected. From the heats of formation of each compound in the ideal gas state, a value for the group C_B–NO_2 (ideal gas) has been derived (Table I). A weighted-average value (C_B–NO_2 (ideal gas)) = 3.0 kcal mol^{-1} was used, and a heat of formation was estimated for each compound. In Table I the difference between observed and estimated heat of formation in the ideal gas state is ±3 kcal mol^{-1}.

The Group Additivity for Solids Method

The larger number of compounds for which the heat of formation of the solid has been measured makes the group additivity for solids an attractive method. From the measured data (Table I), groups were derived by inspection. The values for the groups are (C_B–H) = 0, (C_B–NO_2) = −3, (C_B–NH_2) = −9, and (C_B–CH_3) = −6 kcal mol^{-1}. If the groups had been derived statistically, there would probably be a slight improvement, but the convenience of having (C_B–H) = 0 and integral values for the other groups would be lost in the process. Using these groups, the heats of formation in the solid state for a number of compounds have been calculated. With only one exception (2,4-dinitroaniline), the differences between observed and estimated values are small and in the range expected for group additivity. The exception is interesting because it suggests that there is something wrong with the original data. Consider the series *p*-nitroaniline (PNA), −10.0 kcal mol^{-1}; 2,4-

---

(3) E. S. Domalski, National Bureau of Standards, Washington, D. C., private communication, 1970.

(4) J. J. Englesman, Ph.D. Thesis, Vrije University, Amsterdam, 1955.

(5) S. Marantz and G. T. Armstrong, *J. Chem. Eng. Data*, **13**, 455 (1968).

(6) I. Nitta, S. Seki, M. Momotani, and K. Sato, *Nippon Kagaku Zasshi*, 71, 378 (1950).

(7) J. M. Rosen and C. Dickenson, *J. Chem. Eng. Data*, **14**, 120 (1969).

(8) C. H. Shomate, Naval Ordnance Test Station, China Lake, Calif., private communication, 1970.

(9) D. R. Stull, E. F. Westrum, and G. C. Sinke, "The Chemical Thermodynamics of Organic Compounds," Wiley, New York, N. Y., 1969, pp 671–685.

(10) J. Timmermans, "Physico-Chemical Constants of Pure Organic Compounds," Vol. I and II, Elsevier, New York, N. Y., 1960 and 1965.

dinitroaniline (DNA), −22.4 kcal mol^{-1}; and 2,4,6-trinitroaniline (TNA), −17.8 kcal mol^{-1}. This series is made up by progressively replacing a (C_B–H) with a (C_B–NH_2) group and so the values should form a reasonably progressive series but do not. Because of the good fit to the data for the other amino-nitroaromatics, we conclude that the reported heat of formation of DNA may be in error.

Conclusion

In general, the fit between observed and estimated values suggests that the principle of group additivity can be successfully applied to the heats of formation of solids. At present this approach is more convenient than using ideal gas groups together with heats of sublimation.

Acknowledgments. I thank E. L. Capener, whose enquiries resulted in this research. I am also pleased to thank S. W. Benson, E. S. Domalski, Milton Finger, W. S. McEwan, E. J. McKinney, D. L. Ornellas, J. M. Rosen, Julius Roth, C. H. Shomate, and B. A. Stott for stimulating discussion and for their efforts in finding the origin of the data for DATB and TATB.

Vacuum Vaporization Studies of Lithium Fluoride Single Crystals

by D. L. Howlett, J. E. Lester, and G. A. Somorjai*

Inorganic Materials Research Division, Lawrence Berkeley Laboratory, Department of Chemistry, University of California, Berkeley, California 94720

(Received June 30, 1971)

Publication costs assisted by the U. S. Atomic Energy Commission

The vacuum sublimation kinetics of the (100) face of lithium fluoride single crystals are investigated in the temperature range of 690 to 820° by means of a microbalance. Pure LiF sublimes at about one-sixth of the calculated maximum rate. It has an activation enthalpy of sublimation of 66.7 kcal/mol that is equal to the equilibrium enthalpy of sublimation (ΔH_s = 66.3 kcal/mol). The dependence of the sublimation rates on a calcium ion impurity (Ca^{2+}) that was incorporated in the LiF single crystals is studied. Calcium-doped samples have lower sublimation rates than the sublimation rates of pure LiF crystals. The sublimation rates are not independent of the dislocation density in the various sublimed crystals. The results of this study when combined with the sublimation kinetics studies of other alkali halides (NaCl, KCl) show that surface nonstoichiometry rather than ion diffusion is the rate-controlling process of the sublimation.

Introduction

Alkali halides represent an important group of ionic crystals. They have cubic structures and have melting points in the range of 988° for NaF to 450° for LiI. Monomer and dimer molecules are the vapor species formed when NaCl and KCl sublime. LiF has an appreciable (~4 mol %) trimer concentration in the vapor phase in addition to the monomer and dimer concentrations.[1]

The sublimation kinetics of NaCl have been studied[2] to reveal the mechanism by which ion pairs break away at the subliming surface. The activation enthalpies of sublimation have been determined, and correlations between the sublimation rate and both the divalent cation impurity concentration and the concentration of dislocations in NaCl crystals have been established. To further elucidate the sublimation mechanism of alkali halides and to verify whether the sublimation characteristics of other alkali halides are similar to that of NaCl the sublimation kinetics of LiF single crystals have been investigated. We have measured the vacuum sublimation rate of the (100) crystal face of LiF as a function of temperature. We have also studied the sublimation rate as a function of calcium ion impurity (Ca^{2+}) in the crystal lattice and the effect of dislocation density on the sublimation rates.

Experimental Section

The samples used in this study were pure and impurity-doped lithium fluoride single crystals. The pure and the calcium-doped lithium fluoride crystals were obtained from the Harshaw Chemical Corp.

Studies of the vacuum sublimation of other alkali halides indicate marked effects of small amounts of selected impurities on the sublimation characteristics.[2] The results of spectroscopic analyses of the pure and doped LiF crystals are given in Table I. Analysis was

[1] G. M. Rothberg, M. Eisenstadt, and P. Kusch, *J. Chem. Phys.*, **30**, 517 (1959).

[2] J. E. Lester and G. A. Somorjai, *ibid.*, **49**, 2940 (1968).

Table I: Spectroscopic Analysis for LiF Crystals Used in Experiments[a]

Crystal impurity	Pure LiF	Ca-doped LiF
Ag	ND[b]	1
Al	25	25
B	1	1
Ba	50	50
Ca	50	250
Cu	1	1
Fe	20	20
Mg	22	10
Pb	ND	ND
Si	100	10
Sn	ND	ND

[a] All concentrations are in ppm unless otherwise noted. [b] ND = not detected.

made only for possible cation impurities. Other work on alkali halides has shown that monovalent anion impurities at various concentration levels had no effect on the sublimation rate.[3] Although the accuracy of the analysis is ±30%, this was judged to be satisfactory, since previous alkali halide studies showed detectable changes in the sublimation rate only with order of magnitude changes in impurity concentration.[2]

Lithium fluoride was obtained as large single crystals, and these were cleaved to prepare the samples for sublimation. The samples used in sublimation runs were about 2 × 3 × 5 mm.

To clean the crystal of oil films and possible chemical contamination each lithium fluoride sample was rinsed in a 90% methanol-10% water solution. The sample crystal to be sublimed was then wrapped in a nonreactive (3-mil Pt) metal foil leaving only the face to be sublimed exposed.

A correlation between sublimation rate and dislocation density has been found in studies of the vacuum sublimation of sodium chloride. To measure the dislocation density of lithium fluoride an etching solution, consisting of equal parts concentrated hydrofluoric acid and glacial acetic acid and a 1 vol. % of concentrated HF saturated with $FeCl_3$, was used that specifically develops dislocations as square etch pits.[4] The dislocation etch pits were counted before and after the sublimation. The crystal faces did not have a uniform distribution of etch pits; rather there were regions of large and small etch pit densities. The average value of the etch pit densities could, however, be calculated. A detailed description of the vacuum and microbalance systems is found elsewhere.[3]

The background pressure was kept much lower than the apparent pressure from the subliming sample ($p = 7.4 \times 10^{-6}$ Torr) by at least a factor of 100 (10^{-6} Torr) so that molecules, reactive or nonreactive, in the ambient would rarely impinge on the subliming surface. The capacity of the balance[3] is 1 g, and weight changes as small as 1 μg have been detected. In determining rate through weight loss per time measurements, the balance was used as a null device. A set of wire calibration weights was used to determine the sensitivity of the balance; this sensitivity was about 13.5 mV/mg.

Oven calibration to determine temperature gradients was carried out and results similar to those obtained previously[3] were obtained. After a constant temperature was attained in the hot zone the sample was lowered into the oven and hooked to the balance. Weight loss measurements were then taken. The sublimation runs at the slowest rates took about 7 hr (rate = 3×10^{-2} mg min^{-1} cm^{-2}), and at the fastest about 20 min (rate = 7×10^{-1} mg min^{-1} cm^{-2}).

The measurements carried out using the vacuum microbalance give the absolute weight loss of a subliming crystal as a function of time. This weight loss is normalized by dividing the rate of weight loss by the geometrical surface area of the subliming crystal face. The rate of weight loss, R_s (mg cm^{-2} min^{-1}), is then plotted as the logarithm of R_s *vs.* the reciprocal temperature, $1/T$ (°K). This plot gives a straight line with slope $-\Delta H_s^*/R$, where ΔH_s^* is the activation enthalpy of sublimation.

Experiments in this study utilized three crystal samples from each of the pure LiF single crystals being used in the sublimation runs. Results reported for the evaporation rates of each type of crystal are the average of those sublimed.

Results

A plot of the vacuum sublimation rate, log R_s, *vs.* $1/T$ (°K) for pure LiF (undoped) is shown in Figure 1 along with a curve of the logarithm of the maximum sublimation rate for LiF for comparison. The maximum sublimation rate curve was calculated from the equilibrium vapor pressure data of Pugh and Barrow[5] and the kinetic theory using the formula $R_{max} = P(2\pi mRT)^{-1/2}$ where T is the absolute temperature, R is the gas constant, and m is the molecular weight of the subliming species taken as the weighted average of the various LiF vapor molecules. The weighting factors were obtained from the work of Rothberg, Eisenstadt, and Kusch.[1] The same figure shows the dependence of sublimation rate on temperature for Ca-doped LiF crystals.

In other studies of alkali halide vacuum sublimation the etch pit density at the subliming face was found to influence the rate (*i.e.*, the NaCl sublimation rate increased with increase in etch pit density). Unlike

---

(3) J. E. Lester, Ph.D. Thesis, University of California, Berkeley, 1967.

(4) J. C. Fischer, W. G. Johnston, R. Thomson, and T. Vreeland, "Dislocations and Mechanical Properties of Crystals," New York, N. Y., 1956, p 119.

(5) A. C. P. Pugh and R. F. Barrow, *Trans. Faraday Soc.*, 54, 671 (1958).

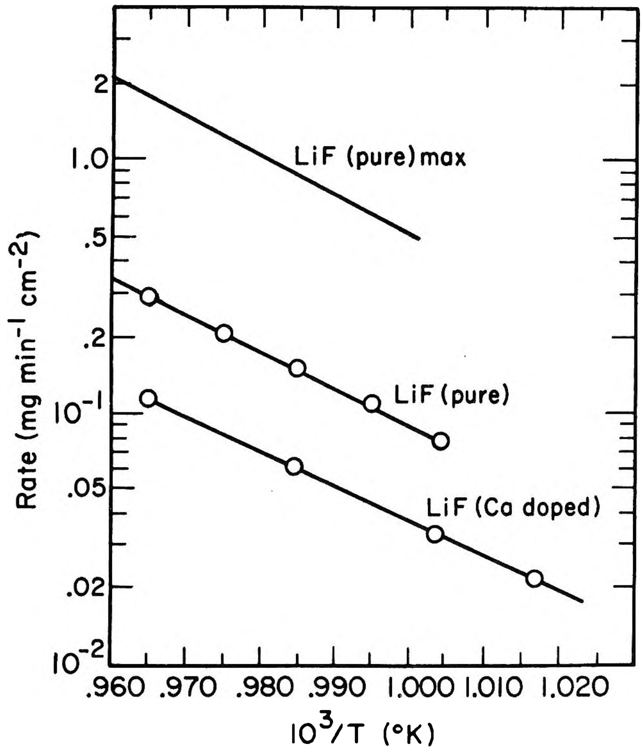

Figure 1. Sublimation rates of pure and Ca-doped LiF crystals.

the etch pit density for NaCl, that for LiF was found to decrease during an experimental run. The etch pit density decreased between 1 × 10^7 and 5 × 10^7 per cm^2 to 1 × 10^6 and 6 × 10^6 per cm^2. The sublimation rates could be reproduced for all of the LiF crystals regardless of their initial dislocation density, indicating that the dislocation density had adjusted to a constant level shortly after the sublimation experiment commenced. Thus, the variation of the dislocation density in the different samples had no effect on the sublimation rates.

The activation enthalpy of sublimation, ΔH_s^*, was calculated for each crystal from the experiment. It should be noted that absolute weight loss measurements determine an average activation enthalpy (per mole of vapor) for the combined vapor flux (monomers, dimers, and trimers).

Discussion

The sublimation characteristics of lithium fluoride single crystals are summarized by the following statements.

(1) The vacuum sublimation rates of the (100) crystal faces of high-purity lithium fluoride were lower by about a factor of 6 ($\alpha_s(730°) = 0.17$) than the vacuum sublimation rates that can be calculated using the equilibrium vapor pressure data.[5] The average activation enthalpy of sublimation (*i.e.*, the weighted average of monomer, dimer, and trimer activation enthalpies) determined by the microbalance studies is $\Delta H_s^* = 66.7$ kcal/mol. This is comparable to the equilibrium enthalpy of sublimation, $\Delta H_s = 66.3$ kcal/mol.

(2) The sublimation rates of Ca-doped (250 ppm) LiF samples are reduced with respect to those of pure LiF crystals (α_s (730°) = 0.07). The activation enthalpy of sublimation is $\Delta H_s^* = 62.6$ kcal/mol for these doped crystals.

(3) High purity LiF crystals that had different dislocation densities (in the range of 10^6 to 10^7 dislocations/cm^2) exhibited identical sublimation rates.

The vacuum sublimation rates of high-purity LiF crystals are lower than the maximum rates, similar to the behavior of NaCl and KCl crystals. Also, the activation enthalpies of sublimation are nearly identical with the enthalpies of sublimation for all of these alkali halide crystals. It would appear that the sublimation mechanisms of these ionic compounds should be similar.

Ca-doped LiF and NaCl exhibit *lower* sublimation rates than that of the undoped crystals. On the other hand, Ca-doped KCl crystals have been found to have *higher* sublimation rates.[6] Ca-doping introduces cation vacancies in the alkali halide crystals in addition to the equilibrium concentration of vacancies that are present in the pure crystal. Although the calcium concentration is in the parts per million range, it has a major effect on the rates of sublimation. The calcium concentration in the crystals is too low to block a large fraction of the surface to prevent sublimation, and there is no experimental evidence for the accumulation of calcium at the surface. Therefore it appears that calcium ions in the alkali halide crystals influence the sublimation rate by changing the vacancy concentrations at the surface, *i. e.*, the surface stoichiometry.

There is strong evidence from the work of Gallon, *et al.*,[7] that the chemical composition of different alkali halide crystal surfaces does not reflect the stoichiometry of the bulk phase. Auger electron spectroscopy studies of LiF and NaF surfaces freshly cleaved in ultrahigh vacuum or cleaved in air have detected the presence of much higher intensity Auger peaks due to the halogen than to the alkali metal.[7] Although calibration of the intensity peaks has not been carried out to permit quantitative surface chemical analysis, the data indicate that the halogen atom concentration is higher than the metal atom concentration.

For KCl, on the other hand, Auger electron spectroscopy studies showed roughly equal intensity peaks due to potassium and chlorine atoms at the surface. Clearly, as indicated by these studies, the alkali metal

---

(6) C. Grimes, J. Hinkley, and J. E. Lester, *J. Chem. Phys.*, to be published.

(7) T. E. Gallon, I. G. Higginbotham, M. Prutton, and H. Tokutaka, *Surface Sci.*, 21, 224 (1970).

concentration was much higher at the KCl surface than at the LiF and NaF surfaces. Mass spectrometric studies[7] have also revealed that upon cleavage the freshly created surface dissociates and alkali metal and halogen vapor atoms are detectable. Dissociation appears to be most marked for LiF and very small in the case of KCl.

These investigations indicate that nonstoichiometry exists at the surface of alkali halides. LiF, NaF, and NaCl (100) surfaces appear to be richer in halogen than in alkali metal atoms; *i.e.*, they are likely to have a larger concentration of cation vacancies than anion vacancies. The introduction of calcium ions into these crystal lattices creates even more cation vacancies and results in an even greater deviation from stoichiometry. Since these ionic crystals sublime as ion pairs (NaCl, Na_2Cl_2, LiF, Li_2F_2, etc.), nonstoichiometry at the subliming surface could readily decrease the sublimation rates. This way, the lowering of the sublimation rates of NaCl and LiF when doped with calcium can be rationalized.

The effect of Ca-doping on the number of cation vacancies in a crystal can also explain the effect of Ca-doping on the sublimation rate of KCl where there was an *increase* in the sublimation rates obtained[6] If one assumes that the potassium atom concentration is greater than the chlorine atom concentration at the (100) surface, there is then a nonstoichiometry that implies a larger surface concentration of anion vacancies than cation vacancies. [The relative intensities of Auger peaks from the potassium and chlorine atoms depend on the probabilities of the various Auger transitions. The roughly equal intensities of the potassium and chlorine Auger peaks for KCl can easily be obtained even if the surface concentration of potassium ions is greater than that of chloride ions at the surface.] For this crystal (*i.e.*, KCl), doping with calcium increases the cation vacancy concentration and improves the stoichiometry. Thus, the sublimation rates increase upon calcium doping of KCl crystals. Based on this model it is expected that the surface concentration of the ions in the minority will control the sublimation rate.

Barr[8] has suggested that the bulk diffusion of more slowly diffusing ions controls the sublimation rate of alkali halides. This suggestion was based on the good agreement found between the activation enthalpies of bulk diffusion of the more slowly diffusing Cl ion and the activation enthalpy of sublimation for NaCl.[8]

The activation enthalpies of sublimation, the activation enthalpies of anion and cation diffusion, and the energies of forming a vacancy pair for NaCl, KCl, and LiF are listed in Table II. Barr's model cannot easily explain the opposite effect of calcium doping on the vacuum sublimation rates of LiF and NaCl, on the one hand, and KCl, on the other, since the more slowly diffusing ion is Cl^- in KCl as well. However, this disagreement can be rationalized since Fuller[9] reported that cation diffusion, which is enhanced by Ca-doping, makes an important contribution to the total diffusion flux in KCl and in fact is dominant at low temperatures (<500°).

Table II: The Activation Energies of Sublimation, ΔH_s^*, Anion and Cation Diffusion, ΔH_D^* Anion and ΔH_D^* Cation, and the Energies of Vacancy Pair Formation, ΔE, of NaCl, KCl, and LiF

	ΔH_s^*	ΔH_D^* anion	ΔH_D^* cation	ΔE vacancy pair
NaCl	55 ± 2[a]	55[b]	41.4[b]	45.5[c]
KCl	47 ± 2[d]	48.8[b]	39.9[b]	53.1[e]
LiF	66.7 ± 2	50.6[f]	43[f]	53.7[f]

[a] Reference 2. [b] Reference 8. [c] N. Laurance, *Phys. Rev.*, **120,** 57 (1960). [d] Reference 6. [e] Reference 9. [f] T. G. Stoebe and P. L. Pratt, *Proc. Brit. Ceram. Soc.*, **9,** (July 1967).

Inspection of Table II reveals that the average activation enthalpy of LiF sublimation (66.7 kcal/mol) is much higher than the activation enthalpies of either anion (50.6 kcal/mol) or cation (43 kcal/mol) diffusion in LiF. The activation enthalpy of sublimation of the monomer (~62 kcal/mol)[1] is already markedly greater than the activation enthalpies of diffusion for either ion.

Thus Barr's model of ion diffusion as a rate-determining step of the sublimation cannot explain the sublimation mechanism of LiF. There must be another step that has a greater energy requirement that controls the rate of sublimation.

Since sublimation involves the formation of ion pairs at the surface that subsequently desorb, the energy of forming a vacancy pair at the surface may also be a rate-determining step. From Table II one can see that for NaCl the energy of forming a vacancy pair (Schottky defect) is less than the activation enthalpy of anion diffusion. On the other hand, for KCl and LiF the energy of vacancy pair formation is greater than ΔH_D^* (anion). Although the energy of vacancy pair formation of LiF (53.7 kcal/mol) was estimated from low-temperature ionic conductivity studies and may be in error, it has to be increased by at least 10 kcal/mol to be of importance in the sublimation mechanism of LiF single crystals.

It appears that the sublimation mechanism of all alkali halides cannot be explained by the simple slow ion diffusion mechanism proposed by Barr.[8] Since sublimation takes place *via* several consecutive reaction steps that include bulk and surface ion diffusion, bond breaking and desorption, it is not surprising that small changes in the energy requirements of any of these reaction steps can change the rate-determining reaction

---

(8) L. W. Barr, *J. Chem. Phys.*, **51,** 1683 (1969).

(9) R. G. Fuller, *Phys. Rev.*, **142,** 524 (1966).

step. It is apparent, however, from our studies and from studies of calcium-doped NaCl and KCl crystals that point defects at the crystal surface play an all important role in the sublimation of alkali halides. Minute changes in the ion vacancy concentrations can markedly change the sublimation rate. *The nonstoichiometry at the surface that is characteristic of the ionic compound or that is created by the incorporation of impurities seems to control the sublimation rates.* This nonstoichiometry appears to remain constant during the sublimation process.

Variation of the dislocation density of LiF apparently has not changed the sublimation rate. Similar insensitivity of the sublimation rate to changes of dislocation density was found for KCl.[6] On the other hand, it was shown that for NaCl the increased concentration of dislocations has increased the sublimation rate. It appears that the annealing rate of excess dislocations that were introduced by stress determines whether high dislocation densities can be maintained at the subliming surface. The annealing rates of excess dislocations are probably more rapid in LiF and KCl crystals than in NaCl.

Acknowledgment. This work was performed under the auspices of the U. S. Atomic Energy Commission.

The Reaction of O(^{3}P) with Dideuterioacetylene[1]

by David G. Williamson

Department of Chemistry, California State Polytechnic College, San Luis Obispo, California 93401

(Received May 21, 1971)

Publication costs assisted by the U. S. Air Force Office of Scientific Research

The reaction of atomic oxygen, O(^{3}P), with C_2D_2 was studied to determine the importance of D atom production in this reaction By measuring the yield of HD from the exchange reaction of D atoms with H_2, the D atom yield was estimated to be (42 ± 10%) based on the number of O(^{3}P) atoms generated.

Introduction

In an earlier study of the reaction of ground-state oxygen atoms with acetylene, various reactions were considered.[2] The possible exothermic reactions, rewritten for deuterated acetylene, are shown below.

$$O + C_2D_2 \longrightarrow (C_2D_2O^*) \tag{1}$$

$$(C_2D_2O^*) \longrightarrow CD_2 + CO \tag{2}$$

$$(C_2D_2O^*) \longrightarrow D + DC_2O \tag{3}$$

$$(C_2D_2O^*) \longrightarrow D_2 + C_2O \tag{4}$$

$$(C_2D_2O^*) \longrightarrow (C_2D_2O) \tag{5}$$

$$M + (C_2D_2O^*) \longrightarrow C_2D_2O + M \tag{6}$$

$(C_2D_2O^*)$ is an unstable complex, analogous to that proposed for oxygen atom–olefin reactions.[3] Reactions 2 and 4 were estimated to account for 25 and 0.3%, respectively, of the original oxygen atoms formed. Reaction 5 was postulated as a possible isomerization or intersystem crossing. The previous work demonstrated the importance of reaction 3, but the yield could not be measured quantitatively.

The object of the present investigation is to estimate the importance of D atom production. If all of the D atoms formed in reaction 3 could be trapped in another compound, this would provide a measure of reaction 3.

Few D atom scavengers which do not react rapidly with O(^{3}P) atoms are known. Therefore, the exchange reaction 7

$$D + H_2 \longrightarrow HD + H \tag{7}$$

was chosen as a way to trap D atoms from reaction 3, since the attack of O(^{3}P) on H_2 is quite slow.[4]

Experimental Section

Ground-state oxygen atoms were generated in a static system by the mercury-photosensitized decomposition of nitrous oxide.[3] All experiments were done at 130.6 ± 0.5° in an air furnace. Two oblong quartz vessels of about 35 cm^3 volume were used.

---

(1) Contribution No. 2844 from the Department of Chemistry, University of California, Los Angeles.

(2) D. G. Williamson and K. D. Bayes, *J. Phys. Chem.*, **73**, 1232 (1969).

(3) R. J. Cvetanovic, *Advan. Photochem.*, **1**, 115 (1963).

(4) K. Schofield, *Planet. Space Sci.*, **15**, 643 (1967).

Table I: N_2/HD Values as a Function of C_2D_2/H_2; Temperature 130.6 ± 0.5°[a]

C_2D_2, Torr	H_2, Torr	N_2, Torr/min	N_2/HD	C_2D_2/H_2	Photolysis time, min
0.95	58	0.127	5.18 ± 0.4	0.0126	3
9.91	56	0.216	25.8 ± 6	0.163	3
1.83	55	0.136	6.03 ± 0.6	0.0282	3
0.96	50	0.0093	5.02 ± 0.5	0.0156	30
6.06	53	0.327	24.6 ± 3	0.103	3
3.27	53	0.163	10.7 ± 1	0.0557	3
0.96	24	0.143	7.58 ± 0.8	0.0287	3
0.96	10.2	0.120	16.3 ± 3.2	0.0735	3
0.96	31	0.110	7.0 ± 0.9	0.0242	3
0.96	19	0.140	9.40 ± 1	0.0363	3
0.95	40	0.113	5.76 ± 1.1	0.0188	3
0.96	25	0.0090	6.45 ± 0.9	0.032	30
1.76	22	0.153	15.7 ± 2	0.0655	3
1.76	104	0.090	3.52 ± 0.4	0.0155	3
0.88	145	0.140	2.01 ± 0.1	0.00517	2
0.88	205	0.100	1.81 ± 0.1	0.00355	2
0.97	88	0.110	3.56 ± 0.5	0.00870	3
0.97	84	0.126	4.36 ± 0.5	0.00865	3
0.95	78	0.113	4.23 ± 0.3	0.00912	3
0.96	104	0.130	3.59 ± 0.3	0.00663	3

[a] The N_2O pressure was 500 ± 65 Torr in all runs.

Both had a freeze-out tube about 10 cm × 0.4 cm which contained a small drop of Hg at the bottom. The freeze-out tubes were at room temperature during photolysis and were shielded from the photolysis light. A GE G25T8 25-watt germicidal lamp provided sufficient 2537-Å light intensity for the experiments.

Measurements of HD and N_2 were made with a CEC 21-620 mass spectrometer. After photolysis, the freeze-out tubes of the reaction vessels were cooled to liquid nitrogen temperature for about 0.5 hr. Samples of noncondensable gases were introduced directly from the cells into the mass spectrometer. Mixtures of H_2–N_2, and D_2–N_2 were used to calibrate the instrument. Using 70-eV ionizing electrons, the sensitivity of the instrument to N_2 was 1.29 ± 0.05 times that of H_2, and 1.25 ± 0.05 that of D_2. An average of these two figures, 1.27 ± 0.05, was used for the sensitivity of N_2 relative to HD.

Result

Mass spectrometric determination of HD yields from reaction 7 and N_2 yields from reaction 8

$$N_2O + Hg(^3P_1) \longrightarrow N_2 + O(^3P) + Hg \qquad (8)$$

showed that the ratio HD/N_2 depends very strongly on the ratio of C_2D_2/H_2. At low C_2D_2/H_2, yield of HD (as measured by HD/N_2) is highest. Increasing C_2D_2/H_2 decreases the HD yield (see Table I). Values of C_2D_2/H_2 in Table I have been corrected for the depletion of C_2D_2 during photolysis. By mass spectral analysis of samples of C_2H_2 and N_2O before and after photolysis, it was determined that for 0.39 Torr of N_2 generated, 0.47 Torr of C_2H_2 was consumed. In Table I, the C_2D_2/H_2 ratios shown are the average values during photolysis. Consumption of C_2H_2 was the same with or without H_2 present. The observed ratio of CO/N_2 = 0.44 at 1 Torr C_2D_2, 500 Torr N_2O, and at 130° was the same as the CO/N_2 ratio measured previously at room temperature.[2] Carbon monoxide yields for C_2D_2 pressures other than 1 Torr were taken to be the same as those found at room temperature. Thus, the contribution by CO to the $m/e = 28$ peak could be calculated. Nitrogen yields in Table I have been corrected for the CO yield, the N_2^+ peak from N_2O and the $m/e = 28$ peak from the background of the instrument.

Discussion

A simple mechanism can account for the dependence of HD/N_2 on the ratio C_2D_2/H_2.

$$O(^3P) + C_2D_2 \longrightarrow D + DC_2O \qquad (3)$$

$$D + C_2D_2 \longrightarrow C_2D_3 \qquad (9)$$

$$D + H_2 \longrightarrow HD + H \qquad (7)$$

$$H + C_2D_2 \longrightarrow C_2D_2H \qquad (10)$$

Applying the steady-state approximation to oxygen atoms and deuterium atoms yields

$$\frac{N_2}{HD} = \frac{1}{f} + \frac{k_9}{fk_7}\left[\frac{(C_2D_2)}{(H_2)}\right] \qquad (I)$$

where

$$f = \frac{k_3}{k_2 + k_3 + k_4 + k_5 + k_6(M)}$$

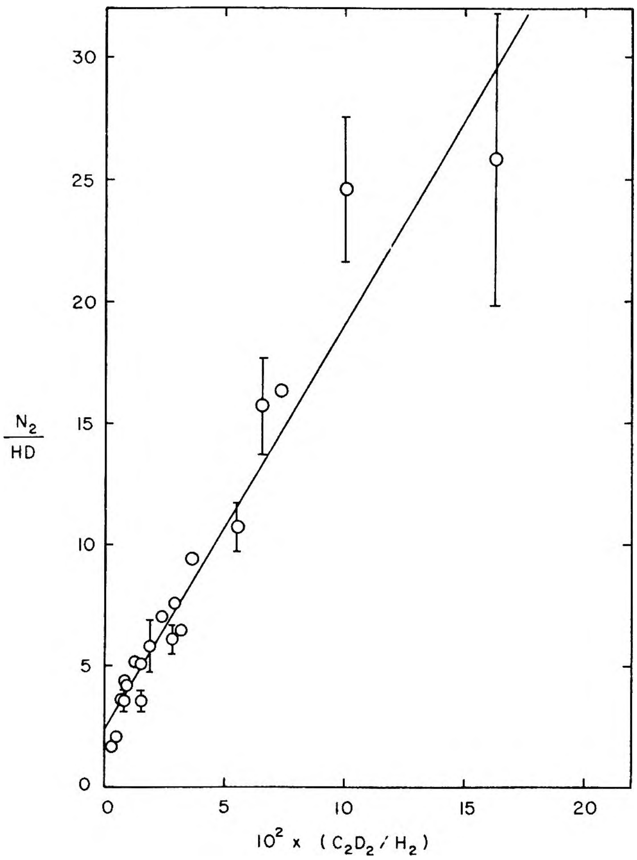

Figure 1.

Figure 1 is a graph of the data in Table I plotted according to eq I. A least-squares line through all the data points has been drawn in Figure 1. Experiments at about 54 Torr of hydrogen and varying C_2D_2 pressures are in reasonable agreement with those points at constant C_2D_2. Therefore, it is the ratio of C_2D_2/H_2 which is important in determining the ratio of N_2/HD as required by eq I. The line in Figure 1 yields $1/f = 2.4 \pm 0.6$ or $f = 0.42 \pm 0.10$ and $k_9/k_7 = 77 \pm 20$. Thus the yield of D atoms from the reaction of O with C_2D_2 is about 40%, which means that reaction 3 is of major importance.

It is not possible to compare directly the ratio of k_9/k_7 determined from Figure 1 with literature values, since the rate constant k_9 has not been observed directly. However, the reaction of D with normal acetylene, reaction 11, has been studied as a function of temperature.[5]

$$D + C_2H_2 \longrightarrow C_2H_2D \qquad (11)$$

Since one would not expect a large isotope effect on the rate of reaction 9 compared to reaction 11, the ratio k_{11}/k_7 should be comparable to k_9/k_7. At 130° the calculated ratio of k_{11}/k_7 is 73, which is to be compared to k_9/k_7 of (70 ± 20) from the slope and intercept of Figure 1. The agreement between these values supports the proposed mechanism.

The points in Figure 1 corresponding to runs with H_2 pressures above 100 Torr tend to fall below the least-squares line. At high H_2 pressures, some additional pathway for the formation of HD appears to become important. One possible disturbance is the sensitized dissociation of H_2, which will generate increasing amounts of hydrogen atoms as the H_2 pressure is increased.

$$Hg^* + H_2 \longrightarrow Hg + 2H \qquad (12)$$

If the H atoms then exchange with C_2D_2 according to eq 13 and 14, this could cause the observed deviations, since the D atoms would go on and exchange with H_2.

$$H + C_2D_2 \longrightarrow C_2D_2H \qquad (13)$$

$$C_2D_2H \longrightarrow C_2DH + D \qquad (14)$$

However, experiments in which the N_2O was replaced with an equivalent pressure of N_2, but with the same high pressures of H_2, showed HD levels that were no greater than 2% of the HD formed during the oxygen atom reactions. Exchange of H with C_2D_2 does not appear to be the cause of the low values of N_2/HD.

Another possible source of HD would be the attack of H on N_2O, reaction 15,[6] followed by the recently suggested reaction 16.[7] This possibility can be ruled out by comparing the known rate of reaction 15 with the rate of the alternate reaction 13. Approximating the rate of combination of H with C_2D_2 by its rate of combination with C_2H_2, one can show that only one H atom in 300 reacts with N_2O according to reaction 15.

$$H + N_2O \longrightarrow OH + N_2 \qquad (15)$$

$$OH + C_2D_2 \longrightarrow DC_2O + HD \qquad (16)$$

The ratio of N_2O to C_2D_2 will have to be several powers of ten larger than those in Table I in order for reactions 15 and 16 to generate more HD than reactions 3 and 7. By similar reasoning, the reaction of oxygen atoms with H_2 can be ruled out as a source of OH in these experiments, since even at the lowest ratio of C_2D_2/H_2 approximately 6% of the O(^{3}P) atoms generated react with H_2.[4]

The excess HD at high H_2 pressures may be coming from exchange reactions of the type

$$DC_2O + H_2 \longrightarrow HC_2O + HD \qquad (17)$$

or the reaction sequence[7,8]

$$CD_2 + H_2 \longrightarrow CD_2H + H \qquad (18)$$

$$H + CD_2H \longrightarrow CD_2H_2 \longrightarrow D + CDH_2 \qquad (19)$$

followed by reaction 7. Another possible source of HD at high H_2 may be reaction 20 followed by reaction

---

(5) K. Houermann, H. Gg. Wagner, and J. Wolfrum, *Ber. Bunsenges. Phys. Chem.*, **72**, 1004 (1968).

(6) G. S. Bahn, "Reaction Rate Compilations for the H-O-N System," Gordon and Breach, New York, N. Y., 1968, p 128.

(7) J. E. Breen and G. P. Glass, *Int. J. Chem. Kinet.*, **3**, 145 (1970).

(8) W. Braun, A. Bass, and M. Pilling, *J. Chem. Phys.*, **52**, 5131 (1970).

7.[9] Since these rate constants have not been measured,

$$CD_2 + H_2 \longrightarrow CDH_2 + D \qquad (20)$$

quantitative estimates of their importance cannot be made at this time.

In conclusion, it has been shown that the yield of D atoms from the reaction of oxygen atoms with C_2D_2 is about 40%, and this yield has been interpreted as a direct measure of the primary reaction 3. This result means that the alternative reaction 2, formation of CD_2 and CO, cannot be the only major primary step in the reaction, as several previous workers have assumed.[10-12] Previous results from similar static-system experiments[2] indicated that approximately 25% of the oxygen atoms generated produced methylene and CO, or C_2O and D_2. Therefore, only about two-thirds of the oxygen atoms produced can be accounted for by gas phase reaction products. Attempts to detect ketene in the gas phase have failed, and so the remaining fraction of oxygen atoms must end up in the polymer, which is observed in the present experiments as well as those at room termperature.

Acknowledgments. The experimental work reported above was carried out in the Department of Chemistry, University of California at Los Angeles. The financial support of the Air Force Office of Scientific Research, under Grant AFOSR 70-1872, is gratefully acknowledged.

---

(9) J. Bell and G. B. Kistiakowsky, *J. Amer. Chem. Soc.*, **84**, 8417 (1962).

(10) C. P. Fenimore and G. W. Jones, *J. Chem. Phys.*, **39**, 1514 (1963).

(11) C. A. Arrington, W. Brennen, G. P. Glass, J. V. Michael, and H. Niki, *ibid.*, **43**, 525 (1965).

(12) J. M. Brown and B. A. Thrush, *Trans. Faraday Soc.*, **63**, 630 (1967).

NOTES

A Nuclear Magnetic Resonance Study of the Protolysis Kinetics of 5-Dimethylaminonaphthalene-1-sulfonic Acid and Its *N*-Methylsulfonamide

by J. F. Whidby,*[1a,c] D. E. Leyden,[1a]
C. M. Himel,[1b] and R. T. Mayer[1b]

Department of Chemistry and Department of Entomology, University of Georgia, Athens, Georgia *(Received March 11, 1971)*

Publication costs borne completely by The Journal of Physical Chemistry

Sulfonamides are an important class of compounds because of their biological activity and use as fluorescent probes in the study of enzyme active sites.[2] We report the results of an nmr study of the protolysis of 5-dimethylaminonaphthalene-1-sulfonic acid (I) and its *N*-methylsulfonamide (II). Proton exchange studies on the 5-dimethylamino group of I and II were performed in aqueous H_2SO_4, whereas proton exchange of the *N*-methylsulfonamide moiety in II was carried out in 16.0 mol % *tert*-butyl alcohol in water. The pK_a of the dimethylamino group of I was determined to be 3.5 in 16% *tert*-butyl alcohol by nmr spectroscopy during this investigation and to be 4.52 ± 0.03 in H_2O by spectrofluorescence measurements.[3] Lagunoff and Ottolenghi[4] report the pK_a for I and II in H_2O to be 4.55 and 3.85, respectively, from spectrofluorometric data. Nmr studies with II in 16% *tert*-butyl alcohol gave a pK_a of 2.1.[3]

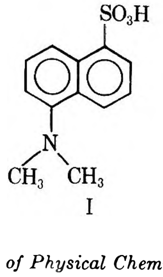
I

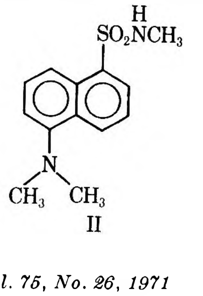
II

Several studies of the site of protonation of carboxylic acid amides have been performed.[5-7] Each study concluded that the major protonation of these compounds occurs at the oxygen atom. However, aliphatic and aromatic *N*-substituted sulfonamides have been shown to protonate on the nitrogen atom[8,9] in concen-

---

(1) (a) Department of Chemistry; (b) Department of Entomology; (c) correspondence should be addressed to 500 B Bexfield Drive, Dugway, Utah 84022. The authors acknowledge support in part by Research Grants from the National Institute of Health ES00207, GM-13935, Agricultural Research Service 12-14-100-9148 (33) and Federal Water Pollution Control Agency 16020 EAO.

(2) C. M. Himel, R. T. Mayer, and L. L. Cook, *J. Polym. Sci. Part A-1*, **8**, 2219 (1970).

(3) C. Himel, R. T. Mayer, J. F. Whidby, and D. E. Leyden, unpublished results.

(4) D. Lagunoff and P. Ottolenghi, *C. R. Trav. Lab. Carlsberg*, **35**, 63 (1966).

(5) R. J. Gillespie and T. Birchall, *Can. J. Chem.*, **41**, 2642 (1963).

(6) D. Herbison-Evans and R. E. Richards, *Trans. Faraday Soc.*, **58**, 845 (1962).

(7) C. A. Bunton, B. N. Figgis, and B. Nayak, *Proc. Int. Meeting Mol. Spectra., 4th, Bologna, 1959*, **3**, 1209 (1962).

(8) R. G. Laughlin, *J. Amer. Chem. Soc.*, **89**, 4268 (1967).

trated H_2SO_4 and have pK_a values of −5 to −7 (Hammet scale).[10,11] The acidity of the neutral sulfonamide moiety has also been determined with various substituents and pK_a values ranging from 4 to 13 have been found.[12-14] These latter pK_a values have been correlated with the biological activity of the compounds and in most cases the most active compounds have pK_a values near 7.[12]

Experimental Section

The nmr spectra were obtained using a Varian HA-100 NMR spectrometer or a Hitachi-Perkin Elmer R-20 high-resolution nuclear magnetic resonance spectrometer, each equipped with a variable temperature probe. The spectrometer settings varied but were checked to ascertain that saturation was not encountered. All temperatures reported are calibrated and are accurate to ±1°. Exchange data for the sulfonamide protolysis are at 30°, and for the 5-dimethylamino group at 56° for I and 78° for II. At temperatures significantly below those given for the latter two, the viscosity of the solutions caused broadening of the nmr lines.

The rate of proton exchange was determined by line shape analysis of the spin–spin doublets observed for the methyl protons in both the 5-dimethylamino and amide methyl protons when the respective hydrogen ion exchange was slow. The values of the coupling constants are 5.0 cps for the amino group in both I and II and 4.95 cps for the methylamide group in II. The chemical shift of the methyl protons in both groups is pH dependent. The amino methyl protons are approximately 3.8 ppm from tetramethylsilane in acid solution, whereas they are only 2.7 ppm in basic solution. The amide methyl protons are found between 2.8 and 2.6 ppm, depending on the acidity of the solution.

The mean lifetime before proton exchange (τ) was obtained by matching computer simulated nmr curves to the experimental spectra with appropriate correction for the natural line width. The natural line width (T_2) of the sample was determined several times during each run. These were assumed to be determined mainly by the inhomogeneity of the magnetic field. The program used to simulate the nmr spectra for proton exchange was written using the equations of Arnold.[15]

All pH measurements were made at room temperature using a Leeds and Northrup Model 7403 line operated pH meter equipped with a glass electrode. The pH meter was standardized using NBS standard buffer solutions. The pH values quoted for the *tert*-butyl alcohol–water mixtures are pH meter readings with no corrections applied. The meter readings taken for equal concentrations of hydrochloric acid in water and 16 mol % *tert*-butyl alcohol in water showed only slight differences. In the 40–60% sulfuric acid solutions used for the studies of the protolysis of the dimethylamino group, the acidity was represented by h_0^{III}, the acidity function for tertiary amines developed by Arnett and Mach.[16] Sulfuric acid solutions were prepared by dilution of concentrated J. T. Baker sulfuric acid. These stock solutions were diluted to approximately 0.1 *M* and titrated with potassium hydroxide for standardization.

A detailed discussion of the preparation of the compounds of the type used in this study has been given.[17] Solutions ranging from 0.1 to 0.5 *M* in I or II were prepared in the various sulfuric acid–water mixtures for obtaining the nmr spectra. The pH adjustments required for the protolysis studies of the sulfonamide group were made by additions of hydrochloric acid or potassium hydroxide as required.

Results and Discussion

Protolysis Kinetics of the 5-Dimethylamino Group. A study of the protolysis of the 5-dimethylamino group was performed in sulfuric acid–water mixtures. A variation of fivefold (0.1 to 0.5 *M*) in the concentration of I and II showed the rate of proton exchange to be first order in the concentration of the respective compounds. However, the rate of the protolysis reaction was found to be inversely proportional to the acidity of the solvent mixture. An earlier, similar study of the protolysis kinetics of iminodiacetic acid and *N*-methyliminodiacetic acid has shown that the only plausible reactions in the solvent medium employed are

$$BH^+ + H_2O \longrightarrow B + H_3O^+ \quad (1)$$

$$BH^+ + H_2SO_4 \longrightarrow B + H_3SO_4^+ \quad (2)$$

$$BH^+ + HSO_4^- \longrightarrow B + H_2SO_4 \quad (3)$$

where BH^+ represents the protonated dimethylamino group.[18] A rate law which fits the observation is

$$1/\tau = k_1[H_2O] + k_2[H_2SO_4] + k_3[HSO_4^-] \quad (4)$$

Unfortunately, it is not feasible to calculate the concentrations of all the species under the varied experimental conditions to test the rate law given by eq 4 and to evaluate the rate constants. However, a plot of $1/\tau$ *vs.* $1/h_0^{\mathrm{III}}$ is linear for the two compounds studied, with slopes of $(9.0 \pm 0.1) \times 10^6$ and $(1.05 \pm 0.03) \times 10^7$, respectively, for I and II; correlation coefficients for these plots are better than 0.998 regardless of con-

---

(9) F. M. Menger and L. Mandell, *J. Amer. Chem. Soc.*, **89**, 4424 (1967).

(10) P. O. I. Vietanen and K. Hunamaki, *Suom. Kemistilehti B*, **42**, 142 (1969).

(11) R. J. Gillespie and T. Birchall, *Can. J. Chem.*, **41**, 148 (1963).

(12) P. H. Bell and R. O. Robin, *J. Amer. Chem. Soc.*, **64**, 2905 (1942).

(13) A. Commarata and R. C. Allen, *J. Pharm. Sci.*, **56**, 640 (1967).

(14) J. K. Seydel, *ibid.*, **57**, 1455 (1968).

(15) J. T. Arnold, *Phys. Rev.*, **102**, 136 (1956).

(16) E. M. Arnett and G. W. Mach, *J. Amer. Chem. Soc.*, **86**, 2671 (1964).

(17) C. M. Himel, W. G. Aboul-Saad, and S. Uk, *J. Agr. Food. Chem.*, **19**, 1171 (1971).

(18) D. E. Leyden and J. F. Whidby, *J. Phys. Chem.*, **73**, 3076 (1969).

centration. These linear plots are evidence for a first-order dependence on the hydrogen ion activity as represented by the acidity function. Further evaluation of kinetic parameters is difficult to justify. Although the acidity function provides a convenient expression of acidity in strongly acid solvent, it does not provide as conveniently the concentrations of chemical species of interest. However, the evidence strongly implies that the proton exchange of the 5-dimethylamino proton is dependent on the transfer of the proton to a base. The most significant species present in solution of the composition used in this work is HSO_4^-.[19] Therefore, it is likely that the principal mechanism for exchange is the reaction represented by eq 3. However, the reaction represented by eq 1 in which water is the base undoubtedly plays an important role and is dominant in dilute acid in which the rate of exchange is extremely rapid.

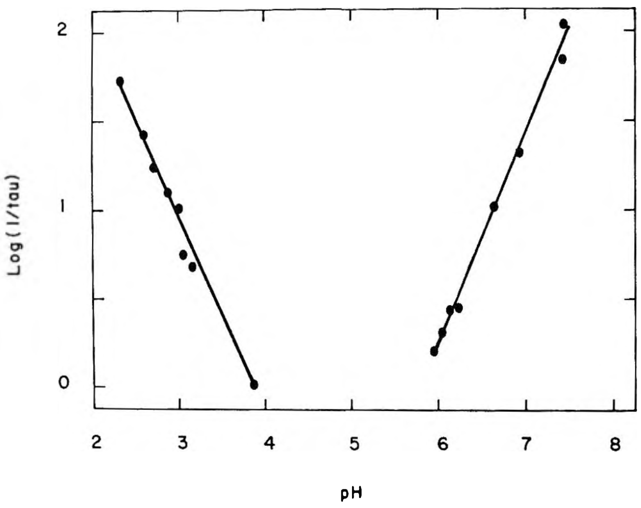

Figure 1. A plot of log $(1/\tau)$ *vs.* pH for the exchange of the sulfonamide proton on II (0.5 M) (τ is in seconds).

Sulfonamide Protolysis. Previous proton exchange systems that have been investigated using nmr which are both acid and base catalyzed have primarily been alcohols,[20,21] thiols,[22] and the amides of carboxylic acids.[23-28] Observations in this work show that exchange of the sulfonamide proton in II is also acid and base catalyzed. A plot of log $(1/\tau)$ *vs.* pH for the proton exchange of the sulfonamide group is shown in Figure 1. The two curves intersect at a pH of 4.8 ± 0.3. At this pH the proton exchange is very slow ($\sim$0.1 sec^{-1}) and is base catalyzed to the same degree as it is acid catalyzed. A plot of the concentration of II *vs.* $1/\tau$ was made in both acidic and basic solutions and a zero slope was obtained in each case. Therefore, it is not necessary to consider reactions which are second order in II. The observed kinetics as a function of pH may therefore be explained as a pH region in which exchange follows the protonation of the nitrogen atom

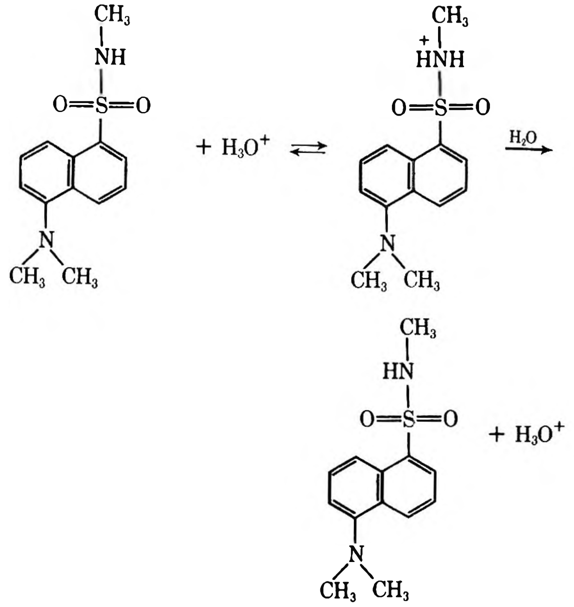

(5)

and a base-catalyzed region involving proton extraction by hydroxide ions

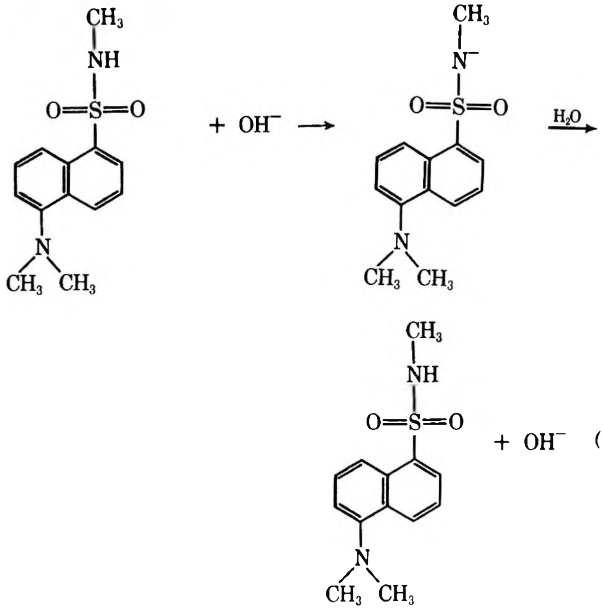

(6)

Variations up to 50 mol % *tert*-butyl alcohol showed no significant effect upon the rate of either reaction which could not be attributed to uncertainties in the pH determination. This is somewhat expected considering the relative basicity of *tert*-butyl alcohol and water, the autoprotolysis constant of *tert*-butyl alcohol,[29] and experimental results of *tert*-butyl alcohol as a means of proton transfer.[30] From the slopes in the plots shown in Figure 1, an acid-catalyzed rate constant of 7.2 × 10^3 M^{-1} sec^{-1} and a base-catalyzed constant of 1.8 × 10^8 M^{-1} sec^{-1} are obtained.

---

[19] T. F. Young, *Rec. Chem. Progr.*, **12**, 81 (1951).

[20] W. G. Patterson, *Can. J. Chem.*, **41**, 2472 (1963).

[21] Z. Luz, D. Gill, and S. Meiboom, *J. Chem. Phys.*, **30**, 1540 (1959).

[22] Reference 14 in M. M. Kreway, D. S. Sappenfield, and W. Schwabacher, *J. Phys. Chem.*, **69**, 2287 (1965).

[23] A. Berger, A. Loweenstein, and S. Meiboom, *J. Amer. Chem. Soc.*, **81**, 62 (1958).

[24] G. Fraenkel and C. Franconi, *ibid.*, **82**, 4478 (1960).

[25] D. G. Kowaleueski and V. J. Kowaleueski, *Ark. Kemi*, **16**, 373 (1960).

[26] J. S. Scarpa, D. D. Mueller, and I. M. Klotz, *J. Amer. Chem. Soc.*, **89**, 6024 (1967), and references cited therein.

[27] J. F. Bundschuck and N. C. Li, *J. Phys. Chem.*, **72**, 1001 (1968).

[28] I. M. Klotz and B. H. Frank, *J. Amer. Chem. Soc.*, **86**, 3889 (1964); **87**, 2721 (1965); **88**, 5103 (1966); **89**, 6024 (1967).

(29) J. Murto, *Acta Chem. Scand.*, **18**, 1043 (1964).

(30) E. Grunwald, R. L. Lipnick, and E. K. Ralph, *J. Amer. Chem. Soc.*, **91**, 4333 (1969).

Raman Spectrum of Purple Sulfur

by Robert E. Barletta and Chris W. Brown*

Department of Chemistry, University of Rhode Island, Kingston, Rhode Island 02881 *(Received April 16, 1971)*

Publication costs assisted by the Petroleum Research Fund

Approximately 35 solid allotropes of sulfur have been reported in the literature.[1] Most of these forms are stable only for short periods of time or under extremely low temperature conditions, and eventually they revert back to stable rhombic sulfur (S_8 rings) at room temperature. Some of the allotropic forms are due to changes in crystal structures, whereas others are due to changes in the molecular composition. Rice and Sparrow[2] first formed purple sulfur by quenching hot sulfur vapor onto a liquid N_2 cold finger. They suggested that the purple color was due to the presence of the S_2 diradical. More recent physical measurements on the purple solid have both confirmed the presence of S_2[3,4] and rejected it.[5]

The infrared spectrum of purple sulfur was recorded by Meyer,[3] who found only one strong band in the 4000–400-cm^{-1} region. This band, at 668 cm^{-1}, was assumed to be the infrared forbidden vibration of S_2. Since other sulfur species such as chains and rings are thought to be present, the activity of this band in the infrared was attributed to an induced dipole moment caused by the environment. In addition to the unexpected observation of this band, its frequency is ~50 cm^{-1} lower than predicted from the electronic spectrum of S_2.[6,7] The band has also been observed in matrix isolation experiments at approximately the same frequency.[4,6,7]

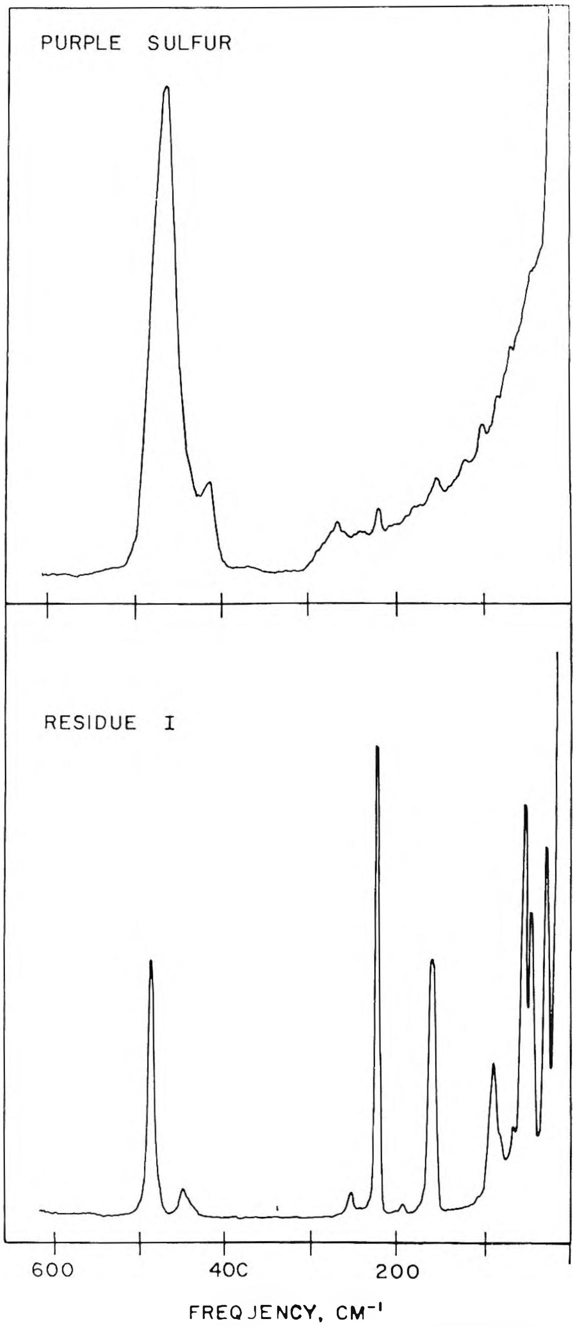

Figure 1. Top, Raman spectrum of purple sulfur at liquid N_2 temperature. Bottom, Raman spectrum of Residue I at room temperature. Spectral slit widths <4 cm^{-1}.

Raman scattering from the S_2 species should be quite strong; thus, we have measured the Raman spectrum of purple sulfur with the intention of solving the dilemma over the existence of S_2 in the purple form. Purple films were formed by heating rhombic sulfur to ~800° in a tube furnace, passing the hot gas through a radiofrequency discharge (~700 W at 10 MHz), and then quenching the gas on a liquid N_2 cold finger in an all-Pyrex dewar. We have formed over 30 films under slightly different conditions of temperature, discharge,

---

(1) B. Meyer, *Chem. Rev.*, **64**, 429 (1964).

(2) F. O. Rice and C. Sparrow, *J. Amer. Chem. Soc.*, **75**, 848 (1953).

(3) B. Meyer and E. Schumacher, *Helv. Chim. Acta*, **43**, 1333 (1960); *Nature*, **186**, 801 (1960).

(4) B. Meyer, *J. Chem. Phys.*, **37**, 1577 (1962).

(5) H. E. Radford and F. O. Rice, *ibid.*, **33**, 774 (1960).

(6) L. Brewer, G. D. Brabson, and B. Meyer, *ibid.*, **42**, 1385 (1965).

(7) L. Brewer and G. D. Brabson, *ibid.*, **44**, 3274 (1966).

Table I: Observed Frequencies (cm^{-1}) in the Raman Spectra of Purple, Rhombic, Residues I, II, and III, and "Crystex" Sulfur

Purple	Rhombic [a]	Rhombic [b]	Residues I	Residues II	Residues III	"Crystex" [c]
	474 m	474 m	474 m	471 m		474 m
466 s						
				456 m	458 vs	456 vs
	441 w	441 w	438 w	440 w		437 w
		430 vw				
418 w				420 w	415 w	416 w
271 w-b				273 vw	271 vw	273 w
				257 vw		
	246 w	247 w	248 vw	244 vw	248 vw	248 vw
218 vw	218 s	218 s	218 s	217 s	218 m	218 m
	215 m	215 m				
	186 vw	188 vw	187 vw	185 vw		187 vw
152 vw	152 m	151 m	154 m	151 m	153 m	151 m
		147 sh				

[a] Present work. [b] Reference 8. (Similar results on rhombic sulfur were first obtained by C. S. Venkateswaran, *Proc. Indian Acad. Sci.*, **4a**, 345 (1936).) [c] Reference 8.

and rate of deposit. The Raman spectra of the samples were recorded *in situ* using a Spex Industries Model 1401 double monochromator with a C.R.L. Model 52-A argon ion laser emitting at 4880 Å.

The observed Raman spectrum of purple sulfur is shown in Figure 1. We did not observe any bands from 500 to 800 cm^{-1}, which suggested that S_2 is not present in any appreciable amounts. Two of the strongest bands in the spectrum of rhombic sulfur (Figure 2) at 218 and 152 cm^{-1} have almost disappeared in the spectrum of purple sulfur, which indicates that very little of the rhombic form (S_8 rings) is present. The three bands at 466, 418, and 271 cm^{-1} are due to a new species or some mixture of species.

In order to determine the cause of the purple color, we recorded Raman spectra at various increments of temperature during the transition back to yellow sulfur. The spectrum of a purple film was recorded, then the film was allowed to warm up slowly until there was a noticeable color change. At that point the temperature was immediately reduced to liquid N_2 temperature and the spectrum was recorded. This experiment was repeated for each change in color. The first change was from purple to greenish yellow and this took place at ~150°K. The next change was from the greenish yellow to a light yellow at ~200°K. Above this temperature there was no detectable color change; however, we recorded spectra at approximately every 25° increment in temperature up to room temperature. Each time the sample was cooled back to liquid N_2 temperature before the spectrum was recorded.

To our surprise, the spectra recorded at each increment in temperature and color change were almost identical. The only observable change was a slight increase in the ratio of the peak heights of the bands at 466 and 418 cm^{-1}. The bands due to rhombic sulfur at 218 and 152 cm^{-1} did not increase in intensity. The film was warmed to room temperature before being immediately cooled to liquid N_2 temperature and the spectrum was practically the same as that for purple sulfur. However, by warming to room temperature and allowing the film to remain at that temperature for about 10 min there were detectable changes in the spectrum which appeared to be directly related to the texture of the purple film.

In about 25% of the experiments the spectra of the room temperature films were that of Residue I (Figure 1), which is the same spectrum as that obtained for rhombic sulfur (Figure 2). The conditions for depositing the purple sulfur which gave these films upon warming were such that an even textured, dark purple deposit was obtained. In all of these cases the film was extremely thin.

In the other 75% of the experiments the spectra of the room temperature films were similar to Residue II or III (Figure 2). In Residue III the bands due to rhombic sulfur at 218 and 154 cm^{-1} are very weak and the bands at 474 and 441 are unresolved from the broad bands at 458 and 415 cm^{-1}. The spectrum of Residue III is very similar to that obtained by Ward[8] for "crystex" sulfur. "Crystex" sulfur is a modification supposedly containing polymeric sulfur chains stablilzed by organic substituents. In "crystex" sulfur as in Residue III the strongest band in the spectrum is at 456 cm^{-1} and there are two new weak bands at 416 and 273 cm^{-1}; all of the bands due to rhombic sulfur are very weak. Our interpretation of Residue III is that it consists of long sulfur chains and is actually the so-called "plastic" form of sulfur. The purple films, which gave Residue III upon warming to room temperature, were much thicker than those that

---

(8) A. T. Ward, *J. Phys. Chem.*, **72**, 4133 (1968).

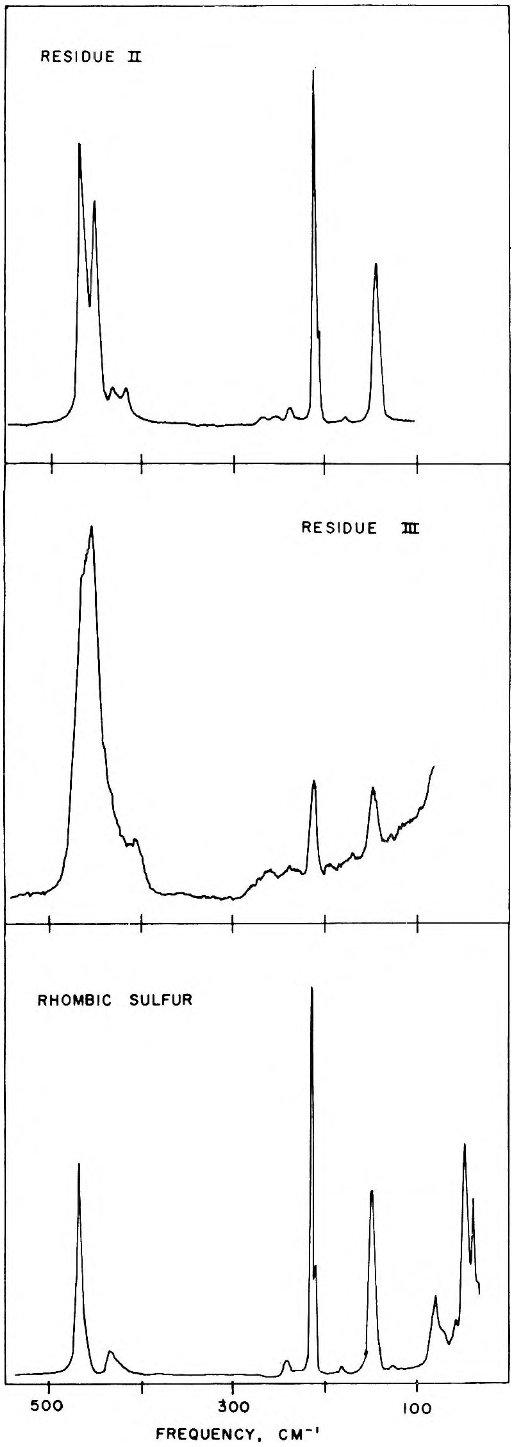

Figure 2. Raman spectra of Residue II, Residue III, and powdered rhombic sulfur. All spectra were recorded at room temperature with spectral slit widths <4 cm^{-1}.

gave Residue I and the films were unevenly distributed over the cold finger. Many times yellow flakes appeared on the surface during the time the film was being deposited. Residue II is obviously a mixture of I and III. After standing for several days the spectrum of Residue III would change to one similar to II.

Rice and Sparrow[2] reported that the yellow sulfur obtained from a purple film was $\sim 40\%$ rhombic and 60% amorphous. In the cases that produced Residue I our results disagree; however, since we are scattering the laser beam off of the front surface of the film, it could be the surface changes to rhombic whereas the interior goes to "plastic." In any event thinner films were more likely to have a spectrum very similar to that of rhombic sulfur. The observed frequencies for purple, rhombic, Residues I, II, and III, and "crystex" sulfur are compared in Table I.

The results of our work on the purple form of sulfur leave open the possibility of small amounts of S_2 giving rise to the purple color. It could well be that the concentration of S_2 is so small that we could not observe it in the Raman spectrum by scattering the laser beam off of the surface of the film. This does not rule out the possibility of observing S_2 in the infrared transmission spectrum of a rather thick film.[3,4] Our evidence suggests that most of the sulfur is present as chains in the purple films, since the rhombic (S_8 rings) bands are very weak. In the experiments which gave Residue I type films, it is likely that the purple films consisted primarily of small chains, S_8 or smaller. In the experiments which led to a plastic, the purple films probably contained more of the longer chain sulfur species.

Acknowledgment. Acknowledgment is made to the donors of The Petroleum Research Fund administered by the American Chemical Society for partial support of this research. We also wish to express our appreciation to the National Science Foundation and to the University of Rhode Island for a grant which made possible the purchase of the Raman instrumentation.

Fluorine Nuclear Magnetic Resonance Study of the Conformation of a Polyethylenimine Derivative[1]

by Timothy W. Johnson[2] and Irving M. Klotz*

Department of Chemistry, Northwestern University,
Evanston, Illinois 60201 *(Received September 9, 1971)*

Publication costs assisted by the National Institute of General Medical Sciences

Polyethylenimine (PEI) is a synthetic, water-soluble polymer with the empirical formula C_2H_5N. Chemical studies show that 25% of the amine nitrogens are tertiary, 50% secondary, and 25% primary. This

---

(1) This investigation was supported in part by a grant (GM-09280) from the National Institute of General Medical Sciences, U. S. Public Health Service.

(2) Postdoctoral Fellow, National Institute of General Medical Sciences, 1969–1971.

distribution indicates that polyethylenimine is a highly branched, fairly compact polymer.[3] Recent experiments with polyethylenimine derivatives containing long-chain hydrophobic residues reveal dramatic binding abilities of the polymers for small molecules, notably methyl orange.[4,5] Interest in the binding ability is augmented additionally by the observation that such derivatives may be modified further to include residues which are potential catalytic groups for hydrolysis reactions. Such bifunctional derivatives have been found to be good catalysts for the hydrolysis of active esters.[6] In view of these features of behavior of the polymers, it becomes important to examine the nature of the environment of the hydrophobic residues attached to these macromolecules.

Recently the fluorine magnetic resonance chemical shift of fluorine-labeled analogs of organic compounds has been demonstrated to give information on the local environment and thus on the location of the fluorine label.[7-10] This method should be applicable to polyethylenimine adducts.

A derivative of 10,10,10-trifluorodecanoic acid (TFD) with PEI-600 (average molecular weight = 50,000) was prepared by reaction of the appropriate nitrophenyl ester with PEI-600 in ethanol. The proton nmr spectrum of the resulting polymer in deuterium oxide indicated that 5.5% of the amine nitrogens had been acylated. Thus the derivative is designated $(TFD)_{.055}$PEI-600. The ability of the polymer derivative to bind methyl orange was measured and found to be similar to that of other hydrophobic derivatives of PEI, with an affinity intermediate between that of hexanoyl and lauroyl polyethylenimines.[5] The similarity in method of preparation and in properties supports the proposed analogy between the fluorinated and unfluorinated derivatives.

Fluorine nmr spectra of the derivative were obtained using a Brucker HFX-90 nmr spectrometer operating at 84.67 MHz with a probe temperature of about 23°. An external capillary of trifluoroacetic acid was used to provide a lock signal and a reference resonance. Multiple scans were obtained and stored in a Fabritek computer of average transients.

Several of the resulting spectra of $(TFD)_{.055}$PEI-600 are displayed in Figure 1. To a good approximation, the spectrum is well represented in each case as either one or two broad, symmetrical resonances, due, respectively, to one or two environments for the fluorine probes. (The resonances are sufficiently broad that the spin-spin multiplet structure is entirely obscured.) Clearly the presence of two resonances is consistent either with slow exchange of fluorines between one environment and the other, or with rapid exchange in a situation in which one fraction of the fluorines experiences a high probability of being in one environment and the remainder have a high probability of being in the other environment. The thermodynamic distinguishability of residues implicit in the second possibility is consistent with the known heterogeneity of PEI and its derivatives.

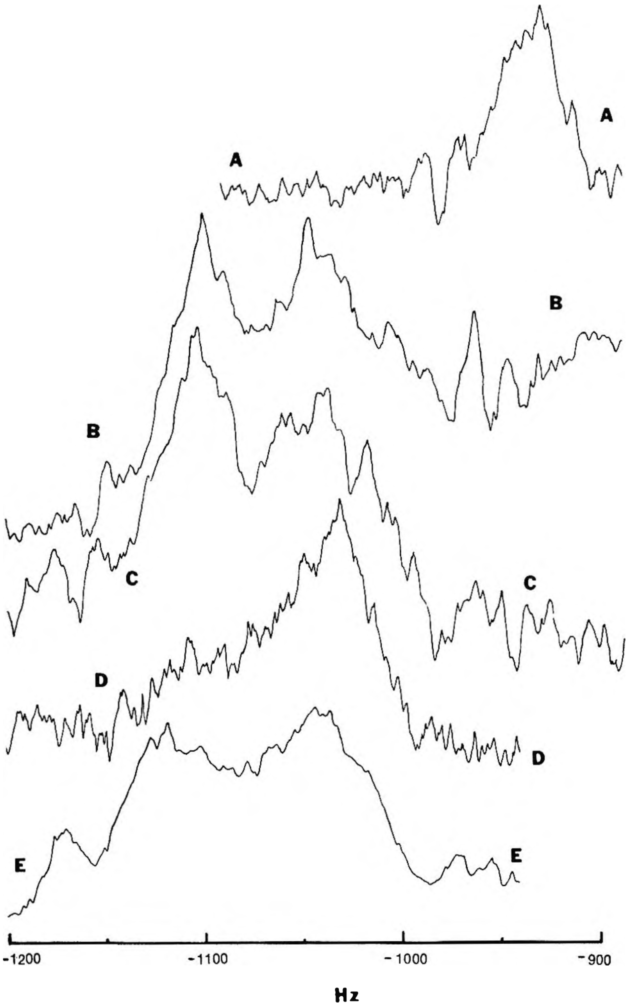

Figure 1. Fluorine nmr spectra of $(TFD)_{.055}$PEI-600: A, 10% solution in absolute ethanol; B, 4% solution in water, pH 7.0; C, 2% solution in water, pH 6.7; D, 2% solution in water, pH 8.9; and E, 1.5% solution in 6 M urea, pH 9.

The substantial line width of the individual resonances, from 20 to 60 Hz apparent half widths, could result from enhanced spin-lattice relaxation due to slow tumbling of the macromolecule, from variability of environments among the fluorines leading to many resonances under one broad peak, or from partial, but incomplete, averaging between the two major classes of fluorines. Proton nmr spectra of methyl protons in the analogous lauroyl PEI display modest line widths of *ca.* 5 Hz. The slight broadening of the proton spectra may be due either to a small enhancement in spin-lattice relaxation or to heterogeneity of environments, to which proton nmr is not particularly sensitive. The lack of substantial spin-lattice relaxation in the unfluorinated compound suggests that this is not a major contributor to the fluorine line widths. Spectra analogous to B and C (Figure 1) at temperatures of 33° display little or no change in line shape as compared to those at the lower temperature. This is inconsistent with the hypothesis that the line width is due to partial but incomplete averaging of environments. Thus it appears that, to a good approximation, each spectrum results from the addition of contributions from fluorines in a large number of environments, resonating at a large number of shifts, but with the environments and shifts in one and sometimes two broad but distinct classes.

---

[3] L. E. Davis in "Water-Soluble Resins," R. L. Davidson and M. Sittig, Ed., Reinhold, New York, N. Y., 1968.

[4] I. M. Klotz and A. R. Sloniewsky, *Biochem. Biophys. Res. Commun.*, **31**, 421 (1968).

[5] I. M. Klotz, G. P. Royer, and A. R. Sloniewsky, *Biochemistry*, **8**, 4752 (1969).

[6] I. M. Klotz, G. P. Royer, and I. S. Scarpa, *Proc. Nat. Acad. Sci., U. S.*, **68**, 263 (1971).

[7] N. Muller and R. H. Birkhahn, *J. Phys. Chem.*, **71**, 957 (1967).

[8] N. Muller and R. H. Birkhahn, *ibid.*, **72**, 583 (1968).

[9] N. Muller and T. W. Johnson, *ibid.*, **73**, 2042 (1969).

[10] T. W. Johnson and N. Muller, *Biochemistry*, **9**, 1943 (1970).

It is appropriate to consider the nature of these classes of environments as revealed by the chemical shifts. *A priori* one may visualize at least three distinct kinds of environment for the fluorines in the derivative: (1) solvent-like, resulting if the pendant groups protrude into the solvent, (2) PEI-core-like, resulting if the pendant groups fold back into the PEI interior, and (3) pendant group-like, resulting if the pendant groups find themselves clustered in contact with one another. The shift expected for (1) is the shift observed for a model, nonassociating fluorine probe in the solvent in question. Such shifts in several solvents are given in Table I. The shift expected for (2) depends somewhat on the model taken for the PEI core. If the PEI core is water-free, an estimate of the shift of a model compound is obtained from the data in Figure 2 as −1175 Hz. In the more likely event that the PEI core is wet, for example containing 50% water, the shift is estimated as −1200 Hz (Table I). In either case the shift is to very low field, lower than for any other environment examined. The shift expected for (3) is that for a micelle-like environment, which has been shown in several studies[7-10] to be −1000 to −1030 Hz, depending on the nature of the aggregating species.

Table I: Chemical Shifts of Model 1,1,1-Trifluoroalkyl Compounds in Several Solvents

Solvent	Chemical shift[a] (Hz at 84.67 MHz)
Ethanol	−905
N-Methylacetamide	−983
Water	−1091
6 *M* Urea	−1118
PEI-6 (extrapolated)	−1175
50% Aqueous PEI-6	−1200

[a] External trifluoroacetic acid was used as reference.

Figure 1A gives the spectrum of the derivative in absolute ethanol. The chemical shift is the same, within a few hertz, as expected for a fluorine probe free in the solution in question. Spectra 1B and 1C display two resonances in each case, one centered at −1045 Hz and the other at −1105 Hz. These shifts are close to being micelle-like and water-like, respectively. Each of the shifts is slightly to low field from what would have been expected for this assignment, positions suggesting that the fluorines in the water-like environment have some limited exposure to the PEI core and that the fluorines in the micelle-like environment have some limited exposure to the PEI core or are exposed to water somewhat more than similar fluorines in detergent micelles. Spectrum 1D displays one dominant resonance at −1030 Hz and a hint of a small resonance at about −1105 Hz. The assignments in this case also are micelle-like and water-like. Spectrum 1E exhibits two resonances, at −1040 and −1120 Hz. Again the shifts can be ascribed to a micelle-like and a water- (or 6 *M* urea-) like environment. In no case is a very low chemical shift found. This indicates that in all of the samples examined, the fluorine probe does not spend an appreciable fraction of the time in the PEI core.

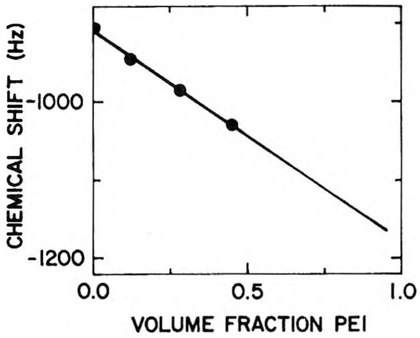

Figure 2. Fluorine chemical shifts of 10,10,10-trifluorodecanoic acid in PEI-6–ethanol mixtures.

Spectra 1B and 1C represent two different concentrations of the same polymer under similar conditions. The absence of a noticeable concentration effect on the relative areas indicates that the micelle-like structure is not an intermolecular one, which could be further dissociated by a reduction in concentration. The effect of pH on the distribution (compare 1C with 1D) is as expected, since the substantial charge on the polymer at pH 7 should expand the polymer and make interactions among the side chains less likely. Similarly, the effect of urea on the distribution (compare

1D with 1E) is as expected, since urea is known to destabilize micelles (see footnote 9 and references contained therein).

Thus the effects of solvent variables on the fluorine spectra not only reveal pH- and urea-induced conformational changes, but they also help confirm the assignment of the resonances to fluorines in micelle-like and solvent-like environments.

COMMUNICATIONS TO THE EDITOR

Electron Spin Resonance Signals of Abnormal Alkyl Radicals Trapped on Porous Vycor Glass Surfaces Coated with Metal Oxides at 77°K

Publication costs assisted by the Faculty of Pharmaceutical Sciences, The University of Tokyo

Sir: As has been reported previously,[1,2] the normal and abnormal methyl radicals ($CH_3(I)$, $g = 2.003$, $A^{H}_{CH_3(I)} = 23.0$ G; $CH_3(II)$, $g = 2.002$, $A^{H}_{CH_3(II)} = 19.3$ G) have been trapped on the surface of porous Vycor glass (PVG, Corning No. 7930) by the photolysis of adsorbed methyl iodide and methane at room temperature and at 77°K, respectively. Although there has been much interest in the adsorbed states of methyl radicals on various solid surfaces,[2-5] the pure signal of the abnormal perdeuteriomethyl radical $CD_3(II)$ has not yet been observed owing to the larger line width and to the overlapping of the signals of both methyl radicals. Quite recently, we have found that the presence of a very small amount (adsorbed fraction $\theta = 10^{-3} \sim 10^{-5}$) of certain metal oxides, such as V_2O_5 and MoO_3, on the surface of PVG exhibits a spectral sensitization to the formation of the $CH_3(II)$ radical from methane at 77°K.[6]

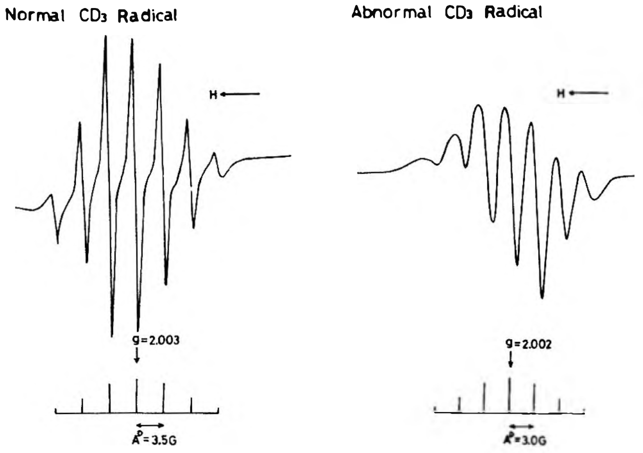

Figure 1. The esr signals of normal and abnormal perdeuteriomethyl radicals trapped on the surfaces of PVG's coated with V_2O_5 at 77°K.

Taking advantage of the spectral sensitizing property of the PVG coated with V_2O_5 ($PVG(V_2O_5)$), we have

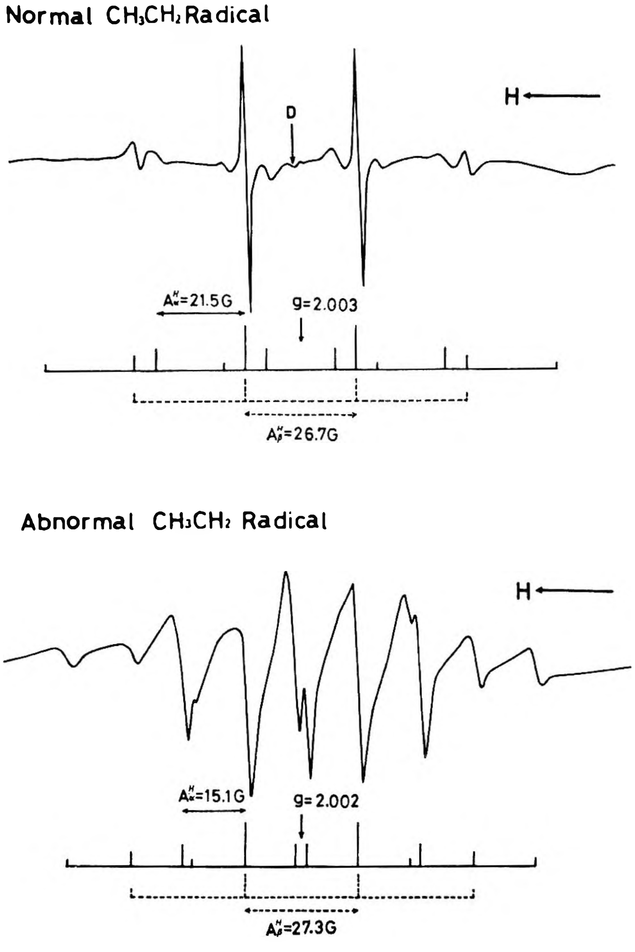

Figure 2. The esr signals of normal and abnormal ethyl radicals trapped on the surfaces of $PVG(V_2O_5)$ at 77°K.

(1) J. Turkevich and Y. Fujita, *Science*, **152**, 1619 (1966).

(2) N. Shimamoto, Y. Fujita, and T. Kwan, *Bull. Chem. Soc. Jap.*, **43**, 580 (1970).

(3) G. B. Garbutt and H. D. Gesser, *Can. J. Chem.*, **48**, 2685 (1970).

(4) C. L. Gardner and E. J. Casey, *ibid.*, **46**, 207 (1968).

(5) G. B. Garbutt, H. D. Gesser, and M. Fujimoto, *J. Chem. Phys.*, **48**, 4605 (1968).

(6) Y. Fujita, K. Hatano, M. Yanagita, T. Katsu, M. Sato, and T. Kwan, *Bull. Chem. Soc. Jap.*, **44**, 2884 (1971).

been able to observe a strong and well resolved esr signal of the abnormal deuteriomethyl radical $CD_3(II)$ ($g = 2.002$, $A^{D}_{CD_3(II)} = 3.0$ G, $A^{H}_{CH_3(II)}/A^{D}_{CD_3(II)} = 6.5$) without overlapping with the normal $CD_3(I)$ ($g = 2.003$, $A^{D}_{CD_3(I)} = 3.5$ G, $A^{H}_{CH_3(I)}/A^{D}_{CD_3(I)} = 6.5$). The esr signal of the $CD_3(II)$ is shown in Figure 1 along with that of the $CD_3(I)$. Experimental methods were similar to those of previous reports.[2,6] This technique to obtain the pure and large signal of abnormal methyl radical has been extended to the photolysis of homologous alkyl hydrocarbons at 77°K, and an abnormal ethyl radical has been trapped. The esr signal of abnormal ethyl radical $C_2H_5(II)$ is shown in Figure 2 together with that of normal ethyl radical $C_2H_5(I)$ trapped on the surface of PVG(V_2O_5) by the photolysis of ethylene at 77°K. The esr constants of the $C_2H_5(II)$ are as follows: $g = 2.002$, $A_{\alpha}^{H}(II) = 15.1$ G, $A_{\beta}^{H}(II) = 27.3$ G, and these parameters can be compared to those of the $C_2H_5(I)$, $g = 2.003$, $A_{\alpha}^{H}(I) = 21.5$ G and $A_{\beta}^{H}(I) = 26.7$ G, respectively.

It is very interesting that the hfc constant of α protons in the $C_2H_5(II)$ differs remarkably from that of the $C_2H_5(I)$, while the hfc constants of β protons in both normal and abnormal ethyl radicals are nearly same. The view that A_{β}^{H} is much less sensitive to the radical geometry than A_{α}^{H} has been recently developed by Norman, *et al.*[7] Experimental evidence to support this contention is also found in the case of the silyl and methyl-substituted silyl radicals,[8] SiH_3, CH_3SiH_2, $(CH_3)_2SiH$, and $(CH_3)_3Si$, whose bent structures, deduced from the ^{29}Si hfc constant in each radical, decrease with increasing methyl substitution owing to the steric effect of the bulky methyl group. The α-proton hfc constant changes from 7.96 G of SiH_3 to 16.99 G of $(CH_3)_2SiH$, while that of methyl protons changes in a small amount less than 2 G going from CH_3SiH_2 to $(CH_3)_3Si$.

The rotational correlation times of the methyl groups in both ethyl radicals, estimated from the line width alternation of methyl proton, hf, are nearly same ($\tau_c \sim 10^{-7}$ sec). This fact indicates that the methyl group does not participate in the strong interaction with the surface, but the methylene group does. Further studies on homologous alkyl radicals are now in progress.

(7) A. J. Dobbs, B. C. Gilbert, and R. O. C. Norman, *J. Chem. Soc. A*, 124 (1971).

(8) P. J. Krusic and J. K. Kochi, *J. Amer. Chem. Soc.*, 91, 3938 (1969).

FACULTY OF PHARMACEUTICAL SCIENCES
THE UNIVERSITY OF TOKYO
HONGO, BUNKYO-KU TOKYO, JAPAN

TAKASHI KATSU
MICHIYASU YANAGITA
YUZABURO FUJITA*

RECEIVED JULY 30, 1971

ADDITIONS AND CORRECTIONS

1965, Volume 69

Robert A. Pierotti: Aqueous Solutions of Nonpolar Gases.

Page 281. In the Abstract the value of σ for water should read 2.75 Å.

Page 287. Equation 20 should read

$$\bar{C}_c = \frac{2\bar{H}_c}{T} + \left(\frac{\bar{H}_c}{\alpha_p}\right)\left(\frac{\partial \alpha_p}{\partial T}\right)_p - \alpha_p\bar{H}_c - \alpha^2{}_pRT^2\left[\frac{y^2}{(1-y)^2}\right]\left\{\frac{12}{(1-y)}\left[2\left(\frac{a_{12}}{a_1}\right)^2 - \left(\frac{a_{12}}{a_1}\right)\right] + \frac{36(1+2y)}{(1-y)^2}\left[\left(\frac{a_{12}}{a_1}\right)^2 - \left(\frac{a_{12}}{a_1}\right) + \frac{1}{2}\right] + 1\right\} \quad (20)$$

The values of $\Delta C_p{}^0$ shown in Table VI were calculated with the correct equation for $\bar{C}_c$.—Robert A. Pierotti.

Raj Mathur and R. Bruce Martin: Effects of Charge and Nickel Ion on Proton Chemical Shifts of Glycyl Peptides.

Page 669. The chemical shift in Table I for the carboxyl terminal residue of dipolar ion glycylglycine should read 1.74 (D). Other values are unchanged with the result that the chemical shifts of the two pairs of methylene hydrogens in glycylglycine cross twice on going from cationic to anionic species.—R. Bruce Martin.

1970, Volume 74

M. H. Gianni, J. Saavedra, R. Myhalyk, and K. Wursthorn: Nuclear Magnetic Resonance Spectral Correlation of Symmetrically Submitted 1,2-Diols and 1,3-Dioxalanes.

Page 210. The authors apologize to Dr. J. Chuche for a missed reference. Enantiotopic relationships in an nmr correlation of stereochemistry for 1,3-dioxalane have been used prior to the publication. See J. Chuche, *C. R. Acad. Sci. Ser. A*, **263**, 779 (1966).—M. H. Gianni.

J. A. Cusumano and M. J. D. Low: Interactions between Surface Hydroxyl Groups and Adsorbed Molecules. I. The Thermodynamics of Benzene Adsorption.

Page 795. Equation 3 should read

$$-\Delta S^\circ{}_{\mathrm{it}} = {}_{\mathrm{g}}S^\circ{}_{\mathrm{tr}} + {}_{\mathrm{g}}S^\circ{}_{\mathrm{rot}} + {}_{\mathrm{g}}S^{\circ 1}{}_{\mathrm{vib}} - {}_{\mathrm{a}}S^\circ{}_{\mathrm{config}} - {}_{\mathrm{a}}S^\circ{}_{\mathrm{rot}} - {}_{\mathrm{a}}S^{\circ 1}{}_{\mathrm{vib}} - {}_{\mathrm{a}}S^\circ{}_{\mathrm{vib}}$$

Equation 4 should read

$$-\Delta S^\circ{}_{\mathrm{mt}} = {}_{\mathrm{g}}S^\circ{}_{\mathrm{tr}} + {}_{\mathrm{g}}S^\circ{}_{\mathrm{rot}} + {}_{\mathrm{g}}S^{\circ 1}{}_{\mathrm{vib}} - {}_{\mathrm{a}}S^\circ{}_{\mathrm{tr}} - {}_{\mathrm{a}}S^\circ{}_{\mathrm{rot}} - {}_{\mathrm{a}}S^\circ{}_{\mathrm{vib}} - {}_{\mathrm{a}}S^{\circ 1}{}_{\mathrm{vib}}$$

Equation 6 should read

$${}_{\mathrm{g}}Q_{\mathrm{tr}} = \left[2\pi\left(\sum_i m_i\right)kT/h^2\right]^{3/2}V^\circ$$

Equation 16 should read

$${}_{\mathrm{a}}S^\circ{}_{\mathrm{rot}} = R\{\ln\,(1/\pi\sigma)[8\pi^3(I_{\mathrm{A}}I_{\mathrm{B}})^{1/2}kT/h^2] + 1\}$$

J. A. Cusumano.

William C. McCabe and Harvey F. Fisher: A Near-Infrared Spectroscopic Method for Investigating the Hydration of a Solute in Aqueous Solution.

Page 2992. In the last sentence to the legend of Figure 1, the phrase, "the absorption cell path length was 0.1 cm" should read, "the absorption cell path length was 0.05 cm."—Harvey F. Fisher.

Cecelia Radlowski and Warren V. Sherman: The γ Radiolysis of 2-Propanol. V. Oxidation by Carbon Tetrachloride.

Page 3046. Equation A should read

$$G(\mathrm{HCl}) = G(\mathrm{CHCl_3}) = G(\mathrm{acetone}) = G(X_i) + 10k_3[\text{2-propanol}]\left\{\frac{G(X_i)}{k_5I}\right\}^{1/2}$$

Warren V. Sherman.

Frederick D. Lewis: On the Photoreduction of Acetophenone.

Page 3333. The curvature in Figure 1 cannot be due to a quenching impurity in the 2-propanol as is evident when eq 8 is rearranged as

$$\frac{1}{\varphi} = 1 + \frac{k_{\mathrm{q}}[\mathrm{Q}]}{k_{\mathrm{r}}[\mathrm{RH}]} + \frac{k_{\mathrm{d}}}{k_{\mathrm{r}}[\mathrm{RH}]}$$

where Q is a quenching impurity in the 2-propanol. We thank Professor C. E. Burchill for bringing this fact to our attention. Experimental data and other conclusions are not affected by this correction.

The observed curvature may be due (*inter alia*) to (a) a polar solvent effect on the carbonyl excited state, (b) departure of eq 4 from pseudo-first-order kinetics at high [RH], or (c) a solvent effect on the free radical reactions described by eq 4 and 5.—Frederick D. Lewis.

Geoffrey Davies and Kay O. Watkins: The Kinetics of Some Oxidation–Reduction Reactions Involving Cobalt(II) in Aqueous Perchloric Acid.

Page 3390. Footnote 21 should read as follows. "For detailed kinetic data, order document NAPS-01286 from ASIS National Auxiliary Publications Service, c/o CCM Information Sciences, Inc., 22 West 34th Street, New York, N. Y. 10001. Remit check or money order for \$5.00 for photocopies or \$2.00 for microfiche."—Geoffrey Davies.

Richard J. Majeste and Edward A. Meyers: The Crystal and Molecular Structure of Bisbipyridyl-μ-dihydroxo-dicopper(II) Nitrate.

Page 3499. There are three errors in Figure 1. (1) The label on the right-hand nitrogen atom in the drawing should be N2, rather than N. (2) The out-of-plane deviation for atom C8 should be −0.048 Å, rather than −0.084 Å. (3) The least-square plane equation should be

$$6.826X + 3.713Y + 2.388Z = 3.0674$$

rather than

$$6.826X - 3.713Y + 2.388Z = -0.047$$

Richard J. Majeste.

A. S. Kertes, O. Levy, and G. Markovits: Aggregation of Alkylammonium Tetrahaloferrates in Benzene.

Page 3569. In Table I, the *t*, °C column should read from the top: 25, 37, 25, 37, 37, 50, 25, 37, 50, 37, 50, 37, 50, 50.—A. S. KERTES.

M. M. Bhasin, C. Curran, and G. S. John: Infrared Study of the Effect of Surface Hydration on the Nature of Acetylenes Adsorbed on γ-Alumina.

Page 3978. The graphical representations of the surface reactions are misrepresented. They should appear as follows.

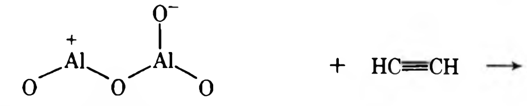

Highly dehydrated
γ-Al_2O_3 (~700–900°) under vacuum

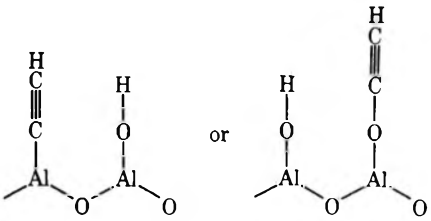

I (Surface aluminum acetylide and proton transfer)

II (Surface aluminum oxyacetylide)

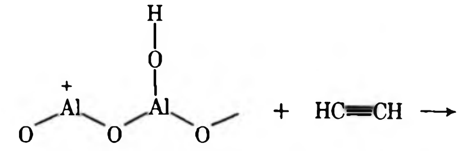

Mildly dehydrated γ-Al_2O_3
(~400–700° under vacuum)

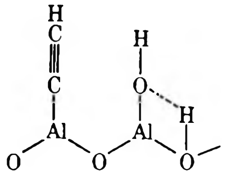

(I′)

MADAN M. BHASIN.

Nora Laiken and George Némethy: A Model for the Binding of Flexible Ligands to the Surfaces of Proteins and Other Macromolecules. I. Statistical-Mechanical Treatment.

Page 4426. Equation 24 should read as follows.

$$t(S) = \mathbf{a}_s^{(1)}\mathbf{W}_s^{-1}\prod_{\rho=1}^{l-1}(\mathbf{W}_s^{s_\rho}\mathbf{W}^{d_\rho}H(d_\rho))\mathbf{W}_s^{s_l}\mathbf{e}$$

Page 4429. The *second line* in eq 55 should read as follows.

$$(1 - \delta_{d_00})\mathbf{a}_d^{(1)}\mathbf{W}_d^{d_0-1} H_0(d_0) \times$$

Page 4430. In the third to last line of text, ε is not to be boldface.—GEORGE NÉMETHY.

1971, Volume 75

Shmuel Weiss, Hartmut Diebler, and Isaac Michaeli: Kinetics of Proton-Transfer Reactions of Polyacrylic and Polymethacrylic Acids with an Indicator.

Page 267. The line above the Abstract concerning publication costs should read as follows: "Publication costs assisted by the Nuclear Research Centre, Negev, Israel Atomic Energy Commission."—SHMUEL WEISS.

Frank J. Millero: The Partial Molal Volumes of Tetraphenylarsonium Tetraphenylboron in Water at Infinite Dilution. Ionic Partial Molal Volumes.

Page 280. The second method used to estimate the $\bar{V}°$ (H^+) from the $\bar{V}°$(Ph_4AsBPh_4) is in error. An incorrect value of 1.81 Å for the r(As) was used in the original calculations. The correct value of r(As) = 1.18 Å yields $\bar{V}°(H^+) = -10.3$ cm³/mol, which is low by 5 cm³/mol compared to the accepted value. Thus, the second method should not be used to estimate the $\bar{V}°(H^+)$ in other solvent systems. The average $\bar{V}°(H^+)$ obtained by methods 1 and 3 are unaffected by the deletion of the second method. I thank Dr. C. V. Krishnan for calling my attention to this error.—FRANK J. MILLERO.

Thomas L. Penner and George S. Hammond: Radiation-Induced Chain Isomerization of *cis*-1,2-Diphenylpropene in Cyclohexane.

Page 294. In the left-hand column, line 3, the expression $G_{c\to t} \approx \phi_{t\to c}$ should read $G_{c\to t}/G_{t\to c} = \phi_{c\to t}/\phi_{t\to c}$.—GEORGE S. HAMMOND.

Noriko Yamaguchi, Yoshihiko Sugiura, Koji Okano, and Eiichi Wada: Non-Newtonian Viscosity and Excluded Volume Effect of Dilute Solutions of Flexible High Polymers.

Page 1142. In the left-hand column, line 14 from the bottom, γ should be β.—Y. SUGIURA.

Terry L. Brewer: Photophysical Processes of *m*-Difluorobenzene.

Page 1235. Equations III, IV, and V should read

$$^1F_{vj} + B \rightarrow {}^1F_{vj-k} + B \quad K_B \tag{III}$$

$$^1F_{vj-k} \rightarrow F + h_{vf} \quad K_f \tag{IV}$$

$$^1F_{vj} \rightarrow {}^1F_{vj-k} \quad K_{vj-k} \tag{V}$$

Page 1236. Equation 1 should read

$$\frac{1}{\Phi_f} = [(K_f + K_y)/K_f][1 + K_x/K_B[\mathrm{B}]]$$

TERRY L. BREWER.

J. L. Borowitz and F. S. Klein: Vapor Pressure Isotope Effects in Methanol.

Page 1815. Statement (e) in the Abstract should read: "There is a direct correlation between deuterium substitution and hydrogen-bond strength. No such correlation is observed in ^{18}O and ^{13}C substitution."

Page 1820. The following paragraph should be added.

Acknowledgment. The subject of this paper was originally suggested by Professor William Spindel. The authors wish to thank him for his suggestion and help.—J. L. BOROWITZ.

Helmut M. Pohlit, Wallace Erwin, Tz-Hong Lin, and Richard M. Lemmon: Hot-Atom Chemistry of Carbon-14 in Solid Benzene at Kinetic Energies between 5 and 100 Electron Volts.

Pages 2555 and 2557. The running titles on these pages incorrectly mention "Carbon-13," whereas the article is concerned only with carbon-14. The same error occurred in the table of contents for this issue.—RICHARD M. LEMMON.

I. M. Kolthoff, E. J. Meehan, and Masaru Kimura: Hydrogen Peroxide Formation upon Oxidation of Oxalic Acid in Presence and Absence of Oxygen and of Manganese(II). I. Manganese(VII), Cerium(IV), Chromium(VI), and Cobalt(III) as Oxidants.

Page 3347. In the left-hand column, line 27, "considerably smaller" should be "a little smaller."

Page 3348. Equation I should read

$$[\mathrm{O}] = \frac{c_0}{k_2\tau}(1 - e^{-k_2t})$$

Page 3348. In the left-hand column, last paragraph, line 11 and following should read: "the value of κ being 2.8, 3.2, and 3.2 × 10^{-4} (t in sec) for $c_0 = 4 \times 10^{-6}$, 2×10^{-5}, and 4×10^{-5} M, respectively. At $c_0 = 2 \times 10^{-4}$ M . . . . κ is only 1.6×10^{-4}."

Page 3348. In Figure 1, the values of c_0 should be multiplied by 2.—I. M. KOLTHOFF.

AUTHOR INDEX *to Volume 75, 1971*

ABELLO L Solvent effect on the dimerization of N-methylaniline 1763

ABRAMOWITZ S The infrared spectrum of matrix-isolated uranium monoxide 2283

ABSAR I Ab initio LCAO-MO-SCF study of the phosphoryl fluoride molecule, OPF_3 1360

ACHE H J Interactions of positrons with defects in sodium chloride crystals 2030

ACQUISTA N The infrared spectrum of matrix-isolated uranium monoxide 2283

ADAMS G F Calculation of inter-ring proton couplings 3765

ADAMSON A W Evaluation of photoluminescence lifetimes 2463

ADATO I Metal-ligand bonding in copper(II) chelates. Electron paramagnetic resonance study 3828

ADLER A J Circular dichroism studies of lysine-rich histone f-1-deoxyribonucleic acid complexes. Effect of salts and dioxane upon conformation 1516

AGRAWAL M C Kinetics of the oxidation of hexacyanoferrate(II) by chloramine-T 838

AHLUWALIA J C Effects of the urea-guanidinium class of protein denaturants on water structure: heats of solution and proton chemical shift studies 815

AHMAD S I Kinetics of the catalysis by reversed micelles of cetyltrimethylammonium bromide in hexanol 2001

AITKEN H W Ionization of trichloroacetic acid in aqueous solutions 2492

AKASAKA K Photoinduced hole-electron recombination in a γ-irradiated single crystal of L-cystine dihydrochloride 3746

AKHTAR S M S γ-Radiolysis of liquid ethanol. Yields of hydrogen and free ions. Solvated electron rate constants 2756

AL-ANI KH Quenching of excited states of fluorobenzene in the gas phase 3662

AL-ANI K Photochemistry of the fluorotoluenes. I. Quantum yields of fluorescence and intersystem crossing in 1-fluoro-2-, 1-fluoro-3-, and 1-fluoro-4-methylbenzenes 3214

ALBRECHT A C Methyl radical formation during photolysis of N,N,N′,N′-tetramethylparaphenylenediamine in 3-methylpentane at 77°K 431

ALBRIDGE R G Study of phosphorus-sulfur compounds by inner-orbital photoelectron spectroscopy. Thiono-thiolo sulfur 3975

ALBRIGHT J G Isotope effects in the diffusion of carbon-14 substituted molecules in the liquid phase. II. Relative diffusion rates of benzene-1-^{14}C and benzene-1,2-^{14}C 1315

ALEI M JR Nitrogen-15 nuclear magnetic resonance shifts and coupling constants for the methylamine hydrochlorides in aqueous solution 1758

ALEI M JR Nitrogen-15 nuclear magnetic resonance shifts in pure methylamines and pure methyl isocyanide-nitrogen-15 932

ALEXANDER M D Electronic absorption spectra and electron paramagnetic resonance of copper(II)-amine complexes 3355

ALEXANDROWICZ Z Intrinsic viscosity of polyelectrolytes 442

ALGER T D Dominance of intramolecular dipole-dipole mechanisms upon carbon-13 relaxation in benzene and cyclohexane 2538

ALGER T D Effect of molecular association on carbon-hydrogen nuclear dipolar relaxation rates 2539

ALLENDOERFER R D Electron spin resonance and electron nuclear double resonance study of the 4-formyl-2,6-di-tert-butylphenoxy radical 2765

ALLENDORF H D Kinetics of the attack of refractory solids by atomic and molecular fluorine 308

ALLRED A L Keto-enol equilibriums in 2,4-pentanedione and 3,3-dideuterio-2,4-pentanedione 433

AMBERG C H Nature of deficiency in nonstoichiometric hydroxyapatites. I. Catalytic activity of calcium and strontium hydroxyapatites 3167

AMBERG C H Nature of deficiency in nonstoichiometric hydroxyapatites. II. Spectroscopic studies of calcium and strontium hydroxyapatites 3172

AMDUR S Mean molal activity coefficient of polymethacrylic acid at various degrees of neutralization 2144

AMES L L Dissociation energies of gaseous gadolinium dicarbide and terbium dicarbide 848

AMEY R L Viscosity and local liquid structure in dimethyl sulfoxide-water mixtures 98

AMPHLETT J C The reaction $2COF_2 \rightarrow CO_2 + CF_4$ and the heat of formation of carbonyl fluoride 3024

AMZEL L M Absolute entropies, conformation, and Debye temperatures of bicyclo[2.2.2]octane- and of bicyclo[3.2.2]nonane-type molecules 1073

ANACKER E W Dependence of micelle aggregation number on polar head structure. I. Light scattering by aqueous solutions of decylammonium salts and related surfactants 369

ANDER P Electrical conductivities of salts of gum arabic and carrageenan in aqueous solutions 1691

ANDERSON D K Tracer and mutual diffusivities in the system chloroform-carbon tetrachloride at 25° 3293

ANDERSON H L Heats of mixing. II. Temperature dependence of aqueous electrolytes with a common ion 1125

ANDERSON K P Complex solubility of silver chloride in methanol-water, acetone-water, and dioxane-water mixtures 93

ANDREWS L Matrix reactions of fluorohalomethanes with alkali metals. Infrared spectrum and bonding in the monofluoromethyl radical 3235

ANGELBERGER P Methylene reactions in photolytic systems involving methyl iodide 2536

ANGELL C A Glass transitions in molecular liquids. I. Influence of proton transfer processes in hydrazine-based solutions 1826

ANGELL C A Corresponding states and the glass transition for alkali metal nitrates 2306

ANGELL C A Two-state thermodynamics and transport properties for water from "bond lattice" model 3698

ANTONIEWICZ P R Coexistence of liquid phases in calcium-ammonia solutions 399

APPLEBY A Scavenging of the molecular hydrogen yield from water irradiated with tritium β particles 601

ARMSTRONG D A Wall effects on concentrations of reactive intermediates in gaseous systems 2883

ARMSTRONG D A Ion lifetimes in gaseous ammonia 444

ASAMI R Nuclear magnetic resonance spectra of carbanions. II. Carbanions produced from α-methylstyrene and cumyl methyl ether 1062

ASHITANI K Diffusion in mixed solvents. II. Iodine in binary solutions of ethanol with hydrocarbons and carbon tetrachloride 963

ATEN C F Relative total scattering cross sections for homologous series of polar and nonpolar molecules 727

ATKINSON G Examination of the Zwanzig theory of dielectric firction. II 239

ATKINSON G Ultrasonic velocity in nonelectrolyte-water mixtures 2336

ATKINSON G Ultrasonic relaxation of tert-butyl alcohol in cyclohexane 3182

ATKINSON G H Absorption spectrum of benzene vapor near 2537 Ang 1564
ATKINSON G H Single vibronic level fluorescence. IV. Its application to the analysis of resonance fluorescence from benzene excited by the 2537-Ang. mercury line 1572
ATKINSON R Vibrational deexcitation of highly excited polyatomic molecules. Amount of energy transferred per collision 3376
ATKINSON T V Electron spin resonance studies of cation radicals produced during oxidation of methylhydrazines 2043
ALTMILLER H G Radiation-induced isomerization of the 1,2-diphenylpropenes in polar liquids 2394
ATTWOOD D Investigations of aqueous mixtures of nonionic surfactants by membrane osmometry 2212
AUBAILLY M Environmental effects on the deprotonation of indole derivatives in alkaline ices 3061
AUBORN J J Spectrophotometric dissociation field effect kinetics of aqueous acetic acid and bromocresol green 2488
AUBORN J J Specific rates in the acid dissociation-ion recombination equilibrium of dilute aqueous hydrazoic acid at 25° 3026
AYRES R L Reactions of iodine with olefins. II. Radiative neutron capture induced reactions of iodine-128 with various C_5 isomers. Evidence for a mechanism other than autoradiolysis in the condensed state 2880
AYSCOUGH P B Kinetic electron spin resonance studies on the photolysis of some carbonyl, nitroso, and nitro compounds 3454
BADDOUR R F Hydrogen promotion of the palladium-catalyzed carbon monoxide oxidation 2065
BAGG J Biionic potentials of a liquid-membrane electrode selective toward calcium 2138
BAILEY A R Heats of dilution and the thermodynamics of dissociation of uranyl and vanadyl sulfates 2368
BAINE P Solvation studies of lithium salts in dimethylformamide 3188
BAJEMA L Spectrum of matrix-isolated carbon disulfide 2204
BALASUBRAHMANYAM K Transport processes in low melting salts. Silver nitrate-thallium nitrate system 4025
BALASUBRAMANIAN D Effects of the urea-guanidinium class of protein denaturants on water structure: heats of solution and proton chemical shift studies 815
BALKAS T I Radiation chemistry of aqueous solutions of trichlorofluoromethane, dichlorodifluoromethane, and chlorotrifluoromethane 455
BANYARD K E Electron correlation and the charge distribution in lithium hydride 416
BARANSKI A Study of the low-temperature hydrogenation of ethylene on zinc oxide by temperature-programmed desorption 208
BARAT F Flash photolysis of chlorate ion in aqueous solution 2177
BARBER N F Mathematical formulations of the effects of cell distortion and liquid column height compression in analytical ultracentrifugation 2507
BARD A J Electron spin resonance studies of cation radicals produced during oxidation of methylhydrazines 2043
BARD A J Simultaneous electrochemical-electron spin resonance measurements. I. Cell design and preliminary results 3281
BAR-ELI K New absorption bands in solutions of alkali metals in amines 286
BARGER H J JR Effect of adsorption potential on the hydrogen-deuterium exchange of benzene at a fuel cell electrode 3715
BARKER N T Behavior of the solvated electron in ethanol-n-hexane mixtures 3639
BARLETTA R E Raman spectrum of purple sulfur 4059
BARRETT R B Ion-exchange selectivity of the synthetic zeolite Linde A in anhydrous and mixed media 85
BATES R G Solute-solvent effects in the ionization of tris(hydroxymethyl)acetic acid and related acids in water and aqueous methanol 826
BATT L Primary and secondary rate processes in the acetone-silane photochemical system 3945
BAUER S H Structure of perchlorocyclopropene 1681
BAUER S H Molecular structure of perfluorocyclopentene and perchlorocyclopentadiene by gas phase electron diffraction 1685
BAUMGARTNER E K Ultrasonic velocity in nonelectrolyte-water mixtures 2336
BAYES K D Predissociation and dissociation energy of HBr^+ 1472
BAYRAKCEKEN F Reactions of fast hydrogen atoms with ethane 841
BEAR J L Kinetics of nickel murexide formation in several solvent systems 3705
BEATTY J W Reactions of fast tritium molecules with 1-butene 2407
BEATTY J W Hydrogen displacement in n-butane by fast T_2 and T_2^+ collisions 2417
BECK G Radiation chemical yield of OH^- as determined by conductometric pulse radiolysis 1759
BECKA L N Absolute entropies, conformation, and Debye temperatures of bicyclo[2.2.2]octane- and of bicyclo[3.2.2]nonane-type molecules 1073
BECSEY J G Hologram interferometry for isothermal diffusion measurements 3374
BEHAR D Investigation of radicals produced in the photolysis of thiosulfate solutions by electron spin resonance 2752
BEKOWIES P J Methyl radical formation during photolysis of N,N,N′,N′-tetramethylparaphenylenediamine in 3-methylpentane at 77°K 431
BELL J A Methylene reaction rates. Quantum yields in the diazomethane-propane photolysis system: effects of photolysis time, reactant ratios, and added gases 1537
BELL T N Reactions of deuterated methyl radicals with methylfluorosilanes. Polar effects in hydrogen abstraction 603
BELLOBONO I R Spontaneous dissolution of metals in aqueous electrolytes. I. Kinetic isotope effects in the reaction of iron with hydrochloric acid solutions in protium and in deuterium oxide 2112
BELLONI J Kinetic study of species formed during the pulsed radiolysis of ammonia 2908
BEN-BASSAT A H I Metal-ligand bonding in copper(II) chelates. Electron paramagnetic resonance study 3828
BENNETT J E Electron spin resonance spectra of some σ-type aromatic radicals 3432
BENNETT S W Quantum yields in the 58.4-nm photolysis of carbon dioxide 3499
BENNETT S W Absorption coefficients and ionization yields of some small molecules at 58.4 nm 719
BENNION D N Transport behavior in dimethyl sulfoxide. II. Viscosity studies 1727
BENNION D N Transport behavior in dimethyl sulfoxide. III. Conductance-viscosity behavior of tetra-N-amylammonium thiocyanate from infinite dilution to molten salt at 55° 3586
BENSON S W Kinetics and thermochemistry of the gas-phase bromination of bromoform. C-H bond dissociation energy in bromoform and the C-Br dissociation energy in carbon tetrabromide 987
BENSON S W Comparison of RRK [Rice-Ramsperger-Kassel] and RRKM [Rice-Ramsperger-Kassel-Marcus] theories for thermal unimolecular processes 1333
BENTLEY M D Micellar effects on the hydrolysis rate of triethylamine-sulfur trioxide 1763
BERGET P B Intrinsic viscosity of short-chain normal alkanes 3120
BERKOWITZ J Photoionization mass spectrometric study of xenon difluoride, xenon tetrafluoride, and xenon hexafluoride 1461
BERLMAN I B Systematics of the electronic spectra of the p-oligophenylenes and their substituted analogs 318
BERMUDEZ V M Infrared study of boron trichloride chemisorbed on silica gel 3249

BERNASCONI C F Intermediates in nucleophilic aromatic substitution. VI. Kinetic evidence of intramolecular hydrogen bonding in Meisenheimer complexes ... 3636
BERNHEIM R A Mercury-sensitized photodecomposition of nitrous oxide in the presence of mixtures of carbon monoxide and methane ... 3205
BERTRAND R D Field-dependent contributions to carbon-13 nuclear relaxation ... 3967
BEST G T Chemistry of barium released at high altitudes ... 1412
BETTS D M Effect of magnetic fields on the pH of water ... 2830
BEZDEK H F Size determination of seawater drops ... 3623
BHACCA N S Structure of nitroform in various solvents ... 499
BHAT S N Vapor phase charge-transfer complexes. V. Blue-shifted iodine band ... 1057
BHAT S N Vapor-phase charge-transfer complexes. VI. Diethyl ether-iodine ... 3682
BIBLER N E Radiolysis of carbon tetrachloride. Radical yields and the formation of tetrachloroethylene as an initial product ... 24
BIBLER N E Dose rate effects in the steady and pulse radiolysis of liquid chloroform ... 2436
BIELSKI B H J Deuterium isotope effect on the decay kinetics of perhydroxyl radical ... 2263
BIERLEIN J A Hologram interferometry for isothermal diffusion measurements ... 3374
BIRRELL G B Role of lipid spin labels in membrane biophysics ... 3417
BIRRELL G B Electron spin resonance study of x-irradiated long-chain alcohols oriented in urea inclusion crystals ... 3489
BISCAR J P Laser-produced oxygen from silicon dioxide ... 2412
BISCAR J P Q-switched laser-induced reactions of thiacyclobutane and thiacyclopentane with oxygen ... 725
BLAKE T D Adsorption on flat surfaces. I. Gas phase autophobicity ... 1887
BLANDER M Bubble nucleation in n-pentane, n-hexane and n-pentane + hexadecane mixtures and water ... 3613
BLANTON C D Protolysis kinetics of ethyl N-methylcarbamate ... 1895
BLAUER J A Kinetics of chlorine monofluoride at high temperatures ... 3939
BLOOMFIELD V A Viscosity of liquid mixtures. 3113
BLOOMFIELD V A Intrinsic viscosity of short-chain normal alkanes ... 3120
BLOOR J E Optical activity of alkyl-substituted cyclopentanones. Intermediate neglect of differential overlap molecular orbital model ... 2466
BLOSSEY D F Aggregation of arylazonaphthols. II. Steric effects on dimer structure in water ... 1227
BLYHOLDER G Photocatalytic reactions on semiconductor surfaces. I. Decomposition of nitrous oxide on zinc oxide ... 1037
BOCKRIS J O'M Ellipsometric investigations of anodic film growth on iron in neutral solution. Prepassive film ... 2823
BOEHM L Transition probabilities of europium in phosphate glasses ... 3980
BOGAN D J Mass spectrum of isocyanic acid ... 1532
BOLOCOFSKY D Ionic radii from scaled particle theory of the salt effect ... 2809
BOND A M Correlation of heterogeneous charge-transfer rate constants and homogeneous rate constants for removal of coordinated water in the a.c. and d.c. polarographic study of some irreversibly reduced complex ions in Aqueous solution ... 2640
BONE L I Gas-phase acidities of alcohols ... 2226
BONE L I Effect of positive ion scavenging by benzene in the radiolysis of propane ... 2272
BONNER O D Ionization of trichloroacetic acid in aqueous solutions ... 2492
BONNER O D Freezing point depression measurements in N-methylacetamide as a solvent ... 2879
BORELLO E Infrared study of surface properties of α-chromia. II. Oxygen chemisorption ... 2783
BORGARDT F G Structure of nitroform in various solvents ... 499
BOROWITZ J L Vapor pressure isotope effects in methanol ... 1815
BOSMANS H J Location of univalent cations in synthetic zeolites of the Y and X type with varying silicon to aluminum ratio. I. Hydrated potassium exchanged forms ... 3327
BOTTENBERG W R JR Enthalpy of transfer of sodium chloride from water to aqueous hydrogen peroxide at 25° ... 2229
BOURNE K H Structure and properties of acid sites in a mixed oxide system. II. tert-Butylbenzee cracking and benzene adsorption ... 220
BOWIE S E Micellar effects on the hydrolysis rate of triethylamine-sulfur trioxide ... 1763
BOWMAN R C JR Cohesive energies of the alkali hydrides and deuterides ... 1251
BOX H C Oxidation and reduction of organic compounds by ionizing radiation. L-Penicillamine hydrochloride ... 2564
BOX H C Electron spin resonance and endor [electron nuclear double resonance] studies of radiation-produced radical pairs ... 3426
BOYD G E Estimation of solute activity coefficients in dilute aqueous mixtures of sodium and zinc bromides at 25°. Comparisons with predictions from the Guggenheim theory of solutions .. 3153
BOYD R H Thermochemistry, thermodynamic functions, and molecular structures of some cyclic hydrocarbons ... 1264
BRADLEY J N Single-pulse shock tube studies of hydrocarbon pyrolysis. II. Pyrolysis of ethane ... 1492
BRADSPIES J I High-yield method for the preparation of anomalous water ... 2976
BRAGIN J Vibrational spectra of trans- and cis-crotononitrile ... 44
BREDIG M A Miscibility of liquid metals with salts. X. Various studies in alkaline earth metal-metal fluoride and rare earth metal-metal difluoride and trifluoride systems ... 2340
BRENNEN W Nitrogen afterglow and the rate of recombination of nitrogen atoms in the presence of nitrogen, argon, and helium ... 1552
BREUER G M Fluorescence decay times of cyclic ketones, acetone, and butanal in the gas phase .. 989
BREWER T Apparent triplet yields of pyrazine. 3769
BREWER T L Photophysical processes of m-difluorobenzene ... 1233
BREY W S JR Electron paramagnetic resonance studies of carbon monoxide adsorbed on thorium oxide ... 895
BRIGGS P R Mass spectra of disilanes. Phenyl-silicon interaction and silicon-silicon bond strength ... 974
BRILL T B Positive temperature coefficients in the bromine nuclear quadrupole resonance spectra of the diethylammonium salts of hexabromoantimony(III) and hexabromobismuth(III) ... 1898
BROCKLEHURST B Ionic species formed from benzene during radiolysis of its solutions in 3-methylpentane at 77°K. Comments ... 1177
BROMAN R F Proton transfer in the two-step electrochemical reduction of oxygen in N,N-dimethylformamide ... 4019
BROOKS J M Rate of the reaction of the ammoniated electron with the ammonium ion at -35° . 986
BROSTOW W Vapor-liquid equilibriums of binary mixtures of carbon-14-labeled hexane with aliphatic ketones ... 4041
BROWN B J Behavior of the solvated electron in ethanol-n-hexane mixtures ... 3639
BROWN C W Raman spectrum of purple sulfur . 4059
BROWN E Energy partitioning on photolysis and pyrolysis of 3-vinyl-1-pyrazoline ... 1640
BROWN L M Mechanism and kinetics of isotopic exchange in zeolites. I. Theory ... 3846
BROWN L M Mechanism and kinetics of isotopic exchange in zeolites. II. Experimental data ... 3855
BROWN R Theory of self-diffusion in three model dense fluids ... 1970
BROWN S C Vibrational spectra and structure of biacetyl ... 1946
BROYDE S B Concentration quenching of proflavine hydrochloride in dry films of sodium deoxyribonucleate and poly(vinyl alcohol) ... 2727
BRUMMER S B High-yield method for the preparation of anomalous water ... 2976

BRUNO G V Electron spin resonance line shapes and saturation in the slow motional region....... 3385
BRUS L E Chemical hydrogen fluoride lasers from flash photolysis of various N_2F_4+RH systems.. 2546
BRUSIC V Ellipsometric investigations of anodic film growth on iron in neutral solution. Prepassive film 2823
BUBERT H Decomposition of ammonia and hydrazine by electron impact 769
BUDZINSKI E E Oxidation and reduction of organic compounds by ionizing radiation. L-Penicillamine hydrochloride...................... 2564
BUDZOL M Radiation chemistry of polyethylene. XI. The molten state 1671
BUETTNER A V Photoreduction of benzophenone in benzene. II. Flash photolysis study of primary photochemical reactions................. 187
BUFFINGTON C W Oxidation of hypophosphorous acid by vanadium(V)......................... 891
BUNTON C A Enhancement of micellar catalysis by added electrolytes...................... 2707
BURCHILL C E Kinetics of isopropyl alcohol radicals by electron spin resonance-flow techniques. Comments 167
BURTON L L Proton magnetic resonance spectra of molten alkali metal acetate solutions of polyhydric alcohols and phenols.................... 1338
BUSI F Effect of olefins on the reactions of nitrous oxide in γ-irradiated liquid cyclopentane... 2560
BUTLER E A Complex solubility of silver chloride in methanol-water, acetone-water, and dioxane-water mixtures 93
BUTLER J N Selective solvation of ions by water in propylene carbonate....................... 1477
BUTT J B Surface diffusion of single sorbates at low and intermediate surface coverage 133
CAFASSO F A Solubility of helium and argon in liquid sodium 2832
CAIRNS E J Structural studies of magnesium halide-potassium halide melts by Raman spectroscopy.. 155
CALA F R Deactivation of vibrationally excited ethane. Comparison of two methods of measuring the pressure dependence..................... 837
CANALES E R Tracer and mutual diffusion coefficients of proteins 379
CANNINGS F R Structure and properties of acid sites in a mixed oxide system. II. tert-Butylbenzee cracking and benzene adsorption 220
CANNON J P Complex formation in aluminum iodide-diethyl ether solutions.................... 282
CANNON P Formation of diamond. IV. Behavior of the diamond-forming reaction with respect to catalyst composition.......................... 2158
CANNON P Formation of diamond. V. Substitution of nitrogen-15 for nitrogen-14 in diamond 2696
CANT N W Catalytic oxidation. IV. Ethylene and propylene oxidation over gold 2914
CAPONECCHI A J Shock tube isomerization of cyclopropane.................................... 2526
CARLSON G A Shock tube study of the tetrafluoroethylene-difluoromethylene equilibrium ... 1625
CARLSON G L Infrared spectra of ground graphite 1149
CARLSON K D Infrared spectra of the aluminum family suboxides................................ 1963
CARR R W JR Use of tubular flow reactors for kinetic studies over extended pressure ranges.... 1593
CARROLL H F Vibrational deexcitation of highly excited polyatomic molecules. Amount of energy transferred per collision 3376
CARSKY P Conjugated radicals. IX. Experimental study and the LCI-SCF open shell calculations on the electronic spectra and the redox equilibria of the nitrogen-containing violenes ... 335
CARSTENSEN E L Low-frequency dielectric dispersion in suspensions of ion-exchange resins 1091
CARTER M K Electron spin resonance of the p-quaterphenyl cation radical................... 902
CASASSA E F Theoretical models for peak migration in gel permeation chromatography....... 3929
CASEY E J Electron spin resonance of atomic silver on porous glass and silica gel surfaces...... 2706
CASPER J M Vibrational spectra and structure of organophosphorus compounds. X. Methyl torsional frequencies and barriers to internal rotation of some CH_3PXY_2 compounds........... 1956
CASPER J M Vibrational spectra and structure of dimethylaminodichlorophosphine 3837
CASTELLS R C Study of the adsorption of insoluble and sparingly soluble vapors at the gas-liquid interface of water by gas chromatography .. 3870
CATLIN A Adsorption of fibrinogen. Electron microscope study 2103
CERRUTI L Infrared study of surface properties of α-chromia. II. Oxygen chemisorption 2783
CESARO A Thermodynamic data for the water-hexamethylenetetramine system 3633
CHAKRABARTI S K Electronic spectra of the heteroaromatics of the type R_2X. I. Diphenylamine and N-methyldiphenylamine.............. 3576
CHAN F S Corresponding state relations for the Newtonian viscosity of concentrated polymer solution. Temperature dependence............. 256
CHANDRA S Dielectric relaxation in α,ω-dibromoalkanes in benzene solution 2616
CHANG C-H Molecular structure of perfluorocyclopentene and perchlorocyclopentadiene by gas phase electron diffraction 1685
CHANG C Y Chain association equilibriums. Nuclear magnetic resonance study of the hydrogen bonding of N-monosubstituted amides. II. In carbon tetrachloride 776
CHANG C Y Chain association equilibriums. Nuclear magnetic resonance study of the hydrogen bonding of N-monosubstituted amines. III. In dioxane 784
CHANG H M Temperature dependence of simple hot atom reactions.............................. 3042
CHANG H W Comparison of energy partitioning from three-centered processes. Bimolecular transfer and unimolecular elimination reactions . 2070
CHANG R Effects of deuterium substitution on the electron-transfer reactions.................. 447
CHANG W M Self-association of butylamines... 938
CHAPMAN I D Effect of the emulsifying agent on the dielectric properties of water-in-oil emulsions 537
CHAUDHRI S A Radiation chemical yield of OH^- as determined by conductometric pulse radiolysis 1759
CHAUDHRI S A Conductometric pulse radiolysis determination of ionic yields and neutralization kinetics in liquid ethanol 3893
CHEN H Raman spectral study of bisulfate-sulfate systems. II. Constitution, equilibriums, and ultrafast proton transfer in sulfuric acid 2672
CHEN H Raman spectral study of bisulfate-sulfate systems. III. Salt effects.................. 2681
CHEN J C H Simultaneous determination of equilibrium and rate constants for first-order reactions 430
CHERVILLE J Molecular conformation of 1,3,5-trinitrohexahydro-s-triazine (RDX) in solution 2056
CHESNUT D B Spin-label investigation of ion-exchange resins 907
CHIANG M H Dynamics of the reactions of O_2^+ with molecular hydrogen and deuterium 1426
CHOHAN R K Oxidation kinetics of 2-mercaptoethylamine hydrochloride by ferricyanide ion in acid medium 2036
CHONG D P Expressions for multiple perturbation energies 1549
CHOU C C Methylene reactions in photolytic systems involving methyl iodide 2536
CHOU C-C Isotope effects in the substitution reaction of 2.8-eV tritium atoms with methane . 1283
CHOW L C Thermodynamics of solutions with liquid crystal solvents. III. Molecular interpretation of solubility in nematogenic solvents 2005
CHRENKO R M Diamond growth rates and physical properties of laboratory-made diamond 1838
CHRISTIAN S D Effects of solvents on molecular complex formation equilibriums. Use of nonpolar analogs for polar solutes...................... 2413
CHRISTIE J R Effects of gas pressure on the viscosities of molten alkali nitrates. II. Potassium nitrate with helium, argon, and nitrogen..... 103
CHRISTOFFERSEN R E Semicontinuum model for the hydrated electron. II. Configurational stability of the ground state 2297

CHRYSOCHOOS J Reactivity of hydrogen atoms and hydrated electrons toward aqueous erythrosine. X-radiolysis 3020
CHUANG T T Infrared studies of adsorption and surface reactions of some secondary alcohols, C_3 to C_5, on γ-alumina and γ-alumina doped with sodium hydroxide 234
CHUNG Y J Electron spin resonance spectra of isocyanatoalkyl radicals 1893
CHUPKA W A Photoionization mass spectrometric study of xenon difluoride, xenon tetrafluoride, and xenon hexafluoride 1461
CHUPKA W A Ion-molecule reactions in ethanol by photoionization 3797
CIFERRI A Thermodynamics of elasticity in open systems. Elastin 142
CILLEY W A Polynuclear complex formation in solutions of calcium ion and 1-hydroxyethylene-1,1-diphosphonic acid. I. Complexometric and pH titrations 676
CIMINO A Structural, magnetic, and optical properties of nickel oxide supported on η- and γ-aluminas 1044
CIMINO A Catalytic activities of nickel oxide supported on γ- and η-aluminas for the nitrous oxide decomposition 1051
CLARK W G Reactions of methylene with 1,2-dichloro ethane and nonequilibrium unimolecular hydrogen chloride elimination from 1,3-dichloropropane, 1,4-dichlorobutane, and 1-chloropropane 2231
CLEARFIELD A Mechanism of ion exchange in crystalline zirconium phosphates. V. Thermodynamic treatment of the hydrogen ion-sodium ion exchange of α-zirconium phosphate 3750
CLEMENT C Molecular conformation of 1,3,5-trinitrohexahydro-s-triazine (RDX) in solution 2056
CLERC M Kinetic study of species formed during the pulsed radiolysis of ammonia 2908
CLEVER H L Excess Gibbs energy of mixing of 1,2,4-trimethylbenzene and 1,3,5-trimethylbenzene with several nitroparaffins by total intensity Rayleigh light scattering at 30° 3728
COCKE D L Mass spectrometric determination of the dissociation energies of the molecules Ho_2, HoAg, and HoAu 3264
COCKS A T Thermal unimolecular decomposition of 1,1,2-trimethylcyclobutane 1437
COETZEE J F Solute-solvent interactions. VI. Specific interactions of tetraphenylarsonium, tetraphenylphosphonium, and tetraphenylborate ions with water and other solvents 3141
COGLEY D R Selective solvation of ions by water in propylene carbonate 1477
COLE B Effect of magnetic fields on the pH of water 2830
COLE D L Kinetics of hydrolysis of ferric ion in dilute aqueous solution 929
COLEMAN A J Effect of adsorption potential on the hydrogen-deuterium exchange of benzene at a fuel cell electrode 3715
COLEMAN D M Complex formation between some acetylenic compounds and benzene 2128
COLLINS R L Organic solid state. IV. Effect of environment on electron transfer in biferrocene[iron(II)iron(III)] picrate 2025
COLON C J Nitrosamine anion radicals 2704
COLUCCIA S Infrared study of surface properties of α-chromia. I. Preparation and adsorption of water, heavy water, and carbon monoxide 2774
COLUCCIA S Infrared study of surface properties of α-chromia. II. Oxygen chemisorption 2783
COLUCCIA S Infrared study of surface properties of α-chromia. III. Adsorption of carbon dioxide 2790
COMBS L L Dielectric constant study of molecular association in polar-polar mixtures. o-Dichlorobenzene-butyl alcohol 2133
COMPANION A L Rittner ionic model study of alkali hydride dimers 984
CONLIN E T II Formation of diamond. IV. Behavior of the diamond-forming reaction with respect to catalyst composition 2158
CONTI L G On the exchange of chromate groups in fresh lead chromate 350
CONWAY B E Polyion hydration. I. Partial molar volumes and electrostriction of polyimine salts 2353
CONWAY B E Polyion hydration. II. Compressibility behavior of polyimine salts 2362
CONWAY B E Extrapolation procedures for evaluation of individual partial gram ionic volumes. Comments 3031
COOMBE R Effects of deuterium substitution on the electron-transfer reactions 447
COOPER G D Photochemistry of the ferrioxalate system 2897
COOPER J N Oxidation of hypophosphorous acid by vanadium(V) 891
COPELAND J L Effects of gas pressure on the viscosities of molten alkali nitrates. II. Potassium nitrate with helium, argon, and nitrogen 103
COPELAND R F Effect of Coulombic fields in the vicinity of metal surfaces upon the entropy and absolute rate of reaction of absorbed molecules 2967
CORIO P L Electron spin resonance studies of adsorbed alkene molecules on synthetic zeolites. Cation radicals of tetramethylethylene and cyclopentene 3475
CORSET J Trifluoracetic acid. Nature of association in diluted solutions in inert and slightly basic solvents 1327
COWAN D O Organic solid state. IV. Effect of environment on electron transfer in biferrocene[iron(II)iron(III)] picrate 2025
COWFER J A Absolute rate constants for the reactions of hydrogen atoms with olefins 1584
CRAIG N C Thermodynamics of cis-trans isomerizations. II. 1-Chloro-2-fluoroethylenes, 1,2-difluorocyclopropanes, and related molecules 1453
CRAIG N C Vibrational relaxation of hydrogen chloride by chlorine atoms and chlorine molecules 1622
CRESCENZI V Thermodynamic data for the water-hexamethylenetetramine system 3633
CRISS C M Viscosity coefficients of ions in various solvents 2532
CROSBY G A Measurement of photoluminescence quantum yields. Review 991
CROSSLEY J Dielectric relaxation of 1-butanol and 1-decanol in several solvents 1790
CROSSLEY R W Shock tube isomerization of cyclopropane 2526
CROWDER G A Vibrational spectra of tert-butyl cyanide 2806
CSILLAG K Transfer diffusion. II. Kinetics of electron exchange reaction between ferrocene and ferricinium ion in alcohols 3303
CUCARELLA M C M Absolute entropies, conformation, and Debye temperatures of bicyclo[2.2.2]octane- and of bicyclo[3.2.2]nonane-type molecules 1073
CUNNINGHAM J Reactions involving electron transfer at semiconductor surfaces. II. Photoassisted dissociation of nitrous oxide over illuminated ferric oxide and zinc oxides 617
CVETANOVIC R J Study of the low-temperature hydrogenation of ethylene on zinc oxide by temperature-programmed desorption 208
CVETANOVIC R J Reaction of oxygen atoms with cyclopentene 3056
CYVIN B N Infrared spectra of lithium tetrafluoroaluminate and sodium tetrafluoroaluminate ... 2609
CYVIN S J Infrared spectra of lithium tetrafluoroaluminate and sodium tetrafluoroaluminate ... 2609
CZAPSKI G Contribution of hydrogen atoms to molecular hydrogen $[G_{H_2}]$ in the radiation chemistry of aqueous solutions 31
CZAPSKI G Competition for e_{aq}^- between several scavengers at high concentrations and its implications on the relevance of dry electrons in the radiation chemistry of aqueous solutions 3626
CZAPSKI G Electron spin resonance studies of short-lived radicals generated by fast flow techniques in aqueous solutions 2957
CZAPSKI G Reactions of organic radicals formed by some "Fenton-like" reagents 3271
DABY E E Mass-spectrometric studies of rate constants for addition reactions of hydrogen and

of deuterium atoms with olefins in a discharge-flow system at 300°K 1601
DACEY J R The reaction $2COF_2 \rightarrow CO_2 + CF_4$ and the heat of formation of carbonyl fluoride 3024
DALE S W Nuclear magnetic spin-lattice relaxation times of phosphorus-31 in some organic and inorganic compounds 3537
D'ALESSANDRO R On the exchange of chromate groups in fresh lead chromate 350
DALLA LANA I G Infrared studies of adsorption and surface reactions of some secondary alcohols, C_3 to C_5, on γ-alumina and γ-alumina doped with sodium hydroxide 234
DANESI P R Electrochemical behavior of liquid anion membranes. Biionic potentials with the NO_3^-–Cl^-, NO_3^-–Br^-, Br^-–Cl^- couples 554
DANIEL S H Recoil tritium reactions with trimethylfluorosilane. A study on parameters affecting hot-atom substitution reactions 301
D'APRANO A Conductance and association behavior of alkali perchlorates in water at 25° 3290
DARBARI G S Correlation between translational and rotational relaxation times for ion pairs in solution 598
DAVIS D D Absolute rate constants for the reaction of atomic oxygen with 1-butene over the temperature range of 259–493°K 3902
DAVIS H T Theory of self-diffusion in three model dense fluids 1970
DAVIS K P Homogeneous and heterogeneous platinum-catalyzed isotopic hydrogen exchange in polycyclic aromatic hydrocarbons 1175
DAVIS S K Shock tube experiments on the pyrolysis of deuterium substituted ethylenes 1
DE S K N-H···π hydrogen bonding 2404
DEARMOND K Photolysis of rhodium(III) 1,10-phenanthroline chelates in glassy solution. Electron spin resonance study 3230
DEBACKER M G Metal-ethylenediamine solutions. Extinction coefficients and equilibriums 3092
DEDINAS J Photoreduction of benzophenone in benzene. II. Flash photolysis study of primary photochemical reactions 187
DEDINAS J Photoreduction of benzophenone in benzene. I. Mechanism of secondary reactions 181
DEES K Reactions of methylene with 1,2-dichloro ethane and nonequilibrium unimolecular hydrogen chloride elimination from 1,3-dichloropropane, 1,4-dichlorobutane, and 1-chloropropane 2231
DEES K Photolysis of ketene-butane mixtures with and without added carbon monoxide 2240
DEGRAFF B A Photochemistry of the ferrioxalate system 2897
DEITZ V R Dynamic adsorption of water vapor by a fiber drawn from a melt of Vycor 2718
DEKOCK R L Spectroscopy of rare earth oxide molecules in inert matrices at 4°K 514
DELBEN F Thermodynamic data for the water-hexamethylenetetramine system 3633
DELEON A Vacuum-ultraviolet photolysis of the C_4H_6 isomers. III. Cyclobutene 3656
DEMAS J N Evaluation of photoluminescence lifetimes 2463
DEMAS J N Measurement of photoluminescence quantum yields. Review 991
DEMETER K Transfer diffusion. II. Kinetics of electron exchange reaction between ferrocene and ferricinium ion in alcohols 3303
DENT A L Butene isomerization over zinc oxide 487
DEO A V Infrared studies of adsorption and surface reactions of some secondary alcohols, C_3 to C_5, on γ-alumina and γ-alumina doped with sodium hydroxide 234
DERRICK M E Excess Gibbs energy of mixing of 1,2,4-trimethylbenzene and 1,3,5-trimethylbenzene with several nitroparaffins by total intensity Rayleigh light scattering at 30° 3728
DESIENO R P Conductance of tetraalkylammonium halides in ethylene glycol 1722
DESNOYERS J E Extrapolation procedures for evaluation of individual partial gram ionic volumes. Comments 3031
DE TROBRIAND A Salting-in of nonpolar gases in aqueous tetraalkylammonium bromide solutions and the apparent molal volume of these salts in water 1803
DEVLIN J P Vibronic effects in the infrared spectrum of the anion of tetracyanoethylene 325
DEVOE H Calculations of the optical properties of 1-methyluracil crystal by an all-order classical oscillator theory 1509
DEWALD R R Rate of the reaction of the ammoniated electron with the ammonium ion at -35° 986
DEWAN R K Viscosity of liquid mixtures 3113
DEWAN R K Intrinsic viscosity of short-chain normal alkanes 3120
DE WET W J Investigations on the ion-exchange and ionic transport properties of glass membranes in molten salts by an electrolytic transport technique 2815
DEWING E W Electrical conductance of gaseous mixtures of aluminum trichloride and sodium tetrachloroaluminate 1260
DHAR S K Solubility of helium and argon in liquid sodium 2832
DIAMOND R M Anion exchange in mixed organic-aqueous solutions. I. Dioxane-water 79
DIEBLER H Kinetics of proton transfer reactions of polyacrylic and polymethacrylic acids with an indicator 267
DIESEN R W Mass spectral study of the decomposition of chlorine fluoride behind shock waves 1765
DILLON J J Electron paramagnetic resonance spectra of pyrrolidino and pyrrolino free radicals. Structure of dialkylamino radicals 3486
DI NAPOLI V On the exchange of chromate groups in fresh lead chromate 350
DIXON R S Second triplet level of 1,5-dichloroanthracene in fluid solutions 845
DO J Energy partitioning on photolysis and pyrolysis of 3-vinyl-1-pyrazoline 1640
DOBLHOFER K Electrosorption of 5-chloro-1-pentanol at the mercury-solution interface 1698
DOEPKER R D Vacuum-ultraviolet photolysis of the C_4H_6 isomers. III. Cyclobutene 3656
DOLE M Radiation chemistry of polyethylene. XI. The molten state 1671
DOLE M Infrared spectrum of polyethylene irradiated at 4°K 3988
DONALDSON G W Radiolysis of colloidal sulfur. Mechanism for solubilization 756
DOREMUS R H Internal hydroxyl groups near the surface of silica 3147
DORER F H Energy partitioning on photolysis and pyrolysis of 3-vinyl-1-pyrazoline 1640
DORER F H Energy partitioning on photolysis of di-tert-butyl peroxide 3651
DORKO E A Shock tube isomerization of cyclopropane 2526
DOYLE L C Reaction of oxygen atoms with cyclopentene 3056
DRAGANIC I Pulse radiolysis of aqueous cyanogen solution 608
DRAGANIC I G Formation of primary yields of hydrogen peroxide and molecular hydrogen ($G_{H_2O_2}$ and G_{H_2}) in the γ radiolysis of neutral aqueous solutions 3950
DRAGANIC Z D Formation of primary yields of hydrogen peroxide and molecular hydrogen ($G_{H_2O_2}$ and G_{H_2}) in the γ radiolysis of neutral aqueous solutions 3950
DRAGANIC Z D Pulse radiolysis of aqueous cyanogen solution 608
DUEWER W H Relative total scattering cross sections for homologous series of polar and nonpolar molecules 727
DUNN L A Electrical conductances and ionization behavior of sodium chloride in dioxane-water solutions at 100° and pressures to 4000 bars 1099
DUNN M R Mass spectrometric study of the reaction of hydrogen atoms with nitrosyl chloride 722
DUNN M R Mass spectrometric study of the reaction of nitrogen atoms with nitrosyl chloride 1172
DUNN M R Mass spectrometric study of the reaction of oxygen atoms with nitrosyl chloride 1320
DUNN M R Photometric and mass spectrometric observations on the reaction of hydrogen atoms with cyanogen 2662

DUNNING B K Photochemical behavior of isocyanides 580
DURIG J R Vibrational spectra of trans- and cis-crotononitrile 44
DURIG J R Vibrational spectra and structure of biacetyl 1946
DURIG J R Vibrational spectra and structure of organophosphorus compounds. X. Methyl torsional frequencies and barriers to internal rotation of some CH_3PXY_2 compounds 1956
DURIG J R Vibrational spectra and structure of dimethylaminodichlorophosphine 3837
DURIG J R Low-frequency modes in molecular crystals. XVII. Torsional motions and barriers to internal rotation in some ethylsilanes, ethylgermanes, and ethanol 3993
DWORKIN A S Miscibility of liquid metals with salts. X. Various studies in alkaline earth metal-metal fluoride and rare earth metal-metal difluoride and trifluoride systems 2340
DYBOWSKI C R Nuclear magnetic relaxation in an homologous series of nematic liquid crystals.. 3834
DYE J L Metal-ethylenediamine solutions. Extinction coefficients and equilibriums 3092
EDGELL W F Hidden degeneracy and the vibration of larger molecules 1343
EDMONDS P D Proton transfer reactions. Mechanism for the absorption of ultrasound in aqueous solutions of proteins 4012
EDWARDS J G High-molecular-weight boron sulfides. VII. Lower temperature studies and metastable decompositions 2410
EDWARDS J O Reactions of acetone and hydrogen peroxide. I. Primary adduct 3004
EDWARDS J O Reaction of acetaldehyde and tert-butyl hydroperoxide 3377
EGLAND R J Origin of complex electron spin resonance spectra of γ-irradiated polycrystalline n-alkyl iodides with even number of carbon atoms per molecule 467
EIBEN K Electron spin resonance studies of transient radicals in aqueous solutions 1186
EICHER L D High-precision viscosity of supercooled water and analysis of the extended range temperature coefficient 2016
EINOLF C W JR Low-frequency dielectric dispersion in suspensions of ion-exchange resins ... 1091
EIRICH F R Interactions of aqueous poly(N-vinylpyrrolidone) with sodium dodecyl sulfate. I. Equilibrium dialysis measurements 3135
EKSTROM A Ionic species formed from benzene during radiolysis of its solutions in 3-methylpentane at 77°K. Reply to comments 1178
EL-AWADY A A Determination of the number of species present in a system. New matrix rank treatment of spectrophotometric data 2954
ELWORTHY P H Investigations of aqueous mixtures of nonionic surfactants by membrane osmometry 2212
ELY J F Statistical mechanical theory of electrostriction in dense gases 771
ENDICOTT J F Ultraviolet photochemistry of acetatopentaamminecobalt(III) in aqueous solution 1914
ENDICOTT J F Ultraviolet photochemistry of ruthenium(III) ammine complexes 3075
ENGLEMAN V S Kinetics of chlorine monofluoride at high temperatures 3939
ENTINE G High-yield method for the preparation of anomalous water 2976
EON C Thermodynamic study of the formation of electron donor-acceptor complexes by gas-liquid chromatography 2632
EPPSTEIN L B Isotope effects in the diffusion of carbon-14 substituted molecules in the liquid phase. II. Relative diffusion rates of benzene-1-^{14}C and benzene-1,2-^{14}C 1315
ERNO B P Molecular association of hydrogen-bonding solutes. Phenol in carbon tetrachloride 3591
ESPENSON J H Electron transfer reactions of ferrocenes 3381
EUSTACE D J Electron spin resonance and electron nuclear double resonance study of the 4-formyl-2,6-di-tert-butylphenoxy radical 2765
EVANS D F Transport properties in hydrogen bonding solvents. VI. The conductance of electrolytes in 2,2,2-trifluoroethanol 1708
EVANS D F Conductance of electrolytes in acetone and in 1-propanol-acetone mixtures at 25° 1714
EVANS R Mechanism of the radiation-induced dechlorination of 1,1,1-trichloro-2,2-bis(p-chlorophenyl)ethane in alcoholic solution 2762
EYLAR E H Dependence of micelle aggregation number on polar head structure. I. Light scattering by aqueous solutions of decylammonium salts and related surfactants 369
EYRING E M Kinetics of hydrolysis of ferric ion in dilute aqueous solution 929
EYRING E M Spectrophotometric dissociation field effect kinetics of aqueous acetic acid and bromocresol green 2488
EYRING E M Specific rates in the acid dissociation-ion recombination equilibrium of dilute aqueous hydrazoic acid at 25° 3026
FANELLI A Outer-sphere association kinetics of magnesium(II), manganese(II), cobalt(II), nickel(II), copper(II), and zinc(II) m-benzenedisulfonates in methanol 2649
FARBER M Mass spectrometric determination of the heats of formation of aluminum oxide chloride(g) and aluminum oxide fluoride(g) 1760
FARISH S H Dielectric constant study of molecular association in polar-polar mixtures. o-Dichlorobenzene-butyl alcohol 2133
FARMER G No evidence for the dimerization of nitromethane in carbon tetrachloride and benzene solutions 3892
FARMER J B Electron spin resonance of free radicals prepared by the reactions of methylene. Deuteriomethyl and formaldiminoxy radicals 2448
FASMAN G D Circular dichroism studies of lysine-rich histone f-1-deoxyribonucleic acid complexes. Effect of salts and dioxane upon conformation 1516
FEDER H M Solubility of helium and argon in liquid sodium 2832
FEHLNER T P Reactions of borane (BH_3). III. Absolute rates of formation of the donor-acceptor adducts phosphorus trifluoride-borane (BH_3PF_3) and trimethylamine-borane ($BH_3N(CH_3)_3$) 2711
FEILLOLAY A Enthalpy of solution of some molecules in aqueous tetraalkylammonium bromide solutions and the apparent expansion coefficient of the aqueous salt solution 2330
FELBER B J Heats of association for divalent transition metal ethylene-maleic acid copolymer complexes 1136
FELDBERG S W Nuances of the ECE mechanism. III. Effects of homogeneous redox equilibrium in cyclic voltammetry 2377
FELDBERG S W Chromium(II)-catalyzed aquation of hexacyanochromate(III) to pentacyanomonohydroxychromate(III) 2381
FENDLER J H Radiation chemistry of aqueous solutions of trichlorofluoromethane, dichlorodifluoromethane, and chlorotrifluoromethane 455
FENDLER J H Solubilization of benzene in aqueous cetyltrimethylammonium bromide measured by differential spectroscopy. Comment 3907
FENG D-F Semicontinuum model for the hydrated electron. II. Configurational stability of the ground state 2297
FENRICK H W Growth and decay of alkyl radicals in γ-irradiated alkyl iodides at 77°K 472
FERNANDEZ-PRINI R Examination of the Zwanzig theory of dielectric firction. II 239
FERREIRA R Bonding properties of diatomic molecular orbitals 3012
FESSENDEN R W Electron spin resonance study of radicals produced in irradiated aqueous solutions of amines and amino acids 738
FESSENDEN R W Electron spin resonance studies of transient radicals in aqueous solutions ... 1186
FESSENDEN R W Electron spin resonance study of the rate constants for reaction of hydrogen atoms with organic compounds in aqueous solution 1654

FESSENDEN R W Electron spin resonance study of radicals produced in irradiated aqueous solutions of thiols 2277

FESSENDEN R W Investigation of radicals produced in the photolysis of thiosulfate solutions by electron spin resonance 2752

FIELD P E Interactions of gases in ionic liquids. I. Solubility of nonpolar gases in molten sodium nitrate 821

FILBY E E Dissociation energies of gaseous gadolinium dicarbide and terbium dicarbide 848

FILHOL A Molecular conformation of 1,3,5-trinitrohexahydro-s-triazine (RDX) in solution 2056

FILIPESCU N Excimer model for fluorene and dibenzofuran 1794

FINCH A Solvation studies. II. Alkaline earth halides in high dielectric solvents 2325

FINK R D Reactions of fast hydrogen atoms with ethane 841

FINNEY C D Low-energy electron radiolysis of methane 2405

FISCHER E Spectra and cis-trans isomerism in highly dipolar derivatives of azobenzene 581

FISCHER H Nuclear and electron spin polarizations during radical reactions 3410

FISHMAN M L Interactions of aqueous poly(N-vinylpyrrolidone) with sodium dodecyl sulfate. I. Equilibrium dialysis measurements 3135

FITZGERALD E A JR Photochemical oxidation of some substituted aromatic amines in chloroform 2737

FLANAGAN T B Self-diffusion of water in uranyl nitrate hexahydrate 1272

FLETCHER A N Self-association of methanol vapor. Evidence for dimers and tetramers 1808

FLETCHER E A Explosion limits of chlorine-fluorine mixtures 867

FLETTERICK R J Crystal and molecular structure of L-alanyl-L-alanine 918

FLIPPEN J L Heptanol as a guest molecule in Dianin's compound 3566

FLORA H B Ionization of trichloroacetic acid in aqueous solutions 2492

FLORENCE A T Micelle formation by some phenothiazine derivatives. II. Nuclear magnetic resonance studies in deuterium oxide 3554

FLORIN A E Nitrogen-15 nuclear magnetic resonance shifts and coupling constants for the methylamine hydrochlorides in aqueous solution 1758

FLORIN A E Nitrogen-15 nuclear magnetic resonance shifts in pure methylamines and pure methyl isocyanide-nitrogen-15 932

FOLMAN M Dielectric absorption of adsorbed sulfur dioxide in the microwave region 532

FOLMAN M Microwave absorption and potential barrier for orientation. Sulfur dioxide adsorbed on sodium chloride and potassium chloride 2602

FOREL M T Molecular conformation of 1,3,5-trinitrohexahydro-s-triazine (RDX) in solution 2056

FORSEN S Nuclear magnetic resonance study of hindered internal rotation in urea in solution 1901

FORSEN S Interaction of halide ions with organic cations containing charged nitrogen, phosphorus, or sulfur in aqueous solutions studied by nuclear quadrupole relaxation 2936

FORT R C JR Proton magnetic resonance study of the hydrogen bonding of alkylated bases to dimethyl sulfoxide 3963

FOYT D C Spin-free quantum chemistry. X. Effective spin Hamiltonian 1866

FOYT D C Linear symmetric helium dihydride. Model superexchange system 1874

FRANKEL L S Nuclear magnetic resonance study of ion-exchange resins. Macroreticular resins, carboxylic acid resins, and line-width effects 1211

FRANKLIN M L Self-diffusion of water in uranyl nitrate hexahydrate 1272

FRAZIER G C JR Recombination of bromine atoms in a laminar hydrogen-bromine flame 3046

FREED J H Electron spin resonance line shapes and saturation in the slow motional region 3385

FREEMAN C G Mass spectrometric study of the reaction of hydrogen atoms with nitrosyl chloride 722

FREEMAN C G Mass spectrometric study of the reaction of nitrogen atoms with nitrosyl chloride 1172

FREEMAN C G Mass spectrometric study of the reaction of oxygen atoms with nitrosyl chloride 1320

FREEMAN C G Photometric and mass spectrometric observations on the reaction of hydrogen atoms with cyanogen 2662

FREEMAN G R Influence of temperature on the γ radiolysis of isopropyl alcohol vapor. Effect of molecular structure on the nonchain and chain decompositions of alcohol vapors 20

FREEMAN G R γ-Radiolysis of liquid ethanol. Yields of hydrogen and free ions. Solvated electron rate constants 2756

FREEMAN G R Effect of olefins on the reactions of nitrous oxide in γ-irradiated liquid cyclopentane 2560

FREND M A Single-pulse shock tube studies of hydrocarbon pyrolysis. II. Pyrolysis of ethane 1492

FREY H M Thermal unimolecular decomposition of 1,1,2-trimethylcyclobutane 1437

FRIBERG S Kinetics of the catalysis by reversed micelles of cetyltrimethylammonium bromide in hexanol 2001

FRIDMANN S A Reactions of borane (BH_3). III. Absolute rates of formation of the donor-acceptor adducts phosphorus trifluoride-borane (BH_3PF_3) and trimethylamine-borane ($BH_3N(CH_3)_3$) 2711

FRIEDEL R A Infrared spectra of ground graphite 1149

FRIEDMAN H L Electron paramagnetic resonance probes for hydrophobic interaction in aqueous solutions 165

FRIEDMAN H L The solvent-isotope effect in the enthalpy of some solutes in methanol 388

FRIEDMAN H L Solvation enthalpies of hydrocarbons and normal alcohols in highly polar solvents 3598

FRIEDMAN H L Solvation enthalpies of electrolytes in methanol and dimethylformamide 3606

FRIEDRICH V J Transfer diffusion. I. Theoretical 3297

FRIEDRICH V J Transfer diffusion. II. Kinetics of electron exchange reaction between ferrocene and ferricinium ion in alcohols 3303

FROBEN F W Paramagnetic species produced by ultraviolet irradiation of lithium, potassium, sodium, magnesium, and cadmium in 3-methylpentane at 77°K 35

FROBEN F W Decomposition of ammonia and hydrazine by electron impact 769

FUEKI K Photoisomerization of maleate radical anions produced in 2-methyltetrahydrofuran by γ-irradiation at 77°K 482

FUEKI K Semicontinuum model for the hydrated electron. II. Configurational stability of the ground state 2297

FUJISAKI N Radiolysis of liquid n-butane 2854

FUJITA Y Electron spin resonance signals of abnormal alkyl radicals trapped on porous Vycor glass surfaces coated with metal oxides at 77°K 4064

FUNABASHI K Effects of optical bleaching on luminescence decay and trapped electron concentrations in γ-irradiated 3-methylpentane at 77°K 3221

FUNK E W Solubilities of hydrocarbons and carbon dioxide in liquid methane and in liquid argon 2345

FUNK E W Entropies of vaporization for fluorocarbons and hydrocarbons from the Hildebrand rule 2530

FUTRELL J H Kinetics of chemical ionization. I. Reaction of tert-$C_4H_9^+$ with benzyl acetate 590

GABOR G New absorption bands in solutions of alkali metals in amines 286

GABOR G Spectra and cis-trans isomerism in highly dipolar derivatives of azobenzene 581

GADEKEN O C Reactions of iodine with olefins. II. Radiative neutron capture induced reactions of iodine-128 with various C_5 isomers. Evidence for a mechanism other than autoradiolysis in the condensed state 2880

GAGNON W F Scavenging of the molecular hydrogen yield from water irradiated with tritium β particles 601

GAIDIS J M Mass spectra of disilanes. Phenyl-silicon interaction and silicon-silicon bond strength 974
GAINEY B W Pure and mixed second virial coefficients of line-core molecules. I. Theory 3687
GAINEY B W Pure and mixed second virial coefficients of line-core molecules. II. Comparison with experiment 3691
GALLAGHER P K Kinetics of the decomposition of freeze-dried iron(II) sulfate 1179
GAMMAGE R B Electron paramagnetic resonance studies of carbon monoxide adsorbed on thorium oxide 895
GANDLER J Reactions of adsorbed organic molecules. II. Bromination of 4-nitrobiphenyl on a silica surface 887
GARDINER W C JR Initiation rate for shock-heated hydrogen-oxygen-carbon monoxide-argon mixtures as determined by OH induction time measurements 1504
GARDNER C L Electron spin resonance of free radicals prepared by the reactions of methylene. Deuteriomethyl and formaldiminoxy radicals 2448
GARDNER C L Electron spin resonance of atomic silver on porous glass and silica gel surfaces 2706
GARDNER P J Solvation studies. II. Alkaline earth halides in high dielectric solvents 2325
GARIBALDO G B Thermodynamics of elasticity in open systems. Elastin 142
GARLAND F Ultrasonic relaxation of tert-butyl alcohol in cyclohexane 3182
GARLAND J K Recoil tritium reactions with propene in the gas phase 1031
GARNETT J L Homogeneous and heterogeneous platinum-catalyzed isotopic hydrogen exchange in polycyclic aromatic hydrocarbons 1175
GASPAR P States of atomic carbon produced in decomposition of organic compounds in a microwave plasma 445
GAY I D Numerical quadrature methods in the analysis of reaction kinetic experiments 1610
GEER R D Dependence of micelle aggregation number on polar head structure. I. Light scattering by aqueous solutions of decylammonium salts and related surfactants 369
GEIGER W E JR Donor-acceptor complexes of phenothiazine and phenoxazine with nickel thiete 2387
GEORGAKAKOS J H Vibrational deexcitation of highly excited polyatomic molecules. Amount of energy transferred per collision 3376
GEORGIEV Z L Tunneling corrections in chemical kinetics 1748
GERA L Catalytic decomposition of perchloric acid vapor on zinc oxide 491
GERMANO N J Aggregation of arylazonaphthols. II. Steric effects on dimer structure in water 1227
GERRY M C L Electron spin resonance of free radicals prepared by the reactions of methylene. Deuteriomethyl and formaldiminoxy radicals 2448
GETOFF N Pulse radiolysis of oxalic acid and oxalates 749
GHIOTTI G Infrared study of surface properties of α-chromia. I. Preparation and adsorption of water, heavy water, and carbon monoxide 2774
GHIOTTI G Infrared study of surface properties of α-chromia. III. Adsorption of carbon dioxide 2790
GHORMLEY J A Production of hydrogen, hydroxide, and hydrogen peroxide in the flash photolysis of ice 40
GIBBONS R M Approximate equation of state. I. Modified Percus-Yevick equation for argon 3568
GILEADI E Adsorption inhibition as a mechanism for the antithrombogenic activity of some drugs. I. Competitive adsorption of fibrinogen and heparin on mica 2107
GILKERSON W R Charge density on the phosphoryl oxygen in a series of phosphate esters. Tributyl phosphate, a monocyclic phosphate, and a bicyclic phosphate ester 3309
GILLES L Flash photolysis of chlorate ion in aqueous solution 2177
GILLES P W High-molecular-weight boron sulfides. VII. Lower temperature studies and metastable decompositions 2410
GINGERICH K A Mass spectrometric determination of the dissociation energies of the molecules Ho_2, HoAg, and HoAu 3264
GISLASON E A Dynamics of the reactions of O_2^+ with molecular hydrogen and deuterium 1426
GISSER H Competitive adsorption of phenol and sodium dinonylnaphthalenesulfonate on nickel oxide powder 1975
GITLIN S N Phase transitions in water adsorbed on silica surfaces 3322
GLOVER M E Intermolecular hydrogen bonding. I. Effects on the physical properties of tetramethylurea-water mixtures 3313
GODDARD N Effect of phosphorus-hydrogen deuterium substitution on the phosphorus-31 nuclear magnetic resonance spectroscopy of several dialkyl phosphonates 3547
GOEL A Distorted hydrogen bonds formed by carbonyl compounds 1744
GOLDBERG I B Simultaneous electrochemical-electron spin resonance measurements. I. Cell design and preliminary results 3281
GOLDEN D M Kinetics and thermochemistry of the gas-phase bromination of bromoform. C-H bond dissociation energy in bromoform and the C-Br dissociation energy in carbon tetrabromide 987
GOLDEN D M Comparison of RRK [Rice-Ramsperger-Kassel] and RRKM [Rice-Ramsperger-Kassel-Marcus] theories for thermal unimolecular processes 1333
GOLDEN S Analysis of broadly overlapping absorption bands according to a two-absorber model 3635
GOLDMAN S Solute-solvent effects in the ionization of tris(hydroxymethyl)acetic acid and related acids in water and aqueous methanol 826
GOLDSCHMIDT C R Intersystem crossing in the charge-transfer quenching of molecular fluorescence 1025
GOLDSCHMIDT C R Laser photolysis of perylene solutions 3894
GOLDSMITH R L Hydrogen promotion of the palladium-catalyzed carbon monoxide oxidation 2065
GOLDSTEIN J H Nuclear magnetic resonance spectra and substituent effects for symmetrically substituted dihalobiphenyls 421
GOLUB M A Photolysis of 1,4-dichlorobutane sensitized by various aliphatic ketones 1168
GORDON L Acid-base equilibriums of fluorescein and 2′, 7′-dichlorofluorescein in their ground and fluorescent states 245
GORDON S Pulse radiolysis of ammonia gas. II. Rate of disappearance of the $NH_2(X^2B_1)$ radical 2087
GORMAN R R Adsorption of fibrinogen. Electron microscope study 2103
GOTTLIEB M H Rates of exchange between free and bound counterions in polyelectrolyte solutions. I. Electroosmotic flows during determinations made by an electrical transference method 1981
GOTTLIEB M H Rates of exchange between free and bound counterions in polyelectrolyte solutions. II. Explanation for the anomalous results obtained by the electrical transference method 1985
GOTTLIEB M H Rates of exchange between free and bound counterions in polyelectrolyte solutions. III. Demonstration that the exchange is not as slow as indicated by the electrical transference measurements 1990
GOUTERMAN M Spectrum of matrix-isolated carbon disulfide 2204
GRABENSTETTER R J Polynuclear complex formation in solutions of calcium ion and 1-hydroxyethylene-1,1-diphosphonic acid. I. Complexometric and pH titrations 676
GRACEFFA P Solvated electron or not 843
GRACEFFA P Solvated electron in any case, but what kind 3905
GRAETZEL M Radiation chemical yield of OH^- as determined by conductometric pulse radiolysis 1759

GRAETZEL M Conductometric pulse radiolysis determination of ionic yields and neutralization kinetics in liquid ethanol 3893
GRAHAM L L Chain association equilibriums. Nuclear magnetic resonance study of the hydrogen bonding of N-monosubstituted amides. II. In carbon tetrachloride 776
GRAHAM L L Chain association equilibriums. Nuclear magnetic resonance study of the hydrogen bonding of N-monosubstituted amines. III. In dioxane 784
GRANT C W M Electron spin resonance of atomic silver on porous glass and silica gel surfaces..... 2706
GRANT D M Dipolar contributions to carbon-13 relaxation times 585
GRANT D M Dominance of intramolecular dipole-dipole mechanisms upon carbon-13 relaxation in benzene and cyclohexane 2538
GRANT D M Effect of molecular association on carbon-hydrogen nuclear dipolar relaxation rates 2539
GRANT D M Field-dependent contributions to carbon-13 nuclear relaxation........ 3967
GRECO P W Conductance of tetraalkylammonium halides in ethylene glycol 1722
GREEN D W Low-lying electronic states of the scandium oxide, yttrium oxide, and lanthanum oxide molecules........ 3103
GREEN M E Noise spectra associated with hydrochloric acid transport through some cation-exchange membranes........ 654
GREEN W J Interactions of gases in ionic liquids. I. Solubility of nonpolar gases in molten sodium nitrate 821
GREENLIEF C M A virial treatment for the adsorption of gases on liquids 344
GREGORY N W Molecular complexes in the vapor of sodium bromide and zinc bromide mixtures 3028
GREGORY N W Spectrophotometric study of the equilibrium between copper(I) bromide, copper(II) bromide, and bromine 592
GRIFFITH O H Role of lipid spin labels in membrane biophysics........ 3417
GRIFFITH O H Electron spin resonance study of x-irradiated long-chain alcohols oriented in urea inclusion crystals........ 3489
GROSSWEINER L I Chemiluminescent reaction of hydrated electrons with optically excited fluorescein dyes........ 764
GRUNDNES J Vapor-phase charge-transfer complexes. VI. Diethyl ether-iodine 3682
GRUNWALD E Selective solvation of ions by water in propylene carbonate........ 1477
GUGLIELMINOTTI E Infrared study of surface properties of α-chromia. I. Preparation and adsorption of water, heavy water, and carbon monoxide 2774
GUGLIELMINOTTI E Infrared study of surface properties of α-chromia. III. Adsorption of carbon dioxide 2790
GUIOCHON G Thermodynamic study of the formation of electron donor-acceptor complexes by gas-liquid chromatography 2632
GUPTA A R Thermodynamic theory of ion-exchange equilibriums in nonaqueous solvents..... 1152
GUPTA S K Thermodynamic investigation of the tungsten-oxygen-bromine system 112
GUPTA Y K Kinetics and mechanism of the reduction of iodate to iodite by bromide in the presence of phenol........ 2516
GUTMAN D Shock-tube study of acetylene-molecular oxygen reaction. Acceleration of reaction in the presence of trace amounts of chromium hexacarbonyl 2402
GUYON P M Photoionization mass spectrometric study of xenon difluoride, xenon tetrafluoride, and xenon hexafluoride........ 1461
GUZZO A V Radical anions of vitamin A aldehyde and related Schiff bases........ 2861
GUZZO A V Singlet-triplet absorption spectrum of all-trans-retinal........ 983
HAAS Y Pathways of radiative and radiationless transitions in europium(III) solutions. Role of solvents and anions........ 3668
HAAS Y Pathways of radiative and radiationless transitions in europium(III) solutions. The role of high energy vibrations........ 3677
HADLEY S G Direct determination of singlet → triplet intersystem crossing quantum yield. II. Quinoline, isoquinoline, and quinoxaline 2083
HAGEGE-TEMMAN J Kinetic study of species formed during the pulsed radiolysis of ammonia. 2908
HAIR M L Reaction of hexamethyldisilazane with silica........ 2181
HALL W K Catalytic oxidation. IV. Ethylene and propylene oxidation over gold 2914
HALPER W Photolysis of rhodium(III) 1,10-phenanthroline chelates in glassy solution. Electron spin resonance study........ 3230
HAMILL W H Electronic processes in the pulse radiolysis of aqueous solutions of halide ions 3081
HAMMOND G S Radiation-induced chain isomerization of cis-1,2-diphenylpropene in cyclohexane........ 292
HAMORI E Kinetics investigation of the amylose-iodine reaction 272
HAN H R Binding states of hydrogen and of nitrogen on the (100) plane of molybdenum...... 227
HAN M Chymotrypsinogen family of proteins. XV. pH and temperature dependence of the α-chymotryptic hydrolysis of N-acetyl-L-tryptophan ethyl ester 1375
HAND C W Mass spectrum of isocyanic acid..... 1532
HANNA E M Ion pairing in 2:2 electrolytes...... 291
HANNUM S E Vibrational spectra and structure of biacetyl 1946
HARBOUR J Radical anions of vitamin A aldehyde and related Schiff bases........ 2861
HARLAND P W Autodetachment lifetimes, attachment cross sections, and negative ions formed by sulfur hexafluoride and sulfur tetrafluoride .. 3517
HARRINGTON P C Electronic absorption spectra and electron paramagnetic resonance of copper(II)-amine complexes........ 3355
HARRIS R K Dipolar contributions to carbon-13 relaxation times 585
HART E J Absorption spectrum of e_{aq}^- in the temperature range -4 to 390° 2798
HARTER D A Photochemistry of the xylenes. Discussion of method 2741
HARTIG R Kinetics of the shock wave thermolysis of 1,1,2,2-tetrafluoroethane........ 3195
HARTKOPF A Study of the adsorption of insoluble and sparingly soluble vapors at the gas-liquid interface of water by gas chromatography........ 3870
HATANO H Photoinduced hole-electron recombination in a γ-irradiated single crystal of L-cystine dihydrochloride........ 3746
HATANO Y Radiolysis of liquid n-butane....... 2854
HATANO Y Gas-phase radiolysis of nitrous oxide. Effect of the addition of several hydrocarbons........ 3178
HATHAWAY E J Structural studies of magnesium halide-potassium halide melts by Raman spectroscopy........ 155
HAUGE R H Matrix-isolation study of the pyrolysis of bromochloromethyl-substituted organomercury compounds. Infrared spectra of the bromochlorocarbene and free radicals CCl_2Br and $CClBr_2$........ 3984
HAUGH M J Predissociation and dissociation energy of HBr^+........ 1472
HAWKE J G Radiation chemistry of crystalline glycollic acid........ 1648
HAWLEY C W Vibrational spectra of trans- and cis-crotononitrile 44
HAWLEY C W Low-frequency modes in molecular crystals. XVII. Torsional motions and barriers to internal rotation in some ethylsilanes, ethylgermanes, and ethanol 3993
HAYASHI K Dissociative electron capture process of methyl vinyl ether in organic glasses..... 476
HAYASHI N Pulse radiolysis of liquid amides... 2267
HAYES D M A potential surface for a nonlinear cheletropic reaction. The decarbonylation of cyclopropanone........ 340
HAYNS M R Electron correlation and the charge distribution in lithium hydride........ 416
HAYON E Spectroscopic investigation of cyclohexanol and cyclohexyl radicals and their corresponding peroxy radicals 1677

HAYON E Intermediates produced in the flash photolysis of acetone and amides in aqueous solution 1910
HAYON E Pulse radiolysis of liquid amides 2267
HEARNE J A Formation of ethane, ethylene, and acetylene from methane on radiolysis with high-intensity electron pulses 1164
HEBERT C Effects of optical bleaching on luminescence decay and trapped electron concentrations in γ-irradiated 3-methylpentane at 77°K 3221
HEICKLEN J Photooxidation of carbon disulfide 854
HEICKLEN J Kinetics and mechanism of the carbon disulfide-oxygen explosion 861
HEICKLEN J Mercury-sensitized photodecomposition of nitrous oxide in the presence of mixtures of carbon monoxide and methane 3205
HELENE C Environmental effects on the deprotonation of indole derivatives in alkaline ices 3061
HELPHREY D B Corresponding states and the glass transition for alkali metal nitrates 2306
HELTON R W Kinetic energy isotope effects of bromine reactions activated by radiative neutron capture in gaseous methyl fluoride and methyl-d_3 fluoride 2072
HEMMES P Kinetics of hydrolysis of ferric ion in dilute aqueous solution 929
HENGLEIN A Radiation chemical yield of OH as determined by conductometric pulse radiolysis 1759
HENGSTENBERG D Bubble nucleation in n-pentane, n-hexane and n-pentane + hexadecane mixtures and water 3613
HENTZ R R Radiation-induced isomerization of the 1,2-diphenylpropenes in polar liquids 2394
HENTZ R R Photolysis of gaseous 1,4-dioxane at 1470 Ang 3899
HEPLER L G Molecular association of hydrogen-bonding solutes. Phenol in carbon tetrachloride 3591
HERLEY P J Effects of radiation on the thermal decomposition induction period in ammonium perchlorate and other pseudostable materials 191
HERMANN R B Theory of hydrophobic bonding. I. The solubility of hydrocarbons in water, within the context of the significant structure theory of liquids 363
HERRON J T Absolute rate constants for the reaction of atomic oxygen with 1-butene over the temperature range of 259-493°K 3902
HERTL W Reaction of hexamethyldisilazane with silica 2181
HESSELINK F TH Theory of the stabilization of dispersions by adsorbed macromolecules. I. Statistics of the change of some configurational properties of adsorbed macromolecules on the approach of an impenetrable interface 65
HESSELINK F TH Theory of the stabilization of dispersions by adsorbed macromolecules. II. Interaction between two flat particles 2094
HICKEL B Flash photolysis of chlorate ion in aqueous solution 2177
HICKS C P Pure and mixed second virial coefficients of line-core molecules. I. Theory 3687
HICKS C P Pure and mixed second virial coefficients of line-core molecules. II. Comparison with experiment 3691
HICKS K W Kinetic studies of permanganate oxidation reactions. III. Reaction with tris(1,10-phenanthroline)iron(II) 1107
HILDEN D L Spectrophotometric study of the equilibrium between copper(I) bromide, copper(II) bromide, and bromine 592
HILTNER P A Diffraction of light by nonaqueous ordered suspensions 1881
HIMEL C M Nuclear magnetic resonance study of the protolysis kinetics of 5-dimethylaminonaphthalene-1-sulfonic acid and its N-methylsulfonamide 4056
HINCHCLIFFE A J Vibrational analysis for the molecules gallium oxide, indium oxide, and thallium oxide. Comment 3908
HOBBS M E Catalysis of the exchange of the ethanol hydroxyl proton by some divalent metallic ions 1994
HOBBS M E Nuclear magnetic spin-lattice relaxation times of phosphorus-31 in some organic and inorganic compounds 3537
HOCHANADEL C J Production of hydrogen, hydroxide, and hydrogen peroxide in the flash photolysis of ice 40
HOFFMAN M Z Ultraviolet photochemistry of acetatopentaamminecobalt(III) in aqueous solution 1914
HOFFMANN R A potential surface for a nonlinear cheletropic reaction. The decarbonylation of cyclopropanone 340
HOLDREN G R Rate constants for reaction of hydrogen atoms in aqueous solutions 449
HOLLOWAY J H Photoionization mass spectrometric study of xenon difluoride, xenon tetrafluoride, and xenon hexafluoride 1461
HOLMES C A Oxidation of hypophosphorous acid by vanadium(V) 891
HOLROYD R A Pulse radiolysis of aqueous cyanogen solution 608
HOMANN K H Structure of fluorine-supported flames. I. Method of investigation. Dichlorodifluoromethane-fluorine flame 3645
HORIE O Recombination of bromine atoms in a laminar hydrogen-bromine flame 3046
HORRELL D R Radiolysis of liquid 1,1,2-trichlorotrifluoroethane 2217
HORRELL D R Radiation-induced oxidation of trichloroethylene 613
HOSAKA A Recoil tritium reactions with cyclobutane-d_8. Excitation energies accompanying substitution of energetic tritium for deuterium 3781
HOWARD L O Conductance study of squaric acid aqueous dissociation 1798
HOWE G R Improved numerical method for evaluating second-order rate constants 1319
HOWER C O Replacement reactions of hot chlorine atoms in chlorofluoromethanes 2685
HOWER J F Spin-label investigation of ion-exchange resins 907
HOWLETT D L Vacuum vaporization studies of lithium fluoride single crystals 4049
HOYT H L Oxidation of hypophosphorous acid by vanadium(V) 891
HUENIG S Conjugated radicals. IX. Experimental study and the LCI-SCF open shell calculations on the electronic spectra and the redox equilibria of the nitrogen-containing violenes 335
HUGGINS M L Thermodynamic properties of liquids, including solutions. IV. Entropy of mixing 1255
HUGHES E JR Effect of varied excitation on the fluorescence spectra of 2-phenylnaphthalene and biphenyl. Photoselection of conformers 3097
HUGHES R E Crystal and molecular structure of L-alanyl-L-alanine 918
HUGUS Z Z JR Determination of the number of species present in a system. New matrix rank treatment of spectrophotometric data 2954
HUIE R E Absolute rate constants for the reaction of atomic oxygen with 1-butene over the temperature range of 259-493°K 3902
HUMMEL R W Formation of ethane, ethylene, and acetylene from methane on radiolysis with high-intensity electron pulses 1164
HUNSTON D L Proton exchange in aqueous urea solutions 2123
HUNT A H Catalysis of the exchange of the ethanol hydroxyl proton by some divalent metallic ions 1994
HUNTSMAN W D Simultaneous determination of equilibrium and rate constants for first-order reactions 430
HUSSEY M Proton transfer reactions. Mechanism for the absorption of ultrasound in aqueous solutions of proteins 4012
HUTCHINS R R Photoelectron-induced decomposition of ethane 2903
IBATA T Pulse radiolysis of liquid amides 2267
ICLI S Nuclear magnetic resonance studies of phenoxy radicals. Hyperfine coupling constants and spin densities of a series of partially fluorinated radicals 3462

IHRIG A M Solvent effects on the fluoroform nuclear magnetic resonance spectra ... 497
IKADA E Dielectric properties of some diols ... 1240
IKEDA T Determination of magnetic moments of paramagnetic ions in microgram quantities using ion-exchange resins ... 2981
INEL Y Photolysis of ethylene at 1216 Ang ... 1317
INOUE Y Pressure jump and isotope replacement studies of acetylene hydrogenation on palladium surface ... 880
IRIE M Dissociative electron capture process of methyl vinyl ether in organic glasses ... 476
IRISH D E Raman spectral study of bisulfate-sulfate systems. II. Constitution, equilibriums, and ultrafast proton transfer in sulfuric acid ... 2672
IRISH D E Raman spectral study of bisulfate-sulfate systems. III. Salt effects ... 2681
IRISH D E Viscosity independence of the half-width of the $\nu_1(A_1)$ Raman line of sulfate ion ... 2684
ISH-SHALOM M Transition probabilities of europium in phosphate glasses ... 3980
IWATA S Electronic spectra of ion-radicals and their molecular orbital interpretation. I. Aromatic nitro-substituted anion-radicals ... 2591
IYENGAR R D Electron spin resonance studies on zinc peroxide and on zinc oxide obtained from a decomposition of zinc peroxide ... 3089
IYER R S Bond energy effects in substitution reactions of fluorine-18 atoms with methyl halides ... 1324
JACKSON D P Wall effects on concentrations of reactive intermediates in gaseous systems ... 2883
JACKSON N R Hologram interferometry for isothermal diffusion measurements ... 3374
JAIN S R Far-infrared absorption of some organic liquids ... 2942
JAMES H J Proton transfer in the two-step electrochemical reduction of oxygen in N,N-dimethylformamide ... 4019
JAMES R E Kinetics of isopropyl alcohol radicals by electron spin resonance-flow techniques ... 1326
JAMESON A K Gas-phase density-dependent directly bonded coupling constant ... 437
JANZ G J Studies of molten lithium chlorate and its aqueous solutions with laser Raman spectroscopy ... 2948
JANZ G J Transport processes in low melting salts. Silver nitrate-thallium nitrate system ... 4025
JANZEN E G Electron spin resonance spectroscopy symposium introduction ... 3383
JEFTIC L Chromium(II)-catalyzed aquation of hexacyanochromate(III) to pentacyanomonohydroxychromate(III) ... 2381
JENNINGS R L Recoil bromine reaction. Isomerization of excited cyclopropyl bromide ... 2698
JENSEN C H Anion exchange in mixed organic-aqueous solutions. I. Dioxane-water ... 79
JENSEN D Color of liquid sulfur ... 912
JESSON J P Electron spin resonance studies of conformations and hindered internal rotation in transient free radicals ... 3438
JEWETT G L Recoil reaction products of carbon-11 in C_5 hydrocarbons ... 3201
JOHNSON C S JR Nuclear spin relaxation in nematic liquid crystals ... 2452
JOHNSON D W Kinetics of the decomposition of freeze-dried iron(II) sulfate ... 1179
JOHNSON S N Energy partitioning on photolysis of di-tert-butyl peroxide ... 3651
JOHNSON T W Fluorine nuclear magnetic resonance study of the conformation of a polyethylenimine derivative ... 4061
JOHNSTON F J Radiolysis of colloidal sulfur. Mechanism for solubilization ... 756
JOLICOEUR C Electron paramagnetic resonance probes for hydrophobic interaction in aqueous solutions ... 165
JONAS L A Sorption properties of activated carbon ... 3526
JONAS V Studies of chemical exchange by nuclear magnetic resonance. VI. Comparison of carbon-nitrogen rotational barriers in amides, thioamides, and amidinium ions ... 3532
JONAS V Studies of chemical exchange by nuclear magnetic resonance. VII. Ion pairing of amididium salts in dimethyl sulfoxide ... 3550
JONATHAN N Infrared spectra of nitric oxide adsorbed on evaporated alkali halide films ... 2930
JONES C H W Iodine-129 Moessbauer studies of the chemical effects of nuclear transformations in compounds of tellurium ... 2867
JONES M T Electron spin resonance line-shape analysis for determination of unresolved metal hyperfine splittings in ion pairs. Application to the benzene anion radical ... 2769
JONES P R Molar absorptivity of carbon trioxide 2991
JONES R W Accuracy of theories of the primitive model of ionic solutions ... 3790
JONES S H Apparent triplet yields of pyrazine ... 3769
JORIS S J Nature of deficiency in nonstoichiometric hydroxyapatites. I. Catalytic activity of calcium and strontium hydroxyapatites ... 3167
JORIS S J Nature of deficiency in nonstoichiometric hydroxyapatites. II. Spectroscopic studies of calcium and strontium hydroxyapatites ... 3172
JOSEPHS R Measurement of the isothermal piezooptic coefficient with the ultracentrifuge ... 716
JOSIEN M L Trifluoracetic acid. Nature of association in diluted solutions in inert and slightly basic solvents ... 1327
JUILLARD J Dissociation and homoconjugation constants of some acids in methyl isobutyl ketone 2496
JUNKER B R Spin-free quantum chemistry. XI. Perturbation theory for interaction energies 1878
KAALHUS O Comparison of the reactivities of dry and mobile electrons ... 1941
KABA R A Electron paramagnetic resonance spectroscopic study of radical cations from hydrazine, methylhydrazine, and dimethylhydrazines . 2048
KAMACHI M Electron spin resonance study of the photolysis of formaldazine ... 164
KANTROWITZ E R Ultraviolet photochemistry of acetatopentaamminecobalt(III) in aqueous solution ... 1914
KAPOOR R C Oxidation kinetics of 2-mercaptoethylamine hydrochloride by ferricyanide ion in acid medium ... 2036
KARAYANNIS N M Infrared and proton nuclear magnetic resonance studies of adducts of tin(II) and-(IV) and titanium(IV) halides with diisopropyl methylphosphonate ... 637
KARGER B L Study of the adsorption of insoluble and sparingly soluble vapors at the gas-liquid interface of water by gas chromatography ... 3870
KARLE J Heptanol as a guest molecule in Dianin's compound ... 3566
KARPEL R L Complexes of nickel(II) with purine bases: relaxation spectra ... 799
KATSU T Electron spin resonance signals of abnormal alkyl radicals trapped on porous Vycor glass surfaces coated with metal oxides at 77°K . 4064
KATSUMATA S Dimerization of the perylene and tetracene radical cations and electronic absorption spectra of their dimers ... 1768
KATZ J L Bubble nucleation in n-pentane, n-hexane and n-pentane + hexadecane mixtures and water ... 3613
KATZ S Medium effects of some denaturing agents on volume changes produced by acid-base reactions ... 1120
KAUFMAN F Organic solid state. IV. Effect of environment on electron transfer in biferrocene[iron(II)iron(III)] picrate ... 2025
KAUL W Thermal decay effects on spatial distributions of radicals in γ-irradiated poly(methyl methacrylate) ... 2443
KAWANO H Thermal negative ion emission from binary cesium halide mixtures on a niobium surface ... 3741
KAYNE S B Investigations of aqueous mixtures of nonionic surfactants by membrane osmometry 2212
KAZANJIAN A R Radiolysis of liquid 1,1,2-trichlorotrifluoroethane ... 2217
KAZANJIAN A R Radiation-induced oxidation of trichloroethylene ... 613
KECKI Z Modified CNDO [complete neglect of differential overlap] method. IV. Ion-molecule interactions in the acetone solutions of electrolytes ... 3581
KEIL D G Absolute rate constants for the reactions of hydrogen atoms with olefins ... 1584
KELLER K H Tracer and mutual diffusion coefficients of proteins ... 379

KELLY C M Tracer and mutual diffusivities in the system chloroform-carbon tetrachloride at 25° 3293
KELLY J J Reactions involving electron transfer at semiconductor surfaces. II. Photoassisted dissociation of nitrous oxide over illuminated ferric oxide and zinc oxides 617
KENNEDY P Competitive adsorption of phenol and sodium dinonylnaphthalenesulfonate on nickel oxide powder 1975
KERN R D Rate of exchange of hydrogen and deuterium behind reflected shock waves. Dynamic analysis by time-of-flight mass spectrometry 1615
KERN R D Dynamic sampling of the deuterium hydride self-exchange behind reflected shock waves 2541
KERN R D JR Complementary shock tube technique study of the exchange of hydrogen chloride and deuterium 171
KERR C M L Electron spin resonance spectrum and structure of the radical anion of phosphorus oxychloride 3023
KERTES A S Molecular association and the dielectric constant of long-chain alkylammonium salts in benzene 542
KEVAN L Semicontinuum model for the hydrated electron. II. Configurational stability of the ground state 2297
KEVAN L Thermal decay effects on spatial distributions of radicals in γ-irradiated poly(methyl methacrylate) 2443
KEVAN L Negative ion-molecule reactions in perfluoropropane 2534
KHORANA S Electronic processes in the pulse radiolysis of aqueous solutions of halide ions 3081
KHRISTOV S G Tunneling corrections in chemical kinetics 1748
KIM H No evidence for the dimerization of nitromethane in carbon tetrachloride and benzene solutions 3892
KIMURA K Dimerization of the perylene and tetracene radical cations and electronic absorption spectra of their dimers 1768
KIMURA M Hydrogen peroxide formation upon oxidation of oxalic acid in presence and absence of oxygen and of manganese(II). I. Manganese(VII), cerium(IV), chromium(VI), and cobalt(III) as oxidants 3343
KING K D Kinetics and thermochemistry of the gas-phase bromination of bromoform. C-H bond dissociation energy in bromoform and the C-Br dissociation energy in carbon tetrabromide 987
KING S T Infrared study of the NH_2 "inversion" vibration for formamide in the vapor phase and in an argon matrix 405
KING T C Ionic reactions at high ionic strengths. Further equilibrium and kinetic measurements on the formation and dissociation of monochloroiron(III) 1113
KIRSZENBAUM M Trifluoracetic acid. Nature of association in diluted solutions in inert and slightly basic solvents 1327
KLEIN D J Spin-free quantum chemistry. IX. Aggregate theory of polyelectronic systems 1860
KLEIN D J Spin-free quantum chemistry. X. Effective spin Hamiltonian 1866
KLEIN F S Vapor pressure isotope effects in methanol 1815
KLOTS C E Reformulation of the quasiequilibrium theory of ionic fragmentation 1526
KLOTZ I M Proton exchange in aqueous urea solutions 2123
KLOTZ I M Fluorine nuclear magnetic resonance study of the conformation of a polyethylenimine derivative 4061
KNOBLER C M Interaction virial coefficients in hydrocarbon-fluorocarbon mixtures 3863
KOBRINSKY P C Pressure dependence of the cross-combination ratio for CF_3 and CH_3 radicals 2225
KOELLING J G Cationic polymerization of vinyl monomers by porous glass 3897
KOHR W Phase transitions in tetraalkylammonium iodide salts 2066
KOKES R J Butene isomerization over zinc oxide 487
KOLB K E Cationic polymerization of vinyl monomers by porous glass 3897
KOLTHOFF I M Dissociation and homoconjugation constants of some acids in methyl isobutyl ketone 2496
KOLTHOFF I M Hydrogen peroxide formation upon oxidation of oxalic acid in presence and absence of oxygen and of manganese(II). I. Manganese(VII), cerium(IV), chromium(VI), and cobalt(III) as oxidants 3343
KOMARYNSKY M Electron spin resonance line-shape analysis for determination of unresolved metal hyperfine splittings in ion pairs. Application to the benzene anion radical 2769
KOMINAMI S Photoinduced hole-electron recombination in a γ-irradiated single crystal of L-cystine dihydrochloride 3746
KONGSHAUG M Comparison of the reactivities of dry and mobile electrons 1941
KOREN R Rapid preequilibriums as a cause for change of activation energy with temperature 2372
KOWALSKI B R Nuclear magnetic resonance spectral interpretation by pattern recognition 1402
KRAMBECK F J Mechanism and kinetics of isotopic exchange in zeolites. I. Theory 3846
KRAMLING R W Linear symmetric helium dihydride. Model superexchange system 1874
KREILICK R W Nuclear magnetic resonance studies of phenoxy radicals. Hyperfine coupling constants and spin densities of a series of partially fluorinated radicals 3462
KREIS R W Freezing points, osmotic coefficients, and activity coefficients of salts in N-methylacetamide. I. Alkali halides and nitrates 2313
KREIS R W Freezing points, osmotic coefficients, and activity coefficients of salts in N-methylacetamide. II. Tetraalkylammonium halides and some alkali metal formates, acetates, and propionates 2319
KRIEGER I M Diffraction of light by nonaqueous ordered suspensions 1881
KRISHNAN C V The solvent-isotope effect in the enthalpy of some solutes in methanol 388
KRISHNAN C V Solvation enthalpies of hydrocarbons and normal alcohols in highly polar solvents 3598
KRISHNAN C V Solvation enthalpies of electrolytes in methanol and dimethylformamide 3606
KROPP J L Effect of propanol upon the absorption and emission of benzoquinolines in 3-methylpentane 2690
KRUKONIS A P Perchlorodiphenylmethyl stable free radical. X-ray analysis of a disordered mixed crystal 1246
KRUSIC P J Electron spin resonance studies of conformations and hindered internal rotation in transient free radicals 3438
KUDER J E Electronic structure of furanquinones. I. Absorption spectra of dinaphtho[2,1-2′,3′]furan-8,13-dione and dinaphtho[1,2-2′,3′]furan-7,12-dione 3257
KULES I Radiation chemistry of supercooled water 2997
KULEVSKY N Molecular complexes of iodine with some mono N-oxide heterocyclic diazines 2504
KUMMER J T Studies of surface reactions of nitric oxide by isotope labeling. II. Deuterium kinetic isotope effect in the ammonia-nitric oxide reaction on a supported platinum catalyst 875
KUNDELL F A Analysis of solution kinetics data coupled with thermal transients in an adiabatic calorimeter. II. First-order reactions 4039
KUNTZ R R Photoelectron-induced decomposition of ethane 2903
KURI Z Photoisomerization of maleate radical anions produced in 2-methyltetrahydrofuran by γ-irradiation at 77°K 482
KURUCSEV T Concentration quenching of proflavine hydrochloride in dry films of sodium deoxyribonucleate and poly(vinyl alcohol) 2727
KUSHNER R Reactions of recoil tritium atoms with 1-butene and cis-2-butene. Average energy of the addition reaction 3771

KUSTIN K Complexes of nickel(II) with purine bases: relaxation spectra 799
KUWATA K Electron spin resonance study of the photolysis of formaldazine 164
LABES M M Infrared and proton nuclear magnetic resonance studies of adducts of tin(II) and -(IV) and titanium(IV) halides with diisopropyl methylphosphonate 637
LACKNER A M Photopolymerization mechanisms. I. Dye-triplet reactions with p-substituted benzenesulfinate ions 3066
LAGERCRANTZ C Spin trapping of some short-lived radicals by the nitroxide method 3466
LAHODNY-SARC O Infrared study of aluminum-deficient zeolites in the region 1300 to 200 cm^{-1} 2408
LAM E Y Y States of atomic carbon produced in decomposition of organic compounds in a microwave plasma 445
LAMPE F W Ion-molecule reactions in dimethylsilane, trimethylsilane, and tetramethylsilane 13
LANG C M Radical anions of vitamin A aldehyde and related Schiff bases 2861
LANG J Effect of urea and other organic substances on the ultrasonic absorption of protein solutions 374
LANGDON A G Self-diffusion studies of gel hydration and the obstruction effect 1821
LARSEN D W Correlation times and reorientation activation energies for tetraalkylammonium ions in aqueous solutions 509
LARSEN D W Proton magnetic resonance study of ion-pairing effects on arsenic-75 quadrupole relaxation in tetraalkylarsonium ions 3880
LARSON J W Heats of dilution and the thermodynamics of dissociation of uranyl and vanadyl sulfates 2368
LASSIGNE C Solvation studies of lithium salts in dimethylformamide 3188
LAU K H Computation of the statistical complexions of molecules and ions 981
LAU K H Application of the method of the steepest descent to the calculation of the translational energy of fragments of ion decomposition 2458
LAURANSAN J Spectroscopic determination of association constants of primary aromatic amines with dimethyl sulfoxide and hexamethylphosphoric triamide 1157
LAURANSAN J Calorimetric determination of enthalpies of association of primary aromatic amines with dimethyl sulfoxide and hexamethylphosphorotriamide 3149
LAWRENCE J Polyion hydration. I. Partial molar volumes and electrostriction of polyimine salts 2353
LAWRENCE J Polyion hydration. II. Compressibility behavior of polyimine salts 2362
LAWSON D R Isomerization of chemically activated n-pentyl radicals 1632
LEE E K C Fluorescence decay times of cyclic ketones, acetone, and butanal in the gas phase 989
LEE E K C Study of the roles of chemical factors in controlling the yields of substitution reactions by energetic tritium atoms. Electronegativity, electron density, and bond energy 1290
LEE S C Replacement reactions of hot chlorine atoms in chlorofluoromethanes 2685
LEE T P Ionic radii from scaled particle theory of the salt effect 2809
LEFFLER A J Axial coordination in the vanadyl ion 599
LEHNIG M Nuclear and electron spin polarizations during radical reactions 3410
LEIGH J S JR Electron paramagnetic resonance studies in frozen aqueous solutions. Elimination of freezing artifacts 1202
LEITNAKER J M High-molecular-weight boron sulfides. VII. Lower temperature studies and metastable decompositions 2410
LEMMON R M Partial degradation of 1,3,5-cycloheptatriene-^{14}C obtained from hot-atom, photolytic, and "thermal" reactions 2558
LEMMON R M Reactions of accelerated carbon-14 with benzene. Degradation of toluene and its mechanism of formation 3524
LEONHARDT H Acid-base equilibriums of fluorescein and 2′, 7′-dichlorofluorescein in their ground and fluorescent states 245
LESIGNE B Flash photolysis of chlorate ion in aqueous solution 2177
LESTER J E Vacuum vaporization studies of lithium fluoride single crystals 4049
LETELIER R J Relative rates of the reactions of hydrogen atoms with hydrogen iodide and hydrogen bromide 835
LEUNG C High-yield method for the preparation of anomalous water 2976
LEVKOV J Phase transitions in tetraalkylammonium iodide salts 2066
LEVY A Photochemically induced isotopic exchange between iodobenzene and molecular iodine 3350
LEVY O Molecular association and the dielectric constant of long-chain alkylammonium salts in benzene 542
LEVY P W Effects of radiation on the thermal decomposition induction period in ammonium perchlorate and other pseudostable materials 191
LEWIS I C Identity of the free radical in solutions of $\Delta^{10,10'}$-bianthrone 290
LEWIS J A Mathematical formulations of the effects of cell distortion and liquid column height compression in analytical ultracentrifugation 2507
LEYDEN D E Nuclear magnetic resonance study of the protolysis kinetics of 5-dimethylaminonaphthalene-1-sulfonic acid and its N-methylsulfonamide 4056
LEYDEN D E Protolysis kinetics of diamines in sulfuric acid 2400
LEYDEN D E Proton exchange and nitrogen inversion of α-phenylethylbenzylmethylamine using nuclear magnetic resonance spectroscopy 3190
LEYENDEKKERS J V Thermodynamics of mixed electrolyte solutions. Ionic entropy correlations and volume fraction statistics 946
LEYENDEKKERS J V Measurement of activity coefficients with liquid ion-exchange electrodes for the system calcium(II)-sodium(I)-chloride(I)-water 957
LI N C Proton exchange between guanidinium ion and water in water-N,N-dimethylacetamide mixtures 688
LIBERTINI L J Role of lipid spin labels in membrane biophysics 3417
LICHTIN N N Pulse radiolysis of liquid amides . 2267
LIMOGES R D Micellar effects on the hydrolysis rate of triethylamine-sulfur trioxide 1763
LIN C T Kinetics of nickel murexide formation in several solvent systems 3705
LIN I J Effect of dissolved paraffinic gases on the surface tension and critical micelle concentration (cmc) of aqueous solutions of dodecylamine hydrochloride (DACl) 3000
LIN M C Chemical hydrogen fluoride lasers from nitrogen fluoride-molecular hydrogen and nitrogen fluoride-ethane systems 284
LIN M C Chemical hydrogen fluoride lasers from flash photolysis of various N_2F_4+RH systems 2546
LIN M C Chemical lasers produced from oxygen(^1D) atom reactions. II. A new hydrogen fluoride elimination laser from the oxygen(^1D) + CH_nF_{4-n} ($n = 1,2,$ and 3) reactions 3642
LIN S H Application of the method of the steepest descent to the calculation of the translational energy of fragments of ion decomposition 2458
LIN S-H Computation of the statistical complexions of molecules and ions 981
LIN T-H Reactions of accelerated carbon-14 with benzene. Degradation of toluene and its mechanism of formation 3524
LINDENBAUM S Estimation of solute activity coefficients in dilute aqueous mixtures of sodium and zinc bromides at 25°. Comparisons with

predictions from the Guggenheim theory of solutions 3153

LINDENBAUM S Thermodynamics of aqueous solutions of tetrabutylammonium carboxylates. Model systems for the hydrophobic interaction in proteins 3733

LINDFORS K R Intermolecular hydrogen bonding. I. Effects on the physical properties of tetramethylurea-water mixtures 3313

LINDMAN B Interaction of halide ions with organic cations containing charged nitrogen, phosphorus, or sulfur in aqueous solutions studied by nuclear quadrupole relaxation 2936

LINDSAY W T JR Osmotic coefficients of one molal alkali metal chloride solutions over a 300° temperature range 3723

LINDSTROM T R Proton magnetic resonance study of the hydrogen bonding of alkylated bases to dimethyl sulfoxide 3963

LINGERTAT H High-yield method for the preparation of anomalous water 2976

LIQUORNIK M Ion exchange in molten salts. V. Potassium zeolite A as an ion exchanger in nitrate melts 2523

LITCHMAN W M Nitrogen-15 nuclear magnetic resonance shifts and coupling constants for the methylamine hydrochlorides in aqueous solution 1758

LITCHMAN W M Nitrogen-15 nuclear magnetic resonance shifts in pure methylamines and pure methyl isocyanide-nitrogen-15 932

LITTLE M J Photopolymerization mechanisms. I. Dye-triplet reactions with p-substituted benzenesulfinate ions 3066

LIU C-T Osmotic coefficients of one molal alkali metal chloride solutions over a 300° temperature range 3723

LIVINGSTON P Electron spin resonance spectroscopy symposium introduction 3383

LIVINTSTON R Acid-base equilibriums of fluorescein and 2', 7'-dichlorofluorescein in their ground and fluorescent states 245

LLOYD R V Electron paramagnetic resonance spectra of pyrrolidino and pyrrolino free radicals. Structure of dialkylamino radicals 3486

LOCKER D J Vibrational eigenvalues. Sine basis sets 1756

LO JACONO M Structural, magnetic, and optical properties of nickel oxide supported on η- and γ-aluminas 1044

LO JACONO M Catalytic activities of nickel oxide supported on γ- and η-aluminas for the nitrous oxide decomposition 1051

LONG G G Positive temperature coefficients in the bromine nuclear quadrupole resonance spectra of the diethylammonium salts of hexabromoantimony(III) and hexabromobismuth(III) 1898

LOU J J Effect of propanol upon the absorption and emission of benzoquinolines in 3-methylpentane 2690

LOWERY K Secondary unimolecular reactions subsequent to substitution reactions by high-energy chlorine-38 and chlorine-39 atoms 440

LUBIN T Primary and secondary rate processes in the acetone-silane photochemical system 3945

LUCAS M Salting-in of nonpolar gases in aqueous tetraalkylammonium bromide solutions and the apparent molal volume of these salts in water 1803

LUCAS M Enthalpy of solution of some molecules in aqueous tetraalkylammonium bromide solutions and the apparent expansion coefficient of the aqueous salt solution 2330

LUMRY R Chymotrypsinogen family of proteins. XV. pH and temperature dependence of the α-chymotryptic hydrolysis of N-acetyl-L-tryptophan ethyl ester 1375

LUMRY R Chymotrypsinogen family of proteins. XVI. Enthalpy-entropy compensation phenomenon of α-chymotrypsin and the temperature of minimum sensitivity 1387

LUNSFORD J H Electron paramagnetic resonance study of Y-type zeolites. III. O_2^- on AlHY, ScY, and LaY zeolites 1165

LURIE S W Transport processes in low melting salts. Silver nitrate-thallium nitrate system 4025

LUTZE W Ion-exchange kinetics in vermiculite. 2484

LYERLA J R JR Dipolar contributions to carbon-13 relaxation times 585

LYERLA J R JR Effect of molecular association on carbon-hydrogen nuclear dipolar relaxation rates 2539

LYERLA J R JR Field-dependent contributions to carbon-13 nuclear relaxation 3967

LYNCH D A JR Infrared spectra of the aluminum family suboxides 1963

LYON R K Equilibrium distributions of some octane and nonane isomers 1486

MCADAMS M J Gas-phase acidities of alcohols. 2226

MCCALL J M JR Protolysis kinetics of diamines in sulfuric acid 2400

MCDOWELL C A Electron spin resonance of free radicals prepared by the reactions of methylene. Deuteriomethyl and formaldiminoxy radicals 2448

MCDOWELL C A Electron spin resonance studies of biradicals of nitro aromatic radical anions and alkali ions 1205

MACEDO P B Dependence of the glass transition temperature on heating rate and thermal history 3379

MCEWAN M J Photometric and mass spectrometric observations on the reaction of hydrogen atoms with cyanogen 2662

MCEWAN M J Mass spectrometric study of the reaction of hydrogen atoms with nitrosyl chloride 722

MCEWAN M J Mass spectrometric study of the reaction of nitrogen atoms with nitrosyl chloride 1172

MCEWAN M J Mass spectrometric study of the reaction of oxygen atoms with nitrosyl chloride.. 1320

MCEWEN R S Crystallographic studies on nickel hydroxide and the higher nickel oxides 1782

MCFARLAND M Initiation rate for shock-heated hydrogen-oxygen-carbon monoxide-argon mixtures as determined by OH induction time measurements 1504

MCGHEE D B Shock tube isomerization of cyclopropane 2526

MCGUIRE R F Energy parameters in polypeptides. IV. Semiempirical molecular orbital calculations of conformational dependence of energy and partial charge in di- and tripeptides. 2286

MCINTYRE J A Mass spectral study of the decomposition of chlorine fluoride behind shock waves 1765

MCINTYRE N S Spectroscopy of titanium oxide and titanium dioxide molecules in inert matrices at 4°K 3243

MACKAY R A Phase transitions in tetraalkylammonium iodide salts 2066

MACKENZIE A P Glass transition in amorphous water. Application of the measurements to problems arising in cryobiology 967

MCKINNEY W J Spectroscopic studies of ionic solvation. VIII. Alkali metal salts in acetone solutions 56

MCLAUGHLIN E Monoisotopic mass spectra of the boranes 3106

MACLEAN D I Structure of fluorine-supported flames. I. Method of investigation. Dichlorodifluoromethane-fluorine flame 3645

MCMAHAN W H JR Dielectric constant study of molecular association in polar-polar mixtures. o-Dichlorobenzene-butyl alcohol 2133

MCNALLY D Thermochemistry, thermodynamic functions, and molecular structures of some cyclic hydrocarbons 1264

MACNEIL K A G Negative ion formation by ethylene and 1,1-difluoroethylene 2584

MCQUARRIE D A Statistical mechanical theory of electrostriction in dense gases 771

MADEC C Spectroscopic determination of association constants of primary aromatic amines with dimethyl sulfoxide and hexamethylphosphoric triamide 1157

MADEC C Calorimetric determination of enthalpies of association of primary aromatic amines with dimethyl sulfoxide and hexamethylphosphorotriamide 3149

MAGEE J L Effects of optical bleaching on luminescence decay and trapped electron concentrations in γ-irradiated 3-methylpentane at 77°K 3221

MAGIERA B Vapor-liquid equilibriums of binary mixtures of carbon-14-labeled hexane with aliphatic ketones 4041

MAGUIRE M M Mercury-sensitized photodecomposition of nitrous oxide in the presence of mixtures of carbon monoxide and methane 3205
MAHAN B H Dynamics of the reactions of O_2^+ with molecular hydrogen and deuterium 1426
MAHAN K I Recoil tritium reactions with propene in the gas phase 1031
MAHLMAN H A Reduction of cerium(IV) by hydrogen peroxide. Dependence of reaction rate on Hammett's acidity function 250
MAIR H J Structure of perchlorocyclopropene .. 1681
MAKI A H Donor-acceptor complexes of phenothiazine and phenoxazine with nickel thiete ... 2387
MAKOWIECKI D M Infrared spectra of the aluminum family suboxides 1963
MALINOWSKI E R Anisotropic solvent shifts determined by factor analysis 1207
MALINOWSKI E R Investigation of the van der Waals effect in nuclear magnetic resonance spectroscopy by factor analysis and the prediction of diamagnetic and paramagnetic susceptibilities ... 3160
MALINOWSKI E R Nuclear magnetic resonance proton shifts of polar solutes 3971
MALTSEV A K Matrix-isolation study of the pyrolysis of bromochloromethyl-substituted organomercury compounds. Infrared spectra of the bromochlorocarbene and free radicals CCl_2Br and $CClBr_2$ 3984
MAMAJEK R C Conductance of tetraalkylammonium halides in ethylene glycol 1722
MANDELKERN L Thermodynamic and morphological properties of crystalline polymers 3909
MANES M Application of the Polanyi adsorption potential theory to adsorption from solution on activated carbon. II. Adsorption of partially miscible organic liquids from water solution 61
MANES M Application of the Polanyi adsorption potential theory to adsorption from solution on activated carbon. III. Adsorption of miscible organic liquids from water solution 3720
MANGELSDORF P C JR Difference chromatography of seawater 1418
MANTAKA A Continuous γ and pulse radiolysis of aqueous benzene solutions. Reactions of the hydroxycyclohexadienyl radical 3886
MARCUS Y Ion exchange in molten salts. V. Potassium zeolite A as an ion exchanger in nitrate melts 2523
MARGERUM J D Photopolymerization mechanisms. I. Dye-triplet reactions with p-substituted benzenesulfinate ions 3066
MARGRAVE J L Levitation calorimetry. IV. Thermodynamic properties of liquid cobalt and palladium 3737
MARGRAVE J L Matrix-isolation study of the pyrolysis of bromochloromethyl-substituted organomercury compounds. Infrared spectra of the bromochlorocarbene and free radicals CCl_2Br and $CClBr_2$ 3984
MARINSKY J A Ion-exchange selectivity of the synthetic zeolite Linde A in anhydrous and mixed media 85
MARINSKY J A Mean molal activity coefficient of polymethacrylic acid at various degrees of neutralization 2144
MARINSKY J A Further examination of the additivity rule 3890
MARKETOS D G Continuous γ and pulse radiolysis of aqueous benzene solutions. Reactions of the hydroxycyclohexadienyl radical 3886
MARKOVIC V M Pulse radiolysis of oxalic acid and oxalates 749
MARKOVITS G Molecular association and the dielectric constant of long-chain alkylammonium salts in benzene 542
MARONI V A Structural studies of magnesium halide-potassium halide melts by Raman spectroscopy 155
MARSHALL H P Structure of nitroform in various solvents 499
MARSHALL W L Electrical conductances and ionization behavior of sodium chloride in dioxane-water solutions at 100° and pressures to 4000 bars 1099
MARTIN R B Zwitterion formation upton deprotonation in L-3,4-dihydroxyphenylalanine and other phenolic amines 2657
MARTINELLI L C Protolysis kinetics of ethyl N-methylcarbamate 1895
MARTIRE D E Thermodynamics of solutions with liquid crystal solvents. III. Molecular interpretation of solubility in nematogenic solvents 2005
MASTERTON W L Ionic radii from scaled particle theory of the salt effect 2809
MASTROIANNI M J Viscosity coefficients of ions in various solvents 2532
MATHIEU M V Infrared study of the surface of titanium dioxides. I. Hydroxyl groups 1216
MATHIEU M V Infrared study of the surface of titanium dioxides. II. Acidic and basic properties 1221
MATSEN F A Spin-free quantum chemistry. IX. Aggregate theory of polyelectronic systems. 1860
MATSEN F A Spin-free quantum chemistry. X. Effective spin Hamiltonian 1866
MATSEN F A Linear symmetric helium dihydride. Model superexchange system 1874
MATSEN F A Spin-free quantum chemistry. XI. Perturbation theory for interaction energies 1878
MATSUDA S Shock-tube study of acetylene-molecular oxygen reaction. Acceleration of reaction in the presence of trace amounts of chromium hexacarbonyl 2402
MATSUMOTO A Pulse radiolysis of liquid amides 2267
MATTHEWS R W Reduction of cerium(IV) by hydrogen peroxide. Dependence of reaction rate on Hammett's acidity function 250
MAYER R T Nuclear magnetic resonance study of the protolysis kinetics of 5-dimethylaminonaphthalene-1-sulfonic acid and its N-methylsulfonamide 4056
MAZZA F Spontaneous dissolution of metals in aqueous electrolytes. I. Kinetic isotope effects in the reaction of iron with hydrochloric acid solutions in protium and in deuterium oxide 2112
MEAKIN P Electron spin resonance studies of conformations and hindered internal rotation in transient free radicals 3438
MEANY J E Iodination of alkyl pyruvates. I. Spontaneous and general base catalyzed iodination of methyl and ethyl pyruvates 150
MEANY J E Reversible hydration of pyruvate esters. Thermodynamic and kinetic studies 792
MEATHERALL R C Viscosity independence of the half-width of the $\nu_1(A_1)$ Raman line of sulfate ion 2684
MEDINA A S Mechanism of ion exchange in crystalline zirconium phosphates. V. Thermodynamic treatment of the hydrogen ion-sodium ion exchange of α-zirconium phosphate 3750
MEEHAN E J Hydrogen peroxide formation upon oxidation of oxalic acid in presence and absence of oxygen and of manganese(II). I. Manganese(VII), cerium(IV), chromium(VI), and cobalt(III) as oxidants 3343
MEEKS F R Viscosity of the cyclohexane-aniline binary liquid system near the critical temperature 2619
MEHRA A Comparative ligand field studies of manganese(II) spectra 435
MEISEL D Reactions of organic radicals formed by some "Fenton-like" reagents 3271
MEISELS G G Photolysis of ethylene at 1216 Ang 1317
MEMMING R Electrochemical investigations on the spectral sensitization of gallium phosphide electrodes 562
METZER A Effect of dissolved paraffinic gases on the surface tension and critical micelle concentration (cmc) of aqueous solutions of dodecylamine hydrochloride (DACl) 3000
MEYER B Spectrum of matrix-isolated carbon disulfide 2204
MEYER B Color of liquid sulfur 912
MEYER E F Cohesive energies in polar organic liquids. II. n-Alkane nitriles and the 1-chloro alkanes 642

MEYER E F Estimation of induction energies using gas-liquid chromatography 831
MEYER F Adsorption of organic gases on clean germanium surfaces 2922
MEYERSTEIN D Photochemically induced isotopic exchange between iodobenzene and molecular iodine 3350
MICHAEL B D Absorption spectrum of e_{aq}^- in the temperature range -4 to 390° 2798
MICHAEL J V Absolute rate constants for the reactions of hydrogen atoms with olefins 1584
MICHAELI I Kinetics of proton transfer reactions of polyacrylic and polymethacrylic acids with an indicator 267
MIEKELEY N Ion-exchange kinetics in vermiculite 2484
MIKNIS F Laser-produced oxygen from silicon dioxide 2412
MIKNIS F P Q-switched laser-induced reactions of thiacyclobutane and thiacyclopentane with oxygen 725
MILE B Electron spin resonance spectra of some σ-type aromatic radicals 3432
MILLER J E Medium effects of some denaturing agents on volume changes produced by acid-base reactions 1120
MILLER M A Nuclear magnetic resonance study of the conformations of valine and phenylalanine derivatives 505
MILLER R L Electronic structure of furanquinones. I. Absorption spectra of dinaphtho[2,1-2',3']furan-8,13-dione and dinaphtho[1,2-2',3']furan-7,12-dione 3257
MILLER W G Liquid crystal-isotropic phase equilibriums in the system poly(γ-benzyl α-L-glutamate)- dimethylformamide 1446
MILLERO F J Partial molal volumes of tetraphenylarsonium tetraphenylboron in water at infinite dilution. Ionic partial molal volumes 280
MILLWARD G E Kinetics of the shock wave thermolysis of 1,1,2,2-tetrafluoroethane 3195
MILLWARD G E Kinetics of the shock wave pyrolysis of pentafluoroethane 3493
MINCH M Enhancement of micellar catalysis by added electrolytes 2707
MINN F L Excimer model for fluorene and dibenzofuran 1794
MINTON A P Measurement of the isothermal piezooptic coefficient with the ultracentrifuge 716
MINTON A P Far-ultraviolet spectrum of ice 1162
MIRSKI U Contribution of hydrogen atoms to molecular hydrogen [G_{H_2}] in the radiation chemistry of aqueous solutions 31
MISTRALI F Thermodynamics of elasticity in open systems. Elastin 142
MIXON A L Charge density on the phosphoryl oxygen in a series of phosphate esters. Tributyl phosphate, a monocyclic phosphate, and a bicyclic phosphate ester 3309
MIYAJIMA G Carbon-13 nuclear magnetic resonance spectroscopy. III. Chloro-substituted ethanes and ethylenes 331
MIYAJIMA G Carbon-13 nuclear magnetic resonance spectroscopy. IV. Bromo-substituted ethanes and ethylenes 3766
MIYAJIMA K Free energy changes on mixing solutions of alkali halides and symmetrical tetraalkylammonium halides 2148
MIYAMA H Ignition of aromatic hydrocarbon-oxygen mixtures by shock waves 1501
MIYAZAKI T Photoisomerization of maleate radical anions produced in 2-methyltetrahydrofuran by γ-irradiation at 77°K 482
MOAN J Photoinduced trapped electrons in rigid polar solution. I. Recombination luminescence 2887
MOAN J Photoinduced trapped electrons in rigid polar solution. II. Kinetics and cross section of two-quantum ionization 2893
MODDEMAN W E Study of phosphorus-sulfur compounds by inner-orbital photoelectron spectroscopy. Thiono-thiolo sulfur 3975
MODELL M Hydrogen promotion of the palladium-catalyzed carbon monoxide oxidation 2065
MOHILNER D M Electrosorption of 5-chloro-1-pentanol at the mercury-solution interface 1698
MOHLING F Accuracy of theories of the primitive model of ionic solutions 3790
MOMANY F A Energy parameters in polypeptides. IV. Semiempirical molecular orbital calculations of conformational dependence of energy and partial charge in di- and tripeptides . 2286
MONAHAN A R Aggregation of arylazonaphthols. II. Steric effects on dimer structure in water 1227
MONTENAY-GARESTIER T Environmental effects on the deprotonation of indole derivatives in alkaline ices 3061
MOORE C B Vibrational relaxation of hydrogen chloride by chlorine atoms and chlorine molecules 1622
MOORE J C Vibronic effects in the infrared spectrum of the anion of tetracyanoethylene 325
MOORE L O Radical reactions of highly polar molecules. Reactivities in atom abstractions from chloroalkanes by fluoroalkyl radicals 2075
MORABITO J M Adsorption of organic gases on clean germanium surfaces 2922
MORGAN W R Proton exchange and nitrogen inversion of α-phenylethylbenzylmethylamine using nuclear magnetic resonance spectroscopy .. 3190
MORINAGA K Initiation rate for shock-heated hydrogen-oxygen-carbon monoxide-argon mixtures as determined by OH induction time measurements 1504
MORRIS E D JR Mass spectrometric study of the reactions of nitric acid with oxygen atoms and hydrogen atoms 3193
MORRIS E D JR Reactivity of hydroxyl radicals with olefins 3640
MORSS L R Thermochemistry of some chlorocomplex compounds of the rare earths. Third ionization potentials and hydration enthalpies of the trivalent ions 392
MORTIER W J Location of univalent cations in synthetic zeolites of the Y and X type with varying silicon to aluminum ratio. I. Hydrated potassium exchanged forms 3327
MORTLAND M M Interlamellar metal complexes on layer silicates. I. Copper(II)-arene complexes on montmorillonite 3957
MOSCINSKI J Correlation of the excess molar volumes of solutions of cadmium and bismuth in their molten halides 3620
MOSER H C Low-energy electron radiolysis of methane 2405
MOUCHARAFIEH N Chemiemission from the cesium-oxygen surface reaction 1928
MOUNTAIN P F Relaxation processes of cholesteryl methyl ether 1237
MOYNIHAN C T Dependence of the glass transition temperature on heating rate and thermal history 3379
MUKHERJEE S $N-H\cdots\pi$ hydrogen bonding 2404
MULAC W Pulse radiolysis of ammonia gas. II. Rate of disappearance of the $NH_2(X^2B_1)$ radical .. 2087
MULLER N Investigation of micelle structure by fluorine magnetic resonance. IV. Fluorine-labeled nonionic detergents 547
MULLER N Investigation of micelle structure by fluorine magnetic resonance. V. Sodium perfluorooctanoate 942
MURAHASHI S Electron spin resonance study of the photolysis of formaldazine 164
MURTHY A S N Distorted hydrogen bonds formed by carbonyl compounds 1744
MURTY T S S R Perfluorinated aliphatic carboxylic acids. Nature of association in dilute solutions in nonpolar solvents 1330
MUSHRAN S P Kinetics of the oxidation of hexacyanoferrate(II) by chloramine-T 838
MYERS L S JR Nanosecond pulse radiolysis studies of aqueous thymine solutions 3815
NADAS J A Transport properties in hydrogen bonding solvents. VI. The conductance of electrolytes in 2,2,2-trifluoroethanol 1708
NADAS J A Conductance of electrolytes in acetone and in 1-propanol-acetone mixtures at 25° 1714
NAGAO M Physisorption of water on zinc oxide surface 3822
NAKANISHI K Diffusion in mixed solvents. II. Iodine in binary solutions of ethanol with hydrocarbons and carbon tetrachloride 963

NAKANISHI K Studies on associated solutions. III. Infrared spectral study of hydrogen bonding in solutions containing hydrogen fluoride 2222

NAKANO F Electron spin resonance studies of biradicals of nitro aromatic radical anions and alkali ions 1205

NAKASHIMA M Intermediates produced in the flash photolysis of acetone and amides in aqueous solution 1910

NANGIA P Pulse radiolysis of ammonia gas. II. Rate of disappearance of the $NH_2(X^2B_1)$ radical 2087

NAUMAN R V Effect of varied excitation on the fluorescence spectra of 2-phenylnaphthalene and biphenyl. Photoselection of conformers 3097

NAZHAT N B Growth and decay of alkyl radicals in γ-irradiated alkyl iodides at 77°K 472

NAZHAT N B Formation of ozonide ions in γ-irradiated aqueous solutions of alkali hydroxides. Reply to comments 3031

NEFEDOV O M Matrix-isolation study of the pyrolysis of bromochloromethyl-substituted organomercury compounds. Infrared spectra of the bromochlorocarbene and free radicals CCl_2Br and $CClBr_2$ 3984

NELSON R E Electrical conductivities of salts of gum arabic and carrageenan in aqueous solutions 1691

NEMETHY G Difference spectrophotometric method for the determination of critical micelle concentrations 804

NEMETHY G Micelle formation by nonionic detergents in water-ethylene glycol mixtures 809

NESYTO E Mechanism of the radiation-induced dechlorination of 1,1,1-trichloro-2,2-bis(p-chlorophenyl)ethane in alcoholic solution 2762

NETA P Electron spin resonance study of the rate constants for reaction of hydrogen atoms with organic compounds in aqueous solution 1654

NETA P Electron spin resonance study of radicals produced in irradiated aqueous solutions of thiols 2277

NETA P Electron spin resonance study of irradiated aqueous solutions of fumarate ion. Use of fumarate for radical trapping 2570

NETA P Rate constants for reaction of hydrogen atoms in aqueous solutions 449

NETA P Electron spin resonance study of radicals produced in irradiated aqueous solutions of amines and amino acids 738

NEUMAN R C JR Studies of chemical exchange by nuclear magnetic resonance. VI. Comparison of carbon-nitrogen rotational barriers in amides, thioamides, and amidinium ions 3532

NEUMAN R C JR Studies of chemical exchange by nuclear magnetic resonance. VII. Ion pairing of amididium salts in dimethyl sulfoxide 3550

NEWMARK R A Nuclear magnetic resonance study of the conformations of valine and phenylalanine derivatives 505

NEWTON T W Kinetics of the reaction between uranium(III) and $Co(NH_3)_4(H_2O)_2^{3+}$ in aqueous perchlorate solutions 2117

NICHOLAS J B Interactions of positrons with defects in sodium chloride crystals 2030

NICHOLAS J E Reactions of fast hydrogen atoms with ethane 841

NICHOLSON O Biionic potentials of a liquid-membrane electrode selective toward calcium 2138

NIELSEN S O Pulse radiolysis of aqueous alkaline sulfite solutions 3510

NIELSEN S O Pulse radiolysis of oxalic acid and oxalates 749

NIKA G G Complementary shock tube technique study of the exchange of hydrogen chloride and deuterium 171

NIKA G G Rate of exchange of hydrogen and deuterium behind reflected shock waves. Dynamic analysis by time-of-flight mass spectrometry 1615

NIKA G G Dynamic sampling of the deuterium hydride self-exchange behind reflected shock waves 2541

NIKI H Mass-spectrometric studies of rate constants for addition reactions of hydrogen and of deuterium atoms with olefins in a discharge-flow system at 300°K 1601

NIKI H Mass spectrometric study of the reactions of nitric acid with oxygen atoms and hydrogen atoms 3193

NIKI H Reactivity of hydroxyl radicals with olefins 3640

NOBLE M Effect of magnetic fields on the pH of water 2830

NOBLE P JR Structure of nitroform in various solvents 499

NORTHROP D A Thermogravimetric investigation of the vaporization of lead telluride, tin telluride, and germanium telluride 118

NOYES W A JR Photochemistry of the xylenes. Discussion of method 2741

NOZAKI H Transient phenomena caused by temperature change on capacitance of rutile film 1279

NUTKOWITZ P M Electron spin resonance spectroscopy of the fluorosulfate radical ($SO_3F.$) in solution. Line width and its temperature dependence 712

NYBERG G Electron spin resonance spectra of copper acetate in acetic acid solutions 2228

O'BRIEN J F Nitrogen-15 nuclear magnetic resonance shifts in pure methylamines and pure methyl isocyanide-nitrogen-15 932

O'DEEN L A Isomerization of vibrationally excited 3-methyl-1-buten-1-yl radicals via hydrogen atom migration. Quantum statistical weight effect 2665

OE S Determination of magnetic moments of paramagnetic ions in microgram quantities using ion-exchange resins 2981

OGDEN J S Vibrational analysis for the molecules gallium oxide, indium oxide, and thallium oxide. Comment 3908

OGREN P J Complex formation in aluminum iodide-diethyl ether solutions 282

OGREN P J Origin of complex electron spin resonance spectra of γ-irradiated polycrystalline n-alkyl iodides with even number of carbon atoms per molecule 467

OGREN P J Growth and decay of alkyl radicals in γ-irradiated alkyl iodides at 77°K 472

OGREN P J Growth patterns of reaction intermediates produced by self-radiolysis of tritiated ethyl iodide at 77°K 3359

OHTAKI H Ionic equilibria in mixed solvents. VI. Dissociation constants of aliphatic diamines in water-methanol solutions 90

OKAMURA S Dissociative electron capture process of methyl vinyl ether in organic glasses 476

OKANO K Non-Newtonian viscosity and excluded volume effect of dilute solutions of flexible high polymers 1141

OLIVER B G Studies of molten lithium chlorate and its aqueous solutions with laser Raman spectroscopy 2948

OLMSTED J III Chemiemission from the cesium-oxygen surface reaction 1928

OMELKA L Radical reactions in the ligand field of metal complexes. I. Electron paramagnetic resonance spectra of complex-bonded radicals formed by reaction of cobalt(II) acetylacetonate with tert-butyl hydroperoxide 2575

OMELKA L Radical reactions in the ligand field of metal complexes. II. Reactions of the tert-butylperoxy radical bound to cobalt(III) 2580

O'NEAL H E Primary and secondary rate processes in the acetone-silane photochemical system 3945

ONG T E Monoisotopic mass spectra of the boranes 3106

OOMMEN T V Color of liquid sulfur 912

OPPERMAN S H Intermolecular hydrogen bonding. I. Effects on the physical properties of tetramethylurea-water mixtures 3313

OSTERLE J F Validity of a simple theory for transport in ion-exchange membranes 3015

OTSUKA A Free energy changes on mixing solutions of alkali halides and symmetrical tetraalkylammonium halides 2148

OTTO K Studies of surface reactions of nitric oxide by isotope labeling. II. Deuterium kinetic isotope effect in the ammonia-nitric oxide reaction on a supported platinum catalyst 875

OTTOLENGHI M Photochemically induced isotopic exchange between iodobenzene and molecular iodine 3350
OTTOLENGHI M Intersystem crossing in the charge-transfer quenching of molecular fluorescence 1025
OTTOLENGHI M Laser photolysis of perylene solutions 3894
OVERBEEK J TH G Theory of the stabilization of dispersions by adsorbed macromolecules. II. Interaction between two flat particles 2094
OWENS C Infrared and proton nuclear magnetic resonance studies of adducts of tin(II) and -(IV) and titanium(IV) halides with diisopropyl methylphosphonate 637
OZASA T Diffusion in mixed solvents. II. Iodine in binary solutions of ethanol with hydrocarbons and carbon tetrachloride 963
PAINTER C E Shock tube isomerization of cyclopropane 2526
PALINO G F Reactions of recoil carbon atoms with oxygen-containing molecules. II. Structural dependence of carbon monoxide yields 2248
PALINO G F Complete retention of configuration during the replacement of hydrogen by energetic tritium in dl- and meso-$(CHFCl)_2$ 1299
PALIT S R $N\text{-}H\cdots\pi$ hydrogen bonding 2404
PANCKURST M H Extrapolation procedures for evaluation of individual partial gram ionic volumes. Reply to comments 3035
PANNETIER G Solvent effect on the dimerization of N-methylaniline 1763
PAPIR Y S Diffraction of light by nonaqueous ordered suspensions 1881
PARFITT R T Micelle formation by some phenothiazine derivatives. II. Nuclear magnetic resonance studies in deuterium oxide 3554
PARKYNS N D Influence of thermal pretreatment on the infrared spectrum of carbon dioxide adsorbed on alumina 526
PARMENTER C S Absorption spectrum of benzene vapor near 2537 Ang 1564
PARMENTER C S Single vibronic level fluorescence. IV. Its application to the analysis of resonance fluorescence from benzene excited by the 2537-Ang. mercury line 1572
PARR C A Potential energy surfaces for atom transfer reactions involving hydrogens and halogens 1844
PARRISH C F Photolysis of gaseous 1,4-dioxane at 1470 Ang 3899
PATTERSON L K Solubilization of benzene in aqueous cetyltrimethylammonium bromide measured by differential spectroscopy. Comment 3907
PATTISON S Kinetics of the proton transfer reactions of serine and threonine 161
PAVIOT J Molecular conformation of 1,3,5-trinitrohexahydro-s-triazine (RDX) in solution 2056
PAVLOU S Primary and secondary rate processes in the acetone-silane photochemical system 3945
PAVLOU S P Energy transfer in thermal isocyanide isomerization. Noble gases in the ethyl isocyanide system 1366
PAVLOU S P Energy transfer in thermal isocyanide isomerization. n-Alkanes and n-alkenes in the ethyl isocyanide system 2171
PAVLOU S P Energy transfer in thermal isocyanide isomerization. General correlations in the ethyl isocyanide system 3037
PEARCE C Effect of mercury on the photolysis of 1,1,1-trifluoroacetone 439
PECHERSKY M J Validity of a simple theory for transport in ion-exchange membranes 3015
PELED E Contribution of hydrogen atoms to molecular hydrogen $[G_{H_2}]$ in the radiation chemistry of aqueous solutions 31
PELED E Competition for e_{aq}^- between several scavengers at high concentrations and its implications on the relevance of dry electrons in the radiation chemistry of aqueous solutions 3626
PELEG M Association equilibriums of silver and chloride ions in liquid ammonium nitrate-water mixtures. I. Molar ratio range water:ammonium nitrate 0.4-1.4 at 110° 2060
PELEG M Association equilibriums of silver and chloride ions in liquid ammonium nitrate-water mixtures. II. Anhydrous melt 3711
PENNER T L Radiation-induced chain isomerization of cis-1,2-diphenylpropene in cyclohexane 292
PENNY A L Reactions involving electron transfer at semiconductor surfaces. II. Photoassisted dissociation of nitrous oxide over illuminated ferric oxide and zinc oxides 617
PENZHORN R D Relative rates of the reactions of hydrogen atoms with hydrogen iodide and hydrogen bromide 835
PERLMUTTER-HAYMAN B Rapid preequilibriums as a cause for change of activation energy with temperature 2372
PERONA M J Comparison of energy partitioning from three-centered processes. Bimolecular transfer and unimolecular elimination reactions 2070
PETERLIN A Molecular mechanism of chain rupture in strained crystalline polymers 3921
PETERS E Kinetics of copper(II)- and copper(I)-catalyzed deuterium exchange in sulfuric and perchloric acid solutions 571
PETERSEN J C Thermodynamic study by infrared spectroscopy of the association of 2-quinolone, some carboxylic acids, and the corresponding 2-quinolone-acid mixed dimers 1129
PETERSON F C Nanosecond pulse radiolysis studies of aqueous thymine solutions 3815
PETHYBRIDGE A D Ion pairing in 2:2 electrolytes 291
PETRONIO M Competitive adsorption of phenol and sodium dinonylnaphthalenesulfonate on nickel oxide powder 1975
PETRUCCI S Correlation between translational and rotational relaxation times for ion pairs in solution 598
PETRUCCI S Outer-sphere association kinetics of magnesium(II), manganese(II), cobalt(II), nickel(II), copper(II), and zinc(II) m-benzenedisulfonates in methanol 2649
PETRUSIS C T Photopolymerization mechanisms. I. Dye-triplet reactions with p-substituted benzenesulfinate ions 3066
PHILIPSON K D Circular dichroism of chlorophyll and related molecules calculated using a point monopole model for the electronic transitions 1440
PHILLIPS D Photochemistry of the fluorotoluenes. I. Quantum yields of fluorescence and intersystem crossing in 1-fluoro-2-, 1-fluoro-3-, and 1-fluoro-4-methylbenzenes 3214
PHILLIPS D Quenching of excited states of fluorobenzene in the gas phase 3662
PHILLIPS L F Photometric and mass spectrometric observations on the reaction of hydrogen atoms with cyanogen 2662
PHILLIPS L F Quantum yields in the 58.4-nm photolysis of carbon dioxide 3499
PHILLIPS L F Absorption coefficients and ionization yields of some small molecules at 58.4 nm 719
PHILLIPS L F Mass spectrometric study of the reaction of hydrogen atoms with nitrosyl chloride 722
PHILLIPS L F Mass spectrometric study of the reaction of nitrogen atoms with nitrosyl chloride 1172
PHILLIPS L F Mass spectrometric study of the reaction of oxygen atoms with nitrosyl chloride 1320
PICHAT P Infrared study of the surface of titanium dioxides. I. Hydroxyl groups 1216
PICHAT P Infrared study of the surface of titanium dioxides. II. Acidic and basic properties 1221
PIKAL M J Ion-pair formation and the theory of mutual diffusion in a binary electrolyte 663
PIKAL M J Theory of the Onsager transport coefficients l_{ij} and R_{ij} for electrolyte solutions 3124
PILETTE Y P Photochemistry of charge-transfer systems. II. Complexes of pyromellitic dianhydride with polynuclear aromatic hydrocarbons 3805
PINION J P Excimer model for fluorene and dibenzofuran 1794
PINNAVAIA T J Interlamellar metal complexes on layer silicates. I. Copper(II)-arene complexes on montmorillonite 3957

PIPER L G Thermodynamics of cis-trans isomerizations. II. 1-Chloro-2-fluoroethylenes, 1,2-difluorocyclopropanes, and related molecules.... 1453
PITKETHLY R C Structure and properties of acid sites in a mixed oxide system. II. tert-Butylbenzee cracking and benzene adsorption 220
PITTS J N JR Photodecomposition of γ-butyrolactone in the vapor phase.......... 2733
PLADZIEWICZ J R Electron transfer reactions of ferrocenes 3381
PLATKO F E Investigation of micelle structure by fluorine magnetic resonance. IV. Fluorine-labeled nonionic detergents.......... 547
PLATT A E Reactions of deuterated methyl radicals with methylfluorosilanes. Polar effects in hydrogen abstraction 603
PLOOSTER M N Phase transitions in water adsorbed on silica surfaces.......... 3322
POBO L G Reactions of fast tritium molecules with 1-butene 2407
POCKER Y Reversible hydration of pyruvate esters. Thermodynamic and kinetic studies 792
POHLIT H M Partial degradation of 1,3,5-cycloheptatriene-^{14}C obtained from hot-atom, photolytic, and "thermal" reactions.......... 2558
POIRIER R V Use of tubular flow reactors for kinetic studies over extended pressure ranges.... 1593
POLNASZEK C F Electron spin resonance line shapes and saturation in the slow motional region 3385
POMMIER C Thermodynamic study of the formation of electron donor-acceptor complexes by gas-liquid chromatography.......... 2632
POPOV A I Spectroscopic studies of ionic solvation. VIII. Alkali metal salts in acetone solutions 56
POTASHNIK R Intersystem crossing in the charge-transfer quenching of molecular fluorescence.......... 1025
POTZINGER P Ion-molecule reactions in dimethylsilane, trimethylsilane, and tetramethylsilane 13
PRAGER S Variational bounds on the intrinsic viscosity.......... 72
PRAKASH J Dielectric relaxation in α,ω-dibromoalkanes in benzene solution 2616
PRATT D W Electron paramagnetic resonance spectra of pyrrolidino and pyrrolino free radicals. Structure of dialkylamino radicals 3486
PRAUSNITZ J M Solubilities of hydrocarbons and carbon dioxide in liquid methane and in liquid argon.......... 2345
PRAUSNITZ J M Entropies of vaporization for fluorocarbons and hydrocarbons from the Hildebrand rule.......... 2530
PRESTON G T Solubilities of hydrocarbons and carbon dioxide in liquid methane and in liquid argon.......... 2345
PRICE F P Transitions in mesophase forming systems. I. Transformation kinetics and pretransition effects in cholesteryl myristate........ 2839
PRICE F P Transitions in mesophase forming systems. II. Transformation kinetics and properties of cholesteryl acetate 2849
PRIMET M Infrared study of the surface of titanium dioxides. I. Hydroxyl groups 1216
PRIMET M Infrared study of the surface of titanium dioxides. II. Acidic and basic properties.. 1221
PRITCHARD G A The reaction $2COF_2 \rightarrow CO_2 + CF_4$ and the heat of formation of carbonyl fluoride 3024
PRITCHARD G O Pressure dependence of the cross-combination ratio for CF_3 and CH_3 radicals 2225
PRITCHARD G O Hexafluoroacetone imine filter for 185 nm.......... 1326
PRITCHARD H O Photochemical behavior of isocyanides.......... 580
PRUE J E Ion pairing in 2:2 electrolytes 291
PURDIE N Heats of association for divalent transition metal ethylene-maleic acid copolymer complexes.......... 1136
PYTLEWSKI L L Infrared and proton nuclear magnetic resonance studies of adducts of tin(II) and -(IV) and titanium(IV) halides with diisopropyl methylphosphonate.......... 637
QUADRIFOGLIO F Thermodynamic data for the water-hexamethylenetetramine system 3633
QUANE D Bond energy terms for methylsilanes and methylchlorosilanes.......... 2480
QUICKENDEN T I Effect of magnetic fields on the pH of water 2830
QUIRING W J Kinetics of the thermally induced dehydrofluorination of 1,1,1-trifluoroethane in shock waves.......... 295
QUIRING W J Kinetics of the shock wave pyrolysis of pentafluoroethane.......... 3493
RABANI J Radiation chemical yield of OH^- as determined by conductometric pulse radiolysis .. 1759
RABANI J Conductometric pulse radiolysis determination of ionic yields and neutralization kinetics in liquid ethanol.......... 3893
RABANI J Pulse radiolytic investigation of O_{aq}^- radical ions 1738
RABINOVITCH B S Energy transfer in thermal isocyanide isomerization. Noble gases in the ethyl isocyanide system 1366
RABINOVITCH B S Intramolecular energy relaxation. Nonrandom decomposition of hexafluorobicyclopropyl.......... 2164
RABINOVITCH B S Energy transfer in thermal isocyanide isomerization. n-Alkanes and n-alkenes in the ethyl isocyanide system 2171
RABINOVITCH B S Energy transfer in thermal isocyanide isomerization. General correlations in the ethyl isocyanide system.......... 3037
RABINOVITCH B S Vibrational deexcitation of highly excited polyatomic molecules. Amount of energy transferred per collision.......... 3376
RABINOVITCH B S Relative total scattering cross sections for homologous series of polar and nonpolar molecules.......... 727
RACK E P Kinetic energy isotope effects of bromine reactions activated by radiative neutron capture in gaseous methyl fluoride and methyl-d_3 fluoride 2072
RACK E P Reactions of iodine with olefins. II. Radiative neutron capture induced reactions of iodine-128 with various C_5 isomers. Evidence for a mechanism other than autoradiolysis in the condensed state.......... 2880
RADLOWSKI C Mechanism of the radiation-induced dechlorination of 1,1,1-trichloro-2,2-bis(p-chlorophenyl)ethane in alcoholic solution 2762
RAGHUNATHAN P Electron spin resonance of free radicals prepared by the reactions of methylene. Deuteriomethyl and formaldiminoxy radicals 2448
RAJENDER S Chymotrypsinogen family of proteins. XV. pH and temperature dependence of the α-chymotryptic hydrolysis of N-acetyl-L-tryptophan ethyl ester.......... 1375
RAJENDER S Chymotrypsinogen family of proteins. XVI. Enthalpy-entropy compensation phenomenon of α-chymotrypsin and the temperature of minimum sensitivity.......... 1387
RAO C N R Distorted hydrogen bonds formed by carbonyl compounds.......... 1744
RAO K G Distorted hydrogen bonds formed by carbonyl compounds.......... 1744
RAO K V S Formation of ozonide ions in γ-irradiated aqueous solutions of alkali hydroxides. Comments 3030
RAO V V S Electron spin resonance studies on zinc peroxide and on zinc oxide obtained from a decomposition of zinc peroxide 3089
RASMUSSEN D H Glass transition in amorphous water. Application of the measurements to problems arising in cryobiology 967
RASSING J Ultrasonic relaxation of tert-butyl alcohol in cyclohexane.......... 3182
RATAICZAK R D Electron spin resonance line-shape analysis for determination of unresolved metal hyperfine splittings in ion pairs. Application to the benzene anion radical.......... 2769
RAUBACH R A Singlet-triplet absorption spectrum of all-trans-retinal.......... 983
RAWSON B J Radiation chemistry of crystalline glycollic acid.......... 1648

RAY A Difference spectrophotometric method for the determination of critical micelle concentrations 804

RAY A Micelle formation by nonionic detergents in water-ethylene glycol mixtures 809

RAYMOND J I Matrix reactions of fluorohalomethanes with alkali metals. Infrared spectrum and bonding in the monofluoromethyl radical 3235

REARDON J D Gas-phase addition reactions of trifluoromethyl and methyl radicals in hexafluoroazomethane-acetone mixtures. I 735

REED E M JR Surface diffusion of single sorbates at low and intermediate surface coverage 133

REED G H Electron paramagnetic resonance studies in frozen aqueous solutions. Elimination of freezing artifacts 1202

REES R Energy partitioning on photolysis and pyrolysis of 3-vinyl-1-pyrazoline 1640

REEVES L W Determination of the hindered rotation barrier in unsym-dimethylselenourea and comparison with similar compounds 3372

REGER J P Gas-phase density-dependent directly bonded coupling constant 437

REHFELD S J Solubilization of benzene in aqueous cetyltrimethyl ammonium bromide measured by differential spectroscopy 3905

REILLY C A Nuclear magnetic resonance spectral interpretation by pattern recognition 1402

REILLY P J Prediction of osmotic and activity coefficients in mixed-electrolyte solutions 1305

REISFELD R Transition probabilities of europium in phosphate glasses 3980

RENNER T A Cohesive energies in polar organic liquids. II. n-Alkane nitriles and the 1-chloro alkanes 642

REUBEN J Electron spin relaxation in aqueous solutions of gadolinium(III). Aquo, cacodylate, and bovine serum albumin complexes 3164

REUCROFT P J Sorption properties of activated carbon 3526

REY-LAFON M Molecular conformation of 1,3,5-trinitrohexahydro-s-triazine (RDX) in solution 2056

RICCIERI P Naphthalene-sensitized photoaquation of some chromium(III)-ammine complex ions 3504

RICH L D Kinetics of hydrolysis of ferric ion in dilute aqueous solution 929

RICHARDSON F S Optical activity of alkyl-substituted cyclopentanones. Intermediate neglect of differential overlap molecular orbital model 2466

RICHARDSON F S Optical activity of trigonally distorted cubic systems 692

RICHERZHAGEN T Identity of the free radical in solutions of $\Delta^{10,10'}$-bianthrone 290

RICHOUX G Molecular conformation of 1,3,5-trinitrohexahydro-s-triazine (RDX) in solution 2056

RICHTOL H H Photochemical oxidation of some substituted aromatic amines in chloroform 2737

RIJKE A M Anomalous freezing behavior of polymer gels and solutions 2623

RING D F Reaction of oxygen atoms with cyclopentene 3056

RING M A Primary and secondary rate processes in the acetone-silane photochemical system 3945

ROBERTS E M Detection of slow motions in solids with wide-line nuclear magnetic resonance spectroscopy 3334

ROBERTS J P Second triplet level of 1,5-dichloroanthracene in fluid solutions 845

ROBINSON E A Solvent and temperature effects on the hydrogen bond 2219

ROBINSON R A Estimation of solute activity coefficients in dilute aqueous mixtures of sodium and zinc bromides at 25°. Comparisons with predictions from the Guggenheim theory of solutions 3153

ROBINSON R A Prediction of osmotic and activity coefficients in mixed-electrolyte solutions 1305

RODDE A F JR Chemiluminescent reaction of hydrated electrons with optically excited fluorescein dyes 764

ROGERS F E Thermochemistry of the Diels-Alder reaction. I. Enthalpy of addition of isoprene to tetracyanoethylene 1734

ROGERS M T Electron spin resonance study of the IO_2F^- radical in γ-irradiated single crystals of potassium oxyfluoroiodate 3479

ROHATGI K K Solvent effect on anthracene monosulfonates in the first excited state 595

RON T Dielectric absorption of adsorbed sulfur dioxide in the microwave region 532

RON T Microwave absorption and potential barrier for orientation. Sulfur dioxide adsorbed on sodium chloride and potassium chloride 2602

ROSEN M J Reactions of adsorbed organic molecules. II. Bromination of 4-nitrobiphenyl on a silica surface 887

ROSENBERG N W Chemistry of barium released at high altitudes 1412

ROSNER D E Effect of rapid homogeneous reaction on the diffusion-limited lifetime of a soluble sphere of arbitrary density 2969

ROSNER D E Kinetics of the attack of refractory solids by atomic and molecular fluorine 308

ROSS D S Kinetics of the unimolecular dehydrofluorination of methyldifluoramine 1170

ROSS R A Estimation of induction energies using gas-liquid chromatography 831

ROTHSCHILD W G Radiation-induced oxidation of liquid sulfur dioxide containing oxygen and water 3631

ROWLAND F S Methylene reactions in photolytic systems involving methyl iodide 2536

ROWLAND F S Relative rates of hydrogen atom abstraction by near-thermal fluorine-18 atoms 2709

ROWLAND F S Reactions of recoil tritium atoms with 1-butene and cis-2-butene. Average energy of the addition reaction 3771

ROWLAND F S Recoil tritium reactions with cyclobutane-d_8. Excitation energies accompanying substitution of energetic tritium for deuterium 3781

ROWLAND F S Isotope effects in the substitution reaction of 2.8-eV tritium atoms with methane 1283

ROWLAND F S Study of the roles of chemical factors in controlling the yields of substitution reactions by energetic tritium atoms. Electronegativity, electron density, and bond energy 1290

ROWLAND F S Complete retention of configuration during the replacement of hydrogen by energetic tritium in dl- and meso-$(CHFCl)_2$ 1299

ROWLAND F S Bond energy effects in substitution reactions of fluorine-18 atoms with methyl halides 1324

ROWLAND F S Secondary unimolecular reactions subsequent to substitution reactions by high-energy chlorine-38 and chlorine-39 atoms 440

ROWLEY J K Ionic reactions at high ionic strengths. Further equilibrium and kinetic measurements on the formation and dissociation of monochloroiron(III) 1113

ROZETT R W Monoisotopic mass spectra of the boranes 3106

RUBINSTEIN G Analysis of broadly overlapping absorption bands according to a two-absorber model 3635

RUFF I Transfer diffusion. I. Theoretical 3297

RUFF I Transfer diffusion. II. Kinetics of electron exchange reaction between ferrocene and ferricinium ion in alcohols 3303

RUSSELL M E Ion-molecule reactions in ethanol by photoionization 3797

RYASON P R Rate of oxidation of lead vapor 2259

RYNBRANDT J D Intramolecular energy relaxation. Nonrandom decomposition of hexafluorobicyclopropyl 2164

RYNBRANDT J D Vibrational deexcitation of highly excited polyatomic molecules. Amount of energy transferred per collision 3376

SADLEJ J Modified CNDO [complete neglect of differential overlap] method. IV. Ion-molecule interactions in the acetone solutions of electrolytes 3581

SAGNER P Solute-solvent effects in the ionization of tris(hydroxymethyl)acetic acid and related acids in water and aqueous methanol 826

ST. PIERRE L E Radiation chemistry of octamethyltrisiloxane 2430

SAITO E Deuterium isotope effect on the decay kinetics of perhydroxyl radical 2263

SALVEMINI F Electrochemical behavior of liquid anion membranes. Biionic potentials with the NO_3^-–Cl^-, NO_3^-–Br^-, Br^-–Cl^- couples 554
SAMUNI A Reactions of organic radicals formed by some "Fenton-like" reagents 3271
SANDOVAL H L Relative rates of the reactions of hydrogen atoms with hydrogen iodide and hydrogen bromide 835
SANGSTER D F Behavior of the solvated electron in ethanol-n-hexane mixtures 3639
SANTUS R Environmental effects on the deprotonation of indole derivatives in alkaline ices.... 3061
SANWAL S N Thermochemistry, thermodynamic functions, and molecular structures of some cyclic hydrocarbons 1264
SAREL S Metal-ligand bonding in copper(II) chelates. Electron paramagnetic resonance study 3828
SARMA T S Effects of the urea-guanidinium class of protein denaturants on water structure: heats of solution and proton chemical shift studies 815
SATATY Y A Complex formation between some acetylenic compounds and benzene 2128
SAUER K Circular dichroism of chlorophyll and related molecules calculated using a point monopole model for the electronic transitions 1440
SAUER M C V Reactions of acetone and hydrogen peroxide. I. Primary adduct 3004
SAUER M C V Reaction of acetaldehyde and tert-butyl hydroperoxide 3377
SAUMAGNE P Spectroscopic determination of association constants of primary aromatic amines with dimethyl sulfoxide and hexamethylphosphoric triamide 1157
SAUMAGNE P Calorimetric determination of enthalpies of association of primary aromatic amines with dimethyl sulfoxide and hexamethylphosphorotriamide 3149
SAVILLE B Use of "concentration-time" integrals in the solutions of complex kinetic equations 2215
SCHAAF D W Molecular complexes in the vapor of sodium bromide and zinc bromide mixtures ... 3028
SCHERAGA H A Energy parameters in polypeptides. IV. Semiempirical molecular orbital calculations of conformational dependence of energy and partial charge in di- and tripeptides . 2286
SCHEUTZOW D Conjugated radicals. IX. Experimental study and the LCI-SCF open shell calculations on the electronic spectra and the redox equilibria of the nitrogen-containing violenes 335
SCHIAVELLO M Structural, magnetic, and optical properties of nickel oxide supported on η- and γ-aluminas 1044
SCHIAVELLO M Catalytic activities of nickel oxide supported on γ- and η-aluminas for the nitrous oxide decomposition 1051
SCHICHMAN S A Viscosity and local liquid structure in dimethyl sulfoxide-water mixtures . 98
SCHILLER R Radiation chemistry of supercooled water 2997
SCHMIDT K H Absorption spectrum of e_{aq}^- in the temperature range -4 to 390° 2798
SCHMIDT L D Binding states of hydrogen and of nitrogen on the (100) plane of molybdenum ... 227
SCHMIDT M Kinetic study of species formed during the pulsed radiolysis of ammonia 2908
SCHMIDT M W Photochemical studies of solid potassium trisoxalatoferrate(III) trihydrate 2986
SCHOENHERR S Radiation-induced oxidation of liquid sulfur dioxide containing oxygen and water 3631
SCHRAGER M Relation between the acentric factor and the entropy of vaporization 166
SCHREIBER H D Solvent and temperature effects on the hydrogen bond 2219
SCHRIER E E Salt effects in alcohol-water solutions. Application of scaled particle theory to the salting-out of polar molecules 3757
SCHUG J C Self-association of butylamines..... 938
SCHULER R H Rate constants for reaction of hydrogen atoms in aqueous solutions............ 449
SCHULER R H Radiation chemistry of aqueous solutions of trichlorofluoromethane, dichlorodifluoromethane, and chlorotrifluoromethane 455
SCHULER R H Electron spin resonance study of the rate constants for reaction of hydrogen atoms with organic compounds in aqueous solution..... 1654
SCHUYLER M W Single vibronic level fluorescence. IV. Its application to the analysis of resonance fluorescence from benzene excited by the 2537-Ang. mercury line 1572
SCHWARTZ L M Conductance study of squaric acid aqueous dissociation 1798
SCHWEIGHARDT F K Proton exchange between guanidinium ion and water in water-N,N-dimethylacetamide mixtures.......................... 688
SCHWOERER F Pulse radiolysis of oxalic acid and oxalates 749
SCIBONA G Electrochemical behavior of liquid anion membranes. Biionic potentials with the NO_3^-–Cl^-, NO_3^-–Br^-, Br^-–Cl^- couples............ 554
SCOTT R L Equilibrium constants for the formation of weak complexes 3843
SCUPPA B Electrochemical behavior of liquid anion membranes. Biionic potentials with the NO_3^-–Cl^-, NO_3^-–Br^-, Br^-–Cl^- couples............ 554
SEALY R C Kinetic electron spin resonance studies on the photolysis of some carbonyl, nitroso, and nitro compounds.......................... 3454
SEARCY A W Demonstration of the existence of lanthanum hexafluoride gas and determination of its stability 108
SEELY G R Chlorophyll-poly(vinylpyridine) complexes. III. Photochemical activity and fluorescence yield................................ 1667
SEESE J D Intermolecular hydrogen bonding. I. Effects on the physical properties of tetramethylurea-water mixtures 3313
SEHESTED K Pulse radiolysis of aqueous alkaline sulfite solutions............................. 3510
SEHESTED K Pulse radiolysis of oxalic acid and oxalates 749
SEIDEL H Radiation-induced oxidation of liquid sulfur dioxide containing oxygen and water...... 3631
SEPULVEDA L Enhancement of micellar catalysis by added electrolytes 2707
SETSER D W Comparison of energy partitioning from three-centered processes. Bimolecular transfer and unimolecular elimination reactions . 2070
SETSER D W Reactions of methylene with 1,2-dichloro ethane and nonequilibrium unimolecular hydrogen chloride elimination from 1,3-dichloropropane, 1,4-dichlorobutane, and 1-chloropropane................ 2231
SETSER D W Photolysis of ketene-butane mixtures with and without added carbon monoxide .. 2240
SEVERSON R G JR Molecular complexes of iodine with some mono N-oxide heterocyclic diazines 2504
SEVILLA M D Electron spin resonance study of the photoionization of thymine. Thymine cation and anion radicals 626
SEWELL P A Study of the adsorption of insoluble and sparingly soluble vapors at the gas-liquid interface of water by gas chromatography........ 3870
SEYFERTH D Matrix-isolation study of the pyrolysis of bromochloromethyl-substituted organomercury compounds. Infrared spectra of the bromochlorocarbene and free radicals CCl_2Br and $CClBr_2$ 3984
SHADDICK R C Determination of the hindered rotation barrier in unsym-dimethylselenourea and comparison with similar compounds 3372
SHAH D O Equilibrium rate of exchange of water molecules at the air-water interface using nuclear magnetic resonance spectroscopy........... 2694
SHANE E C Nitrogen afterglow and the rate of recombination of nitrogen atoms in the presence of nitrogen, argon, and helium 1552
SHANNON T W Mass spectra of disilanes. Phenyl-silicon interaction and silicon-silicon bond strength................ 974
SHARMA D N Kinetics and mechanism of the reduction of iodate to iodite by bromide in the presence of phenol................................ 2516
SHARPE W R Solute-solvent interactions. VI. Specific interactions of tetraphenylarsonium, tetraphenylphosphonium, and tetraphenylborate ions with water and other solvents 3141
SHARY-TEHRANY S Thermochemistry, thermodynamic functions, and molecular structures of some cyclic hydrocarbons...................... 1264

SHAW D H Photochemical behavior of isocyanides ... 580
SHAW K N Determination of the hindered rotation barrier in unsym-dimethylselenourea and comparison with similar compounds ... 3372
SHAW R Kinetics of the unimolecular dehydrofluorination of methyldifluoramine ... 1170
SHAW R Heats of formation of nitroaromatics. Group additivity for solids ... 4047
SHELEF M Studies of surface reactions of nitric oxide by isotope labeling. II. Deuterium kinetic isotope effect in the ammonia-nitric oxide reaction on a supported platinum catalyst ... 875
SHERER S Proton magnetic resonance spectra of molten alkali metal acetate solutions of polyhydric alcohols and phenols ... 1338
SHERMAN W V Mechanism of the radiation-induced dechlorination of 1,1,1-trichloro-2,2-bis(p-chlorophenyl)ethane in alcoholic solution ... 2762
SHERRY H S Mechanism and kinetics of isotopic exchange in zeolites. I. Theory ... 3846
SHERRY H S Mechanism and kinetics of isotopic exchange in zeolites. II. Experimental data ... 3855
SHIDA S Radiolysis of liquid n-butane ... 2854
SHIDA S Gas-phase radiolysis of nitrous oxide. Effect of the addition of several hydrocarbons ... 3178
SHIDA T Electronic spectra of ion-radicals and their molecular orbital interpretation. I. Aromatic nitro-substituted anion-radicals ... 2591
SHIH S Electron spin resonance studies of adsorbed alkene molecules on synthetic zeolites. Cation radicals of tetramethylethylene and cyclopentene ... 3475
SHIHABI D S Reactivity of hydrogen atoms and hydrated electrons toward aqueous erythrosine. X-radiolysis ... 3020
SHILLADY D D Optical activity of alkyl-substituted cyclopentanones. Intermediate neglect of differential overlap molecular orbital model ... 2466
SHIMODA H Studies on associated solutions. III. Infrared spectral study of hydrogen bonding in solutions containing hydrogen fluoride ... 2222
SHIN H K Dependence of vibrational transition probabilities on the rotation angles and impact parameter in BC + A collisions ... 923
SHIN H K De-Excitation of molecular vibration on collision: vibration-to-rotation energy transfer in hydrogen halides ... 1079
SHIN H K Vibrational energy transfer in hydrogen plus helium ... 4001
SHIN K K Excitation of molecular vibration on collision. Dependence of the rotation-averaged transition probability on the impact parameter .. 3185
SHINE H J The electron spin resonance spectra of some bis(4-alkoxyphenyl) sulfides and ethers . 411
SICILIO F Kinetics of isopropyl alcohol radicals by electron spin resonance-flow techniques ... 1326
SIDDIQI A Photolysis of ethylene at 1216 Ang .. 1317
SIEBERT E M D Interaction virial coefficients in hydrocarbon-fluorocarbon mixtures ... 3863
SIEGENTHALER H Transport processes in low melting salts. Silver nitrate-thallium nitrate system ... 4025
SIGAL P Photolytic reactions of 1,3-diphenylpropene ... 2079
SILVERMAN J Perchlorodiphenylmethyl stable free radical. X-ray analysis of a disordered mixed crystal ... 1246
SIMHA R Corresponding state relations for the Newtonian viscosity of concentrated polymer solution. Temperature dependence ... 256
SIMIC M Spectroscopic investigation of cyclohexanol and cyclohexyl radicals and their corresponding peroxy radicals ... 1677
SIMMONS E L Photochemistry of solid layers. Reaction rates ... 588
SIMONAITIS R Photodecomposition of γ-butyrolactone in the vapor phase ... 2733
SIMONAITIS R Mercury-sensitized photodecomposition of nitrous oxide in the presence of mixtures of carbon monoxide and methane ... 3205
SIMPSON W H Sorption properties of activated carbon ... 3526
SIMSOHN H Investigation of micelle structure by fluorine magnetic resonance. V. Sodium perfluorooctanoate ... 942
SINGER L S Identity of the free radical in solutions of $\Delta^{10,10'}$-bianthrone ... 290
SINGH B P Solvent effect on anthracene monosulfonates in the first excited state ... 595
SINHA B P Oxidation kinetics of 2-mercaptoethylamine hydrochloride by ferricyanide ion in acid medium ... 2036
SISTER MARY A. MATESICH Transport properties in hydrogen bonding solvents. VI. The conductance of electrolytes in 2,2,2-trifluoroethanol ... 1708
SISTER MARY A. MATESICH Conductance of electrolytes in acetone and in 1-propanol-acetone mixtures at 25° ... 1714
SKINNER G B Shock tube experiments on the pyrolysis of deuterium substituted ethylenes ... 1
SKINNER H B Demonstration of the existence of lanthanum hexafluoride gas and determination of its stability ... 108
SLUTSKY L J Kinetics of the proton transfer reactions of serine and threonine ... 161
SLUYTERS J H Interpretation of electrode admittance in the case of specific reactant adsorption. Application to the bis(ethylenediamine) cobalt(III-II) system ... 2209
SLUYTERS-REHBACH M Interpretation of electrode admittance in the case of specific reactant adsorption. Application to the bis(ethylenediamine) cobalt(III-II) system ... 2209
SMAIL T Bond energy effects in substitution reactions of fluorine-18 atoms with methyl halides ... 1324
SMITH B A Nuclear magnetic relaxation in an homologous series of nematic liquid crystals ... 3834
SMITH C F JR Complex formation in aluminum iodide-diethyl ether solutions ... 282
SMITH D Vibronic effects in the infrared spectrum of the anion of tetracyanoethylene ... 325
SMITH D E Heats of mixing. II. Temperature dependence of aqueous electrolytes with a common ion ... 1125
SMITH E A Rate of oxidation of lead vapor ... 2259
SMITH P Electron paramagnetic resonance spectroscopic study of radical cations from hydrazine, methylhydrazine, and dimethylhydrazines ... 2048
SMITH W B Solvent effects on the fluoroform nuclear magnetic resonance spectra ... 497
SMITH W S Secondary unimolecular reactions subsequent to substitution reactions by high-energy chlorine-38 and chlorine-39 atoms ... 440
SNELSON A Infrared spectra of lithium tetrafluoroaluminate and sodium tetrafluoroaluminate 2609
SOLLY R K Comparison of RRK [Rice-Ramsperger-Kassel] and RRKM [Rice-Ramsperger-Kassel-Marcus] theories for thermal unimolecular processes ... 1333
SOLMS D J Anomalous freezing behavior of polymer gels and solutions ... 2623
SOLOMON W C Kinetics of chlorine monofluoride at high temperatures ... 3939
SOLTZBERG L J Perchlorodiphenylmethyl stable free radical. X-ray analysis of a disordered mixed crystal ... 1246
SOLYMOSI F Catalytic decomposition of perchloric acid vapor on zinc oxide ... 491
SOMORJAJ G A Vacuum vaporization studies of lithium fluoride single crystals ... 4049
SPENCER H E Photochemical studies of solid potassium trisoxalatoferrate(III) trihydrate ... 2986
SPENCER J N Solvent and temperature effects on the hydrogen bond ... 2219
SPOHR R Photoionization mass spectrometric study of xenon difluoride, xenon tetrafluoride, and xenon hexafluoride ... 1461
SPRINGBORN R L Chemical effects of the nuclear reaction $^{14}N(n,p)^{14}C$ in potassium azide ... 2551
SRINIVASAN S Adsorption inhibition as a mechanism for the antithrombogenic activity of some drugs. I. Competitive adsorption of fibrinogen and heparin on mica ... 2107

SRIVASTAVA R D Mass spectrometric determination of the heats of formation of aluminum oxide chloride(g) and aluminum oxide fluoride(g) 1760

STARKIE H C Electron spin resonance of atomic silver on porous glass and silica gel surfaces. Comments 2705

STEADMAN C J Solvation studies. II. Alkaline earth halides in high dielectric solvents 2325

STEC K S Cohesive energies in polar organic liquids. II. n-Alkane nitriles and the 1-chloro alkanes 642

STEC W J Effect of phosphorus-hydrogen deuterium substitution on the phosphorus-31 nuclear magnetic resonance spectroscopy of several dialkyl phosphonates 3547

STEC W J Study of phosphorus-sulfur compounds by inner-orbital photoelectron spectroscopy. Thiono-thiolo sulfur 3975

STEEN H B Comparison of the reactivities of dry and mobile electrons 1941

STEEN H B Photoinduced trapped electrons in rigid polar solution. I. Recombination luminescence 2887

STEEN H B Photoinduced trapped electrons in rigid polar solution. II. Kinetics and cross section of two-quantum ionization 2893

STEIN G Pathways of radiative and radiationless transitions in europium(III) solutions. Role of solvents and anions 3668

STEIN G Pathways of radiative and radiationless transitions in europium(III) solutions. The role of high energy vibrations 3677

STEIN G Continuous γ and pulse radiolysis of aqueous benzene solutions. Reactions of the hydroxycyclohexadienyl radical 3886

STEINGRABER O J Systematics of the electronic spectra of the p-oligophenylenes and their substituted analogs 318

STERN J H Enthalpy of transfer of sodium chloride from water to aqueous hydrogen peroxide at 25° 2229

STERN K H Dynamic method for measuring decomposition pressures of salts. Comments 721

STEVENS R D Electron paramagnetic resonance spectroscopic study of radical cations from hydrazine, methylhydrazine, and dimethylhydrazines 2048

STEVENSON G R Nitrosamine anion radicals 2704

STILBS P Nuclear magnetic resonance study of hindered internal rotation in urea in solution 1901

STONER G E Adsorption of fibrinogen. Electron microscope study 2103

STONER G E Adsorption inhibition as a mechanism for the antithrombogenic activity of some drugs. I. Competitive adsorption of fibrinogen and heparin on mica 2107

STRAUSS G Concentration quenching of proflavine hydrochloride in dry films of sodium deoxyribonucleate and poly(vinyl alcohol) 2727

STRONG H M Diamond growth rates and physical properties of laboratory-made diamond 1838

STUDENCKI A Rittner ionic model study of alkali hydride dimers 984

SU T Negative ion-molecule reactions in perfluoropropane 2534

SUBRAMANIAN S Electron spin resonance study of the IO_2F^- radical in γ-irradiated single crystals of potassium oxyfluoroiodate 3479

SUBRAMANIAN S Effects of the urea-guanidinium class of protein denaturants on water structure: heats of solution and proton chemical shift studies 815

SUGIURA Y Non-Newtonian viscosity and excluded volume effect of dilute solutions of flexible high polymers 1141

SULLIVAN P D The electron spin resonance spectra of some bis(4-alkoxyphenyl) sulfides and ethers 411

SULLIVAN P D Temperature-dependent splitting constants in the electron spin resonance spectra of cation radicals. III. Hydroxyl group 2195

SUSKI L Correlation of the excess molar volumes of solutions of cadmium and bismuth in their molten halides 3620

SUTTER E J Glass transitions in molecular liquids. I. Influence of proton transfer processes in hydrazine-based solutions 1826

SUTTER J R Kinetic studies of permanganate oxidation reactions. III. Reaction with tris(1,10-phenanthroline)iron(II) 1107

SUTTON J Continuous photolysis at 253.7 nm of acetone in aqueous solution in the presence of nitromethane 851

SUTTON M M Mass spectrometric study of the reaction of hydrogen atoms with nitrosyl chloride 722

SUZUKI T Photoisomerization of maleate radical anions produced in 2-methyltetrahydrofuran by γ-irradiation at 77°K 482

SVIRBELY W J Analysis of solution kinetics data coupled with thermal transients in an adiabatic calorimeter. I 4029

SVIRBELY W J Analysis of solution kinetics data coupled with thermal transients in an adiabatic calorimeter. II. First-order reactions 4039

SWEET R C Shock tube experiments on the pyrolysis of deuterium substituted ethylenes 1

SWORSKI T J Reduction of cerium(IV) by hydrogen peroxide. Dependence of reaction rate on Hammett's acidity function 250

SYMONS M C R Electron spin resonance of atomic silver on porous glass and silica gel surfaces. Comments 2705

SYMONS M C R Formation of ozonide ions in γ-irradiated aqueous solutions of alkali hydroxides. Comments 3030

SYMONS M C R Case for solvated electrons 3904

TACHIKAWA E Study of the roles of chemical factors in controlling the yields of substitution reactions by energetic tritium atoms. Electronegativity, electron density, and bond energy 1290

TAKAHASHI K Carbon-13 nuclear magnetic resonance spectroscopy. III. Chloro-substituted ethanes and ethylenes 331

TAKAHASHI K Nuclear magnetic resonance spectra of carbanions. II. Carbanions produced from α-methylstyrene and cumyl methyl ether 1062

TAKAHASHI K Carbon-13 nuclear magnetic resonance spectroscopy. IV. Bromo-substituted ethanes and ethylenes 3766

TAKAKI M Nuclear magnetic resonance spectra of carbanions. II. Carbanions produced from α-methylstyrene and cumyl methyl ether 1062

TAKAO S Gas-phase radiolysis of nitrous oxide. Effect of the addition of several hydrocarbons 3178

TAKEYAMA T Initiation rate for shock-heated hydrogen-oxygen-carbon monoxide-argon mixtures as determined by OH induction time measurements 1504

TALLMADGE J A Liquid film which occurs in a draining vessel 583

TAMAI Y Effect of surface groups of carbon on the adsorption and catalytic base hydrolysis of a hexaamminecobalt(III) ion 649

TAMRES M Vapor phase charge-transfer complexes. V. Blue-shifted iodine band 1057

TAMRES M Vapor-phase charge-transfer complexes. VI. Diethyl ether-iodine 3682

TANAKA K Photocatalytic reactions on semiconductor surfaces. I. Decomposition of nitrous oxide on zinc oxide 1037

TANAKA N Ionic equilibria in mixed solvents. VI. Dissociation constants of aliphatic diamines in water-methanol solutions 90

TANG Y-N Recoil tritium reactions with trimethylfluorosilane. A study on parameters affecting hot-atom substitution reactions 301

TANG Y-N Secondary unimolecular reactions subsequent to substitution reactions by high-energy chlorine-38 and chlorine-39 atoms 440

TANG Y-N Study of the roles of chemical factors in controlling the yields of substitution reactions by energetic tritium atoms. Electronegativity, electron density, and bond energy 1290

TANNO K Radiolysis of liquid n-butane 2854

TANNY G B Radiation chemistry of octamethyltrisiloxane 2430

TARPLEY A R JR Nuclear magnetic resonance spectra and substituent effects for symmetrically substituted dihalobiphenyls ... 421
TAUBE H Molar absorptivity of carbon trioxide. 2991
TELLINGHUISEN J B Absorption coefficients and ionization yields of some small molecules at 58.4 nm ... 719
TELLINGHUISEN J B Quantum yields in the 58.4-nm photolysis of carbon dioxide ... 3499
TEOH H Coexistence of liquid phases in calcium-ammonia solutions ... 399
TESTA A C Modification of nitrobenzene photochemistry by molecular complexation ... 2415
TEWARI K C Proton exchange between guanidinium ion and water in water-N,N-dimethylacetamide mixtures ... 688
THEARD L M Nanosecond pulse radiolysis studies of aqueous thymine solutions ... 3815
THOMAS H C Self-diffusion studies of gel hydration and the obstruction effect ... 1821
THOMAS J Conductance of electrolytes in acetone and in 1-propanol-acetone mixtures at 25° 1714
THOMPSON D S Inelastic light scattering from log normal distributions of spherical particles in liquid suspension ... 789
THOMPSON D W Keto-enol equilibriums in 2,4-pentanedione and 3,3-dideuterio-2,4-pentanedione ... 433
THOMPSON J C Coexistence of liquid phases in calcium-ammonia solutions ... 399
THOMPSON J C Kinetics investigation of the amylose-iodine reaction ... 272
THOMPSON K R The infrared spectrum of matrix-isolated uranium monoxide ... 2283
THOMPSON K R Spectroscopy of titanium oxide and titanium dioxide molecules in inert matrices at 4°K ... 3243
THRUSH B A Vibrational deexcitation of highly excited polyatomic molecules. Amount of energy transferred per collision ... 3376
THYNNE J C J Negative ion formation by ethylene and 1,1-difluoroethylene ... 2584
THYNNE J C J Autodetachment lifetimes, attachment cross sections, and negative ions formed by sulfur hexafluoride and sulfur tetrafluoride .. 3517
TIERNAN T O Negative ion-molecule reactions in perfluoropropane ... 2534
TKAC A Radical reactions in the ligand field of metal complexes. I. Electron paramagnetic resonance spectra of complex-bonded radicals formed by reaction of cobalt(II) acetylacetonate with tert-butyl hydroperoxide ... 2575
TKAC A Radical reactions in the ligand field of metal complexes. II. Reactions of the tert-butylperoxy radical bound to cobalt(III) ... 2580
TOBY S Pressure dependence of the cross-combination ratio for CF_3 and CH_3 radicals ... 2225
TOBY S Deactivation of vibrationally excited ethane. Comparison of two methods of measuring the pressure dependence ... 837
TOBY S Hexafluoroacetone imine filter for 185 nm ... 1326
TOKIWA F Nuclear magnetic resonance study of interaction between anionic and nonionic surfactants in their mixed micelles ... 3560
TOMITA A Effect of surface groups of carbon on the adsorption and catalytic base hydrolysis of a hexaamminecobalt(III) ion ... 649
TOMKINS R P T Transport processes in low melting salts. Silver nitrate-thallium nitrate system ... 4025
TONDRE C Effect of urea and other organic substances on the ultrasonic absorption of protein solutions ... 374
TONDRE C Ultrasonic absorption as a probe for the study of site binding of counterions in polyelectrolyte solutions ... 3367
TONG C K Vibrational spectra of trans- and cis-crotononitrile ... 44
TORIKAI A Photoisomerization of maleate radical anions produced in 2-methyltetrahydrofuran by γ-irradiation at 77°K ... 482
TORRENCE G Mean molal activity coefficient of polymethacrylic acid at various degrees of neutralization ... 2144
TOTH L M Coordination effects on the spectrum of uranium(IV) in molten fluorides ... 631
TOU J C Loose and tight activated complexes in the ion fragmentations of a dimethylthiocarbamate and a phosphorothioate ... 1903
TOUHARA H Studies on associated solutions. III. Infrared spectral study of hydrogen bonding in solutions containing hydrogen fluoride ... 2222
TRAN DINH SON Continuous photolysis at 253.7 nm of acetone in aqueous solution in the presence of nitromethane ... 851
TRAVERS J G Molecular association of hydrogen-bonding solutes. Phenol in carbon tetrachloride ... 3591
TREVERTON J A Levitation calorimetry. IV. Thermodynamic properties of liquid cobalt and palladium ... 3737
TRIBUTSCH H Electrochemical investigations on the spectral sensitization of gallium phosphide electrodes ... 562
TRINQUECOSTE C Molecular conformation of 1,3,5-trinitrohexahydro-s-triazine (RDX) in solution ... 2056
TROTTER W Modification of nitrobenzene photochemistry by molecular complexation ... 2415
TRUHLAR D G Potential energy surfaces for atom transfer reactions involving hydrogens and halogens ... 1844
TSAI C C Crystal and molecular structure of L-alanyl-L-alanine ... 918
TSAI S C Circular dichroism of chlorophyll and related molecules calculated using a point monopole model for the electronic transitions ... 1440
TSAO C W Dynamics of the reactions of O_2^+ with molecular hydrogen and deuterium ... 1426
TSCHUIKOW-ROUX E Kinetics of the thermally induced dehydrofluorination of 1,1,1-trifluoroethane in shock waves ... 295
TSCHUIKOW-ROUX E Kinetics of the shock wave thermolysis of 1,1,2,2-tetrafluoroethane .. 3195
TSCHUIKOW-ROUX E Kinetics of the shock wave pyrolysis of pentafluoroethane ... 3493
TSCHUIKOW-ROUX E Kinetics of the thermally induced dehydrofluorination of 1,1,1-trifluoroethane in shock waves ... 295
TSUJII K Nuclear magnetic resonance study of interaction between anionic and nonionic surfactants in their mixed micelles ... 3560
TUCKER E E Effects of solvents on molecular complex formation equilibriums. Use of nonpolar analogs for polar solutes ... 2413
TULLI P Naphthalene-sensitized photoaquation of some chromium(III)-ammine complex ions.... 3504
TUMOSA C S Interactions of positrons with defects in sodium chloride crystals ... 2030
TURNER N H Dynamic adsorption of water vapor by a fiber drawn from a melt of Vycor ... 2718
TUTTLE T R JR Analysis of broadly overlapping absorption bands according to a two-absorber model ... 3635
TUTTLE T R JR Solvated electron in any case, but what kind ... 3905
TUTTLE T R JR Solvated electron or not ... 843
TYNDALL J R Rittner ionic model study of alkali hydride dimers ... 984
TYRRELL J Complex formation between some acetylenic compounds and benzene ... 2128
VALYOCSIK E W Photolytic reactions of 1,3-diphenylpropene ... 2079
VANARTSDALEN E R Proton magnetic resonance spectra of molten alkali metal acetate solutions of polyhydric alcohols and phenols 1338
VAN DEN ENDEN J Nuclear magnetic resonance line shape of solid heptane ... 3901
VAN DER LINDE H J Influence of temperature on the γ radiolysis of isopropyl alcohol vapor. Effect of molecular structure on the nonchain and chain decompositions of alcohol vapors ... 20
VAN GEMERT M J C Dielectric measurements with time-domain reflectometry when large conductivities are involved ... 1323
VAN HEUVELEN A Electronic absorption spectra and electron paramagnetic resonance of copper(II)-amine complexes ... 3355

VAN NIEKERK M Investigations on the ion-exchange and ionic transport properties of glass membranes in molten salts by an electrolytic transport technique 2815
VAN PUTTE K Nuclear magnetic resonance line shape of solid heptane 3901
VAN REENEN T J Investigations on the ion-exchange and ionic transport properties of glass membranes in molten salts by an electrolytic transport technique 2815
VAN WAZER J R Ab initio LCAO-MO-SCF study of the phosphoryl fluoride molecule, OPF_3 1360
VAN WAZER J R Effect of phosphorus-hydrogen deuterium substitution on the phosphorus-31 nuclear magnetic resonance spectroscopy of several dialkyl phosphonates 3547
VAN WAZER J R Study of phosphorus-sulfur compounds by inner-orbital photoelectron spectroscopy. Thiono-thiolo sulfur 3975
VASLOW F Salt-induced critical-type transitions in aqueous solutions. Heats of dilution of the lithium and sodium halides 3317
VASUDEV P Iodine-129 Moessbauer studies of the chemical effects of nuclear transformations in compounds of tellurium 2867
VAUGHAN J D Chemical effects of the nuclear reaction $^{14}N(n,p)^{14}C$ in potassium azide 2551
VAUGHAN V L Chemical effects of the nuclear reaction $^{14}N(n,p)^{14}C$ in potassium azide 2551
VELAPOLDI R A Transition probabilities of europium in phosphate glasses 3980
VELECKIS E Solubility of helium and argon in liquid sodium 2832
VERRALL R E Extrapolation procedures for evaluation of individual partial gram ionic volumes. Comments 3031
VESELY K Radical reactions in the ligand field of metal complexes. I. Electron paramagnetic resonance spectra of complex-bonded radicals formed by reaction of cobalt(II) acetylacetonate with tert-butyl hydroperoxide 2575
VESELY K Radical reactions in the ligand field of metal complexes. II. Reactions of the tert-butylperoxy radical bound to cobalt(III) 2580
VESLEY G F Role of singlet and triplet states in aromatic substitution reactions 1775
VINCOW G Identity of the free radical in solutions of $\Delta^{10,10'}$-bianthrone 290
VINCOW G Electron spin resonance spectroscopy of the fluorosulfate radical ($SO_3F.$) in solution. Line width and its temperature dependence 712
VINCOW G Spin-restricted SCF-CI[configuration interaction] theory and calculations of contact hyperfine splittings 3400
VINEN R Biionic potentials of a liquid-membrane electrode selective toward calcium 2138
VIRMANI Y P Electron paramagnetic resonance studies of carbon monoxide adsorbed on thorium oxide 895
VIRMANI Y P Electron paramagnetic resonance study of hydrogen atoms trapped in γ-irradiated calcium phosphates 1936
VOIGT A F Reactions of recoil carbon atoms with oxygen-containing molecules. II. Structural dependence of carbon monoxide yields 2248
VOIGT A F Reactions of recoil carbon atoms with oxygen-containing molecules. III. Reaction mechanisms in methanol 2253
VOIGT A F Recoil reaction products of carbon-11 in C_5 hydrocarbons 3201
VOLMAN D H Interpretation of electron spin resonance evidence for the mechanism of free-radical-induced reactions of methylenecyclobutane and methylenecyclopentane 714
VOLPIN D Thermodynamics of elasticity in open systems. Elastin 142
VON HAHN H E A Kinetics of copper(II)- and copper(I)-catalyzed deuterium exchange in sulfuric and perchloric acid solutions 571
VREDENBERG S Kinetics of chemical ionization. I. Reaction of tert-$C_4H_9^+$ with benzyl acetate 590
VRIJ A Theory of the stabilization of dispersions by adsorbed macromolecules. II. Interaction between two flat particles 2094
WADA E Non-Newtonian viscosity and excluded volume effect of dilute solutions of flexible high polymers 1141
WADDINGTON D J Pyrolysis of 2-nitropropane 2427
WADE C G Nuclear magnetic relaxation in an homologous series of nematic liquid crystals 3834
WADE W H Adsorption on flat surfaces. I. Gas phase autophobicity 1887
WAI C M Recoil bromine reaction. Isomerization of excited cyclopropyl bromide 2698
WALKER B F Initiation rate for shock-heated hydrogen-oxygen-carbon monoxide-argon mixtures as determined by OH induction time measurements 1504
WALKER M S Electronic structure of furanquinones. I. Absorption spectra of dinaphtho[2,1-2',3']furan-8,13-dione and dinaphtho[1,2-2',3']furan-7,12-dione 3257
WALKER S Relaxation processes of cholesteryl methyl ether 1237
WALKER S Far-infrared absorption of some organic liquids 2942
WALLACE R A Equivalent conductivity of potassium halides in molten acetamide 2687
WANG K M Electron paramagnetic resonance study of Y-type zeolites. III. O_2^- on AlHY, ScY, and LaY zeolites 1165
WARING C E Gas-phase addition reactions of trifluoromethyl and methyl radicals in hexafluoroazomethane-acetone mixtures. I 735
WARREN J L Iodine-129 Moessbauer studies of the chemical effects of nuclear transformations in compounds of tellurium 2867
WARRICK P JR Spectrophotometric dissociation field effect kinetics of aqueous acetic acid and bromocresol green 2488
WARRICK P JR Specific rates in the acid dissociation-ion recombination equilibrium of dilute aqueous hydrazoic acid at 25° 3026
WARRIS M A Pyrolysis of 2-nitropropane 2427
WARSHAY M Effects of laminar and turbulent boundary layer buildup in shock tubes upon chemical rate measurements 2700
WATANABE N Studies on associated solutions. III. Infrared spectral study of hydrogen bonding in solutions containing hydrogen fluoride 2222
WATERMAN D C Infrared spectrum of polyethylene irradiated at 4°K 3988
WATKINS C L Nuclear spin relaxation in nematic liquid crystals 2452
WATKINS K W Isomerization of chemically activated n-pentyl radicals 1632
WATKINS K W Isomerization of vibrationally excited 3-methyl-1-buten-1-yl radicals via hydrogen atom migration. Quantum statistical weight effect 2665
WEBBER S E External heavy-atom effect on the quantum yield of sensitized phosphorescence of some aromatic molecules 1921
WEE E L Liquid crystal-isotropic phase equilibriums in the system poly(γ-benzyl α-L-glutamate)-dimethylformamide 1446
WEI L Y Effect of positive ion scavenging by benzene in the radiolysis of propane 2272
WEINER P H Anisotropic solvent shifts determined by factor analysis 1207
WEINER P H Investigation of the van der Waals effect in nuclear magnetic resonance spectroscopy by factor analysis and the prediction of diamagnetic and paramagnetic susceptibilities 3160
WEINER P H Nuclear magnetic resonance proton shifts of polar solutes 3971
WEINSTOCK B Mass-spectrometric studies of rate constants for addition reactions of hydrogen and of deuterium atoms with olefins in a discharge-flow system at 300°K 1601
WEISS J J Formation of ozonide ions in γ-irradiated aqueous solutions of alkali hydroxides. Reply to comments 3031
WEISS K Photochemistry of charge-transfer systems. II. Complexes of pyromellitic dianhydride with polynuclear aromatic hydrocarbons 3805
WEISS S Kinetics of proton transfer reactions of polyacrylic and polymethacrylic acids with an indicator 267

WELLS. W. L. Ultraviolet photochemistry of ruthenium(III) ammine complexes 3075
WELTNER W JR Spectroscopy of titanium oxide and titanium dioxide molecules in inert matrices at 4°K 3243
WELTNER W JR Spectroscopy of rare earth oxide molecules in inert matrices at 4°K 514
WEN W-Y Free energy changes on mixing solutions of alkali halides and symmetrical tetraalkylammonium halides 2148
WENDORFF J H Transitions in mesophase forming systems. I. Transformation kinetics and pretransition effects in cholesteryl myristate 2839
WENDORFF J H Transitions in mesophase forming systems. II. Transformation kinetics and properties of cholesteryl acetate 2849
WENNERSTROM H Interaction of halide ions with organic cations containing charged nitrogen, phosphorus, or sulfur in aqueous solutions studied by nuclear quadrupole relaxation 2936
WENTORF R H JR Diamond growth rates 1833
WERNER A S Dynamics of the reactions of O_2^+ with molecular hydrogen and deuterium 1426
WEST E D Analysis of solution kinetics data coupled with thermal transients in an adiabatic calorimeter. I 4029
WEST E D Analysis of solution kinetics data coupled with thermal transients in an adiabatic calorimeter. II. First-order reactions 4039
WEXLER S Reactions of fast tritium molecules with 1-butene 2407
WEXLER S Hydrogen displacement in n-butane by fast T_2 and T_2^+ collisions 2417
WHARTON J H Effect of varied excitation on the fluorescence spectra of 2-phenylnaphthalene and biphenyl. Photoselection of conformers 3097
WHEELER V L Thermodynamics of cis-trans isomerizations. II. 1-Chloro-2-fluoroethylenes, 1,2-difluorocyclopropanes, and related molecules 1453
WHIDBY J F Protolysis kinetics of ethyl N-methylcarbamate 1895
WHIDBY J F Nuclear magnetic resonance study of the protolysis kinetics of 5-dimethylaminonaphthalene-1-sulfonic acid and its N-methylsulfonamide 4056
WHITE J D Kinetics of the reaction between uranium(III) and $Co(NH_3)_4(H_2O)_2^{3+}$ in aqueous perchlorate solutions 2117
WHITE J L Infrared study of aluminum-deficient zeolites in the region 1300 to 200 cm^{-1} 2408
WHITE R D Kinetics of the proton transfer reactions of serine and threonine 161
WHITFIELD M Measurement of activity coefficients with liquid ion-exchange electrodes for the system calcium(II)-sodium(I)-chloride(I)-water 957
WHYTOCK D A Effect of mercury on the photolysis of 1,1,1-trifluoroacetone 439
WICKER R K II Freezing points osmotic coefficients, and activity coefficients of salts in N-methylacetamide. I. Alkali halides and nitrates 2313
WIEDEMEIER H High-molecular-weight boron sulfides. VII. Lower temperature studies and metastable decompositions 2410
WIERS B H Polynuclear complex formation in solutions of calcium ion and 1-hydroxyethylene-1,1-diphosphonic acid. II. Light scattering, sedimentation, mobility, and dialysis measurements 682
WIERSMA S J Explosion limits of chlorine-fluorine mixtures 867
WILCOX F L Salt effects in alcohol-water solutions. Application of scaled particle theory to the salting-out of polar molecules 3757
WILLARD J E Paramagnetic species produced by ultraviolet irradiation of lithium, potassium, sodium, magnesium, and cadmium in 3-methylpentane at 77°K 35
WILLARD J E Origin of complex electron spin resonance spectra of γ-irradiated polycrystalline n-alkyl iodides with even number of carbon atoms per molecule 467
WILLARD J E Growth and decay of alkyl radicals in γ-irradiated alkyl iodides at 77°K 472
WILLARD J E Growth patterns of reaction intermediates produced by self-radiolysis of tritiated ethyl iodide at 77°K 3359
WILLIAMS F Electron spin resonance spectra of isocyanatoalkyl radicals 1893
WILLIAMS F Electron spin resonance spectrum and structure of the radical anion of phosphorus oxychloride 3023
WILLIAMS G J Relative total scattering cross sections for homologous series of polar and nonpolar molecules 727
WILLIAMS J L Secondary unimolecular reactions subsequent to substitution reactions by high-energy chlorine-38 and chlorine-39 atoms 440
WILLIAMS R L Reactions of recoil carbon atoms with oxygen-containing molecules. II. Structural dependence of carbon monoxide yields 2248
WILLIAMS R L Reactions of recoil carbon atoms with oxygen-containing molecules. III. Reaction mechanisms in methanol 2253
WILLIAMS R L Relative rates of hydrogen atom abstraction by near-thermal fluorine-18 atoms 2709
WILLIAMSON D G Reaction of $O(^3P)$ with dideuterioacetylene 4053
WILSON D E Ion lifetimes in gaseous ammonia 444
WILSON N K Hindered rotation about the S_2C–NR_2 bond in N,N,N′,N′-tetraalkylthiuram disulfides and monosulfides 1067
WILSON R D Heats of mixing. II. Temperature dependence of aqueous electrolytes with a common ion 1125
WILSON T R S Difference chromatography of seawater 1418
WINKLER C A Quantum yields in the 58.4-nm photolysis of carbon dioxide 3499
WIRTH G B Tracer and mutual diffusivities in the system chloroform-carbon tetrachloride at 25° 3293
WIRTH H O Systematics of the electronic spectra of the p-oligophenylenes and their substituted analogs 318
WOHLEBER D A Application of the Polanyi adsorption potential theory to adsorption from solution on activated carbon. II. Adsorption of partially miscible organic liquids from water solution 61
WOHLEBER D A Application of the Polanyi adsorption potential theory to adsorption from solution on activated carbon. III. Adsorption of miscible organic liquids from water solution 3720
WOJCIK L H Kinetics of chemical ionization. I. Reaction of tert-C_4H_9+ with benzyl acetate 590
WOLF A P States of atomic carbon produced in decomposition of organic compounds in a microwave plasma 445
WOLFF H Concentration dependence of vapor pressure isotope effect of methylamine and N-deuteriomethylamine in hexane 160
WOLFF M A Complexes of nickel(II) with purine bases: relaxation spectra 799
WOLFGANG R Temperature dependence of simple hot atom reactions 3042
WONG M K Spectroscopic studies of ionic solvation. VIII. Alkali metal salts in acetone solutions 56
WONG P K Electron spin resonance study of trapped radicals produced by the radiolysis of hydrogenous materials on porous glasss 201
WOOD B J Rate and mechanism of interaction of oxygen atoms and hydrogen atoms with silver and gold 2186
WOOD D E Electron paramagnetic resonance spectra of pyrrolidino and pyrrolino free radicals. Structure of dialkylamino radicals 3486
WOOD R H Freezing points, osmotic coefficients, and activity coefficients of salts in N-methylacetamide. I. Alkali halides and nitrates 2313
WOOD R H Freezing points, osmotic coefficients, and activity coefficients of salts in N-methylacetamide. II. Tetraalkylammonium halides and some alkali metal formates, acetates, and propionates 2319
WOOD R H Prediction of osmotic and activity coefficients in mixed-electrolyte solutions 1305

WOOD W P Photooxidation of carbon disulfide 854
WOOD W P Kinetics and mechanism of the carbon disulfide-oxygen explosion 861
WOODS D E Kinetic electron spin resonance studies on the photolysis of some carbonyl, nitroso, and nitro compounds 3454
WOODS R Oxidation of ethyl xanthate on platinum, gold, copper, and galena electrodes. Relation to the mechanism of mineral flotation 354
WOODWARD A J Infrared spectra of nitric oxide adsorbed on evaporated alkali halide films 2930
WOOLLEY E M Complex solubility of silver chloride in methanol-water, acetone-water, and dioxane-water mixtures 93
WOOLLEY E M Molecular association of hydrogen-bonding solutes. Phenol in carbon tetrachloride 3591
WOOLSEY G B Freezing point depression measurements in N-methylacetamide as a solvent 2879
WROBLOWA H Ellipsometric investigations of anodic film growth on iron in neutral solution. Prepassive film 2823
WUELFING P JR Photochemical oxidation of some substituted aromatic amines in chloroform 2737
YAFUSO M Noise spectra associated with hydrochloric acid transport through some cation-exchange membranes 654
YAMAGUCHI N Non-Newtonian viscosity and excluded volume effect of dilute solutions of flexible high polymers 1141
YAMANARI K Determination of magnetic moments of paramagnetic ions in microgram quantities using ion-exchange resins 2981
YAMAZAKI M Transient phenomena caused by temperature change on capacitance of rutile film 1279
YAMAZAKI T Dimerization of the perylene and tetracene radical cations and electronic absorption spectra of their dimers 1768
YAN J F Energy parameters in polypeptides. IV. Semiempirical molecular orbital calculations of conformational dependence of energy and partial charge in di- and tripeptides 2286
YANAGITA M Electron spin resonance signals of abnormal alkyl radicals trapped on porous Vycor glass surfaces coated with metal oxides at 77°K 4064
YANG C C Viscosity of the cyclohexane-aniline binary liquid system near the critical temperature 2619
YANNONI N F Perchlorodiphenylmethyl stable free radical. X-ray analysis of a disordered mixed crystal 1246
YAO N-P Transport behavior in dimethyl sulfoxide. II. Viscosity studies 1727
YAO N-P Transport behavior in dimethyl sulfoxide. III. Conductance-viscosity behavior of tetra-N-amylammonium thiocyanate from infinite dilution to molten salt at 55° 3586
YASUMORI I Pressure jump and isotope replacement studies of acetylene hydrogenation on palladium surface 880
YEATTS L B Electrical conductances and ionization behavior of sodium chloride in dioxane-water solutions at 100° and pressures to 4000 bars 1099
YEH C Absolute rate constants for the reactions of hydrogen atoms with olefins 1584
YEO K O Effects of solvents on molecular complex formation equilibriums. Use of nonpolar analogs for polar solutes 2413
YOONG M Kinetic energy isotope effects of bromine reactions activated by radiative neutron capture in gaseous methyl fluoride and methyl-d_3 fluoride 2072
YOSHIDA H Dissociative electron capture process of methyl vinyl ether in organic glasses 476
YOUHNE Y Vibronic effects in the infrared spectrum of the anion of tetracyanoethylene 325
YUM S I Tracer and mutual diffusion coefficients of proteins 379
ZADOROJNY C Reversible hydration of pyruvate esters. Thermodynamic and kinetic studies 792
ZAGORSKI Z P Pulse radiolysis of aqueous alkaline sulfite solutions 3510
ZAHRADNIK R Conjugated radicals. IX. Experimental study and the LCI-SCF open shell calculations on the electronic spectra and the redox equilibria of the nitrogen-containing violenes 335
ZANA R Effect of urea and other organic substances on the ultrasonic absorption of protein solutions 374
ZANA R Ultrasonic absorption as a probe for the study of site binding of counterions in polyelectrolyte solutions 3367
ZECCHINA A Infrared study of surface properties of α-chromia. I. Preparation and adsorption of water, heavy water, and carbon monoxide 2774
ZECCHINA A Infrared study of surface properties of α-chromia. II. Oxygen chemisorption 2783
ZECCHINA A Infrared study of surface properties of α-chromia. III. Adsorption of carbon dioxide 2790
ZEHAVI D Pulse radiolytic investigation of O_{aq}^- radical ions 1738
ZEISS C A A potential surface for a nonlinear cheletropic reaction. The decarbonylation of cyclopropanone 340
ZELLER E J Electron paramagnetic resonance study of hydrogen atoms trapped in γ-irradiated calcium phosphates 1936
ZIMBRICK J D Electron paramagnetic resonance study of hydrogen atoms trapped in γ-irradiated calcium phosphates 1936
ZINATO E Naphthalene-sensitized photoaquation of some chromium(III)-ammine complex ions 3504
ZWOLINSKI B J High-precision viscosity of supercooled water and analysis of the extended range temperature coefficient 2016

KEYWORD INDEX *to Volume 75, 1971*

Abs entropies bicyclooctane 1073
Absorption band overlap analysis 3635
Absorption benzoquinoline propanol effect 2690
Absorption carbon disulfide matrix 2204
Absorption coeffs gaseous mols 719
Absorption emission spectra carbon 445
Absorption excited singlet perylene 3894
Absorption IR org liqs 2942
Absorption optical radiolysis erythrosin 3020
Absorption perylene tetracene dimers 1768
Absorption spectra cyanogen ion radicals 608
Absorption spectra dipolar azobenzenes 581
Absorption spectra europium 3668
Absorption spectra methanol polymer 1808
Absorption spectra methyluracil 1509
Absorption spectrum aq electron 2798
Absorption spectrum benzene vapor 1564
Absorption spectrum cyclohexyl radical 1677
Absorption spectrum singlet triplet retinal 983
Abstraction hydrogen fluorine 18 2709
Abstraction hydroxyl aliph alc 1186
Acceptor donor electron complexes 2632
Acentric factor vaporization 166
Acetaldehyde peroxide addn mechanism 3377
Acetamide dimethyl pulse radiolysis 2267
Acetamide molten conductance potassium halide 2687
Acetate copper soln ESR 2228
Acetate potassium heat mixing 1125
Acetates alkali activity coeffs 2319
Acetates metal fused PMR solvent 1338
Acetato ammine cobalt UV photochemistry 1914
Acetic acid dissocn kinetics 2488
Acetic acid soln copper acetate 2228
Acetic acids hydroxymethyl ionization 826
Acetone addn trifluoromethyl radical 735
Acetone adsorption 3720
Acetone aq solvent 93
Acetone diphenylpropene irradn isomerization 2394
Acetone flash photolysis 1910
Acetone fluoro imine extinction coeffs 1326
Acetone hydrated electron scavenger 3626
Acetone hydrogen peroxide adduct 3004
Acetone lithium interaction 3581
Acetone photolysis 837
Acetone photolysis aq solns 851
Acetone silane photodecompn 3945
Acetone soln electrolyte conductance 1714
Acetone solvation alkali ions 56
Acetonitrile adsorption 3720
Acetonitrile soln viscosity coeff ion 2532
Acetylacetonate cobalt complex bonded radicals 2575
Acetylene hydrogen deuterium exchange 4053
Acetylene hydrogenation palladium surfaces 880
Acetylene oxygen reaction 2402
Acetylene prodn photolysis ethylene 1317
Acetylene yield methane radiolysis 2405
Acetylene yield radiolysis methane 1164
Acetylenic compds benzene complex 2128
Acetyltryptophan chymotrypsin hydrolysis 1375
Acid base reaction denaturing agent 1120
Acid hydrazoic dissocn recombination 3026
Acid oxalic oxidn 3343
Acid perchloric catalytic decompn 491
Acid sites catalyst 220
Acid strengths resolution medium 2496
Acidity alcs 2226
Acidity consts detn 2657
Acidity function reaction rate 250
Acidity titanium dioxide surface 1221
Acids hydroxymethyl acetic ionization 826
Acids polymeric proton transfer 267
Acrylamides photopolymn 3066
Acrylic acid polymer proton transfer 267
Activated carbon adsorbent 61 3720
Activated carbon sorbent 3526
Activation energies tetraalkylammonium ions 509
Activation energy alkyldifluoroamine dehydrofluorination 1170
Activation energy preequil temp 2372
Activity coeff bromide 3153
Activity coeff hexane ketone system 4041
Activity coeff polymethacrylic acid 2144
Activity coeffs alkali propionates 2319
Activity coeffs ion exchange electrodes 957
Activity coeffs mixed electrolytes 1305
Activity coeffs salts methylacetamide 2313
Activity polyelectrolyte salt soln 3890
Acylated polyethylenimine NMR fluorine 4061
Additivity group thermodns 4047
Addn hydrogen hydroxyl benzene benzoate 1186
Addn isoprene tetracyanoethylene enthalpy 1734
Addn reactions hydrogen olefin 1601
Addn tritium recoil butene 3771
Adenine nickel complexes 799
Adenines PMR 3963
Adiabatic calorimetry reaction kinetics 4029 4039
Adiabatic compressibility polyethylenimine hydration 2362
Admittance electrode reactant adsorption 2209
Adsorbate hydrogenous radiolysis 201
Adsorbed mol entropy 2967
Adsorbed nitric oxide IR 2930
Adsorbed org mols reactions 887
Adsorbent activated carbon 61
Adsorbent alkali chloride 2602
Adsorbent alumina 234
Adsorbent aluminum 1887
Adsorbent molybdenum sulfide 133
Adsorbent silica 201 3322
Adsorption benzene 220
Adsorption carbon dioxide chromia 2790
Adsorption carbon dioxide IR 526
Adsorption carbon monoxide EPR 895
Adsorption chloropentanol mercury 1698
Adsorption chromia 2774
Adsorption cobalt hexaammine carbon 649
Adsorption fibrinogen 2103
Adsorption fibrinogen heparin mica 2107
Adsorption fibrinogen mica 2107
Adsorption gas liq 344
Adsorption isotherm calcn 61
Adsorption macromol 65
Adsorption org gas germanium 2922
Adsorption phenol 1975
Adsorption polymer dispersion stabilization 2094
Adsorption potential theory 3720
Adsorption reactant electrode admittance 2209
Adsorption sulfur dioxide 532 2602
Adsorption water 3322
Adsorption water vapor Vycor fiber 2718
Adsorption xanthate 354
Afterglow nitrogen 1552
Agar gel ion diffusion 1821
Aggregate theory mols 1860
Aggregation arylazonaphthols 1227
Aging lead chromate ppt 350
Air water interface NMR 2694
Alanine alanyl structure 918
Alanines NMR conformations 505
Alanyl alanine structure 918
Albumin soln diffusion 379
Albumin soln ultrasound urea 374
Alc aliph hydroxyl abstraction 1186
Alc aq salt effect 3757
Alc butyl dichloro benzene assocns 2133
Alc ethyl ion mol reaction 3797
Alc propyl radicals polemic 167
Alc propyl radiolysis 20

Alc solvation enthalpy 3598
Alc urea inclusion compds 3489
Alc water glass transition 3379
Alc water ion exchange medium 85
Alcs acidity equil const 2226
Alcs adsorbed IR 234
Alcs adsorption 1887 3720
Alcs atom recoil carbon 2248
Alcs dielec absorption solvent effects 1790
Aliph alc hydroxyl abstraction 1186
Aliph hydrocarbon soly water 363
Aliph ketone photolysis sensitizer 1168
Aliphatic ketone fluorescence decay times 989
Alk earths fluorides soly 2340
Alk earths solvation studies 2325
Alkali chloride adsorbent 2602
Alkali chlorides osmotic coeffs 3723
Alkali fluoroaluminate IR 2609
Alkali formates osmotic coeffs 2319
Alkali halide film adsorbents 2930
Alkali halides heat mixing 1125
Alkali halides nitrates freezing points 2313
Alkali hydrides cohesive energies 1251
Alkali ions acetone solvation 56
Alkali ions ESR 1205
Alkali metal amine solns 286
Alkali metal hydride dimers 984
Alkali metal hydroxide gamma irradn 3030 3031
Alkali metal reactions halomethane 3235
Alkali metal soln amine ESR 843
Alkali metal UV irradn 35
Alkali nitrate glass transition 2306
Alkali perchlorate ion pairs 3290
Alkali tetraalkylammonium halides mixing 2148
Alkane isomers equil distribution 1486
Alkanenitriles cohesive energies 642
Alkanes dibromo dielec relaxation 2616
Alkanes normal intrinsic viscosity 3120
Alkanoate hydroxyl abstraction 1186
Alkanoic acid perfluorodimerization 1330
Alkene zeolite adsorbed ESR 3475
Alkoxy phenyl radical ESR 411
Alkyl iodides polycryst ESR 467
Alkyl isocyanides photochemistry 580
Alkyl pyruvates iodination 150
Alkyl radicals growth decay 472
Alkylammonium bromide solns enthalpy 2330
Alkylammonium salts mol assocn 542
Alkyldifluoroamine dehydrofluorination kinetics 1170
Allene prodn photolysis ethylene 1317
Alumina adsorbent 234
Alumina adsorbents carbon dioxide 526
Alumina supports catalysts 1044
Aluminate fluoro alkali IR 2609
Aluminosilicate cracking catalyst 220
Aluminum adsorbent 1887
Aluminum deficient zeolite IR 2408
Aluminum iodide ethyl ether complex 282
Aluminum oxide halide heat formation 1760
Aluminum suboxide IR 1963
Aluminum trichloride sodium tetrachloroaluminate cond 1260
Amide hydrogen bond NMR 784
Amide rotational barrier 3532
Amides hydrogen bonding NMR 776
Amidinium ion pairing 3550
Amidinium rotational barrier 3532
Amine adamantane radicals EPR 3486
Amine alkali metal solns 286
Amine arom assocn consts 1157
Amine copper complexes absorption EPR 3355
Amine fluorescence quencher 1025
Amine nitrobenzenes complex 3636
Amine nitroso anion radical 2704
Amine soln alkali metal ESR 843
Amines arom photochem oxidn 2737
Amines butyl self assocn 938
Amines complex 3149
Amines ionic equil solvent 90
Amines methyl NMR 932
Amines proton exchange NMR 3190
Amines zwitterions micellar hydrolysis 1763
Amino acid radical ESR 738
Aminoalkanes protolysis kinetics 2400
Aminonaphthalenesulfonic acid protolysis 4056
Ammine chromium photoaquation 3504
Ammine cobalt acetato UV photochemistry 1914
Ammine cobalt carbon hydrolysis 649
Ammine cobalt complex uranium reaction 2117
Ammine ruthenium complex photochemistry 3075
Ammonia calcium phase diagram 399
Ammonia excited fluorescence 769
Ammonia gaseous ion lifetimes 444
Ammonia nitric oxide reactions 875
Ammonia radiolysis 2087
Ammonia radiolysis kinetics 2908
Ammonia sodium optical absorption 3635
Ammonium alkyl iodide phase transition 2066
Ammonium bromide tetraalkyl gas salting in 1803
Ammonium ionic radii 2809
Ammonium ions electrons reaction 986
Ammonium methyl nitrogen NMR 1758
Ammonium perchlorate thermolysis 191
Ammonium quaternary micelle solubilization benzene 3905
Ammonium quaternary micelle solubilization polemic 3907
Ammonium quaternary salt micelle 369
Ammonium quaternary thiocyanate soln 3586
Amylose iodine kinetics 272
Aniline cyclohexane viscosity 2619
Anilines complex 3149
Anilines methyl dimerization review 1763
Anion benzene dimer 1177 1178
Anion exchange lead chromate 350
Anion exchange solvent medium 79
Anion liq membrane potential 554
Anion radical benzene 2769
Anion radical thymine irradn 3815
Anion radicals nitro aroms 2591
Anions maleate radicals photoisomerization 482
Anisotropic solvent shifts factor anal 1207
Anodic film iron ellipsometry 2823
Anomalous water prodn 2976
Anthracene dichloro triplet level 845
Anthracene energy transfer perylene 3894
Anthracene pyromellitic dianhydride complexes 3805
Anthracenes fluorescence quenching 1025
Anthracenesulfonates fluorescence solvent effects 595
Anthraquinone electrochem ESR 3281
Antimonate bromo NQR 1898
Antithrombogenic drugs 2107
AO energy matching 3012
Apatite deficiency 3172
Aq electron absorption spectrum 2798
Aq soln viscosity coeff ion 2532
Aqueous org adsorption isotherm 61
Argon collision oxygen vibration 3185
Argon ionization yields absorption coeffs 719
Argon methane solvents 2345
Argon mixts shock waves 1504
Argon nitrogen afterglow 1552
Argon soly sodium 2832
Argon state equation 3568
Arom amines assocn consts 1157
Arom amines photochem oxidn 2737
Arom amines proton donors 2404
Arom hydrocarbon shock wave ignition 1501
Arom mols sensitized phosphorescence 1921
Arom pyromellitic dianhydride complexes 3805
Arom radical sigma ESR 3432
Arom substitution singlet triplet states 1775
Aroms nitro anion radicals 2591
Arsenic 75 quadrupole relaxation 3880
Arsonium phenyl ions soln 3141
Arsonium phenylboron molal vol 280
Arsoniums NMR 3880
Artifact freezing elimination EPR 1202
Aryl mercury halogenated pyrolysis 3984
Arylazonaphthols dimer structure 1227
Assocn alkylammonium salts 542
Assocn butyl alc cyclohexane 3182
Assocn consts arom amines 1157
Assocn consts ions water 1477
Assocn methanol vapor 1808
Assocn quinolone thermodynamics 1129
Assocn self butyl amines 938
Assocn transition metal polyelectrolyte 1136

Atom alcs recoil carbon 2248
Atom transfer reactions 1844
Atomic interaction energies calcn 1878
Atomic motions solids NMR 3334
Atomic oxygen reaction butene 3902
Atoms hydrogen reactions hydrogen halides 835
Attachment electron sulfur fluoride 3517
Axial coordination vanadyl ion NMR 599
Azide hydrogen dissocn recombination 3026
Azide potassium nuclear reaction 2551
Azo dyes dimer structure 1227
Azobenzene electrochem ESR 3281
Azobenzenes dipolar absorption spectra 581
Azoxybenzene alkoxy relaxation 3834
Band overlap spectral analysis 3635
Barium effect ionosphere 1412
Barium strontium exchange vermiculite 2484
Base pairing energy detn 3963
Basicity series solvents 3606
Basicity titanium dioxide surface 1221
Benzene acetylenic compds complex 2128
Benzene anion radical 2769
Benzene benzoate hydrogen hydroxyl addn 1186
Benzene decompn microwave plasma 445
Benzene dichloro butyl alc assocns 2133
Benzene dimerization nitromethane 3892
Benzene effect propane irradn 2272
Benzene hydrogen deuterium exchange 3715
Benzene labeled diffusion coeff 1315
Benzene nitrous oxide irradn 3886
Benzene piezooptic coeffs 716
Benzene resonance fluorescence 1572
Benzene shock wave ignition 1501
Benzene soln radiolysis 1177 1178
Benzene solubilization cetyltrimethylammonium bromide 3905
Benzene solubilization micelle polemic 3907
Benzene vapor absorption spectrum 1564
Benzenedisulfonate metal assocn 2649
Benzenes cracking catalyst 220
Benzenes nitroparaffins mixing energy 3728
Benzenesulfonate surfactant 3560
Benzisoxazole carboxylate decarboxylation catalysis 2705
Benzoate benzene hydrogen hydroxyl addn 1186
Benzofuran excimer SCF MO 1794
Benzophenone photoredn 181 187
Benzopinacol photoprodn 181
Benzoquinoline methyl pentane 2690
Benzoquinone rotational barrier 2195
Benzoyl peroxide irradn radical 3426
Benzoyloxy radical ESR 3426
Benzyl acetate butyl reaction kinetics 590
Benzylglutamate poly DMF system 1446
Biacetyl vibrational spectra 1946
Bianthrone free radical 290
Bicyclononane Debye temp 1073
Bicyclooctane conformation 1073
Bicyclopropyl hexafluoro decompn 2164
Binding state adsorbed mols 227
Biphenyl fluorescence 3097
Biphenyl photoprodn 181
Biphenyls bromination 887
Biphenyls fluoro NMR 421
Bismuth halide melt excess vol 3620
Bisulfate proton equil 2672 2681
Bond dissocn energies bromoform 987
Bond lattice model water 3698
Bonding copper 2 ligand 3828
Bonding MO 3012
Borane adducts kinetics 2711
Boranes mass spectra 3106
Borate phenyl ions soln 3141
Boron chloride chemisorption 3249
Boron chloride nitrobenzene photooxidn 2415
Boron sulfides mass spectra 2410
Boundary turbulent kinetics shock tube 2700
Bounds intrinsic viscosity 72
Bovine serum albumin gadolinium ESR 3164
Bovine serum albumin proton transfer 4012
Bragg diffraction polystyrene latex 1881
Bromide activity coeff 3153
Bromide cetyltrimethylammonium solubilization benzene 3905
Bromide cetyltrimethylammonium solubilization polemic 3907
Bromide copper 2 decompn thermodn 592
Bromide cyclopropyl hot chem 2698
Bromide hydrogen ion predissocn 1472
Bromide hydrogen reaction hydrogen atoms 835
Bromide methyl fluorine 18 reaction 1324
Bromide redn iodate kinetics 2516
Bromide sodium zinc complex 3028
Bromination bromoform bond dissocn energies 987
Bromination nitrobiphenyl silica surfaces 887
Bromine hydrogen flame 3046
Bromine reaction isotope effect 2072
Bromine 80m reaction 2698
Bromo antimonate NQR 1898
Bromo ethanes ethylenes NMR 3766
Bromoform bromination bond dissocn energies 987
Bromomethane tritium reaction 1290
Bubble nucleating hydrocarbon 3613
Butane butenes tritiated 2407
Butane hydrogen tritium exchange 2417
Butane ketene photolysis 2240
Butane propane chloro methylene 2231
Butane radiolysis scavenger effects 2854
Butane tritium reaction 3042
Butanol dielec relaxation 1790
Butanol enthalpy soln alkylammonium bromide 2330
Butanol photoprodn mechanism 3945
Butene reaction atomic oxygen 3902
Butene reaction fast tritium mol 2407
Butene tritium recoil 3771
Butenes isomerization 487
Butenyl radical isomerization 2665
Butyl alc assocn cyclohexane 3182
Butyl alc dichloro benzene assocns 2133
Butyl amines self assocn 938
Butyl cyanides vibrational spectrum 2806
Butyl nitroxide membrane biophys 3417
Butyl peroxide photodecompn 3651
Butyl radical deexcitation polemic 3376
Butyl reaction benzyl acetate kinetics 590
Butylbenzene cracking catalyst 220
Butylium ion benzyl acetate 590
Butyne dichloro benzene complex 2128
Butyrolactone vapor photodecompn 2733
Cacodylate gadolinium ESR 3164
Cadmium hydrated electron scavenger 3626
Cadmium UV irradn 35
Calcium ammonia phase diagram 399
Calcium ethylenediphosphonic acids complexation 676
Calcium ethylenediphosphonic acids complexes 682
Calcium hydroxylapatite catalytic activity 3167
Calcium phosphate gamma irradn 1936
Calcium selective electrode potential 2138
Calcium sodium chloride water system 957
Calorimetry adiabatic reaction kinetics 4029 4039
Calorimetry levitation 3737
Capacitance rutile film 1279
Capillary nos liq film profile 583
Capture electrons Me vinyl ether 476
Carbamate protolysis kinetics 1895
Carbanion NMR 1062
Carbides gadolinium terbium dissocn energies 848
Carbon activated sorbent 3526
Carbon adsorption cobalt hexaammine 649
Carbon atom alcs recoil 2248
Carbon contact hyperfine splitting 3400
Carbon dioxide adsorption chromia 2790
Carbon dioxide adsorption IR 526
Carbon dioxide hydrocarbons solys 2345
Carbon dioxide photolysis 3499
Carbon disulfide matrix isolated spectra 2204
Carbon disulfide oxygen explosion 861
Carbon disulfide photooxidn 854
Carbon monoxide adsorption chromia 2774
Carbon monoxide adsorption EPR 895
Carbon monoxide ionization yields 719
Carbon monoxide ketene butane 2240
Carbon monoxide mixts shock waves 1504
Carbon monoxide nitrous oxide photolysis 3205
Carbon monoxide oxidn catalysis 2065
Carbon monoxide reaction ethylene 340
Carbon monoxide Taft const 2248
Carbon nuclear spin relaxation 2538
Carbon recoil methanol mechanism 2253

Carbon states decompn organics 445
Carbon tetrabromide bond dissocn energy 987
Carbon tetrachloride chloroform diffusivity 3293
Carbon tetrachloride dimerization nitromethane 3892
Carbon tetrachloride ethanol iodine diffusion 963
Carbon tetrachloride phenol mol assocn 3591
Carbon tetrachloride piezooptic coeffs 716
Carbon tetrachloride radiolysis 24
Carbon trioxide IR absorptivity 2991
Carbon 11 recoil reactions 3201
Carbon 13 NMR chloroethane chloroethylene 331
Carbon 13 NMR haloethanes haloethylenes 3766
Carbon 13 nuclear relaxation 3967
Carbon 14 cycloheptatriene 2558
Carbonate propylene water PMR 1477
Carbonyl chromium acceleration reaction 2402
Carbonyl compds distorted hydrogen bonds 1744
Carbonyl compds photolysis ESR 3454
Carbonyl fluoride formation enthalpy 3024
Carboxylates tetrabutylammonium excess thermodns 3733
Carrageenan salt soln cond 1691
Catalysis detergent salt effect 2707
Catalysis iodination 150
Catalysis platinum homogeneous heterogeneous 1175
Catalyst diamond formation 2158
Cation exchange membranes hydrogen transport 654
Cation radical quaterphenyl ESR 902
Cation radicals ESR splitting 2195
Cations locations zeolite 3327
Cations radical hydrazines EPR 2048
CD chlorophyll electronic transition 1440
CD nucleic acid protein 1516
Cell distortion ultracentrifugation 2507
Cerium 4 redn kinetics 250
Cesium ethylenediamine solns 3092
Cesium halide thermionic emission 3741
Cesium oxygen surface reactions 1928
Cetyltrimethylammonium bromide solubilization benzene 3905
Cetyltrimethylammonium bromide solubilization polemic 3907
Chain assocn equil 776 784
Chain isomerization diphenylpropene 292
Chain rupture cryst polymer 3921
Chain scissioning polydimethylsiloxane 2430
Charge distribution lithium hydride 416
Charge transfer complexes vapor phase 1057
Charge transfer ether iodine 3682
Charge transfer iodine iodobenzene 3350
Charge transfer pyromellitic dianhydride 3805
Charge transfer quenching fluorescence 1025
Chem kinetics tunneling correction 1748
Chem laser hydrogen fluoride 3642
Chem lasers hydrogen fluoride 284
Chemical laser hydrogen fluoride 2546
Chemiemission cesium oxygen surface reactions 1928
Chemiluminescence fluorescein dyes 764
Chemiluminescence IR hydrogen halide 2070
Chloramine T oxidn cyanoferrate 2 kinetics 838
Chlorate aq flash photolysis 2177
Chlorate lithium solns 2948
Chloride alkali adsorbent 2602
Chloride calcium sodium water system 957
Chloride hydrogen deuterium exchange 171
Chloride hydrogen fluorescence IR 1622
Chloride methyl fluorine 18 reaction 1324
Chloride nitrosyl nitrogen reaction kinetics 1172
Chloride nitrosyl oxygen reaction 1320
Chloride nitrosyl reaction mass spectra 1320
Chloride oxide aluminum heat formation 1760
Chloride silver ions assocn 2060 3711
Chloride sodium polyacrylate water 3890
Chloride sodium solns elec conductance 1099
Chlorides alkali osmotic coeffs 3723
Chlorides nitrosyl hydrogen reactions 722
Chlorine energetic substitutions orgs 440
Chlorine fluoride thermal decompn 1765
Chlorine fluoride thermolysis kinetics 3939
Chlorine fluorine mixts explosion limits 867
Chlorine hot replacement chlorofluoromethanes 2685
Chlorine quenching hydrogen chloride 1622
Chloro ethane ethylene NMR 331
Chloro ethylene radiation induced oxidn 613
Chloro iron ions dissocn 1113
Chloro sulfonamide oxidn cyanoferrate 2 838
Chloroalkanes cohesive energies 642
Chloroamminechromium photoaquation 3504
Chlorobutane photolysis sensitizer ketone 1168
Chlorocomplex lanthanide heat soln 392
Chlorocyclopentadiene per mol structure 1685
Chlorocyclopropene per structure 1681
Chloroethane methylene 2231
Chloroethylenes radiolytic prodn 24
Chlorofluorescein acid base equil 245
Chlorofluoroethanes radiolysis 2217
Chlorofluoroethylenes cis trans isomerizations 1453
Chlorofluoromethanes hot chlorine replacement 2685
Chloroform carbon tetrachloride diffusivity 3293
Chloroform enthalpy soln alkylammonium bromide 2330
Chloroform radiolysis 2436
Chloromethane tetrafluoroethylene telomerization reactivity 2075
Chloromethane tritium reaction 1290
Chloropentanol electrosorption mercury 1698
Chlorophyll CD electronic transition 1440
Chlorophyll pyro fluorescence quantum yield 1667
Chlorosilanes bond energy terms 2480
Cholesteric smectic transformation 2839
Cholesteryl acetate transformation kinetics 2849
Cholesteryl myristate transformation kinetics 2839
Chrmisorption oxygen chromia 2783
Chromate lead anion exchange 350
Chromatog difference sea water 1418
Chromatog gas liq complexes 2632
Chromatog gas liq induction energies 831
Chromatog gel permeation peak migration 3929
Chromia surface IR 2774 2783 2790
Chromium ammine photoaquation 3504
Chromium carbonyl acceleration reaction 2402
Chymotrypsin acetyltryptophan hydrolysis 1375
Chymotrypsin thermodynamics 1387
Circular dichroism lysine histone 1516
Clathrate hexamethylenetetramine water 3633
Cobalt acetato ammine UV photochemistry 1914
Cobalt acetylacetonate complex bonded radicals 2575
Cobalt ammine complex uranium reaction 2117
Cobalt benzenedisulfonate assocn 2649
Cobalt ethylenediamine system admittance 2209
Cobalt hexaammine carbon adsorption 649
Cobalt hydroxyacetylacetonate bound radical 2580
Cobalt melt thermodns 3737
Cohesive energies alkali hydrides 1251
Cohesive energies alkanenitriles 642
Collectors xanthate 354
Collision deexcitation mol vibrations 1079
Collision helium hydrogen 4001
Collision mol energy transfer polemic 3376
Collisions impact parameters 923
Colloidal dispersion stabilization 65
Colloidal sulfur radiolysis 756
Colloidal suspensions light scattering 789
Color liq sulfur 912
Column compression ultracentrifugation 2507
Complex ammine ruthenium photochemistry 3075
Complex photoaquation ammine chromium 3504
Complex sodium zinc bromide 3028
Complexation ethylenediphosphonic acids calcium 676
Complexation phosphonic acids calcium 682
Complexes ethylenediphosphonic acids calcium 682
Complexes ligand field transitions 692
Complexes phosphonic acids calcium 676
Compressibility adiabatic polyethylenimine hydration 2362
Concn quenching proflavine dye 2727
Concn time integrals kinetic equation 2215
Cond aluminum trichloride sodium tetrachloroaluminate 1260
Cond dielec detn time reflectometry 1323
Cond sat soln 1691
Conductance electrolyte acetone soln 1714
Conductance electrolyte trifluoroethanol 1708
Conductance potassium halide molten acetamide 2687
Conductance squaric acid soln 1798
Conductance tetraalkylammonium halide soln 1722
Conductance tetraamylammonium thiocyanate soln 3586

Configuration tritium exchange dichlorodifluoroethane 1299
Conformation bicyclooctane 1073
Conformation free radicals ESR 3438
Conformation mol trinitrohexahydrotriazine 2056
Conformations alanines valine phenylalanines NMR 505
Conformers fluorescence photoselection 3097
Const cholesteryl methyl dielec 1237
Contact hyperfine splittings 3400
Coordination complexes consts detn 3843
Coordination effects uranium 4 spectra 631
Copper acetate soln ESR 2228
Copper arene interlamellar montmorillonite 3957
Copper benzenedisulfonate assocn 2649
Copper catalyzed deuterium exchange 571
Copper polyamine complexes spectra 3355
Copper scavenge hydrogen yield 601
Copper 2 bromide decompn thermodn 592
Copper 2 ligand bonding 3828
Core line mols virial coeffs 3687 3691
Correlation decay tetraalkylammonium ions 509
Corresponding state alkali nitrate 2306
Corresponding state viscosity 256
Coulombic interaction metal adsorbed mol 2967
Counterion binding site polyelectrolyte 3367
Counterion exchange polyacrylate polyelectrolyte 1985
Counterion sodium counterion 1990
Coupling consts gases silicon fluorides 437
Coupling proton naphthalene ring 3765
Cracking butylbenzene catalyst 220
Crit micelle concn detn 804
Cross sections scattering gases 727
Crotononitrile vibrational spectra 44
Cryobiol glass transition water 967
Crystal field calcns manganese complexes 435
Crystallog nickel oxide 1782
Crystals liq nematic 2452
Crystn polymer review 3909
Cubic systems distorted optical activity 692
Cumyl methyl ether carbanions 1062
Current step ESR 3281
Cyanic acids mass spectrum 1532
Cyanides butyl vibrational spectrum 2806
Cyanoethylene IR vibronic effect 325
Cyanoferrate 2 oxidn chloramine T kinetics 838
Cyanogen hydrogenation 2662
Cyanogen solns radiolysis 608
Cyclic hydrocarbons thermodn 1264
Cyclic voltammetry homogeneous redox equil 2377
Cyclobutane tritium deuterium substitution 3781
Cyclobutene photodecompn 3656
Cycloheptatriene carbon 14 2558
Cycloheptatriene vibrational deexcitation polemic 3376
Cyclohexane aniline viscosity 2619
Cyclohexane butyl alc assocn 3182
Cyclohexanol absorption spectrum 1677
Cyclohexyl radical absorption spectrum 1677
Cyclopentane nitrous oxide irradn 2560
Cyclopentanones INDO MO 2466
Cyclopentene oxygen addn rearrangement 3056
Cyclopentene radical ESR 3475
Cyclopentenes perfluoro perchloro 1685
Cyclopropane bromine 80m reaction 2698
Cyclopropane shock tube isomerization 2526
Cyclopropane vinyl photolysis pyrolysis energy partitioning 1640
Cyclopropanes fluoro cis trans isomerizations 1453
Cyclopropanone decarbonylation 340
Cyclopropene perchloro structure 1681
Cyclopropyl bromide hot chem 2698
Cystine dihydrochloride irradn 3746
Cytosines PMR 3963
DDD radiation induced dichlorination 2762
DDT radiation induced dichlorination 2762
Deactivation vibrationally excited ethane 837
Debye temp bicyclononane 1073
Decanol dielec relaxation 1790
Decarbonylation cyclopropanone 340
Decarboxylation benzisoxazole carboxylate catalysis 2705
Decay growth alkyl radicals 472
Decay perhydroxyl radical isotope effect 2263
Decompn catalytic perchloric acid 491
Decompn hexafluoro bicyclopropyl 2164
Decompn kinetics iron sulfate 1179
Decompn kinetics iron 2 sulfate 1179
Decompn nitrous oxide 1037 1051
Decompn organics carbon states 445
Decompn thermal chlorine fluoride 1765
Decylammonium salt micelle aggregation 369
Deexcitation mol vibrations collision 1079
Defect sodium chloride positron interaction 2030
Degeneracy hidden vibration large mols 1343
Dehydrofluorination kinetics alkyldifluoroamine 1170
Dehydrogenation hydrogen malonate 3426
Denaturants protein 815
Denaturation protein model 3733
Denaturing agent acid base reaction 1120
Dense fluids self diffusion 1970
Density effect coupling consts 437
Density tetraamylammonium thiocyanate soln 3586
Deoxyribonucleate sodium film proflavine 2727
Deprotonation indoles fluorescence 3061
Detergent catalysis salt effect 2707
Detergents crit micelle concn 804
Detergents micelle formation 809
Detergents nonionic micelle structure 547
Deuterated ethane decompn 837
Deuterated methanol vapor pressure 1815
Deuteration arom platinum catalyst 1175
Deuteride alkali cohesive energies 1251
Deuterioethyl bromide irradn 472
Deuterioethyl iodide ESR 467
Deuteriomethyl radical ESR 2448
Deuterium effect electron transfer naphthalene 447
Deuterium exchange copper catalyzed 571
Deuterium exchange hydrogen chloride 171
Deuterium hydride self exchange 2541
Deuterium hydrogen exchange acetylene 4053
Deuterium hydrogen exchange benzene 3715
Deuterium hydrogen exchange hydroquinone 1775
Deuterium hydrogen reaction shock wave 1615
Deuterium isotope effect 2263
Deuterium keto enol equil 433
Deuterium oxide adsorption chromia 2774
Deuterium oxygen mol ion reaction 1426
Deuterium photochem excited reaction ethane 841
Deuterium tritium substitution cyclobutane 3781
Deuteroethylene pyrolysis 1
Dialysis equil polyvinylpyrrolidinone 3135
Diamines ionic equil solvent 90
Diamond crystn 1833 1838
Diamond formation 2158
Diamond synthetic ESR nitrogen 15 2696
Dianins compd heptanol crystals 3566
Diat MO bonding 3012
Diazine oxide iodine complexes 2504
Diazomethane photolysis 2448
Diazomethane propane photolysis system 1537
Dibenzofuran excimer model 1794
Dibromoalkanes dielec relaxation 2616
Dichlorination DDT radiation induced 2762
Dichloro benzene butyl alc assocns 2133
Dichloro dimethylamino phosphine IR 3837
Dichloroanthracene second triplet level 845
Dichlorobutyne benzene complex 2128
Dichlorodifluoroethane configuration tritium exchange 1299
Dielec absorption sulfur dioxide 532
Dielec const cholesteryl methyl ether 1237
Dielec const diol 1240
Dielec const polar mixts 2133
Dielec consts alkylammonium salts 542
Dielec detn time reflectometry cond 1323
Dielec dispersion ion exchange resins 1091
Dielec friction theory 239
Dielec orientational relaxation ion pairs 598
Dielec props emulsions 537
Dielec relaxation butanol decanol 1790
Dielec relaxation dibromoalkanes 2616
Diels Alder reaction thermochemistry 1734
Difference chromatog sea water 1418
Diffraction light polystyrene latex 1881
Diffusion binary electrolytes theory 663
Diffusion coeff labeled benzene 1315
Diffusion hemoglobin albumin soln 379
Diffusion iodine mixed solvents 963
Diffusion ion gel hydration 1821
Diffusion loss radical 2883

Diffusion soln hologram interferometry 3374
Diffusion surface sorbate 133
Diffusion theory 1970
Diffusion transfer 3303
Diffusion transfer theory 3297
Diffusion water uranyl nitrate hexahydrate 1272
Diffusivity carbon tetrachloride chloroform 3293
Difluoroethylene ion prodn 2584
Dihydroxyanthracene rotational barrier 2195
Dihydroxynaphthalene rotational barrier 2195
Diln heats uranyl vanadyl sulfates 2368
Dimerization energy alkali metal hydride 984
Dimerization methyl anilines review 1763
Dimerization nitromethane carbon tetrachloride 3892
Dimerization perfluoroalkanoic acid solvent 1330
Dimerization perylene tetracene 1768
Dimerization trifluoroacetic acid solvent 1327
Dimethyl acetamide pulse radiolysis 2267
Dimethyl formamide pulse radiolysis 2267
Dimethyl sulfoxide amines assocn 1157
Dimethyl sulfoxide soln viscosity 1727
Dimethylamino dichloro phosphine IR 3837
Dimethylpropane surface diffusion 133
Dinaphthofurandiones spectra 3257
Dinitrobenzene photoredn 1667
Diol dielec const 1240
Dioxane adsorption 3720
Dioxane aq solvent 93
Dioxane gaseous UV photolysis 3899
Dioxane water anion exchange medium 79
Dioxide carbon adsorption chromia 2790
Dioxide sulfur liq photooxidn 3631
Dipeptides MO conformation 2286
Diphenylamine electronic spectra 3576
Diphenylpropene chain isomerization 292
Diphenylpropene irradn isomerization 2394
Diphenylpropene photolysis 2079
Dipolar azobenzenes absorption spectra 581
Dipolar contributions carbon 13 relaxations 585
Dipolar relaxation mol assocn 2539
Dipole effects intramol relaxation 2538
Discharge flow systems addn reactions 1601
Disilanes mass spectra 974
Disilazane hexamethyl hydroxyl reaction 2181
Disordered mixed crystal x ray 1246
Dispersion ion exchange resin 1091
Dispersion stabilization 65
Dispersion stabilization adsorption polymer 2094
Dispersions polytetrafluoroethylene 789
Dissocn energies gadolinium terbium dicarbides 848
Dissocn hydrogen bromide ion 1472
Dissocn kinetics acetic acid 2488
Dissocn monochloroiron III ion 1113
Dissocn photoassisted nitrous oxide 617
Dissocn pressures liq salts polemic 721
Dissocn recombination hydrazoic acid 3026
Dissocn squaric acid 1798
Dissoln metals aq electrolytes 2112
Disulfide carbon matrix isolated spectra 2204
Divinylbenzene styrene copolymer 1211
DMF adsorption 3720
DMF oxygen electroredn 4019
DMF polybenzylglutamate system 1446
DMF solvation 3606
DMF solvation lithium ion 3188
Dodecyl sulfate sodium interactions 3135
Dodecyl sulfate surfactant 3560
Dodecylamine hydrochloride aq surface tension 3000
Donor acceptor electron complexes 2632
DOPA deprotonation 2657
Drainage vessel liq film 583
Drop size sea water 3623
Duroquinone radical rotational barrier 2195
Dye proflavine concn quenching 2727
Dyes fluorescein optically excited 764
Dyes sensitization semiconductor electrodes 562
Dynamic adsorption water Vycor 2718
Dynamic method dissocn pressures 721
ECE mechanism nuances 2377
Elasticity thermodns 142
Elastin elasticity 142
Elec cond calcium ammonia 399
Elec conductance sodium chloride solns 1099
Electrode admittance reactant adsorption 2209
Electrode benzene isotope exchange 3715
Electrode ion exchange potential 554
Electrode liq membrane potential 2138
Electrode potential ferrocenes 3381
Electrodes gallium phosphide spectral sensitization 562
Electrodes ion exchange activity coeffs 957
Electrolyte conductance acetone soln 1714
Electrolyte conductance trifluoroethanol 1708
Electrolyte micellar catalysis enhancement 2707
Electrolyte mixed solns thermodn 946
Electrolyte soln dimethyl sulfoxide 1727
Electrolyte soln viscosity coeff 2532
Electrolyte solns 3124
Electrolyte solvation 3606
Electrolytes aq metals dissoln 2112
Electrolytes binary diffusion theory 663
Electrolytes ion pairing 291
Electrolytes relaxation times ion pairs 598
Electrolytic growth prepassive film iron 2823
Electrolytic transport technique 2815
Electron aq absorption spectrum 2798
Electron attachment sulfur fluoride 3517
Electron correlation lithium hydride 416
Electron d phosphoryl oxygen 3309
Electron diffraction gas phase perhalocyclopentenes 1685
Electron donor acceptor complexes 2632
Electron ds phosphoryl fluoride 1360
Electron exchange ferrocene ferricinium 3303
Electron hydrated scavenger 3626
Electron hydrated semicontinuum model 2297
Electron impact decompn ammonia hydrazine 769
Electron irradn polyethylene 3988
Electron irradn thymine 3815
Electron photoinduced trapped 2893
Electron pulse radiolysis methane 1164
Electron radiolysis methane 2405
Electron reactivity 1941
Electron recombination cystine dihydrochloride 3746
Electron solvated ethanol hexane 3639
Electron solvated polemic 3904 3905
Electron solvated theory sodium soln 843
Electron solvation ethylenediamine 3092
Electron spin polarization radical reaction 3410
Electron spin relaxation macromol 3164
Electron transfer ferrocene salts 2025
Electron transfer ferrocenes 3381
Electron transfer kinetics naphthalene ESR 447
Electron transfer semiconductor surfaces 617
Electron trapped concn decay 3221
Electronic absorption perylene tetracene dimers 1768
Electronic spectra amine 3576
Electronic spectra anion radicals 2591
Electronic spectra copper amines 3355
Electronic spectra hydrogen bromide ion 1472
Electronic spectrum oligo phenylenes 318
Electronic spectrum violenes 335
Electronic state rare earth oxide 3103
Electronic transition CD chlorophyll 1440
Electrons ammonium ions reaction 986
Electrons capture Me vinyl ether 476
Electrons hydrated reaction fluorescein dyes 764
Electrons photoinduced trapped solns 2887
Electroosmotic flow polyelectrolyte 1981
Electroredn oxygen DMF 4019
Electrosorption chloropentanol mercury 1698
Electrostriction gases statistical mechanics 771
Electrostriction polyethylenimine 2353 2362
Ellipsometry anodic film iron 2823
Emission absorption spectra carbon 445
Emission carbon disulfide matrix 2204
Emission spectra europium 3668
Emulsions dielec props 537
ENDOR ESR phenoxy radical 2765
Energetic chlorine substitutions orgs 440
Energies activation tetraalkylammonium ions 509
Energies dissocn gadolinium terbium dicarbides 848
Energies induction gas liq chromatog 831
Energy activation temp preequil 2372
Energy eigenvalues computation 1756
Energy intramol relaxation 2164
Energy levels calcns manganese complexes 435
Energy matching AO 3012
Energy partition photodecompn peroxide 3651
Energy partitioning photolysis pyrolysis vinylpyrazoline 1640

Energy transfer anthracene perylene 3894
Energy transfer isocyanide thermal isomerization 2171
Energy transfer mol collision polemic 3376
Energy transfer thermal isomerization 1366
Enthalpy addn isoprene tetracyanoethylene 1734
Enthalpy copper 2 bromide decompn 592
Enthalpy diln hexamethylenetetramine water 3633
Enthalpy formation carbonyl fluoride 3024
Enthalpy hydration lanthanide ion 392
Enthalpy solvation 3606
Enthalpy solvation hydrocarbon 3598
Enthalpy sublimation tungsten compds 112
Enthalpy transfer aq sodium chloride 2229
Enthalpy transfer solute methanol 388
Entropies abs bicyclooctane 1073
Entropy adsorbed mol 2967
Entropy assocn metal polyelectrolyte 1136
Entropy copper 2 bromide decompn 592
Entropy enzymic hydrolysis 1387
Entropy hexamethylenetetramine water 3633
Entropy ionic correlations 946
Entropy mixing polymer soln 1255
Entropy vaporization 166
Entropy vaporization hydrocarbons fluorocarbons 2530
Enzymic hydrolysis entropy 1387
EPR carbon monoxide adsorption 895
EPR cobalt acetylacetonate reaction 2575
EPR copper amines 3355
EPR copper 2 ligand 3828
EPR freezing artifact elimination 1202
EPR hydrophobic solutes 165
EPR pyrrolidino pyrrolino free radicals 3486
EPR radical cations hydrazines 2048
EPR radicals short lived 2957
EPR trapped hydrogen atoms 1936
Equation state argon 3568
Equil const alcs 2226
Equil consts detn 3843
Equil dialysis polyvinylpyrrolidinone 3135
Equil distribution alkane isomers 1486
Equil ion exchange thermodn 1152
Equil keto enol pentanediones 433
Equil rates relations 430
Equiv cond salt soln 1691
Equiv conductance squaric acid soln 1798
Erythrosin reactivity hydrogen electron 3020
ESR adsorbed alkene zeolite 3475
ESR alkoxyphenyl sulfide ether 411
ESR amine radical 738
ESR carbonyl compds photolysis 3454
ESR copper acetate soln 2228
ESR detection radicals polemic 167
ESR deuteriomethyl formaldiminoxy radical 2448
ESR ENDOR phenoxy radical 2765
ESR fluoroiodate radical 3479
ESR fluorosulfate radicals temp 712
ESR formaldazine photolysis 164
ESR free radicals conformation 3438
ESR fumarate irradn 2570
ESR glycolic acid 1648
ESR ion exchange resins 907
ESR ion pair 2769
ESR kinetics hydrogen atom org compds 1654
ESR line shapes 3385
ESR membrane model system 3417
ESR methyl ethyl radical 4064
ESR methyl hydrazine oxidn products 2043
ESR methyl isocyanate 1893
ESR methylenecyclobutanes hydroxyl radicals reactions 714
ESR naphthalene electron transfer kinetics 447
ESR nitro arom radical anions 1205
ESR ozonide formation comment 3030 3031
ESR penicillamine hydrochloride irradn 2564
ESR phosphorus oxytrichloride radical anion 3023
ESR photoionization thymine 626
ESR polycryst alkyl iodides 467
ESR propanol radical comments 1326
ESR quaterphenyl cation radical 902
ESR radical 1186
ESR radical pair irradn 3426
ESR radicals irradiated thiols 2277
ESR radiolysis ethyl iodide 3359
ESR rhodium phenanthroline photolysis 3230
ESR sigma arom radical 3432
ESR silver glass silica 2705 2706
ESR simultaneous electrochem cell 3281
ESR sodium soln THF naphthalene 843
ESR spectra 3383
ESR splitting temp dependence 2195
ESR synthetic diamond nitrogen 15 2696
ESR tetramethylphenylenediamines 431
ESR trapped radicals 201 3466
ESR vitamin A aldehyde 2861
ESR Y zeolites superoxide adsorption 1165
ESR zinc peroxide 3089
Ester hydration pyruvate kinetics 792
Ethane chloro NMR 331
Ethane fluoro thermolysis kinetics 295
Ethane nitrogen fluoride laser 284
Ethane photoelectron induced decompn 2903
Ethane pyrolysis single pulse shock tube 1492
Ethane reaction photochem excited deuterium 841
Ethane vibrationally excited deactivation 837
Ethane yield methane radiolysis 2405
Ethane yield radiolysis methane 1164
Ethanes bromo NMR 3766
Ethanol diphenylpropene irradn isomerization 2394
Ethanol fluoro electrolyte conductance 1708
Ethanol hexane solvated electron 3639
Ethanol hydrocarbons iodine diffusion 963
Ethanol hydroxyl proton exchange 1994
Ethanol pulse radiolysis 3893
Ethanol radiolysis liq 2756
Ethene yield methane radiolysis 2405
Ether alkoxyphenyl ESR 411
Ether cumyl methyl carbanions 1062
Ether diphenylpropene irradn isomerization 2394
Ether ethyl aluminum iodide complex 282
Ether iodine charge transfer 3682
Ether vinyl Me electrons capture 476
Ethyl alc ion mol reaction 3797
Ethyl alc torsion rotation 3993
Ethyl ether aluminum iodide complex 282
Ethyl iodide gamma irradn 472
Ethyl iodide tritiated radiolysis 3359
Ethyl isocyanate ESR 1893
Ethyl methylcarbamate protolysis NMR 1895
Ethyl radical ESR 4064
Ethyl xanthate oxidn 354
Ethylamine mercapto ferricyanide oxidn 2036
Ethylbenzene shock wave ignition 1501
Ethylene chloro NMR 331
Ethylene chloro radiation induced oxidn 613
Ethylene glycol soln tetraalkylammonium halide 1722
Ethylene hydrogenation 208
Ethylene ion prodn 2584
Ethylene maleic acid copolymer complexes 1136
Ethylene oxidn gold catalyst 2914
Ethylene photolysis 1317
Ethylene pyrolysis 1
Ethylene reaction carbon monoxide 340
Ethylene tetracyano IR 325
Ethylene yield radiolysis methane 1164
Ethylenediamine cobalt system admittance 2209
Ethylenediamine solvation electron 3092
Ethylenediamines copper complexes spectra 3355
Ethylenediphosphonic acids calcium complexation 676
Ethylenediphosphonic acids calcium complexes 682
Ethylenes bromo NMR 3766
Ethylenes chlorofluoro cis trans isomerizations 1453
Europium absorption emission spectra 3668
Europium soln fluorescence 3677
Europium spectral transition 3980
Excess vol halide melt 3620
Exchange counterion polyelectrolyte 1981
Exchange deuterium copper catalyzed 571
Exchange resin ion NMR 1211
Exchange self deuterium hydride 2541
Exchanger sodium polystyrene 1990
Excimer model fluorene dibenzofuran 1794
Excimer perylene fluorescence absorption 3894
Excitation barium ionosphere 1412
Excitation cyclobutane tritium substitution 3781
Excitation pyromellitic dianhydride complexes 3805
Excited ammonia hydrazine fluorescence 769
Excited optically fluorescein dyes 764
Excited singlet absorption perylene 3894
Excluded vol effect polymers 1141

Explosion carbon disulfide oxygen 861
Explosion limits chlorine fluorine mixts 867
Extinction coeffs hexafluoroacetone imine 1326
Far uv water ice 1162
Fast flow technique radicals generation 2957
Fast tritium mol reaction butene 2407
Fenton reagents org radical formation 3271
Ferric ion hydrolysis kinetics 929
Ferric oxide dissocn nitrous oxide 617
Ferricinium ferrocene electron exchange 3303
Ferricyanide mercaptoethylamine oxidn 2036
Ferrocene ferricinium electron exchange 3303
Ferrocene salts electron transfer 2025
Ferrocenes electron transfer 3381
Ferrocyanide oxidn chloramine T kinetics 838
Fiber Vycor water vapor adsorption 2718
Fibrinogen adsorption 2103
Fibrinogen heparin adsorption mica 2107
Film alkali halide adsorbents 2930
Film liq vessel drainage 583
Filter hexafluoroacetone imine 1326
Flame hydrogen bromine 3046
Flames fluorine supported 3645
Flash excitation pyromellitic dianhydride 3805
Flash photolysis acetone 1910
Flash photolysis aq chlorate 2177
Flash photolysis dichloroanthracene 845
Flash photolysis fluorescein dyes 764
Flash photolysis nitrogen fluoride 2546
Flotation minerals xanthate collectors 354
Fluids self diffusion 1970
Fluorene excimer model 1794
Fluorescein dyes optically excited 764
Fluoresceins acid base equil 245
Fluorescence absorption perylene excimer 3894
Fluorescence anthracenesulfonates solvent effects 595
Fluorescence benzoquinoline propanol effect 2690
Fluorescence decay times aliphatic ketone 989
Fluorescence europium soln 3668 3677
Fluorescence excited ammonia hydrazine 769
Fluorescence fluorobenzene 3662
Fluorescence fluorotoluene photoyield 3214
Fluorescence indoles 3061
Fluorescence IR hydrogen chloride 1622
Fluorescence photoselection conformers 3097
Fluorescence pyrochlorophyll quantum yield 1667
Fluorescence quenching charge transfer 1025
Fluorescence vibronic level 1572
Fluorescent state fluorescein 245
Fluoride chlorine thermal decompn 1765
Fluoride chlorine thermolysis kinetics 3939
Fluoride hydrogen chem laser 3642
Fluoride hydrogen chem lasers 284
Fluoride hydrogen chemical laser 2546
Fluoride hyrogen org solvents IR 2222
Fluoride lanthanum gas dimer 108
Fluoride lithium vaporization 4049
Fluoride methyl fluorine 18 reaction 1324
Fluoride oxide aluminum heat formation 1760
Fluoride phosphoryl MO calcns 1360
Fluorides fluorides mass spectrometry 1461
Fluorides metals soly 2340
Fluorides silicon coupling consts gases 437
Fluorinated ethane thermolysis 3195
Fluorine chlorine mixts explosion limits 867
Fluorine NMR acylated polyethylenimine 4061
Fluorine reaction refractory solid 308
Fluorine supported flames 3645
Fluorine 18 hydrogen abstraction 2709
Fluorine 18 methyl halide reaction 1324
Fluoro biphenyls NMR 421
Fluoro octyl glycol ethers 547
Fluoroacetone imine extinction coeffs 1326
Fluoroacetone photolysis mercury effect 439
Fluoroalkanoic acid dimerization solvent 1330
Fluoroaluminate alkali IR 2609
Fluorobenzene excited state quenching 3662
Fluorobenzene photophysical processes 1233
Fluorocarbon hydrocarbon virial coeff 3863
Fluorocarbons entropy vaporization 2530
Fluorocarbons neg ions reactions 2534
Fluorochloroethanes gamma radiolysis 2217
Fluorochloromethanes solns radiochemistry 455
Fluorocyclopentene per mol structure 1685
Fluorocyclopropanes cis trans isomerizations 1453
Fluoroethane thermolysis shock induced 295
Fluoroethanol electrolyte conductance 1708
Fluoroethylene methylene equils 1625
Fluoroethylenes ion prodn 2584
Fluoroform NMR solvent effect 497
Fluoroiodate radical ESR 3479
Fluoromethane tritium reaction 1290
Fluoromethyl addn acetone mass spectra 735
Fluoromethyl radical matrix IR 3235
Fluorosilane reaction tritium 301
Fluorosulfate radicals ESR temp 712
Fluorotoluene photoyield fluorescence 3214
Formaldazine photolysis ESR 164
Formaldiminoxy radical ESR 2448
Formamide dimer MO 1744
Formamide inversion vibration 405
Formamide pulse radiolysis 2267
Formate catalysis iodination 150
Formates alkali osmotic coeffs 2319
Formation heat aluminum oxide halide 1760
Formation heat nitroarom 4047
Fragmentation ionic quasiequil theory 1526
Free radical bianthrone 290
Free radicals conformation ESR 3438
Free radicals pyrrolidino pyrrolino EPR 3486
Freezing artifact elimination EPR 1202
Freezing depression detn methylacetamide 2879
Freezing depression polymethacrylate 2623
Freezing points alkali halides nitrates 2313
Freezing points tetraalkylammonium halides 2319
Friction dielec theory 239
Fuel cell isotope exchange 3715
Fumarate irradn ESR 2570
Fumarate radical anions prodn 482
Fumarate radical ion 2570
Furan dibenzo excimer SCF MO 1794
Furanquinones spectra 3257
Gadolinium complexes ESR 3164
Gadolinium dicarbide dissocn energy 848
Gallium oxide IR 3908
Gallium phosphide electrodes spectral sensitization 562
Gallium suboxide IR 1963
Gamma irradn calcium phosphate 1936
Gamma irradn Et iodide 467
Gamma irradn sulfur dioxide oxidn 3631
Gamma radiolysis fluorochloroethanes 2217
Gammas irradn ethyl iodides 472
Gammas irradn maleate radical anions 482
Gas adsorption liq 344
Gas liq chromatog induction energies 831
Gas liq interface soly 3870
Gas org adsorption germanium 2922
Gas phase autophobicity 1887
Gas phase electron diffraction perhalocyclopentenes 1685
Gas pressure melt viscosity 103
Gaseous ammonia ion lifetimes 444
Gases coupling consts 437
Gases electrostriction statistical mechanics 771
Gases nonpolar soly molten salts 821
Gases scattering cross sections 727
Gel hydration ion diffusion 1821
Gel permeation chromatog peak migration 3929
Gelatin proton transfer 4012
Germanes torsion rotation 3993
Germanium org gas adsorption 2922
Germanium telluride vaporization thermogravimetry 118
Glass membranes ion exchange 2815
Glass polymn vinyl monomers 3897
Glass surface silver ESR 2705 2706
Glass surface trapped radical 4064
Glass transition alkali nitrate 2306
Glass transition amorphous water 967
Glass transition mol liqs 1826
Glass transition water alc 3379
Glasses methyltetrahydrofuran 482
Globulin soln ultrasound urea 374
Glycerol water glass transition 967
Glycine soln ultrasound urea 374
Glycol ethers micellization NMR 547
Glycol water glass transition 967
Glycolic acid radiation chemistry 1648

Gold holmium dissocn energy 3264
Gold reaction oxygen hydrogen 2136
Gradient temp effect calorimetry 4029 4039
Graphite ground IR 1149
Ground graphite IR 1149
Group additivity thermodns 4047
Group III zeolite superoxide adsorption 1165
Growth decay alkyl radicals 472
Growth prepassive film iron 2823
Guanides PMR 3963
Guanidinium ion water proton exchange 688
Gum arabic salt soln cond 1691
Halide alkali film adsorbents 2930
Halide alkali heat mixing 1125
Halide cesium thermionic emission 3741
Halide hydrogen abstraction elimination 2070
Halide hydrogen vibrations 1079
Halide ion interactions NQR 2936
Halide magnesium potassium melt structure 155
Halide melt excess vol 3620
Halide oxide aluminum heat formation 1760
Halide potassium conductance molten acetamide 2687
Halide soln radiolysis 3081
Halide tetraalkylammonium soln conductance 1722
Halides alkali tetraalkylammonium mixing 2148
Halides hydrogen reactions hydrogen atoms 835
Halides nitrates alkali freezing points 2313
Halides tetraalkylammonium freezing points 2319
Halides tin titanium IR 637
Haloethylenes cyclopropanes isomerizations 1453
Halogen transfer reactions 1844
Halogenated aryl mercury pyrolysis 3984
Halomethae tritium reaction 1290
Halomethane fluorine flame 3645
Halomethanes nuclear relaxation 3967
Hard intermol function 3568
Harned coeffs calcium chloride 957
Heat assocn metal polyelectrolyte 1136
Heat capacity water adsorbed 3322
Heat diln alkali halide 3317
Heat formation aluminum oxide halide 1760
Heat formation nitroarom 4047
Heat formation tungsten compds 112
Heat mixing aq electrolytes 1125
Heat soln hexamethylenetetramine water 3633
Heat soln lanthanide chlorocomplex 392
Heat soln ureas quanidinum chloride 815
Heating glass transition temp 3379
Helium hydride superexchange model 1874
Helium hydrogen collision 4001
Helium nitrogen afterglow 1552
Helium soly sodium 2832
Hemoglobin proton transfer 4012
Hemoglobin soln diffusion 379
Heparin fibrinogen adsorption mica 2107
Heparin fibrinogen mica 2107
Heptane solid NMR 3901
Heptanol Dianins compd crystals 3566
Heterogeneous homogeneous platinum catalysis 1175
Hexabromoantimonate nuclear quadrupole resonance 1898
Hexaethylene glycol ethers 547
Hexafluoro bicyclopropyl decompn 2164
Hexafluoroacetone imine extinction coeffs 1326
Hexahydrate uranyl nitrate water diffusion 1272
Hexamethyldisilazane silica hydroxyl reaction 2181
Hexamethylenetetramine water heat soln 3633
Hexamethylphosphorotriamide amines assocn 1157
Hexane ethanol solvated electron 3639
Hexane ketone vapor liq equil 4041
Hidden degeneracy vibration large mols 1343
Hindered rotation thiuram disulfide 1067
Histone lysine circular dichroism 1516
Hole cystine dihydrochloride crystal 3746
Hole defect synthetic diamond 2696
Holmium mol dissocn energy 3264
Hologram interferometry diffusion soln 3374
Homoconjugation consts acids 2496
Homogeneous heterogeneous platinum catalysis 1175
Homogeneous reaction soly 2969
Homogeneous redox equil cyclic voltammetry 2377
Hot atom reaction 3042
Hot atom reaction fluorine 18 1324
Hot atom tritium reaction 1290
Hot chem cyclopropyl bromide 2698
Hot chlorine replacement chlorofluoromethanes 2685
Hot methyl radicals methylene 2536
Hydrated electron scavenger 3626
Hydrated electron semicontinuum model 2297
Hydrated electrons reaction fluorescein dyes 764
Hydration enthalpy lanthanide ion 392
Hydration gel ion diffusion 1821
Hydration polyethylenimine adiabatic compressibility 2362
Hydration polyethylenimine molar vol 2353
Hydration pyruvate ester kinetics 792
Hydrazine based solns 1826
Hydrazine excited fluorescence 769
Hydrazine methyl oxidn products ESR 2043
Hydrazines radical cations EPR 2048
Hydrazobenzene photoredn dinitrobenzene 1667
Hydrazoic acid dissocn recombination 3026
Hydride alkali cohesive energies 1251
Hydride alkali metal dimers 984
Hydride deuterium self exchange 2541
Hydride helium superexchange model 1874
Hydride lithium charge distribution 416
Hydride titanium wide line NMR 3334
Hydrobromide polyethylenimine hydration 2353 2362
Hydrocarbon aliph soly water 363
Hydrocarbon arom shock wave ignition 1501
Hydrocarbon bubble nucleating 3613
Hydrocarbon fluorocarbon virial coeff 3863
Hydrocarbon nitrous oxide radiolysis 3178
Hydrocarbon pyrolysis single pulse shock tube 1492
Hydrocarbon solvation enthalpy 3598
Hydrocarbons adsorbed radiolysis 201
Hydrocarbons carbon dioxide solys 2345
Hydrocarbons cyclic thermodn 1264
Hydrocarbons effect surface tension 3000
Hydrocarbons entropy vaporization 2530
Hydrocarbons ethanol iodine diffusion 963
Hydrocarbons fluorescence quenching 1025
Hydrochlorides methylamine NMR 1758
Hydrogen abstraction fluorine 18 2709
Hydrogen abstraction polar effects 603
Hydrogen adsorbed binding state 227
Hydrogen atom concns mass spectrometry 722
Hydrogen atom effect radiolysis 31
Hydrogen atom org compds kinetics ESR 1654
Hydrogen atom photolytic prodn 40
Hydrogen atom reaction nitric acid 3193
Hydrogen atoms kinetics aq solns 449
Hydrogen atoms olefin reactions 1584
Hydrogen atoms trapped EPR 1936
Hydrogen azide dissocn recombination 3026
Hydrogen bond amide NMR 784
Hydrogen bond Meisenheimer complex 3636
Hydrogen bonding amides NMR 776
Hydrogen bonding effect 3547
Hydrogen bonding intermol 3313
Hydrogen bonding naphthylamines pi bases 2404
Hydrogen bonding phenols IR 2219
Hydrogen bonding propanol benzoquinoline 2690
Hydrogen bonds distorted carbonyl compds 1744
Hydrogen bromide ion predissocn 1472
Hydrogen bromine flame 3046
Hydrogen chloride deuterium exchange 171
Hydrogen chloride fluorescence IR 1622
Hydrogen contact hyperfne splitting 3400
Hydrogen deuterium exchange acetylene 4053
Hydrogen deuterium exchange benzene 3715
Hydrogen deuterium exchange hydroquinone 1775
Hydrogen deuterium reaction shock wave 1615
Hydrogen effect carbon monoxide oxidn 2065
Hydrogen fluoride chem laser 3642
Hydrogen fluoride chem lasers 284
Hydrogen fluoride chemical laser 2546
Hydrogen halide abstraction elimination 2070
Hydrogen halides reactions hydrogen atoms 835
Hydrogen halides vibrations 1079
Hydrogen helium collision 4001
Hydrogen hydrated electron scavenger 3626
Hydrogen hydroxyl addn benzene benzoate 1186
Hydrogen ionization yields absorption coeffs 719
Hydrogen ions transport noise spectra 654
Hydrogen isotopes excited reaction ethane 841
Hydrogen migration isomerization 2665

Hydrogen mixts shock waves 1504
Hydrogen mol yield scavenge 601
Hydrogen olefin addn reactions 1601
Hydrogen oxygen mol ion reaction 1426
Hydrogen peroxide acetone adduct 3004
Hydrogen peroxide hydrogen yield 3950
Hydrogen peroxide oxidn kinetics 250
Hydrogen peroxide photolytic prodn 40
Hydrogen peroxide prodn oxidant 3343
Hydrogen radiolytic prodn 201
Hydrogen reaction silver gold 2186
Hydrogen transfer reaction tunneling correction 1748
Hydrogen transfer reactions 1844
Hydrogen tritium exchange butane 2417
Hydrogen vibrational energy 1756
Hydrogenation acetylene palladium surfaces 880
Hydrogenation cyanogen 2662
Hydrogenation ethylene 208
Hydrogenous adsorbate radiolysis 201
Hydrolysis chymotrypsin acetyltryptophan 1375
Hydrolysis cobalt ammine carbon 649
Hydrolysis enzymic entropy 1387
Hydrolysis kinetics ferric ion 929
Hydrolysis micellar amines zwitterions 1763
Hydrolysis nitrophenyl laurate 2001
Hydroperoxide cobalt acetylacetonate reaction 2575
Hydrophobic solutes EPR 165
Hydroquinone hydrogen deuterium exchange 1775
Hydroquinone radical rotational barrier 2195
Hydroxide alkali metal gamma irradn 3030 3031
Hydroxide ion radiation yield 1759
Hydroxide ionic radii 2809
Hydroxide nickel oxidn 1782
Hydroxide sodium doped alumina 234
Hydroxy hydroperoxy propane prepn 3004
Hydroxyacetylacetonate cobalt bound radical 2580
Hydroxyapatite deficiency 3172
Hydroxyl abstraction aliph alc 1186
Hydroxyl group ESR splitting 2195
Hydroxyl group internal silica surface 3147
Hydroxyl induction times shock waves 1504
Hydroxyl proton exchange ethanol 1994
Hydroxyl radical olefin 3640
Hydroxyl radical photolytic prodn 40
Hydroxyl radicals methylenecyclobutanes reactions ESR 714
Hydroxyl silica hexamethyldisilazane reaction 2181
Hydroxyl surface titanium dioxide 1216
Hydroxylapatite calcium catalytic activity 3167
Hydroxymethyl acetic acids ionization 826
Hyperfine splitting metal 2769
Hyperfine splittings contact 3400
Hypophosphorus acid oxidn 891
Hyrogen fluoride org solvents IR 2222
Hyrogen peroxide transfer sodium chloride 2229
Ice photolysis 40
Ice water far uv 1162
Ignition arom hydrocarbon shock wave 1501
Illuminated surfaces dissocn nitrous oxide 617
Imine hexafluoroacetone extinction coeffs 1326
Impact electron decompn ammonia hydrazine 769
Inclusion compds alc urea 3489
Indium oxide IR 3908
Indium suboxide IR 1963
INDO MO cyclopentanones 2466
Indoles fluorescence 3061
Induction energies gas liq chromatog 831
Induction period thermolysis 191
Interaction energy 1878
Interactions halide ion NQR 2936
Intercolation compd 3566
Interface gas liq soly 3870
Interface macromol impenetrable 65
Interfacial props water 3870
Interferometry hologram diffusion soln 3374
Interlamellar copper arene montmorillonite 3957
Intermol function division 3568
Intramol dipole effects relaxation 2538
Intramol energy relaxation 2164
Intrinsic viscosity bounds 72
Intrinsic viscosity polyelectrolyte solns 442
Inversion nitrogen amines NMR 3190
Iodate redn kinetics 2516
Iodide alkylammonium phase transition 2066
Iodide aluminum ethyl ether complex 282
Iodide ethyl gamma irradn 472
Iodide hydrogen reaction hydrogen atoms 835
Iodide methyl fluorine 18 reaction 1324
Iodides alkyl polycryst ESR 467
Iodination alkyl pyruvates 150
Iodine amylose kinetics 272
Iodine band blue shifted 1057
Iodine diazine oxide complexes 2504
Iodine diffusion mixed solvents 963
Iodine ether charge transfer 3682
Iodine iodobenzene photoexchange 3350
Iodine radiolysis pentene 2880
Iodine 129 Moessbauer spectrum 2867
Iodobenzene iodine photoexchange 3350
Iodomethane tritium reaction 1290
Ion butylium benzyl acetate 590
Ion decompn fragments energy 2458
Ion diffusion gel hydration 1821
Ion exchange electrode potential 554
Ion exchange electrodes activity coeffs 957
Ion exchange equil thermodn 1152
Ion exchange glass membranes 2815
Ion exchange kinetics vermiculite 2484
Ion exchange mechanism 3750
Ion exchange membrane transport 3015
Ion exchange resin dispersion 1091
Ion exchange resin magnetic moment 2981
Ion exchange resin NMR 1211
Ion exchange resins ESR 907
Ion exchanger selectivity 85
Ion exchanger zeolite 2523
Ion fragmentation dimethylthiocarbamate 1903
Ion lifetimes gaseous ammonia 444
Ion mobility dielec friction 239
Ion mol reaction ethyl alc 3797
Ion mol reactions methylsilanes 13
Ion pair ESR 2769
Ion pair formation diffusion 663
Ion pairing amidinium 3550
Ion pairing effects PMR 3880
Ion pairing electrolytes 291
Ion pairs alkali perchlorate 3290
Ion pairs relaxation times correlation 598
Ionic entropy correlations 946
Ionic equil solvent compn 90
Ionic fragmentation quasiequil theory 1526
Ionic partial vol calcn polemic 3031 3035
Ionic radii scaled particle theory 2809
Ionic soln model theory 3790
Ionic solvation spectra 56
Ionic transport glass membranes 2815
Ionization aluminum trichloride sodium tetrachloroaluminate 1260
Ionization barium ionosphere 1412
Ionization chem kinetics tert butyl 590
Ionization hydroxymethyl acetic acids 826
Ionization potential lanthanide plutonium 392
Ionization sodium chloride 1099
Ionization trichloroacetic acid soln 2492
Ionization yields gaseous mols 719
Ionosphere barium effect 1412
Ions mols quantum states 981
Ions neg fluorocarbons reactions 2534
Ions silver chloride assocn 3711
Ions tetraalkylammonium PMR 509
Ions water assocn consts 1477
IR absorption org liqs 2942
IR absorptivity carbon trioxide 2991
IR acetone lithium interaction 3581
IR adsorbed alcs 234
IR adsorbed nitric oxide 2930
IR alkali fluoroaluminate 2609
IR aluminum deficient zeolite 2408
IR aluminum suboxide 1963
IR butyl cyanides 2806
IR carbon dioxide adsorption 526
IR chemiluminescence hydrogen halide 2070
IR chromia surface 2774 2783 2790
IR crotononitrile 44
IR dimethylamino dichloro phosphine 3837
IR fluorescence hydrogen chloride 1622
IR formamide 405

IR gallium indium oxide 3908
IR ground graphite 1149
IR hyrogen fluoride org solvents 2222
IR ionic solvation 56
IR lithium ion DMF 3188
IR matrix fluoromethyl radical 3235
IR phenols hydrogen bonding 2219
IR silica boron chloride 3249
IR tetracyanoethylene vibronic effect 325
IR tin titanium halides complexes 637
IR titanium dioxide matrix 3243
IR titanium dioxide surface 1221
IR uranium oxide 2283
Iron anodic film ellipsometry 2823
Iron chloro ions dissocn 1113
Iron dissoln aq electrolytes 2112
Iron ions hydrolysis 929
Iron phenanthrolene complexes oxidn 1107
Iron 2 sulfate decompn kinetics 1179
Iron 3 oxalate photochem 2897
Iron 3 oxalato 2986
Irradiated polymethacrylate radical 2443
Irradn aq solns yields 3950
Irradn benzene nitrous oxide 3886
Irradn cystine dihydrochloride 3746
Irradn electron polyethylene 3988
Irradn electron thymine 3815
Irradn fluorochloromethanes solns 455
Irradn gamma Et iodide 467
Irradn gammas ethyl iodides 472
Irradn glycolic acid 1648
Irradn hydrated electron scavenger 3626
Irradn hydrocarbon nitrous oxide 3178
Irradn isomerization diphenylpropene 2394
Irradn liq amides 2267
Irradn nitrous oxide cyclopentane 2560
Irradn octamethyltrisiloxane chain scission 2430
Irradn pentane methyl luminescence 3221
Irradn propane benzene effect 2272
Irradn radical pair ESR 3426
Irreversible redn complexes polarog 2640
Isobutyl methyl ketone effect 2496
Isocyanatoalkyl radical ESR 1893
Isocyanic acid mass spectrum 1532
Isocyanide isomerization 3037
Isocyanide methyl NMR 932
Isocyanide thermal isomerization 1366
Isocyanide thermal isomerization energy transfer 2171
Isocyanides photochemistry 580
Isomerization butenyl radical 2665
Isomerization chain diphenylpropene 292
Isomerization cyclopropane shock tube 2526
Isomerization diphenylpropene irradn 2394
Isomerization dipolar azobenzenes 581
Isomerization isocyanide 3037
Isomerization isocyanides photolysis 580
Isomerization pentyl radical 1632
Isomerization thermal isocyanide 1366
Isomerization thermal isocyanide energy transfer 2171
Isomerizations cis trans thermodn 1453
Isoprene addn tetracyanoethylene enthalpy 1734
Isopropanol enthalpy soln alkylammonium bromide 2330
Isopropyl alcohol radiolysis 1759
Isopropyl methylphosphonates titanium tin halides complexes 637
Isoquinoline singlet triplet crossing 2083
Isotope effect benzene diffusion rate 1315
Isotope effect bromine reaction 2072
Isotope effect concn 160
Isotope effect deuterium 2263
Isotope effect electron transfer 447
Isotope effect methanol solvent 388
Isotope effects ammonia nitric oxide 875
Isotope effects tritium methane 1283
Isotope effects vapor presure methanol 1815
Isotope exchange zeolite 3846
Isotope exchange zeolites 3855
Isotope replacement acetylene hydrogenation 880
Isotropic liq cholesteric transformation 2839
Ketene butane photolysis 2240
Keto enol equil pentanediones 433
Ketone aliphatic fluorescence decay times 989
Ketone hexane vapor liq equil 4041
Ketone methyl isobutyl effect 2496
Ketone sensitizer chlorobutane photolysis 1168
Kinetic equation soln 2215
Kinetic studies tubular flow reactors 1593
Kinetics alkyldifluoroamine dehydrofluorination 1170
Kinetics aminoalkanes protolysis 2400
Kinetics carbon recoil methanol 2253
Kinetics chem tunneling correction 1748
Kinetics chlorine fluoride decompn 1765
Kinetics cyanogen reactions 608
Kinetics decompn iron sulfate 1179
Kinetics dissocn acetic acid 2488
Kinetics dissocn monochloroiron III ion 1113
Kinetics enzymic hydrolysis 1375
Kinetics ethane pyrolysis 1492
Kinetics first order reactions 430
Kinetics hydrogen atom org compds ESR 1654
Kinetics hydrogen atoms aq solns 449
Kinetics hydrolysis ferric ion 929
Kinetics ion exchange vermiculite 2484
Kinetics nitrogen nitrosyl chloride reaction 1172
Kinetics numerical quadrature methods 1610
Kinetics oxalates pulse radiolysis 749
Kinetics photochemistry solid layer 588
Kinetics propanol radical comments 1326
Kinetics protolysis carbamate 1895
Kinetics pyruvate ester hydration 792
Kinetics rate const evaln 1319
Kinetics redn iodate 2516
Kinetics transformation cholesteryl acetate 2849
Kinetics transformation cholesteryl myristate 2839
Kinetics trimethylcyclobutane thermolysis 1437
Kinetics turbulent boundary shock tube 2700
Labeling tritium recoil butene 3771
Laminar boundary kinetic shock tube 2700
Lanthanide ion hydration enthalpy 392
Lanthanum fluoride gas dimer 108
Laser chem hydrogen fluoride 3642
Laser chemical hydrogen fluoride 2546
Laser photolysis perylene soln 3894
Laser produced oxygen silica 2412
Laser Raman spectroscopy 2948
Lasers chem hydrogen fluoride 284
Lasers induced reactions oxygen thiacyclobutane 725
Latex polystyrene light diffraction 1881
Laurate nitrophenyl hydrolysis 2001
Layer solid photochemistry kinetics 588
Lead chromate anion exchange 350
Lead telluride vaporization thermogravimetry 118
Lead vapor oxidn rate 2259
Level second triplet dichloroanthracene 845
Levitation calorimetry 3737
Lifetime sol sphere diffusion 2969
Lifetime spectra positron sodium chloride 2030
Lifetimes ions gaseous ammonia 444
Ligand copper 2 bonding 3828
Ligand field calcns manganese compds 435
Ligand field radical reactions 2575
Ligand field transitions optical activity 692
Light diffraction polystyrene latex 1881
Light scattering colloidal suspensions 789
Linde A zeolite 85
Line core mols virial coeffs 3687 3691
Line shape NMR heptane 3901
Line shapes ESR 3385
Lipid spin label biophys 3417
Liq adsorption gas 344
Liq anion membrane potential 554
Liq assocn shifts NMR amines 932
Liq crystal isotropic phase equil 1446
Liq crystal NMR relaxation 3834
Liq crystal solvents thermodn 2005
Liq crystals nematic 2452
Liq film vessel drainage 583
Liq membrane electrode potential 2138
Liq mixts viscosity 3113
Liq salts dissocn pressures polemic 721
Liq structure viscosity 98
Liq sulfur dioxide photooxidn 3631
Liq vapor equil ketone hexane 4041
Liq vapor exchange water 2694
Lithium acetone interaction 3581
Lithium chlorate solns 2948

Lithium fluoride vaporization 4049
Lithium halide diln heat 3317
Lithium hydride charge distribution 416
Lithium hydride dimer vibrational frequencies 984
Lithium ion acetone solvation 56
Lithium ion solvation DMF 3188
Luminescence irradn methyl pentane 3221
Luminescence photo lifetime detn 2463
Luminescence recombination 2887
Lysine histone circular dichroism 1516
Lysozyme soln ultrasound urea 374
Macromol adsorption 65
Macromol electron spin relaxation 3164
Macroreticular ion exchange resin 1211
Magnesium benzenedisulfonate assocn 2649
Magnesium potassium halide melt structure 155
Magnesium stearate emulsifiers 537
Magnesium UV irradn 35
Magnetic field vs pH 2830
Magnetic moment ion exchange resin 2981
Magnetic props nickel oxide 1044
Magnetic susceptibility prediction 3160
Maleate radical anions photoisomerization 482
Maleic acid copolymer metal assocn 1136
Malonate potassium hydrogen irradn 3426
Manganese benzenedisulfonate assocn 2649
Manganese compds ligand field calcns 435
Mass spectra boranes 3106
Mass spectra boron sulfides 2410
Mass spectra disilanes 974
Mass spectra fluoromethyl addn acetone 735
Mass spectra nitrogen nitrosyl chloride 1172
Mass spectra nitrosyl chloride reaction 1320
Mass spectrometry chlorine fluoride 1765
Mass spectrometry hydrogen atom concns 722
Mass spectrometry xenon fluorides 1461
Mass spectrum isocyanic acid 1532
Matrix IR fluoromethyl radical 3235
Matrix rank treatment spectrophotometry 2954
Matrix spectra titanium oxide 3243
Mechanism platinum catalysis 1175
Mechanism recoil carbon alcs 2248
Meisenheimer complex hydrogen bond 3636
Melt halide excess vol 3620
Melt structure magnesium potassium halide 155
Melt viscosity gas pressure 103
Melts lithium chlorate 2948
Membrane biophys spin label 3417
Membrane ion exchange transport 3015
Membrane liq anion potential 554
Membrane liq electrode potential 2138
Membranes cation exchange hydrogen transport 654
Membranes glass ion exchange 2815
Mercaptoethylamine ferricyanide oxidn 2036
Mercury chloropentanol electrosorption 1698
Mercury effect fluoroacetone photolysis 439
Mercury halogenated aryl pyrolysis 3984
Mercury liq adsorption xenon 344
Metal adsorbed mol Coulombic interaction 2967
Metal assocn ethylene copolymer 1136
Metal benzenedisulfonate assocn 2649
Metal complexes redn mechanism 2640
Metal hyperfine splitting 2769
Metal ion binding DOPA 2657
Metal ions ethanol proton exchange 1994
Metals dissoln aq electrolytes 2112
Metals salts miscibility 2340
Methacrylic acid polymer proton transfer 267
Methane argon solvents 2345
Methane electron radiolysis 2405
Methane nitro dimerization benzene 3892
Methane nitrous oxide photolysis 3205
Methane radiolysis electron pulse 1164
Methane tritium isotope effects 1283
Methanes halo alkali metal reactions 3235
Methanol carbon recoil mechanism 2253
Methanol enthalpy transfer solute 388
Methanol polymer absorption spectra 1808
Methanol soln viscosity coeff ion 2532
Methanol vapor presure isotope effects 1815
Methanol water glass transition 967
Methylacetamide freezing depression 2879
Methyl alc aq solvent 93
Methyl alc solvation 3606
Methyl alc water solvent medium 90
Methyl amines NMR 932
Methyl fluoride bromine reaction 2072
Methyl halide fluorine 18 reaction 1324
Methyl hydrazine oxidn products ESR 2043
Methyl iodide photolysis methylene 2536
Methyl isobutyl ketone effect 2496
Methyl isocyanate ESR 1893
Methyl pentane benzoquinoline 2690
Methyl pentane irradn luminescence 3221
Methyl radical ESR 4064
Methyl radical tetramethylphenylenediamines 431
Methyl sulfoxide complex 3149
Methyl sulfoxide water viscosity 98
Methyl sulfoxides octyl fluoro 547
Methyl trifluoromethyl radicals combination 2225
Methyl uracil optical props 1509
Methyl vinyl ether electron capture 476
Methylamine hydrochlorides NMR 1758
Methylamine vapor pressure 160
Methylbutenyl radical isomerization 2665
Methylcarbamate ethyl protolysis NMR 1895
Methylcyclopropane prodn photolysis ethylene 1317
Methylene chloride axial coordination vanadyl 599
Methylene chloroethane 2231
Methylene photolysis methyl iodide 2536
Methylene reaction rates 1537
Methylenecyclobutanes hydroxyl radicals reactions ESR 714
Methylenecyclopentane hydroxyl radical reactions ESR 714
Methylfluorosilane reaction tritium 301
Methylfluorosilanes 603
Methylpentane matrix metals 35
Methylphosphonates titanium tin halides complexes 637
Methylpropanes surface diffusion 133
Methylpropionamide NMR protolysis 1895
Methylsilanes adsorption 1887
Methylsilanes bond energy terms 2480
Methylsilanes ion mol reactions 13
Methylstyrene carbanions 1062
Methyltetrahydrofuran glasses 482
Methylureas water system 3313
Mica adsorption fibrinogen heparin 2107
Mica heparin fibrinogen 2107
Micellar catalysis electrolyte enhancement 2707
Micellar effects hydrolysis zwitterions 1763
Micellar wt surfactant 2212
Micelle aggregation decylammonium salt 369
Micelle crit concn detn 804
Micelle dodecylamine hydrochloride aq 3000
Micelle formation detergents 809
Micelle hydrolysis nitrophenyl laurate 2001
Micelle quaternary ammonium solubilization benzene 3905
Micelle solubilization benzene polemic 3907
Micelle structure NMR 942
Micelle structure nonionic detergents 547
Micelle surfactant NMR 3560
Micelles phenothazines NMR 3554
Microwave absorption 2602
Microwave plasma decompn org compds 445
Migration hydrogen isomerization 2665
Minerals flotation xanthate collectors 354
Miscibility metals salts 2340
Mixing energy benzenes nitroparaffins 3728
Mixing entropy polymer soln 1255
Mixing halides alkali tetraalkylammonium 2148
MO bonding 3012
MO calcns phosphoryl fluoride 1360
MO conformation peptides 2286
MO formamide dimer 1744
MO INDO cyclopentanones 2466
Moessbauer spectrum iodine 129 2867
Mol assocn alkylammonium salts 542
Mol assocn phenol carbon tetrachloride 3591
Mol assocns dielec const 2133
Mol collision vibrational excitation 3185
Mol conformation trinitrohexahydrotriazine 2056
Mol hydrogen radiolytic yield 31
Mol ion reactions methylsilanes 13
Mol liqs glass transition 1826
Mol structure perfluorocyclopentene perchlorocyclopentadiene 1685

Mol structure radiolysis 20
Mol symmetry vaporization 166
Mol vibrational deexcitation polemic 3376
Mol vibrations deexcitation collision 1079
Mol wt viscosity 256
Molal vol phenylarsonium phenylborate 280
Molar vol polyethylenimine hydration 2353
Mols ions quantum states 981
Mols line core virial coeffs 3687 3691
Mols polar salting out 3757
Molten salt glass membranes 2815
Molten salt ion exchange 2523
Molten salts soly nonpolar gases 821
Molybdenum adsorbed binding state 227
Molybdenum reaction atomic fluorine 308
Molybdenum sulfide adsorbent 133
Monoxide carbon reaction ethylene 340
Montmorillonite copper arene interlamellar 3957
Motions solids detection NMR 3334
Multiple perturbation energies 1549
Murexide nickel formation kinetics 3705
Myristate cholesteryl transformation kinetics 2839
Naphthalene electron transfer kinetics ESR 447
Naphthalene excimer SCF MO 1794
Naphthalene ring proton coupling 3765
Naphthalene sulfonamide protolysis NMR 4056
Naphthalene THF sodium soln ESR 843
Naphthalenesulfonate sodium adsorption 1975
Naphthols arylazo dimer structure 1227
Naphthylamines proton donors aromatics 2404
Neg ions reactions xenon mols 2534
Nematic liq crystal relaxation 3834
Nematic liq crystals 2452
Nematogenic solvents 2005
Neutron activated bromine reaction 2072
Neutron bombardment nitrogen 14 2551
Neutron capture iodine pentene 2880
Newtonian viscosity polymer solns 256
Nickel benzenedisulfonate assocn 2649
Nickel murexide formation kinetics 3705
Nickel oxide adsorbent 1975
Nickel oxide catalysts 1051
Nickel oxide catalysts structure 1044
Nickel oxide crystallog 1782
Nickel purine complexes spectra 799
Nickel thiete phenoxazine phenothiazine 2387
Niobium thermionic emission 3741
Nitrate alkali glass transition 2306
Nitrate ionic radiies 2809
Nitrate melt ion exchange 2523
Nitrate potassium melt viscosity 103
Nitrate silver thallium melt 4025
Nitrate uranyl hexahydrate water diffusion 1272
Nitrates halides alkali freezing points 2313
Nitric acid reaction hydrogen atom 3193
Nitric oxide adsorbed IR 2930
Nitric oxide surface reactions 875
Nitro arom radical anions ESR 1205
Nitro aroms anion radicals 2591
Nitro compds photolysis ESR 3454
Nitroarom formation heat 4047
Nitrobenzene complex photooxidn nitrosobenzene 2415
Nitrobenzene electrochem ESR 3281
Nitrobenzene soln radiolysis 1759
Nitrobenzenes amine complex 3636
Nitrobiphenyl bromination silica surfaces 887
Nitroform structure solvents NMR 499
Nitrogen adsorbed binding state 227
Nitrogen atoms recombination 1552
Nitrogen contg org cations 2936
Nitrogen fluoride chem lasers 284
Nitrogen fluoride laser 2546
Nitrogen inversion amines NMR 3190
Nitrogen ionization yields absorption coeffs 719
Nitrogen nitrosyl chloride reaction kinetics 1172
Nitrogen NMR methyl ammonium 1758
Nitrogen yield radiolysis 3178
Nitrogen 14 neutron bombardment 2551
Nitrogen 15 synthetic diamond ESR 2696
Nitromethane dimerization carbon tetrachloride 3892
Nitromethane scavanger photolysis acetone 851
Nitroparaffins benzenes mixing energy 3728
Nitrophenyl laurate hydrolysis 2001
Nitropropane pyrolysis 2427
Nitroso amine anion radical 2704
Nitroso compds photolysis ESR 3454
Nitrosobenzene photooxidn nitrobenzene complex 2415
Nitrosyl chloride nitrogen reaction kinetics 1172
Nitrosyl chloride reaction mass spectra 1320
Nitrosyl chlorides hydrogen reactions 722
Nitrous oxide benzene irradn 3886
Nitrous oxide cyclopentane irradn 2560
Nitrous oxide decompn 1037 1051
Nitrous oxide photoassisted dissocn 617
Nitrous oxide photodecompn 3205
Nitrous oxide radiolysis 3178
Nitrous oxide reaction 1738
Nitroxide butyl membrane biophys 3417
Nitroxide interaction ESR 3417
Nitroxide method radical spectra 3466
NMR air water interface 2694
NMR alanines valine phenylalanines conformations 505
NMR amidinium ion 3550
NMR amines proton exchange 3190
NMR bromo ethanes ethylenes 3766
NMR carbanions 1062
NMR carbon 13 chloroethane chloroethylene 331
NMR detection motions solids 3334
NMR fluorine acylated polyethylenimine 4061
NMR fluoro biphenyls 421
NMR fluoroform solvent effect 497
NMR hydrogen bond amide 784
NMR hydrogen bonding amides 776
NMR interpretation pattern recognition 1402
NMR ion exchange resin 1211
NMR lithium ion DMF 3188
NMR methyl amines 932
NMR micelle structure 942
NMR micelle structure detergents 547
NMR nitroform structure solvents 499
NMR nitrogen methyl ammonium 1758
NMR phenothazines micelles 3554
NMR phenoxy radical 3462
NMR phosphorus 31 phosphonate 3547
NMR protolysis ethyl methylcarbamate 1895
NMR protolysis naphthalene sulfonamide 4056
NMR proton chem shift 3971
NMR relaxation liq crystal 3834
NMR rotational barrier selenoureas 3372
NMR silicon tetrafluoride coupling consts 437
NMR solid heptane 3901
NMR spin lattice relaxation 2539
NMR surfactant micelle 3560
NMR tin titanium halides complexes 637
NMR urea internal rotation 1901
NMR van der Waals effect 3160
NMR vanadyl ion axial coordination 599
Noise spectra hydrogen ions transport 654
Nonane isomers equil distribution 1486
Nonelectrolyte water system ultrasonic velocity 2336
Nonionic detergents micelle structure 547
Nonpolar gases soly molten salts 821
Nonpolar in salting gases alkylammonium 1803
Nonpolar mols scattering cross section 727
Nonpolar solvent polar solute model 2413
NQR halide ion interactions 2936
Nuclear activation iodine pentene 2880
Nuclear Overhauser effect mol assocn 2539
Nuclear Overhauser effects relaxations 585
Nuclear polarization radical reaction 3410
Nuclear quadrupole resonance hexabromoantimonate 1898
Nuclear reaction potassium azide 2551
Nuclear relaxation carbon 13 3967
Nuclear spin relaxation 2452
Nuclear spin relaxation carbon 2538
Nuclear transformation tellurium compd 2867
Nucleating bubble hydrocarbon 3613
Nucleic acid protein CD 1516
Numerical quadrature methods kinetics 1610
Octamethyltrisiloxane irradn chain scission 2430
Octane isomers equil distribution 1486
Octyl fluoro methyl sulfoxides 547
Olefin effect nitrous oxide irradn 2560
Olefin hydrogen addn reactions 1601
Olefin hydrogen atoms reactions 1584

Olefin hydroxyl radical 3640
Olefine quenching fluorobenzene 3662
Oligo phenylenes electronic spectrum 318
Oligomerization mechanism butyl alc 3182
Onsager transport coeff theory 3124
Optical absorption alkali metal amine 286
Optical absorption radiolysis erythrosin 3020
Optical absorption sodium ammonia 3635
Optical activity distorted cubic systems 692
Optical bleaching luminescence decay 3221
Optical props methyl uracil 1509
Optical props nickel oxide 1044
Optically excited fluorescein dyes 764
Org aq adsorption isotherm 61
Org cations halide ion interactions 2936
Org gas adsorption germanium 2922
Org liqs IR absorption 2942
Org mols reactions adsorbed 887
Org radical formation Fenton reagents 3271
Org solid state 2025
Organics decompn carbon states 445
Organophosphorus compds vibrational spectra 1956
Osmometry polymethacrylic acid 2144
Osmotic coeff hexamethylenetetramine water 3633
Osmotic coeff polyelectrolyte soln 3890
Osmotic coeffs alkali chlorides 3723
Osmotic coeffs alkali formates 2319
Osmotic coeffs mixed electrolytes 1305
Overhauser effect mol assocn 2539
Overhauser effects nuclear relaxations 585
Overlap absorption band analysis 3635
Oxalate iron 3 photochem 2897
Oxalates pulse radiolysis 749
Oxalatoferrate potassium photolysis 2986
Oxalic acid oxidn 3343
Oxalic acid pulse radiolysis 749
Oxidant oxalic acid 3343
Oxide gallium indium IR 3908
Oxide halide aluminum heat formation 1760
Oxide mixt catalyst 220
Oxide nickel catalysts 1051
Oxide nickel crystallog 1782
Oxide nitrous cyclopentane irradn 2560
Oxide nitrous radiolysis 3178
Oxide nitrous reaction 1738
Oxide titanium spectra matrix 3243
Oxide uranium IR 2283
Oxide zinc 3822
Oxide zinc catalyst 491
Oxides carbon decompn microwave plasma 445
Oxides illuminated dissocn nitrous oxide 617
Oxides rare earth spectroscopy 514
Oxidizing radical reactivity 1738
Oxidn carbon monoxide catalysis 2065
Oxidn ethyl xanthate 354
Oxidn hypophosphorus acid vanadium 891
Oxidn iron phenanthrolene complexes 1107
Oxidn mercaptoethylamine ferricyanide 2036
Oxidn methyl hydrazine products ESR 2043
Oxidn oxalic acid 3343
Oxidn photochem arom amines 2737
Oxidn rate lead vapor 2259
Oxidn sulfur dioxide gamma irradn 3631
Oxidn trichloroethylene radiation induced 613
Oxychloride phosphorus radical anion ESR 3023
Oxyethylene ether micellar wt 2212
Oxygen acetylene reaction 2402
Oxygen addn cyclopentene rearrangement 3056
Oxygen atom reaction laser 3642
Oxygen atom reaction nitric acid 3193
Oxygen atomic reaction butene 3902
Oxygen carbon disulfide explosion 861
Oxygen carbon recoil methanol 2253
Oxygen cesium surface reactions 1928
Oxygen chrmisorption chromia 2783
Oxygen deuterated acetylene reaction 4053
Oxygen electroredn DMF 4019
Oxygen ionization yields absorption coeffs 719
Oxygen laser produced silica 2412
Oxygen mixts shock waves 1504
Oxygen mol ion hydrogen reaction 1426
Oxygen nitrosyl chloride reaction 1320
Oxygen phosphoryl charge d 3309
Oxygen quenching fluorobenzene 3662
Oxygen reaction silver gold 2186
Oxygen thiacyclobutane lasers induced reactions 725
Oxygen vibration collision argon 3185
Oxygen 18 methanol vapor pressure 1815
Ozone extinction coeffs 1326
Ozonide formation ESR comment 3030 3031
Pairing ion electrolytes 291
Palladium catalyst carbon monoxide oxidn 2065
Palladium melt thermodns 3737
Palladium surfaces acetylene hydrogenation 880
Partial ionic vol calcn polemic 3031 3035
Particle interaction polymer adsorption 2094
Pattern recognition NMR interpretation 1402
Peak migration gel permeation chromatog 3929
Penicillamine hydrochloride irradn ESR 2564
Pentafluoroethane shock wave pyrolysis 3493
Pentane carbon 11 recoil 3201
Pentane methyl benzoquinoline 2690
Pentane methyl irradn luminescence 3221
Pentanediones keto enol equil 433
Pentanol chloro electrosorption mercury 1698
Pentanone quenching fluorobenzene 3662
Pentene carbon 11 recoil 3201
Pentene iodine radiolysis 2880
Pentyl radical isomerization 1632
Perchlorate alkali ion pairs 3290
Perchlorate ammonium thermolysis 191
Perchloric acid catalytic decompn 491
Perchloric acid soln deuterium exchange 571
Perchlorocyclopropene structure 1681
Perfluoroalkanoic acid dimerization solvent 1330
Perfluorooctanoate sodium NMR 942
Perfluoropropane neg ions 2534
Perhalocyclopentenes gas phase electron diffraction 1685
Perhydroxyl radical decay isotope effect 2263
Permanganate oxidn reactions kinetics 1107
Peroxide acetaldehyde addn mechanism 3377
Peroxide benzoyl irradn radical 3426
Peroxide butyl photodecompn 3651
Peroxide hydrogen oxidn kinetics 250
Peroxide hydrogen photolytic prodn 40
Peroxide zinc ESR 3089
Peroxy tert butyl radical 2580
Peroxycyclohexanol radical 1677
Perturbation energies multiple 1549
Perturbation theory 1878
Perylene dimerization 1768
Perylene excited singlet absorption 3894
PH vs magnetic field 2830
Phase diagram ammonia calcium 399
Phase transition alkylammonium iodide 2066
Phase transition lead chromate 350
Phenanthrolene iron complexes oxidn 1107
Phenanthroline rhodium glass photolysis 3230
Phenol adsorption 1975
Phenol mol assocn carbon tetrachloride 3591
Phenols hydrogen bonding IR 2219
Phenols PMR 1338
Phenothazines micelles NMR 3554
Phenothiazine nickel thiete complexes 2387
Phenoxazine nickel thiete complexes 2387
Phenoxy radical ESR ENDOR 2765
Phenoxy radical NMR 3462
Phenyl alkoxy radical ESR 411
Phenyl isocyanides photochemistry 580
Phenyl radical ESR 3432
Phenyl silicon interaction mass spectra 974
Phenylalanines NMR conformations 505
Phenylarsonium ions soln 3141
Phenylarsonium phenylborate molal vol 280
Phenylborate phenylarsonium molal vol 280
Phenylcarbinols photoprodn 181
Phenylenediamines tetramethyl ESR 431
Phenylenes oligo electronic spectrum 318
Phenylnaphthalene fluorescence 3097
Phenylpropenes chain isomerization 292
Phloroglucinol PMR acetate melt 1338
Phosphate calcium gamma irradn 1936
Phosphate ester NMR 3537
Phosphate glass europium doped 3980
Phosphate zirconium ion exchange 3750
Phosphide gallium electrodes spectral sensitization 562
Phosphine dimethylamino dichloro IR 3837
Phosphite ester NMR 3537

Phospholene oxide NMR 3537
Phosphonate phosphorus 31 NMR 3547
Phosphonates titanium tin halides complexes 637
Phosphonic acids calcium complexation 682
Phosphonic acids calcium complexes 676
Phosphonium phenyl ions soln 3141
Phosphorescence arom mols 1921
Phosphorescence benzoquinoline propanol effect 2690
Phosphorothioate ion fragmentation 1903
Phosphorotriamide complex 3149
Phosphorus acid hypo oxidn 891
Phosphorus contg org cations 2936
Phosphorus halide NMR 3537
Phosphorus organo compds spectra 1956
Phosphorus oxytrichloride radical anion ESR 3023
Phosphorus spin lattice relaxation 3537
Phosphorus sulfur compds 3975
Phosphorus trifluoride borane adduct 2711
Phosphorus 31 NMR phosphonate 3547
Phosphoryl fluoride MO calcns 1360
Phosphoryl oxygen charge d 3309
Photoaquation ammine chromium 3504
Photoassisted dissocn nitrous oxide 617
Photocatalytic reactions semiconductor surfaces 1037
Photochem excited deuterium reaction ethane 841
Photochem hydrogen deuterium exchange hydroquinone 1775
Photochem hydroxyl radical 3640
Photochem oxidn arom amines 2737
Photochem xylenes 2741
Photochemistry ruthenium ammine complex 3075
Photochemistry UV acetato ammine cobalt 1914
Photocurrents semiconductor electrodes 562
Photodecompn acetone silane 3945
Photodecompn butyl peroxide 3651
Photodecompn cyclobutene 3656
Photodecompn vapor butyrolactone 2733
Photoelectron induced decompn ethane 2903
Photoelectron spectroscopy 3975
Photoexchange iodine iodobenzene 3350
Photoinduced trapped electrons solns 2887
Photoionization barium ionosphere 1412
Photoionization mass spectrometry 1461
Photoionization thymine ESR 626
Photoionization 2 quantum 2893
Photoisomerization isocyanides 580
Photoisomerization maleate radical anions 482
Photoluminescence lifetime detn 2463
Photoluminescence quantum yields review 991
Photolysis acetone 837
Photolysis acetone aq solns 851
Photolysis benzophenone 187
Photolysis carbon dioxide 3499
Photolysis carbonyl compds ESR 3454
Photolysis chlorobutane sensitizer ketone 1168
Photolysis diazomethane 2448
Photolysis diazomethane propane 1537
Photolysis diphenylpropene 2079
Photolysis energy partitioning vinylpyrazoline 1640
Photolysis ethylene 1317
Photolysis flash aq chlorate 2177
Photolysis flash dichloroanthracene 845
Photolysis flash fluorescein dyes 764
Photolysis flash nitrogen fluoride 2546
Photolysis fluoroacetone mercury effect 439
Photolysis formaldazine ESR 164
Photolysis ice 40
Photolysis ketene butane 2240
Photolysis laser perylene soln 3894
Photolysis potassium oxalatoferrate 2986
Photolysis rhodium phenanthroline glass 3230
Photolysis thiosulfate 2752
Photolysis UV gaseous dioxane 3899
Photometry crit micelle concn 804
Photoneutron carbon 11 recoil reactions 3201
Photooxidn carbon disulfide 854
Photooxidn liq sulfur dioxide 3631
Photooxidn nitrobenzene boron chloride 2415
Photophysical fluorobenzene processes 1233
Photopolymn acrylamides 3066
Photoredn benzophenone 181 187
Photoredn dinitrobenzene 1667
Photoselection conformers fluorescence 3097
Photoyield fluorescence fluorotoluene 3214
Physisorption water 3822
Pi electron radical calcn 3400
Piezooptic coeffs detns ultracentrifuge 716
Plasma microwave decompn org compds 445
Platinum catalysis homogeneous heterogeneous 1175
Plutonium lanthanide ionization potential 392
PMR ionic solvation 56
PMR proton exchange 688
PMR solvent fused metal acetates 1338
PMR tetraalkylammonium ions 509
PMR water propylene carbonate 1477
Polar effects hydrogen abstraction 603
Polar mols salting out 3757
Polar mols scattering cross section 727
Polar solute nonpolar solvent model 2413
Polarization nuclear electron spin reaction 3410
Polarization nuclear radical reaction 3410
Polarog irreversible redn complexes 2640
Polarog oxygen redn 4019
Polemic viscosity polyelectrolyte solns 442
Polyacrylate polyelectrolyte counterion exchange 1985
Polyacrylate polyelectrolyte exchange 1981
Polyacrylate sodium chloride water 3890
Polyacrylate sodium exchange 1990
Polybenzylglutamate DMF system 1446
Polybutadiene freezing depression 2623
Polydimethylsiloxane chain scissioning 2430
Polyelectrolyte counterion binding site 3367
Polyelectrolyte counterion exchange polyacrylate 1985
Polyelectrolyte electroosmotic flow 1981
Polyelectrolyte salt soln activity 3890
Polyelectrolyte salt solns viscosity 442
Polyelectrolyte transition metal assocn 1136
Polyelectronic systems 1860
Polyethylene electron irradn 3988
Polyethylene molten radiation chemistry 1671
Polyethylenimine acylated NMR fluorine 4061
Polyethylenimine hydration adiabatic compressibility 2362
Polyethylenimine hydration molar vol 2353
Polyhydric alcs PMR 1338
Polyion hydration 2353 2362
Polymer cryst chain rupture 3921
Polymer crystn review 3909
Polymer soln thermod props 1255
Polymer solns Newtonian viscosity 256
Polymer solns viscosity 72
Polymeric acids proton transfer 267
Polymethacrylate freezing depression 2623
Polymethacrylate radical spatial distribution 2443
Polymethacrylic acid activity coeff 2144
Polymn vinyl monomers glass 3897
Polyoxyethylene surfactant 3560
Polystyrene exchanger sodium 1990
Polystyrene latex light diffraction 1881
Polystyrene soln viscosity 1141
Polytetrafluoroethylene dispersions 789
Polyvinyl alc film proflavine 2727
Polyvinyl alc freezing depression 2623
Polyvinylpyridine pyrochlorophyll complex 1667
Polyvinylpyrrolidinone interactions 3135
Polywater prodn 2976
Positron sodium chloride defect interaction 2030
Potassium azide nuclear reaction 2551
Potassium fluoroiodate radiolysis 3479
Potassium halide conductance molten acetamide 2687
Potassium hydrogen malonate irradn 3426
Potassium ion acetone solvation 56
Potassium magnesium halide melt structure 155
Potassium nitrate melt viscosity 103
Potassium oxalatoferrate photolysis 2986
Potential energy surfaces 1844
Potential liq anion membrane 554
Potential liq membrane electrode 2138
Potential step ESR 3281
Potentiometric titrn polymethacrylic acid 2144
Powder pattern x ray interpretation 1782
Predissocn hydrogen bromide ion 1472
Preequil activation energy temp 2372
Prepassive film growth iron 2823
Pressure dependence combination radicals 2225
Pressure dependence ethane decompn 837
Pressures dissocn liq salts polemic 721
Presure vapor isotope effects methanol 1815

Probabilities vibrational transition 923
Proflavine dye concn quenching 2727
Propane butane chloro methylene 2231
Propane diazomethane photolysis system 1537
Propane hydroxy hydroperoxy prepn 3004
Propane irradn benzene effect 2272
Propanes surface diffusion 133
Propanol acetone electrolyte soln cond 1714
Propanol effect absorption emission 2690
Propanol photoprodn mechanism 3945
Propanol radical kinetics comments 1326
Propargyl halides benzene complex 2128
Propene diphenyl photolysis 2079
Propene tritium recoil reaction 1031
Propenes chain isomerization 292
Propionates alkali activity coeffs 2319
Propyl alc radicals polemic 167
Propyl alc radiolysis 20
Propylbenzene shock wave ignition 1501
Propylene carbonate water PMR 1477
Propylene oxidn gold catalyst 2914
Propylenediamine aminoethyl complex spectra 3355
Protein denaturants 815
Protein denaturation model 3733
Protein nucleic acid CD 1516
Protein proton transfer reaction 4012
Protein soln ultrasound urea 374
Protolysis aminonaphthalenesulfonic acid 4056
Protolysis ethyl methylcarbamate NMR 1895
Protolysis kinetics aminoalkanes 2400
Proton chem shift NMR 3971
Proton chem shifts protein denaturants 815
Proton coupling naphthalene ring 3765
Proton donors naphthylamines aromatics 2404
Proton exchange amines NMR 3190
Proton exchange aq urea solns 2123
Proton exchange guanidinium ion water 688
Proton exchange hydroxyl ethanol 1994
Proton shift solutes 3160
Proton transfer effect 1826
Proton transfer polymeric acids 267
Proton transfer reaction 4012
Proton transfer reaction kinetics 161
Proton transfer sulfuric acid 2672 2681
Pulse radiolysis alk sulfite 3510
Pulse radiolysis benzene nitrous 3886
Pulse radiolysis chloroform 2436
Pulse radiolysis cyanogen solns 608
Pulse radiolysis electron methane 1164
Pulse radiolysis ethanol 3893
Pulse radiolysis fluoroescein dyes 764
Pulse radiolysis formamide 2267
Pulse radiolysis halide soln 3081
Pulse radiolysis nitrous oxide 1738
Pulse radiolysis oxalic acid 749
Pulse radiolysis thymine 3815
Purine nickel complexes spectra 799
Pyrazine triplet quantum yield 3769
Pyrazoline vinyl photolysis pyrolysis energy partitioning 1640
Pyrene pyromellitic dianhydride complexes 3805
Pyridine adsorption 3720
Pyridyl radical ESR 3432
Pyrimidinyl radical ESR 3432
Pyrochlorophyll fluorescence quantum yield 1667
Pyrolysis energy partitioning vinylpyrazoline 1640
Pyrolysis nitropropane 2427
Pyrolysis shock tube 1
Pyromellitic dianhydride complexes 3805
Pyrrolidino pyrrolino free radicals EPR 3486
Pyrrolino pyrrolidino free radicals EPR 3486
Pyruvate ester hydration kinetics 792
Pyruvates alkyl iodination 150
Quadrupole relaxation arsenic 75 3880
Quanidine hydrochloride acid base reaction 1120
Quanidinium urea protein denaturants 815
Quantum chem spin free 1860 1866 1878
Quantum states mols ions 981
Quantum yield carbon monoxide 3499
Quantum yield fluorescence pyrochlorophyll 1667
Quantum yield phosphorescence aroms 1921
Quantum yield triplet pyrazine 3769
Quantum yields photochem reactions 588
Quantum yields photoluminescence review 991
Quasiequil theory ionic fragmentation 1526
Quaternary ammonium salt micelle 369
Quaternary ammonium thiocyanate soln 3586
Quaterphenyl cation radical ESR 902
Quenching concn proflavine dye 2727
Quenching excited state fluorobenzene 3662
Quenching fluorescence charge transfer 1025
Quenching glass transition temp 3379
Quinoline singlet triplet crossing 2083
Quinolone assocn thermodynamics 1129
Quinoxaline singlet triplet crossing 2083
Radiation chemistry glycolic acid 1648
Radiation chemistry molten polyethylene 1671
Radiation damage dehydrogenation 3426
Radiation field satn ESR 3385
Radiation induced dichlorination DDT 2762
Radiation induced oxidn trichloroethylene 613
Radiation yield hydroxide ion 1759
Radical alkoxy phenyl ESR 411
Radical anion thymine irradn 3815
Radical anions maleate photoisomerization 482
Radical anions nitro arom ESR 1205
Radical arom sigma ESR 3432
Radical benzene anion 2769
Radical butenyl isomerization 2665
Radical butyl deexcitation polemic 3376
Radical cations hydrazines EPR 2048
Radical cyclohexyl absorption spectrum 1677
Radical electron pi calcn 3400
Radical ESR 1186
Radical fluoroiodate ESR 3479
Radical fluoromethyl matrix IR 3235
Radical formaldiminoxy deuteriomethyl ESR 2448
Radical free bianthrone 290
Radical hydroxyl olefin 3640
Radical hydroxyl photolytic prodn 40
Radical methyl ethyl ESR 4064
Radical olefin ESR 3475
Radical oxidizing reactivity 1738
Radical pair irradn ESR 3426
Radical pentyl isomerization 1632
Radical phenoxy NMR 3462
Radical polymethacrylate spatial distribution 2443
Radical quaterphenyl ESR 902
Radical reaction ligand field 2580
Radical reaction nuclear polarization 3410
Radical spectra nitroxide method 3466
Radical trapping fumarate 2570
Radical wall diffusion loss 2883
Radicals alkyl growth decay 472
Radicals anion nitro aroms 2591
Radicals cation ESR splitting 2195
Radicals cobalt acetylacetonate reaction 2575
Radicals complex bonded cobalt acetylacetonate 2575
Radicals fluorosulfate ESR temp 712
Radicals generation fast flow technique 2957
Radicals irradiated thiols ESR 2277
Radicals propyl alc polemic 167
Radicals trapped ESR 201
Radicals trifluoromethyl methyl combination 2225
Radii ionic scaled particle theory 2809
Radiolysis alc inclusion compds 3489
Radiolysis ammonia 2087
Radiolysis ammonia kinetics 2908
Radiolysis aq solns 31
Radiolysis benzene soln polemic 1177 1178
Radiolysis butane scavenger effects 2854
Radiolysis carbon tetrachloride 24
Radiolysis chlorofluoroethanes 2217
Radiolysis chloroform 2436
Radiolysis colloidal sulfur 756
Radiolysis cyanogen solns 608
Radiolysis electron methane 2405
Radiolysis erythrosin optical absorption 3020
Radiolysis halide soln 3081
Radiolysis hydrated electron scavenger 3626
Radiolysis hydrogenous adsorbate 201
Radiolysis induction period 191
Radiolysis iodine pentene 2880
Radiolysis liq ethanol 2756
Radiolysis methane electron pulse 1164
Radiolysis nitrobenzene soln 1759

Radiolysis nitrous oxide 3178
Radiolysis potassium fluoroiodate 3479
Radiolysis propyl alc 20
Radiolysis pulse alk sulfite 3510
Radiolysis pulse ethanol 3893
Radiolysis pulse fluoroescein dyes 764
Radiolysis pulse formamide 2267
Radiolysis pulse nitrous oxide 1738
Radiolysis pulse oxalic acid 749
Radiolysis pulse thymine 3815
Radiolysis supercooled water 2997
Radiolysis tritiated ethyl iodide 3359
Radiolysis water hydrogen yield 601
Radiolytic chain isomerization 292
Radiolytic hydrogen peroxide hydrogen 3950
Raman butyl cyanides 2806
Raman crotononitrile 44
Raman dimethylamino dichloro phosphine 3837
Raman halide melt structure 155
Raman laser spectroscopy 2948
Raman line sulfate viscosity 2684
Raman purple sulfur 4059
Raman sulfuric acid equil 2672 2681
Raman trichloroacetric acid soln 2492
Random walk adsorption polymer 2094
Rank matrix treatment spectrophotometry 2954
Rare earth oxide electronic state 3103
Rare earth oxides spectroscopy 514
Rare earths fluorides soly 2340
Rare gas matrixes spectra 3243
Rate const evaln method 1319
Rate correction shock tube 2700
Rate hydrogen abstraction reaction 2709
Rate ketene butane 2240
Rates equil relations 430
Reactant adsorption electrode admittance 2209
Reaction acetylene oxygen 2402
Reaction electrons ammonium ions 986
Reaction kinetics adiabatic calorimetry 4029 4039
Reaction rate adsorbed mol 2967
Reactions hydrogen halides hydrogen atoms 835
Reactivity chloromethane tetrafluoroethylene telomerization 2075
Reactivity electron 1941
Reactivity oxidizing radical 1738
Reactor tubular flow 1593
Recoil carbon atom alcs 2248
Recoil carbon methanol mechanism 2253
Recoil reaction tritium 1031
Recoil reactions 11 recoil 3201
Recoil tritium butene 3771
Recombination bromine atoms 3046
Recombination cystine dihydrochloride holes 3746
Recombination dissocn hydrazoic acid 3026
Recombination kinetics acetic acid 2488
Recombination luminescence 2887
Recombination nitrogen atoms 1552
Recombination radical 2883
Redn irreversible complexes polarog 2640
Redn kinetics iodate 2516
Redn nitroso amine 2704
Redox equil cyclic voltammetry 2377
Redox equil violenes 335
Reflection spectra methyluracil 1509
Reflectometry time dielec detn cond 1323
Refractive index methyluracil 1509
Relaxation dielec dibromoalkanes 2616
Relaxation intramol dipole effects 2538
Relaxation intramol energy 2164
Relaxation NMR liq crystal 3834
Relaxation nuclear carbon 13 3967
Relaxation nuclear spin 2452
Relaxation process cholesteryl methyl ether 1237
Relaxation spectra nickel purine complexes 799
Relaxation spin lattice NMR 2539
Relaxation spin lattice phosphorus 3537
Relaxation times correlation ion pairs 598
Relaxations dipolar contributions carbon 13 585
Replacement hot chlorine chlorofluoromethanes 2685
Resin ion exchange ESR 907
Resin ion exchange magnetic moment 2981
Resonance fluorescence benzene 1572
Retinal singlet triplet absorption spectrum 983
Review crystn polymer 3909
Review dimerization methyl anilines 1763
Review photoluminescence quantum yields 991
Rhodium phenanthroline glass photolysis 3230
Rice Ramsperger Kassel theory 1333
Rotational barrier carbon nitrogen 3532
Rotational barrier selenoureas NMR 3372
Rotational diffusion rate ESR 3385
Rubber freezing depression 2623
Rupture chain cryst polymer 3921
Ruthenium ammine complex photochemistry 3075
Rutile film capacitance 1279
Salt effect aq alc 3757
Salt effect bisulfate equil 2681
Salt effect detergent catalysis 2707
Salt polyelectrolyte soln activity 3890
Salt polyelectrolyte solns viscosity 442
Salting in nonpolar gases alkylammonium bromide 1803
Salting out polar mols 3757
Salts liq dissocn pressures polemic 721
Salts metals miscibility 2340
Salts methylacetamide activity coeffs 2313
Sat soln cond 1691
Scaled particle theory 3757
Scaled particle theory ionic radii 2809
Scattering cross sections gases 727
Scavenge mol hydrogen yield 601
Scavenger hydrated electron 3626
SCF MO excimers fluorene dibenzofuran naphthalene 1794
Sea water difference chromatog 1418
Sea water drop size 3623
Selenoureas NMR rotational barrier 3372
Self diffusion theory 1970
Self radiolysis ethyl iodide 3359
Semiconductor electrodes spectral sensitization 562
Semiconductor surfaces electron transfer 617
Semiconductor surfaces photocatalytic reactions 1037
Semicontinuum model hydrated electron 2297
Sensitization spectral gallium phosphide electrodes 562
Sensitized phosphorescence arom mols 1921
Serine proton transfer 161
Shear rate intrinsity viscosity 1141
Shock induced thermolysis fluoroethane 295
Shock tube 171
Shock tube isomerization cyclopropane 2526
Shock tube pyrolysis 1
Shock tube study tetrafluoroethylene difluoromethylene 1625
Shock wave chlorine fluoride decompn 1765
Shock wave deuterium hydride 2541
Shock wave hydrogen deuterium reaction 1615
Shock wave ignition arom hydrocarbon 1501
Shock wave pyrolysis pentafluoroethane 3493
Shock wave thermolysis kinetics 3939
Shock waves hydroxyl induction times 1504
Silane acetone photodecompn 3945
Silane trimethylfluoro reaction tritium 301
Silanes bond energy terms 2480
Silanes ion mol reactions 13
Silanes methylfluoro 603
Silanes torsion rotation 3993
Silica adsorbent 201 3322
Silica gel chemisorbent 3249
Silica hydroxyl hexamethyldisilazane reaction 2181
Silica laser produced oxygen 2412
Silica surface internal hydroxyl group 3147
Silica surface silver ESR 2705 2706
Silica surfaces bromination nitrobiphenyl 887
Silicate alumino IR 2408
Silicon fluorides coupling consts gases 437
Silicon silicon bond strength disilanes 974
Siloxane chain scission 2430
Silver chloride aq org soly 93
Silver chloride ions assocn 2060 3711
Silver ESR glass silica 2705 2706
Silver holmium dissocn enery 3264
Silver reaction oxygen hydrogen 2186
Silver rutile titanium sandwich 1279
Silver thallium nitrate melt 4025
Sine basis vibrational eigenvalues 1756
Singlet excited absorption perylene 3894
Singlet states arom substitution 1775

Singlet triplet absorption spectrum retinal 983
Singlet triplet crossing quinolines 2083
Singlet triplet methylene 2536
Size drop sea water 3623
Smectic solid transformation 2839
Sodium aq enthalpy transfer 2229
Sodium ammonia optical absorption 3635
Sodium bromide activity coeff 3153
Sodium calcium chloride water system 957
Sodium chloride defect positron interaction 2030
Sodium chloride polyacrylate water 3890
Sodium chloride solns elec conductance 1099
Sodium counterion exchange 1990
Sodium dinonylnaphthalenesulfonate adsorption 1975
Sodium dodecyl sulfate interactions 3135
Sodium halide diln heat 3317
Sodium helium argon soly 2832
Sodium hydroxide doped alumina 234
Sodium ion acetone solvation 56
Sodium nitrate molten soly gases 821
Sodium perfluorooctanoate NMR 942
Sodium soln THF naphthalene ESR 843
Sodium tetrachloroaluminate aluminum trichloride cond 1260
Sodium zinc bromide complex 3028
Soft intermol function 3568
Solid layer photochemistry kinetics 588
Solid smectic transformation 2839
Solid state org 2025
Solid transformation cholesteryl acetate 2849
Soln dimethyl sulfoxide viscosity 1727
Soln ionic model theory 3790
Soln mixing thermodn 4041
Soln tetraalkylammonium halide conductance 1722
Solns fluorochloromethanes radiochemistry 455
Solns mixed electrolyte thermodn 946
Solns thermodn liq crystal solvents 2005
Solubilization benzene cetyltrimethylammonium bromide 3905
Solubilization cetyltrimethylammonium bromide polemic 3907
Solubilization colloidal sulfur 756
Solute polar nonpolar solvent model 2413
Solute solvent interactions 3141
Solvated electron ethanol hexane 3639
Solvated electron polemic 3904 3905
Solvated electron theory sodium soln 843
Solvation alkali ions acetone 56
Solvation effect anion exchange 79
Solvation electron ethylenediamine 3092
Solvation enthalpy 3606
Solvation enthalpy hydrocarbon 3598
Solvation lithium ion DMF 3188
Solvation studies alk earths 2325
Solvent compn ionic equil 90
Solvent effect fluoroform NMR 497
Solvent effect hydrogen bonding phenols 2219
Solvent effects anthracenesulfonates fluorescence 595
Solvent effects dielec absorption alcs 1790
Solvent effects dimerization review 1763
Solvent exchange water resin 1211
Solvent methanol isotope effect 388
Solvent nonpolar polar solute model 2413
Solvent perfluoroalkanoic acid dimerization 1330
Solvent PMR fused metal acetates 1338
Solvent polar hydrocarbon solvation 3598
Solvent shifts anisotropic factor anal 1207
Solvent solute interactions 3141
Solvent trifluoroacetic acid dimerization 1327
Solvents basicity series 3606
Solvents shifts gases coupling consts 437
Soly aliph hydrocarbon water 363
Soly helium argon sodium 2832
Soly homogeneous reaction 2969
Soly nonpolar gases molten salts 821
Solys hydrocarbons carbon dioxide 2345
Sorbate surface diffusion 133
Sorbent activated carbon 3526
Span 80 emulsifiers 537
Spatial distribution polymethacrylate radical 2443
Species no system detn 2954
Spectra absorption methanol polymer 1808
Spectra ESR 3383
Spectra polyethylene electron irradn 3988
Spectra radical nitroxide method 3466
Spectral sensitization gallium phosphide electrodes 562
Spin free quantum chem 1860 1866 1878
Spin Hamiltonian 1866
Spin label lipid biophys 3417
Spin lattice relaxation NMR 2539
Spin lattice relaxation phosphorus 3537
Spin relaxation nuclear 2452
Splittings hyperfine contact 3400
Squaric acid dissocn 1798
Stabilization dispersion 65
State equation argon 3568
States quantum mols ions 981
Statistical mechanics electrostriction gases 771
Statistics vol fraction 946
Steady radiolysis chloroform 2436
Stearates magnesium emulsifiers 537
Steric effects azonaphthols dimers 1227
Strontium barium exchange vermiculite 2484
Strontium hydroxylapatite catalytic activity 3167
Structure alanyl alanine 918
Structure biacetyl 1946
Structure micelle nonionic detergents 547
Structure nickel oxide catalysts 1044
Structure perchlorodiphenylmethyl radical 1246
Structure thermodn polymer review 3909
Styrene divinylbenzene copolymer 1211
Styrene methyl carbanions 1062
Sublimation enthalpy tungsten compds 112
Sublimation rate control 4049
Suboxide aluminum IR 1963
Substitution arom singlet triplet states 1775
Substitution reaction tritium 1290
Substitution tritium recoil butene 3771
Substitutions energetic chlorine orgs 440
Sulfate dodecyl sodium interactions 3135
Sulfate iron 2 decompn kinetics 1179
Sulfate Raman line viscosity 2684
Sulfates ion pairing 291
Sulfates uranyl vanadyl diln heats 2368
Sulfide alkoxyphenyl ESR 411
Sulfide carbon photooxidn 854
Sulfide thiuram hindered rotation 1067
Sulfides boron mass spectra 2410
Sulfite alk pulse radiolysis 3510
Sulfonamide chloro oxidn cyanoferrate 2 838
Sulfonamide naphthalene protolysis NMR 4056
Sulfonate naphthalene adsorption 1975
Sulfoxide dimethyl soln viscosity 1727
Sulfoxide methyl complex 3149
Sulfoxide methyl water viscosity 98
Sulfoxides methyl octyl fluoro 547
Sulfur colloidal radiolysis 756
Sulfur contg org cations 2936
Sulfur dioxide adsorption 532 2602
Sulfur dioxide liq photooxidn 3631
Sulfur fluoride ion prodn 3517
Sulfur liq color 912
Sulfur phosphorus compds 3975
Sulfur purple Raman 4059
Sulfur trioxide zwitterions hydrolysis 1763
Sulfuric acid equil Raman 2672 2681
Sulfuric acid soln deuterium exchange 571
Supercooled water viscosity 2016
Superexchange model helium hydride 1874
Superheating fluids 3613
Superoxide adsorption Y zeolites ESR 1165
Surface diffusion sorbate 133
Surface glass trapped radical 4064
Surface reactions cesium oxygen 1928
Surface silica internal hydroxyl group 3147
Surface tension dodecylamine hydrochloride aq 3000
Surfaces semiconductor electron transfer 617
Surfactant micellar wt 2212
Surfactant micelle aq soln 369
Surfactant micelle NMR 3560
Surfactants micellar hydrolysis zwitterions 1763
Suspensions colloidal light scattering 789
Taft const carbon monoxide 2248
Tellurides vaporization thermogravimetry 118
Tellurium compd nuclear transformation 2867
Telomerization tetrafluoroethylene chloromethane reactivity 2075

Temp effect absorption aq electron 2798
Temp effect hot reaction 3042
Temp glass transition heating 3379
Temp gradient effect calorimetry 4029 4039
Temp preequil activation energy 2372
Terbium dicarbide dissocn energy 848
Tert butyl peroxy radical 2580
Tetraalkylammonium alkali halides mixing 2148
Tetraalkylammonium halide soln conductance 1722
Tetraalkylammonium halides freezing points 2319
Tetraalkylammonium ions PMR 509
Tetraalkylarsonium NMR 3880
Tetrabutylammonium carboxylates excess thermodns 3733
Tetrabutylammonium ionic radies 2809
Tetracene dimerization 1768
Tetrachloroaluminate sodium aluminum trichloride cond 1260
Tetrachloroethylene radiolytic prodn 24
Tetracyanoethylene addn isoprene enthalpy 1734
Tetrafluoroethylene chloromethane telomerization reactivity 2075
Tetramethylammonium ionic radiies 2809
Tetramethylethylene radical ESR 3475
Tetramethylphenylenediamines ESR 431
Tetramethylsilane adsorption 1887
Tetramethylurea water system 3313
Tetraphenylarsonium ions soln 3141
Tetrapropylammonium ionic radiies 2809
Thallium silver nitrate melt 4025
Thallium suboxide IR 1963
Theory Onsager transport coeff 3124
Theory self diffustion 1970
Thermal decompn chlorine fluoride 1765
Thermal isocyanide isomerization energy transfer 2171
Thermal isomerization isocyanide 1366
Thermal unimal processes theories 1333
Thermionic emission cesium halide 3741
Thermochemistry Diels Alder reaction 1734
Thermod props polymer soln 1255
Thermodn acetaldehyde peroxide addn 3377
Thermodn alkylammonium salt transition 2066
Thermodn cis trans isomerizations 1453
Thermodn cyclic hydrocarbons 1264
Thermodn ether iodine complex 3682
Thermodn hexane ketone soln 4041
Thermodn hydrocarbon solvation 3598
Thermodn hydrocarbon water soln 363
Thermodn ion exchange equil 1152
Thermodn micellization detergents 547
Thermodn mixed electrolyte solns 946
Thermodn soln mixing 4041
Thermodn structure polymer review 3909
Thermodns donor acceptor complexes 2632
Thermodns elasticity 142
Thermodynamics assocn quinolone 1129
Thermodynamics chymotrypsin 1387
Thermoelasticity elastin 142
Thermolysis fluorinated ethane 3195
Thermolysis fluoroethane shock induced 295
Thermolysis kinetics chlorine fluoride 3939
Thermolysis kinetics trimethylcyclobutane 1437
THF naphthalene sodium soln ESR 843
Thiacyclobutane lasers induced reactions oxygen 725
Thiacyclopentane lasers induced reactions oxygen 725
Thiete nickel phenoxazine phenothiazine 2387
Thioamide rotational barrier 3532
Thiocarbamate ion fragmentation 1903
Thiocyanate quaternary ammonium soln 3586
Thiolo thiono photoelectron spectra 3975
Thiols irradiated radicals ESR 2277
Thiono thiolo photoelectron spectra 3975
Thiophosphate ester NMR 3537
Thiosulfate photolysis 2752
Thiuram disulfide hindered rotation 1067
Thorium oxide adsorbents 895
Threonine proton transfer 161
Thrombogenic activity drug mechanism 2107
Thymine photoionization ESR 626
Thymine pulse radiolysis 3815
Time reflectometry dielec detn cond 1323
Tin halides complexes 637
Tin telluride vaporization thermogravimetry 118
Titanium dioxide surface hydroxyl 1216
Titanium dioxide surface IR 1221
Titanium halides complexes 637
Titanium hydride wide line NMR 3334
Titanium oxide spectra matrix 3243
Titanium rutile silver sandwich 1279
Toluene degrdn 3524
Toluene piezooptic coeffs 716
Toluene shock wave ignition 1501
Transfer diffusion 3303
Transfer diffusion theory 3297
Transfer vibrational energy 4001
Transformation kinetics cholesteryl acetate 2849
Transformation kinetics cholesteryl myristate 2839
Transition europium soln 3668
Transition glass water alc 3379
Transition metal assocn polyelectrolyte 1136
Transition pathway europium soln 3677
Transition phase lead chromate 350
Transition probabilities vibrational 923
Transition probability vibration collision 3185
Translational energy ion fragments 2458
Transport coeff theory Onsager 3124
Transport hydrogen ions noise spectra 654
Transport ion exchange membrane 3015
Transport props nitrate melt 4025
Transport props water 3698
Trapped electrons photoinduced solns 2887
Trapped hydrogen atoms EPR 1936
Trapped radical glass surface 4064
Trapped radicals ESR 201
Triazine trinitro hexahydro conformation 2056
Trichloride aluminum sodium tetrachloroaluminate cond 1260
Trichloroacetic acid soln ionization 2492
Trichloroethylene oxidn radiation induced 613
Trifluoride phosphorus borane adduct 2711
Trifluoroacetic acid dimerization solvent 1327
Trifluorodecanoate polyethylenimine NMR 4061
Trifluoromethyl methyl radicals combination 2225
Trimethylamine borane adduct 2711
Trimethylbenzene shock wave ignition 1501
Trimethylcyclobutane thermolysis kinetics 1437
Tripeptides MO conformation 2286
Triphenylene pyromellitic dianhydride complexes 3805
Triplet excitation transfer isomerization 2394
Triplet pyrazine quantum yield 3769
Triplet singlet absorption spectrum retinal 983
Triplet singlet crossing quinolines 2083
Triplet singlet methylene 2536
Triplet states arom substitution 1775
Tritiated ethyl iodide radiolysis 3359
Tritium butane reaction 3042
Tritium deuterium substitution cyclobutane 3781
Tritium exchange dichlorodifluoroethane configuration 1299
Tritium hydrogen exchange butane 2417
Tritium methane isotope effects 1283
Tritium mol fast reaction butene 2407
Tritium radiolysis water hydrogen yield 601
Tritium reaction trimethylfluorosilane 301
Tritium recoil butene 3771
Tritium recoil reaction 1031
Tritium substitution reaction 1290
Tryptophan fluorescence 3061
Tryptophan photoionization 2893
Tubular flow reactors 1593
Tungsten bromide oxide thermodns 112
Tungsten reaction atomic fluorine 308
Tunneling correction chem kinetics 1748
Turbulent boundary kinetics shock tube 2700
Ultracentrifuge piezooptic coeffs detns 716
Ultracentrifuge technique 2507
Ultrasonic longitudinal relaxation ion pairs 598
Ultrasonic velocity nonelectrolyte water system 2336
Ultrasound absorption polyelectrolyte counterion 3367
Ultrasound protein soln urea 374
Ultrasound proton transfer reaction 4012
Unimal processes thermal theories 1333
Unimol decompn theory 1526
Uracil methyl optical props 1509
Uracils PMR 3963
Uranium cobalt ammine complex reaction 2117
Uranium oxide IR 2283
Uranium 4 spectra 631

Uranyl nitrate hexahydrate water diffusion 1272
Uranyl vanadyl sulfates diln heats 2368
Urea alc inclusion compds 3489
Urea aq solns proton exchange 2123
Urea NMR internal rotation 1901
Urea quanidinium protein denaturants 815
Urea ultrasound protein soln 374
Urea volume change reaction 1120
Ureas water system 3313
Uv far water ice 1162
UV irradn metals 35
UV photochemistry acetato ammine cobalt 1914
UV photochemistry ruthenium complex 3075
UV photolysis gaseous dioxane 3899
UV spectra methyluracil 1509
UV titanium oxide 3243
Valine NMR conformations 505
Van der Waals effect NMR 3160
Vanadium oxidn hypophosphorus acid 891
Vanadyl ion axial coordination NMR 599
Vanadyl uranyl sulfates diln heats 2368
Vapor lead oxidn rate 2259
Vapor liq equil ketone hexane 4041
Vapor phase charge transfer 3682
Vapor phase charge transfer complexes 1057
Vapor pressure isotope effect 160
Vapor presure isotope effects methanol 1815
Vaporization entropy 166
Vaporization entropy hydrocarbons fluorocarbons 2530
Vaporization lithium fluoride 4049
Vaporization tellurides thermogravimetry 118
Vermiculite ion exchange kinetics 2484
Vessel drainage liq film 583
Vibration inversion formamide 405
Vibration large mols hidden degeneracy 1343
Vibration mols deexcitation 1079
Vibration transition europium soln 3677
Vibrational deexcitation mol polemic 3376
Vibrational eigenvalues sine basis 1756
Vibrational energy transfer 4001
Vibrational excitation hexafluorobicyclopropyl 2164
Vibrational excitation mol collision 3185
Vibrational frequencies lithium hydride dimer 984
Vibrational spectra biacetyl 1946
Vibrational spectra crotononitrile 44
Vibrational spectra organophosphorus compds 1956
Vibrational spectrum butyl cyanides 2806
Vibrational transition probabilities 923
Vibrationally excited ethane deactivation 837
Vibronic effect IR tetracyanoethylene 325
Vibronic level fluorescence 1572
Vinyl Me ether electrons capture 476
Vinyl monomers polymn glass 3897
Vinylpyrazoline photolysis pyrolysis energy partitioning 1640
Vinylpyridine polymer pyrochlorophyll complex 1667
Violenes electronic spectrum 335
Virial coeff hydrocarbon fluorocarbon 3863
Virial coeffs line core mols 3687 3691
Viscosity coeff electrolyte soln 2532
Viscosity dimethyl sulfoxide soln 1727
Viscosity flexible polymer soln 1141
Viscosity intrinsic bounds 72
Viscosity intrinsic normal alkanes 3120
Viscosity liq mixts 3113
Viscosity liq structure 98
Viscosity melt gas pressure 103
Viscosity Newtonian polymer solns 256
Viscosity polyelectrolyte salt solns 442
Viscosity Raman line sulfate 2684
Viscosity supercooled water 2016
Viscosity tetraamylammonium thiocyanate soln 3586
Viscosity vs crit temp 2619
Vitamin A aldehyde ESR 2861
Vol fraction statistics 946
Vol molar polyethylenimine hydration 2353
Vol partial ionic calcn polemic 3031 3035
Voltammetry cyclic ESR 3281
Volume change acid base reaction 1120
Vycor fiber water vapor adsorption 2718
Vycor glass adsorbents 532
Wall diffusion loss radical 2883
Water adsorbed radiolysis 201
Water adsorption 1887 3322
Water adsorption chromia 2774
Water alc glass transition 3379
Water alc ion exchange medium 85
Water amorphous glass transition 967
Water anomalous prodn 2976
Water calcium sodium chloride system 957
Water catalysis iodination 150
Water diffusion uranyl nitrate hexahydrate 1272
Water dioxane anion exchange medium 79
Water guanidinium ion proton exchange 688
Water hexamethylenetetramine heat soln 3633
Water ice far uv 1162
Water interfacial props 3870
Water liq vapor exchange 2694
Water methyl alc solvent medium 90
Water methyl sulfoxide viscosity 98
Water nonelectrolyte system ultrasonic velocity 2336
Water photooxidn sulfur dioxide 3631
Water physisorption 3822
Water PMR propylene carbonate 1477
Water radiolysis hydrogen yield 601
Water sea difference chromatog 1418
Water sea drop size 3623
Water sodium chloride polyacrylate 3890
Water solvent exchange resin 1211
Water soly aliph hydrocarbon 363
Water supercooled radiolysis 2997
Water supercooled viscosity 2016
Water superheating 3613
Water vapor absorption silica 3147
Water vapor adsorption Vycor fiber 2718
Water 2 state thermodns 3698
X ray induced trapped electrons 1941
X ray perchlorodiphenylmethyl radical 1246
X ray powder pattern interpretation 1782
Xanthate ethyl oxidn 354
Xenon adsorption liq mercury 344
Xenon fluorides mass spectrometry 1461
Xenon ionization yields absorption coeffs 719
Xenon mols reactions neg ions 2534
Xylene shock wave ignition 1501
Xylenes photochem 2741
Yield hydrogen peroxide hydrogen 3950
Yield nitrogen radiolysis 3178
Yield quantum carbon monoxide 3499
Zeolite adsorbed alkene ESR 3475
Zeolite aluminum deficient IR 2408
Zeolite cations locations 3327
Zeolite ion exchanger 85 2523
Zeolite isotope exchange 3846
Zeolites isotope exchange 3855
Zeolites Y superoxide adsorption ESR 1165
Zinc benzenedisulfonate assocn 2649
Zinc bromide activity coeff 3153
Zinc hydrated electron scavenger 3626
Zinc oxide catalyst 491
Zinc oxide catalysts 1037
Zinc oxide hydrogenation catalyst 208
Zinc oxide physisorbent 3822
Zinc oxides dissocn nitrous oxide 617
Zinc peroxide ESR 3089
Zinc sodium bromide complex 3028
Zirconium phosphate ion exchange 3750
Zwanzig theory dielec friction 239
Zwitterions amines micellar hydrolysis 1763

COMPOUND INDEX *to Volume 75, 1971*[1]

acetaldehyde
adsorption–desorption isotherm data for vapors on activated carbon, 3526; prodn. in recoil C atom reaction in methanol, 2253; prodn. of in γ radiolysis of 2-propanol, 20; reaction w/ *t*-BuOOH by nmr, 3377; reaction w/ H atoms: kinetics by esr; 1654; reactivity w/ OH radicals, 3640
acetamide
esr of radical prod. in irradiated aq. soln. of, 738; flash photolysis in aq. soln., 1910; molten: equivalent conductivity of potassium halides in, 2687; reaction of H atoms in aq. solns. of, 449; reaction w/ H atoms: kinetics by esr, 1654
acetamide, *N*-*tert*-butyl-
H bonding of, in CCl_4 and dioxane studied by nmr, 776, 784
acetamide, *N*,*N*-dimethyl-
flash photolysis in aq. soln., 1910; proton exchg. between guandiinium ion and H_2 in aq., 688; pulse radiolysis, 2267
acetamide, *N*-isopropyl-
H bonding of, in CCl_4 and dioxane studied by nmr, 776, 784
acetamide, *N*-methyl-
–alkali halide and nitrate solns: freezing pts., osmotic coeffs., and act. coeffs., 2313; esr of radical prod. in irradiated aq. soln. of, 738; flash photolysis in aq. soln., 1910; freezing pt. depression measurements in, 2879; freezing pts., osmotic coeff., and act. coeffs. of salts in, 2313, 2319; H bonding of, in CCl_4 and dioxane studied by nmr, 776, 784
acetamide-d_3, *N*,*N*-dimethyl-
C–N rotational barriers, 3532
acetamidinium bromide, *N*,*N*-dimethyl
ion pairing by nmr, 3550
acetamidinium chloride, *N*,*N*-dimethyl
ion pairing by nmr, 3550
acetamidinium-d_3 chloride, *N*,*N*-dimethyl-
C–N rotational barriers, 3532
acetamidinium iodide, *N*,*N*-dimethyl
ion pairing by nmr, 3550
acetamidinium-d_3 nitrate, *N*,*N*-dimethyl-
C–N rotational barriers, 3532
acetate
effect on $G(X_2^-)$ in radiolysis of aq. halide solns., 3081; radical anion ($CH_2CO_2^-$); esr in aq. soln., 1186; salts containing: enhancement of micellar catalysis, 2707
acetate, chloro-
radical anion ($CHClCO_2\cdot^-$); esr in aq. soln., 1186
acetic acid
adsorption from H_2O soln. onto activated carbon: exptl. and calcd. data, 3720; adsorption on TiO_2 by ir, 1221; –hydrazine binary sys.: glass transition, 1826; mol. assocn. effects on C–H nuclear dipolar relaxation rates, 2539; polarographic redn. of O_2 in presence of, 4019; prod. from irradn. of crys. glycolic acid, 1648; reaction of H atoms in aq. solns. of, 449; reaction w/ H atoms: kinetics by esr, 1654; spectrophotometric dissocn. field effect kinetics of aq., 2488
acetic acid, bromo-
reaction of H atoms in aq. solns. of, 449; reaction w/ H atoms: kinetics by esr, 1654
acetic acid, chloro-
CIDNP during photolysis of mixts. containing, 3410
use e^- scavenging efficiency in aq. solns., 1941
acetic acid, cyano-
reaction w/ H atoms: kinetics by esr, 1654
acetic acid, iminodi-
see iminodiacetic acid
acetic acid, iodo-; methyl ester
prod. in recoil C atom reaction in methanol, 2253
acetic acid, mercapto-
radicals produced in irradn. of aq. solns. of, 2277
acetic acid, nitrilotri-
see nitrilotriacetic acid
acetic acid, phenyl-
polarographic redn. of O_2 in presence of, 4019
acetic acid, trichloro-
ionization in aq. solns. using Raman, 2492
use e^- scavenging efficiency in aq. solns., 1941; recombination luminescence of tryptophan, 2887
acetic acid, trifluoro-
assocn. in dil. solns., 1327, 1330
acetic acid, trifluoro-; alkali salts
enthalpy in methanol: solv.–isotope effect, 388
acetic acid, tris(hydroxymethyl)-
ionization in H_2O and aq. MeOH: solute–solv. effects, 826
acetone
adsorption from H_2O soln. onto activated carbon: exptl. and calcd. data, 3720; adsorption–desorption isotherm data for vapors on activated carbon, 3526; cohesive energy, 642; competition for e_{aq}^- between e_{aq}^- scavengers, 3626; effect on epr of complex-bonded *t*-$BuO_2\cdot$, 2580; flash photolysis in aq. solns., 1910; fluorescence decay time in gas phase, 989; –hexafluoroazomethane mixts.: addn. reactions of CF_3 and CH_3 radicals in, 735; induction energy for, in Apiezon M estimated by glc, 831; ion–mol. interactions in acetone solns. of: modified CNDO method, 3581; nmr of polar solutes in: nature of solv. effect, 3971; photolysis in aq. soln. at 253.7 nm in presence of CH_3NO_2, 851; photolysis kinetics at 313 nm in presence of silane, 3945; photolysis of 1,4-dichlorobutane sensitized by, 1168; prod. in photolysis of di-*t*-butyl peroxide, 3651; prod. in pyrolysis of nitropropane, 2427; prodn. of in γ radiolysis of 2-propanol, 20; reaction of H atoms in aq. solns. of, 449; reaction w/ H atoms: kinetics by esr, 1654; reactions w/ H_2O_2, 3004; vapor–liq. equil. of binary mixts. of *n*-hexane-^{14}C w/, 4041; yields of H_2O_2 in radiolysis of aq. solns. containing, 3950
use deactivation of vibrationally excited C_2H_6: measuring pressure dependence, 837
acetone-d_6
photolysis of 1,4-dichlorobutane sensitized by, 1168
use deactivation of vibrationally excited C_2H_6: measuring pressure dependence, 837
acetone, 1,1,1-trifluoro-
photolysis of: effect of Hg, 439
acetone imine, hexafluoro-
filter for 185 nm, 1326
acetonitrile
adsorption from H_2O soln. onto activated carbon: exptl. and calcd. data, 3720; adsorption–desorption isotherm data for vapors on activated carbon, 3526; cohesive energy, 642; energy transfer efficiency in thermal isomerization of C_2H_5NC, 3037; nmr in various solvents: nature of solv. effect, 3971; prod. in pyrolysis of nitropropane, 2427; reaction of H atoms in aq. solns. of, 449; reaction w/ H atoms: kinetics by esr, 1654; relative total scattering cross section of mols. *vs.*, 727; solute–solv. interactions studied by nmr, 3141
acetonitrile-N^{15}
^{15}N chem. shift, 932
acetyl chloride, dichloro-
oxidn. prod. of C_2HCl_3, 613
acetyl radical
decompn.: comparison of RRK and RRKM theories, 1333
acetylene
energy transfer efficiency in thermal isomerization of C_2H_5NC, 3037; H abstraction reaction by near-thermal ^{18}F atoms, 2709; hydrogenation on Pd: pressure jump and isotope replacement, 880; ion decompn.: translational energy of fragments calcd., 2458; –O_2 reaction: shock-tube study, 2402; prod. from CH_4 on radiolysis w/ high-intensity e^- pulses, 1164; prod. in photolysis of *c*-C_4H_6, 3656; prod. in pyrolysis of ethane, 1492; prod. in recoil ^{11}C reactions w/ C_5 hydrocarbons, 3201; reaction w/ H atoms: abs. rate const., 1584; relative total scattering cross section, 727
acetylene, diphenyl-
quantum yield of sensitized phosphorescence: external heavy-atom effect, 1921
acetylene, phenyl-
product of reaction of energetic ^{14}C ions w/ solid benzene, 2555
acetylene, vinyl-
prod. in photolysis of *c*-C_4H_6, 3656
acetylenedicarboxylic acid, dimethyl ester
use degradn. of cycloheptatriene, 2558
acetylenes, subst.
complex formation w/ benzene, 2128

---

(1) Index prepared by Maxine Heinitz.

acetylene-d_2
  reaction w/ $O(^3P)$, 4053
acrolein
  oxidn. prod. from propene over gold, 2914; prod. in pyrolysis of nitropropane, 2427; prod. of reaction of c-C_5H_8 w/ O atoms, 3056
acrylamide
  use dye-triplet reactions w/ p-substd. benzenesulfinates, 3066
acrylic acid, polymer
  proton-transfer reactions of, 267
adamantane
  Debye temp., 1073; thermochem., thermodn. fcns. and mol. structure, 1264
adenine
  complexes w/ Ni^{2+}: relaxation spectra, 799
adenine, 9-ethyl-
  H-bonding of, in dimethyl sulfoxide-d_6 by nmr, 3963
adenosine triphosphate
  –Mn^{2+} complex: epr in frozen aq. soln., 1202
agar gels
  self-diffusion studies of gel hydration, 1821
air
  –water interface: equil. rate of exchange of water at, using nmr, 2694
α-alanine
  esr of radicals prod. in irradiated aq. soln. of, 738; reaction w/ H atoms: kinetics by esr, 1654
β-alanine
  esr of radicals prod. in irradiated aq. soln. of, 738; reaction w/ H atoms: kinetics by esr, 1654; vol. change in protonation: medium effects, 1120
alanine, *N*-acetyl-
  reaction w/ H atoms: kinetics by esr, 1654
alanine, *N*-acetyl-; methyl ester
  nmr, 505
alanine, phenyl-; derivatives
  conformations by nmr, 505
alanine, phenyl-; L-3,4-dihydroxy-
  zwitterion formation upon deprotonation, 2657
L-alanine amide, *N*-acetyl-*N′*-methyl-
  conformational dependence of energy and partial charge, 2286
L-alanyl-D-alanine, *N*-methyl-*C′*-methyl-
  conformational dependence of energy and partial charge, 2286
L-alanyl-L-alanine
  crystal and molecular structure, 918
L-alanyl-L-alanine, *N*-methyl-*C′*-methyl-
  conformational dependence of energy and partial charge, 2286
alcohols
  cohesive energies, 642; enthalpies of soln. in various polar solvents, 3598; esr of X-irradiated long-chain, in urea inclusion crys., 3489; gas-phase acidities of, 2226; ir study of H-bonding in solns. of HF in, 2222; products of radiolysis of N_2O–hydrocarbon mixts., 3178; reactions of recoil C atoms w/, 2248
alcohols, polyhydric
  nmr of molten alkali acetate solns. of, 1338
alkali metal
  absorption bands in solns. of, in amines, 286; absorption bands in solns. of, in liq. ammonia: analysis of band into two components, 3635; –ethylenediamine solns.: extinction coeff. and equilibria, 3092; matrix reactions w/ fluorohalomethanes, 3235
alkali metal acetate
  –*N*-methylacetamide solns.: freezing pts., osmotic coeffs., and act. coeffs., 2319; nmr of molten, solns. of polyhydric alcohols, 1338
alkali metal chloride
  effect on circular dichroism of lysine-rich histone f-1-DNA complexes, 1516; osmotic coeffs. of 1 *M* solns., 3723; ultrasonic absorption of polyelectrolyte solns. upon addition of, 3367
alkali metal deuterides
  isotopic substitution effects on cohesive energies, 1251
alkali metal formate
  –*N*-methylacetamide solns.: freezing pts., osmotic coeffs., and act. coeffs., 2319
alkali metal halides
  films: ir of NO adsorbed on, 2930; free energy changes mixing solns. of, and tetraalkyl halides, 2148; ionic radii, 2809; –*N*-methylacetamide solns.: freezing pts., osmotic coeffs., and act. coeffs., 2313
  use salt effects in Raman study of bisulfate–sulfate sys., 2681
alkali metal hydride
  dimers: Rittner ionic model study, 984; isotopic substitution effects on cohesive energies, 1251
alkali metal hydroxide
  formation of C_3^- in γ-irradiated aq. solns. of, 3030, 3031
alkali metal ions
  ionic mobility: Zwanzig theory of dielectric friction, 239; –nitro aromatic radical anion clusters; esr, 1205
alkali metal nitrate
  corresponding states and glass transition, 2306; –*N*-methylacetamide solns.: freezing pts., osmotic coeffs., and act. coeffs., 2313; viscosities of fused, pressurized w/ gasses, 103
alkali metal perchlorate
  conductance and assocn. behavior in H_2O at 25°, 3290
alkali metal propionate
  –*N*-methylacetamide solns.: freezing pts., osmotic coeffs., and act. coeffs., 2319
alkali metal salts
  ionic solvation in acetone: spectroscopic studies, 56
alkaline earth fluorides
  –alkaline earth metals: miscibility of liq. metals w/ salts, 2340
alkaline earth halides
  solvation studies in high dielectric solvents, 2325
alkaline earth metals
  –metal fluoride sys.: miscibility of liq. metals w/ salts, 2340
alkaline earth perchlorates
  –HCl mixts.: act. coeffs., 1305
n-alkanes
  acentric factor and entropy of vaporization, 166; effect on thermal isomerization of ethyl isocyanide, 2171; enthalpies of soln. in various polar solvents, 3598; interaction virial coeffs. in binary mixts. w/ fluorocarbons, 3863; intrinsic viscosity calcns. for short chains, 3120; relative total scattering cross section, 727
alkanes, 1-chloro-
  cohesive energies, 642
alkanes, chloro-
  reactivities in atom abstractions by fluoroalkyl radicals, 2075
alkanes, cyclic
  thermochem., thermodn. fcns. and mol. structure of some, 1264
alkanes, α,ω-dibromo-
  dielectric relaxation in C_6H_6 solns., 2616
alkanes, iodo-
  γ-irradn. of polycrystalline w/ even no. of C atoms, 467
alkanes, perfluoro-
  interaction virial coeffs. in binary mixts. w/ hydrocarbons, 3863
n-alkenes
  effect on thermal isomerization of ethyl isocyanide, 2171
alkyl radicals
  γ-irradn. of iodoalkanes: growth and decay of, 472
alkyl radicals, fluoro-
  atom abstraction from chloroalkanes, 2075
alkynes
  relative total scattering cross section, 727
allyl bromide
  see propene, 3-bromo-
alumina
  ir of CO_2 adsorbed on, 526; polymerization of styrene and of methyl methacrylate on, 3897
γ-alumina
  adsorption and surface reactions of sec. alcohols on, and NaOH doped; by ir, 234; NiO supported on: catalytic act. of, for N_2O decompn., 1051; NiO supported on: structural, magnetic, and opt. props., 1044
γ-alumina, NaOH doped
  adsorption and surface reactions of sec. alcohols, 234
η-alumina
  NiO supported on: catalytic act. of, for N_2O decompn., 1051; NiO supported on: structural, magnetic, and opt. props., 1044
aluminate, sodium tetrachloro-
  conductivity of gaseous $AlCl_3$–Al_2Cl_6 mixts. containing, 1260
aluminum
  atoms in silica: benzene adsorption and *t*-butylbenzene cracking, 220; -doped NaCl crys.: interactions of positrons w/, 2030; impurity in lab-made diamond, 1838; sys. Ho–Au–: equilibria involving gaseous species over, 3264
aluminum, foil
  surface adsorption of species on oxidized foil, 1887
aluminum, triethyl-
  reaction w/complex-bonded *t*-butylperoxyl; epr, 2580
aluminum, triisobutyl-
  reaction w/complex-bonded *t*-butylperoxyl; epr, 2580
aluminum bromide ($AlBr_3$)
  catalyst in isomerization of octanes, 1486
aluminum iodide (AlI_3)
  –diethyl ether solns: complex formation in, 282
aluminum oxide (Al_2O)
  infrared, 1963

aluminum oxychloride (AlOCl)
  heat of formation of gaseous, by mass spec., 1760
aluminum oxyfluoride (AlOF)
  heat of formation of gaseous, by mass spec., 1760
Amberlite
  nmr study of macroreticular and carboxylic acid resins, 1211
amides
  pulse radiolysis, 2267
amides, *N*-alkyl-
  H-bonding of, in CCl_4 and dioxane studied by nmr, 776, 784
amines
  –alkali metal solns.: new absorption bands, 286; aromatic: assocn. consts. w/ proton acceptors by ir, 1157; aromatic: enthalpies of assocn. of, w/ proton acceptors, 3149; radicals prod. in irradiated aq. solns. of: esr, 738; substd. aromatic: photochem. oxidn. in $CHCl_3$, 2737
amino acids
  radicals prod. in irradiated aq. solns. of: esr, 738
amino radical
  rate of disappearance of, produced by irradn. of NH_3 vapor, 2087
aminyl dioxide radical anion, methyl-
  esr of, and its mercapto- analogs, 2752
ammonia
  absorption coeff. and ionization yield at 58.4 nm, 719; adsorption on TiO_2 by ir, 1221; –calcium solns.: coexistence of liq. phases in, 399; decompn. by e^- impact, 769; ion lifetimes in gaseous, 444; –NO reaction on Pt: deuterium kinetic isotope effect, 875; pulse radiolysis of vapor: disappearance of NH_2 radical, 2087; pulsed radiolysis: kinetic study of species formed, 2908; relative total scattering cross section, 727
  use radiolysis of CCl_4, 24
ammonia-d_3
  –NO reaction on Pt: kinetic isotope effect, 875; photolysis at 123.6 nm in presence of c-C_4H_6, 3646; relative total scattering cross section, 727
ammonia-^{15}N
  ^{15}N chem. shift, 932
ammonium acetate
  effect on circular dichroism of lysine-rich histone f-1–DNA complexes, 1516
ammonium bisulfate
  use redn. of Ce(IV) by H_2O_2, 250
ammonium bromide
  use salt effects in Raman study of bisulfate–sulfate sys., 2681
ammonium chloride
  effect of circular dichroism of lysine-rich histone f-1–DNA complexes, 1516
  use salt effects in Raman study of bisulfate–sulfate sys., 2681
ammonium ion
  ionic radius from scaled particle theory of salt effect, 2809; reaction rate of ammoniated e^- w/, at $-35°$, 986; viscosity coeffs., B_η, in various solvents, 2532
ammonium nitrate
  assocn. equil. of Ag^+ and Cl^- in, 3711; –$Cd(NO_3)_2$ glass transition temps., 2306; –H_2O mixts: assocn. equil. of Ag^+ and Cl^- in, 2060
ammonium perchlorate
  decompn. of, over ZnO, 491; thermal decompn. induction period: radn. effects, 191
ammonium-^{15}N chloride
  ^{15}N nmr, 1758

Ammonium compounds, substituted
butyltriisoamylammonium iodide
  conductance in acetone, 1714; conductance in CF_3CH_2OH, 1708
butyltriisoamylammonium tetraphenylborate
  conductance in acetone, 1714
tert-butyltrimethylammonium ion
  correlation time and reorientation activation energy in aq. soln., 509
cetyltrimethylammonium bromide
  kinetics of catalysis by reversed micelles of, in hexanol, 2001; solubilization of benzene in aq., by differential spectroscopy, 3905, 3907
decylammonium salts
  micelle aggregation number: dependence on polar head structure, 369
n-decyltrimethylammonium ion
  correlation time and reorientation activation energy in aq. soln., 509
2-(*N*,*N*-dimethylamino)ethyltrimethylammonium sulfate
  protolysis kinetics in sulfuric acid, 2400
dodecyltrimethylammonium bromide
  micellar effects on triethylamine–SO_3 hydrolysis, 1763
eicosanyltrimethylammonium bromide
  micellar effects on triethylamine–SO_3 hydrolysis, 1763
ethyltrimethylammonium ion
  correlation time and reorientation activation energy in aq. soln., 509
n-hexadecyltrimethylammonium ion
  correlation time and reorientation activation energy in aq. soln., 509
n-hexyltrimethylammonium ion
  correlation time and reorientation activation energy in aq. soln., 509
isopropyltrimethylammonium ion
  correlation time and reorientation activation energy in aq. soln., 509
n-octyltrimethylammonium ion
  correlation time and reorientation activation energy in aq. soln., 509
tetraalkylammonium bromides
  enthalpy of soln. of molecules in aq. solns. of, 2330
tetraalkylammonium halides
  conductance in ethylene glycol, 1722; free energy changes mixing solns. of, and alkali metal halides, 2148; –*N*-methylacetamide solns: freezing pts., osmotic coeffs., and act. coeffs., 2319
tetraalkylammonium ions
  correlation times and reorientation activation energies in aq. solns., 509; ion mobility: Zwanzig theory of dielectric friction, 239
tetraalkylammonium salts
  mol. assocn. and dielectric consts. of long-chain salts in C_6H_6, 542
tetrabutylammonium bromide
  apparent molal vol. in H_2O and salting-in of gases in aq. soln., 1803; conductance in acetone and in 1-propanol–acetone mixts., 1714; conductance in CF_3CH_2OH, 1708; conductance in ethylene glycol, 1722; enthalpy of soln. of molecules in aq. solns. of, 2330; epr probe into hydrophobic interaction in aq. soln., 165; interaction w/ halide ions studied by nuclear quadrupole relaxation, 2936
tetrabutylammonium carboxylates
  thermodyns. of aq. solns: apparent molal heat contents and osmotic and activity coeffs. 3733
tetrabutylammonium chloride
  conductance in acetone and in 1-propanol–acetone mixts., 1714; conductance in CF_3CH_2OH, 1708
tetrabutylammonium halides
  free energy changes mixing solns. of alkali metal halide and, 2148; –*N*-methylacetamide solns: freezing pts. and osmotic and activity coeffs., 2319
tetrabutylammonium iodide
  conductance in acetone and in 1-propanol–acetone mixts., 1714; conductance in CF_3CH_2OH, 1708; conductance in ethylene glycol, 1722; phase transitions, 2066
tetrabutylammonium ion
  enthalpies of transfer to propylene carbonate from methanol or dimethylformamide, 3606; ionic radius ffom scaled particle theory of salt effect, 2809; viscosity coeffs., B_η, in various solvents, 2532
tetrabutylammonium perchlorate
  conductance in acetone and in 1-propanol–acetone mixts., 1714; conductance in CF_3CH_2OH, 1708
tetrabutylammonium tetraphenylborate
  conductance in acetone, 1714
tetraethylammonium bromide
  apparent molal vol. in H_2O and salting-in of gases in aq. soln., 1803; conductance in acetone, 1714; conductance in CF_3CH_2OH, 1708; conductance in ethylene glycol, 1722; enthalpy of soln. of molecules in aq. solns. of, 2330
tetraethylammonium chloride
  interaction w/ halide ions studied by nuclear quadrupole relaxation, 2936; solute–solv. interactions studied by nmr, 3141
tetraethylammonium halides
  free energy changes mixing solns. of alkali halide and, 2148; –*N*-methylacetamide solns: freezing pts. and osmotic and activity coeffs., 2319
tetraethylammonium iodide
  conductance in acetone, 1714; conductance in CF_3CH_2OH, 1708; conductance in ethylene glycol, 1722; phase transition, 2066
tetraethylammonium ion
  assocn. const. of H_2O w/, in propylene carbonate by nmr, 1477; enthalpies of transfer to propylene carbonate from methanol or dimethylformamide, 3606; ionic radius from

  scaled particle theory of salt effect, 2809; viscosity coeffs., B_η, in various solvents, 2532

tetraethylammonium perchlorate
  solute–solv. interactions studied by nmr, 3141

tetraheptylammonium iodide
  conductance in CF_3CH_2OH, 1708; phase transitions, 2066

tetraheptylammonium salts
  membrane potentials of C_6H_6 solns. of NO_3^-, Cl^-, and Br^- salts between 2 aq. electrolyte solns., 554; mol. assocn. and dielectric consts. in benzene, 542

tetrahexylammonium iodide
  phase transitions, 2066

tetrahexylammonium ion
  enthalpies of transfer to propylene carbonate from methanol or dimethylformamide, 3606

tetra(hydroxyethyl)ammonium chloride
  interaction w/ halide ions studied by nuclear quadrupole relaxation, 2936

tetramethylammonium bromide
  conductance in CF_3CH_2OH, 1708; conductance in ethylene glycol, 1722

tetramethylammonium chloride
  conductance in CF_3CH_2OH, 1708; effect of micellar catalysis, 2707

tetramethylammonium halides
  free energy changes mixing solns. of, and alkali metal halide, 2148; –*N*-methylacetamide solns: freezing pts. and osmotic and activity coeffs., 3219

tetramethylammonium hydroxide
  use study of complexation between Ca^{2+} and $CH_3C(OH)(PO_3H_2)_2$, 676, 682

tetramethylammonium iodide
  conductance in CF_3CH_2OH, 1708; conductance in ethylene glycol, 1722; phase transition, 2066

tetramethylammonium ion
  correlation time and reorientation activation energy in aq. soln., 509; enthalpies of transfer to propylene carbonate from methanol or dimethylformamide, 3606; ionic radius from scaled particle theory of salt effect, 2809; viscosity coeffs., B_η, in various solvents, 2532

tetramethylammonium perchlorate
  conductance in acetone, 1714; conductance in CF_3CH_2OH, 1708

tetramethylammonium perfluorooctanoate
  critical micelle concn. by ^{19}F nmr, 942

tetramethylammonium polyphosphate
  site binding of counterions in solns. of: ultrasonic absorption, 3367

tetramethylammonium tetraphenylborate
  conductance in acetone, 1714

tetrapentylammonium chloride
  enthalpy in methanol: solv.–isotope effect, 388

tetrapentylammonium iodide
  phase transitions, 2066

tetrapentylammonium thiocyanate
  conductance–viscosity behavior from infinite dilution to molten salt at 55°, 3586

tetraphenylammonium ion
  enthalpies of transfer to propylene carbonate from methanol or dimethylformamide, 3606

tetrapropylammonium bromide
  apparent molal vol. in H_2O and salting-in of gases in aq. soln., 1803; conductance in acetone, 1714; conductance in CF_3CH_2OH, 1708; conductance in ethylene glycol, 1722; enthalpy of soln. of molecules in aq. solns. of, 2330

tetrapropylammonium halides
  free energy changes mixing solns. of alkali metal halide and, 2148; –*N*-methylacetamide solns.: freezing pts. and osmotic and activity coeffs., 2319

tetrapropylammonium iodide
  conductance in acetone, 1714; conductance in CF_3CH_2OH, 1708; conductance in ethylene glycol, 1722; phase transitions, 2066

tetrapropylammonium ion
  enthalpies of transfer to propylene carbonate from methanol or dimethylformamide, 3606; ionic radius from scaled particle theory of salt effect, 2809; viscosity coeffs., B_η, in various solvents, 2532

tetramethylammonium-^{15}N chloride
  ^{15}N nmr, 1758

tridodecylammonium salts
  see tridodecylamine salts

amylose
  –iodine reaction: kinetics, 272

anatase
  surface props. by ir, 1216, 1221

aniline
  complexes w/ proton acceptors: calorimetric detn. of enthalpies of assocn., 3149; sys. cyclohexane–: viscosity near critical temp., 2619

aniline, *N*,*N*-diethyl-
  fluorescent quencher in flash photolysis of anthracenes, 1025

aniline, 2,4-dinitro-
  heat of formation estd. by group additivity, 4047

aniline, *N*-methyl-
  solv. effect on dimerization, 1763

aniline, *N*-methyl-*N*-nitroso-
  redn. by potassium: esr of nitrosamine anion rad., 2704

aniline, *p*-nitro-
  heat of formation estd. by group additivity, 4047

aniline, *p*-nitrosodiethyl-
  reaction w/ complex-bonded *t*-butylperoxyl; epr, 2580

aniline, substd.
  assocn. consts. w/ proton acceptors by ir, 1157; complexes w/ proton acceptors: calorimetric detn. of enthalpies of assocn., 3149

aniline, 2,4,6-trinitro-
  heat of formation estd. by group additivity, 4047

anilinium ion
  dissocn. const. in isobutyl methyl ketone, 2496

anthracene
  charge-transfer quenching of mol. fluorescence: intersystem crossing, 1025; complex w/ pyromellitic anhydride: photochem., 3805; –perylene mixts. in toluene: pulsed laser irradn., 3894; Pt-cat. isotopic H exchange, 1175

anthracene, 1,5-dichloro-
  second triplet level of, in fluid solns., 845

anthracene, diphenyl-
  charge-transfer quenching of mol. fluorescence: intersystem crossing, 1025

anthracene, 9-methyl-
  charge-transfer quenching of mol. fluorescence: intersystem crossing, 1025

anthracene, 1,2,3,4,5,6,7,8-octahydro-
  see octhracene

anthracene sulfonates
  solvent effect on fluorescence spectra, 595

anthraquinone
  esr of cation radicals, 2195; simultaneous electrochem.–esr expts., 3281

antimonate(III), hexabromo-; tris(diethylammonium) salt
  ^{79}Br nqr spectra, 1898

Apiezon M
  use estimation of induction energies using glc, 831

arabate, alkali salts
  conductivity in aq. soln., 1691

argon
  absorption coeff. and ionization yield at 58.4 nm, 719; effect on thermal isomerization of C_2H_5NC, 1366; initiation rate for shock-heated mixts. of O_2–CO–H_2–, 1504; ir study of formamide in matrix of, 405; liquid: soly. of hydrocarbons and CO_2 in, 2345; modified Percus–Yevick equation for, 3568; nitrogen afterglow and recombn. of N atoms in presence of, 1552; –O_2 sys.: vibrational transitions in collisions, 923; soly. in liq. Na, 2832; soly. of, in molten $NaNO_3$, 82
  use ignition of aromatic hydrocarbon–O_2 mixts. by shock waves, 1501; ir of matrix-isolated UO, 2283; photolysis of CH_2N_2–propane mixts., 1537; spectrum of matrix-isolated CS_2, 2204

arsonium, tetramethyl-; various salts
  ^{75}As nmr, 3880

arsonium, tetraphenyl-; chloride
  enthalpy in methanol: solv.–isotope effect, 388; epr probe into hydrophobic interaction in aq. soln., 165; solute–solv. interactions studied by nmr, 3141

arsonium, tetraphenyl-; ion
  enthalpies of transfer to propylene carbonate from methanol or dimethylformamide, 3606; interactions w/ water and other solvents studied by nmr, 3141

arsonium, tetraphenyl-; tetraphenylborate
  partial molal vol. of, in H_2O at infinite dilution, 280

3-azabicyclo[3.3.3]nonane
  absolute entropies, comformation, Debye temp., and ir, 1073

1-azabicyclo[2.2.2]octane
  see quinuclidine

1-azanaphthalene
  see quinoline

2-azanaphthalene
  see isoquinoline

azide ion (N_3^-)
acid dissocn.–ion recombn. equilibrium: specific rates, 3026; radn. chem. of aq. solns. of, 31

azobenzene
simultaneous electrochem.–esr expts., 3281

azobenzene, derivatives
spectra and cis–trans isomerism, 581

azomethane, hexafluoro-
–acetone mixts.: addn. reactions, 735

azonaphthols, aryl-
steric effects on dimer structure, 1227

azo-*n*-propane
use isomerization of *n*-pentyl radicals, 1632

p-azoxyanisole
nematogenic solv: mol. interpretation of soly. in, 2005; proton spin–lattice relaxation, 2452

azoxybenzene, 4,4′-bis(alkoxy)-
nuclear magnetic relaxations in solid liq. crys., 3834

azoxybenzene, 4,4′-dihexoxy-
nematogenic solv: mol. interpretation of soly. in, 2005

bacteriochlorophyll
circular dichroism calcd., 1440

barium
metal–BaF_2 phase diagram, 2340; vapor: chem. of, released at high altitudes, 1412

barium azide (BaN_6)
thermal decompn. induction period: radn. effects, 191

barium bromide
solvation studies in high dielectric solvents, 2325

barium chloride
solvation studies in high dielectric solvents, 2325; sys. HCl–CsCl–: osmotic and act. coeffs. predicted, 1305; sys. LiCl–NaCl–: osmotic and act. coeffs., 1305; sys. NaCl–KCl–: osmotic and act. coeffs. predicted, 1305

barium fluoride
—Ba metal phase diagram, 2340

barium ion (Ba^{2+})
produced in release of Ba vapor at high altitudes, 1412

barium ion ($^{133}Ba^{2+}$)
—Sr^{2+} ion-exchange kinetics in vermiculite, 2484

barium oxide
chem. of Ba vapor at high altitudes; visible spectrum, 1412

barium perchlorate
–HCl mixts.: act. coeffs. 1305

benzene
adsorption of vapor on water by glc, 3870; adsorption on copper(II) montmorillonite: spectroscopic study, 3957; adsorption on mixed oxide sys., 220; absorption spectrum of vapor near 253.7 nm, 1564; adsorption–desorption isotherm data for vapors on activated carbon, 3526; anion radical: determination of unresolved metal hyperfine splittings, 2769; assignments in 253.7-nm fluorescence spectrum, 1572; ^{13}C relaxation mechanism, 2538; continuous γ and pulse radiolysis of aq. solns., 3886; e^- donor–acceptor complexes by glc: thermodn. study, 2632; effect of positive ion scavenging by, in radiolysis of propane, 2272; enthalpies of soln. in various polar solvents, 3598; enthalpy in methanol: solv.–isotope effect, 388; –ethanol mixts.: viscosity coeff. data of, and diffusion coeffs. of I_2 in, 963; π H-bonding w/ naphthylamine, 2404; H–D exchange of, at fuel cell electrode: effect of adsorption potential, 3715; hot-atom chem. of ^{14}C in solid, 2555; ignition of, –O_2 mixts by shock waves, 1501; ionic species formed during radiolysis of, 1177, 1178; isothermal piezooptic coeff. w/ ultracentrifuge, 716; photochem., 2741; solubilization in cetyltrimethylammonium bromide by differential spectroscopy, 3905, 3907; solute–solv. interactions studied by nmr, 3141; viscosity of liq. mixts. containing: calcd., 3113
use matrix isolation of phenyl radical: esr ^{13}C spectra, 3432

benzene, bromo-
enthalpies of soln. in various polar solvents, 3598; far-ir, 2942

benzene, butyl-
thermodns. of soln. in liq. crys. solvents for *n*-, *sec*-, and *tert*-, 2005

benzene, *tert*-butyl-
cracking of: kinetics, 220

benzene, chloro-
adsorption of vapor on water by glc, 3870; enthalpies of soln. in various polar solvents, 3598; far-ir, 2942; π H-bonding w/ naphthylamine, 2404

benzene, *p*-diamino-; dihydrochloride
interaction w/ halide ions studied by nuclear quadrupole relaxation, 2936

benzene, 1,3-diamino-2,4,6-trinitro-
heat of formation estd. by group additivity, 4047

benzene, *m*-dibromo-
far-ir, 2942

benzene, *o*-dibromo-
far-ir, 2942

benzene, *p*-dibromo-
enthalpy of fusion, 2066

benzene, dichloro-
far-ir of *o*-, *m*-, and *p*-, 2942; thermodns. of soln. in liq. crys. solvents for *o*-, *m*-, and *p*-, 2005

benzene, *o*-dichloro-
–butyl alcohol mixts: mol. assocn. in, by dielectric consts., 2133

benzene, dicyano-
use quencher in photolysis of pyrene, 1025

benzene, difluoro-
far-ir of *o*-, *m*-, and *p*-, 2942

benzene, *m*-difluoro-
absorption and fluorescent spectra, 1233

benzene, *o*-dihalo-
far-ir, 2942

benzene, 1,4-dihydroxy-2,3,5,6-tetramethyl-
see duroquinol

benzene, *o*-diiodo-
far-ir, 2942

benzene, 1,3-dimethyl-2-nitro-
anion radical: electronic spectra and MO interpretation, 2591

benzene, *m*-dinitro-
heat of formation estd. by group additivity, 4047; radical anion: electronic spectra and MO interpretation, 2591; radical anion–Na^+ clusters: esr, 1205

benzene, *o*-dinitro-
radical anion: electronic spectra and MO interpretation, 2591

benzene, *p*-dinitro-
photoredn. by hydrazobenzene sensitized by chlorophyll–poly(vinylpyridine) complex, 1667; radical anion: electronic spectra and MO interpretation, 2591

benzene, ethyl-
enthalpies of soln. in various polar solvents, 3598; enthalpy in methanol: solv.–isotope effect, 388; π H-bonding w/ naphthylamine, 2404; ignition of, –O_2 mixts by shock waves, 1501; prod. in radiolysis of propane containing traces of benzene, 2272

benzene, fluoro-
adsorption of vapor on water by glc, 3870; adsorption–desorption isotherm data for vapors on activated carbon, 3526; far-ir, 2942; quenching of excited states in gas phase, 3662

benzene, *p*-fluoronitro-
far-ir, 2942

benzene, halo-
enthalpies of soln. in various polar solvents, 3598; far-ir, 2942

benzene, hexafluoro-
far-ir, 2942

benzene, hydrazo-
see hydrazobenzene

benzene, iodo-
enthalpies of soln. in various polar solvents, 3598; far-ir, 2942; photochem. induced isotopic exchange between, and $I^{131}I$, 3350
use prepn. of phenyl radical, 3432

benzene, *m*-iodonitro-
radical anion–Na^+ clusters esr, 1205

benzene, isobutyl-
thermodns. of soln. in liq. crys. solvents, 2005

benzene, isopropyl-
see cumene

benzene, *p*-[*N*-(*p*-methoxybenzylidene)amino]-*n*-butyl-
proton spin–lattice relaxation, 2452

benzene, nitro-
esr of radicals from, in aq. soln., 1186; far-ir, 2942; heat of formation estd. by group additivity, 4047; kinetic esr study on photolysis of, 3454; photochem. modified by mol. complexation, 2415; radical anion: electronic spectra and MO interpretation, 2591; radical anion–alkali ion clusters: esr, 1205; simultaneous electrochem.–esr expts., 3281

benzene, nitroso-
kinetic esr study on photolysis of, 3454

benzene, *n*-propyl-
ignition of, –O_2 mixts. by shock waves, 1501

benzene, sexiphenyl-
electronic spectra, 318

benzene, 2,3,5,6-tetramethyl-1,4-dinitro-
see durene, dinitro-

benzene, 1,3,5-triamino-2,4,6-trinitro-
heat of formation estd. by group additivity, 4047

benzene, 1,2,4-trimethyl-
  excess Gibbs energy of mixing, w/ nitroalkanes by total intensity Rayleigh light scattering at 30°, 3728
benzene, 1,3,5-trimethyl-
  see mesitylene
benzene, 1,3,5-trinitro-
  heat of formation estd. by group additivity, 4047; Meisinheimer complex formation w/ aliph. amines: kinetic evidence of intramol. H-bonding, 3636
benzene-1-^{14}C
  relative diffusion rates of, and benzene-1,2-^{14}C, 1315
benzene-1,2-^{14}C
  relative diffusion rate of, and benzene-1-^{14}C, 1315
benzene-d_5, bromo-
  use prepn. of phenyl-d_5 radical, 3432
benzene-d_6
  use matrix isolation of σ-type aromatic radicals: ^{13}C esr spectra, 3432
benzene-d_n
  prod. at fuel cell electrode (n = 1–6), 3715
1,2-benzenedicarboxylic acid
  see phthalic acid
1,2-benzenediol
  see pyrocatehcol
1,3-benzenediol
  see resorcinol
1,4-benzenediol
  see hydroquinone
benzenesulfinate, para-substituted
  dye–triplet reactions w/: substituent effects, 3066
benzenesulfonic acid, 2,4,6-trinitro-
  dissocn. const. in isobutyl methyl ketone, 2496
1,3-5-benzenetricarboxylic acid
  reaction w/ H atoms: kinetics by esr, 1654
1,2,3-benzenetriol
  see pyrogallol
1,3,5-benzenetriol
  see phloroglucinol
benzisoxazole-3-carboxylate anion, 3-nitro-
  decarboxylation: micellar catalyzed, 2707
benzoate
  effect on micellar catalysis, 2707
  use chemiluminescent reaction of hydrated e$^-$, 764
benzoic acid
  polarographic redn. of O_2 in presence of, 4019; –2-quinolone dimer: thermodn. by ir, 1129; reaction of H atoms in aq. solns. of, 449; reaction w/ H atoms: kinetics by esr, 1654
benzoic acid, 3,5-dinitro-
  dissocn. and homoconjugation consts. in isobutyl methyl ketone, 2496
benzoic acid, pentafluoro-
  assocn. behavior in dil. solns., 1330
benzonitrile
  far-ir, 2942
benzophenone
  photoredn. in C_6H_6, 181, 187
  use sensitized phosphorescence of aromatic mol., 1921
benzopinacol
  prodn. of, in photoredn. of benzophenone, 181
benzoyl peroxide
  CIDNP during photolysis, 3410; esr and endor studies of radical pair formation in, 3426
benzoyl radical
  decompn. to Ph– + CO: comparison of RRK and RRKM theories, 1333
benzoyloxy radical
  esr and endor studies of, pairs from benzoyl peroxide, 3426
benzquinolines
  effect of 1-propanol on the absorption and emission of, in 3-methylpentane, 2690
benzyl acetate
  reaction w/ t-$C_4H_9^+$: kinetics, 590
beryllium fluoride (BeF_2)
  –LiF molten soln.: coordn. effects on spectrum of U(IV) in, 631
biacetyl
  see 2,3-butanedione
$\Delta^{10,10'}$-bianthrone
  identity of free radical in solns. of, 290
10,10'-bi-9-anthranoxy radical
  evidence for, in $\Delta^{10,10'}$-bianthrone solns., 290
bicyclo[2.2.1]heptane
  see norbornane
bicyclo[2.2.2]octane
  absolute entropies, conformation and Debye temp., 1073; thermochem., thermodn. fcns. and mol. structure, 1264
bicyclo[2.2.2]octane, 1-oxo-4-ethyl-2,6,7-trioxa-1-phospha-
  charge density on phosphoryl oxygen, 3309
bicyclopropyl-d_2, hexafluoro-
  nonrandom decompn. of vibrationally excited, 2164
biferrocene[Fe(II)Fe(III)] fluoroborate
  synthesis and phys. props; electronic, nmr, and Mössbauer spectra, 2025
biferrocene[Fe(II)Fe(III)] picrate
  effect of environment of e$^-$ transfer in; electronic, nmr, and Mössbauer spectra, 2025
biphenyl
  fluorescence spectrum: effect of varied excitation, 3097; prodn. of, in photoredn. of benzophenone, 181; product of reaction of energetic ^{14}C ions w/ solid benzene, 2555; Pt-cat. isotopic H exchange, 1175; quantum yield of sensitized phosphorescence: external heavy-atom effect, 1921
  use radiolysis of H_2O on porous glass, 201
biphenyl, 2- and 4-bromo-4'-nitro-
  products in bromination of nitrobiphenyl on silica, 887
biphenyl, dihalo-
  nmr spectra and substituent effects for 12 symmetrically substd., 421
biphenyl, dinitro-
  anion radicals of various isomers: electronic spectra and MO interpretation, 2591
biphenyl, o-nitro-
  anion radical: electronic spectra and MO interpretation, 2591
biphenyl, p-nitro-
  anion radical: electronic spectra and MO interpretation, 2591; bromination of, on Cab-O-Sil, 887
4-biphenyldiphenylcarbinol
  prodn. of, in photoredn. of benzophenone, 181
bismuth
  excess molar volume of solns. of, in its molten halides, 3620
bismuth(III) halides
  correlation of excess molar volume of Bi in molten, 3620
bismuthate(III), hexabromo-; tris(diethylammonium)salt
  ^{79}Br nqr spectra, 1898
bisulfate
  –sulfate sys: Raman study, 2672, 2681
borane (BH_3)
  reaction w/ PF_3 and Me_3N, 2711
borane, trifluorophosphine-
  abs. rate of formation, 2711
borane, trimethylamine-
  abs. rate of formation, 2711
boranes
  monoisotopic mass spectra, 3106

Borates
(contg. some ligands other than oxo or hydroxy)
tetrafluoroborate ion
  assocn. const. of H_2O w/, in propylene carbonate by nmr, 1477
tetraphenylborate, butyltriisoamylammonium salt
  conductance in acetone, 1714; viscosity study in dimethyl sulfoxide, 1727
tetraphenylborate, cesium salt
  conductance in acetone, 1714
tetraphenylborate, ion
  assocn. const. of H_2O w/, in propylene carbonate by nmr, 1477; interactions w/ water and other solvents studied by nmr, 3141; viscosity coeffs., B_η, in various solvents, 2532
tetraphenylborate, lithium salt
  ionic solvation in acetone: spectroscopic study, 56
tetraphenylborate, potassium salt
  conductance in acetone, 1714
tetraphenylborate, sodium salt
  conductance in acetone, 1714; epr probe into hydrophobic interaction in aq. soln., 165; ionic solvation in acetone: spectroscopic study, 56; solute–solv. interactions studied by nmr, 3141; viscosity study in dimethyl sulfoxide, 1727
tetraphenylborate, tetrabutylammonium salt
  conductance in acetone, 1714
tetraphenylborate, tetramethylammonium salt
  conductance in acetone, 1714
tetraphenylborate, tetraphenylarsonium salt
  partial molal vol. of, in H_2O at infinite dilution, 280

boron
  impurity in lab-made diamond, 1838
boron, amorphous
  attack of, by atomic fluorine, 308

boron oxide (B_2O_3)
  –SiO_2 disk: polymerization of styrene and methyl methacrylate on, 3897
boron sulfides, high mol. wt.
  lower temp. studies and metastable decompns., 2410
boron trichloride
  chemisorbed on silica gel: ir, 3249; photochem. of $PhNO_2$ modified by mol. complexation w/, 2415
bovine serum albumin
  ultrasonic absorption due to proton transfer for solns. of, 4012; ultrasonic absorption of solns. of, 374
bromcresol green
  spectrophoto. dissocn. field effect kinetics of aq. CH_3CO_2H and, 2488
bromide ion
  –Cl^- and –NO_3^- couples: electrochem. behavior of liq. anion membranes, 554; ionization efficiency of, emitted from CsBr, 3741; salts containing: enhancement of micellar catalysis, 2707; viscosity coeffs., B_η in various solvents, 2532; yields of H_2 in radiolysis of aq. solns. containing, 3950
  use pulse radiolytic study of O^-, 1738
bromine (Br_2)
  bromination of 4-nitrobiphenyl on Cab-O-Sil, 887; –H_2 laminar flame: recombn. of Br atoms in, 3046; sys.: tungsten–oxygen–; thermodn. study, 112
  use gas-phase bromination of $CHBr_3$: kinetics and thermochem., 987; reaction of fast H atoms w/ C_2H_6, 841; reactions of recoil C atoms in MeOH, 2253; recoil tritium reactions w/ $(CH_3)_3SiF$, 301; scavenger in radiolysis of CCl_4, 24; scavenger in recoil T reactions w/ CH_3F, 1290
bromine, atomic
  isotope effects between (n,γ)-activated Br isotopes in gaseous CH_3F and CD_3F, 2072; potential energy surfaces for atom transfer reactions, 1844; recombn. of, in laminar H_2–Br_2 flame, 3046
bromine, isotope of mass 80
  isotope effects of (n,γ)-activated Br reactions in gaseous CH_3F, 2072; recoil Br^{80m} reactions: isomerization of c-C_3H_5Br, 2698
bromine, isotope of mass 82
  isotope effects of (n,γ)-activated Br reactions in gaseous CH_3F, 2072
bromoform
  ^{13}C spin–lattice relaxation time: effect of field-dependent relaxation mechanisms, 3967; far-ir, 2942; gas-phase bromination: kinetics and thermochem., 987; nmr in various solvents: nature of solv. effect, 397[illegible]
1,3-butadiene
  prod. from cyclobutene: comparison of RRK and RRKM theories, 1333; prod. in photolysis of *c*-C_4H_6, 3656; prod. of photolysis and pyrolysis of 4-vinyl-1-pyrazoline, 1640; quenching of excited states of C_6H_5F by, 3662; reaction w/ H and D atoms: rate consts. by mass spec., 1601; soly. and activity coeffs. in liq. methane and argon, 2345
  use scavenger in recoil T reaction w/ $(CHFCl)_2$, 1299; 1,3-
1,3-butadiene, hexafluoro-
  use prepn. of hexafluorobicyclopropane, 2164
butadiene, (*Z*)-1,4-polymer
  –benzene soln: anomalous freezing behavior, 2623
butanal
  fluorescence decay time in gas phase, 989
n-butane
  acentric factor and entropy of vaporization, 166; decompn. to C_2H_5 radicals: comparison of RRK and RRKM theories, 1333; effect on gas-phase radiolysis of N_2O, 3178; entropy of vaporization from Hildebrand rule, 2530; H displacement in, by fast T_2 and T_2^+ collisions, 2417; interaction virial coeffs. in binary mixts. w/ fluorocarbons, 3863; –ketene mixts.: photolysis w/ and w/o added CO, 2240; prod. in photolysis of CH_2N_2–propane mixts., 1537; radiolysis of liquid, 2854; reaction w/ H atoms: kinetics by esr, 1654; reactivity w/ OH radicals, 3640; recoil tritium reactions: temp. dependence 3042; second virial coeffs.: exptl. and calcd. for pure and mixed sys., 3691; sys. $^{14}CH_3I$–: methylene reactions in photolysis of, 2536; theory of hydrophobic bonding, 363
  use energy transfer in thermal isomerization of Et—N═C, 2171
butane, 1-chloro-
  cohesive energy, 642
butane, 1,4-dibromo-
  dielectric relaxation in benzene soln., 2616
butane, 1,4-dichloro-
  elimination of HCl from, 2231; photolysis sensitized by aliph. ketones, 1168
butane, 2,3-dimethyl-
  entropy of vaporization from Hildebrand rule, 2530; prod. in photolysis of CH_2N_2–propane mixts., 1537; soly. and activity coeffs. in liq. methane and argon 2345
butane, 2-methyl-
  see isopentane
butane, perfluoro-
  entropy of vaporization from Hildebrand rule, 2530; interaction virial coeffs. in binary mixts. w/ hydrocarbons, 3863 second virial coeffs.: exptl. and calcd. for pure and mixed sys., 3691
butane, perfluoro-2,3-dimethyl-
  entropy of vaporization from Hildebrand rule, 2530
butane, *N*,*N*,*N*′,*N*′-tetramethyl-1,4-diamino-
  protolysis kinetics in H_2SO_4, 2400
butane, 2,2,3-trimethyl-
  acentric factor and entropy of vaporization, 166
n-butane-d_{10}
  radiolysis of *n*-C_4H_{10} mixts. of, 2854
2,3-butanediol, 2,3-dimethyl-
  prodn. of, in γ radiolysis of 2-propanol, 20
2,3-butanedione
  kinetic esr study on photolysis of, 3454; quenching of excited states of C_6H_5F by, 3662; vibrational spectra and structure, 1946
2,3-butanedione-d_6
  vibrational spectra and structure, 1946
butanenitrile
  cohesive energy, 642; energy transfer efficiency in thermal isomerization of C_2H_5NC, 3037
butanes
  production of isomeric, in photolysis of CH_2N_2–propane mixts., 1537
butanoic acid
  reaction of H atoms in aq. solns. of, 449; reaction w/ H atoms: kinetics by esr, 1654
butanoic acid, 4-cyclohexyl-
  –2-quinolone dimer: thermodn. by ir, 1129
butanoic acid, heptafluoro-
  assocn. in dil. solns., 1330
butanoic acid, 4-hydroxy-; γ-lactone
  photodecompn. in vapor phase, 2733
butanoic acid, tetrabutylammonium salt
  thermodns. of aq. solns. of, 3733
1-butanol
  adsorption on oxidized Al foil, 1887; catalytic dehydration by Ca and Sr hydroxyapatites, 3167; –*o*-dichlorobenzene mixts.: mol. assocn. in, by dielectric consts., 2133; dielectric relaxation in several solvents, 1790; enthalpies of soln. in various polar solvents, 3598; enthalpy of soln. in aq. alkylammonium bromide solns., 2330; gas-phase acidity, 2226; reaction of recoil C atoms w/, 2248; reaction w/ H atoms: kinetics by esr 1654
2-butanol
  adsorption and surface reaction on γ-alumina: ir study, 234; –*o*-dichlorobenzene mixts.: mol. assocn. in, by dielectric consts., 2133; reaction of H atoms in aq. solns. of, 449; reaction of recoil C atoms w/, 2248; reaction w/ H atoms: kinetics by esr, 1654
2-butanone
  CIDNP during formation of, 3410; cohesive energy, 642; photolysis of 1,4-dichlorobutane sensitized by, 1168; vapor–liq. equil. of binary mixts. of *n*-hexane-^{14}C w/, 4041
2-butanone, 4,4-dichloro-
  CIDNP during formation of, 3410
2-butanone, 3-methyl-3-nitroso-
  spin trapping of short-lived radicals by nitroxide method, 3466
2-butanone, 4,4,4-trifluoro-
  prod. in reaction of hexafluoroazomethane–acetone mixts., 735
butanonitrile
  see butanenitrile
(*E*)-2-butene
  isomerization in pyrazine–butene sys., 3769
1-butene
  isomerization over ZnO, 487; prod. of radiolysis of butane, 2854; reaction w/ atomic oxygen: abs. rate consts., 3902; reaction w/ recoil tritium atoms: average energy of addn. reaction, 3771; reactions w/ fast T_2 mols., 2407; reaction w/ H atoms: abs. rate const., 1584, 1601; reactivity w/ OH radicals, 3640
  use energy transfer in thermal isomerization of Et—N═C, 2171
1-butene, 2-methyl-
  reaction w/ H and D atoms: rate consts. by mass spec., 1601; reactivity w/ OH radicals, 3640

1-butene, 3-methyl-
reaction w/ H and D atoms: rate consts. by mass spec., 1601
1-butene, polymer
thermodn. and morphological props. of cryst., 3909
(*E*)-2-butene
prod. of radiolysis of butane, 2854; quenching of excited states of C_6H_5F by, 3662; reaction w/ H atoms: abs. rate const., 1584, 1601; reactivity w/ OH radicals, 3640
use photochem. of fluorotoluenes, 3214
(*Z*)-2-butene
effect on gas-phase radiolysis of N_2O, 3178; isomerization over ZnO, 487; prod. of radiolysis of butane, 2854; quenching of excited states of C_6H_5F by, 3662; reaction w/ H atoms: abs. rate const., 1584, 1601; reactions w/ recoil tritium atoms: average energy of addn. reaction, 3771; reactivity w/ OH radicals, 3640
use photochem. of fluorotoluenes, 3214
2-butene, 2,3-dimethyl-
esr of, adsorbed on synthetic zeolites, 3475; reaction w/ H and D atoms: rate consts. by mass spec., 1601; reactivity w/ OH radicals, 3640
2-butene, 2-methyl-
prod. in thermal decompn. of 1,1,2-trimethylcyclobutane, 1437; reaction w/ H and D atoms: rate consts. by mass spec., 1601; reactivity w/ OH radicals, 3640
2-butene, perfluoro-
quenching of excited states of C_6H_5F by, 3662
1-buten-1-yl radical, 3-methyl-
isomerization of vibrationally excited, 2665
tert-butoxyl radical
decompn.: comparison of RRK and RRKM theories, 1333; epr of complex-bonded, 2575; exptl. and calcd. decompn. rate constants, 3651
sec-butyl alcohol
see 2-butanol
tert-butyl alcohol
–*o*-dichlorobenzene mixts.: mol. assocn. in, by dielectric consts., 2133; effect on epr of complex-bonded *t*-$BuO_2\cdot$, 2580; epr probe into hydrophobic interaction in aq. soln., 165; prod. in photolysis of acetone–silane mixts., 3945; prod. in photolysis of di-*tert*-butyl peroxide, 3651; reaction of recoil C atoms w/, 2248; reaction w/ H atoms: kinetics by esr, 1654; ultrasonic relaxation in *c*-C_6H_{12}, 3182; ultrasonic velocity in aq. solns., 2336
butylamines
self-assocn. in the four isomeric cpds. by nmr, 938
tert-butyl bromide
far-ir, 2942
tert-butyl cation
reaction of, w/ benzyl acetate; kinetics, 590
tert-butyl chloride
far-ir, 2942
butyl *p*-(*p*-ethoxyphenoxycarbonyl)phenyl carbonate
proton spin–lattice relaxation, 2452
tert-butyl hydroperoxide
epr of complex-bonded radicals formed by reaction of cobalt(II) acetylacetonate w/, 2575
tert-butyl nitroxide
see di-*tert*-butyl nitroxide
tert-butylperoxyl radical
epr of, complex-bonded to Co(II), 2575; reactions of, complex-bonded to Co(III), 2580
n-butyl radical
decay of, in γ-irradiated C_4H_9I, 472
sec-butyl radical, 2,3-dimethyl-
equilibrium conformation and rotational barrier by esr, 3438
2-butyne, 1,4-dichloro-
complex formation w/ benzene, 2128
butyric acid
see butanoic acid
γ-butyrolactone
see butanoic acid, 4-hydroxy; γ-lactone
butyronitrile
see butanenitrile

Cab-O-Sil
see silica, Cab-O-Sil
cadmium
excess molar volume of solns. of, in its molten halides, 3620; uv irradn. of, in 3-methylpentane matrix: esr, 35
cadmium halides
correlation of excess molar volume of Cd in molten, 3620
cadmium iodide (CdI_2)
isothermal diffusivity of aq. solns. by hologram interferometry, 3374
cadmium ion (Cd^+)
formation in radiolysis of solns. containing Cd^{2+} and halide, 3081
cadmium ion (Cd^{2+})
competition for e_{aq}^- between e_{aq}^- scavengers, 3626
cadmium nitrate $Cd(NO_3)_2\cdot 4H_2O$
–alkali metal nitrate glass transition temps., 2306
calcium
–ammonia solns: coexistence of liq. phases in, 399; metal–CaF_2 phase diagram, 2340
calcium bromide
solvation studies in high dielectric solvents, 2325
calcium chloride
ionic entropy correlations of mixed electrolyte solns., 946; solvation studies in high dielectric solvents, 2325
calcium fluoride
–Ca phase diagram, 2340
calcium hydroxyapatite
nature of deficiency in nonstoichiometry: catalytic activity, 3167; spectroscopic studies, 3172
calcium ion (Ca^{2+})
biionic potentials of liq.-membrane electrode selective toward, 2138; catalysis of exchange of ethanol hydroxyl proton, 1994; complexation w/ $CH_3C(OH)(PO_3H_2)_2$, 676, 682; in sea water by difference chromatography, 1418; –Na^+–Cl^-–H_2O sys.: act. coeffs. by liquid ion-exchng. electrodes, 957; sublimation rate of LiF as fcn. of, impurity, 4049
calcium nitrate
–methylamine binary sys.: glass transitions, 1826
calcium oxide (CaO)
decompn. of $HClO_4$ over, 491
calcium perchlorate
–HCl mixts.: act. coeffs., 1305
calcium phosphate $[Ca_{10}(PO_3)_6(OH)_2]$
epr of H atoms in γ-irradiated, 1936
caprinitrile
see decanenitrile
caproic acid
see hexanoic acid
capronitrile
see hexanenitrile
caprylonitrile
see octanenitrile
carbene, bromochloro-
infrared spectrum, 3984
carbene, difluoro-
shock tube study of C_2F_4–CF_2 equil., 1625
carbene radical ($CH\cdot$)
nonempirical calcns. of contact hyperfine splittings, 3400
carbon
adsorption and hydrolysis of $[Co(NH_3)_6]^{3+}$ on, 649; adsorption of fibrinogen on, studied by e^- microscope, 2103
carbon, activated
adsorption of org. liq. from H_2O soln., 61; Polanyi adsorption potential theory applied to adsorption of organic liq. on, 3720; sorption properties, 3526
carbon, atomic
states of, produced in decompn. of org. cpds. in microwave plasma, 445
carbon, diamond
effect of catalyst composition on formation and props. of, 2158; formation: substitution of ^{15}N for ^{14}N in, 2696; phys. props. of lab-made, 1838; studies of growth rates, 1833, 1838
carbon, graphite
attack of, by atomic fluorine, 308; ir spectrum after intense grinding, 1149
carbon, isotope of mass 11
reaction of recoil C atoms w/ oxygen-containing molecules, 2248, 2253; reactions of recoil C in C_6 hydrocarbons, 3201
carbon, isotope of mass 14
hot-atom chem. of, in solid benzene between 5 and 100 eV, 2555; reaction of accelerated ^{14}C w/ benzene, 3524
carbon dioxide
adsorption coeff. and ionization yield at 58.4 nm, 719; adsorption on α-Cr_2O_3 using ir, 2790; adsorption on TiO_2 by ir, 1221; energy transfer efficiency in thermal isomerization of C_2H_5NC, 3037; ir of, adsorbed on alumina, 526; photodecompn. prod. of γ-butyrolactone, 2733; photolysis at 58.4 nm: quantum yields, 3499; second virial coeffs.: exptl. and calcd. for pure and mixed sys., 3691; soly. and activity coeffs. in liq. methane and argon, 2345; soly. of, in molten $NaNO_3$, 821
use relative rates of reaction of H atoms w/ HI and HBr, 835
carbon disulfide
absorption and emission spectra of matrix-isolated, 2204; ^{13}C spin–lattice relaxation time: effect of field-dependent relaxa-

tion mechanisms, 3967; nmr of polar solutes in: nature of solv. effect, 3971; $-O_2$ explosion: kinetics and mech., 861; photo-oxidn., 854
carbon monoxide
  addn. to C_2H_4: potential energy surface for nonlinear cheletropic reaction, 340; absorption coeff. and ionization yield at 58.4 nm, 719; adsorbed on ThO_2: epr, 895; adsorption on α-chromia using ir, 2774; Hg-sensitized photodecompn. in presence of, and CH_4, 3205; initiation rate for shock-heated mixts. of O_2–H_2–Ar–, 1504; Pd-catalyzed oxidn. promoted by H_2, 2065; photodecompn. prod. of γ-butyrolactone, 2733; photolysis of ketene–butane mixts. containing, 2240; prod. in photolysis of di-*tert*-butyl peroxide, 3651; prod. in photolysis of CS_2–O_2 mixts., 854; prod. in photolysis of gaseous dioxane, 3899; prod. in γ radiolysis of 2-propanol, 20; prod. in reaction of hexafluoroazomethane–acetone mixt., 735; prod. in recoil C atom reaction in methanol, 2253; prod. in recoil C atom reactions w/ alcohols and ethers, 2248; second virial coeffs.: exptl. and calcd. for pure and mixed sys., 3691
carbon tetrabromide
  prod. in bromination of $CHBr_3$, 987
carbon tetrachloride
  adsorption–desorption isotherm data for vapors on activated carbon, 3526; atom abstraction from, by fluoroalkyl radicals, 2075; –ethanol mixts.: diffusion coeffs. of I_2 in, 963; far-ir, 2942; intermol. assocn. of phenol in, 3591; isothermal piezo-optic coeff. w/ ultracentrifuge, 716; nmr of polar solutes in: nature of solv. effect, 3971; radiolysis of, 24; reaction kinetics of solvated e^- in solns. containing, 2756; reaction w/ H atoms: kinetics by esr, 1654; replacement reactions of hot Cl atoms, 2685; sys. $CHCl_3$–: traces and mutual diffusivities in, at 25°, 3293; viscosity of liq. mixts. containing: calcd., 3113
carbon tetrafluoride
  entropy of vaporization from Hildebrand rule, 2530; interaction virial coeffs. in binary mixts. w/ hydrocarbons, 3863; prod. in $CCl_2F_2 + F_2$ combustion reaction, 3645; replacement reactions of hot Cl atoms, 2685
carbon trioxide
  molar absorptivity, 2991
carbonate radical ion ($CO_2\cdot^-$)
  esr in aq. fumarate soln., 2570; short-lived transient in photolysis of ferrioxalate sys., 2897
carbonyl fluoride (COF_2)
  thermal decompn. and heat of formation, 3024
carbonyl sulfide (OCS)
  prod. in photolysis of CS_2-O_2 mixts., 854
carboxymethylcellulose
  site binding of counterions in solns. of: ultrasonic absorption, 3367
carrageenan, salts
  conductivity in aq. soln., 1691
catechol
  solv. and temp. effects on ir of OH group, 2219
cation-exchange membranes
  noise spectra associated w/ HCl transport across, 654
cerate, hexachloro-; dicesium sodium salt
  thermochem., 392
cerium
  soly. in CeF_3, 2340
cerium fluoride (CeF_3)
  soly. of liq. Ce in, 2340
cerium ion (Ce^{3+})
  use pulse radiolytic study of O^-, 1738
cerium ion (Ce^{4+})
  oxidn. of oxalic acid by, in presence and absence of O_2 and Mn(II), 3343; redn. of, by H_2O_2, 250; sys. containing: short lived radicals generated by fast flow techniques, 2957
  use oxidn. of methylhydrazines, 2043
cerium oxide (CeO), (CeO_2)
  spectroscopy of, molecules in inert matrix, 514
cesium
  –ethylenediamine solns.: extinction coeff. and equilibria, 3092; $-O_2$ surface reaction: chemiemission, 1928
cesium acetate
  nmr of molten alkali acetate solns. of polyhydric alcohols, 1338
cesium bromide
  –*N*-methylacetamide solns.: freezing pts., osmotic coeffs., and act. coeffs., 2313; thermal negative ion emission from, mixts. on Nb wire, 3741
cesium chloride
  activity coeff. *vs.* concentration: comparison of theory and exptl., 3790; conductance in CF_3CH_2OH, 1708; effect on circular dichroism of lysine-rich histone f-1-DNA complexes, 1516; film: ir of NO adsorbed on, 2930; –*N*-methylacetamide solns.: freezing pts., osmotic coeffs., and act. coeffs., 2313; osmotic coeffs. of 1 *M* soln., 3723; sys. HCl–$BaCl_2$–: osmotic and act. coeffs. predicted, 1305; sys. H_2O–NaCl–: volume fraction statistics, 946; sys. KCl–H_2O–: heats of mixing, 1125; sys. LiCl–H_2O–: heats of mixing, 1125; sys. LiCl–NaCl–: osmotic and act. coeffs., 1305; sys. NaCl–H_2O–: heats of mixing, 1125; thermal negative ion emission from, mixts. on Nb wire, 3741; ultrasonic absorption of polyelectrolyte solns. upon addition of, 3367
  use salt effects in Raman study of bisulfate–sulfate sys., 2681
cesium deuteride
  cohesive energy, 1251
cesium fluoride
  thermal negative ion emission from, mixts. on Nb wire, 3741
cesium halide
  thermal negative ion emission from, mixts. on Nb wire, 3741
cesium hydride
  cohesive energy: isotopic substitution effect, 1251; dimer: Rittner ionic model study, 984
cesium hydroxide
  formation of O_3^- in γ-irradiated aq. solns. of, 3030, 3031
cesium iodide
  activity coeff. *vs.* concentration: comparison of theory and exptl., 3790; –*N*-methylacetamide solns.: freezing pts., osmotic coeffs., and act. coeffs., 2313; thermal negative ion emission from, mixts. on Nb wire, 3741
cesium ion
  enthalpies of transfer to propylene carbonate from methanol or dimethylformamide, 3606; ion-exchg. selectivity coeffs. for, w/ NaA and KA zeolites, 85; viscosity coeffs., B_η, in various solvents, 2532
cesium nitrate
  corresponding states and glass transition, 2306
cesium perchlorate
  conductance and assocn. behavior in H_2O at 25°, 3290
cesium permanganate
  thermal decompn. induction period: radn. effects, 191
Cetomacrogol
  effect on nmr of phenothiazines, 3554
chloramine-T
  oxidn. of $Fe(CN)_6{}^{4-}$ by: kinetics, 838
chlorate ion
  flash photolysis in aq. soln., 2177
chloride ion
  assocn. const. of H_2O w/, in propylene carbonate by nmr, 1477; assocn. equil. of, and Ag^+ in liq. NH_4NO_3–H_2O mixts., 2060; assocn. equil. w/ Ag^+ in NH_4NO_3 melt, 3711; $-Ca^{2+}$–Na^+–H_2O sys.: act. coeffs. by liq. ion-exchange electrodes, 957; heats of mixing of electrolytes containing, 1125; ionization efficiency of, emitted from CsCl, 3741; $-NO_3^-$ and $-Br^-$ couples: electrochem. behavior of liq. anion membranes, 554; pulse radiolysis in aq. solns., 3081; reactions at high ionic strengths: $FeCl^{2+}$ equilibrium, 1113; salts containing: enhancement of micellar catalysis, 2707; salts containing: thermodns. of mixed electrolyte solns., 946; self-diffusion in gels, 1821; viscosity coeffs., B_η, in various solvents, 2532
chloride ion, di- (Cl_2^-)
  see dichloride ion
chlorine (Cl_2)
  $-F_2$ mixts.: explosion limits, 867; prod. in $CCl_2F_2 + F_2$ combustion reaction, 3645; vibrational relaxation of HCl by, and Cl atoms, 1622
  use scavenger in radiolysis of CCl_4, 24
chlorine, atomic
  potential energy surfaces for atom transfer reactions, 1844; prod. of oxidn. of penicillamine HCl by ionizing radn., 2564; vibrational relaxation of HCl by, and Cl_2, 1622
chlorine, isotope of mass 38
  hot atom replacement reactions in chlorofluoromethanes, 2685
chlorine fluoride (ClF)
  decompn. behind shock waves studied by mass spec., 1765; kinetics of, at high temp., 3939; prod. in $CCl_2F_2 + F_2$ combustion reaction, 3645; prod. in explosion of Cl_2–F_2 mixts., 867
chloroform
  adsorption–desorption isotherm data for vapors on activated carbon, 3526; atom abstraction from, by fluoroalkyl radicals, 2075; ^{13}C spin-lattice relaxation time: effect of field-dependent relaxation mechanisms, 3967; elimination of HCl from vib. excited, 2070; enthalpy of soln. in aq. alkylammonium bromide solns., 2330; far-ir, 2942; nmr in various solvents: nature of solv. effect, 3971; radiolysis, 2436; reaction w/ H atoms: kinetics by esr, 1654; sys. CCl_4–: tracer and mutual diffusivities in, at 25°, 3293
  use scavenger in radiolysis of CCl_4, 24
chlorophyll
  see also pyrochlorophyll

chlorophyll a
  circular dichroism of, and related mols. calcd., 1440
chlorpromazine HCl
  micelle formation: nmr in D_2O, 3554
cholate
  effect on micellar catalysis, 2707
cholesteryl acetate
  transformation kinetics and props. of, 2849
cholesteryl methyl ether
  relaxation processes, 1237
cholesteryl myristate
  transformation kinetics and pretransition effects, 2839
chromate ion ($^{51}CrO_4^{2-}$)
  exchange of, in fresh $PbCrO_4$, 350
α-chromia
  ir study of surface props., 2774, 2783, 2790
chromium(II)
  -catalyzed aquation of $Cr(CN)_6^{3-}$ to $Cr(CN)_5(OH)^{3-}$, 2381; reaction w/ H_2O_2 in presence of 2-propanol using esr flow technique, 3271
chromium(III)
  reactions w/ organic radicals formed by "Fenton-like" reagents, 3271
chromium(VI)
  oxidn. of oxalic acid by, in presence and absence of O_2 and Mn(II), 3343

Chromium complexes
cis-aquochlorotetraamminechromium(III) ion
  photoaquation prod. of $Cr(NH_3)_5Cl^{2+}$, 3504
chloropentaamminechromium(III) ion
  naphthalene-sensitized photoaquation, 3504
hexaamminechromium(III) ion
  naphthalene-sensitized photoaquation, 3504
hexacarbonylchromium
  effect on combustion of C_2H_2, 2402
hexacyanochromate(III) ion
  Cr(II)-catalyzed aquation of, 2381
pentacyanomonohydroxychromate(II) ion
  –catalyzed aquation of $Cr(CN)^{3-}$, 3281

chromium nitrate [$Cr(NO_3)_3$]
  epr of frozen aq. soln., 1202
chromium oxide (α-Cr_2O_3)
  see α-chromia
α-chymotrypsin
  enthalpy–entropy compensation phenomenon of, and temp. of minimum sensitivity, 1387; hydrolysis of *N*-acetyl-L-tryptophan ethyl ester: pH and temp. dependence, 1375
cobalt
  liquid: thermodn. props., 3737
cobalt(II)
  see cobalt ion (Co^{2+})
cobalt(III)
  oxidn. of oxalic acid by, in presence and absence of O_2 and Mn(II), 3343
cobalt acetylacetonate
  see cobalt complexes: bis(acetylacetonato)cobalt(II)
cobalt(II) *m*-ibenzenedisulfonate
  outer-sphere assocn. kinetics in MeOH by ultrasonic relaxation, 2649

Cobalt complexes
acetatoaquotetraamminecobalt(III) ion
  prodt. in photolysis of [$Co(NH_3)_5O_2CCH_3$]$^{2+}$, 1914
acetatopentaamminecobalt(III) ion
  uv photochem. in aq. soln., 1914
aquo-cobalt(II) complexes
  correlation of heterogeneous charge-transfer rate consts., 2640
bis(acetylacetonato)cobalt(II)
  epr of complex-bonded radicals formed by reaction of, w/ *t*-BuOOH, 2575
bis(ethylenediamine)cobalt(III–II) electrode
  interpretation of electrode admittance, 2209
diaquotetraamminecobalt(III) ion
  reaction w/ U^{3+} in aq. ClO_4^-, 2117
hexaamminecobalt(III) ion
  adsorption and hydrolysis of, on carbon, 649
hydroxopentaamminecobalt(III) ion
  hydrolysis prodt. of [$Co(NH_3)_6$]$^{3+}$ on carbon, 649
trioxalatocobaltate(III), tripotassium salt
  oxidn. of oxalic acid by, in presence and absence of O_2 and Mn(II), 3343

cobalt ion (Co^{2+})
  catalysis of exchange of ethanol hydroxyl proton, 1994; –C_2H_4–maleic acid copolymer complexes: heats of assocn., 1136; magnetic moment using ion-exchange resin, 2981; prod. in photolysis of [$Co(NH_3)_5O_2CCH_3$]$^{2+}$, 1914; prod. in reaction $U^{3+} + Co(NH_3)_4(H_2O)_2^{3+}$, 2117
copper
  electrode: oxidn. of ethyl xanthate on, 354; –Mn catalyst alloy: effect on diamond-forming reaction, 2158; –Ni catalyst alloy: effect on diamond-forming reaction, 2158
copper acetate [$Cu(ac)_2$]
  esr in acetic acid solns., 2228
copper(II)–amine complexes
  absorption spectra and epr data, 3355; formation on montmorillonite, 3957
copper(II) *m*-benzenedisulfonate
  outer-sphere assocn. kinetics in MeOH by ultrasonic relaxation, 2649
copper(II), *N*,*N*′-bis(2-aminoethyl)-1,3-propanediamine-; chloride and nitrate
  absorption spectra and epr data, 3355
copper bromide (CuBr), ($CuBr_2$)
  equilibrium between, and Br_2: spectrophotometric study, 592
copper(II) chelates
  bonding parameters from epr data, 3828
copper(II), 4,7-diaza-1,10-decanediamine-; dichloride
  prepn., absorption spectrum, and epr data, 3355
copper(II), 4,7-diaza-1,10-decanediamine-; dinitrate
  prepn., absorption spectrum, and epr data, 3355
copper ion (Cu^+)
  kinetics of, -catalyzed D exchng. in H_2SO_4 and $HClO_4$ solns., 571
copper ion (Cu^{2+})
  catalysis of exchange of ethanol hydroxyl proton, 1994; –C_2H_4–maleic acid copolymer complexes: heats of assocn., 1136; kinetics of, -catalyzed D exchange in H_2SO_4 and $HClO_4$ solns., 571; magnetic moment using ion-exchange resin, 2981; scavenging of H_2 yield from water irradiated w/ β particles by, 601; yields of H_2 in radiolysis of aq. solns. containing, 3950
copper(II) montmorillonite
  adsorption of methylbenzenes on: spectroscopic study, 3957
copper nitrate [$Cu(NO_3)_2$]
  epr of frozen aq. soln., 1202
crotononitrile
  vibrational spectra of *E*- and *Z*-, 44
crystal violet
  use spectral sensitization of GaP electrodes, 562
crytocyanine
  use spectral sensitization of GaP electrodes, 562
cumene
  πH-bonding w/ naphthylamine, 2404; prod. in radiolysis of propane containing traces of benzene, 2272
cyanamide ion ($^{14}CN_2^{2-}$)
  prod. from nuclear reaction $^{14}N(n,p)^{14}C$ in KN_3, 2551
cyanide ion ($^{14}CN^-$)
  prod. from nuclear reaction $^{14}N(n,p)^{14}C$ in KN_3, 2551
cyanogen
  pulse radiolysis of aq. soln. Absorption spectra of ion radical, 608; reaction w/ H atoms: photometric and mass spec. observations, 2662
cyclobutane
  recoil tritium reactions: excitation energies accompanying T for H substitution, 3781; substitution reaction by recoil T atoms: chem. factors controlling yield, 1290
cyclobutane, methylene-
  mech. of free-radical-induced reactions: interpretation of esr, 714
cyclobutane, perfluoro-
  quenching of excited states of C_6H_5F by, 3662
cyclobutane, 1,1,2-trimethyl-
  thermal unimolecular decompn., 1437
cyclobutane-d_6
  recoil tritium reactions: excitation energies accompanying T for D substitution, 3781
cyclobutanecarboxylic acid
  prod. of reaction of c-C_5H_8 w/ O atoms, 3056
1,3-cyclobutanediol, 2,2,4,4-tetramethyl-
  nmr of molten alkali acetate solns. of *cis*- and *trans*-, 1338
cyclobutanone
  fluorescence decay time in gas phase, 989
cyclobutene
  isomerization to butadiene: comparison of RRK and RRKM theories, 1333; vacuum-uv photolysis, 3656
cyclobutene, perfluoro-
  substitution reaction by recoil T atoms: chem. factors controlling yield, 1290

cycloheptane
adsorption of vapor on water by glc, 3870
1,3,5-cycloheptatriene
collisional quenching of vibrationally excited, 3376
1,3,5-cycloheptatriene-^{14}C
partial degradn. of, obtained from hot-atom, photolytic, and thermal reactions, 2558; product of reaction of energetic ^{14}C ions w/ solid benzene, 2555
1,3,5-cycloheptatriene-^{14}C, phenyl-
product of reaction of energetic ^{14}C ions w/ solid benzene, 2555
1,3,5-cycloheptatriene-d_8
collisional quenching of vibrationally excited, 3376
cyclohexadienyl radicals, hydroxy-
esr of, derived from C_6H_6 and benzoate ion, 1186; spectrum and reactions of, in aq. benzene solns., 3886
cyclohexane
anisotropic solv. shifts by factor anal., 1207; ^{13}C relaxation mechanism, 2538; –ethanol mixts.: viscosity coeff. data of, and diffusion coeffs. of I_2 in, 963; intermeds. in pulse radiolysis of, in presence of Ar, N_2O, O_2, 1677; nmr in various solvents: nature of solv. effect, 3971; reaction w/ H atoms: kinetics by esr, 1654; soly. and activity coeffs. in liq. methane and argon, 2345; sys. aniline–: viscosity near critical temp., 2619; viscosity of liq. mixts. containing: calcd., 3113
cyclohexane, methyl-
acentric factor and entropy of vaporization, 166; soly. and activity coeffs. in liq. methane and argon, 2345
cyclohexanecarboxylic acid
–2-quinolone dimer: thermodyn. by ir, 1129
cyclohexanol
intermeds. in pulse radiolysis of, in presence of Ar, N_2O, O_2, 1677
cyclohexanone
fluorescence decay time in gas phase, 989; photolysis of 1,4-dichlorobutane sensitized by, 1168
cyclohexylamine
effect on epr of complex-bonded t-$BuO_2\cdot$, 2580
cyclonite
see *s*-triazine, 1,3,5-trinitrohexahydro-
cyclooctane
adsorption of vapor on water by glc, 3870; anisotropic solv. shifts by factor anal., 1207
cyclopentadiene
e^- donor–acceptor complexes by glc: thermodn. study, 2632
cyclopentadiene, perchloro-
mol. structure by gas phase e^- diffraction, 1681
cyclopentane
entropy of vaporization from Hildebrand rule, 2530; reactions of N_2O in γ-irradiated liq., 2560; reaction w/ H atoms: kinetics by esr, 1654; recoil ^{11}C reactions w/, 3201; soly. and activity coeffs. in liq. methane and argon, 2345
cyclopentane, 1,2-epoxy-
prod. of reaction of c-C_5H_8 w/ O atoms, 3056
cyclopentane, ethyl-
acentric factor and entropy of vaporization, 166
cyclopentane, methyl-
soly. and activity coeffs. in liq. methane and argon, 2345
cyclopentane, methylene-
mech. of free-radical-induced reactions: interpretation of esr, 714
cyclopentane, perfluoro-
entropy of vaporization from Hildebrand rule, 2530
cyclopentanone
fluorescence decay time in gas phase, 989; opt. activity using INDO MO model, 2466; photolysis of 1,4-dichlorobutane sensitized by, 1168; prod. of reaction of c-C_5H_8 w/ O atoms, 3056
cyclopentanone, 2,3-dimethyl-
opt. activity using INDO MO model, 2466
cyclopentanone, 2,5-dimethyl-
fluorescence decay times in gas phase for both isomers, 989
cyclopentanone, 2-methyl-
opt. activity using INDO MO model, 2466
cyclopentanone, (+)-3-methyl-
opt. activity using INDO MO model, 2466
cyclopentene
e^- donor–acceptor complexes by glc: thermodn. study, 2632; effect of, on reactions of N_2O in γ-irradiated cyclopentane, 2560; esr of, adsorbed on synthetic zeolites, 3475; reaction w/ atomic O, 3056; recoil ^{11}C reactions w/, 3201
cyclopentene, perfluoro-
mol. structure by gas phase e^- diffraction, 1681
cyclopropane
ion decompn: translational energy of fragments calcd., 2458; photodecompn. prod. of γ-butyrolactone, 2733; reaction w/ H atoms: kinetics by esr, 1654; recoil Br reactions, 2699; shock tube isomerization, 2526
cyclopropane, bromo-
isomerization induced by recoil Br reaction, 2698
cyclopropane, 1,2-difluoro-
thermodns. of cis–trans isomerization, 1453
cyclopropane, 1,2-diphenyl-
prods. in photolysis of 1,3-diphenylpropene, 2079
cyclopropanone
decarbonylation: potential energy surface for nonlinear cheletropic reaction, 340
cyclopropene, perchloro-
structure by e^- diffraction, 1681
cyclopropylcarbinyl radical
equilibrium conformation and rotational barrier by esr, 3438
cyclotetrasiloxane, octamethyl-
prod. of irradn. of octamethyltrisiloxane, 2430
cysteine
radicals produced in irradn. of aq. solns., 2277
L-cystine dihydrochloride
photoinduced hole–electron recombn. in γ-irradiated single crys., 3746
cytosine, 1-methyl-
H-bonding of, in dimethyl sulfoxide-d_6 by nmr, 3963

p,p'-DDD
prod. of dechlorination of DDT, 2762
p,p'-DDT
radn. induced dechlorination, 2762
n-decane
acentric factor and entropy of vaporization, 166; adsorption of vapor by glc, 3870; thermodns. of soln. in liq. crys. solvents, 2005
decane, 1-chloro-
cohesive energy, 642
decanenitrile
cohesive energy, 642
decanoic acid, calcium salt
use complexometric titrn. study of complexation between Ca^{2+} and $CH_3C(OH)(PO_3H_2)_2$—solubility prodt. determination, 676
decanoic acid, 10,10,10-trifluoro-
derivative of, w/ polyethylenimine: ^{19}F nmr study of conformation, 4061
1-decanol
dielectric relaxation in several solvents, 1790; –urea inclusion compound: esr of X-irradiated, 3489
deca-2,4,6,8-tetraenal
triplet state energies and total band widths, 983
n-1-decene
thermodns. of soln. in liq. crys. solvents, 2005
denaturants
effects of urea–guanidinium class of, on H_2O structure, 815; medium effects of, 1120
deoxyribonucleic acid
–lysine-rich histone f-1 complexes: effect of salts on circular dichroism, 1516
deoxyribonucleic acid, sodium salt
concn. quenching of proflavine HCl in dry films of, 2727
deuteriobromonium ion (DBr^+)
predissocn. and dissosn. energy, 1472
deuterium
exchg. in H_2SO_4 and HCl_4 solns.; Cu^I and Cu^{II} catalyzed, 571; –hydrogen exchange of benzene at fuel cell electrode: effect of adsorption potential, 3715; –hydrogen exchange photoinduced in p-hydroquinone, 1775
deuterium (D_2)
dynamics of reaction w/ O_2^+, 1426; exchange of, and HCl, 171; exchange of surface OH groups in TiO_2 w/, 1216; H abstraction reaction by near-thermal ^{18}F atoms, 2709; HD self-exchange: dynamic sampling of reflected shock zone, 2541; hydrogenation of C_2H_2 on Pd: pressure jump and isotope replacement, 880; prod. in the reaction of fast D atoms w/ C_2H_6, 841; rate of exchange of, and H_2 behind reflected shock waves, 1615
deuterium, atomic
addn. reactions w/ olefins: rate consts. by mass spec., 1601; reaction of fast, w/ C_2H_6, 841
deuterium bromide
cation derived from: predissocn. and dissocn. energy of DBr^+, 1472
use reaction of fast H atoms w/ C_2H_6, 841
deuterium chloride
vibrational relaxation: vibration-to-rotation energy transfer, 1079

deuterium hydride
  see hydrogen-d_1
deuterium oxide
  see water (D_2O)
diamines
  ionic equilibria in mixed solv., 90; protolysis kinetics in H_2SO_4, 2400
1,4-diaminobutane
  dissocn. consts. of, in water–methanol mixts., 90
1,2-diaminoethane
  dissocn. consts. of, in water–methanol mixts., 90
1,3-diaminopropane
  dissocn. consts. of, in water–methanol mixts., 90
diamond
  see carbon, diamond
1,4-diazabicyclo[2.2.2]octane
  absolute entropies, conformation and Debye temp., 1073
diazabicyclo[2.2.2]octanium bromide, decyl-
  micelle aggregation number: dependence on polar head structure, 369
1,4-diazanaphthalene
  see quinoxaline
diazene, difluoro- (N_2F_2)
  thermodns. of cis–trans isomerization, 1453
diazomethane
  –propane mixts.: quantum yields in photolysis of, 1537
  use esr of radicals prepared by reactions of methylene, 2448
diazomethane-^{14}C
  use degradn. of cycloheptatriene, 2558
dibenzofuran
  MO calcns. for excimer model, 1794
di-*tert*-butyl nitroxide
  high-freq. esr expts. on, partitioned between aq. and membrane phases, 3417
dichloride ion (Cl_2^-)
  formation in radiolysis of Cl^-, 3081
dichromate
  oxidn. of oxalic acid by, in presence and absence of O_2 and Mn(II), 3343
dicyclopentadiene, tetrahydro-
  see tricyclo[5.2.1.0^{2,6}]decane
diethylamine
  mol. complex formation equil: solv. effects, 2413
diethylamine, *N*-nitroso-
  redn. by potassium: esr of nitrosamine anion rad., 2704
diglycolic acid, dithio-
  radicals produced in irradn. of aq. solns., 2277
diglycolic acid, thio-
  radicals produced in irradn. of aq. solns., 2277
diholmium (Ho_2)
  dissocn. energy determined by mass spec., 3264
diiodide ion (I_2^-)
  formation in radiolysis of I^-, 3081
diisopropylamine, *N*-nitroso-
  redn. by potassium: esr of nitrosamine anion radical, 2704
dimethylamine
  esr study of radicals prod. in irradiated aq. soln. of, 738; Meisenheimer complex formation w/ trinitrobenzene: evidence for intramol. H-bonding, 3636
dimethylamine-N^{15}
  ^{15}N chem. shift, 932
dimethylamine-N^{15} hydrochloride
  ^{15}N nmr, 1758
dimethylcarbamic acid, aryl ester
  activated complexes in ion fragmentation, 1903
dimethylisopropylcarbinyl radical
  see *sec*-butyl radical, 2,3-dimethyl-
dinaphtho[1,2-2′,3′]furan-7,12-dione
  absorption spectrum, 3257
dinaphtho[2,1-2′,3′]furan-8,13-dione
  absorption spectrum, 3257
dinonylnaphthalenesulfonic acid, Na salt
  competitive adsorption of PhOH and, on NiO, 1975
diols
  nmr of molten alkali acetate solns. of, 1338
diols, alkyl
  dielectric props. of four, 1240
1,4-dioxane
  adsorption from H_2O soln. onto activated carbon: exptl. and calcd. data, 3720; adsorption–desorption isotherm data for vapors on activated carbon, 3526; anion exchange in, –water solns., 93; effect on circular dichroism of lysine-rich histone f-1-DNA complexes, 1516; photolysis of gaseous, at 147 nm, 3899; reaction of recoil C atoms w/, 2248; reaction w/ H atoms: kinetic by esr, 1654; –water solns: conductivity and ionization behavior of NaCl in, 1099
1,3-dioxaphosphorinanyl derivatives
  inner-orbital photoelectron spectroscopic study—^{31}P nmr data, 3975
dioxonium ion (O_2^+)
  reaction w/ H_2 and D_2, 1426
diphenylamine
  electronic spectra, 3576
diphenylmethyl radical, perchloro-
  see methyl radical, perchlorodiphenyl-
disilane, substituted
  mass spectra of 7 cpds.: phenyl–Si interaction and Si–Si bond strength, 974
disilazane, hexamethyl-
  surface reaction w/ silica, 2181
disiloxane, hexamethyl-
  prod. of irradn. of octamethyltrisiloxane, 2430
n-dodecane
  acentric factor and entropy of vaporization, 166
dodecane, 1-chloro-
  cohesive energy, 642
dodecanenitrile
  cohesive energy, 642
dodeca-2,4,6,8,10-pentaenal
  triplet state energies and total band widths, 983
n-dodecyl hexaoxyethylene monoether
  membrane osmometry of aq. mixts., 2212
dodecylamine hydrochloride
  surface tension and critical micelle concn. of aq. solns: effect of paraffinic gases, 3000
dopamine
  zwitterion formation upon deprotonation, 2657
Dowex 50W
  spin-label investigation, 907
durene, dinitro-
  radical anion: electronic spectra and MO interpretation, 2591
duroquinol
  esr of cation radicals, 2195
dysprosate, hexachloro-; dicesium sodium salt
  thermochem., 392
dysprosium oxide (DyO)
  spectroscopy of, molecules in inert matrix, 514

n-eicosane
  acentric factor and entropy of vaporization, 166
elastin
  thermodns. of elasticity in open sys., 142
electrolytes
  conductance in CF_3CH_2OH, 1708; effect on circular dichroism of lysine-rich histone f-1-DNA complexes, 1516; enhancement of micellar catalysis, 2707; heats of mixing; temp. dependence of aq., w/ common ion, 1125; ionic entropy correlations and vol. fraction statistics in mixed solns. of, 946; ion–mol. interactions in acetone solns. of: modified CNDO method, 3581; osmotic and act. coeffs. predicted for mixed sys., 1305; theory of Onsager transport coeffs. for solns. of, 3124
electrolytes, poly-
  –salt mixtures: additivity rule, 3890
electron, ammoniated
  reaction rate w/ NH_4^+ at $-35°$, 986
electron, hydrated
  absorption spectrum in range -4 to 390°, 2798; reactivity toward aq. erythrosin, 3020; semicontinuum model, 2297
electron, solvated
  rate constants in γ radiolysis of ethanol, 2756
emulsifier
  effect of nature of, on dielectric props. of water-in-oil emulsion, 537
eosin
  chemiluminescent reaction of hydrated e^- w/ opt. excited, 764
epinephrine
  zwitterion formation upon deprotonation, 2657
erbate, hexachloro-; dicesium sodium salt
  thermochem., 392
erbium oxide (ErO)
  spectroscopy of, molecules in inert matrix, 514
erythrosin
  reactivity of H atoms and e_{aq}^- toward; X-radiolysis, 3020
ethane
  acentric factor and entropy of vaporization, 166; absorption coeff. and ionization yield at 58.4 nm, 719; anisotropic solv. shifts by factor anal., 1207; deactivation of vibrationally excited: measuring pressure dependence, 837; decompn. to

$CH_3\cdot$: comparison of RRK and RRKM theories, 1333; effect on gas-phase radiolysis of N_2O, 3178; effect on surface tension and critical micelle concn. of aq. dodecylamine·HCl solns., 2000; entropy of vaporization from Hildebrand rule, 2530; H abstraction reaction by near-thermal ^{18}F atoms, 2709; hydrophobic bonding: theory, 363; interaction virial coeffs. in binary mixts. w/ fluorocarbons, 3863; $-NF_3$ sys.: chem. HF lasers from, 284; nmr in various solvents: nature of solv. effect, 3971; photoelectron-induced decompn., 2903; prod. from CH_4 on radiolysis w/ high-intensity e^- pulses, 1164; prod. in hydrogenation of C_2H_2 on Pd: pressure jump and isotope replacement, 880; prod. in photolysis of ketene–butane mixts., 2240; prod. in radiolysis of butane, 2854; prod. in γ radiolysis of 2-propanol, 20; pyrolysis using single-pulse shock tube technique, 1492; radiolysis of, on porous glass: esr, 201; reaction w/ H atoms: kinetics by esr, 1654; reactions of fast H atoms w/, 841; second virial coeffs: exptl. and calcd. for pure and mixed sys., 3691; sys. N_2F_4–: chem. HF laser from flash photolysis of, 2546
use energy transfer in thermal isomerization of Et—N≡C, 2171

ethane, bromo-
^{13}C nmr, 3766; nmr interpretation by pattern recognition, 1402; prod. of recoil Br reaction w/ c-C_3H_6 and c-C_3H_5Br, 2698; reaction w/ H atoms: kinetics by esr, 1654

ethane, chloro-
^{13}C nmr, 331; cohesive energy, 642; reaction w/ H atoms: kinetics by esr, 1654; thermal elimination of HCl, 295

ethane, chloro-substd.
^{13}C nmr, 331

ethane, 1,1-dibromo-
^{13}C nmr, 3766

ethane, 1,1-dichloro-
^{13}C nmr, 331

ethane, 1,2-dichloro-
adsorption of, from water soln., 61; adsorption of vapor on water by glc, 3870; ^{13}C nmr, 331

ethane, 1,1-dichloro-2,2-bis(p-chlorophenyl)-
prod. of dechlorination of DDT, 2762

ethane, 1,2-dichloro-1,2-difluoro-
stereochem. of substitution of energetic T for H in *dl*- and *meso*-, 1299

ethane, 2,2-dimethoxy-
prod. in recoil C atom reaction in methanol, 2253

ethane, dimethoxy-
use esr of nitro aromatic radical anions and alkali ions, 1205

ethane, 1,1-dinitro-
nmr in various solvents, 499

ethane, fluoro-
sys. N_2F_4–: chem. HF laser from flash photolysis of, 2546

ethane, hexachloro-
^{13}C nmr, 331; prod. in radiolysis of $CHCl_3$, 2436

ethane, hexafluoro-
entropy of vaporization from Hildebrand rule, 2530; interaction virial coeffs. in binary mixts. w/ hydrocarbons, 3863

ethane, iodo-
esr of 6 isotopically different γ-irradiated cpds., 467; sys. N_2F_4–: chem. HF laser from flash photolysis of, 2546

ethane, 1-iodo-2,2-dimethoxy-
prod. in recoil C atom reaction in methanol, 2253

ethane, nitro-
excess Gibbs energy of mixing binary solns. of, by total intensity Rayleigh light scattering, 3728

ethane, pentachloro-
^{13}C nmr, 331; prod. in radiolysis of $CHCl_3$, 2436

ethane, pentafluoro-
kinetics of shock wave pyrolysis, 3493

ethane, 1,1,1,2-tetrabromo-
^{13}C nmr, 3766

ethane, 1,1,2,2-tetrabromo-
^{13}C nmr, 3766

ethane, tetrachloro-
adsorption–desorption isotherm data for vapors on activated carbon, 3526; ^{13}C nmr, 331; prod. in radiolysis of $CHCl_3$, 2436

ethane, 1,1,2,2-tetrafluoro-
shock wave thermolysis kinetics, 3195

ethane, N,N,N',N'-tetramethyldiamino-
protolysis kinetics in H_2SO_4, 2400

ethane, 1,1,2-tribromo-
^{13}C nmr, 3766

ethane, 1,1,1-trichloro-
^{13}C nmr, 331; far-ir, 2942

ethane, 1,1,1-trichloro-2,2-bis(p-chlorophenyl)-
radn. induced dechlorination, 2762

ethane, 1,1,2-trichloro-
^{13}C nmr, 331

ethane, 1,1,2-trichlorotrifluoro-
radiolysis, 2217

ethane, 1,1,1-trifluoro-
H abstraction reaction by near-thermal ^{18}F atoms, 2709; thermal decompn., 295

ethane-d_6
photoinduced decompn., 2903

ethane-2-t, 1-iodo-
self-radiolysis: growth patterns of reaction intermeds—esr of polycryst., 3359

ethanol
absorption coeff. and ionization yield at 58.4 nm, 719; adsorption on oxidized Al foil, 1887; binary solns.: viscosity coeff. data of, and diffusion coeffs. of I_2 in, 963; conductometric pulse radiolysis determination of ionic yields and neutralization kinetics, 3893; effect on epr of complex-bonded t-$BuO_2\cdot$, 2580; enthalpies of soln. in various polar solvents, 3598; esr of radical from, and CH_3NO_2 in aq. soln., 1186; far-ir of solid, 3993; gas-phase acidity, 2226; ion–molecule reactions by photoionization, 3797; kinetics of e^- exchg. between ferrocene and ferricinium ion in, 3303; nmr study of exchange of hydroxyl H catalyzed by divalent metal ions, 1994; prod. in γ radiolysis of 2-propanol, 20; radiolysis of liquid, 2756; reaction of H atoms in aq. solns. of, 449; reaction of recoil C atoms w/, 2248; reaction w/ H atoms: kinetics by esr, 1654; salt effects in aq. solns: scaled particle theory applied to salting-out polar mol., 3757; solute–solv. interactions studied by nmr 3141; yields of H_2O_2 in radiolysis of aq. solns. containing, 3950
use pulse radiolytic study of O^-, 1738

ethanol, p-*tert*-alkylphenoxy(polyethoxy)-
critical micelle concns. of several, in water–ethylene glycol mixts., 809

ethanol, 2-iodo-
prod. in recoil C atom reaction in methanol, 2253

ethanol, 2,2,2-trifluoro-
conductance of electrolytes in, 1708

ethanol-d_6
far-ir of solid, 3993

ether, bis(4-alkoxyphenyl)
esr of hydroxy- and methoxy- cpds., 411

ether, cholesteryl methyl
relaxation processes, 1237

ether, cumyl methyl
carbanions derived from: nmr, 1062

ether, ethyl
absorption coeff. and ionization yield at 58.4 nm, 719; adsorption of, from water soln., 61; $-AlI_3$ solns.: complex formation in, 282; e^- donor–acceptor complexes by glc: thermodn. study, 2632; $-I_2$ complex in vapor phase: spectral and thermodn. props., 3682; reaction of recoil C atoms w/, 2248; reaction w/ H atoms: kinetics by esr, 1654

ether, isobutyl vinyl
polymerization on porous glass: ir, 3897

ether, isopropyl
prodn. of in γ radiolysis of 2-propanol, 20; reaction of recoil C atoms w/, 2248

ether, methyl
adsorption on clean germanium surfaces, 2922

ether, methyl vinyl
dissociative e^- capture process of, in org. glasses, 476

ether, propyl
reaction of recoil C atoms w/, 2248

ether, n-propyl
adsorption of vapor on water by glc, 3870

ether, vinyl
e^- donor–acceptor complexes by glc: thermodn. study, 2632

ethers
ir study of H-bonding in solns. of HF in, 2222; reactions of recoil C atoms w/, 2248

ethyl acetate
adsorption of, from water soln., 61; adsorption–desorption isotherm data for vapors on activated carbon, 3526

ethyl radical
esr of normal and abnormal, trapped on V_2O_5 coated porous Vycor, 4064; growth and decay of, in γ-irradiated C_2H_5I and C_2D_5I, 472; prod. from n-C_4H_{10} decompn.: comparison of RRK and RRKM theories, 1333

ethyl radical, 1,2-dihydroxy-
esr in aq. fumarate soln., 2570

ethyl radical, 1-hydroxy-
esr in aq. fumarate soln., 2570

- ethyl radical, 1-hydroxy-1-methyl-
  - esr in aq. soln., 1186; H-abstraction reaction from silane in photolysis of acetone–silane mixts., 3945; kinetics of, by esr-flow techniques, 167, 1326; reactions of, formed by "Fenton-like" reagents, 3271
- ethyl xanthate
  - oxidn. of, on Pt, Au, Cu, and galena electrodes, 354
- ethylamine
  - –alkali metal metal solns.: new absorption bands, 286
- ethylamine hydrochloride, 2-mercapto-
  - oxidn. kinetics of, by $[Fe(CN)_6]^{3-}$, 2036
- ethylene
  - CO addn. to: potential energy surface for nonlinear cheletropic reaction, 340; effect on gas-phase radiolysis of N_2O, 3178; hydrogenation of, on ZnO, 208; –maleic acid copolymer–metal ion complexes: heats of assocn., 1136; negative ion formation, 2584; oxidn. over gold catalysts, 2914; photodecompn. prod. of γ-butyrolactone, 2733; photolysis at 121.6 nm, 1317; photolysis of HI and HBr in presence of, 835; prod. from CH_4 on radiolysis w/ high-intensity e pulses, 1164; prod. in hydrogenation of C_2H_2 on Pd: pressure jump and isotope replacement, 880; prod. in photolysis of c-C_4H_6, 3656; prod. in photolysis of gaseous dioxane, 3899; prod. in photolysis of ketene-butane–CO mixts., 2240; prod. in pyrolysis of ethane, 1492; prod. in radiolysis of butane, 2854; prod. in γ radiolysis of 2-propanol, 20; prod. in recoil tritium reactions w/ $(CH_3)_3SiF$, 301; prod. in thermal decompn. of 1,1,2-trimethylcyclobutane, 1437; prod. of reaction of c-C_5H_8 w/ O atoms, 3056; reaction w/ H atoms: abs. rate const., 1584; reaction w/ H atoms: kinetics by esr, 1654; reactivity w/ OH radicals, 3640; sys. $^{14}CH_3I$–: methylene reactions in photolysis of, 2536; *use* energy transfer in thermal isomerization of Et—N≡C, 2171; radiolysis of CCl_4, 24; scavenger in recoil T reaction w/ $(CHFCl)_2$, 1299
- ethylene, bromo-
  - ^{13}C nmr, 3766
- ethylene, 1-chloro-2-fluoro-
  - thermodns. of cis–trans isomerization, 1453
- ethylene, chloro-substd.
  - ^{13}C nmr, 331
- ethylene, 1,1-dibromo-
  - ^{13}C nmr, 3766
- ethylene, 1,2-dibromo-
  - ^{13}C nmr for both isomers, 3766; thermodns. of cis–trans isomerization, 1453
- ethylene, 1,1-dichloro-
  - ^{13}C nmr, 331
- ethylene, 1,2-dichloro-
  - ^{13}C nmr of *cis*- and *trans*-, 331; thermodns. of cis–trans isomerization, 1453
- ethylene, 1,1-difluoro-
  - negative ion formation, 2584; prodn. of, in thermal decompn. of CH_3CF_3, 295; quenching of excited states of C_6H_5F by, 3662
- ethylene, 1,2-diiodo-
  - thermodns. of cis–trans isomerization, 1453
- ethylene, 1,1-diphenyl-
  - carbanions derived from: nmr, 1062
- ethylene, fluoro-
  - photolysis of HI and HBr in presence of, 835
- ethylene, halo-
  - thermodns. of cis–trans isomerizations, 1453
- ethylene, polymer
  - ir spectrum of irradiated, at 4°K, 3988; mol. mechanism of chain rupture in strained cryst. polymers, 3921; radn. chem. in molten state, 1671; thermodn. and morphological props. of cryst., 3909
- ethylene, polytetrafluoro-
  - inelastic light scattering of, in liq. suspension, 789
- ethylene, tetrachloro-
  - ^{13}C nmr, 331
- ethylene, tetracyano-
  - addn. of isoprene to, 1734; anion: vibronic effects in ir spectrum of, 325; vibronic effects in ir spectrum of, 325
  - *use* radiolysis of H_2 on porous glass, 201
- ethylene, tetrafluoro-
  - photolysis of HI and HBr in presence of, 835; prod. in shock wave pyrolysis of C_2HF_5, 3493; shock tube study of C_2F_4–CF_2 equil., 1625
  - *use* radical reactions of chloroalkanes, 2075
- ethylene, tribromo-
  - ^{13}C nmr, 3766
- ethylene, trichloro-
  - ^{13}C nmr, 331; radn.-induced oxidn., 613
- ethylene, trifluoro-
  - prod. in thermal decompn. of CHF_2CHF_2, 3195
- ethylene glycol
  - conductance of tetralkylammonium halides in, 1722; effect of, on nonionic micelles, 809; glass transition temp. of aq. solns., 967, 3379; prod. from irradn. of crys. glycollic acid, 1648; reaction w/ H atoms: kinetics by esr, 1654; salt effects in aq. solns: scaled particle theory applied to salting-out polar mol., 3757
- ethylene oxide, trichloro-
  - oxidn. prod. of C_2HCl_3, 613
- ethylene sulfonate, polymer
  - site binding of counterions in solns. of: ultrasonic absorption, 3367
- ethylene-1,2-d_2
  - pyrolysis of: shock tube expts., 1
- ethylene-d_4
  - pyrolysis of: shock tube expts., 1
- ethylenediamine
  - –alkali metal solns: extinction coeffs. and equilibria, 3092
- ethylenimine polymer
  - ^{19}F nmr of conformation of a derivative of, 4061
- ethylenimine polymer hydrobromides
  - compressibility behavior, 2362; partial molar vols. and electrostriction, 2353
- europium
  - transition probabilities of, in phosphate glasses, 3980
- europium(III) ion
  - pathways of radiative and radiationless transitions in soln., 3668, 3677
- europium(III) nitrate
  - absorption and emission spectra in various solvents, 3668
- europium(III) perchlorate
  - adsorption and emission spectra in various solvents, 3668; fluorescence of $^5D_0$ level, 3677

- ferrate(II), hexacyano- ($Fe(CN)_6^{4-}$)
  - oxidn. by chloramine-T: kinetics, 838
- ferrate(II), hexacyano-; potassium salt
  - *use* pulse radiolytic study of O^-, 1738
- ferrate(III), hexacyano- ($Fe(CN)_6^{3-}$)
  - oxidn. kinetics of 2-mercaptoethylamine HCl by, 2036
- ferrate(II), oxalato-; complex ions
  - products of photolysis of ferrioxalate sys., 2897
- ferrate(III), tetrahalo-; tetraheptylammonium
  - mol. assocn. and dielectric consts. in benzene, 542
- ferrate(III), trisoxalato-; potassium
  - photochem. studies, 2986
- ferricinium ion
  - kinetics of e^- exchg. between, and ferrocene in alcohols, 3303
- ferricyanide ion
  - *see* ferrate(III), hexacyano-
- ferrioxalate system
  - *see* iron(III)–oxalate system
- ferrocene
  - kinetics of e^- exchg. reaction between, and ferricinium ion in alcohols, 3303
  - *use* scavenger in radiolysis of CCl_4, 24
- ferrocene[Fe(II)Fe(III)], bi-
  - *see* biferrocene
- ferrocenes, substituted
  - e^- transfer reactions, 3381
- ferrocyanide ion
  - *see* ferrate(II), hexacyano-
- fibrinogen
  - adsorption studied by e^- microscope, 2103; competitive adsorption of, and heparin on mica, 2107
- fluorene
  - fluorescence spectrum: effect of varied excitation, 3097; MO calcns. for excimer model, 1794; quantum yield of sensitized phosphorescence: external heavy-atom effect, 1921
- fluorescein
  - acid–base equil. of, and 2′-7′-, in their grnd. and fluorescent states, 245; chemiluminescent reaction of hydrated e^- w/ opt. excited, 764
- fluorescein, 2′,4′,5′,7′-tetraiodo-
  - *see* erythrosin
- fluoride ion
  - ionization efficiency of, emitted from CsF, 3741; pulse radiolysis in aq. solns., 3081; salts containing: enhancement of micellar catalysis, 2707
- fluorides, molten
  - coordn. effects on spectrum of U(IV) in, 631
- fluorine (F_2)
  - –CCl_2F_2 combustion reaction, 3645; –Cl_2 mixts.: explosion limits, 867; kinetics of attack of solids by, 308

fluorine, atomic
  H abstraction from alkanes by, 2070; kinetics of attack of solids by, 308
fluorine, isotope of mass 18
  near-thermal stoms: relative rates of H abstraction reactions by, 2709; substitution reactions of ^{18}F atoms w/ halomethanes: bond energy effects, 1324
fluorocarbons
  entropies of vaporization from Hildebrand rule, 2530; interaction virial coeffs. in binary mixts. w/ hydrocarbons, 3863
fluoroform
  elimination of HF from vib. excited, 2070; HF elimination laser from reaction of O(^{1}D) w/, 3642; prod. in reaction of hexafluoroazomethane–acetone mixt., 735; solv. effects on nmr spectra of, 497
formaldazine
  esr study of photolysis of, 164
formaldehyde
  photodecompn. prod. of γ-butyrolactone, 2733; prod. from irradn. of crys. glycollic acid, 1648; prod. in photolysis of gaseous dioxane, 3899; prod. in reaction of hexafluoroazomethane–acetone mixts., 735; –water sys.: mol. orbital calcns., 1744
formaldehydesulfoxalate, sodium salt
  use dye-triplet reactions w/ *p*-substd. benzenesulfinates, 3066
formaldiminoxyl radical
  esr, 2448
formamide
  flash photolysis in aq. solns., 1910; ir study of, in vapor phase and Ar matrix, 405; open trans dimer: mol. orbital calcns., 1744; pulse radiolysis, 2267; solvation studies of alkaline earth halides in, 2325
formamide, *N*,*N*-dimethyl-
  adsorption from H_2O soln. onto activated carbon: exptl. and calcd. data, 3720; enthalpy of transfer of electrolytes to propylene carbonate from, 3606; flash photolysis in aq. soln., 1910; polarographic redn. of O_2 in presence of H^+ donors, 4019; pulse radiolysis, 2267; solvation studies of alkaline earth halides in, 2325; solvation studies of lithium salts in, 3188; sys. poly-γ-benzyl-α,L-glutamate–: liq. crys.-isotropic phase equilibria, 1446
formamide, *N*-methyl-
  pulse radiolysis, 2267; solvation studies of alkaline earth halides in, 2325
formate
  yields of H_2O_2 in radiolysis of aq. solns. containing, 3950
  use chemiluminescent reaction of hydrated e$^-$, 764
formic acid
  –hydrazine binary sys.: glass transition, 1826; mol. assocn. effects on C–H nuclear dipolar relaxation rate, 2539; reaction w/ H atoms: kinetics by esr, 1654; reactivity w/ OH radicals, 3640
fumarate ion
  esr or irradiated aq. solns. of; use of, for radical trapping, 2570
fumaric acid, esters
  radical anions: photoisomerization, 482
furan
  e$^-$ donor–acceptor complexes by glc: thermodn. study, 2632
furan, 2,5-dihydro-
  e$^-$ donor–acceptor complexes by glc: thermodn. study, 2632
furan, 2-methyl-
  e$^-$ donor–acceptor complexes by glc: thermodn. study, 2632
furan, tetrahydro-
  reaction of recoil C atoms w/, 2248; reaction w/ H atoms: kinetics by esr, 1654; ultrasonic velocity in aq. solns., 2336
2-furanone
  the lactones which might be classed as furanones are found under their respective acids
furanquinones
  absorption spectra, 3257

gadolinate, hexachloro-; dicesium sodium salt
  thermochem., 392
gadolinium(III) complexes
  aquo, cacodylate, and bovine serum albumin complexes: electron spin relaxation in aq. solns., 3164
gadolinium dicarbide (GdC_2)
  dissosn. energy, 848
gadolinium oxide (GdO)
  spectroscopy of, molecules in inert matrix, 514
galena electrode
  oxidation of ethyl xanthate on, 354
gallium indium oxide (GaInO)
  infrared, 1963
gallium oxide (Ga_2O)
  infrared, 1963; vibrational analysis, 3908
gallium phosphide, electrodes
  spectral sensitization of: electrochem. study, 562
gelatin
  ultrasonic absorption due to proton transfer for solns. of, 4012
gels
  anomalous freezing behavior, 2623
germane, ethyl-
  far-ir and low freq. Raman of solid, 3993
germane, ethyltrichloro-
  far-ir and low freq. Raman of solid, 3993
germanium
  adsorption of organic gases on clean surfaces of, 2922
germanium telluride
  vaporization, 118
glass, porous
  see also Vycor, porous
  esr of atomic Ag on, 2705, 2706; polymerization of vinyl monomers by, 3897; radiolysis of hydrogenous material on: esr, 201
glass membranes
  ion-exchg. and ionic transport props. in molten salts, 2815
glucose
  use chemiluminescent reaction of hydrated e$^-$, 764
α,L-glutamate, poly-γ-benzyl-
  sys. dimethylformamide–: liq. crys.-isotropic phase equilibria, 1446
glutamic acid, polymer
  ultrasonic absorption due to proton transfer for solns. of, 4012
glycerol
  epr probe into hydrophobic interaction in aq. soln., 165; glass transition temp. of aq. solns., 967, 3379
glycine
  esr of radicals prod. in irradiated aq. solns. of, 738; reaction w/ H atoms: kinetics by esr, 1654; vol. change for neutralization: medium effects, 1120
glycine, *N*-acetyl-
  effect of, on ultrasonic absorption of protein solns., 374; esr of radicals prod. in irradiated aq. solns. of, 738; reaction w/ H atoms: kinetics by esr, 1654
glycine, di-
  effect of, on ultrasonic absorption of protein solns., 374
glycine, sodium salt
  vol. change in protonation: medium effects, 1120
glycine amide, *N*-acetyl-*N*′-methyl-
  conformational dependence of energy and partial charge, 2286
glycolaldehyde
  prod. in recoil C atom reaction in methanol, 2253
glycolate
  radical anion derived from: esr in aq. soln., 1186
glycolic acid
  radn. chem. of crys., 1648; reaction w/ H atoms: kinetics by esr, 1654
glycylglycine, *N*-methyl-*C*′-methyl-
  conformational dependence of energy and partial charge, 2286
glycylphenalanylglycine
  nmr, 505
glyoxylic acid
  esr of radicals from, in aq. soln., 1186
gold
  catalysts Au/α-Al_2O_3, Au/SiO_2, and Au sponge: oxidn. of olefins over, 2914; electrode: oxidn. of ethyl xanthate on, 354; rate of O atom and H atom interaction on, 2186; sys. Ho–Al–: equilibria involving gaseous species over, 3264
graphite
  see carbon, graphite
guaiacol
  solv. and temp. effects of ir of OH group, 2219
guanidinium chloride
  effect on circular dichroism of lysine-rich histone f-1–DNA complexes, 1516; effect of, on vol. change resulting in acid–base reaction, 1120; effects of, on water structure: heats of soln. and nmr, 815
guanidinium ion
  proton exchg. between, and H_2O in aq. dimethylacetamide by nmr, 688
guanidinium ion, diphenyl-
  dissocn. const. in isobutyl methyl ketone, 2496
guanidinium ion, tetramethyl-
  dissocn. const. in isobutyl methyl ketone, 2496
guanine, 9-ethyl-
  H-bonding of, in dimethyl sulfoxide-d_6 by nmr, 3963
gum arabic, salts
  conductivity in aq. soln., 1691

halide ions
interaction w/ organic cations studied by nuclear quadrupole relaxation, 2936; pulse radiolysis in aq. solns., 3081
halogen, atomic
potential energy surfaces for atom transfer reactions, 1844
helium
effect on thermal isomerization of C_2H_5NC, 1366; nitrogen afterflow and recombn. of N atoms in presence of, 1552; soly. in liq. Na, 2832; soly. of, in molten $NaNO_3$, 821; vibrational energy transfer w/ He, 4001
helium hydride (HeH_2)
model for study of superexchange, 1874
hemoglobin, human
ultrasonic absorption due to proton transfer for solns. of, 4012
heparin
competitive absorption of, and fibrinogen on mica, 2107
n-heptadecane
acentric factor and entropy of vaporization, 166
n-heptane
acentric factor and entropy of vaporization, 166; adsorption of vapor on water by glc, 3870; enthalpies of soln. in various polar solvents, 3598; enthalpy in methanol: solv.–isotope effect, 388; entropy of vaporization from Hildebrand rule, 2530; intrinsic viscosity of solns. containing: calcd., 3113; nmr line shape of solid, 3901; second virial coeffs: exptl. and calcd. for pure and mixed sys., 3691; soly. and activity coeffs. in liq. methane and argon, 2345; thermodns. of soln. in liq. crys. solvents, 2005
heptane, 1-chloro-
thermodns. of soln. in liq. crys. solvents, 2005
heptane, dimethyl-
thermodns. of soln. in liq. crys. solvents for various isomers, 2005
heptane, 3-ethyl-
thermodyns. of soln. in liq. crys. solvents, 2005
heptane, 2-methyl-
adsorption of vapor on water by glc, 3870
heptane, perfluoro-
entropy of vaporization from Hildebrand rule, 2530
heptanes, methyl-
equilibrium distributions of various octane isomers, 1486
heptanoic acid, tetrabutylammonium salt
thermodns. of aq. solns., 3733
2-heptanone
cohesive energy, 642
heptanones
photolysis of 1,4-dichlorobutane sensitized by 2-, 3-, and 4-, 1168
heptasiloxane, dodecamethyl-
prod. of irradn of octamethyltrisiloxane, 2430
1-heptene
second virial coeffs: exptl. and calcd. for pure and mixed sys., 3691; thermodyns. of soln. in liq. crys. solvents, 2005
n-hexadecane
acentric factor and entropy of vaporization, 166
n-hexadecane
bubble nucleation, 3613
n-hexadecyl nonaoxyethylene monoether
membrane osmometry of aq. mixts., 2212
hexadecylsulfonic acid, sodium salt
micellar effects on triethylamine–SO_3 hydrolysis, 1763
hexamethylenetetramine
Debye temp., 1073; sys. H_2O–: thermodn. data, 3633
hexamethylphosphorotriamide
see phosphorotriamide, hexamethyl-
n-hexane
acentric factor and entropy of vaporization, 166; adsorption–desorption isotherm data for vapors on activated carbon, 3526; adsorption of vapor on water by glc, 3870; bubble nucleation, 3613; enthalpies of soln. in various polar solvents, 3598; enthalpy in methanol: solv.–isotope effect, 388; entropy of vaporization from Hildebrand rule, 2530; –ethanol mixts.: viscosity coeff. data of, and diffusion coeffs. of I_2 in, 963; induction energy for, in Apiezon M estimated by glc, 831; interaction virial coeffs. in binary mixts. w/ fluorocarbons, 3863; reaction w/ H atoms: kinetics by esr, 1654; soly. and activity coeffs. in liq. methane and argon, 2345
use energy transfer in thermal isomerization of Et—N≡C, 2171
hexane, 1-bromo-
thermodns. of soln. in liq. crys. solvents, 2005
hexane, 1-chloro-
cohesive energy, 642; thermodns. of soln. in liq. crys. solvents, 2005
hexane, 1,6-dibromo-
dielectric relaxation in benzene soln., 2616
hexane, dimethyl-
equilibrium distributions of various octane isomers, 1486
hexane, 2,4-dimethyl-
adsorption of vapor on water by glc, 3870
hexane, 3,4-dimethyl-
prod. in photolysis of ketene–butane mixts., 2240
hexane, 1-iodo-
thermodns. of soln. in liq. crys. solvents, 2005
hexane, 3-methyl-
acentric factor and entropy of vaporization, 166; soly. and activity coeffs. in liq. methane and argon, 2345
hexane, perfluoro-
entropy of vaporization from Hildebrand rule, 2530; interaction virial coeffs. in binary mixts. w/ hydrocarbons, 3863; second virial coeffs: exptl. and calcd. for pure and mixed sys., 3691
n-hexane-^{14}C
vapor–liq. equil. of binary mixts. of, w/ ketones, 4041
1,3-hexanediol, 2-ethyl-
dielectric props., 1240
hexanenitrile
cohesive energy, 642; induction energy for, in Apiezon M estimated by glc, 831
hexanes
prod. in recoil ^{11}C reactions w/ C_5 hydrocarbons, 3201
hexanoic acid
reaction w/ H atoms: kinetics by esr, 1654
hexanoic acid, *p*-(*p*-ethoxyphenylazo)phenyl ester
proton spin–lattice relaxation, 2452
hexanoic acid, tetrabutylammonium salt
thermodns. of aq. solns., 3733
1-hexanol
enthalpies of soln. in various polar solvents, 3598; gas-phase acidity, 2226; reaction w/ H atoms: kinetics by esr, 1654
hexanone
photolysis of 1,4-dichlorobutane sensitized by 2-, and 3-, 1168
1-hexene
use energy transfer in thermal isomerization of Et—N≡C, 2171
hexogen
see *s*-triazine, 1,3,5-trinitrohexahydro-
n-hexyl radical
decay of, in γ-irradiated $C_6H_{13}I$, 472; decompn. to *sec*-hexyl rad.: comparison of RRK and RRKM theories, 1333
sec-hexyl radical
prod. from *n*-hexyl rad.: comparison of RRK and RRKM theories, 1333
holmium
sys. Al–Au–Ho and Ag–Ho: equilibria involving gaseous species over, 3264
holmium gold (HoAu)
mass spec. determination of dissocn. energy, 3264
holmium oxide (HoO)
spectroscopy of, molecules in inert matrix, 514
holmium silver (HoAg)
mass spec. determination of dissocn. energy, 3264
hydrazine
decompn. by e^- impact, 769; epr of cation radicals from, 2048; –protonic acid binary sys.: glass transitions, 1826
hydrazine, 1,1-dimethyl-
esr of cation radicals from, 2043, 2048
hydrazine, 1,2-dimethyl-
epr of cation radicals from, 2048
hydrazine, 1,2-diphenyl-
see hydrazobenzene
hydrazine, methyl-
epr of cation radicals from, 2048; esr of cation radicals from, 2043
hydrazine, tetrafluoro-
flash-photolyzed mixts. of, w/ various hydrogen sources, 2546
use CH_3NF_2 degydrofluorination kinetics, 1170
hydrazobenzene
photoredn. of dinitrobenzene sensitized by chlorophyll–poly(vinylpyridine) complex, 1667
hydrazoic acid
acid dissocn.–ion recombn. equilibrium: specific rates, 3026
hydrazyl, diphenylpicryl-
use scavenger in radiolysis of CCl_4, 24
hydrobromonium ion (HBr^+)
predissocn. and dissocn. energy, 1472

hydrocarbons
  see also *n*-alkanes, *n*-alkenes, and olefins
  acentric factor and entropy of vaporization, 166; effect on gas-phase radiolysis of N_2O, 3178; enthalpies of soln. in various polar solvents, 3598; interaction virial coeffs. in binary mixts. fluorocarbons, 3863; recoil ^{11}C reactions in C_5, 3201; theory of hydrophobic bonding, 363
hydrogen
  –deuterium exchange of benzene at fuel cell electrode: effect of adsorption potential, 3715; displacement in butane by fast T_2 and T_2^+ collisions, 2417; exchange photoinduced in *p*-hydroquinone, 1775
hydrogen (H_2)
  absorption coeff. and ionization yield at 58.4 nm, 719; binding states of, on (100) plane of Mo, 227; –Br_2 laminar flame: recombn. of Br atoms in, 3046; dynamics of reaction w/ O_2^+, 1426; energy transfer efficiency in thermal isomerization of C_2H_5NC, 3037; formation of primary yields of, in ν-radiolysis of neutral aq. solns., 3950; H abstraction reaction by near-thermal ^{18}F atoms, 2709; HD self-exchange: dynamic sampling of reflected shock zone, 2541; hydrogenation of C_2H_2 on Pd: pressure jump and isotope replacement, 850; hydrogenation of C_2H_4 on ZnO, 208; initiation rate for shock-heated mixts. of O_2–CO–Ar–, 1504; –NF_3 sys.: chem. HF lasers from, 284; potential energy surfaces for atom transfer reactions, 1844; prod. in photolysis of c-C_4H_6, 3656; prod. in photolysis of gaseous dioxane, 3899; prod. in γ-radiolysis of 2-propanol, 20; promotion of Pd-catalyzed CO oxidn., 2065; rate of exchange of, and D_2 behind reflected shock waves, 1615; scavenging of, yield from H_2 irradiated w/ T β particles, 601; second virial coeffs: exptl. and calcd. for pure and mixed sys., 3691; vibrational energy transfer w/ He, 4001; yields in γ-radiolysis of ethanol, 2756; yields of, from solns. of N_2O in γ-irradiated c-C_5H_{10}), 2560
hydrogen, atomic
  addn. reactions w/ olefins: rate consts. by mass spec., 1601; epr study of, trapped in γ-irradiated calcium phosphates, 1936; esr in aq. fumarate soln., 2570; potential energy surfaces for atom transfer reactions, 1844; prodn. of, in flash photolysis of ice, 40; radiation chem. of aq. solns.: contribution of, to G_{H_2}, 31; rate of interaction w/ Au, 2186; reaction of fast, w/ ethane, 841; reaction of, in aq. solns.: rate consts., 449; reaction w/ cyanogen: photometric and mass spec. observations, 2662; reactions w/ HI and HBr: relative rates, 835; reaction w/ HNO_3: mass spec. study, 3193; reaction w/ olefins: absolute rate consts., 1584; reaction w/ ONCL: mass spect. study, 722; reaction w/ organic cpds. in aq. soln. by esr, 1654; reactivity toward aq. erythrosin, 3020
hydrogen bromide
  cation derived from: predissocn. and dissocn. energy of HBr^+, 1472; –hydrazine binary sys.: glass transitions, 1826; recombn. of Br atoms w/, 3046; relative rate of reaction of H atoms w/ HI and, 835; vibrational relaxation: vibration-to-rotation energy transfer, 1079
hydrogen chloride
  –alkaline earth perchlorate mixts.: act. coeffs., 1305; –D_2 exchange kinetics, 1615; elimination of, from chloroalkanes, 2231; exchange of, and D_2, 171; –hydrazine binary sys.: glass transitions, 1826; ir chemiluminescence from, produced in 3-centered reactions, 2070; Onsager transport coeffs. for aq. solns. of: comparison of exptl. and theory, 3124; radiolysis of, on porous glass: esr, 201; sys. CsCl–$BaCl_2$–: osmotic and act. coeffs. predicted, 1305; sys. KCl–H_2O–: heats of mixing, 1125; sys. N_2F_4–: chem. HF laser from flash photolysis of, 2546; transport through cation-exchg. membranes; noise sepctra, 654; vibrational relaxation by Cl atoms and Cl_2, 1622; vibrational relaxation: vibration-to-rotation energy transfer, 1079
  use e^- scavenging efficiency in aq. solns., 1941; recombination luminescence of tryptophan, 2887
hydrogen cyanide
  –D_2 exchange kinetics, 1615; energy transfer efficiency in thermal isomerization of C_2H_5NC, 3037; prod. in decompn. of CH_3-NF_2, 1170; relative total scattering cross section, 727
hydrogen fluoride
  chemical, elimination lasers from $O(^1D)$ atom reactions, 3642; chem. lasers from flash photolysis of various N_2F_4 + RH sys., 2546; chemical lasers from NH_3 sys., 284; elimination from C_2HF_5, 3493; elimination of, from CHF_2CHF_2, 3195; ir chemiluminescence from, produced in 3-centered reactions, 2070; ir study of H-bonding in solns. containing, 2222; kinetics of expulsion of, from methyldifluoramine, 1170; prodn. of, in thermal decompn. of CH_3CF_3, 295
hydrogen halides
  potential energy surfaces for atom transfer reactions, 1844; vibrational relaxation: vibration-to-rotation energy transfer, 1079
hydrogen iodide
  H abstraction reaction by near-thermal ^{18}F atoms, 2709; reaction rate w/ H atoms relative to HBr, 835; vibrational relaxation: vibration-to-rotation energy transfer, 1079
  use scavenger in reaction of ^{18}F atoms w/ halomethane, 1324
hydrogen ion
  competition for e_{aq}^- between e_{aq}^- scavengers, 3626; exchange in aq. urea solns., 2123; –Na^+ exchange of α-zirconium phosphate: thermodn. treatment, 3750; transport across cation-exchg. membrane; noise spectra, 654
hydrogen peroxide
  enthalpy of transfer of NaCl from water to aq., 2229; formation of primary yields of, in γ-radiolysis of neutral aq. solns., 3950; formation upon oxidn. of oxalic acid in presence and absence of O_2 and Mn(II), 3343; influence on spectral sensitization of GaP electrodes, 562; prodn. of, in flash photolysis of ice, 40; reaction w/ Fe^{2+}, Cr^{2+}, V^{4+}, and Ti^{3+} in presence of 2-propanol, 3271; reactions w/ acetone, 3004; redn. of Ce^{IV} by, 250; sys. containing: short-lived radicals generated by fast flow techniques, 2957
  use e^- scavenging efficiency in aq. solns., 1941; epr of hydrazines, 2048
hydrogen sulfide
  use reactions of recoil T atoms w/ 1-butene and (*Z*)-2-butene, 3771; recoil tritium reactions w/ cyclobutane, 3781; scavenger in recoil T reaction w/ $(CHFCl)_2$, 1299
hydrogen-d_1
  dynamic sampling of, self-exchange behind reflected shock waves, 2541; prod. in the reaction of fast D atoms w/ C_2H_6, 841; self-exchange reaction: dynamic sampling of reflected shock zone, 2541
hydrogen sulfide-d_2
  photolysis of c-C_4H_6 in presence of, 3656
p-hydroquinone
  esr of cation radicals, 2195; nmr of molten alkali acetate solns. of, 1338; role of singlet and triplet states in arom. substitution reactions, 1775
hydroxide ion
  ionic radius from scaled particle theory of salt effect, 2809; radn. chem. yield by conductometric pulse radiolysis, 1759
hydroxyapatites, calcium and strontium
  nature of deficiency in nonstoichiometry: catalytic activity 3167; spectroscopic studies, 3172
hydroxycyclohexadienyl radicals
  esr of, derived from C_6H_6 and benzoate ion, 1186
hydroxyl radical
  decay kinetics, 1593; esr in aq. fumarate soln., 2570; prod. in flash photolysis of aq. ClO_3^-, 2177; prodn. of, in flash photolysis of ice, 40; reactivity w/ olefins, 3640
hyperoxide ion (O_2^-)
  esr of, on Y-type zeolites, 1165; observed in esr studies of ZnO_2 and ZnO, 3089
hypophosphorous acid
  oxidn. by vanadium(V), 891
hypoxanthine
  complexes w/ Ni^{2+}: relaxation spectra, 799

imidazole
  vol. change in protonation: medium effects, 1120
iminodiacetic acid
  esr of radical prod. in irradiated aq. soln. of, 738
indium gallium oxide (InGaO)
  infrared, 1963
indium oxide (In_2O)
  infrared, 1963; vibrational analysis, 3908
indole derivatives
  environmental effects on deprotonation of, 3061
iodate ion
  reduction to iodite by Br^- in presence of phenol, 2516
iodide ion
  effect on circular dichroism of lysine-rich histone f-1-DNA complexes, 1516; –iodine–amylose reaction: kinetics, 272; ionization efficiency of, emitted from CsI, 3741; pulse radiolysis in aq. solns., 3081; self-diffusion in gels, 1821; viscosity coeffs., B_η, in various solvents, 2532; yields of H_2 in radiolysis of aq. solns. containing, 3950
  use pulse radiolytic study of O^-, 1738
iodine (I_2)
  –amylose reaction: kinetics, 272; diffusion coeffs. of, in binary solns., 963; –ethyl ether complex in vapor phase: spectral and thermodn. props., 3682; mol. complexes w/ heterocyclic diazine *N*-oxides, 2504; photochem. induced isotopic exchange between PhI and, using $I^{131}I$, 3350; photolysis of HI and HBr in pres-

ence of, 835; scavenger in reaction of hot T w/ n-C_4H_{10}: temp. dependence, 3042; vapor phase charge-transfer complexes w/ diethyl sulfide, 1057
use effect on self-radiolysis of C_2H_4TI, 3359; reactions of recoil C atoms in MeOH, 2253; scavenger in recoil T reactions w/ CH_3F, 1290; scavenger in recoil T reaction w/ $(CHFCl)_2$, 1299; scavenger in radiolysis of CCl_4, 24
iodine, atomic
potential energy surfaces for atom transfer reactions, 1844
iodine, isotope of mass 128
radiative neutron capture induced reactions of, w/ olefins, 2880
iodine, isotope of mass 129
Mössbauer studies of chem. effects of nuclear transformations in Te cpds., 2867
iodine, isotope of mass 131
photochem, induced isotopic exchange between PhI and mol. iodine, 3350
iodite
prod. in reduction of iodate by Br^- in presence of phenol, 2516
iodoform
nmr in various solvents: nature of solv. effect, 3971
ion-exchange membranes
validity of a simple theory for transport in, 3015
ion-exchange resins
low-freq. dielectric dispersion in suspension of, 1091; magnetic moments of paramagnetic ions using, 2981; nmr study of macroreticular and carboxylic acid resins, 1211; spin-label investigation, 907; thermodn. theory of ion-exchng. equilibira in noneq. solv., 1152
iron
anodic film growth on: ellipsometric study, 2823; reaction w/ HCl in H_2O and D_2O, 2112
iron(II) aquo complexes
correlation of heterogeneous charge-transfer rate consts., 2640
iron hydroxide $[Fe(OH)_2]$
anodic film growth of the prepassive film growth on Fe, 2823
iron ion (Fe^{2+})
catalysis of exchange of ethanol hydroxyl proton, 1994; magnetic moment using ion-exchange resin, 2981; reaction w/ H_2O_2 in presence of 2-propanol using esr flow technique, 3271
use pulse radiolytic study of O^-, 1738
iron ion (Fe^{3+})
kinetics of hydrolysis in dil. aq. soln., 929; reactions at high ionic strengths: $FeCl^{2+}$ equilibrium, 1113; reactions w/ organic radicals formed by "Fenton-like" reagents, 3271; secondary redn. by oxalate radical anion 2897
iron(III), monochloro- $(FeCl^{2+})$
formation and dissocn., 1113
iron oxide (Fe_2O_3)
photoassisted dissocn. of N_2O over, 617; prod. by freeze-dried $FeSO_4$ decompn., 1179
iron oxide sulfate $(Fe_2O_2SO_4)$
intermed. in decompn. of $FeSO_4$, 1179
iron perchlorate $[Fe(ClO_4)_3]$
dil. aq. solns. of, studied by electric field jump relaxation kinetics, 929
iron sulfate $(FeSO_4)$
freeze-dried: decompn. kinetics 1179
use dye-triplet reactions w/ p-substd. benzenesulfinates, 3066
iron(II), tris(1,10-phenanthroline)-; ion
kinetic study of reaction w/ MnO_4^-, 1107
iron(III)-oxalate system
photochem., 2897
isobutane
prod. in photolysis of CH_2N_2-propane mixts., 1537; prod. in photolysis of di-*tert*-butyl peroxide, 3651; reaction w/ H atoms: kinetics by esr, 1654
use reaction of t-$C_4H_9^+$ w/ benzyl acetate, 590
isobutyl alcohol
–o-dichlorobenzene mixts: mol. assocn. in, by dielectric consts., 2133; reaction of H atoms in aq. solns. of, 449; reaction of recoil C atoms w/, 2248
isobutyl radical
equilibrium conformation and rotational barrier by esr, 3438
isobutylamine
self-assocn. by nmr, 938
isobutylene
induction energy for, in Apiezon M estimated by glc, 831; prod. in thermal decompn. of 1,1,2-trimethylcyclobutane, 1437; reaction w/ H atoms: abs. rate const., 1584, 1601; reactivity w/ OH radicals, 3640
isobutyric acid
reaction w/ H atoms: kinetics by esr, 1654
isobutyric acid, α-amino-
esr of radicals prod. in irradiated aq. solns. of, 738; reaction w/ H atoms: kinetics by esr, 1654
isobutyronitrile
see propiononitrile, 2-methyl-
isocyanatoalkyl radicals
esr, 1893
isocyanic acid
mass spectrum, 1532
isocyanic acid, methyl and ethyl esters
esr of radicals derived from, 1893
isocyanide, ethyl
energy transfer in thermal isomerization, 1366, 3037; photochem. behavior, 580; thermal isomerization of; effect of n-alkanes and alkenes, 2171
isocyanide, methyl
photochem. behavior, 580; relative total scattering of molecules *vs.*, 727
isocyanide, phenyl
photochem. behavior, 580
isooctane
adsorption of vapor on water by glc, 3870; adsorption–desorption isotherm data for vapors on activated carbon, 3526; soly. and activity coeffs. in liq. methane and argon, 2345
isopentane
entropy of vaporization from Hildebrand rule, 2530; prod. in photolysis of ketene-butane-CO mixts., 2240; recoil ^{11}C reactions w/, 3201; soly. and activity coeffs. in liq. methane and argon, 2345
isopentane, perfluoro-
entropy of vaporization from Hildebrand rule, 2530
isoprene
addn. to tetracyanoethylene, 1734
isopropoxyl radical
esr in aq. soln., 1186
isopropyl alcohol
see 2-propanol
isopropyl alcohol radical
see ethyl radical, 1-hydroxy-1-methyl-
isoquinoline
singlet → triplet intersys. crossing quantum yield, 2083

ketene
–butane mixts: photolysis w/ and w/o added CO, 2240
ketones, aliphatic
photolysis of 1,4-dichlorobutane sensitized by, 1168; vapor–liq. equil. of binary mixts. of n-hexane-^{14}C w/, 4041
ketones, cyclic
fluorescence decay times in gas phase, 989
krypton
effect on thermal isomerization of C_2H_5NC, 1366

lactic acid
reaction w/ H atoms: kinetics by esr, 1654
β-lactoglobuline
ultrasonic absorption of solns. of, 374
lanthanate, hexachloro-; dicesium sodium salt
thermochem., 392
lanthanum
soly. in LaF_3, 2340
lanthanum chloride $(LaCl_3)$
ion-pair formation and mutual diffusion in aq. soln., 663
lanthanum fluoride (LaF_3)
soly. of liq. La in, 2340; vaporization and mass spec. data, 108
lanthanum fluoride (La_2F_6)
stability of the gas, 108
lanthanum oxide (LaO)
low-lying electronic states, 3103
latex, monodisperse
diffraction of light by nonaq. suspensions of, 1881
lauronitrile
see dodecanenitrile
lead
vapor: rate of oxidn., 2259
lead chromate $(PbCrO_4)$
exchange of chromate between fresh ppt. of, and soln. containing $^{51}CrO_4^{2-}$, 350
lead oxide (PbO_2)
prod. in oxidn. of Pb vapor, 2259
lead sulfide
electrode: oxidn. of ethyl xanthate on, 354
lead telluride (PbTe)
vaporization, 118
leucoerythrosin
prod. of prolonged irradn. of erythrosin, 3020

liquid crystals, nematic
  nuclear spin relaxation, 2452
lithium
  matrix reactions w/ fluorohalomethanes, 3235; uv irradn. of, in 3-methylpentane matrix: esr, 35
lithium acetate
  –*N*-methylacetamide solns: freezing pts. and osmotic and activity coeffs., 2319
lithium albuminum fluoride ($LiAlF_4$)
  ir of matrix isolated, 2609
lithium bromide
  activity coeff. *vs.* concentration: comparison of theory and exptl., 3790; heat of dilution, 3317; –*N*-methylacetamide solns: freezing pts., osmotic coeffs., and act. coeffs., 2313
lithium carbonate
  dynamic method of measuring decompn. press., 721
lithium chlorate
  laser Raman spectrum of molten and of aq. solns., 2948
lithium chloride
  activity coeff. *vs.* concentration: comparison of theory and exptl., 3790; conductance in CF_3CH_2OH, 1708; conductance in 1-propanol–acetone mixts., 1714; effect on circular dichroism of lysine-rich histone f-1–DNA complexes, 1516; effect on micellar catalysis, 2707; heat of dilution, 3317; ion pair: assocn. const. of H_2O w/, in propylene carbonate by nmr, 1477; –*N*-methylacetamide solns: freezing pts., osmotic coeffs., and act. coeffs. 2313; Onsager transport coeffs. in solns. of: comparison of exptl. and theory, 3124; osmotic coeffs. of 1 *M* soln., 3723; sys. CsCl–H_2O–: heats of mixing, 1125; sys. H_2O–$LiNO_3$–: volume fraction statistics, 946; sys. NaCl–$BaCl_2$–: osmotic and act. coeffs., 1305; sys. NaCl–CsCl–: osmotic and act. coeffs., 1305; sys. NaCl–KCl–: osmotic and act. coeffs., 1305
  use salt effects in Raman study of bisulfate–sulfate sys., 2681
lithium deuteride
  cohesive energy, 1251
lithium fluoride
  –BeF_2 molten soln.: coordn. effects on spectrum of U(IV) in, 631; sys. $^4LiF + AlF_3$ or $^6LiF + AlF_3$: ir, 2609; vaporization studies of single crys., 4049
lithium formate
  –*N*-methylacetamide solns: freezing pts. and osmotic and activity coeffs., 2319
lithium halide
  heats of dilution, 3317
lithium hydride
  cohesive energy: isotopic substitution effect, 1251; dimer: Rittner ionic model study, 984
lithium hydroxide
  formation of O_3^- in γ-irradiated aq. solns. of, 3030
lithium iodide
  activity coeff. *vs.* concentration: comparison of theory and exptl., 3790; heat of dilution, 3317; ion–mol. interactions in acetone solns. of: modified CNDO method, 3581
lithium ion
  assocn. const. of H_2O w/, in propylene carbonate by nmr, 1477; enthalpies of transfer to propylene carbonate from methanol or dimethylformamide, 3606; exchange between nitrate melt and potassium zeolite A, 2523; –Na^+ ion-exchg. and ionic transport props. of glass membranes, 2821; –nitroaromatic radical anion clusters; esr, 1205; viscosity coeffs., B_η, in various solvents, 2532
lithium nitrate
  corresponding states and glass transition, 2306; –*N*-methylacetamide solns: freezing pts., osmotic coeffs, and act. coeffs. 2313; nmr of molten, –KNO_3 solns. of pentaerythritol, 1338; sys. H_2O–LiCl–: volume fraction statistics, 946
lithium perchlorate
  conductance and assocn. behavior in H_2O at 25°, 3290; ion–mol. interactions in acetone solns. of: modified CNDO method, 3581; solvation studies in dimethylformamide, 3188
lithium propionate
  –*N*-methylacetamide solns: freezing pts. and osmotic and activity coeffs., 3219
lithium salts
  ionic solvation in acetone: spectroscopic studies, 56
lithium tetraphenylborate
  ionic solvation in acetone: spectroscopic study, 56
lutetate, hexachloro-; dicesium sodium salt
  thermochem., 392
lutetium oxide (LuO)
  spectroscopy of, molecules in inert matrix, 514
lutidinium bromide
  interaction w/ halide ions studied by nuclear quadrupole relaxation, 2936
lysine, poly-
  ultrasonic absorption due to proton transfer for solns. of, 4012
lysine-rich histone f-1
  –deoxyribonucleic acid complexes: effect of salts on circular dichroism, 1516
lysozyme
  ultrasonic absorption of solns. of, 374

magnesium
  soly. of liq., in MgF_2, 2340; uv irradn. of, in 3-methylpentane matrix: esr, 35
magnesium *m*-benzenedisulfonate
  outer-sphere assocn. kinetics in MeOH by ultrasonic relaxation, 2649
magnesium chloride
  effect of circular dichroism of lysine-rich histone f-1–DNA complexes, 1516
magnesium fluoride
  soly. of liq. Mg in, 2340
magnesium halide
  –potassium halide melts: Raman spectra, 155
magnesium ion (Mg^{2+})
  catalysis of exchange of ethanol hydroxyl proton, 1994; in sea water by difference chromatography, 1418
magnesium oxide (MgO)
  decompn. of $HClO_4$ over, 491; radiolysis of hydrogenous material on: esr, 201
magnesium perchlorate
  –HCl mixts.: act. coeffs., 1305
magnesium stearate
  effect on dielectric props. of water-in-oil emulsions, 537
magnesium sulfate
  ion-pair formation and mutual diffusion in aq. soln., 663
maleic acid
  –ethylene copolymer–metal ion complexes: heats of assocn., 1136
maleic acid, esters
  radical anions: photoisomerization, 482
malic acid
  prod. from irradn. of crys. glycollic acid, 1648
malonate
  radical anion derived from: esr in aq. soln., 1186
malonic acid
  reaction of H atoms in aq. solns. of, 449; reaction w/ H atoms: kinetics by esr, 1654
malonic acid, diethyl-
  use reversible hydration of pyruvate esters, 792
malonic acid, monopotassium salt
  esr and endor studies of radical pair formation in, 3426
manganese
  –Cu catalyst alloy: effect on diamond-forming reaction, 2158; –Ni catalyst alloys: effect on diamond-forming reaction, 2158
manganese(II)
  H_2O_2 formation upon oxidn. of oxalic acid in presence and absence of, 3343
manganese(VII)
  oxidn. of oxalic acid by, in presence and absence of O_2 and Mn(II), 3343
manganese(II) adenosine triphosphate complex
  epr in frozen aq. soln., 1202
manganese(II) aquo complexes
  correlation of heterogeneous charge-transfer rate consts., 2640
manganese(II) *m*-benzenedisulfonate
  outer-sphere assocn. kinetics in MeOH by ultrasonic relaxation, 2649
manganese chloride ($MnCl_2$)
  epr of frozen aq. soln., 1202
manganese ion (Mn^{2+})
  catalysis of exchange of ethanol hydroxyl proton, 1994; –C_2H_4–maleic acid copolymer complexes: heats of assocn., 1136; comparative ligand field studies of spectra of, 435; magnetic moment using ion-exchange resin, 2981
mercury
  effect of, on photolysis of trifluoroacetone, 439; electrosorption of 5-chloro-1-pentanol on, 1698; xenon adsorption on: virial treatment, 344
mercury, (bromodichloromethyl)phenyl-
  matrix-isolation study of pyrolysis: ir, 3984
mercury, (chlorodibromomethyl)phenyl-
  matrix-isolation study of pyrolysis: ir, 3984
mesitylene
  adsorption on Cu(II) montmorillonite: spectroscopic study, 3957; excess Gibbs energy of mixing w/ nitroalkanes by total intensity Rayleigh light scattering at 30°, 3728; far-ir, 2942;

π H-bonding w/ naphthylamine, 2404; ignition of, $-O_2$ mixts. by shock waves, 1501

mesitylene, dinitro-
  anion radical: electronic spectra and MO interpretation, 2591

mesitylene, nitro-
  anion radical: electronic spectra and MO interpretation, 2591

metaphosphate
  transition probabilities of Eu in, glasses, 3980

metatelluric acid, poly-
  see telluric acid $(H_2TeO_4)_n$

methacrylic acid, polymer
  mean molal activity coeff. at various degrees of neutralization, 2144; proton-transfer reactions of, 267

methane
  absorption coeff. and ionization yield at 58.4 nm, 719; anisotropic solv. shifts by factor anal., 1207; enthalpy of soln. in aq. alkylammonium bromide solns., 2330; entropy of vaporization from Hildebrand rule, 2530; H abstraction reaction by near-thermal ^{18}F atoms, 2709; Hg-sensitized photodecompn. in presence of, and CO, 3205; hydrophobic bonding: theory, 363; interaction virial coeffs. in binary mixts. w/ fluorocarbons, 3863; isotope effects in substitution reaction of 2.8-eV T atoms w/, 1283; liquid: soly. of hydrocarbons and CO_2 in, 2345; low-energy electron radiolysis, 2405; nmr in various solvents: nature of solv. effect, 3971; prod. in photolysis of di-*tert*-butyl peroxide, 3651; prod. of radiolysis of butane, 2854; prod. of γ radiolysis of 2-propanol, 20; prod. of recoil tritium reactions w/ $(CH_3)_3SiF$, 301; radiolysis of, on porous glass: esr, 201; radiolysis w/ high-intensity e^- pulses, 1164; reaction w/ H atoms: kinetics by esr, 1654; salting-out consts. for tetraalkylammonium bromide solns., 1803; second virial coeffs: exptl. and calcd. for pure and mixed sys., 3691; sys. N_2F_4-: chem. HF laser from flash photolysis of, 2546
  use competitive expts. in recoil tritium reactions w/ cyclobutane, 3781; energy transfer in thermal isomerization of Et—N≡C, 2171; photolysis of CH_2N_2–propane mixts., 1537; spectrum of matrix-isolated CS_2, 2204

methane, bromo-
  adsorption on clean germanium surfaces, 2922; ^{13}C spin–lattice relaxation time: effect of field-dependent relaxation mechanisms, 3967; nmr in various solvents: nature of solv. effect, 3971; prod. of recoil Br reaction w/ c-C_3H_6 and c-C_3H_5Br, 2698; prod. of recoil tritium reactions w/ $(CH_3)_3SiF_3$, 301; substitution reaction by recoil T atoms: chem. factors controlling yield, 1290; substitution reaction of ^{18}F atoms: bond energy effects, 1324; sys. N_2F_4-: chem. HF laser from flash photolysis of, 2546

methane, bromochloro-
  matrix reactions w/ Li: ir, 3235

methane, bromochloro(perchlorodiphenyl)-
  X-ray anal. of disordered mixed crys. containing, 1246

methane, bromofluoro-
  matrix reactions w/ Li: ir, 3235

methane, bromotrichloro-
  use radiolysis of CCl_4, 24

methane, chloro-
  adsorption on clean germanium surfaces, 2922; atom abstraction from, by fluoroalkyl radicals, 2075; cohesive energy, 642; nmr in various solvents: nature of solv. effect, 3971; radn. chem. in aq. soln., 455; reaction w/ H atoms: kinetics by esr, 1654; substitution reaction by recoil T atoms: chem. factors controlling yield, 1290; substitution reaction of ^{18}F atoms: bond energy effects, 1324
  use radiolysis of CCl_4, 24

methane, chloro(perchlorodiphenyl)-
  X-ray anal. of disordered mixed crys. containing, 1246

methane, chlorotrifluoro-
  radn. chem. in aq. soln., 455; reaction w/ H atoms: kinetics by esr, 1654; replacement reactions of hot Cl atoms, 2685

methane, dibromo-
  ^{13}C spin–lattice relaxation time: effect of field-dependent relaxation mechanisms, 3967; nmr in various solvents: nature of solv. effect, 3971

methane, dichloro-
  adsorption of, from water soln., 61; atom abstraction from, by fluoroalkyl radicals, 2075; ^{13}C spin-lattice relaxation time: effect of field-dependent relaxation mechanisms, 3967; CIDNP during photolysis of mixts. containing, 3410; nmr in various solvents: nature of solv. effect, 3971; prod. in radiolysis of $CHCl_3$, 2436; reaction w/ H atoms: kinetics by esr, 1654
  use radiolysis of CCl_4, 24

methane, dichlorodifluoro-
  $-F_2$ combustion reaction, 3645; radn. chem. in aq. soln., 455; reaction w/ H atoms: kinetics by esr, 1654; replacement reactions of hot Cl atoms, 2685

methane, dichlorofluoro-
  elimination of HX from vib. excited, 2070

methane, difluoro-
  HF elimination laser from reaction of $O(^1D)$ w/, 3642; sys. N_2F_4-: chem. HF laser from flash photolysis of, 2546

methane, diiodo-
  ^{13}C spin–lattice relaxation time: effect of field-dependent relaxation mechanisms, 3967; nmr in various solvents: nature of solv. effect, 3971

methane, diphenyl-
  product of reaction of energetic ^{14}C ions w/ solid benzene, 2555

methane, fluoro-
  HF elimination laser from reaction of $O(^1D)$ w/, 3642; isotope effects of (n,γ)-activated Br reactions in gaseous, and CD_3F, 2072; substitution reaction by recoil T atoms: chem. factors controlling yield, 1290; substitution reaction of ^{18}F atoms: bond energy effects, 1324; sys. N_2F_4-: chem. HF laser from flash photolysis of, 2546

methane, fluorotrichloro-
  prod. in $CCl_2F_2 + F_2$ combustion reaction, 3645; reaction w/ H atoms: kinetics by esr, 1654; replacement reactions of hot Cl atoms, 2685

methane, halo-
  ^{13}C spin–lattice relaxation time: effect of field-dependent relaxation mechanisms, 3967; elimination of HX from vib. excited 2070; nmr in various solvents: nature of solv. effect, 3971; substitution reactions by recoil T atoms: chem. factors controlling yields, 1290; substitution reactions of ^{18}F atoms: bond energy effects, 1324

methane, iodo-
  ^{13}C spin–lattice relaxation time: effect of field-dependent relaxation mechanisms, 3967; CIDNP during photolysis of mixts. containing, 3410; far-ir, 2942; methylene reactions in photolytic sys. containing, 2536; nmr in various solvents: nature of solv. effect, 3971; reaction w/ H atoms: kinetics by esr, 1654; substitution reaction by recoil T atoms: chem. factors controlling yield, 1290; substitution reaction of ^{18}F atoms: bond energy effects, 1324

methane, nitro-
  adsorption–desorption isotherm data for vapors on activated carbon, 3526; excess Gibbs energy of mixing binary solns. of, by total intensity Rayleigh light scattering, 3728; freezing pt. depression in CCl_4 and benzene, 3892; photolysis of aq. acetone in presence of, 851; prod. in pyrolysis of nitropropane, 2427; radicals from, in aq. soln.: esr, 1186; reaction w/ H atoms: kinetics by esr, 1654
  use photolysis of $S_2O_3^{2-}$ solns., 2752

methane, tetranitro-
  reaction kinetics of solvated e^- in solns. containing, 2756

methane, trichlorofluoro-
  radn. chem. in aq. soln., 455

methane, trinitro-
  structure in various solvents, 499

methane, tris(hydroxymethyl)amino-
  vol. change in protonation: medium effects, 1120

methane-^{14}C, iodo-
  methylene reactions in photolytic sys. containing, 2536

methane-d_2
  isotope effects in substitution reaction of 2.8-eV T atoms w/, 1283

methane-d_2, bromofluoro-
  matrix reactions w/ Li: ir, 3235

methane-d_3
  isotope effects in substitution reaction of 2.8-eV T atoms w/, 1283

methane-d_3, fluoro-
  isotope effects of (n,γ)-activated Br reactions in gaseous, 2072

methane-d_4
  H abstraction reaction by near-thermal ^{18}F atoms, 2709; isotope effects in substitution reaction of 2.8-eV T atoms w/, 1283; radiolysis of, on porous glass; esr, 201; relative total scattering cross section, 727

methanesulfenyl radical anion, nitro-
  esr, 2752

methanethiol
  adsorption on clean germanium surfaces, 2922

methanol
  absorption coeff. and ionization yield at 58.4 nm, 719; adsorption on clean germanium surfaces, 2922; adsorption on oxidized Al foil, 1887; adsorption–desorption isotherm data for vapors on activated carbon, 3526; effect on epr of complex-bonded *tert*-$BuO_2\cdot$, 2580; enthalpies of soln. in various polar solvents, 3598; enthalpy of transfer of electrolytes to propylene carbonate from, 3606; gas-phase acidity, 2226; glass transition temp. of aq. solns., 967, 3379; kinetics of e^- exchg. between ferrocene

and ferricinium ion in, 3303; mol. complex formation equil: solv. effects, 2413; prod. from irradn. of crys. glycollic acid, 1648; radical and anion radical derived from: esr of aq. soln., 1186; reaction of H atoms in aq. solns. of, 449; reaction of recoil C atoms in, 2248, 2253; reaction w/ H atoms: kinetics by esr, 1654; salt effects in aq. solns: scaled particle theory applied to salting-out polar mol., 3757; self-assocn. of vapor; ir, 1808; solute–solv. interactions studied by nmr, 3141; solv.-isotope effect in enthalpy of some solutes in, 388; vapor pressure isotope effects, 1815
use pulse radiolytic study of O^-, 1738
methanol-*d*
solv.-isotope effect in enthalpy of some solutes in, 388; vapor press isotope effects in CH_3OD, CD_3OH, and CD_3OD, 1815
methemoglobin
tracer and mutual diffusion coeffs., 379
methoxyl radical
esr in aq. soln., 1186
methyl acetate
mol. assoc. effects on C–H nuclear dipolar relaxation rates, 2539; prod. in recoil C atom reaction in methanol, 2253
methyl formate
adsorption of vapor on water by glc, 3870; mol. assocn. effects on C–H nuclear dipolar relaxation rate, 2539
methyl methacrylate
polymerization on Al_2O_3 and B_2O_3–SiO_2, 3897
use scavenger in radiolysis of CCl_4, 24
methyl methacrylate, polymer
–benzene soln: anomalous freezing behavior, 2623; thermal decay effects on spatial distribution of radicals in γ-irradiated, 2443
methyl radical
addn. reactions in $CF_3N{=}NCF_3$ acetone mixts., 735; esr in aq. fumarate soln., 2570; formation during photolysis of *N,N,N′,N′* tetramethyl-*p*-phenylenediamine, 431; H-abstraction reaction from silane in photolysis of acetone–silane mixts., 3945; nonempirical calcns. of contact hyperfine splittings, 3400; press. dependence of cross-combination ratio for, and CF_3, 2225; prod. from *tert*-BuO decompn.: comparison of RRK and RRKM, 1333; prod. from C_2H_6 decompn.: comparison of RRK and RRKM theories, 1333
methyl radical, amino-
esr in aq. fumarate soln., 2570
methyl radical, bromodichloro-
infrared spectrum, 3984
methyl radical, chloro-
esr in aq. fumarate soln., 2570
methyl radical, chlorodibromo-
infrared spectrum, 3984
methyl radical, fluoro-
ir spectrum and bonding, 3235
methyl radical, hydroxy-
esr in aq. fumarate soln., 2570; esr in aq. soln., 1186; temp. dependent esr: experimental and calculated, 3438
methyl radical, methoxy-
temp. dependent esr: experimental and calculated, 3438
methyl radical, perchlorodiphenyl-
X-ray anal of disordered mixed crys., 1246
methyl radical, trifluoro-
addn. reactions in $CF_3N{=}NCF_3$ acetone mixts., 735; esr in aq. fumarate soln., 2570; press. dependence of cross-combination ratio for, and CH_3, 2225
methyl-^{13}C radical, hydroxy-
temp. dependent esr, 3438
methyl-*d* radical
esr, 2448
methyl-d_2 radical
esr, 2448
methyl-d_2 radical, fluoro-
ir spectrum, 3235
methyl-d_3 radical
esr of normal and abnormal, trapped on V_2O_5 coated porous Vycor, 4064; reaction w/ $(CH_3)_3SiF$: polar effects in H abstraction, 603
methylamine
–alkali metal solns.: new absorption bands, 286; –$Ca(NO_3)_2$ binary sys.: glass transitions, 1826; esr study of radicals prod. in irradiated aq. soln. of, 738; vapor pressure isotope effect of, and *N*-deuterio-, 160
methylamine-^{14}C
prod. from nuclear reaction $^{14}N(n,p)^{14}C$ in KN_3, 2551
methylamine, *N*-d_2
vapor press. isotope effect, 160
methylamine-^{15}N
^{15}N chem. shift, 932
methylamine-^{15}N hydrochloride
^{15}N nmr, 1758
methylcarbamic acid, ethyl ester
protolysis kinetics, 1895
methyldifluoramine
kinetics of unimol. dehydrofluorination, 1170
N-methyldiphenylamine
electronic spectra, 3576
methylene
esr of radicals prepared by reactions of, 2448; reactions in photolytic sys. involving CH_3I, 2536; reactions of, w/ 1,2-dichloroethane, 2231; reaction rates: photolysis of CH_2N_2–propane mixts., 1537
methylene blue
reaction of *p*-substd. benzenesulfinates w/ photoactivated, 3066
use spectral sensitization of GaP electrodes, 562
methylhydrazine
decompn. to $NH_3 + CH_2{=}NH$: comparison of RRK and RRKM theories, 1333
methylideneamine
prod. from CH_3NHNH_2 decompn: comparison of RRK and RRKM theories, 1333
methylsulfonic acid; trifluoro-; sodium salt
viscosity study in dimethyl sulfoxide, 1727
mica
adsorption of fibrinogen on, studied by e^- microscope, 2103; competitive adsorption of fibrinogen and heparin on, 2107
molecular sieve
radiolysis of hydrogenous material on: esr, 201
molten acetamide
equivalent conductivity of potassium halides in, 2687
molten fluorides
coordn. effects on spectrum of U(IV) in, 631
molten lithium chlorate
laser Raman spectrum, 2948
molten nitrates
Na^+ and K^+ exchange between, and zeolite, 2523
molten salts
ion-exchg. and ionic transport props., of glass membranes in, 2815; pmr of solns. of, 1338
molten sodium nitrate
soly. of nonpolar gases in, 821
molybdenum
attack of, surfaces by atomic fluorine, 308; binding states of H_2 and N_2 on (100) plane, 227
molybdenum sulfide
surface diffusion rates, 153
montmorillonite
Cu(II)–arene complexes formed on, 3957

naphthalene
electron-transfer reactions: effects of deuterium substitution, 447; enthalpy of fusion, 2066; inter-ring nmr coupling calcd., 3765; MO calcns. for excimer model, 1794; Pt-cat. isotopic H exchange, 1175; quantum yield of sensitized phosphorescence: external heavy-atom effect, 1921; -sensitized photoaquation of some Cr(III)-ammine complexes, 3504
naphthalene, 1-bromo-
far-ir, 2942
naphthalene, 1-chloro-
far-ir, 2942
naphthalene, 1,4-dihydroxy-
esr of cation radicals, 2195
naphthalene, 1,4-dihydroxy-2,3-dimethyl-
esr of cation radicals, 2195
naphthalene, 1-fluoro-
far-ir, 2942
naphthalene, 2-phenyl-
fluorescence spectrum: effect of varied excitation, 3097
naphthalene, 1,2,3,4-tetrahydro-
see tetralin
naphthalene, 2-*o*-tolyl-
fluorescence spectrum: effect of varied excitation, 3097
1-naphthalenesulfonamide, 5-dimethylamino-*N*-methyl-
protolysis kinetics by nmr, 4056
naphthalenesulfonate, sodium dinonyl-
see dinonylnaphthalenesulfonic acid, Na salt
β-naphthalenesulfonate
effect on micellar catalysis, 2707
1-naphthalenesulfonic acid, 5-dimethylamino-
protolysis kinetics by nmr, 4056
naphthalenide, potassium
electron-transfer reactions: effects of deuterium substitution, 447

3-naphthoic acid, 3′-alkyl-4′-chloro-6′-sulfophenylazo-2-hydroxyl-
  steric effects on dimer structure, 1227
α-naphthylamine
  assocn. consts. w/ proton acceptors by ir, 1157; π hydrogen bonding, 2404
β-naphthylamine
  assocn. consts. w/ proton acceptors by ir, 1157
β-naphthylamine, *N*-phenyl-
  reaction w/ complex-bonded *t*-butylperoxyl; epr, 2580
nematic liquid crystals
  nuclear magnetic relaxation in an homologous series of, 3834
neodymate, hexachloro-; dicesium sodium salt
  thermochem., 392
neodymium
  soly. in NdF_3, 2340
neodymium fluoride (NdF_3)
  soly. of liq. Nd in, 2340
neodymium oxide (NdO)
  spectroscopy of, molecules in inert matrix, 514
neon
  effect on thermal isomerization of C_2H_5NC, 1366; relative total scattering cross section, 727
  use ir of matrix-isolated UO, 2283
neopentane
  acentric factor and entropy of vaporization, 166; anisotropic solv. shifts by factor anal., 1207; nmr in various solvents: nature of solv. effect, 3971; soly. and activity coeffs. in liq. methane and argon, 2345; surface diffusion rate of, thru solid sorbate, 133; viscosity of liq. mixts. containing: calcd., 3113
neopentyl alcohol
  reaction w/ H atoms: kinetics by esr, 1654
nickel
  –copper catalyst alloy: effect on diamond-forming reaction, 2158; –Mn catalyst alloy: effect on diamond-forming reaction, 2158
nickel(II) *m*-benzenedisulfonate
  outer-sphere assocn. kinetics in MeOH by ultrasonic relaxation, 2649
nickel, bis-*cis*-(1,2-perfluoromethylethylene-1,2-dithiolato)-
  see nickel thiete
nickel hydroxide [$Ni(OH)_2$]
  crystallographic study, 1782
nickel ion (Ni^{2+})
  catalysis of exchange of ethanol hydroxyl proton, 1994; –C_2H_4–maleic acid copolymer complexes: heats of assocn., 1136; complexes w/ purine bases: relaxation spectra, 799; magnetic moment using ion-exchange resin, 2981
nickel(II) murexide
  kinetics of formation in several solvents, 3705
nickel oxide (NiO)
  adsorption of phenol on, 1975; on η- and γ-aluminas: catalytic activities of, for N_2O decompn., 1051; on η- and γ-aluminas: structural, magnetic, and opt. props., 1044
nickel oxides, higher
  crystallographic studies, 1782
nickel thiete
  donor–acceptor complexes of phenothiazine and phenoxazine w/; opt. absorption spectrum, magnetic susceptibility, esr, 2387
niobium
  thermal negative ion emission from binary cesium halide mixts. on, 3741
nitrate ion
  –Cl^- and –Br^- couples: electrochem. behavior of liq. anion membranes, 554; ionic radius from scaled particle theory of salt effect, 2809; salts containing: thermodns. of mixed electrolyte solns., 946; yields of H_2 in radiolysis of aq. solns. containing, 3950
nitric acid
  –hydrazine binary sys.: glass transitions, 1826; reactions w/ O atoms and H atoms: mass spec. study, 3193
  use acid–base equil. of fluorescein, 245
nitric oxide
  see nitrogen oxide (NO)
nitriles
  cohesive energies, 642; relative total scattering cross section, 727
nitrilotriacetic acid
  esr of radical prod. in irradiated aq. soln. of, 738
nitroform
  see methane, trinitro-
nitrogen
  afterglow and recombn. rate of N atoms, 1552; impurity in lab-made diamond, 1838
nitrogen (N_2)
  absorption coeff. and ionization yield at 58.4 nm, 719; afterglow and recombn. of N atoms in presence of, 1552; binding state of, on (100) plane of Mo, 227; energy transfer efficiency in thermal isomerization of C_2H_5NC, 3037; prod. in NH_3–NO reaction on Pt, 875; prod. in reaction of hexafluoroazomethane–acetone mixt., 735; relative total scattering cross section, 727; second virial coeffs.: exptl. and calcd. for pure and mixed sys., 3691; soly. of, in molten $NaNO_3$, 821; yields of, from solns. of N_2O in γ-irradiated *c*-C_5H_{10}, 2560
  use decompn. of $FeSO_4$ in presence of, 1179; effect on CS_2–O_2 explosion, 861; photolysis of CH_2N_2–propane mixts., 1537; spectrum of matrix-isolated CS_2, 2204
nitrogen, atomic
  reaction of w/ ONCl: mass spec. study, 1172; recombn. rate in presence of N_2, Ar, and He, 1552
nitrogen, isotope of mass 15
  substitution of, for ^{14}N in diamond, 2696
nitrogen fluoride (NF_3)
  –H_2 and –C_2H_6 sys.: chem. HF lasers from, 284
nitrogen oxide (N_2O)
  absorption coeff. and ionization yield at 58.4 nm, 719; catalytic act. of NiO supported on γ- and η-aluminas for decompn. of, 1051; decompn. on ZnO, 1037; gas-phase radiolysis: effect of hydrocarbons, 3178; Hg-sensitized photodecompn. in CO–CH_4 mixts., 3205; photoassisted dissocn. over Fe_2O_3 and ZnO, 617; prod. in NH_3–NO reaction on Pt, 875; radn. chem. of aq. benzene solns. in presence of, 3886; reaction kinetics of solvated e^- in solns. containing, 2756; reactions in γ-irradiated *c*-C_5H_{10}, 2560
  use pulse radiolysis of aq. $(CN)_2$ soln., 608
nitrogen oxide (NO)
  adsorbed on alkali halide films: ir, 2930; absorption coeff. and ionization yield at 58.4 nm, 719; –NH_3 reaction on Pt: deuterium kinetic isotope effect, 875
  use photoinduced decompn. of C_2H_6, 2903; prepn. of CH_2NO radical, 2448
nitrogen oxide (^{15}NO)
  use esr of CH_2NO radical, 2448
nitrogen oxide (NO_2)
  prod. in pyrolysis of nitropropane, 2427
nitrosamine anion radicals
  esr, 2704
nitrosyl chloride (ONCl)
  reaction of N atoms w/: mass spec. study, 1172; reaction w/ H atoms: mass spec. study, 722; reaction w/ O atoms by mass spec., 1320
nitrosyl-^{15}N chloride
  reaction of N atoms w/: mass spec. study, 1172
nitrous oxide
  see nitrogen oxide (N_2O)
nitroxide, di-*tert*-butyl
  see di-*tert*-butyl nitroxide
noble gases
  effect on thermal isomerization of C_2H_5NC, 1366
n-nonane
  acentric factor and entropy of vaporization, 166; adsorption of vapor on water by glc, 3870; thermodns. of soln. in liq. crys. solvents, 2005
nonanoic acid, tetrabutylammonium salt
  thermodns. of aq. solns., 3733
2-nonanone
  cohesive energy, 642
n-1-nonene
  thermodns. of soln. in liq. crys. solvents, 2005
norbornane
  thermochem., thermodn. fcns. and mol. structure, 1264
norepinephrine
  zwitterion formation upon deprotonation of, and isopropyl-, 2657
nylon
  mol. mechanism of chain rupture in strained cryst. polymers, 3921

octane
  equilibrium distributions of various isomers upon isomerization, 1486
n-octane
  acentric factor and entropy of vaporization, 166; adsorption of vapor on water by glc, 3870; equilibrium distribution upon isomerization, 1486; second virial coeffs.: exptl. and calcd. for pure and mixed sys., 3691; soly. and activity coeffs. in liq. methane and argon, 2345; thermodns. of soln. in liq. crys. solvents, 2005

octane, 1-chloro-
  cohesive energy, 642; thermodns. of soln. in liq. crys. solvents, 2005
octane, 2-methyl-
  thermodyns. of soln. in liq. crys. solvents, 2005
octanenitrile
  cohesive energy, 642
octanoate, perfluoro-; salts
  critical micelle concn. from ^{14}F chem. shift data, 942
octanoic acid, perfluoro-
  assocn. in dil. solns., 1330
p-octaphenyl, tetramethyl-
  electronic spectra, 318
n-1-octene
  thermodns. of soln. in liq. crys. solvents, 2005
n-2-octene, (*E*)- and (*Z*)-
  thermodns. of soln. in liq. crys. solvents, 2005
n-3-octene, (*E*)- and (*Z*)-
  thermodns. of soln. in liq. crys. solvents, 2005
n-4-octene, (*E*)- and (*Z*)-
  thermodns. of soln. in liq. crys. solvents, 2005
octhracene
  thermochem., thermodn. fcns. and mol. structure, 1264
octyl hexaoxyethylene glycol monoether, 8,8,8-trifluro-
  micelle structure by ^{19}F nmr; prepn., m.p., 547
n-octyl trimethylene phosphate
  charge density on phosphoryl oxygen, 3309
oil
  -water emulsion: effect of emulsifying agent on dielectric props. of, 537
olefins
  addn. reactions of H and D atoms, 1601; effect of, on reactions of N_2O in γ-irradiated cyclopentane, 2560; quenching of excited states of C_6H_5F by, 3662; reactions of ^{128}I w/ various C_5 isomers, 2880; reaction w/ H atoms, 1584; reactivity w/ OH radicals, 3640
p-oligophenylenes
  electronic spectra, 318
orthotelluric acid
  see telluric acid (H_6TeO_6)
3-oxabicyclo[3.2.2]nonane
  absolute entropies, conformation and Debye temp., 1073
oxalate ions
  pulse radiolysis, 749
oxalate radical anion ($C_2O_4\cdot^-$)
  short-lived transient in photolysis of ferrioxalate sys., 2897
oxalic acid
  H_2O_2 formation upon oxidn. of, in presence and absence of O_2 and Mn(II), 3343; pulse radiolysis of, and its anions, 749; reaction of H atoms in aq. solns. of, 449; reaction w/ H atoms: kinetics by esr, 1654
oxide ion (O_{aq}^-)
  pulse radiolytic study, 1738
oxirane, 2-methyl-
  see propane, 1,2-epoxy-
oxyfluoroiodite radical (IO_2F^-)
  esr study, 3479
oxygen
  laser-produced, from SiO_2, 2412
oxygen (O_2)
  absorption coeff. and ionization yield at 58.4 nm, 719; –Ar sys.: vibrational transitions in collisions, 923; cation derived from: dynamics of reaction w/ H_2 and D_2, 1426; –cesium surface reaction: chemiemission, 1928; –C_2H_2 reaction: Shock-tube study, 2402; chemisorption on α-Cr_2O_3 using ir, 2783; –CS_2 explosion: kinetics and mech., 861; –CS_2 mixts.: photolysis at 313 nm, 854; H_2O_2 formation upon oxidn. of oxalic acid in presence and absence of, 3343; influence on spectral sensitization of GaP electrodes, 562; initiation rate for shock-heated mixts. of H_2–Ar–CO–, 1504; polarographic redn. in presence of H^+ donors, 4019; pulse radiolysis of thymine in presence of, 3815; quenching of excited states of C_6H_5F by, 3662; radn.-induced oxidn. of liq. SO_2 containing, 3631
  use decompn of $FeSO_4$ in presence of, 1179; ignition of aromatic hydrocarbon–O_2 mixts. by shock waves, 1501; quencher in photolysis of pyrene, 1025; reactions of recoil T atoms w/ 1-butene and (*Z*)-2-butene, 3771; recoil tritium reactions w/ $(CH_3)_3SiF$, 301; recoil tritium reactions w/ cyclobutane, 3781; recoil tritium reactions w/ propene in gas phase, 1031; scavenger in radiolysis of butane, 2854; scavenger in reaction of ^{18}F atoms w/ halomethanes, 1324; scavenger in recoil T reaction w/ $(CHFCl)_2$, 1299
oxygen, atomic
  rate of interaction w/ Ag and Au, 2186; reaction of, w/ acetylene-d_2, 4053; reaction w/ 1-butene: abs. rate const., 3902; reaction w/ cyclopentene, 3056; reaction w/ HNO_3: mass spec. study, 3193; reaction w/ ONCl by mass spec., 1320
ozonide ion (O_3^-)
  formation in γ-irradiated aq. alkali hydroxide solns., 3030,3031

palladium
  -catalyzed CO oxidn. promoted by H_2, 2065; hydrogenation of C_2H_2 on: pressure jump and isotope replacement, 880; liquid: thermodn. props., 3737
pelargonic acid
  see nonanoic acid
L-penicillamine hydrochloride
  oxidn. and redn. of, by ionizing radn.; esr, 2564
n-pentadecane
  acentric factor and entropy of vaporization, 166
1,3-pentadiene
  prod. of photolysis and pyrolysis of 4-vinyl-1-pyrazoline, 1640
1,4-pentadiene
  prod. of photolysis and pyrolysis of 4-vinyl-1-pyrazoline, 1640
2,4-pentadione
  keto–enol equilibria, in, and 3,3-dideuterio-, 433
pentaerythritol
  nmr of molten alkali acetate solns. of, 1338
n-pentane
  acentric factor and entropy of vaporization, 166; adsorption of vapor on water by glc, 3870; bubble nucleation in pure, and in mixts. w/ hexadecane, 3613; enthalpies of soln. in various polar solvents, 3598; enthalpy in methanol: solv.–isotope effect, 388; entropy of vaporization from Hildebrand rule, 2530; interaction virial coeffs. in binary mixts. w/ fluorocarbons, 3863; prod. in photolysis of ketene–butane mixts., 2240; reaction w/ H atoms: kinetics by esr, 1654; reaction w/ ^{128}I, 2880; recoil ^{11}C reactions w/, 3201; second virial coeffs.: exptl. and calcd. for pure and mixed sys., 3691; soly. and activity coeffs. in liq. methane and argon, 2345
  use energy transfer in thermal isomerization of Et—N≡C, 2171
pentane, 1-chloro-
  induction energy for, in Apiezon M estimated by glc, 831; thermodns. of soln. in liq. crys. solvents, 2005
pentane, 1,5-dibromo-
  dielectric relaxation in benzene soln., 2616
pentane, 2,2-dimethyl-
  acentric factor and entropy of vaporization, 166
pentane, 2,4-dimethyl-
  acentric factor and entropy of vaporization, 166
pentane, 3,3-dimethyl-
  acentric factor and entropy of vaporization, 166; thermodns. of soln. in liq. crys. solvents, 2005
pentane, 3-ethyl-
  acentric factor and entropy of vaporization, 166
pentane, 2-methyl-
  entropy of vaporization from Hildebrand rule, 2530; soly. and activity coeffs. in liq. methane and argon, 2345
pentane, 3-methyl-
  entropy of vaporization from Hildebrand rule, 2530; luminescence decay of γ-irradiated, 3221; soly. and activity coeffs. in liq. methane and argon, 2345
pentane, perfluoro-
  entropy of vaporization from Hildebrand rule, 2530; interaction virial coeffs. in binary mixts. w/ hydrocarbons, 3863; second virial coeffs.: exptl. and calcd. for pure and mixed sys., 3691
pentane, perfluoro-2-methyl-
  entropy of vaporization from Hildebrand rule, 2530
pentane, perfluoro-3-methyl-
  entropy of vaporization from Hildebrand rule, 2530
pentane, 1,1,5-trimethyl-
  see isooctane
2,4-pentanediol, 2-methyl-
  dielectric props., 1240
pentanoic acid, tetrabutylammonium salt
  thermodns. of aq. solns. of, 3733
1-pentanol
  adsorption on oxidized Al foil, 1887; enthalpies of soln. in various polar solvents, 3598; gas-phase acidity, 2226
1-pentanol, 5-chloro-
  electrosorption on Hg, 1698
3-pentanol
  adsorption and surface reactions on γ-alumina: ir study, 234
2-pentanone
  cohesive energy, 642; quenching of excited states of C_6H_5F by, 3662; vapor–liq. equil. of binary mixts. of *n*-hexane-^{14}C w/, 4041
2-pentanone, 4-methyl-
  dissocn. and homoconjugation consts. of acids in, 2496

3-pentanone
  vapor–liq. equil. of binary mixts. of n-hexane-^{14}C w/, 4041
pentanones
  photolysis of 1,4-dichlorobutane sensitized by 2-, 3-, and 2,4-dimethyl-3-, 1168
4-pentenal
  prod. of reaction of c-C_5H_8 w/ O atoms, 3056
1-pentene
  reaction w/ H atoms: abs. rate const., 1584; reaction w/ ^{128}I, 2880; reactivity w/ OH radicals, 3640; recoil ^{11}C reactions w/, 3201
  use energy transfer in thermal isomerization of Et—N≡C, 2171
2-pentene
  reactivity w/ OH radicals, 3640
(*E*)-2-pentene
  reaction w/ ^{128}I, 2880
(*Z*)-2-pentene
  reaction w/ ^{128}I, 2880
n-pentyl radical
  decay of, in γ-irradiated $C_5H_{11}I$, 472; isomerization of chem. activated, 1632
sec-pentyl radical
  prod. from chem. activated *n*-pentyl, 1632
tert-pentyl radical
  equilibrium conformation and rotational barrier by esr, 3438
peptides, poly-
  ultrasonic absorption due to proton transfer for solns. of, 4012
perchlorate ion
  assocn. const. of H_2O w/, in propylene carbonate by nmr, 1477; effect on circular dichroism of lysine-rich histone f-1–DNA complexes, 1516; transport behavior in dimethyl sulfoxide, 1727
  use pulse radiolysis of aq. halide solns., 3081
perchloric acid
  Cu^{I}- and Cu^{II}-catalyzed D exchg. in solns. of, 571; decompn. of, over ZnO, 491; dissocn. const. in isobutyl methyl ketone, 2496
  use acid–base equil. of fluorescein, 245; reactions at high ionic strengths, 1113; reaction $U^{3+} + Co(NH_3)_4(H_2O)_2^{3+}$ in aq., 2117
perhydroxyl radical
  decay kinetics: deuterium isotope effect, 2263
permanganate
  oxidn. of oxalic acid by, in presence and absence of O_2 and Mn(II), 3343; reaction w/ tris(1,10-phenathroline)iron(II), 1107
peroxide ion (O_2^{2-})
  evidence of, on surface of ZnO_2, 3089
peroxide, *tert*-butyl hydro-
  reaction w/ acetaldehyde by nmr, 3377
peroxide, *tert*-butyl isopropyl
  energy partitioning on photolysis, 3651
peroxide, di-*tert*-butyl
  energy partitioning on photolysis, 3651
  use CH_3NF_2 dehydrofluorination kinetics, 1170
peroxide, (1-hydroxy-1-methyl)ethyl hydro-
  prod. of reaction between acetone and H_2O_2, 3004
peroxydisulfuryl difluoride ($S_2O_6F_2$)
  esr of $SO_3F\cdot$ in, 712
perylene
  laser photolysis, 3894; radical cation dimers: formation and electronic absorption spectra, 1768
phenanthrene
  quantum yield of sensitized phosphorescence: external heavy-atom effect, 1921
phenol
  adsorption on TiO_2 by ir, 1221; competitive adsorption on NiO, 1975; intermol. assocn. of, in CCl_4, 3591; polarographic redn. of O_2 in presence of, 4019; reaction w/ complex-bonded *tert*-butylperoxyl; epr, 2580; reduction of iodate to iodite by Br^- in presence of, 2516; solv. and temp. effects on ir of OH group, 2219
phenol, 2-chloro-
  polarographic redn. of O_2 in presence of, 4019
phenol, 2,6-di-*tert*-butyl-4-(fluorophenyl)-
  nmr of radicals derived from, 3462
phenol, 2,6-di-*tert*-butyl-4-(fluorotolyl)-
  nmr of radicals derived from, 3462
phenol, 2,6-dimethyl-
  see 2,6-xylenol
phenol, 2,6-dinitro-
  dissocn. const. in isobutyl methyl ketone, 2496
phenol, *p*-(*p*-ethoxyphenylazo)-; ester of
  proton spin–lattice relaxation, 2452
phenol, nitro-
  esr of radicals from *o*, *m*-, and *p*-, in aq. soln., 1186
phenol, *o*-nitro-
  solv. and temp. effects on ir of OH group, 2219
phenol, tri-*tert*-butyl-
  reaction w/ complex-bonded *tert*-butylperoxyl; epr, 2580
phenol, *sym*-trichloro-
  solv. and temp. effects on ir of OH group, 2219
phenol red indicator
  proton-transfer reactions between polyacrylic acid and, 267
phenols
  nmr of molten alkali acetate solns. of, 1338
phenothiazine
  donor–acceptor complex w/ nickel thiete; opt. absorption spectrum, magnetic susceptibility, esr, 2387
phenothiazine derivatives
  micelle formation: nmr in D_2O, 3554
phenoxazine
  donor–acceptor complex w/ nickel thiete; opt. absorption spectrum, magnetic susceptibility, esr, 2387
phenoxyl radical, 2,6-di-*tert*-butyl-4-formyl-
  esr and endor study, 2765
phenoxyl radicals, 2,6-di-*tert*-butyl-4-(fluorophenyl)-
  nmr studies, 3462
phenyl radical
  esr and endor studies of, pairs from benzoyl peroxide, 3426; esr: ^{13}C spectra, 3432; prod. from PhCO decompn.: comparison of RRK and RRKR theories, 1333
p-phenylenediamine, *N*-substituted-
  photochem. oxidn. in $CHCl_3$, 2737
p-phenylenediamine, *N*,*N*,*N'*,*N'*-tetramethyl-
  photochem. in 3-methylpentane glass, 431
α-(phenylethyl)benzylmethylamine
  proton exchange and N inversion using nmr, 3190
phenylphosphate dianion
  effect on micellar catalysis, 2707
phloroglucinol
  nmr of molten alkali acetate solns. of, 1338
phosgene
  oxidn. prod. of C_2HCl_3, 613
phosphate esters
  charge density of phosphoryl oxygen in a series of, 3309
phosphine, dimethylaminodichloro-
  vibrational spectra and structure of, and deuterio analog, 3837
3-phospholene 1-oxide, 1,3-dimethyl-
  nuclear magnetic spin–lattice relaxation and viscosity data, 3547
phosphonic acid, dialkyl esters
  ^{31}P nmr, 3547
phosphonic acid, (1-hydroxyethylidene)di-
  complexation w/ Ca^{2+}, 676, 682
phosphonic acid, methyl-; diisopropyl ester
  adduct w/ Sn(II), Sn(IV), and Ti(IV) halides: ir and pmr, 637
phosphonic acid-*d*, dialkyl esters
  ^{31}P nmr, 3547
phosphonic chloride fluoride, methyl-
  vibrational spectra and structure, 1956
phosphonic dichloride, methyl-
  vibrational spectra and structure, 1956
phosphonic difluoride, methyl-
  vibrational spectra and structure, 1956
phosphonium, tetrabutyl-; bromide
  interaction w/ halide ions studied by nuclear quadrupole relaxation, 2936
phosphonium, tetraphenyl-; chloride
  interaction w/ halide ions studied by nuclear quadrupole relaxation, 2936; solute–solv. interactions studied by nmr, 3141
phosphonium, tetraphenyl-; ion
  enthalpies of transfer to propylene carbonate from methanol or dimethylformamide, 3606; interactions w/ water and other solvents studied by nmr, 3141
phosphonothioic dichloride, methyl-
  vibrational spectra and structure, 1956
phosphonous dichloride, methyl-
  vibrational spectra and structure, 1956
phosphoric acid
  –hydrazine binary sys.: glass transitions, 1826; nuclear magnetic spin–lattice relaxation and viscosity data, 3547
phosphoric acid, trialkyl esters
  nuclear magnetic spin–lattice relaxation and viscosity data, 3547
phosphorothioate, *O*-(3,6-dichloro-2-pyridyl)-*O*,*O*-dimethyl-
  activated complexes in ion fragmentation, 1903

phosphorothionic acid, trimethyl ester
nuclear magnetic spin–lattice relaxation and viscosity data, 3547
phosphorotriamide, hexamethyl-
assocn. consts. of aromatic amines w/, by ir, 1157; complexes w/ aromatic amines: calorimetric detn. of enthalpies of assocn., 3149
phosphorous acid, trialkyl esters
nuclear magnetic spin–lattice relaxation and viscosity data, 3547
phosphorus chloride (PCl_3)
nuclear magnetic spin–lattice relaxation and viscosity data, 3547
phosphorus fluoride (PF_3)
reaction w/ BH_3, 2711
phosphorus oxide (P_4O_6)
nuclear magnetic spin–lattice relaxation and viscosity data, 3547
phosphorus oxychloride radical anion ($POCl_3\cdot^-$)
esr spectrum and structure, 3023
phosphoryl fluoride (OPF_3)
LCAO–MO–SCF study, 1360
phthalic acid, dimethyl ester
product in degradn. of cycloheptatriene-^{14}C, 2558
phthalic acid, tetrachloro-; dibutyl ester
e^- donor–acceptor complexes by glc: thermodn. study, 2632
phthalonitrile
radical anion–sodium ion clusters: esr, 1205
picrate ion
viscosity coeffs., B_η, in various solvents, 2532
picric acid
dissocn. and homoconjugation consts. in isobutyl methyl ketone, 2496
piperidine
Meisenheimer complex formation w/ trinitrobenzene: evidence for intramol. H-bonding, 3636
4-piperidine-1-oxyl, 2,2,6,6-tetramethyl-
epr probe for hydrophobic interaction in various aq. solns., 165
piperidine-*N*-oxyl-4-ol, 2,2,6,6-tetramethyl-
epr of frozen aq. soln., 1202
use spin-label investigation of ion-exchange resins, 907
piperidinium picrates
effect of adding phosphate esters on conductivity of chlorobenzene solns. of, and N-substd., 3309
platinum
electrode: oxidn. of ethyl xanthate on, 354; surface reaction of NH_3–NO on, 875
plutonate, hexachloro-; dicesium sodium salt
thermochem., 392
polyelectrolytes
site binding of counterions in solns. of: ultrasonic absorption, 3367
polymer
Newtonian viscosity of concd. solns. of, 256; solutions: anomalous freezing behavior, 2623
polymers, crystalline
mol. mechanism of chain rupture in strained, 3921; thermodn. and morphological props., 3909
polymetatelluric acid
see telluric acid $(H_2TeO_4)_n$
potassium
absorption bands in solns. of, in amines, 286; -ethylenediamine solns: extinction coeff. and equilibria, 3092; uv irradn. of, in 3-methylpentane matrix: esr, 35
use reduction of nitrosoamines; esr, 2704
potassium acetate
-*N*-methylacetamide solns.: freezing pts. and osmotic and activity coeffs., 2319; sys. $KCl–H_2O$–: heats of mixing, 1125; sys. $KF–H_2O$–: heats of mixing, 1125
potassium azide
nuclear reaction $^{14}N(n,p)^{14}C$ in, 2551
potassium bromide
conductance in CF_3CH_2OH, 1708; equivalent conductivity in molten acetamide, 2687; -*N*-methylacetamide solns.: freezing pts., osmotic coeffs., and act. coeffs., 2313; sys. $KCl–H_2O$–: heats of mixing, 1125
potassium chloride
activity coeff. *vs.* concentration comparison of theory and exptl., 3790; conductance in CF_3CH_2OH, 1708; effect on circular dichroism of lysine-rich histone f-1-DNA complexes, 1516; equivalent conductivity in molten acetamide, 2687; film: ir of NO adsorbed on, 2930; isothermal diffusivity of aq. solns. by hologram interferometry, 3374; -*N*-methylacetamide solns.: freezing pts., osmotic coeffs, and act. coeffs., 2313; Onsager transport coeffs. in aq. solns. of: comparison of exptl. and theory, 3124; SO_2 adsorbed on: microwave absorption, 2602; sys. $CsCl–H_2O$–: heats of mixing, 1125; sys. $HCl–H_2O$–: heats of mixing, 1125; sys. $KBr–H_2O$–: heats of mixing, 1125; sys. $KC_2H_3O_2–H_2O$–: heats of mixing, 1125; sys. $KF–H_2O$–: heats of mixing, 1125; sys. LiCl–NaCl–: osmotic and act. coeffs., 1305; sys. $NaCl–BaCl_2$–: osmotic and act. coeffs. predicted, 1305; ultrasonic absorption of polyelectrolyte solns. upon addition of, 3367
use salt effects in Raman study of bisulfate–sulfate sys., 2681
potassium deuteride
cohesive energy, 1251
potassium fluoride
effect on circular dichroism of lysine-rich histone f-1–DNA complexes, 1516; enthalpy in methanol: solv.–isotope effect, 388; sys. $KC_2H_3O_2–H_2O$–: heats of mixing, 1125; sys. $KCl–H_2O$–: heats of mixing, 1125
potassium halide
equivalent conductivity in molten acetamide, 2687; -magnesium halide melts: Raman spectra, 155
potassium hydride
cohesive energy: isotopic substitution effect, 1251; dimer: Rittner ionic model study, 984
potassium hydroxide
formation of O_3^- in γ-irradiated aq. solns. of, 3030
potassium iodide
conductance in CF_3CH_2OH, 1708; enthalpy in methanol: solv.-isotope effect, 388; equivalent conductivity in molten acetamide, 2687; -*N*-methylacetamide solns: freezing pts., osmotic coeffs., and act. coeffs., 2313
use amylose–iodine reaction: kinetics, 272
potassium ion
assocn. const. of H_2O w/, in propylene carbonate by nmr, 1477; enthalpies of transfer to propylene carbonate from methanol or dimethylformamide, 3606; exchange of, and Na^+ between nitrate melts and zeolite, 2523; in sea water by difference chromatography, 1418; viscosity coeffs., B_η, in various solvents, 2532
potassium naphthalenide
electron-transfer reactions: effects of deuterium substitution, 447
potassium nitrate
corresponding states and glass transition, 2306; -*N*-methylacetamide solns: freezing pts., osmotic coeffs., and act. coeffs., 2313; nmr of molten, $-LiNO_3$ solns. of pentaerythritol, 1338; viscosities of fused w/ He, Ar, and N_2, 103
potassium oxyfluoroiodate (KIO_2F_2)
esr study of IO_2F^- radical in γ irradiated, 3479
potassium perchlorate
conductance and assocn. behavior in H_2O at 25°, 3290
potassium perfluorooctanoate
critical micelle concn. by ^{19}F nmr, 942
potassium permanganate
thermal decompn. induction period: radn. effects, 191
potassium propionate
-*N*-methylactamide solns: freezing pts. and osmotic and activity coeffs., 2319
potassium thiocyanate
effect on circular dichroism of lysine-rich histone f-1-DNA complexes, 1516; ionic solvation in acetone: spectroscopic studies, 56; nmr of molten, -NaSCN solns. of pentaerythritol, 1338
praseodymium oxides (PrO, PrO_2)
spectroscopy of, molecules in inert matrix, 514
proflavine hydrochloride
concn. quenching of, in dry films of DNA and poly(vinyl alcohol), 2727
promazine HCl
micelle formation: nmr in D_2O, 3554
promethazine HCl
micelle formation: nmr in D_2O, 3554
propane
acentric factor and entroxy of vaporization, 166; $-CH_2N_2$ mixts.: quantum yields in photolysis of, 1537; effect on gas-phase radiolysis of N_2O, 3178; effect on surface tension and critical micelle concn. of aq. dodecylamine·HCl solns., 3000; enthalpy of soln. in aq. alkylammonium bromide solns., 2330; entropy of vaporization from Hildebrand rule, 2530; hydrophobic bonding: theory, 363; interaction virial coeffs. in binary mixts. w/ fluorocarbons, 3863; prod. of radiolysis of butane, 2854; radiolysis of: effect of positive ion scavenging by benzene, 2272; reaction w/ H atoms: kinetics by esr, 1654; relative total scattering of mols. *vs.* 727; salting-out consts. for tetraalkylammonium bromide solns., 1803; second virial coeffs: exptl. and calcd. for pure and mixed sys., 3691;

surface diffusion rate of, thru solid sorbate, 133; sys. $^{14}CH_3I$–: methylene reactions in photolysis of, 2536
use energy transfer in thermal isomerization of Et—N=C, 2171
propane, 1-bromo-
reaction kinetics of solvated e^- in solns. containing, 2756
propane, 2-bromo-2-methyl-
see tert-butyl bromide
propane, 1-chloro-
cohesive energy, 642; elimination of HCl from, 2231
propane, 2-chloro-2-methyl-
see tert-butyl chloride
propane, 1,3-dibromo-
dielectric relaxation in benzene soln., 2616
propane, 1,3-dichloro-
elimination of HCl from, 2231
propane, 2,2-dimethyl-
see neopentane
propane, 1,1-dinitro-
nmr in various solvents, 499
propane, 1,2-diphenyl-
prod. in radiolysis of propane containing traces of benzene, 2272
propane, 2,2-diphenyl-
prod. in radiolysis of propane containing traces of benzene, 2272
propane, 1,2-epoxy-
prod. in pyrolysis of nitropropane, 2427; ultrasonic velocity in aq. solns., 2336
propane, 2-hydroxy-2-hydroperoxy-
prod. of reaction between acetone and H_2O_2, 3004
propane, 2-methyl-2-nitroso
spin trapping of short-lived radicals by nitroxide method, 3466
propane, 1-nitro-
nmr interpretation by pattern recognition, 1402
propane, 2-nitro-
excess Gibbs energy of mixing binary solns. of, by total intensity Rayleigh light scattering, 3728; pyrolysis, 2427
propane, perfluoro-
entropy of vaporization from Hildebrand rule, 2530; interaction virial coeffs. in binary mixts. w/ hydrocarbons, 3863; negative ion–molecule reactions in, 2534
propane, *N,N,N',N'*-tetramethyl-1,3-diamino-
protolysis kinetics in H_2SO_4, 2400
1,2-propanediol
prod. in recoil C atom reaction in methanol, 2253
1,3-propanediol
prod. in recoil C atom reaction in methanol, 2253
1,3-propanediol, 2-amino-2-hydroxymethyl-
nmr of molten alkali acetate solns. of, 1338
1,3-propanediol, 2-amino-2-methyl-
nmr of molten alkali acetate solns. of, 1338
1,3-propanediol, 2,2-dimethyl-
nmr of molten aklali acetate solns. of, 1338
1,3-propanediol, 2-hydroxymethyl-2-methyl-
nmr of molten alkali acetate solns. of, 1338
1-propanol
adsorption from H_2O soln. onto activated carbon: exptl. and calcd. data, 3720; adsorption on oxidized Al foil, 1887; effect on absorption and emission of benzquinolines, 2690; enthalpies of soln. in various polar solvents, 3598; gas-phase acidity, 2226; kinetics of e^- exchg. between ferrocene and ferricinium ion in, 3303; reaction of H atoms in aq. solns. of, 449; reaction of recoil C atoms w/, 2248; reaction w/ H atoms: kinetics by esr, 1654; salt effects in aq. solns: scaled particle theory applied to salting-out polar mol., 3757
1-propanol, 2,2-dimethyl-
see neopentyl alcohol
1-propanol, 1-methyl-
see sec-butyl alcohol
1-propanol, 2-methyl-
see isobutyl alcohol
2-propanol
adsorption and surface reactions on γ-alumina: ir study, 234; adsorption coeff. and ionization yield at 58.4 nm, 719; adsorption from H_2O soln. onto activated carbon: exptl. and calcd. data, 3720; enthalpy of soln. in aq. alkylammonium bromide solns., 2330; prod. in photolysis of acetone–silane mixts., 3945; prod. in photolysis of di-*tert*-butyl peroxide, 3651; radical and anion radical derived from: esr in aq. soln., 1186; radicals from: kinetics by esr-flow techniques, 167, 1326; γ radiolysis of vapro: influence of temperature, 20; radn. chem. of aq. solns. of, 31; reaction of H atoms in aq. solns. of, 449; reaction of recoil C atoms w/, 2248; reaction w/ H atoms: kinetics by esr, 1654; reactions of "Fenton-like" reagents in presence of, using esr flow techniques, 3271; yields of H_2O_2 in radiolysis of aq. solns. containing, 3950
use kinetic esr study of photolysis of $PhNO_2$, 3454
2-propanol, 2-methyl-
see tert-butyl alcohol
2-propanol-*d*
reaction of H atoms in aq. solns. of, 449
propargyl halides
complex formation w/ benzene, 2128
propene
effect on gas-phase radiolysis of N_2O, 3178; effect on reactions of N_2O in γ-irradiated cyclopentane, 2560; oxidn. over gold catalysts, 2914; photodecompn. prod. of γ-butylrolactone, 2733; prod. in pyrolysis of nitropropane, 2427; prod. in radiolysis of butane, 2854; prod. in thermal decompn. of 1,1,2-trimethylcyclobutane, 1437; prod. of recoil T atom reactions w/ 1- and 2-butene, 3771; prodn. of in γ radiolysis of 2-propanol, 20; reaction w/ H atoms: abs. rate const., 1584, 1601; reactivity w/ OH radicals, 3640; recoil tritium reaction w/, in gas phase, 1031; second virial coeffs: exptl. and calcd. for pure and mixed sys., 3691
use energy transfer in thermal isomerization of Et—N≡C, 2171; scavenger in radiolysis of NH_3, 2087
propene, 3-bromo-
prod. of recoil Br reaction w/ *c*-C_3H_6 and *c*-C_3H_5Br, 2698
propene, 1,2-diphenyl-
radn.-induced chain isomerization of, 292; radn.-induced isomerization in polar liqs., 2394
propene, 1,3-diphenyl-
photolytic reactions, 2079
propene, 2-phenyl-
polymerization on porous glass: ir, 3897
propene, 3-phenyl-
prod. in radiolysis of propane containing traces of benzene, 2272
propene-1-^{13}C
oxidn. over gold, 2914
propene-d_6
reactivity w/ OH radicals, 3640
propionaldehyde
adsorption–desorption isotherm data for vapors on activated carbon, 3526; reactivity w/ OH radicals, 3640
propionamide, *N*-methyl-
pulse radiolysis, 2267
propionic acid
reaction of H atoms in aq. solns. of, 449; reaction w/ H atoms: kinetics by esr, 1654
propionic acid, 2-hydroxy-
prod. from irradn. of crys. glycollic acid, 1648
propionic acid, 3-mercapto-
radicals produced in irradn. of aq. solns., 2277
propionic acid, pentafluoro-
assocn. in dil. solns., 1330
propionic acid, 2,3,3-trichloro-
CIDNP during formation of, 3410
propionitrile
adsorption of, from water soln., 61; reaction w/ H atoms: kinetics by esr, 1654
propionitrile, 2,2-dimethyl-
vibrational spectra, 2806
propionitrile, 2-methyl-
nmr interpretation by pattern recognition, 1402; reaction w/ H atoms: kinetics by esr, 1654
n-propyl radical
addn. to C_2H_4, 1632; decay of, in γ-irradiated C_3H_7I, 472; equilibrium conformation and rotational barrier by esr, 3438
1-propyl radical, 2-hydroxy-
kinetics of, by esr-flow techniques, 167, 1326; reactions of, formed by "Fenton-like" reagents, 3271
2-propyl radical, 2-hydroxy-
see ethyl radical, 1-hydroxy-1-methyl-
propylene carbonate
selective solvation of ions by H_2O in, 1477; single-ion enthalpy of transfer to, from other solvents, 3606
propylene glycol, di-
dielectric props., 1240
propylene oxide
see propane, 1,2-epoxy-
protein denaturants
effects of urea–guanidinium glass of, on H_2O structure, 815
proteins
chymotrypsinogen family, 1375, 1387; tracer and mutual diffusion coeffs., 379; ultrasonic absorption due to proton transfer for solns. of, 4012; ultrasonic absorption of solns. of, 374

pseudoisocyanine
use spectral sensitization of GaP electrodes, 562
purine, 9-methyl-
complexes w/ Ni^{2+}: relaxation spectra, 799
pyran, dihydro-
prod. of reaction of c-C_5H_8 w/ O atoms, 3056
pyrazine
apparent triplet yields, 3769; mol. complex w/ I_2, 2504
1-pyrazoline, 3-vinyl-
energy partitioning on photolysis and pyrolysis of, 1640
pyrene
charge-transfer quenching of mol. fluorescence: intersystem crossing, 1025; complex w/ pyromellitic anhydride: photochem., 3805; Pt-cat. isotopic H exchange, 1175
Pyrex membrane
ion-exchg. and ionic transport props. in molten salts, 2815
pyridazine *N*-oxide
mol. complex w/ I_2, 2504
pyridine
adsorption from H_2O soln. onto activated carbon: exptl. and calcd. data, 3720; adsorption on TiO_2 by ir, 1221; effect on epr of complex-bonded *tert*-BuO_2·, 2580; ir study of H-bonding in solns. of HF in, 2222
pyridine, amino-
assocn. consts. of 2-, 3-, and 4-, w/ proton acceptors by ir, 1157; complexes w/ proton acceptors: calorimetric detn. of enthalpies of assocn., 3149
pyridine, 4-vinyl-; polymer
–pyrochlorophyll complexes: photochem. activity, 1667
pyridine-d_5
use prepn. of 2-pyridyl-d_4 radical, 3432
pyridine *N*-oxide
mol. complex w/ I_2, 2504
pyridinium bromide
interaction w/ halide ions studied by nuclear quadrupole relaxation, 2936
2-pyridyl radical
esr: ^{13}C spectra, 3432
pyrimidine, amino-
assocn. consts. of, 2-, 4-, and 5-, w/ proton acceptors by ir, 1157
pyrimidine, 5-amino-
complexes w/ proton acceptors: calorimetric detn. of enthalpies of assocn., 3149
pyrimidine, 2-bromo-
use prepn. of 2-pyrimidinyl radical, 3432
pyrimidine *N*-oxide
mol. complex w/ I_2, 2504
2-pyrimidinyl radical
esr: ^{13}C spectra, 3432
pyrobacteriochlorophyll
circular dichroism calcd., 1440
pyrocatechol
nmr of molten alkali acetate solns. of, 1338
pyrochlorophyll
–poly(vinylpyridine) complexes: photochem. activity, 1667
pyrochlorophyll a
circular dichroism calcd., 1440
pyrogallol
nmr of molten alkali acetate solns. of, 1338
pyromellitic dianhydride
complexes w/ aromatic hydrocarbons: photochem., 3805
pyrrole
e$^-$ donor–acceptor complexes by glc: thermodn. study, 2632
pyrrole, 1-methyl-
e$^-$ donor–acceptor complexes by glc: thermodn. study, 2632
pyrrolidine
Meisenheimer complex formation w/ trinitrobenzene: evidence for intramol. H-bonding, 3636
pyrrolidino radical
epr spectrum, 3486
pyrrolidone, *N*-vinyl-; polymer
interactions of sodium dodecyl sulfate and aq., studied by equil. dialysis, 3135
pyrrolino radical
epr spectrum, 3486
pyruvic acid, alkyl esters
iodination of, 150; reversible hydration: thermodn. and kinetic studies, 792

p-quaterphenyl
cation radical: esr, 902; electronic spectra of, and substituted, 318
quinoline
singlet → triplet intersys. crossing quantum yield, 2083
2-quinolone
self assocn. and mixed dimers w/ carboxylic acid: thermodn. by ir, 1129
quinoxaline
singlet → triplet intersys. crossing quantum yield, 2083
p-quinquephenyl, substituted
electronic spectra, 318
quinuclidine
absolute entropies, conformation, and Debye temp., 1073
quinuclidinium bromide, decyl-
micelle aggregation number: depence on polar head structure, 369

rare earth chloro complex compounds
thermochem. of, 392
rare earth fluorides
–rare earth metals: miscibility of liq. metals w/ salts, 2340
rare earth metals
–metal fluoride sys.: miscibility of liq. metals w/ salts, 2340
rare earth oxides
spectroscopy of, molecules in inert matrices, 514
RDX
see *s*-triazine 1,3,5-trinitrohexahydro-
resorcinol
nmr of molten alkali acetate solns. of, 1338; solv. and temp. effects on ir of OH group, 2219
all-trans-retinal
radical anion: esr, 2861; singlet–triplet absorption spectrum, 983
N-retinylidene Schiff bases
esr, 2861
rhodamine B
use spectral sensitization of GaP electrodes, 562
rhodium(III) 2,2′-dipyridyl chelates
photolytic decompn: esr, 3230
rhodium(III) 1,10-phenanthroline chelates
photolytic decompn: esr, 3230
rose bengal
use spectral sensitization of GaP electrodes, 562
rubber, natural
–benzene soln: anomalous freezing behavior, 2623
rubidium
absorption bands in solns. of, in amines, 286
rubidium acetate
nmr of molten alkali acetate solns. of polyhydric alcohols, 1338
rubidium chloride
ultrasonic absorption of polyelectrolyte solns. upon addition of, 3367
use salt effects in Raman study of bisulfate–sulfate sys., 2681
rubidium deuteride
cohesive energy, 1251
rubidium hydride
cohesive energy: isotopic substitution effect, 1251; dimer: Rittner ionic model study, 984
rubidium ion
enthalpies of transfer to propylene carbonate from methanol or dimethylformamide, 3606; viscosity coeffs., B_η, in various solvents, 2532
rubidium nitrate
corresponding states and glass transition, 2306
rubidium perchlorate
conductance and assocn. behavior in H_2O at 25°C, 3290
rubidium permanganate
thermal decompn. induction period: radn. effects, 191
ruthenium(III) ammine complexes
uv photochem., 3075
rutile
surface props. by ir, 1216, 1221; temp. change on capacitance of film of, 1279

salicylic acid
–hydrazine binary sys.: glass transitions, 1826
samarium
metal–SmF_2 phase diagram, 2340
samarium fluoride (SmF_2)
–Sm phase diagram, 2340
samarium oxide (SmO)
spectroscopy of, molecules in inert matrix, 514
scandium oxide (ScO)
low-lying electronic states, 3103
Sephadex G-25-80
use epr studies in frozen aq. solns., 1202
serine
proton-transfer reactions: kinetics, 161
serum albumin
tracer and mutual diffusion coeffs., 379

p-sexiphenyl, tetremethyl-
  electronic spectra, 318
silane
  photolysis kinetics of acetone at 313 nm in presence of, 3945
silane, di-
  see disilane
silane, difluorodimethyl-
  reaction of CD_3 radicals w/, 603
silane, dimethyl-
  ion–molecule reactions in, 13
silane, ethyl-
  far-ir and low freq. Raman of solid, 3993
silane, ethyltrichloro-
  far-ir and low freq. Raman of solid, 3993
silane, fluorodimethyl-
  prodn. of, in recoil tritium reactions w/ $(CH_3)_3SiF$, 301
silane, fluorotrimethyl-
  reaction of CD_3 radicals w/, 603; recoil tritium reactions: parameters affecting substitution, 301
silane, tetramethyl-
  adsorption on oxidized Al foil, 1887; anisotropic solv. shifts by factor anal., 1207; ion–molecule reactions in, 13; nmr in various solvents: nature of solv. effect, 3971; reaction of CD_3 radicals w/, 603
silane, trifluoromethyl-
  reaction of CD_3 radicals w/, 603
silane, trimethyl-
  ion–molecule reactions in, 13
silane-d_3, ethyl-
  far-ir and low freq. Raman of solid, 3993
silanes, chloromethyl-
  bond energy terms, 2480
silanes, fluoromethyl-
  reaction of CD_3 radicals w/, 603
silanes, methyl-
  bond energy terms, 2480
silanes, phenyl-substd.-
  ionization potential and heats of formation of various cpds., 974
silica
  aluminum in: benzene adsorption and *tert*-butylbenzene cracking, 220; esr of atomic Ag on, 2705, 2706; internal hydroxyl groups near the surface, 3147; phase transitions in water adsorbed on, 3322; surface reaction of hexamethyldisilazane w/, 2181
silica, aerosil
  ir of BCl_3 chemisorbed on, 3249
silica, Cab-O-Sil
  –B_2O_3 disk: polymerization of styrene and methyl methacrylate on, 3897; bromination of 4-nitrobiphenyl on, 887; phase transitions in water adsorbed on, 3322; radiolysis of hydrogenous material on: esr, 201
silicate
  transition probabilities of Eu in, glass, 3980
silicates, layer
  see montmorillonite
silicon dioxide
  laser-produced oxygen from, 2412
silicon tetrafluoride
  gas-phase density-dependent directly bonded coupling constant, 437
silk
  mol. mechanism of chain rupture in strained cryst. polymers, 3921
silver
  atomic: esr of, on porous glass and silica gel 2705, 2706; rate of O atom interaction on, 2186; sys. Ho–: equilibria involving gaseous species over, 3264; –Ti–TiO_2 film: temp. change on capacitance of, 1279
silver chloride
  solubility in aq.–nonaq. solv. mixts., 93
silver ion (Ag^+)
  assocn. equil. of, and Cl^- in liq. NH_4NO_3–H_2O mixts., 2060; assocn. equil. w/ Cl^- in NH_4NO_3 melt, 3711; exchange between nitrate melt and potassium zeolite A, 2523
silver nitrate
  sys. $TlNO_3$–: viscosity and conductance props. and laser Raman spectrum for molten mixts., 4025
silyl ions, phenyl-substd.
  energetics of formation, 974
silyl radicals, phenyl-substd.-
  energetics of formation, 974
sodium
  –ethylenediamine solns: extinction coeff. and equilibria, 3092; soly. of He and Ar in liq., 2832; –THF-d_8–naphthalene-d_8 solns.: esr, 843; uv irradn. of, in 3-methylpentane matrix: esr, 35
sodium, isotope of mass 22
  isotopic exchange in zeolites: kinetics and mechanism using radioactive tracer technique, 3855
sodium acetate
  effect on circular dichroism of lysine-rich histone f-1–DNA complexes, 1516; –*N*-methylacetamide solns.: freezing pts. and osmotic and activity coeffs., 2319; nmr of molten alkali acetate solns. of polyhydric alcohols, 1338; vol. change in protonation: medium effects, 1120
sodium aluminum fluoride ($NaAlF_4$)
  ir of matrix isolated, 2609
sodium bromide
  enthalpy in methanol: solv.–isotope effect, 388; film: ir of NO adsorbed on, 2930; heat of dilution, 3317; –*N*-methylacetamide solns.: freezing pts., osmotic coeffs., and act. coeffs., 2313; salt effects in water–alcohol solns.: scaled particle theory applied to salting-out polar mol., 3757; sys. H_2O–$ZnBr_2$–: solute activity coeffs. estd. and compared w/ predictions of Guggenheim theory of solns., 3153; –$ZnBr_2$ mixts.: mol. complexes in the vapor, 3028
soldium chloride
  activity coeff. *vs.* concentration: comparison of theory and exptl., 3790; effect on micellar catalysis, 2707; effect on vol. change resulting in acid–base reaction, 1120; electrical conductances and ionization behavior in dioxane–H_2O solns., 1099; enthalpy of transfer from H_2O to aq. H_2O_2, 2229; film: ir of NO adsorbed on, 2930; heat of dilution, 3317; interactions of positrons w/ defects in crys., 2030; –*N*-methylacetamide solns: freezing pts., osmotic coeffs., and act. coeffs., 2313; Onsager transport coeffs. in aq. solns. of: comparison of exptl. and theory, 3124; osmotic coeffs. of 1 *M* soln., 3723; salt effects in water–alcohol solns.: scaled particle theory applied to salting-out polar mol., 3757; SO_2 adsorbed on: microwave absorption, 2602; sys. CsCl–H_2O–: heats of mixing, 1125; sys. H_2O–CsCl–: volume fraction statistics, 946; sys. KCl–$BaCl_2$–: osmotic and act. coeffs. predicted, 1305; sys. LiCl–$BaCl_2$–: osmotic and act. coeffs., 1305; sys. LiCl–CsCl–: osmotic and act. coeffs., 1305; sys. –LiCl–KCl–: osmotic and act. coeffs., 1305; sys. sodium polyacrylate–H_2O–: additivity rule, 3890; ultrasonic absorption of polyelectrolyte solns. upon addition of, 3367
  use slat effects in Raman study of bisulfate–sulfate sys., 2681
sodium deuteride
  cohesive energy, 1251
sodium dodecyl sulfate
  interactions w/ aq. poly(*N*-vinylpyrrolidone) studied by equil. dialysis, 3135
sodium fluoride
  activity coeff. *vs.* concentration: comparison of theory and exptl., 3790; sys. NaF + AlF_3: ir, 2609
sodium formate
  –*N*-methylacetamide solns.: freezing pts. and osmotic and activity coeffs., 2319
sodium glycinate
  vol. change in protonation: medium effects, 1120
sodium halide
  effect on circular dichroism of lysine-rich histone f-1–DNA complexes, 1516; films: ir of NO adsorbed on, 2930; heats of dilution, 3317;
sodium hydride
  cohesive energy: isotopic substitution effect, 1251; dimer: Rittner ionic model study, 984
sodium hydroxide
  formation of O_3^- in γ-irradiated aq. solns. of, 3030, 3031
sodium iodide
  activity coeff. *vs.* concentration: comparison of theory and exptl., 3790; enthalpy in methanol: solv.–isotope effect, 388; film: ir of NO adsorbed on, 2930; heat of dilution, 3317; –*N*-methylacetamide solns: freezing pts., osmotic coeffs., and act. coeffs., 2313; salt effects in water–alcohol solns: scaled particle theory applied to salting-out polar mol., 3757
sodium ion
  assocn. const. of H_2O w/, in propylene carbonate by nmr, 1477; –Ca^{2+}–Cl^-–H_2O sys.: act. coeffs. by liq. ion-exchange electrodes, 957; enthalpies of transfer to propylene carbonate from methanol or dimethylformamide, 3606; exchange of, and K^+ between nitrate melts and zeolite, 2523; –H^+ exchange of α-zirconium phosphate: thermodn. treatment, 3750; in sea water by difference chromatography, 1418; ion-exch. selectivity coeff. for, w/ KA zeolite, 85; –Li^+: ion-exchg. and ionic transport props. of glass membranes, 2821; –nitro aromatic radical anion clusters; esr, 1205; self-diffusion in gels, 1821; viscosity coeffs., B_η, in various solvents, 2532

sodium ion, isotope of mass, 22
exchange rates between free and bound couterions in polyelectrolyte solns., 1990

sodium nitrate
corresponding states and glass transition, 2306; –*N*-methylacetamide solns.: freezing pts., osmotic coeffs., and act. coeffs., 2313; soly. of nonpolar gases in molten, 821; yields of H_2O_2 in radiolysis of aq. solns. containing, 3950
use e^- scavenging efficiency in aq. solns., 1941; recombination luminescence of tryptophan, 2887

sodium perchlorate
conductance and assocn. behavior in H_2O at 25°, 3290; effect on circular dichroism of lysine-rich histone f-1–DNA complexes, 1516; solute–solv. interactions studied by nmr, 3141; viscosity study in dimethyl sulfoxide, 1727

sodium perfluorooctanoate
micelle structure by ^{19}F nmr, 942

sodium permanganate
thermal decompn. induction period: radn. effects, 191

sodium polyacrylate
exchange rates between free and bound counterions in, 1981, 1985, 1990; sys. $NaCl–H_2O$–: additivity rule, 3890

sodium polyphosphate
exchange rates between free and bound couterions in, 1981

sodium propionate
–*N*-methylacetamide solns: freezing pts. and osmotic and activity coeffs., 2319

sodium salts
ionic solvation in acetone: spectroscopic studies, 56

sodium tetraphenylborate
ionic solvation in acetone: spectroscopic study, 56

sodium thiocyanate
nmr of molten, –KSCN solns. of pentaerythritol, 1338; viscosity study in dimethyl sulfoxide, 1727

sodium trifluoromethanesulfonate
viscosity study in dimethyl sulfoxide, 1727

Sorbitan monooleate
effect on dielectric props. of water-in-oil emulsions, 537

squaric acid
conductance stucy of aq. dissocn., 1798

stearic acid, magnesium salt
effect on dielectric props. of water-in-oil emulsions, 537

(*E*)-stilbene
heat of formation estd. by group additivity, 4047

(*E*)-stilbene, *p,p'*-dinitro-
anion radical: electronic spectra and MO interpretation, 2591

stilbene, 2,2'4,4'6,6'-hexanitro-
heat of formation estd. by group additivity, 4047

strontium bromide
solvation studies in high dielectric solvents, 2325

strontium chloride
ionic entropy correlations of mixed electrolyte solns., 946; ion-pair formation and mutual diffusion in aq. soln., 663; solvation studies in high dielectric solvents, 2325

strontium hydroxyapatite
nature of deficiency in nonstoichiometry: catalytic activity, 3167; spectroscopic studies, 3172

strontium ion ($^{85}Sr^{2+}$)
–Ba^{2+} ion-exchange kinetics in vermiculite, 2484

strontium perchlorate
–HCl mixts.: act. coeffs., 1305

styrene
polymerization on porous glass: ir, 3897

styrene, *o*-chloro-
polymerization on porous glass: ir, 3897

styrene, methyl-
polymerization on porous glass: ir, 3897

styrene, α-methyl-
carbanions derived from: nmr, 1062

styrene, polymer
Newtonian viscosity of conc. solns. of: corresponding state relations, 256; non-Newtonian viscosity and excluded vol. effect of dilute solns., 1141

styrene sulfonate, polymer
site binding of counterions in solns. of: ultrasonic absorption, 3367

succinaldehyde
photodecompn. prod. of γ-butyrolactone, 2733

succinic acid
reaction of H atoms in aq. solns. of, 449; reactions w/ H atoms: kinetics by esr, 1654

succinic acid, mercapto-
radicals produced in irradn. of aq. solns., 2277

sulfate
–bisulfate sys: Raman study, 2672; salts containing: enhancement of micellar catalysis, 2707; viscosity independence of half-width of $\nu_1(A_1)$ Raman line, 2684
use pulse radiolysis of aq. halide solns., 3081

sulfate, fluoro-; radical ($SO_3F\cdot$)
esr in soln.: temp.-dependent line width, 712

sulfide, bis(4-alkoxyphenyl)
esr of hydroxy- and methoxy- cpds., 411

sulfide, diethyl
vapor phase charge-transfer complexes w/ I_2, 1057

sulfite
pulse radiolysis of aq. alk. solns. of, 3510

sulfolane
solute–solv. interactions studied by nmr, 3141

sulfonium, triethyl-; bromide
interaction w/ halide ions studied by nuclear quadrupole relaxation, 2936

sulfonium, trimethyl-; bromide
interaction w/ halide ions studied by nuclear quadrupole relaxation, 2936

sulfoxide, dimethyl
assocn. consts. of aromatic amines w/, by ir, 1157; complexes w/ aromatic amines: calorimetric detn. of enthalpies of assocn., 3149; nmr of polar solutes in: nature of solv. effect, 3971; solute–solv. interactions studied by nmr, 3141; transport behavior: conductance–viscosity behavior of tetrapentylammonium thiocyanate in, 3586; transport behavior: viscosity of electrolyte solns., 1727; –water mixts.: viscosity and local liq. structure in, 98

sulfoxide, 8,8,8-trifluorooctyl methyl
micelle structure by ^{19}F nmr; prepn., m.p., 547

sulfur, colloidal
radiolysis of,: mech. for solubilization, 756

sulfur, liquid
color, spectra and composition at various temp., 912

sulfur, purple
Raman spectrum, 4059

sulfur dioxide
adsorbed on NaCl and KCl: microwave absorption, 2602; dielectric absorption of adsorbed, in microwave region, 532; mol. complex formation equil.: solv. effects, 2413; prod. in photolysis of $CS_2–O_2$ mixts., 854; radn.-induced oxidn. of liquid, containing O_2 and H_2O, 3631

sulfur hexafluoride
autodetachment lifetimes, attachment cross section, and negative ions formed by, 3517; quenching of excited states of C_6H_5F by, 3662
use scavenger in radiolysis of butane, 2854

sulfur tetrafluoride
autodetachment lifetimes, attachment cross section and negative ions formed by, 3517

sulfur trioxide
–triethylamine; micellar effects on hydrolysis of 1763

sulfuric acid
constitution, equilibria, and ultrafast H^+ transfer; Raman, 2672; Cu^I- and Cu^{II}-catalyzed D exchg. in solns. of, 571; protolysis kinetics of diamines in, 2400
use acid–base equil. of fluorescein, 245

superoxide ion
see hyperoxide ion

surfactants, cationic
micellar effects on triethylamine–SO_3 hydrolysis, 1763

surfactants, nonionic
critical micelle concn. by difference spectrophotometry, 804; investigation of aq. mixts. by membrane osmometry, 2212; micelle formation by, in water–ethylene glycol mixts., 809; micelle structure by nmr of fluorine-labeled, 547

tartaric acid
prod. from irradn. of crys. glycollic acid, 1648; reaction w/ H atoms: kinetics by esr, 1654

telluric acid (H_2TeO_3)
^{129}I Mössbauer studies of chem. effects of nuclear transformations, 2867

telluric acid $(H_2TeO_4)_n$
^{129}I Mössbauer studies of chem. effects of nuclear transformations, 2867

telluric acid (H_6TeO_6)
^{129}I Mössbauer studies of chem. effects of nuclear transformations, 2867

tellurium oxide (tetragonal TeO_2)
^{129}I Mössbauer studies of chem. effects of nuclear transformations, 2867

tellurium oxide (α-TeO_3)
  ^{129}I Mössbauer studies of chem. effects of nuclear transformations, 2867
terbium dicarbide (TbC_2)
  dissocn. energy, 848
terbium oxides (TbO, TbO_2)
  spectroscopy of, molecules in inert matrix, 514
m-terphenyl
  Pt-cat. isotopic H exchange, 1175; quantum yield of sensitized phosphorescence: externa heavy-atom effect, 1921
p-terphenyl
  Pt-cat. isotopic H exchange, 1175
p-terphenyl, bridged
  electronic spectra, 318
p-terphenyl, substituted
  electronic spectra, 318
tetracene
  radical cation dimers: formation and electronic absorption spectra, 1768
n-tetradecane
  acentric factor and entropy of vaporization, 166
tetralin
  thermochem., thermodn. fcns., and mol. structure, 1264
tetrasiloxane, decamethyl-
  prod. of irradn. of octamethyltrisiloxane, 2430
thallium nitrate
  sys. $AgNO_3$–: viscosity and conductance props. and laser Raman spectrum for molten mixts., 4025
thallium oxide (Tl_2O)
  infrared, 1963; vibrational analysis, 3908
thiacyclobutane
  laser-induced reactions w/ O_2, 725
thiacyclopentane
  laser-induced reactions w/ O_2, 725
thioacetamide-d_3, *N*,*N*-dimethyl-
  C–N rotational barriers, 3532
thiocyanate ion
  effect on circular dichroism of lysine-rich histone f-1–DNA complexes, 1516; transport behavior in dimethyl sulfoxide, 1727; yields of H_2 in radiolysis of aq. solns. containing, 3950
  use pulse radiolytic study of O^-, 1738
thiodiglycol
  dielectric props., 1240
thiols
  radicals produced in irradn. of aq. solns. of, 2277
thiophene
  e^- donor–acceptor complexes by glc: thermodn. study, 2632
thiophene, substituted
  e^- donor–acceptor complexes by glc: thermodn. study, 2632
thiophene, tetrahydro-
  see thiacyclopentane
thioridazine HCl
  micelle formation: nmr in D_2O, 3554
thiosulfate
  photochem. of alkaline, aq. solns. in a flow sys.: esr of radicals prod., 2752
thiuram disulfides and monosulfides, *N*,*N*,*N*′,*N*′-tetralkyl-
  hindered rotation about S_2C–NR_2 bond by nmr, 1067
thorium
  soly. in ThF_4, 2340
thorium fluoride
  soly. of liq. Th in, 2340
thorium oxide (ThO_2)
  epr of CO adsorbed on, 895
threonine
  proton-transfer reactions: kinetics, 161
thulium oxide (TmO)
  spectroscopy of, molecules in inert matrix, 514
thymine
  nanosecond pulse radiolysis of aq. solns., 3815; photoionization studied by esr: cation and anion radicals of, 626
tin halides (SnX_2, SnX_4)
  adducts w/ diisopropyl methylphosphonate: ir and pmr, 637
tin telluride (SnTe)
  vaporization, 118
titanium
  attack of, by atomic fluorine, 308; –TiO_2–Ag film: temp. change on capacitance of, 1279
titanium chloride ($TiCl_3$)
  use epr of hydrazines, 2048
titanium halides (TiX_4)
  adducts w/ diisopropyl methylphosphonate: ir and pmr, 637
titanium ion (Ti^{3+})
  reaction w/ H_2O_2 in presence of 2-propanol using esr flow technique, 3271; sys. containing: short-lived radicals generated by fast flow techniques, 2957
titanium ion (Ti^{4+})
  reactions w/ organic radicals formed by "Fenton-like" reagents, 3271
titanium oxide (TiO)
  spectroscopy in inert matrices at 4°K, 3243
titanium oxide (TiO_2)
  spectroscopy in inert matrices at 4°K, 3243; surface properties by ir, 1216, 1221; –Ti–Ag film: temp. change on capacitance of, 1279
toluene
  adsorption of vapor on water by glc, 3870; adsorption on Cu(II) montmorillonite: spectroscopic study, 3957; enthalpies of soln. in various polar solvents, 3598; enthalpy in methanol: solv.-isotope effect, 388; –ethanol mixts.: viscosity coeff. data of, and diffusion coeffs. of I_2 in, 963; far-ir, 2942; π H-bonding w/ naphthylamine, 2404; ignition of, –O_2 mixts. by shock waves, 1501; isothermal piezooptic coeff. w/ ultracentrifuge, 716; product of reaction of energetic ^{14}C ions w/ solid benzene, 2555
toluene, chloro-
  thermodns. of soln. in liq. crys. solvents for *o*-, *m*-, and *p*-, 2005
toluene, dinitro-
  anion radicals of the various isomers: electronic spectra and MO calcns., 2591
toluene, 2,6-dinitro-
  heat of formation estd. by group additivity, 4047
toluene, fluoro-
  photochem. of *o*-, *m*-, and *p*-, 3214
toluene, nitro-
  anion radicals of *o*-, *m*-, and *p*-: electronic spectra and MO interpretation, 2591
toluene, 2,4,6-trinitro-
  heat of formation estd. by group additivity, 4047
toluene-^{14}C
  degradn. of, and its mechanism of formation, 3524
p-toluenesulfonamide, *N*-chloro-
  see chloramine-T
toluenesulfonate
  effect on micellar catalysis, 2707
transition metal complexes
  opt. act. of trigonally distorted cubic sys., 692
s-triazine, 1,3,5-trinitrohexahydro-
  mol. conformation in soln.; ir, Raman, nmr, mol. opt. anisotropy, 2056
tributyl phosphate
  charge density on phosphoryl oxygen, 3309
tricyclo[3.3.1.1^{3,7}]decane
  see adamantane
tricyclo[5.2.1.0^{2,6}]decane
  thermochem., thermodn. fcns., and mol. structure, 1264
tricyclo[3.2.2.0^{2,4}]nona-6,8-diene-6,7-dicarboxylate, dimethyl-
  intermed. prod. in degradn. of cycloheptatriene-^{14}C, 2558
n-tridecane
  acentric factor and entropy of vaporization, 166
2-tridecanone
  cohesive energy, 642
tridodecylamine salts
  mol. assocn. and dielectric consts. in benzene, 542
triethanolamine hydrobromide
  interaction w/ halide ions studied by nuclear quadrupole relaxation, 2936
triethylaluminum
  see aluminum, triethyl-
triethylamine
  –SO_3; micellar effects on hydrolysis of, 1763
triethylamine hydrobromide
  interaction w/ halide ions studied by nuclear quadrupole relaxation, 2936
triethylenediamine
  see 1,4-diazabicyclo[2.2.2]octane
triisobutylaluminum
  see aluminum, triisobutyl-
trimethylamine
  adsorption on TiO_2 by ir, 1221; esr study of radicals prod. in irradiated aq. soln. of, 738; mol. complex formation equil: solv. effects, 2413; reaction w/ BH_3, 2711
trimethylamine hydrobromide
  interaction w/ halide ions studied by nuclear quadrupole relaxation, 2936
trimethylamine-^{15}N
  ^{15}N chem. shift, 932
trimethylamine-^{15}N hydrochloride
  ^{15}N nmr, 1758

triphenylamine
use radiolysis of H_2O on porous glass, 201
triphenylene
complex w/ pyromellitic anhydride: photochem., 3805
trisiloxane, octamethyl-
radiation chem., 2430
tritium
recoil reactions w/ 1-butene and (*Z*)-2-butene, 3771; recoil reactions w/ *c*-C_4D_8: excitation energies accompanying T for D substitution, 3781
tritium (T_2)
H displacement in butane by, and T_2^+ collisions, 2417; reactions of fast, w/ 1-butene, 2407
tryptophan
afterglow and thermoluminescence in ethylene glycol–water glass, 2887; environmental effects on deprotonation of, 3061; kinetics of photoionization, 2887
L-tryptophan ethyl ester, *N*-acetyl-
α-chymotryptic hydrolysis of, 1375, 1387
tungsten
attack of, surface by atomic fluorine, 308; sys.: oxygen–bromine–; thermodn. study, 112
tungsten oxybromides
thermodn. study, 112
p-tyramine
zwitterion formation upon deprotonation, 2657
tyrosine
zwitterion formation upon deprotonation of, and its ethyl ester, 2657

n-undecane
acentric factor and entropy of vaporization, 166; thermodns. of soln. in liq. crys. solvents, 2005
6-undecanol
–urea inclusion compound: esr of X-irradiated, 3489
n-1-undecene
thermodns. of soln. in liq. crys. solvents, 2005
undecylenoic acid, *p*-(*p*-ethoxyphenylazo)phenyl ester
proton spin–lattice relaxation, 2452
uracil, 1-methyl-
calcns. of opt. props. of crys., 1509; H-bonding of, in dimethylsulfoxide-d_6 by nmr, 3963
uranium ion (U^{3+})
reaction w/ $[Co(NH_3)_4(H_2O)_2]^{3+}$ in aq. ClO_4^-, 2117
uranium ion (U^{4+})
coordn. effects on spectrum of, in molten fluorides, 631; prod. in reaction $U^{3+} + Co(NH_3)_4(H_2O)_2^{3+}$, 2117
uranium oxide (UO)
ir spectrum of matrix-isolated, 2283
uranium oxide (UO_2)
ir spectrum of matrix-isolated, 2283
uranyl nitrate
ionic entropy correlations of mixed electrolyte solns., 946
uranyl nitrate hexahydrate
self-diffusion of water in, 1272
uranyl sulfate
heat of dilution and thermodns. of dissocn., 2368
urea
–alcohol inclusion compounds: esr of X-irradiated, 3489; effect of, on ultrasonic absorption of protein solns., 374; effect on vol. change resulting in acid–base reaction, 1120; effects of, on water structure: heats of soln. and nmr, 815; micelle structure in aq. soln. of: ^{19}F nmr, 547; nmr study of hindered internal rotation in soln., 1901; proton exchange in aq. solns., 2123; reaction w/ H atoms: kinetics by esr, 1654
urea, 1,3-dimethyl-
effects of, on water structure: heats of soln. and nmr, 815
urea, *unsym*-dimethylseleno-
hindered rotation barriers by nmr, 3372
urea, tetramethyl-
effects of, on water structure: heats of soln. and nmr, 815; –water mixts: effects of H-bonding on vapor press., viscosities, densities, surface tensions, heat of mixing, and molar refractivities, 3313
urea, thio-
effects of, on water structure: heats of soln. and nmr, 815

valeric acid
see pentanoic acid
valine, derivatives
conformations by nmr, 505
vanadium(IV)
reaction w/ H_2O_2 in presence of 2-propanol using esr flow technique, 3271
vanadium(V)
oxidn. of H_3PO_2 by, 891
vanadium oxide (V_2O_5)
esr of abnormal alkyl radicals on porous Vycor coated w/, 4064
vanadyl, bispicolinato-
epr probe for hydrophobic interaction in various aq. solns., 165
vanadyl ion (VO^{2+})
axial coordn., 599
vanadyl sulfate
heat of dilution and thermodns. of dissocn., 2368
vermiculite
ion-exchange kinetics, 2484
vinyl alcohol, polymer
concn. quenching of proflavine HCl in dry films of, 2727; –water soln.: anomalous freezing behavior, 2623
violenes, nitrogen containing
electronic spectra and LCI–SCF calcns., 335
vitamin A aldehyde
see all-trans-retinal
Vycor, fiber
dynamic adsorption of H_2O vapor on, 2718
Vycor, porous
dielectric absorption in microwave region of CO_2 adsorbed on, 532; esr of abnormal alkyl radicals trapped on V_2O_5 coated, 4064; radiolysis of hydrogenous material on: esr, 201

water
adsorbed on silica: phase transitions, 3322; absorption coeff. and ionization yield at 58.4 nm, 719; adsorption of sparingly sol. vapors on, 3870; adsorption on α-chromia using ir, 2774; adsorption on oxidized Al foil, 1887; bubble nucleation, 3613; –dimethyl sulfoxide mixts.: viscosity and local liq. structure in, 98; effects of some protein denaturants on, structure, 815; effect on epr of complex-bonded *tert*-$BuO_2\cdot$, 2580; equil. rate of exchange of, at air–water interface using nmr, 2694; flash photolysis of, at −10°, 40; –formaldehyde sys.: mol. orbital calcns., 1744; high-precision viscosity of supercooled, and anal. of extended range temp. coeff., 2016; ion decompn.: translational energy of fragments calcd., 2458; mol. complex formation equil.: solv. effects, 2413; –nonelectrolyte mixts.: ultrasonic velocity, 2336; –oil emulsion: effect of emulsifying agent on dielectric props. of, 537; pH: effect of magnetic field, 2830; physisorption on ZnO, 3822; proton exchg. between guanidium ion and, in aq. dimethylacetamide by nmr; radiolysis of, on porous glass: esr, 201; radn.-induced oxidn. of liq. SO_2 containing, 3631; reaction of Fe in aq. HCl kinetic isotope effects, 2112; salt effects in, alcohol solns : scaled particle theory applied to salting-out polar mol., 3757; solute–solv. interactions studied by nmr, 3141; supercooled: radn. chem., 2997; sys. hexamethylenetetramine–: thermodn. data, 3633; –tetramethylurea mixts: effects of H-bonding on vapor press., viscosities, densities, surface tensions, heat of mixing, and molar refractivities, 3313; "two-state" thermodns. and transport props., 3698
water (D_2O)
absorption on α-chromia using ir, 2774; exchange of surface OH groups in TiO_2 w/, 1216; isothermal diffusivity of aq. solns. by hologram interferometry, 3374; radiolysis of, on porous glass: esr, 201; reaction of Fe w/ HCl in: kinetic isotope effects, 2112
use micelle formation of phenothiazene derivatives: nmr in, 3554; prepn. of CH_2D and CHD_2 radicals, 2448; self-diffusion of water in uranyl nitrate hexahydrate, 1272
water, amorphous
glass transition temperature, 967, 3379
water, anomalous
prepn.: a high-yield method, 2976
water, ice
far-uv, 1162
water, sea
difference chromatography, 1418; size determination of drops, 3623
water, vapor
dynamic adsorption on Vycor fiber, 2718

xanthate, ethyl
oxidn. of on Pt, Au, Cu, and galena electrodes, 354
xenon
absorption coeff. and ionization yield at 58.4 nm, 719; adsorption on liq. Hg: virial treatment, 344; effect on thermal isomerization of C_2H_5NC, 1366
use photolysis of CH_2N_2–propane mixts., 1537
xenon fluorides XeF_2, XeF_4, XeF_6
photoionization mass spec. study, 1461
xylene
reactivity w/ OH radicals, 3640
m-xylene
adsorption on Cu(II) montmorillonite: spectroscopic study,

3957; ignition of, –O_2 mixts. by shock waves, 1501; photochem., 2741; thermodns. of soln. in liq. crys. solvents, 2005

o-xylene
adsorption on Cu(II) montmorillonite: spectroscopic study, 3957; ignition of, –O_2 mixts. by shock waves, 1501; photochem, 2741; thermodns. of soln. in liq. crys. solvents, 2005

p-xylene
adsorption on Cu(II) montmorillonite: spectroscopic study, 3957; π H-bonding w/ naphthylamine, 2404; ignition of, –O_2 mixts. by shock waves, 1501; photochem., 2741; thermodns. of soln. in liq. crys. solvents, 2005

2,6-xylenol
polarographic redn. of O_2 in presence of, 4019; reaction w/ complex-bonded *tert*-butylperoxyl; epr, 2580

ytterbium
metal–YbF_2 phase diagram, 2340

ytterbium fluoride (YbF_2)
–Yb phase diagram, 2340

yttrate, hexachloro-; dicesium sodium salt
thermochem., 392

yttrium oxide (YO)
low-lying electronic states, 3103

zeolite
Al deficient: ir study, 2408; esr of O_2^- on AlHY, ScY, and LaY, 1165; esr study of adsorbed alkene molecules on synthetic, 3475; isotopic exchange kinetics and mechanism, 3846, 3855; structure of potassium-exchanged synthetic X and Y type using X-ray diffraction, 3327

zeolite A, potassium
ion exchanger in nitrate melts, 2523

zeolite Linde A
ion-exchange selectivity of, in nonaq. and mixed media, 85

zinc(II) *m*-benzenedisulfonate
outer-sphere assocn. kinetics in MeOH by ultrasonic relaxation, 2649

zinc bromide ($ZnBr_2$)
–NaBr mixts.: mol. complexes in the vapor, 3028; sys. H_2O–NaBr–: solute activity coeffs. estd. and compared w/ predictions of Guggenheim theory of solns. 3153

zinc ion (Zn^{2+})
catalysis of exchange of ethanol hydroxyl proton, 1994; –C_2H_4–maleic acid copolymer complexes: heats of assocn., 1136; competition for e_{aq}^- between e_{aq}^- scavengers, 3626

zinc oxide (ZnO)
decompn. of $HClO_4$ over, 491; decompn. of N_2O on, 1037; esr of, formed from decompn. of ZnO_2, 3089; hydrogenation of C_2H_4 on, 208; isomerization of butene over, 487; photoassisted dissocn. of N_2O over, 617; physisorption of water on, 3822

zinc perchlorate [$Zn(ClO_4)_2$]
prodn. of in decompn. of $HClO_4$ over, 491

zinc peroxide (ZnO_2)
esr study, 3089

zinc sulfate
ion-pair formation and mutual diffusion in aq. soln., 663; Onsager transport coeffs. in aq. solns. of: comparison of exptl. and theory, 3124

α-zirconium phosphate
thermodn. treatment of H^+–Na^+ exchange of, 3750

what's happening

on the frontiers

of chemical research?

ACCOUNTS
OF CHEMICAL
RESEARCH
LETS YOU KNOW...

in short, critical articles

that cover all areas *of*

chemical research.

Whether you are a practicing chemist, professor or student, you want to keep up with the latest developments. Yet few of you have the time to read thoroughly all the journals of primary publications. ACCOUNTS fills the gap.

Written by investigators active in the fields reviewed, ACCOUNTS' concise, brief articles place recent developments in perspective—and relate them to earlier work and their probable future significance.

Once you start relying on ACCOUNTS to keep you informed, you'll wonder how you got along without its monthly arrival.

Complete and mail back
the form below. We'll
prove how valuable this
publication can be to you.

American Chemical Society / 1155 Sixteenth Street, N.W., Washington, D.C. 20036

Please send me ACCOUNTS OF CHEMICAL RESEARCH at the following subscription rates:

ACS members:	☐ U.S. $ 5.00	☐ Canada, PUAS $ 8.00	☐ Other Nations $ 8.50
Nonmembers:	☐ U.S. $10.00	☐ Canada, PUAS $13.00	☐ Other Nations $13.50

Name ______________________ Title ______________________

Employer ______________________

Address: ☐ Home ☐ Business ______________________

City ______________ State/Country ______________ Zip ______________

Nature of employer's business? ☐ Manufacturing or processing ☐ Academic ☐ Government
☐ Other ______________________
(Please indicate)

Note: Subscriptions at ACS Member Rates are for personal use only.

☐ I am an ACS member ☐ I am not an ACS member

Payment must be made in U.S. currency, by international money order, UNESCO coupons, U.S. bank draft; or order through your book dealer.

need to know about…

The most advanced theory?
The latest applications?
Newest chemicals and reagents?

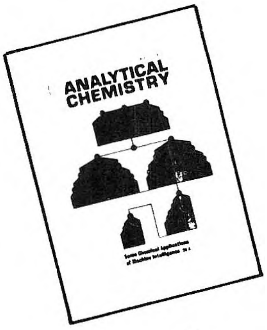
ANALYTICAL CHEMISTRY

Then ANALYTICAL CHEMISTRY is designed for you.

Each month you receive information that is fresh, current and relevant to *today's needs*. Brand new ideas are introduced. One of them might be the answer to one of your problems.

Two other good reasons for starting your ANALYTICAL CHEMISTRY subscription now are the 1971-72 *LABORATORY GUIDE* to Instruments, Equipment and Chemicals and the valuable *ANNUAL REVIEWS* issue.

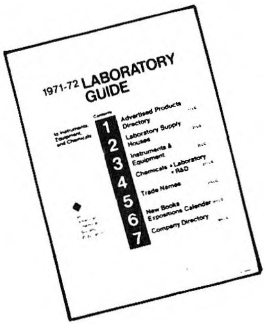
1971-72 LABORATORY GUIDE
1 Advertised Products Directory
2 Laboratory Supply Houses
3 Instruments & Equipment
4 Chemicals • Laboratory • R&D
5 Trade Names
6 New Books Expositions Calendar
7 Company Directory

The 500-page LABORATORY GUIDE gives you 20,000 separate entries with more than 1000 manufacturers selling over 600 products.

The special April ANNUAL REVIEWS issue presents authoritative researchers reviewing the latest methodology and applications of analytical science.

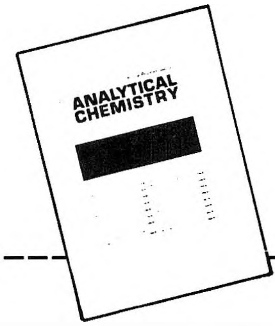
ANALYTICAL CHEMISTRY

Be sure to benefit from AC's thorough coverage of the analytical sciences. Just complete the form below and mail it back to us today.

American Chemical Society / 1155 Sixteenth Street, N.W., Washington, D.C. 20036

Please send me ANALYTICAL CHEMISTRY at the following subscription rates:

ACS members:	☐ U.S. $5.00	☐ Canada $7.00	☐ PUAS $ 7.50	☐ Other Nations $ 8.50
Nonmembers:	☐ U.S. $7.00	☐ Canada $9.50	☐ PUAS $17.50	☐ Other Nations $18.50

Note: Subscriptions at ACS Member Rates are for personal use only.

NAME ____________________ POSITION ____________________

ADDRESS ____

CITY ____________________ STATE/COUNTRY ____________ ZIP ________

YOUR COMPANY ____________________ NATURE OF COMPANY'S BUSINESS ____________________

☐ **I am an ACS member** ☐ **I am not an ACS member** ☐ **Bill me for $**____________________

☐ Payment enclosed in the amount of $______________(payable to American Chemical Society). Payment must be made in U.S. currency by international money order, UNESCO coupons or U.S. bank draft; or order through your book dealer.

A2A